Le rôle du pergélisol dans le cycle du carbone mondial sur les échelles de temps des siècles à plusieurs millénaires : une étude de modélisation

Katherine Crichton

UNIVERSITÉ DE GRENOBLE

THÈSE

Pour obtenir le grade de

DOCTEUR DE L'UNIVERSITÉ DE GRENOBLE

Spécialité : **Terre, Univers, Environnement**

Arrêté ministériel : 7 août 2006

Présentée par

Katherine CRICHTON

Thèse dirigée par **Jerome CHAPPELLAZ**
codirigée par **Didier ROCHE**

préparée au sein du **Laboratoire de Glaciologie et Géophysique de l'Environnement**
dans **l'École Doctorale TUE Océan Atmosphère Hydrologie**

The role of permafrost soils in the global carbon-cycle on the timescales of centuries to multi-millennia. A modelling study.

Thèse soutenue publiquement le **« 17 octobre 2014 »**,
devant le jury composé de :

M. Victor BROVKIN
Associate Professor, Max Planck Institute for Meteorology (Rapporteur)
M. Yves GODDERIS
Directeur de Recherche Observatoire Midi-Pyrénées (Rapporteur)
M. Didier SWINGEDOUW
Charge de Recherches, CNRS, EPOC (Examinateur)
M. Jean BRAUN
Professeur UJF, (Président du jury)
M. Jerome CHAPPELLAZ
Directeur de recherche, LGGE (Directeur de thèse)
M. Didier ROCHE
Charge de Recherches, LSCE (Co-encadrant)
M. Gerhard KRINNER
Directeur de recherche, LGGE (Invité)

Université Joseph Fourier / Université Pierre Mendès France /
Université Stendhal / Université de Savoie / Grenoble INP

Acknowledgements

This work was possible thanks to funding as of the European Commission's "GREENCYCLES II" Marie Curie Initial Training Network

Thanks to all the people involved with Greencycles II, for the workshops, meetings, events and general inspiration. Without this network, the results would have been no results at all.

Thanks to Nathaelle Bouttes for invaluable and generous help and advice. Thanks also to Didier Roche, Jerome Chappellaz, Gerhard Krinner and Gilles Delaygue. Also thanks for various supervision and advice from anyone who agreed to talk, particularly Victor Brovkin, Andrey Ganopolski, Guy Munhoven and Peter Cox.

Many thanks especially to Patrice Cumin for support and for being very patient.

The research leading to these results has received funding from the European Community's Seventh Framework Programme (FP7 2007-2013) under Grant 238366 (GREENCYCLES II) and under grant GA282700 (PAGE21, 2011-2015).

Ocean, atmosphere, land and cryosphere

Greenland. K Crichton, 2011

Resume

Cette étude visait à développer un modèle dynamique du pergélisol-carbone à intégrer dans le modèle CLIMBER-2 et d'effectuer des simulations en vue de contribuer à la connaissance du cycle du carbone. Ce travail pourrait, pour la première fois, permettre une étude de modélisation avec un modèle de système terrestre qui comprendrait l'atmosphère dynamique, l'océan dynamique, la végétation dynamique et les composantes de la cryosphere, y compris les terres gelées, afin d'étudier le paléoclimat. La disponibilité des données récentes du CO_2 et de $\delta^{13}C$ de CO_2 dans l'atmosphère fourni un moyen de valider les résultats du modèle pour déterminer si une dynamique pergélisol-carbone pourrait avoir joué un rôle important au cours des climats changeants.

La preuve du changement du carbone-13 dans l'océan profond a indiqué que le changement de la concentration de CO_2 dans l'atmosphère pendant les périodes glaciaires n'a pas été causé par l'absorption du carbone par la biosphère terrestre (Broecker et Denton, 1989). Le fractionnement de carbone lors de la photosynthèse provoque une signature de $\delta^{13}C$ de matière organique végétale d'environ -25‰ (Maslin et Thomas 2003) par rapport à la source. Le changement de $\delta^{13}C$ de l'océan entier est d'environ -0.35‰ entre le LGM et le PI. Afin de réaliser ce changement dans l'océan, une source de carbone de ~500GtC avec la signature de $\delta^{13}C$ de -25 ‰ est nécessaire, par exemple une réduction de la biosphère terrestre. Cette source augmenterait le CO_2 atmosphérique d'environ 25ppmv (Archer, 2010). La conclusion était que entre les périodes interglaciaires et les périodes glaciaires, les changements de CO_2 atmosphérique devaient être causée par l'absorption de carbone dans l'océan. Cette absorption de carbone par l'océan devait être suffisamment forte pour compenser le CO_2 atmosphérique de 25ppmv supplémentaire (par biosphère terrestre) au dessus de ~100ppmv vu dans l'atmosphère entre interglaciaire et périodes glaciaires. Les reconstructions de la variation de la taille de la biosphère terrestre, par

pollen, entre la dernière période glaciaire et l'actuel, indiquent qu'elles avaient augmenté d'environ 1000GtC (Crowley, 1995). Cela semble confirmer que l'océan était la source de carbone de l'atmosphère au cours de la terminaison glacial. Toutefois, un mécanisme qui n'est ni représenté dans les études de modélisation couplés paléo-climatiques, ni dans les reconstructions de la biosphère terrestre (comme NPP, Productivité Primaires Nette) est l'effet des sols gelés. Les concentrations élevées de carbone dans les sols gelés aujourd'hui (Tarnocai et al 2009) et des études de paleosols (Zimov et al 2006, Ciais et al 2012) soulignent l'importance du pergélisol dans le climat qui est à la fois directement et indirectement lié au cycle du carbone. De plus, les données de $\delta^{13}C$ atmosphérique tout au long de la terminaison glaciaire montre une chute rapide de $\delta^{13}C$ atmosphérique puis une reprise (Schmitt et al 2012). Les différences entre les estimations de l'évolution de la biosphère terrestre a base de $\delta^{13}C$ de l'océan et à base de pollen, les sols dans les régions de pergélisol riche en carbone et la baisse rapide de $\delta^{13}C$ atm pendant le début de terminaison se combinent afin de créer le début de cette étude.

Les modèles complexes sont concentrées sur l'océan en tant que contrôleur principal de dioxyde de carbone dans l'atmosphère sur des échelles de temps glaciaires et millénaires. La profondeur de l'océan Austral est une zone d'intérêt particulière concernant la variabilité de CO_2 glaciaire-interglaciaires. Les efforts de modélisation actuels visent à recréer les changements de CO_2 observées en utilisant les mécanismes de l'océan. Ceux-ci sont souvent liés au stockage et libération de carbone dans l'océan Austral profond. Jusqu'à présent, la biosphère terrestre n'a pas été bien prise en compte dans les simulations transitoires du cycle du carbone dans les modèles du système terrestre.

Un mécanisme pergélisol-carbone simplifié a été développé et validé et à été réglé en utilisant les données de la terminaison 1. Il a été constaté que, pour reproduire des données de CO_2 et $\delta^{13}C$ atmosphériques (pour l'atmosphère et l'océan) au cours de la terminaison, une combinaison des mécanismes océaniques-glaciaires et pergélisol-carbone ont été nécessaires. Suite à cette constatation, plusieurs cycles glaciaires ont été modélisés pour étudier la sensibilité du mécanisme pergélisol-carbone aux forçages de CO_2, les calottes glaciaires et l'insolation. l'étendue des calottes glaciaires a été jugée particulièrement importante pour le contrôle de la superficie des terres disponibles pour le pergélisol, et donc aussi pour la dynamique du carbone du pergélisol-carbone. La libération du carbone dans les sols de dégel en

réponse à l'augmentation de l'insolation d'été dans les hautes latitudes, a été jugée très probable comme la source des hausses initiales de CO_2 dans l'atmosphère au cours des terminaisons glaciaires.

Les données CO_2 de terminaison 1 peuvent être bien reproduits, y compris le plateau de CO_2 BA / YD, quand le forçage de l'eau douce est appliqué à l'Atlantique nord. Il a été constaté que l'augmentation du CO_2 atmosphérique au début de la terminaison n'a pas besoin d'une coupure et reprise de l'AMOC. La source de la hausse initiale de CO_2 atmosphérique était terrestre, et l'océan n'est devenu une source de carbone qu'après environ 15kyrBP. En réduisant la salinité de l'Atlantique nord au cours de la B-A/YD, l'hémisphère nord a refroidi, le pergélisol a avancé et le carbone a été repris dans les pergélisols. A la reprise de l'AMOC, le transport rapide de la chaleur vers l'hémisphère Nord a causé la fonte du pergélisol et une augmentation rapide du CO_2 atmosphérique.

Expériences avec forçage de l'eau douce ont souligné l'importance du mécanisme du pergélisol-carbone dans l'évolution rapide des climats. Les augmentations très rapides des niveaux de CO_2 dans l'atmosphère peuvent être expliqués par la libération rapide des sols en carbone en réponse à l'augmentation du transport de chaleur vers l'hémisphère nord. C'est en réponse à la reprise de l'AMOC suite d'un événement AMOC arrêt/réduction, tels que des événements D/O vu dans les données du δ18O Groenland. Les projections de changement climatique représentent des événements de réchauffement rapide. La conduite du modèle par des projections d'émissions (base de données RCP) a prédit l'augmentation du CO_2 de pic et une plus longue période a des niveaux élevées de CO_2 par rapport aux sorties du modèle qui ne comprennent pas les évaluations du pergélisol-carbone.

L'analyse de $\delta^{13}C$ de l'océan doit tenir compte de la dynamique du pergélisol et du carbone de la terre en général et de son effet sur les niveaux de $\delta^{13}C$ atmosphériques. Si ce n'est pas pris en compte alors la circulation océanique peut être trop invoquée pour tenter d'expliquer les changements de $\delta^{13}C$ de l'océan et du CO_2 atmosphérique. Le système Terre n'est pas tout simplement l'atmosphère et l'océan. Les conclusions de ce travail soulignent qu'il est essentiel de considérer la dynamique du carbone des sols lors de l'interprétation paléo-indicateurs pour le cycle du carbone.

Le mécanisme pergélisol-carbone réagit aux changements de température et amplifie la réponse du cycle du carbone. Il est fortement dépendant non seulement de l'apport d'énergie (qui détermine la température du sol et de l'emplacement du

pergélisol), mais également de la surface de terres disponible à l'échelle mondiale sur laquelle le pergélisol peut exister. Afin de modéliser et de comprendre correctement la réponse du système terrestre dans les climats futurs et passés, le mécanisme de rétroaction pergélisol-carbone est un élément important du système. Ce travail a été une première étape pour aborder le rôle que la cryosphere terrestre joue dans le cycle du carbone et du système climatique sur de longues échelles de temps, et que d'autres études sont essentielles.

Abstract

This study aimed to develop a permafrost-carbon dynamic model to incorporate into the CLIMBER-2 Earth system model and to carry out simulations with a view to contributing to the knowledge of the carbon cycle. The work would, for the first time, allow a fully coupled modelling study with an earth system model which included dynamic atmosphere, ocean, vegetation and cryosphere components including frozen land to study paleoclimates. The availability of recent ice core data for CO_2 and $\delta^{13}C$ of atmospheric CO_2 was to provide a means of validating model findings to identify whether a permafrost-carbon dynamic could have played a significant role in past changing climates.

Evidence from the change in deep ocean carbon-13, via $\delta^{13}C$ signature of foraminifera shells in ocean sediment cores, indicated that the CO_2 draw-down in the atmosphere during glacial periods was not caused by the terrestrial biosphere carbon uptake (Broecker and Denton 1989). The fractionation of carbon during photosynthesis results in a $\delta^{13}C$ signature of terrestrial plant organic matter of around -25‰ (Maslin and Thomas 2003) with respect to the source. The estimated whole ocean change in $\delta^{13}C$ is around -0.35‰ between the last glacial maximum and the present interglacial. In order to achieve this change a source of carbon with $\delta^{13}C$ signature of -25‰ the size of around 500Gt is required, for example a reduction in the terrestrial biosphere. This source would increase atmospheric CO_2 by around 25ppmv (Archer 2010). The conclusion from this was that changes in atmospheric CO_2 between the interglacial and the glacial periods must be due to the ocean uptake. This uptake of carbon by the ocean must also be strong enough to overcome the extra 25ppmv atmospheric CO_2. Pollen based reconstructions of the change in the size of the terrestrial biosphere between the last glacial period and the present-day indicated it had grown by around 1000GtC (Crowley 1995). This seemed to confirm the $\delta^{13}C$ indication of the ocean as the carbon source during the glacial termination. However, one mechanism that is not represented in the palaeo-climate coupled modelling studies, nor in the NPP (pollen) based reconstructions of terrestrial biosphere is the effect of frozen soils. High carbon concentrations in frozen soils of the present day

(Tarnocai et al 2009) and some studies of past soils (Zimov et al 2006, Ciais et al 2012) point to the importance of permafrost in climate. Both directly and indirectly linked to the carbon cycle. As well as this, a recent record of atmospheric $\delta^{13}C$ throughout the termination period shows a fast drop in $\delta^{13}C$ atm then a recovery (Schmitt et al 2012). The difference between ocean-based and pollen-based estimates of changes in the terrestrial biosphere, the high carbon soils in permafrost regions and the fast drop in $\delta^{13}C$ atm during the termination lead into this study: The role of permafrost soils in the global carbon-cycle on the timescales of centuries to multi-millennia.

Complex models have focussed on the ocean as the main controller of atmospheric carbon dioxide on glacial and millennial timescales. Different vegetation models used with GCMs generally show far more model spread than different ocean models, which complicates comparison of paleoclimate land biosphere studies. The deep Southern Ocean is an area of particular interest for glacial-interglacial CO_2 variability, and current modelling efforts aim to recreate the observed CO_2 changes using ocean mechanisms. These are often related to deep southern ocean carbon storage and release. Sea-ice extent, and its transient changes, in the southern ocean seem to be an important mechanism that may provide a control on the capability of the southern ocean to store carbon. So far the terrestrial biosphere has not been well-considered in transient simulations of the carbon cycle in Earth system models.

A simplified permafrost-carbon mechanism was developed and validated (chapter 3) and tuned using data from termination 1 (chapter 4). It was found that in order to reproduce atmospheric CO_2 and $\delta^{13}C$ data (for atmosphere and ocean) during the termination, a combination of glacial ocean mechanisms and the permafrost-carbon mechanism was required. Following this finding, several glacial cycles were modelled to study the sensitivity of the permafrost-carbon mechanisms to CO_2, ice sheets and insolation (chapter 5). Ice sheet extent was found to be particularly important in controlling the land area available for permafrost and therefore the carbon dynamics of permafrost-carbon. The permafrost-carbon mechanism, via carbon release from thawing soils responding to increasing summer insolation in higher northern latitudes, was found to very likely be the source of initial rises in CO_2 on glacial terminations.

Termination 1 CO_2 data could be well reproduced, including the B-A/YD CO_2 plateau, when fresh water forcing was applied to the north Atlantic. Freshening the

north Atlantic in the B-A/YD period resulted in northern hemisphere cooling and a permafrost advance and soil carbon uptake. On AMOC resumption fast heat transport to the northern hemisphere caused permafrost thaw and a fast rise in atmospheric CO_2. It was found that the rise in CO_2 at the start of the termination did not require an AMOC switch-off and resumption event as the source of the initial CO_2 rise was from the land, and the ocean only became a carbon source after around 15kyrBP.

Fresh water forcing experiments pointed to the importance of the permafrost-carbon mechanism in fast changing climates. Very fast increases in atmospheric CO_2 levels may be explained by fast soil-carbon release responding to increased heat transport to the northern hemisphere on AMOC resumption following an AMOC switch-off/reduction event, such as D/O events seen in the Greenland δ18O record. Future climate change projections represent fast warming events. Driving the model by emissions projections (RCP database) predicted increased peak CO_2 and much longer term elevated CO_2 levels relative to model outputs which did not include the permafrost carbon feedback.

Analysis of ocean $\delta^{13}C$ must take into account the dynamics of permafrost and land carbon in general and its effect on atmospheric $\delta^{13}C$ levels. If this is not taken into account then ocean circulation may be over-invoked in attempting to explain changes in ocean $\delta^{13}C$ and atmospheric CO_2. The Earth system is not simply atmosphere and ocean. The findings in this work highlight that it is essential to consider land carbon dynamics when interpreting paleo-indicators for the carbon cycle.

The permafrost-carbon mechanism reacts to temperature changes and amplifies the carbon cycle's response. It is stongly dependent not only on energy input (that determines soil temperature and permafrost location), but also on the area of land available globally on which it can exist. In order to properly model and understand the Earth system response to forcing in both future and past climates, the permafrost-carbon feedback mechanism is an important system component. This work has been a first step to address the role that the land cryosphere plays in the carbon cycle and climate system on long timescales, and further studies are essential.

"Le rôle du pergélisol dans le cycle du carbone mondial sur les échelles de temps des siècles à plusieurs millénaires. Une étude de modélisation"

Table des matières

1. Introduction et contexte

Échelles de temps et mécanismes du cycle du carbone

Les mécanismes actifs dans le cycle du carbone fonctionnent sur une variété des échelles de temps, de quelques jours à plusieurs millénaires et plus. Ces mécanismes sont représentées sur la figure 1. Les trois mécanismes principaux qui stabilises à long terme le cycle de carbone sont: le homéostat d'oxygène, le thermostat de érosion-CO_2, et le carbonate de calcium pH-stat de l'océan. L'orbite de la terre autour du soleil et le mouvement des plaques tectoniques influent sur le climat parce qu'ils fixent les conditions limites du système terrestre. D'autres mécanismes sont contrôlées par la système entiere, et fournir une rétroaction vers la système entiere, et donc affecte la température et le climat de la surface de la terre. La figure 1 montre des échelles de temps intéressante pour cette étude: de siècles à plusieurs millénaires.

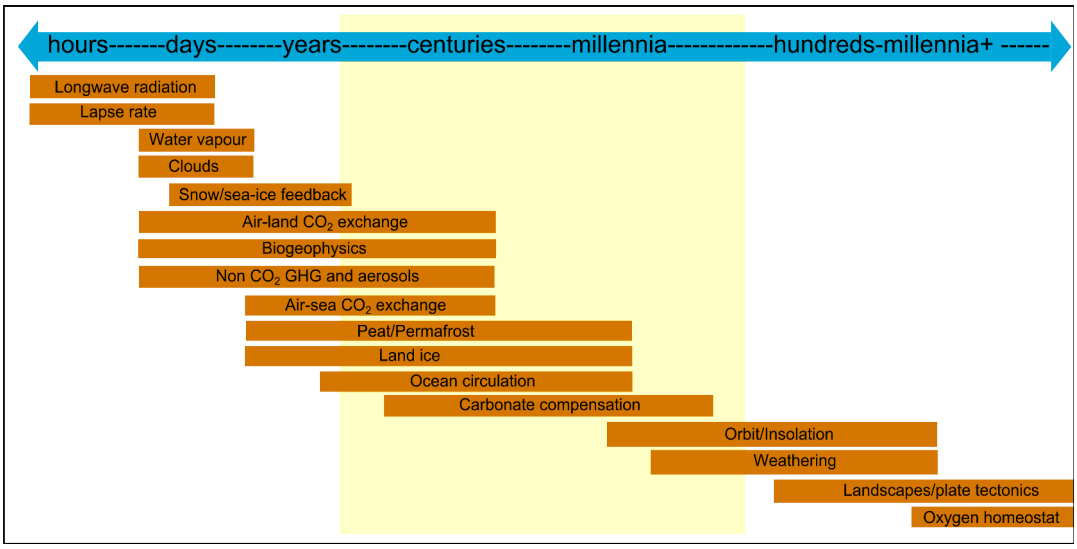

Figure 1: Évaluations et mécanismes dans le système climatique, avec indication des échelles de temps dans lequel ils agissent. Adapté du GIEC AR5 (Stocker et al. 2013) avec les mécanismes de l'échelle de temps plus longues ajouté. Zone surlignée en jaune est l'échelle de temps dans lequel cette étude est intéressé.

Actuel cycle du carbone organique

La figure 2 montre les composants du cycle du carbone le plus actif sur l'échelle de temps prise en compte pour cette étude. Le plus grand réservoir de carbone est l'océan qui contiens ~38000 GtC (un Gigatonne (Gt) de carbone est égal à un Petagramme (Pg)), largement sous la forme inorganique: CO_2 dissous, d'acide carbonique H_2CO_3, ions bicarbonate HCO_3^- et ions carbonate CO_3^{2-}, qui dépendent directement du pH de l'eau. Le deuxième plus grand réservoir est le sol, qui contient

~3970 ± 325GtC (Ciais et al 2012), dont 2370±125GtC qui est considéré comme actif dans le cycle du carbone rapide. Le stock de carbone du pergélisol estimé a 1672GtC (Tarnocai et al 2009) n'est pas prise en compte dans la figure 2, et il a été souvent négligé dans les études de modélisation du cycle du carbone. Actuellement l'atmosphère contient ~780GtC (~390ppmv CO_2) (Archer, 2010). Le mouvement de carbone entre ces réservoirs lors des changements climatiques, et les mécanismes qui le contrôle, sont encore soumis à des incertitudes. Par l'étude des données indirectes, les carottes de sédiments marins et de glace et les études de modélisation, une meilleure compréhension de la fonction du système carbone-climat peut être abordée.

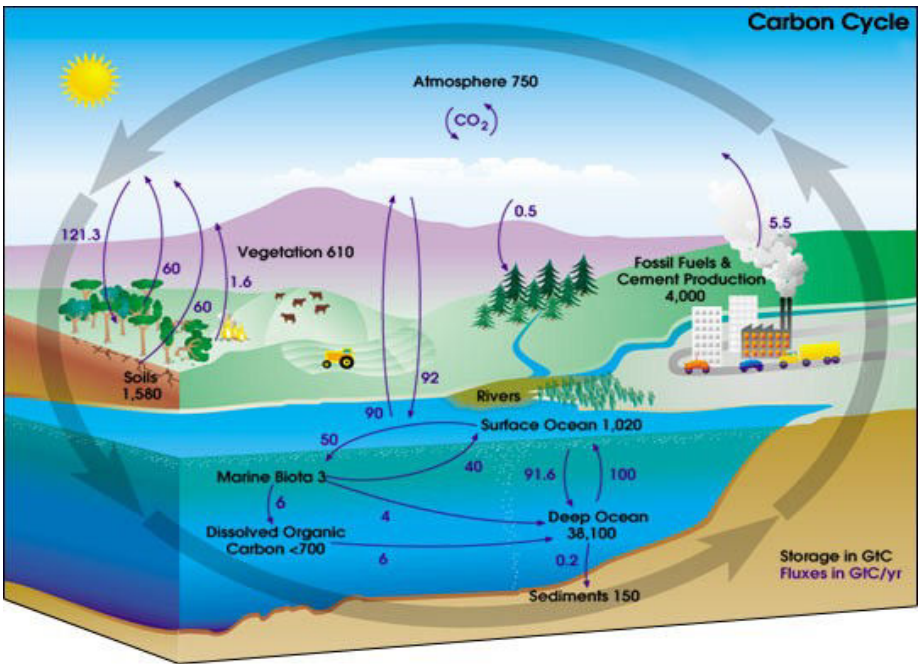

Figure 2: cycle du carbone organique (NASA Geo Science Enterprise). N.B. ce schéma ne tient pas compte le réservoir de carbone dans les pergélisols.

Les Mécanismes

1.1 homéostat d'oxygène

La trasnformation du carbone en dioxyde de carbone repose sur la présence d'oxygène. Le homéostat d'oxygène a la plus longue échelle de temps des trois principaux mécanismes de stabilisation. Les détails de son fonctionnement ne sont pas bien connu, mais à des périodes de temps géologiques, des parties de l'océan sont devenus anoxiques. En raison de la connaissance limitée du fonctionnement du homéostat d'oxygène et des échelles de temps très longues qui lui sont associés, nous considerons qu'il est inactif sur les échelles de temps prise en compte dans cette étude.

1.2 Géologie et tectonique des plaques

La position des continents sur la surface de la terre a un effet sur le système climatique par les circulations océaniques, l'albédo de la surface et la circulation atmosphérique. La quantité ou la force du volcanisme affecte directement la quantité de dioxyde de carbone dans l'atmosphère, car les volcans émettent du carbone qui était enterré dans la profondeurs terrestre. La formation des montagnes affecte également l'équilibre du carbone entre l'atmosphère et l'océan (Raymo et al., 1988). Avec plus de terre exposé à l'atmosphère, les effets de l'altération/érosion par la pluie peuvent augmenter l'absorption du carbone de l'atmosphère dans l'océan. L'effet des changements du terrain sur l'échelle de temps des plaques-tectonique et la formation des montagnes ne sont pas prise en compte dans cette étude. Nous considerons que ces mécanismes sont fixés sur l'échelle de temps de plusieurs millénaires.

1.3 Érosion

Le thermostat d'erosion-CO_2 fonctionne sur des dizaines à des centaines de milliers d'années. Son principe fondamental est que, lorsque le cycle hydrologique accélère (en raison de l'énergie supplémentaire dans le système) il augmente l'érosion des roches calcaires (CaO). L'altération des roches, par moyens mécanique et chimique et l'écoulement d'eau vers l'océan, provoque l'absorption du CO_2 de l'atmosphère par l'océan (Archer, 2010).

Réaction de Urey:

$CaSiO_3 + CO_2 \leftrightarrow CaCO_3 + SiO_2$ équation 1 (Urey, 1952)

$CaO + CO_2 \leftrightarrow CaCO_3$ équation 2 (Archer, 2010)

Équations 1 et 2 donnent les constituants de base du processus chimique du thermostat d'erosion-CO_2. En supprimant le silicate des deux côtés de la réaction, il laisse un processus très simplifié (équation 2): l'équilibre entre les roches ignées, dioxyde de carbone et calcaire.

Ce thermostat est également régie par la position des continents et le soulèvement des montagnes qui ont un effet sur l'échelle de quelques dizaines à des centaines de millions d'années. De nos jours, les cycles glaciaires sont plus froid que d'autres périodes de l'histoire de la terre (Zachos et al, 2001). Une théorie qui explique cette phénomène est le soulèvement de l'Himalaya qui a augmenté l'érosion de CaO et mis en place les conditions pour pousser le système dans les cycles glacial-interglaciaires (Raymo et al 1988).

L'érosion des roches se produit de deux façons: altération mécanique et chimique. Les deux moyens d'altération sont accélérés en présence d'eau. En générale, dans des conditions chaudes l'altération chimique est augmenté, et dans des conditions froides altération mécanique est augmenté (due en grande partie aux effets du gel et de l'expansion de l'eau par le gel).

1.4 Insolation

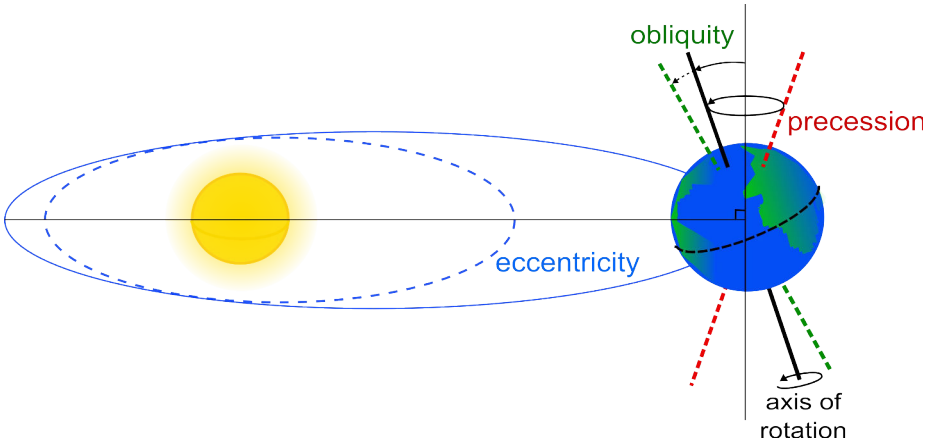

Figure 3: facteurs orbitaux affectant le climat sur des échelles de temps de plusieurs millénaires. "Eccentricity" est la forme de l'orbite, soit plus circulaire ou plus elliptique. "Obliquity" est l'angle d'inclinaison de l'axe de rotation de la Terre par rapport au plan de l'orbite. "Precession" est l'oscillation de l'axe de rotation de la Terre qui change le position de l'axe de rotation par rapport au cadre de référence des étoiles (la direction dans laquelle l'axe de rotation du Nord est confrontée à des changements).

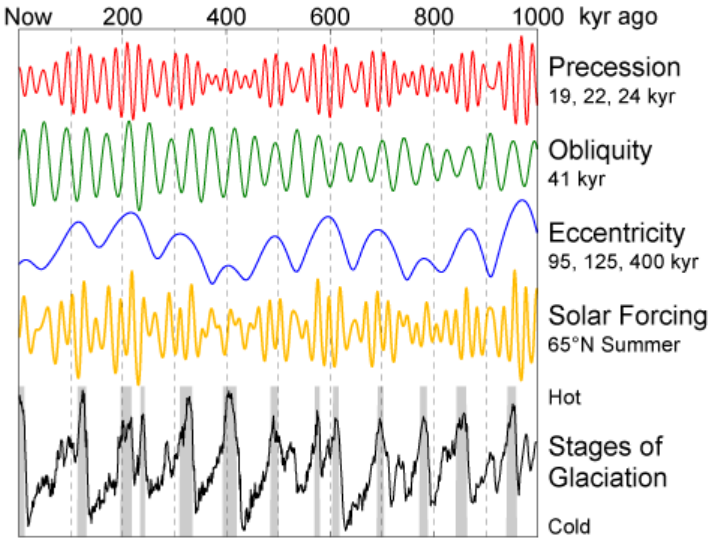

Figure 4: Fréquences dominantes de chaque paramètres orbitaux (Quinn et al, 1991). En jaune, l'insolation (entrée de l'énergie solaire) reçu à 65°N le 1er Juillet, et la ligne noire sont les données ^{18}O à partir des carottes de glace de l'Antarctique montrant les changements climatiques au cours des mêmes périodes (Lisiecki et Raymo 2005) avec interglaciaire (plus chaud) périodes en gris. (Wikipedia 2013).

L'orbite de la terre autour du soleil détermine la quantité totale d'énergie (rayonnement solaire) reçu par le système terrestre par le rayonnement solaire. Il est donc le moteur principal du système climatique de la terre. La figure 3 montre les trois composantes principales de l'orbite de la terre définie par la théorie de Milankovitch. Chacun de ces paramètres a une fréquence dominante particulière (représentée sur la figure 4) qui, lorsqu'elles sont combinées, se traduisent par une exposition par latitude qui varie avec l'orbite. L'insolation est le seul apport d'énergie important pour le système terre, et les études qui considèrent la relation statistique entre l'évolution de l'orbite et le record mondial de température peut indiquer le mécanisme de contrôle de la réponse du système terrestre.

1.5 Compensation des carbonates

Le troisième des principaux mécanismes de stabilisation est la compensation des carbonate dans l'océan. La concentration de carbone dissous dans l'eau de mer modifie le pH de l'océan. Cela affecte la capacité de l'eau de mer a dissoudre le carbone inorganique. L'effet est que la quantité de carbone dans l'océan est stabilisé sur l'échelle de temps de quelques milliers d'années par des ajustements du pH de l'océan. La profondeur de compensation des carbonates est le point où l'ajoute de carbonate de calcium est équilibrée par sa dissolution dans l'eau de l'océan. En dessous de ce niveau, il n'y a pas de carbonates déposés sous forme de sédiments sur les fonds marins.

Les variations du niveau de la mer en raison de la font (ou la formation) des calotte glaciaire a également un effet sur le mécanisme de compensation des carbonates. Les récifs coralliens localiser en eau peu profondes qui ont été inondées pendant l'élévation du niveau de la mer sont considérés comme un mécanisme important qui augmente le CO_2 atmosphérique. Ce mécanisme a peut-être réduit la capacité des océans à retenir le CO_2 en solution par la production de carbonate dans ces plateau inondées

1.6 Les calottes de glace

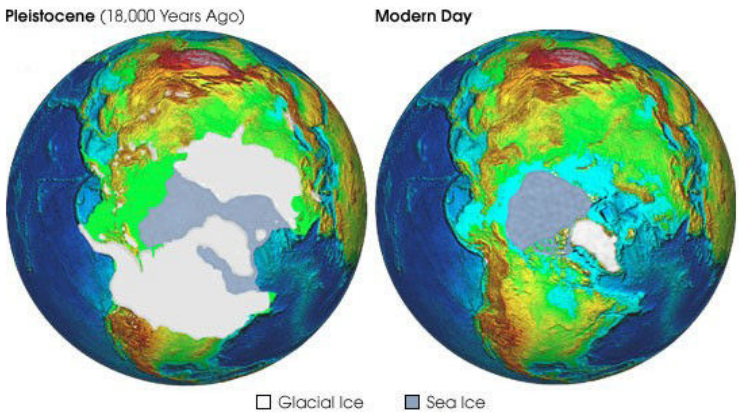

Figure 5: Les calottes de glace de l'hémisphère nord pour 18kyr BP (gauche) et moderne (NOAA) (droite)

Les études des terrains, des carottes des sédiments marins et de glaces montrent que les calottes de glace avaient existé sur les masses terrestres de l'hémisphère nord pendant les (froides) périodes glaciaires. La calotte glaciaire de l'hémisphère sud a également augmenté pendant les périodes froides. La figure 5 montre une représentation graphique des calottes glaciaires de l'hémisphère nord à 18kyr BP (« Before Present » avant le présent) et l'époque moderne (NOAA, National Oceanic and Atmospheric Administration). La présence de ces grandes calottes glaciaires changer l'élévation de surface et les flux d'énergie de surface, qui à son tour affecte la circulation atmosphérique. Ces grandes calottes de glace reflètent l'énergie solaire dans l'espace et augment l'albédo global. Cela provoque une chute de la température mondiale. La croissance des calottes glaciaires emprisonne de l'eau sur la terre qui réduit le niveau de la mer et le volume de l'océan.

1.7 Température, salinité et pression de l'océan

Le température de l'océan, la salinité et la pression affectent la capacité de l'eau à dissoudre le CO_2. Dans l'eau froide plus de dioxyde de carbone peut être maintenue en solution. Dans les eaux plus salées moins de dioxyde de carbone peut être maintenue en solution. En eau douce, une pression croissante augmente la capacité de l'eau à dissoudre le CO_2. Pendant les périodes glaciaires une quantité d'eau douce plus importante a été emprisonné dans les calottes glaciaires et donc l'eau de mer aurait été plus salée, mais aussi plus froide. L'équilibre relatif de ces effets sont étudié en général en utilisant des modèles océan-atmosphère.

1.8 La circulation océanique

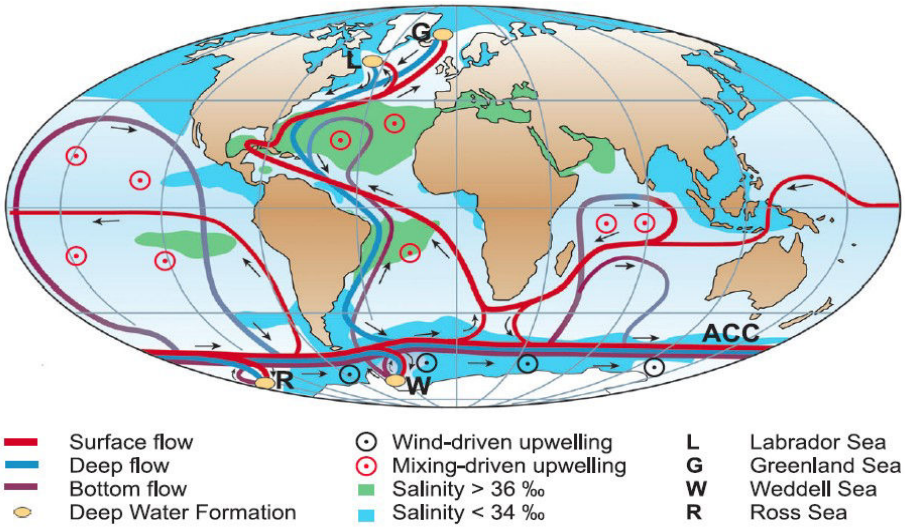

Figure 6: circulation thermohaline mondiale (Rahmsdorf 2002), d'aujourd'hui. "Représentation schématique de la circulation thermohaline mondiale. Les courants des eaux de surface sont représentés en rouge, les eaux profondes en bleu claire et les eaux de fond en bleu foncé. Les principaux sites de formation d'eau profonde sont indiquées en orange " ACC est le courant circumpolaire antarctique.

Les changements de circulation océanique sont important parce qu'ils contrôlent une partie du climat mondiale, mais aussi régionale et locale, ce qui modifie des modes de transport de l'énergie partout dans le monde. La circulation océanique est une combinaison de l'effet de Coriolis due à la rotation de la terre autour de son axe, et les effets combinés de la température et de la salinité de l'eau qui déterminent la flottabilité de l'eau. Elle dépend également de la configuration des continents.

La figure 6 montre la circulation thermohaline mondiale actuelle. Un facteur important de cette circulation est la circulation méridienne océanique de l'Atlantique (AMOC). Les eaux chaudes et salées, portées en Atlantique Nord par le Gulf Stream, se refroidissent et s'enfoncent au fond. Cela crée le flux de retour de l'AMOC et l'eau profonde de l'Atlantique-Nord (NADW). Pendant les périodes de fonte des calottes glaciaire de l'hémisphère nord, l'eau douce a été libéré dans cette région. Cela peut avoir réduit la capacité des eaux a plonger en profondeur (parce que l'eau douce est plus flottable que l'eau salée). Cela peut avoir affecté la puissance de l'AMOC et les circulation océanique globale.

Pendant la période glaciaire, on pense que l'océan austral profond peut avoir agi comme un grand réservoir de carbone. Les mécanismes qui auraient pu causer ce stockage de carbone sont encore des sujets d'étude. Ce réservoir profond de carbone dans l'océan est une hypothèse de premier plan pour le rabattement de CO_2 de l'atmosphère au cours des périodes glaciaires, ainsi que la température des océans et la réponse de compensation des carbonates à des changements de pH dans l'océan.

1.9 Fertilisation en fer des organismes marins

Bio-productivité dans l'océan dépend de la disponibilité des éléments nutritifs fournis aux phytoplancton et zooplancton pour se nourrir. Dans la période glaciaire l'atmosphère contenait plus de particules de poussière, y compris le fer qui est un élément nutritif limité pour la productivité des océans. Si ce fer atmosphérique a été mis à la surface de l'océan, il peut avoir augmenté la productivité des océans. La augmentation de productivité de l'océan peut avoir augmenté la "pompe biologique" causant plus de carbone stocké dans l'océan profond (Bopp et al 2003). L'hypothèse de la fertilisation par le fer fournit un mécanisme qui aurait pu entraîner un réservoir de carbone dans l'océan austral profond.

1.10 Biosphère terrestre

Réagissant aux conditions climatiques, la végétation terrestre subit des changement des biomes, et du stockage de carbone. Pendants des conditions froides et inhospitalières la croissance de végétation est limitée. Selon les données de pollen, la dernière période glaciaire a vu la végétation terrestre réduite en manière important par rapport à aujourd'hui. Avec réduction de l'apport de la végétation, l'accumulation de carbone dans les sols aurait également été touché.

Carbone-13 (^{13}C) a été utilisé pour estimer l'évolution du stock de carbone terrestre. Des carottes de sédiments de l'océan profond sont considérés largement indépendantes des facteurs biologiques qui affectent ^{13}C, en raison du lent mélange des

eaux de l'océan profond. Cela signifie que les changements $\delta^{13}C$ vu dans les coquilles des foraminifères des eaux profondes peuvent être utilisés pour indiquer le changement de $\delta^{13}C$ dans l'océan entier. En 1977, en analysant les foraminifères, Shackleton a calculé le changement de $\delta^{13}C$ de l'océan entre la dernière période glaciaire (LGM) ~21kyr BP et la pré-industrielle ~ 1850 CE (PI) a 0.7 ‰.

Method: Change in ocean $\delta^{13}C$	Delta ocean $\delta^{13}C$ (‰)	terrestrial biomass increase (GtC)
Shackelton (1977)	0.70*	1000
Duplessy et al (1984)	0.15	220
Berger and Vincent (1986)	0.40	570
Curry et al (1988)	0.46	650
Duplessy et al (1988)	0.32	450
Broecker and Peng (1993)	0.35	425
Bird et al (1994)		270-720

*from only one sediment core

Method: Palaeo and terrestrial vegetation data analysis	Range, growth in terrestrial biosphere (GtC)	Mean growth in terrestrial biosphere (GtC)
Adams et al (1990)*		1350
Van Campo et al (1993)	430-930	715
Crowley (1995)	750-1050	900

*Considered to be an overestimate

Method: Vegetation models	Details	Range, growth in terrestrial biosphere (GtC)	Mean growth in terrestrial biosphere (GtC)
Friedlingstein et al (1992)	Climate (biosphere) model		300
Peng et al (1995)	Palaeoecological data and biosphere model	470-1014	742
Francois et al (1998)	Biosphere model	134-606	370
Beerling (1999)	Biosphere model and modelled $\delta^{13}C$	550-680	615
Otto et al (2002)	DGVM	828-1106	967
Kaplan et al (2002)	DGVM		821

Tableau 1, les estimations de changement de la biosphère terrestre entre LGM et PI, disposés par type d'étude. Adapté de Maslin et Thomas 2003

En équilibrant les changements dans l'océan et l'atmosphère des stocks de carbone, il a été possible d'estimer la quantité de carbone qui devra avoir été libéré de l'océan depuis le LGM pour créer ce changement de $\delta^{13}C$. De cela, ainsi que du changement de carbone de l'atmosphère connu à partir des carottes de glace, une estimation de la croissance dans la biosphère terrestre de LGM à PI a été faite à 1000GtC.

Une revue de littérature sur l'équilibre entre les réservoirs de carbone de l'atmosphère, des océans, et de la biosphère terrestre de la LGM à nos jours (pour les études jusqu'à 2002) est montrée dans le tableau 1 (adapté de Maslin et Thomas 2003). L'interprétation de $\delta^{13}C$ de l'océan profond par des études de foraminifères est toujours problématique: la circulation océanique et le mélange des eaux affecte la distribution du carbone dans les bassins océaniques. Ainsi, afin d'obtenir une estimation du changement de carbone de l'océan, il est nécessaire d'estimer (ou connaître) les circulations à LGM. La fourchette des estimations pour le changement de $\delta^{13}C$ dans l'océan est 0.15‰ à 0.46‰, et crée des estimations de croissance de la biosphère terrestre de 220Gt à 650Gt (voir tableau 1). Une autre méthode pour estimer la taille de la variation de la biosphère terrestre est l'analyse des sols, pollens fossiles et la sédimentologie, comme Adams et al (1990). Leurs estimation représente une augmentation de 1350Gt dans la biosphère terrestre depuis LGM. Une mise à jour sur cette estimation a donné une gamme de croissance de 900 à 1900GtC. Cette méthode est indirecte, et les estimations (connaissances) des assemblages de plantes à LGM sont également nécessaires. A partir de ces deux approches, il semble y avoir un décalage entre l'estimation de la croissance de la biosphère par l'analyse des pollens et et celles des changements du $\delta^{13}C$ de l'océan. L'océan est le plus grand réservoir de carbone pertinent à cette échelle de temps. Donc, on a supposé que tout le carbone ajouté à l'atmosphère et la biosphère depuis LGM est tiré de l'océan. Une réévaluation de cette hypothèse peut être en mesure de fournir une raison pour le décalage. Une région qui peut avoir fourni une source de carbone dans l'atmosphère au cours de la dernière terminaison glaciaire est la zone des pergélisols du LGM.

Pergélisol et paléosols

Les paléosols sont généralement utilisés pour reconstituer les conditions climatiques. Les reconstructions du contenu du carbone dans les sols sont difficiles en raison de l'absence d'écosystèmes et de sols actuelles similaires de nos jours par rapport aux conditions glaciaires. L'étendue du pergélisol pour le climat plus froid de LGM a laissé des caractéristiques encore visibles dans le paysage d'aujourd'hui. La superficie totale du pergélisol (continue et discontinue) pour les périodes de LGM et PI sont plus fiables que les estimations des stocks de carbone du sol. Actuellement, il n'existe pas d'estimations de carbone du sol fiables pour la dernière période glaciaire maximale provenant de données indirectes et d'analyses de carottes de sédiments. Dans le climat actuel les estimations du carbone du sol total sont déjà difficiles. Les stocks de carbone du sol de pergélisol et du sols tourbeux ont pris en compte qu'assez récemment. Les conclusions des études présentées dans le texte principal montrent que les sols dans la

région de pergélisol ne sont pas déserts a LGM. Ils montrent aussi que les sols de LGM (les plus haut sédiments) ne peuvent pas être utilisés comme un bon indicateur de la quantité totale de carbone dans tous les sols (en profondeur) à la fin de la période glaciaire, en raison des effets transitoires du changement climatique au cours du temps et des sols aux taux lents d'accumulation de carbone. Ciais et al. (2012) ont estimé la taille de la réserve de carbone de la terre à l'époque LGM en combinant des études de modélisation du cycle de carbone océanique et des données isotopiques de l'oxygène à déduire la productivité primaire brute (GPP) de l'océan et de la terre à LGM. Ils ont constaté que le taux de GPP terrestre s'élève à ~40±10 PgCyr-1, ce qui représente la moitié de la quantité durant la période de l'Holocène. Malgré le taux GPP bas, ils ont estimé que l'augmentation totale dans le réservoir du carbone de la biosphère terrestre entre LGM et PI était 330GtC. Grâce à ces résultats, ils ont proposé que à LGM, le réservoir de carbone inerte dans la biosphère terrestre était 700GtC supérieure qu'à PI. Ceci permet d'obtenir une explication du décalage des estimations du changement de la biosphère terrestres entre les méthodes océan et pollens. Estimations à base de pollen n'inclut pas la forte concentration de carbone dans les pergélisols. Les études des pollens estimer les changements du stock de carbone des sols actif (la végétation et les sols non-gelée) de l'ordre de 1000GtC (Adams et al 1990, Van Campo et al 1993, Crowley et al 1995...). Les études de l'océan indiquent la variation totale de carbone dans la biosphère terrestre depuis LGM, de l'ordre de 400GtC à 500GtC (Duplessy et al. 1988, Broecker et Peng 1993). La différence entre ces estimations peut être le réservoir de carbone inerte sur la terre qui ne seraient pas pris en compte dans les estimations indiquées par pollens.

1.11 Résumé

Les modèles complexes sont concentrées sur l'océan en tant que contrôleur principal de dioxyde de carbone dans l'atmosphère sur des échelles de temps glaciaires et millénaires. Les modèles de végétation utilisés avec GCMs (modelés des systèmes terrestre complexe) montrent une plus vaste gammes de résultats que les modèles océaniques, ce qui rends la comparaison des études de la biosphère terrestre paléoclimatiques difficile. La profondeur de l'océan Austral est une zone d'intérêt particulière concernant la variabilité de CO_2 glaciaire-interglaciaires. Les efforts de modélisation actuels visent à recréer les changements de CO_2 observées en utilisant les mécanismes de l'océan. Ceux-ci sont souvent liés au stockage et libération de carbone dans l'océan Austral profond. La glace de mer, et ses changements transitoires, dans l'océan Austral semblent être un mécanisme important qui peut fournir un contrôle sur la capacité de l'océan Austral à stocker le carbone. Jusqu'à présent, la biosphère terrestre n'a pas été bien prise en compte dans les simulations transitoires du cycle du carbone dans les modèles du système terrestre.

2. Fondations de cette étude

La preuve du changement du carbone-13 dans l'océan profond, par la signature de $\delta^{13}C$ de coquilles de foraminifères dans les carottes de sédiments marins, a indiqué que le changement de la concentration de CO_2 dans l'atmosphère pendant les périodes glaciaires n'a pas été causé par l'absorption du carbone par la biosphère terrestre (Broecker et Denton, 1989). Le fractionnement de carbone lors de la photosynthèse provoque une signature de $\delta^{13}C$ de matière organique végétale d'environ -25‰ (Maslin et Thomas 2003) par rapport à la source. Le changement de $\delta^{13}C$ de l'océan entier est d'environ -0.35‰ entre le LGM et le PI. Afin de réaliser ce changement, une source de carbone de ~500GtC avec la signature de $\delta^{13}C$ de -25 ‰ est nécessaire, par exemple une réduction de la biosphère terrestre. Cette source augmenterait le CO_2 atmosphérique d'environ 25ppmv (Archer, 2010). La conclusion était que entre les périodes interglaciaires et les périodes glaciaires, les changements de CO_2 atmosphérique devaient être causée par l'absorption de carbone dans l'océan. Cette absorption de carbone par l'océan devait être suffisamment forte pour compenser le CO_2 atmosphérique de 25ppmv supplémentaire (par biosphère terrestre) au dessus de ~100ppmv vu dans l'atmosphère entre interglaciaire et périodes glaciaires. Les reconstructions de la variation de la taille de la biosphère terrestre, par pollen entre la dernière période glaciaire et l'actuel, indiquent qu'elles avaient augmenté d'environ 1000GtC (Crowley, 1995). Cela semble confirmer que l'océan était la source de carbone de l'atmosphère au cours de la terminaison glacial. Toutefois, un mécanisme qui n'est ni représenté dans les études de modélisation couplés paléo-climatiques, ni dans les reconstructions de la biosphère terrestre (comme NPP, Productivité Primaires Nette) est l'effet des sols gelés. Les concentrations élevées de carbone dans les sols gelés aujourd'hui (Tarnocai et al 2009) et des études de paleosols (Zimov et al 2006, Ciais et al 2012) soulignent l'importance du pergélisol dans le climat qui est à la fois directement et indirectement lié au cycle du carbone. De plus, les données de $\delta^{13}C$ atmosphérique tout au long de la terminaison glaciaire montre une chute rapide de $\delta^{13}C$ atmosphérique puis une reprise (Schmitt et al 2012). Les différences entre les estimations de l'évolution de la biosphère terrestre a base de $\delta^{13}C$ de l'océan et à base de pollen, les sols dans les régions de pergélisol riche en carbone et la baisse rapide de $\delta^{13}C_{atm}$ pendant le début de terminaison se combinent afin de créer le début de cette étude: Le rôle du pergélisol dans le cycle du carbone mondial sur les échelles de temps de siècles à plusieurs millénaires. Une étude de modélisation.

3. Questions de recherche

1. Les preuves suggèrent que pendant les périodes de réchauffement rapide, la fonte du pergélisol libère du carbone dans l'atmosphère. Jusqu'à présent, les études de modélisation axée sur les causes de la hausse des émissions de CO_2 au cours de la dernière déglaciation ont omis le mécanisme de pergélisol. L'insolation pourrait entraîné la libération du pergélisol-carbone, et aurait contribué à l'augmentation des émissions de CO_2 dans l'atmosphère entre 18kyr a 12kyr BP?

2. Jusqu'à présent les données de $\delta^{13}C$ atmosphérique n'ont pas été expliquées par des mécanismes de l'océan, le mécanisme pergélisol-carbone pourrait expliquer la baisse rapide de $\delta^{13}C$ atm au début de la dernière terminaison glaciaire?

3. De peut il que le mécanisme pergélisol-carbone explique aussi les données de la terminaison glaciaire précédente, TII?

4. Si le pergélisol-carbone joue un rôle important dans l'augmentation du CO_2 atmosphérique pendant la terminaison glaciaire, agit-il à chaque cycle de précession et quelle est la puissance de l'effet dans les périodes non-terminaison?

5. Les changements climatiques rapides qui peuvent avoir affectés l'hémisphère nord, auraient un effet sur l'étendue du pergélisol. Le mécanisme pergélisol-carbone pourrait avoir joué un rôle dans ces changements climatiques rapides?

4. Méthode de recherche

Un mécanisme simplifié de pergélisol-carbone a été développé pour une utilisation avec le modèle dynamique de végétation dans le CLIMBER-2 EMIC (Crichton et al 2014). Le réservoir de carbone de la biosphère terrestre totale a été réglé en utilisant des estimations de Ciais et al (2012). Les littératures ont identifié qu'il existe des grandes incertitudes pour la réponse dynamique du sol-carbone du pergélisol pendant le changement climatique. Par conséquent, la partie dynamique du mécanisme simplifié a été réglé en utilisant les données des carottes de glace de CO_2 et $\delta^{13}C$ pour la dernière terminaison glaciaire (TI). Ce réglage de TI inclus la libération du carbone de l'océan austral comme un mécanisme important pour expliquer l'élévation du CO_2 atm pendant la déglaciation. Ceci a été basé sur les études de Bouttes et al (2012). Le modèle CLIMBER-2P, avec un mécanisme de pergélisol inclus et entièrement couplé en fonctionnement, a été utilisé pour effectuer des simulations climatiques pour répondre aux questions de recherche posées ci-dessus.

5. Résultats et discussion

Dans la section suivante, chacune des questions de recherche posées seront adressées individuellement. Les résultats des simulations avec CLIMBER-2P sont examinées en premier, suivi par une discussion des limites du modèle et / ou des données, et leurs implications pour l'interprétation de nos résultats.

5.1 L'évolution de CO_2 au cours de la dernière terminaison glaciaire

1. Les preuves suggèrent que pendant les périodes de réchauffement rapide, la fonte du pergélisol libère du carbone dans l'atmosphère. Jusqu'à présent, les études de modélisation axée sur les causes de la hausse des émissions de CO_2 au cours de la dernière déglaciation ont omis le mécanisme de pergélisol. L'insolation pourrait entraîné la libération du pergélisol-carbone, et aurait contribué à l'augmentation des émissions de CO_2 dans l'atmosphère entre 18kyr a 12kyr BP?

Afin de répondre à cette question, un mécanisme pergélisol-carbone simplifié a été développé pour CLIMBER-2. Le mécanisme repose sur le contrôleur de premier ordre pour les pergélisols riches en carbone: une réduction de la vitesse de la décomposition du sol. Le modèle CLIMBER-2 n'a pas de profondeur de sol, et la décomposition du carbone dans les sols n'est contrôlée que par le total des stocks de carbone et la température dans une cellule de la grille. Cela nous a permis de modéliser une réduction de la décomposition du sol en augmentant le temps de séjour de carbone au sol avec un multiplicateur pour le carbone dans les pergélisols. Le modèle « re-mixing », décrit dans le chapitre 3 (texte principal), s'est avéré représenter le mieux les effets combinés d'une croissance de la profondeur de la couche active et de la réduction de longueur de la saison de croissance le long d'un gradient de pergélisol. Ces deux caractéristiques ont créé une relation non-linéaire entre la fraction de pergélisol d'une cellule de la grille e CLIMBER-2 et l'équilibre de la concentration de carbone au sol. Le modèle du pergélisol-carbone a été réglé pour le total des stocks de carbone dans les sols à LGM et PI avec les estimations de Ciais et al (2012). Un total de quatre paramètres dynamiques, qui déterminent le taux d'accumulation et de décomposition du carbone dans les pergélisol et les pergélisol-dégelé, ont été retenus pour utilisation dans des simulations de T1 (terminaison-glaciaire 1).

T1 a été simulée dans les chapitres 4 et 6 (texte principal). Le chapitre 4 présente les simulations T1 avec les quatre paramètres dynamiques du pergélisol et un climat de l'évolution des calottes glaciaires, évolution CO_2, changements d'orbite et une réduction de carbone stocké dans l'océan Austral profond. La libération d'eau douce dans la région de l'Atlantique Nord, qui a affecté la circulation AMOC, a été inclus dans la simulation de T1 dans le chapitre 6.

Événements terminaison 1

Le modèle CLIMBER-2P, avec un mécanisme de pergélisol-carbone incorporé, a été utilisé pour exécuter des simulations de la dernière terminaison. Les mécanismes d'océan glaciaire, qui ont été développés et testés par Bouttes et al (2011), ont été appliqués conjointement pour trouver un climat LGM et le cycle du carbone qui s'est montré être en accord avec les données de CO_2 atmosphérique, $\delta^{13}C$ atmosphérique et données $\delta^{13}C$ océaniques. En utilisant une version d'évolution relativement lente pour le réservoir de carbone de l'océan profond, les résultats suggèrent que les émissions de carbone des pergélisols-dégel peut avoir un rôle important à jouer dans l'élévation du CO_2 atmosphérique pendant la déglaciation.

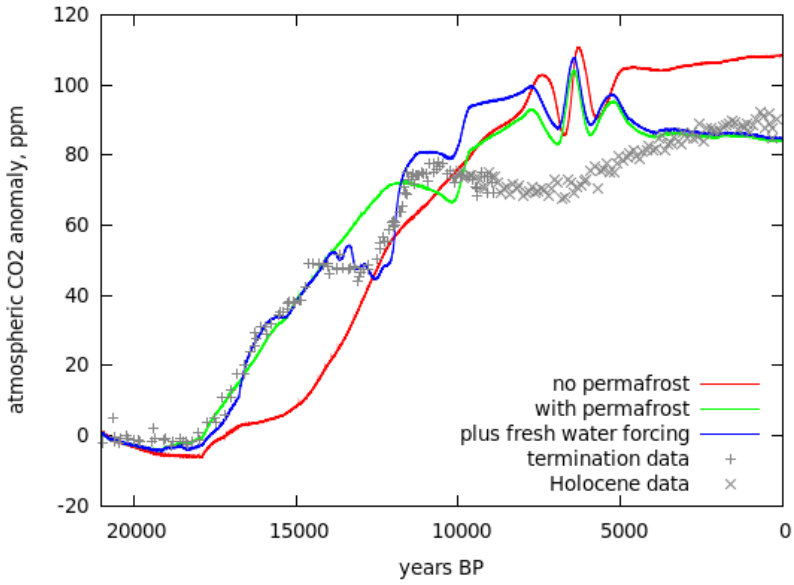

Figure 7, les concentrations de dioxyde de carbone de l'atmosphère des simulations de terminaison 1, modèle standard sans pergélisol (rouge), avec le pergélisol (vert) et le pergélisol et l'eau douce de forçage (bleu). Les données de Monnin et al 2001 tracées sur Parrenin et al 2013 échelle d'âge.

21kyr BP à 14kyr BP

L'augmentation de l'insolation d'été de latitudes nord, moyennes et hautes, a entraîné une réduction de la superficie du pergélisol et une libération de carbone de la terre dans l'atmosphère de 18kyr BP. Il en est résulté une absorption nette de carbone entre 18k à 15kyr BP dans l'océan, malgré la réorganisation de la circulation océanique dans le même temps (et une libération de carbone des eaux profondes de l'océan par la réduction des plongée des saumures). Lorsque la même simulation a été réalisée dans le chapitre 6, cette fois avec forçage d'eau douce dans l'Atlantique nord, la première partie de la terminaison n'a pas été grandement affectée. Pas d'arrêt d'AMOC, comme cela a

été proposé par McManus et al (2004), a été nécessaire pour créer une augmentation du CO_2 atmosphérique de 18kyr à 14kyr BP. Le CO_2 atmosphérique modélisé est présenté dans la figure 7.

14kyr BP à 10kyr BP

A 14kyr BP l'océan est devenu une source de carbone dans l'atmosphère. De environ 13kyr BP les pergélisols ont commencé à devenir un puits de carbone, grâce à l'augmentation NPP et, un peu plus tard, par un élargissement de la zone de pergélisol. Cette augmentation de la zone de pergélisol a été le résultat de nouvelles terres étant exposée sous calottes de glace se retirèrent, et plus tard en réponse à la baisse de l'insolation d'été (~11kyr BP). L'absorption de carbone du pergélisol combinée avec l'augmentation de la taille de la biosphère terrestre, tirée par l'amélioration du climat et l'augmentation de productivité primaire nette (NPP), a changé la biosphère d'une source de carbone en un puits de carbone. Maintenant que la biosphère terrestre avait commencé à absorber le carbone de l'atmosphère, l'océan était le seul contributeur à la hausse du CO_2 dans l'atmosphère en l'absence de forçage de l'eau douce en atlantique nord.

Le plateau de CO_2, vu dans les données entre 14kyr et 12kyr BP (le Bolling-Allerod/Younger Dryas ou B-A/YD), a été simulée dans le chapitre 6 en forçant l'océan Atlantique Nord avec de l'eau douce. Ce forçage de l'eau douce a réduit la force de l'AMOC qui a entraîné un refroidissement de l'hémisphère nord. Ce refroidissement a entraîné une augmentation de la superficie du pergélisol et une augmentation du taux d'absorption du carbone dans la biosphère terrestre. Lorsque le forçage de l'eau douce a cessé, le dépassement et la reprise de l'AMOC ont provoqué un réchauffement rapide dans l'hémisphère nord, le dégel du pergélisol, et une émissions de carbone de courte durée de la biosphère. Cela a provoqué une hausse rapide du CO_2 atmosphérique après plateau B-A/YD.

Une période de l'augmentation de CO_2 rapide qui se produisent avant YD au cours de la Bolling-Allerod (BA) juste avant 14kyr BP n'a pas été modélisée de façon explicite dans le chapitre 6. Selon Lourantou et al (2010), cette augmentation des émissions de CO_2 était de plus de 10 ppm en quelques dizaines à centaines d'années. Dans leur données, ce saut de CO_2 est précédée par un ralentissement du taux d'augmentation de CO_2 atmosphérique. Selon la simulation dans le chapitre 6, il est possible que ce saut de CO_2 de BA peut avoir été causée par un mécanisme similaire à la BA / YD: une augmentation de l'AMOC provoquer un dégel du pergélisol et les émissions de carbone, bien que nous ne proposons pas un arrêt fort ou de longue durée de l'AMOC avant cet événement.

Après 10kyr BP

A partir de 10kyr BP le modèle ne peut plus bien reproduire les données. C'est probablement le résultat des simplifications du modèle et de l'absence d'un mécanisme

tourbières / terres humides. Selon Yu et al (2011) les tourbières de l'hémisphère nord ont commencé à accumuler des sommes importantes de carbone à ~10kyrBP. Si cette dynamique avait été incluse dans le modèle, il serait probablement possible d'expliquer la décalage entre modèle et données.

Dans tous les résultats des simulations, la déstabilisation et la disparition de la végétation dans la région du Sahara provoque une forte perturbation dans le cycle du carbone. Le mécanisme pergélisol-carbone amplifie l'effet de cette perturbation.

Discussion de T1, le modèle et les données

La reconstruction de la température par des données proxy pour la dernière terminaison (Clarke et al 2012, Shakun et al 2012) est pauvre pour les endroit de pergélisol continentales, comme le montre la figure 8. Le bande des latitudes de 30 à 60 degrés nord, qui en Eurasie était probablement les lieux des grandes quantités de carbone dans les pergélisols, est fortement biaisées en faveur du climat de l'Atlantique nord et les lieux océaniques en général. Selon Clark et al (2012) les endroits Beringia (environ de l'Alaska) ont vu la température montée de 18kyr BP durablement tout au long de la période de terminaison. Actuellement il n'y a pas suffisamment de données de température pour rejeter l'hypothèse d'un dégel des pergélisols qui a provoqué l'augmentation de CO_2 atmosphérique. En effet, d'après des reconstructions globales actuellement utilisées pour déterminer les conducteurs des changements et les conséquences, il n'y a pas du tout de données pour l'Eurasie continentale.

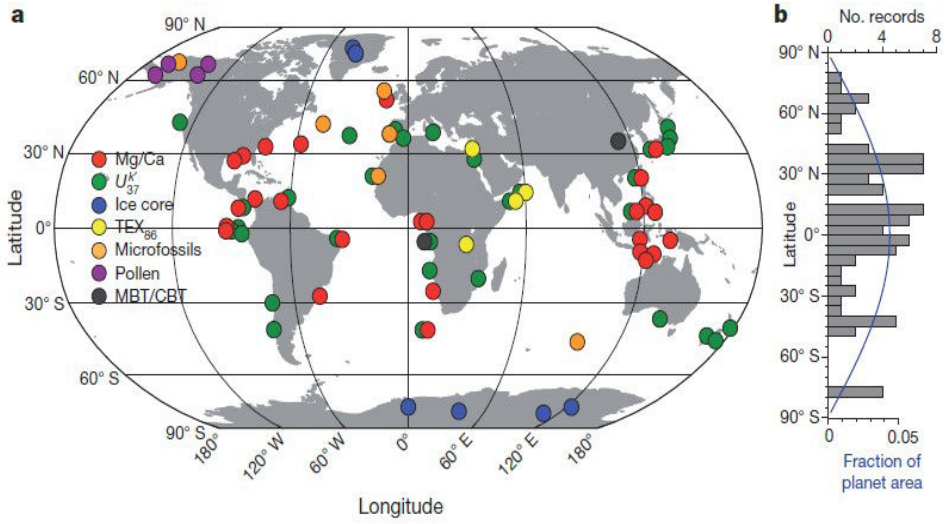

Fig 8, a) Lieux et types des données proxy de température utilisé par Shakun et al (2012) pour reconstruire les changements de la température mondiale au cours de la dernière terminaison. Il n'existe pas de données pour l'Eurasie continentale, où d'importants stocks de carbone de sol étaient probablement présents au LGM (chapitre 3), b) nombre d'enregistrements par bande de latitude. (de Shakun et al 2012).

Le fonctionnement du mécanisme de pergélisol-carbone développé est très simplifiée par rapport au monde réel. Comme un paramétrage, il ne modélise pas spécifiquement la dynamique de dégel qui dépend des conditions locales (Riseborough et al 2008). Toutefois, la dynamique du cycle de carbone, réglé avec les données de T1 donnent une indication de la possible réponse générale du pergélisol-carbone (couplé dans la système entier). Même si l'étendue du pergélisol est en équilibre avec le climat instantané dans le modèle CLIMBER-2P, la dynamique du cycle du carbone entraîne un retard de perte de carbone (par rapport au climat) des sols qui avait été pergélisol. Cela imite la combinaisons des mécanismes du monde réel tels que la formation des taliks, le taux d'épaississement de la couche active, la conduction thermique à travers le pergélisol et le taux de décomposition du carbone du sol lui-même. Une autre simplification importante est que les côtes de la terre sont fixes. La dynamique du carbone sur les plateaux continentaux est un mécanisme qui doit être étudié. Le rôle des tourbières et des terres humides a également été identifié dans tous les chapitres comme mécanisme important et serait liée à la dynamique du pergélisol-carbone.

Afin de simuler la terminaison 1, la contribution de l'océan a été choisi comme la réduction linéaire de la plongée de saumures entre 18kyr à 12kyrBP (Bouttes et al 2012). Selon les résultats du modèle, en l'absence de mécanismes de l'océan glacial, une libération de carbone à partir du pergélisol-dégel pourrait expliquer l'augmentation initiale de CO_2 dans l'atmosphère. Cependant, cette hausse initiales n'a pas besoin d'être expliquée par l'océan. Pour toutes les simulations, de 18kyr à 12kyr BP la réduction linéaire des plongées de saumures n'a pas été modifiée. Différents points de début / fin et différentes fonctions (par exemple exponentielle, parabolique, contrôlé par un autre paramètre du modèle, etc) pour le changement des plongées de saumures auraient un impact sur le cycle du carbone. Selon la comparaison avec la reconstruction du changement climatique par Shakun et al (2012) (chapitre 6 texte principal, Figure 6.18) pour l'hémisphère sud, le modèle simule le début de la montée en température se produisant autour de 1k ans plus tard que les données le suggèrent. Il montre également un pic de température se produisant autour de 2k ans plus tôt que les données suggèrent. Cela peut laisser entendre que le contrôleur pour le mécanisme glaciaire de l'océan sud aurait été plus lent que celui utilisé, peut-être de 19kyr à 10kyrBP. Si tel était le cas, alors l'implication serait que la perte de carbone du dégel du pergélisol devrait être légèrement plus rapide de 18kyr à 14kyr BP, afin de reproduire les données. Le record de $\delta^{13}C$ dans les profondeur de l'océan Atlantique Sud suggère également que la libération de carbone stocké dans l'océan profond a peut-être commencé plus tôt que 18kyr BP de plusieurs milliers d'années (chapitre 4 texte principal, figure 9).

Le réglage des dynamiques du pergélisol-carbone déterminé dans le chapitre 3 a été destiné à donner une large gamme de dynamiques pour effectuer des simulations de la terminaison 1. Parmi les quatre paramètres, la dynamique « medium », où la taille du réservoir de sol total « rapide » était d'environ la même taille que le réservoir de sol « lent », a montré le meilleur ajustement par rapport aux données. Comme indiqué dans le paragraphe précédent, en ce qui concerne les mécanismes de l'océan, le réglage dynamique du mécanisme pergélisol-carbone peut être l'objet d'ajustements dans les

études futures. Le forçage de l'eau douce figurant dans la simulation du chapitre 6 s'appuie sur les dynamiques du cycle du carbone, à la fois de l'océan et de la terre, afin de produire le meilleur ajustement. Si la dynamique du pergélisol-carbone étaient plus rapide (les émissions de carbone se produisent plus rapidement pendant le dégel), cela aurait un impact sur la réponse du système pendant les événements d'arrêt et de redémarrage de l'AMOC.

Dans le chapitre 4, les rôles combinés des cycles de carbone océaniques et terrestres ont été étudiés. Il a été constaté que l'augmentation de la productivité des organismes marins dans l'océan Austral n'était pas nécessaire pour recréer le climat LGM ou les donnes de CO_2 atmosphérique pour la T1. La meilleure combinaison de mécanismes choisie était un maximum de 80% de plongées de saumures créées sur la formation de glace, qui réduit de façon linéaire à partir de 18k à 0% à 12k yrBP lors de la terminaison. Cela a été combiné avec la dynamique « medium » pergélisol-carbone pour aboutir à une bon correspondance avec les changements de CO_2 vu dans les données. Selon d'autres études (Haarpainter et al, 2001 Bouttes et al 2011), le montant maximal de plongées de saumures devrait être plus proche de 60%. Il est connu que le cycle du carbone dans CLIMBER-2 est moins sensible à l'étendue de glace de mer dans l'océan Austral que les données d'observation le suggèrent (Brovkin et al 2012). Si il était plus sensible, alors la fraction de saumures rejetée qui plonge n'aurait pas besoin d'être aussi élevée que 80%. Brovkin et al (2012) a constaté que l'amélioration de la sensibilité du modèle à la couverture de glace de mer pour l'océan sud, a entraîné une augmentation de 10 ppm de CO_2 dans l'atmosphère à la fin d'une terminaison glaciaire, par rapport au modèle standard. Ces 10ppm supplémentaire signifient que le maximum nécessaire des saumures qui plonge est inférieure a 80%; soit environ 60%. Selon les simulations d'équilibre LGM dans le chapitre 4, les paramètres de l'océan des plongées de saumures a 0.6, et le paramètre de stratification «alpha» a 0.5 conduit à un climat LGM de ~200ppm, où les données montrent ~190ppm, voila la différence de 10 ppm.

La simulation du plateau de CO_2 de B-A/YD ne tient pas compte des changements climatique pour le contrôleur des plongées de saumures. L'inversion froide de l'Antarctique (Antarctic cold reversal) vu dans les données des carottes de glace, n'a pas été vu dans la sortie de simulation dans le chapitre 6. Si le mécanisme de l'océan glacial a été couplé à des changements climatiques, causés par un rafraîchissement de l'océan Atlantique nord et la réponse AMOC, ce renversement froid peut être en mesure d'être modéliser. Le contrôleur des plongées de saumures reste une réduction linéaire entre 18kyr et 12kyrBP. Il se peut que l'évolution de la glace de mer ait eu un effet sur les plongées de saumures, et donc sur le stock de carbone de l'océan profond.

5.2 L'évolution de $\delta^{13}C$ en cours de la dernière terminaison

2. Jusqu'à présent les données de $\delta^{13}C$ atmosphérique n'ont pas été expliquées par des mécanismes de l'océan, le mécanisme pergélisol-carbone pourrait expliquer la baisse rapide de $\delta^{13}C$ atm au début de la dernière terminaison glaciaire?

Comme pour la comparaison des données de CO_2 atmosphérique et les données du sortie du modèle, les paramètres du modèle pour T1 de la dynamique du pergélisol et les paramètres de l'océan glaciaires ont été choisis pour convenir au mieux aux données. Ainsi, l'hypothèse est qu'il n'y a pas d'autres mécanismes que ceux modélisés qui sont responsables ou qui ont joué un rôle majeur dans l'évolution de $\delta^{13}C$ de CO_2 atmosphérique.

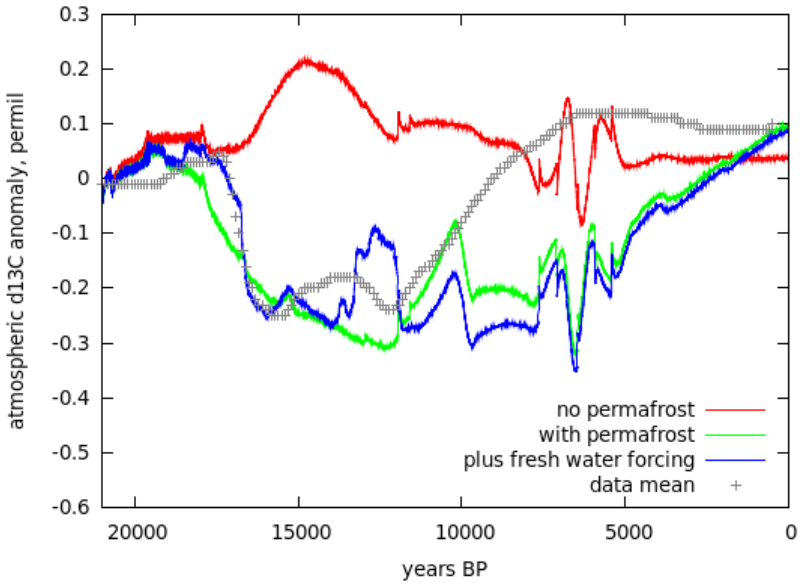

Figure 9, $\delta^{13}C$ de dioxyde de carbone atmosphérique pour des simulations de terminaison glaciaire 1, modèle standard sans pergélisol (rouge), avec le pergélisol (vert) et du pergélisol et l'eau douce de forçage (bleu). Données de Schmitt et al 2012.

21kyr à 14kyr BP

La baisse des $\delta^{13}C$ vu dans les données entre 18kyr et 16kyr BP pourrait bien être modélisé quand le pergélisol-carbone est inclus comme source de carbone dans l'atmosphère (figure 9). Lorsqu'il n'y a pas un forçage de l'eau douce appliqué dans la région de l'Atlantique nord, la baisse de $\delta^{13}C$ atmosphérique modélisé est produite plus tôt que vu dans les données (ligne verte). L'application de forçage d'eau douce pauvre qui a retardé l'augmentation de la puissance de l'AMOC jusqu'à 17.5kyrBP a entraîné la hausse de $\delta^{13}C$ dans le modèle en accord avec les données (ligne bleue), mais aussi en

accord avec les données de CO_2 (fig 8). Pour créer le profil de forçage de l'eau douce, seule l'émission de CO_2 a été utilisée pour ajuster le profil (chapitre 6, texte principal). Par conséquent, le fait qu'il corresponde très bien aux données de $\delta^{13}C$ conforte dans l'hypothèse de pergélisol-carbone.

14-10kyr BP

A 14kyr BP, quand le forçage de l'eau douce est appliqué et le record du CO_2 est mieux modélisé (figure 8), la variabilité vu dans le $\delta^{13}C$ modélisée ne se voit pas dans les données de moyenne $\delta^{13}C$. Dans le chapitre 6 (texte principal), tous les points de données de $\delta^{13}C$ atmosphérique mesurés sont tracés avec la sortie du modèle (figure 6.17 texte principal). Lorsque le CO_2 commence à plateau, les données de Lourantou et al (2010) montre une augmentation de la $\delta^{13}C$ comme le fait notre modèle. Lorsque le CO_2 commence à monter rapidement à nouveau après le plateau, les données de Lourantou et al (2010) montre une chute rapide dans $\delta^{13}C$, tout comme notre modèle. Le profil de forçage de l'eau douce a été obtenu en l'ajustant jusqu'à ce que les données CO_2 puisse être bien reproduites par le modèle. Un total de 10 itérations a été faite. Dans la figure 8, nous pouvons voir que les changements de CO_2 modélisés montrent un léger décalage par rapport aux données. Ce décalage est également visible dans la sortie modèle de $\delta^{13}C$ par rapport aux données de Lourantou et al. Si le profil de forçage était affiné alors les changements de CO_2 et $\delta^{13}C$ pourraient très probablement être mieux modélisés.

Après 10kyr BP

Après ~10kyr BP, le modèle $\delta^{13}C$ s'écarte notablement des données. Lorsque des données montrent une hausse soutenue, la sortie du modèle montre une baisse suivie d'une hausse 5kyrs plus tard que les données. En ce qui concerne le CO_2, cette différence peut être expliquée par l'absence d'une représentations des tourbières/terres humides dans le modèle. Un autre problème peut être la dynamique de la végétation, qui ne présentent pas une réponse forte à l'Holocène optimum climatique, car les données suggèrent était l'expansion de la végétation (Prentice et al 1998, Gallimore et al 2005) ou le modèle de végétation a atteint un plateau (de contenu de carbone). La déstabilisation et la disparition de la végétation dans le Sahara avant 5kyrBP est également évidente dans la sortie du modèle, mais visible moins clairement aux données $\delta^{13}C$.

Discussion pour T1, le modèle et les données

La discussion de T1 pour les paramètres du modèle et les simplifications par rapport aux considérations des données de CO_2, tiennent aussi au regard de la comparaison modèles-données $\delta^{13}C$. Si la libération de carbone de l'océan a eu lieu sur une période plus longue que celle modélisée dans notre étude, comme suggéré par les données, elle aurait un impact sur le $\delta^{13}C$. Dans les simulations du modèle dans lequel aucun mécanisme de l'océan glacial était inclus (chapitre 4, texte principal) la dynamique mieux adaptée pour les données de $\delta^{13}C$ était une dynamique pergélisol-

carbone beaucoup plus rapide que dans le cas où les mécanismes de l'océan glacial étaient inclus. Une réduction linéaire de plongées des saumures entre 18kyr à 12kyr BP a donné un correspondance des données de CO_2 et $\delta^{13}C$ avec le dynamique « medium » pergélisol-carbone. Un mécanisme de l'océan glacial qui évoluerait plus lentement devrait être combiné une dynamique du pergélisol-carbone plus rapide afin de faire correspondre avec les données de CO_2 et $\delta^{13}C$.

Il existe des mécanismes qui ont pu affecter le $\delta^{13}C$ atmosphérique qui ne sont pas inclus dans notre simulation. Il s'agit notamment de: la déstabilisation des hydrates de gaz dans l'océan; inondations des plateaux continentaux sur l'élévation du niveau de la mer; changements de taux d'émission de méthane sur la terre; changements de la productivité d'organismes marins dans l'océan; tourbières/terres humides. Tel que discuté, les tourbières/terres humides avaient probablement affectés le $\delta^{13}C$ atmosphérique dés 10kyrBP et sont des puits de carbone important, estimé d'une croissance de plus de 500GtC depuis le début de la période interglaciaire actuelle. Les changements dans la productivité des organismes marins peuvent avoir eu un certain effet sur $\delta^{13}C$, mais selon Fischer et al (2009) il est probable que peu d'effet, en accord avec les résultats de notre étude (chapitre 4). Les données du méthane des carottes de glace indique les changements rapides de la concentration atmosphérique de méthane pendants la terminaison (Chappellaz et al 1990). Le méthane est fortement appauvrie en carbone-13 et des changements dans les sources seraient suffisante pour affecter $\delta^{13}C$ atmosphérique de CO_2. Selon Melton et al (2012), qui a mesuré $\delta^{13}C$ de CH_4 dans les carottes de glace, les sources de hausse de méthane observées dans les données au cours de la période de réchauffement de Younger Dryas ont été probablement dominées par combustion de la biomasse, suivi de l'importance des lacs thermokarstiques (indiquant le dégel du pergélisol). Cela suggère que la contribution des terres humides tropicales ou des hydrates de gaz méthane dans l'océan n'a pas joué un rôle important. Fischer et al (2008) conclue également que les hydrates de méthane n'ont pas joué un grand rôle dans les données de méthane vu dans l'atmosphère pendant T1. L'inondation des plateaux continentaux peut avoir entraîné la libération de carbone dans le reste du système et avait affecté $\delta^{13}C$, CO_2 et CH_4 atmosphérique.

Les relevés de $\delta^{13}C$ des carottes de glace représente ce qui a été enregistré du vrai signal de $\delta^{13}C$ atmosphérique. Ils dépendent des taux de changement, parce que le processus de fermeture névé permet des échanges de gaz entre la neige / glace et l'atmosphère jusqu'à son achèvement. Kohler et al (2011) a considéré le réchauffement de B-A entre 15 et 14 kyrBP et le saut en CO_2 atmosphérique pour les processus d'action rapide dans lequel l'enregistrement des carottes de glace ne serait pas représenter la véritable ampleur des changements qui se sont produits. Le processus de fermeture névé devrait également atténuer le signal de $\delta^{13}C$. Ils concluent que ~125GtC a été libéré ce qui a produit une augmentation des émissions de CO_2 de 20-35ppm, soit de 2 à 3,5 fois plus élevé que les relevés des carottes de glace ont montré, au cours d'une période de moins de 200 années. Au moment de leur étude, les données de $\delta^{13}C$ a haute-résolution n'étaient pas disponibles et ils ne pouvaient pas conclure si l'augmentation du CO_2 atmosphérique a été en grande partie de source océanique ou terrestre, mais ils

suggèrent que l'inondation des plateaux continentaux à ce moment peut avoir causé la libération de 125GtC dans l'atmosphère. Dans les climats de changement rapide, l'atténuation du signal atmosphérique dans les carottes de glace doit être pris en compte lors de l'exécution des comparaisons modèle-données.

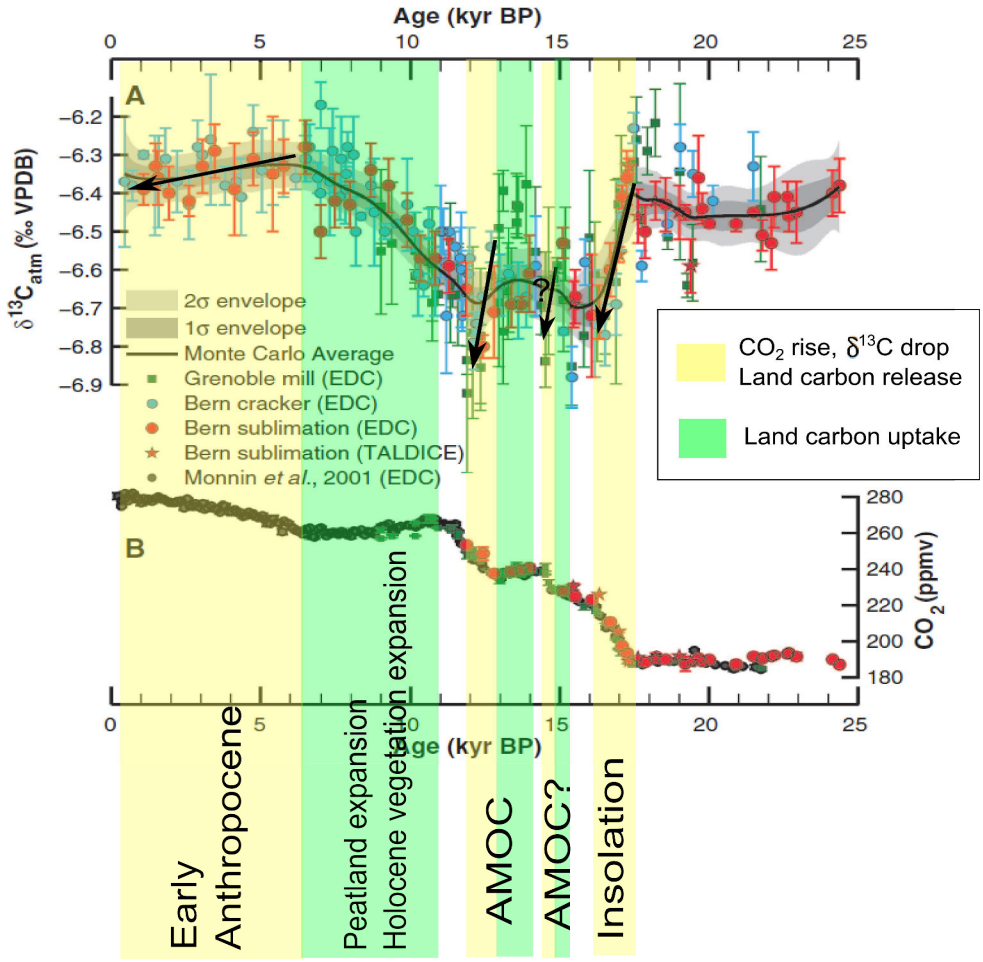

Figure 10, les données de CO_2 et $\delta^{13}C$ rapportées par Schmitt et al (2012) avec les mécanismes proposés superposées. Les flèches indiquent la tendance générale qui peut être vu dans les données

Les données de Lourantou et al (2010) pour $\delta^{13}C$ montrent une plus grande variabilité que les autres ensembles de données présentés par Schmitt et al (2012) (montre a la figure 10). Entre la période 16kyr et 12kyr BP l'ensemble de données Grenoble Mill a beaucoup plus de points de données que l'ensemble de données de la méthode Bern Sublimation. L'ensemble de Bern Sublimation est utilisé par Schmitt et al comme l'ensemble de référence pour effectuer l'analyse des résiduelles pour d'autres ensembles, et la détermination de ces résiduelles en comparant les données au même point dans le temps. Étant donné que les données de Lourantou et al Grenoble Mill sont

de plus haute résolution, cette comparaison avec des points correspondant en temps avec les données de Bern Sublimation est problématique. Comme décrit dans le paragraphe précédent, les changements rapides de $\delta^{13}C$ dans l'atmosphère ne sont pas tous pris dans les enregistrements de données dans les carottes de glace. Une plus haute résolution comme Grenoble Mill doit donner des points de données qui sont plus proches de la réalité, bien que, la méthode de Bern sublimation est plus précise que les méthodes Grenoble Mill et Bern Cracker. Cependant, les modèles d'âge de carottes de glace sont un facteur très important à considérer lors de la création des séries de données chronologiques, en particulier pour leurs l'évolution rapide. Le création de résidus en comparant les points de données qui ne sont pas au même point dans le temps peut avoir entraîné un faux lissage pour la moyenne Monte Carlo de $\delta^{13}C$ rapporté par Schmitt et al (2012). Nos résultats montrent que les changements très rapides dans $\delta^{13}C$ atmosphérique peuvent être causés en réponse à des événements liés a la puissance d'AMOC (chapitre 6, texte principal), les ±200 d'années entre les points de données rapportées par Schmitt et al pour le calcul des résidus est probablement beaucoup trop long. Pour cette raison, nous ne considérons pas que les données de $\delta^{13}C$ moyenne, de la méthode Monte Carlo, invalide les résultats de notre modèle, dans lequel les changements de puissance d'AMOC entraînent des changements rapides dans $\delta^{13}C$ modélisé.

Selon les résultats de CLIMBER-2P et la comparaison avec les données, une explication proposée pour les changements de CO_2 et $\delta^{13}C$ atmosphérique est présenté dans la figure 10. L'augmentation de l'insolation d'été dans les hautes latitudes a provoqué un dégel du pergélisol qui avait produit la libération (décomposition) de carbone du sol vers l'atmosphère résultant de l'apparition de la hausse de CO_2 atmosphérique à ~17.5kyrBP. En parallèle, des changements dans l'océan Austral causaient lentement la réduction de la masse de l'eau de fond de l'Antarctique. Entre 17.5kyr à 15kyrBP, malgré ce changement de la circulation océanique, l'océan était un puits de carbone. A partir de 16kyrBP la perte de carbone des terres ralenti, et de 13kyrBP la terre est devenue un puits de carbone, parce que l'expansion de la biosphère avait compensé les pertes de pergélisol-dégel. Se produisant aussi autour 15kyr BP, la fonte des calottes glaciaires et de l'eau s'écoulant dans l'Atlantique nord a peut-être ralenti la hausse de température de l'hémisphère nord. Lors de l'événement de réchauffement de B-A, survenant de 14.7kyrBP, une augmentation rapide d'AMOC peut avoir provoqué un dégel rapide du pergélisol libérant de nouveaux des sols de haute concentrations de carbone qui a décomposé rapidement et vu comme une augmentation des émissions de CO_2, et la chute de $\delta^{13}C$. Le plateau de CO_2 vu juste après cette hausse rapide et qui a duré plusieurs milliers d'années était probablement le résultat d'un événement de dégel fort de la calotte glaciaire, qui a provoqué une réduction drastique de la puissance de l'AMOC, et à causé un ré-expansion du pergélisol. A la reprise d'AMOC après cet événement, le réchauffement très rapide de l'hémisphère nord a provoqué un dégel du pergélisol rapide et la libération de carbone via la décomposition du carbone du sol, l'augmentation de CO_2 dans l'atmosphère et une chute de $\delta^{13}C$. Tout au long de ces événements, le réarrangement lent de la circulation océanique a entraîné

une tendance à la hausse des émissions de CO_2 dans l'atmosphère dans les périodes où la terre était un puits de carbone. Les tourbières ont commencé à de créer et de développés de manière significative de 11kyrBP, et une expansion de la végétation dans l'approche de l'optimum climatique de l'Holocène a provoqué une chute lente à long terme de CO_2 atmosphérique et l'augmentation $\delta^{13}C$. A 10kyr BP, l'insolation d'été de l'hémisphère nord de haute latitude a commencé à réduire et en réponse la zone de pergélisol a commencé à augmenter. A 6kyr BP, le système de terre peut déjà avoir été perturbé en raison d'interventions anthropiques, et cela se voit dans les données de CO_2 et $\delta^{13}C$.

5.3 Terminaison II, l'évolution de CO_2 et $\delta^{13}C$

3. De peut il que le mécanisme pergélisol-carbone explique aussi les données de la terminaison glaciaire précédente, TII?

Des données de CO_2 de Terminaison II (T2, ~135kyr BP) pourraient être généralement reproduites, et s'appuyer aussi sur les mécanismes glaciaires de l'océan, comme la terminaison 1, pour produire la hausse d'environ 100 ppm de CO_2 entre les périodes glaciaire et interglaciaire. Pour $\delta^{13}C$ (et CO_2) les données pourraient être reproduites mais uniquement si la sortie du modèle était déplacé d'environ 2.5kyrs. Cela peut être dû à des incertitudes dans le modèle d'âge utilisé pour les données de CO_2 et de $\delta^{13}C$. Pour modéliser correctement T2, la simulation doit être réalisée à nouveau en utilisant un modèle d'âge déplacé pour les données de CO_2 pour conduire CLIMBER-2P. Si cela est fait, la sortie du modèle de $\delta^{13}C$ peut montrer une meilleure correspondance aux données que celle présentés au chapitre 4 (texte principal). Une autre explication qui peut contribuer, est que l'élévation initiale du niveau de la mer a été causée par la fonte des calottes glaciaires de l'hémisphère sud, et pas seulement celle de l'hémisphère nord (voir section 8.5.1 texte principal). Les modèles d'âge et leurs synchronisation des ensembles de données, même pour la terminaison 1, sont toujours un exercice non-trivial. Dans ce sens, il est considéré comme raisonnable de suggérer que la sortie du modèle décalé peut représenter les données mesurées pour la fin 2.

Avant T2 la terre peut avoir stocké moins de carbone dans le pergélisol qu'au T1, en raison d'une grande calotte de glace Eurasienne, ce qui peut être en mesure d'expliquer pourquoi une baisse rapide du $\delta^{13}C$ au début de l'augmentation de l'insolation des haute latitude nord n'est pas vu aussi clairement dans données de T2 que dans les données T1. Cette question est examinée plus en détail dans la section 8.5 (texte principal). Aucunes expériences sur le forçage de l'eau douce n'a été réalisée pour la période T2, mais comme T1 il se peut que la fonte des calottes de glaces et l'apport d'eau douce dans l'Atlantique nord ait eu un impact sur le cycle du carbone, principalement par la biosphère terrestre.

Comme T1, l'importance des tourbières / terres humides pour la dynamique du cycle de carbone a été identifié. Pour les deux terminaisons, lorsque les niveaux de CO_2 atteint autour de 250 ppm, le $\delta^{13}C$ modélise a divergé des données, et le CO_2 modélisé a

augmenté trop vite. Cela suggère un mécanisme d'absorption de carbone des sols ce qui manque au modèle: les tourbières et les terres humides de l'hémisphère nord. Les discussions des simulations pour T1 concernant l'interdépendance entre les réactions des océans et le cycle du carbone des sols sont également valables pour T2.

5.4 dynamique du pergélisol sur des échelles de temps glaciaires

4. Si le pergélisol-carbone joue un rôle important dans l'augmentation du CO_2 atmosphérique pendant la terminaison glaciaire, agit-il à chaque cycle de précession et quelle est la puissance de l'effet dans les périodes non-terminaison?

Les mécanismes pergélisol-carbone ont changé la dynamique du carbone des sols par rapport au modèle standard. Les stocks totaux de carbone dans les sols modélisés au cours de la dernière période de cycle glaciaire sont présentés dans la figure 11, et le carbone du pergélisol pour la même simulation est montré dans la figure 12. Dans le modèle standard, la réponse de la biosphère terrestre n'est vraiment sensible qu'au CO_2 et a la température annuelle moyenne. Cela a juste agit que comme un retour négative pendant les périodes de changements climatiques, dans lesquelles le réchauffement et l'augmentation de CO_2 atmosphérique induisent l'augmentation du carbone dans la biosphère terrestre. Avec le mécanisme de pergélisol-carbone le stock de carbone des sols est maintenant beaucoup plus sensible à la surface des calottes de glace et aux changements de l'insolation d'été dans les hautes latitudes.

La superficie de pergélisol est sensible à l'insolation à tous les cycles d'insolation, mais aussi fortement influencé par la superficie des calottes glaciaire sur la terre, et le concentrations atmosphérique de CO_2. Pas toutes les terminaisons, telles qu'elles sont définies, sont associés à une réduction de la superficie du pergélisol et une libération de carbone des sols, indiqué par les résultats du modèle. Au T3 (~ 250kyr BP) l'augmentation de CO_2 atmosphérique provient en totalité de l'océan. Au cours des terminaisons (T3 exception) le dégel du pergélisol a contribué à la hausse initiale du CO_2 atmosphérique. Cependant, des baisses importantes dans le total des stocks de carbone dans les sols sont vus dans d'autres périodes que les terminaisons. Les extensions des calottes de glace dans les phases de refroidissement, associées à des cycles d'insolation, ont causé des pertes de superficie de la zone du pergélisol et des pertes de carbone du sol. Cela s'est produit en même temps que les conditions climatiques sont devenues plus défavorable pour la croissance de la végétation et donc la perte de carbone du sol a été aggravée par la réduction de NPP. Pour le dernier cycle glaciaire, une réduction de l'ordre de 800GtC a été observée entre 80kyr et 65kyrBP, cet ordre de chute serait évident dans les données $\delta^{13}C$. Par contre, la plus longue et la plus rapide des réductions dans les stocks de carbone du pergélisol a eu lieu pendant les périodes de terminaison glaciaire.

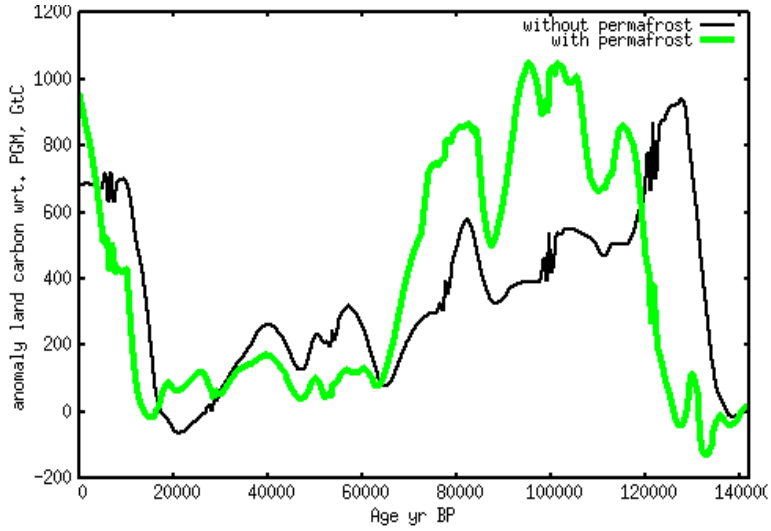

Figure 11, anomalie de carbone des sols par rapport au PGM pour CLIMBER-2P (ligne verte) et le CLIMBER-2 modèle standard (ligne noire, pas de carbone du pergélisol).

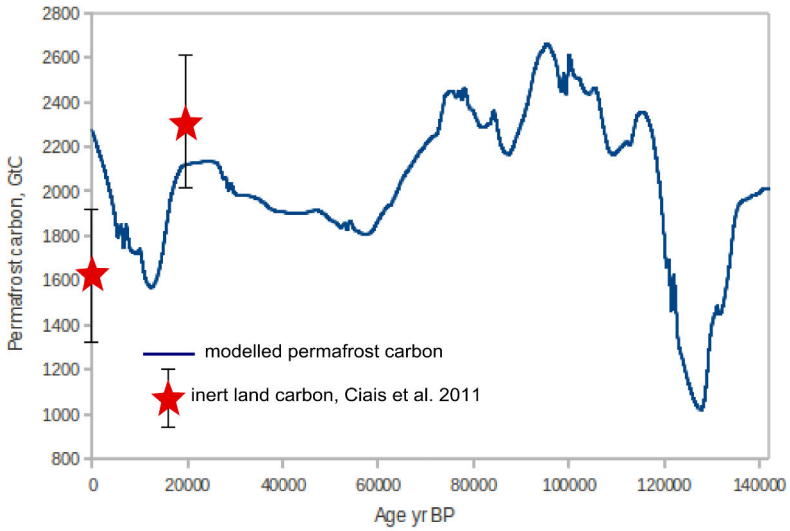

Figure 12, modélisation des stocks de carbone du pergélisol pour le dernier cycle glaciaire. Estimation du stock de carbone inerte des terres de Ciais et al (2012) a marqué avec les étoiles rouges.

Les simulations présentées dans le chapitre 5 (texte principal) ne comprennent pas une contribution d'un mécanisme de l'océan glacial. C'est la raison pour laquelle les données de CO_2 ne peuvent pas être reproduites en sortie du modèle. Cependant, les résultats des simulations de terminaison 1 et 2 suggèrent que le mécanisme de l'océan

glacial produit des changements des stocks de carbone de l'océan répondants plutôt lentement. Pour la terminaison 2, l'inclusion du mécanisme de l'océan glaciaire produit une anomalie maximale de 140GtC dans la quantité de carbone dans l'océan ou la terre par rapport à la simulation sans mécanismes de l'océan glaciaires (chapitre 4, fig 4.3 texte principal). Selon les données de carottes de glace, les périodes de terminaison représentent les plus grands et les plus rapides changements climatiques sur un cycle glaciaire, peut-être à l'exception de la variabilité du climat à l'échelle millénaire (pour la vitesse). Pour ces raisons, les dynamique et période de changement vu dans le stocks de carbone dans la terre et l'océan a la figure 5.8 (chapitre 5, texte principal) sont considérés comme fiables pour la réponse du système entraîné par insolation, à une confiance estimée de ± 140GtC. Le de forçage de l'eau douce n'a pas été inclus dans les simulations de cycles glaciaires complets, par conséquent, l'effet sur l'AMOC n'est pas pris en compte dans les résultats. Les mécanismes de l'océan glaciaire se traduirait par des tendances à long terme qui ne figurent pas dans nos simulations du modèle (mais observées dans les données). La dynamique des tourbières / terres humides, qui ne figure pas dans notre modèle, aurait un effet sur les stocks de carbone dans les sols. Selon la comparaison modèle-données de périodes terminaisons il se peut que les tourbières et les terres humides soient plus importantes dans les climats chauds, où le CO_2 est supérieur à ~ 250 ppm, cette idée est soutenue par les dates d'âge basales des tourbières actuelles (Yu et al 2010).

5.5 variabilité du climat a l'échelle millénaire

5. Les changements climatiques rapides qui peuvent avoir effectuées l'hémisphère nord, auraient une effet sur l'étendue du pergélisol. Le mécanisme pergélisol-carbone pourrait avoir joué un rôle dans ces changements climatiques rapides?

Aucune donnée $\delta^{13}C$ n'est encore disponible pour variabilité du climat a l'échelle millénaire pendant la dernière période glaciaire, mais la comparaison avec les données de CO_2 et la température pourrait être faite. Les résultats du modèle dans le chapitre 6 (texte principal) pour les événements d'arrêt et redémarrage d'AMOC (avec un climat de base a l'équilibre) montre que le CO_2 modélisé a augmenté plus rapidement et plus tard que les données (pour des événements comparables). Les simulations réalisées ont été très simplifiée, et un fond de climat de base à l'équilibre n'est pas représentatif des conditions réelles de l'époque. Cependant, comme avec d'autres études quand l'AMOC a entraîné les changements climatiques rapides, l'importance du climat de fond sur la réponse du système était très évidente. Au cours d'une série de forçages de l'eau douce, les événements de grandeur décroissante mis en œuvre dans le modèle, le décalage entre le CO_2 modélisé et les données peut être expliqué par un manque de tourbières, le feu et la réponse de mécanisme de l'océan glacial dans le modèle. Si le pergélisol-carbone, ou une source de carbone des sols, ont un rôle à jouer lors de ces événements a l'échelle millénaire alors il serait visible dans les données $\delta^{13}C$ atmosphérique. Pour nos

paramètres du modèle un événement AMOC arrêt-reprise qui dure 1500 années a entraîné une baisse de $\delta^{13}C$ de 0,3 ‰. Le refroidissement dans l'hémisphère nord a entraîné une absorption de carbone des sols et une augmentation de $\delta^{13}C$ plus tard. Le réchauffement a provoqué une libération de carbone des sols et une baisse rapide de $\delta^{13}C$ pour les simulations de climat de fond LGM.

6. projections futures pour les scénarios d'émissions de carbone d'origine anthropique

Ainsi que les questions de recherche initialement posées sur les paléoclimats, le modèle CLIMBER-2P entièrement couplé a été utilisé pour simuler les changements climatiques futurs sur la base des émissions de dioxyde de carbone provenant de sources humaines. La conduite du modèle avec les projections d'émissions de la base de données RCP a permis une première estimation de l'ampleur de la rétroaction pergélisol-carbone pour des scénarios du futurs dans le chapitre 7 (texte principal). Identifiés à partir des simulations d'échelle de temps longues (plusieurs cycles glaciaires), pendant les périodes interglaciaires le modèle n'est pas fortement conduit par des mécanismes de l'océan glaciaires, par la suite ceux-ci n'ont pas figure dans le modèle pour les changement au futurs. Le CO_2 modélisé pour 1850 CE dans le modèle était 274ppm, moins de 5 ppm d'écart de données. Cela permet au modèle d'être entièrement couplé et au CO_2 atmosphérique calculé dans le cycle de carbone de conduire le code radiatif et le modèle de la végétation.

En comparant les sorties CLIMBER-2P avec les modèles CMIP et une ensemble des modèles EMIC (Zickfeld et al 2013), le CO_2 atmosphérique calculé par CLIMBER-2P est plus élevé, en raison du carbone émis par le pergélisol qui dégèle. Pour le plus haut forçage, RCP 8.5, cela équivaut à environ 500ppm de plus de CO_2 atmosphérique au pic de température. Le taux du carbone émis à partir du pergélisol qui dégèle dépend de la vitesse de montée en température. C'est une caractéristique des mécanismes avec un long temps à l'équilibre, et rend la rétroaction du pergélisol-carbone (PCF) difficile à comparer avec la description du GIEC des rétroactions qui sont considérées comme linéaire et d'agir vite dans les projections futures. Le PCF crée également un plus longue traîne dans la réponse du système climatique, le CO_2 atmosphérique reste plus élevé dans l'atmosphère sur de plus longues échelles de temps.

Là encore, comme avec d'autres simulations, les tourbières et les terres humides dans les latitudes nordiques sont importante pour le système terrestre. Le modèle CLIMBER-2P ne représente que la réponse pour le sol gelé, pas les tourbières étroitement liés, dans les hautes latitudes. Par rapport à d'autres modèles, CLIMBER-2P projette beaucoup plus des pertes de carbone du sol. Les résultats du modèle montre un bon accord avec les estimations de Schuur et al (2011) pour la libération de carbone du pergélisol et Harden et al (2012) pour le carbone vulnérables au dégel du sol. Il se peut que la différence entre les projections CLIMBER-2P et d'autres modèles soit largement expliquée par l'augmentation d'absorption du carbone dans les tourbières. Notre modèle

a été réglé aux données de la terminaison 1, en tant que tel, il représente toute la dynamique de dégel tels que la formation talik, la couche actifs épaississants et le taux de libération de carbone du pergélisol-dégel. Afin de déterminer si la différence entre notre modèle et les sorties de modèles plus complexes est due à l'absorption des tourbières / terres humides, elle devrait être intégrée dans le modèle CLIMBER-2P pour des études suivantes.

Le traitement du pergélisol dans notre modèle considère que son rôle dans le cycle de carbone, mais pas son rôle avec le flux de l'énergie du surface. Le gel et le dégel du matériau aurait un effet fort sur le budget de l'énergie tout au long de l'année, et pendant les périodes de l'évolution des climats. Cette chaleur latente de dégel de la cryosphere, notamment le pergélisol qui représente une quantité importante d'énergie en fonction de l'estimation dans le chapitre 7 (texte principal), doit être prise en compte dans le calcul du budget énergétique dans les modèles complexe.

Les simulations pour les projections futurs ont seulement l'impact de l'augmentation du CO_2 sur le système actuel, y compris des calottes de glace fixes. Dans le cas réel du monde, et en particulier pour les échelles de temps plus longues et les plus forts forçages, l'impact de la fonte des calottes glaciaire serait important pour la réponse du système Terre. Ces effets seraient le changement de l'albédo, la superficie des terres (nouvelles terres exposées actuellement sous les calottes glaciaires) et l'élévation du niveau de la mer, et la réponse de l'AMOC. Des données récentes suggèrent déjà un ralentissement de la puissance de l'AMOC depuis les années 1990 (Robson et al 2014), qui coïncide avec la fonte de la calotte glaciaire du Groenland (Hanna et al 2008). Une puissant forçage de l'eau douce dans l'océan Atlantique nord peut induire une réduction forte de l'AMOC (selon le chapitre 6, texte principal) qui peut temporairement refroidir l'hémisphère nord et affecter la concentration de CO_2 dans l'atmosphère. D'autres études de la réponse futur du système qui incluent la fonte des calottes des glaces ainsi que forçage du CO_2 et le changement en utilisation des terres permettra de mieux représenter la réponse éventuelle du système que les projections actuelles.

7. Conclusions

Cette étude visait à développer un modèle dynamique du pergélisol-carbone à intégrer dans le modèle CLIMBER-2 et d'effectuer des simulations en vue de contribuer à la connaissance du cycle du carbone. Ce travail pourrait, pour la première fois, permettre une étude de modélisation avec un modèle de système terrestre qui comprendrait l'atmosphère dynamique, l'océan dynamique, la végétation dynamique et les composantes de la cryosphere, y compris les terres gelées, afin d'étudier le paléoclimat. La disponibilité des données récentes du CO_2 et de $\delta^{13}C$ de CO_2 dans l'atmosphère fourni un moyen de valider les résultats du modèle pour déterminer si une dynamique pergélisol-carbone pourrait avoir joué un rôle important au cours des climats changeants.

Un mécanisme pergélisol-carbone simplifié a été développé et validé (chapitre 3, texte principal) et à été réglé en utilisant les données de la terminaison 1 (chapitre 4, texte principal). Il a été constaté que, pour reproduire des données de CO_2 et $\delta^{13}C$ atmosphériques (pour l'atmosphère et l'océan) au cours de la terminaison, une combinaison des mécanismes océaniques-glaciaires et pergélisol-carbone ont été nécessaires. Suite à cette constatation, plusieurs cycles glaciaires ont été modélisés pour étudier la sensibilité du mécanisme pergélisol-carbone aux forçages de CO_2, les calottes glaciaires et l'insolation (chapitre 5). l'étendue des calottes glaciaires a été jugée particulièrement importante pour le contrôle de la superficie des terres disponibles pour le pergélisol, et donc aussi pour la dynamique du carbone du pergélisol-carbone. La libération du carbone dans les sols de dégel en réponse à l'augmentation de l'insolation d'été dans les hautes latitudes, a été jugée très probable comme la source des hausses initiales de CO_2 dans l'atmosphère au cours des terminaisons glaciaires.

Les données CO_2 de terminaison 1 peuvent être bien reproduits, y compris le plateau de CO_2 BA / YD, quand le forçage de l'eau douce est appliqué à l'Atlantique nord. Il a été constaté que l'augmentation du CO_2 atmosphérique au début de la terminaison n'a pas besoin d'une coupure et reprise de l'AMOC. La source de la hausse initiale de CO_2 atmosphérique était terrestre, et l'océan n'est devenu une source de carbone qu'après environ 15kyrBP. En réduisant la salinité de l'Atlantique nord au cours de la B-A/YD, l'hémisphère nord a refroidi, le pergélisol a avancé et le carbone a été repris dans les pergélisols. A la reprise de l'AMOC, le transport rapide de la chaleur vers l'hémisphère Nord a causé la fonte du pergélisol et une augmentation rapide du CO_2 atmosphérique.

Expériences avec forçage de l'eau douce ont souligné l'importance du mécanisme du pergélisol-carbone dans l'évolution rapide des climats. Les augmentations très rapides des niveaux de CO_2 dans l'atmosphère peuvent être expliqués par la libération rapide des sols en carbone en réponse à l'augmentation du transport de chaleur vers l'hémisphère nord. C'est en réponse à la reprise de l'AMOC suite d'un événement AMOC arrêt/réduction, tels que des événements D/O vu dans les données du δ18O Groenland. Les projections de changement climatique représentent des événements de réchauffement rapide. La conduite du modèle par des projections

d'émissions (base de données RCP) a prédit l'augmentation du CO_2 de pic et une plus longue période a des niveaux élevées de CO_2 par rapport aux sorties du modèle qui ne comprennent pas les évaluations du pergélisol-carbone.

L'analyse de $\delta^{13}C$ de l'océan doit tenir compte de la dynamique du pergélisol et du carbone de la terre en général et de son effet sur les niveaux de $\delta^{13}C$ atmosphériques. Si ce n'est pas pris en compte alors la circulation océanique peut être trop invoquée pour tenter d'expliquer les changements de $\delta^{13}C$ de l'océan et du CO_2 atmosphérique. Le système Terre n'est pas tout simplement l'atmosphère et l'océan. Les conclusions de ce travail soulignent qu'il est essentiel de considérer la dynamique du carbone des sols lors de l'interprétation paléo-indicateurs pour le cycle du carbone.

Le mécanisme pergélisol-carbone réagit aux changements de température et amplifie la réponse du cycle du carbone. Il est fortement dépendant non seulement de l'apport d'énergie (qui détermine la température du sol et de l'emplacement du pergélisol), mais également de la surface de terres disponible à l'échelle mondiale sur laquelle le pergélisol peut exister. Afin de modéliser et de comprendre correctement la réponse du système terrestre dans les climats futurs et passés, le mécanisme de rétroaction pergélisol-carbone est un élément important du système. Ce travail a été une première étape pour aborder le rôle que la cryosphere terrestre joue dans le cycle du carbone et du système climatique sur de longues échelles de temps, et que d'autres études sont essentielles.

Table of Contents

Chapter 1: Background and literature review

Chapter 2: The CLIMBER-2 model

Chapter 3: Permafrost model development

Chapter 4: Glacial-interglacial transitions, tuning the carbon dynamics

Chapter 5: Glacial cycles

Chapter 6: Fresh water forcing and millennial scale variability

Chapter 7: Future Projections

Chapter 8: Discussion and Conclusions

Chapter 1: Introduction and Background

This chapter presents an overview of the carbon cycle within the earth system, and identifies a possible area which would benefit from further study: The role of permafrost and high carbon soils in high northern latitudes. This presents a start point for this study, aiming to estimate the permafrost-carbon feedback within the earth system via paleoclimate coupled modelling studies and constraining the estimate using ice core atmospheric CO_2 and $\delta^{13}C$ data.

1.1 Introduction

During the 19th century the study of landscape features suggested that in the past the world had been much wetter or much colder. At the time the presence of large rocks, which originated in mountainous areas, but presently deposited on lowlands posed questions about mechanisms that could have carried them there. Their existence were either thought to be as a result of large floods, on which ice rafts carried the rocks to distance, or due to action of very large glaciers which extended as far as these lower areas. The existence of post-glacial moraines far from glaciers, and striations and grooves in both inland and coastal valleys in Scotland strongly suggested that in the past glaciers covered a lot more of the land surface than they do today (Thomas Francis Jamieson 1862). In the 1870s James Croll extended formulae on the Earth's eccentricity of orbit around the sun, and presented an explanation for glaciation periods as a result of eccentricity forcing including the ice-albedo feedback and ocean current feedback as important factors. In 1895 Svente Arrenhius published a study which considered the effects of changes in atmospheric CO_2 concentrations and its effect on the thermal balance of the Earth surface temperature, highlighting the importance of atmospheric chemistry in regulating the climate. In 1941 Milankovitch linked the changes in summer insolation, dependent on the Earth's orbit around the Sun, at high latitudes (65° North) to glacial-interglacial oscillations, concluding that high northern latitudes exerted control on glacial cycles. Today, work on identifying the mechanisms which are responsible for the changes in climate and in the concentration of atmospheric CO_2, and other gases, which then feedback to effect climate are still subjects of study.

1.2. Tools and indicators

The study of the present-day climate can be carried out using direct measurement data of the subject of interest, for example using satellite data, field study methods and models to interpret data to the global scale. The study of past climates does not generally allow for the direct measurement of data, but rather relies on the study and measurement of indicators which can provide some information about the climate during the period of interest.

1.2.1 Landscapes

Landscape features visible today provide a record of mechanical and chemical processes which that landscape has experienced. An example of this are the first studies which provided clues to glacial cycles as carried out in the 19th century. Landscape features provide the main source of information on the extent of the cryosphere in the past, as post glacial moraines and evidence of frozen and patterned ground in present day temperate regions (French and Millar 2013) for example. In the longer term, the study of geology has provided insight in long past climates on the time-scale of millions

of years, and evidence of the orbital pacing of geological scale climate changes (Lourens et al 2005).

1.2.2 Proxies

A proxy record is one which is determined from an indirect source of information to provide the data of interest. For example a source that shows variability dependent on precipitation may be used as a rainfall proxy, provided there is a good understanding of the control that rainfall has on the source (proxy). Some examples of proxy data are listed next.

The study of pollen trapped in sediments can provide information of plant assemblages present at the time. By reconstructing the biomes (types of vegetation assemblages) the general climatic conditions can be determined, as different plants are suited to different climatic conditions. The study of the soils and paleosols themselves can also provide information on the conditions of the time. The presence of burnt material in soils or sediments is the main means of reconstructing paleo-fire regimes. Trees grow annually causing the appearance of rings through their cross section. The study of the size and density of these rings can provide a means of reconstructing temperature or climate at the location in which the tree grew. Very slow growing and long lived trees can provide thousands of years worth of proxy temperature data, and fossil trees can provide information on temperature on longer timescales. The study of speloethems and patterns of accumulation by looking at cross sections can be used to reconstruct a temporal record of climate conditions.

Proxy records determined from ocean sediment cores are used extensively in the reconstruction of past climates through very long timescales (millions of years). Some more details on these are given next. Many other methods of the use of proxies to reconstruct climate and other local conditions are available, and new proxies are being established frequently.

1.2.3 Ice and ocean sediment cores

Ocean cores

Prior to the more widespread use of models as a research tool, palaeo proxy data measurements were carried out that provided clues about the glacial carbon cycle. Sediment cores from the sea bed hold fossils of foraminifera whose shells formed in the palaeo-Ocean. The constituents of the shells can give information on local conditions. Ocean core drilling is the leading method of studying past climates, particularly climates on the timescales of millions of years before the present day.

Ice cores

In ice, air is trapped in bubbles that form when snow compacts on an ice cap as it is covered with fresher layers of snow fall. This process of bubble closure (trapping the

air) takes a certain amount of time depending upon the local conditions such as snowfall rates and temperature. When drilled and analysed, these trapped bubbles of air provide a direct record of the constituents of the palaeoclimate's atmosphere. Antarctic ice cores have generally less (snow) accumulation than Greenland ice cores and so, because of ice sheet dynamics, longer time-scale records have been obtained from Antarctic ice cores. Analysis of the constituents of the ice (water) also provide indicators of climate, the longest of these records being from EDC in Antarctica, this provides a 800,000 year deuterium record, a proxy for temperature (Jouzel et al 2007). Currently, records for atmospheric CO_2 are only available from Antarctic ice cores, because in Greenland ice biological activity has effected the CO_2 levels trapped in the ice.

When investigations of the carbon cycle using models and/or other methods are carried out, the results can be compared against the data from ice cores and proxy records, bearing in mind that there are margins for error both record types. When air is trapped between ice crystals it takes some time for it to be fully closed off from the surrounding atmosphere. This bubble closure process means that some very fast processes' signatures are lost as the gases in the ice continue to exchange with the atmosphere for a period of time.

Fractionation of isotopes

Fractionation of isotopes is the process that occurs during the transfer of material between different pools via chemical and biochemical reactions. An isotope is an atom of the element (material) that has the same number of protons in its nucleus, but a different number of neutrons which give it a slightly different atomic weight. The stable isotopes of Carbon, Oxygen and Hydrogen commonly provide a means to study past climates.

Carbon-14 (^{14}C), also known as radiocarbon, is the isotope of carbon which contains 2 more neutrons in its nucleus than (regular) ^{12}C. ^{14}C makes up around 1 part per trillion of all carbon on the Earth. The natural source of ^{14}C is the action of cosmic rays on nitrogen-14 in the upper atmosphere that creates carbon-14, which is therefore a cosmogenic nuclide. ^{14}C is commonly used to date biological material, it is unstable and has a half-life of 5730±40 years (Godwin 1962). When a biological entity has died and no-longer builds itself from carbon in its environment, the ^{14}C fraction of carbon within it gradually reduces (via radioactive decay). Measurement of the amount of ^{14}C fraction remaining can provide an age estimate for that biological material. The same method can be used to measure the age of biologically derived carbon in atmospheric carbon-dioxide, and combined with other ice core data can provide clues to the sources and sink of the carbon passing through the atmosphere.

Carbon-13 (^{13}C) is a stable isotope of carbon and contains 1 more neutron than carbon-12 (^{12}C). It makes up around 1.1% of all carbon. During biological uptake of carbon, the photosynthesis reaction preferentially uptakes ^{12}C, causing the ratio between ^{13}C and ^{12}C to be lower in the biological entity than in the source. Measuring the ratio of ^{13}C to ^{12}C in a carbon pool can give information about the sources and sinks of the carbon passing through that pool.

Oxygen-18 (^{18}O) is a stable isotope of oxygen containing 2 more neutrons than oxygen-16 (^{16}O). Evaporation of ocean water preferentially uptakes ^{16}O water molecules, as it is slightly less heavy than ^{18}O. As well as this, precipitation of water vapour occurs first with ^{18}O water molecules, again because it is heavier. Due to this, ice in ice cores is depleted in ^{18}O compared to ocean water. Measuring the ratio between ^{18}O and ^{16}O of the water trapped in ice in Arctic and Antarctic ice cores can provide information about the temperature of the precipitation and also how much ice existed globally at that point in time. Oxygen is also present in the shells of sea creatures as $CaCO_3$, measuring the ratio of ^{18}O to ^{16}O in these shells can also provide information on the conditions of the sea water in which the creatures lived.

Deuterium (D) is an isotope of hydrogen containing an extra neutron. Measurements of the ratio of deuterium to hydrogen in water trapped as ice in ice cores can give information about the temperature at which the precipitation of that water occurred because the enrichment in D of precipitation-water is sensitive to temperature.

1.2.4 Computational models

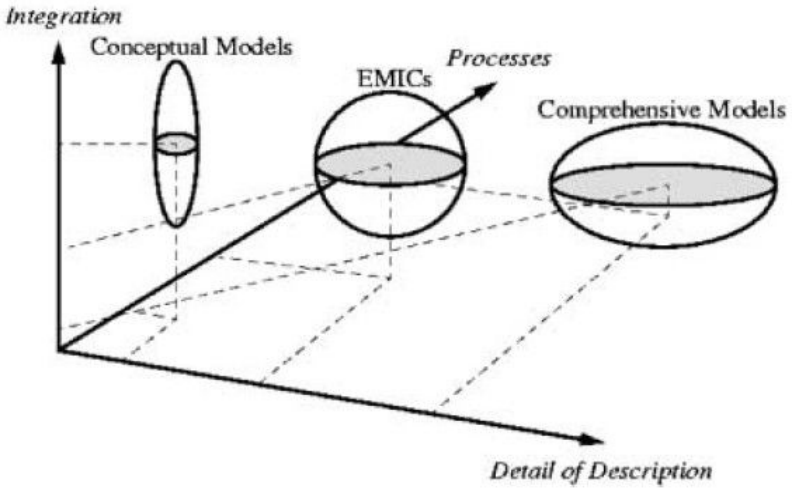

Fig 1.1: Computational models complexities and characteristics on an integration of processes, detail of description and processes space (Claussen et al 2002).

Proxy and measurement data provide important information on conditions (generally) local to the measurement point. In order to study a system, the use of models, both as process and global Earth system models, is employed. For Earth system model operation there are three main class of models: Box models, Earth system Model of Intermediate Complexity (EMICs) and Atmosphere-Ocean General Circulation Models (AOGCMs) known also as GCMs. Figure 1.1 shows how these three types are organised in terms of integration between processes, detail of process description and

how processes themselves are represented (Claussen et al 2002).

Box models can provide important insights into the major driving processes that effect climate on long timescales, but cannot easily provide insights on unforeseen feedbacks in the system because every processes is parametrised. More sophisticated model which use physical process representation can study these feedbacks. Using more complex and coupled models may provide greater insight into the processes at work as they require fewer parametrisations and assumptions and rely more on physical properties of processes in the systems. Figure 1.2 shows the development of state of the art models. Starting with atmosphere models in the mid 1970s, and gradually adding the processes as scientific understanding of their function improved, resulting in coupled AOGCMs. The EMICs present the opportunity to study the system fully coupled, where feedbacks from mechanisms act on the earth system. Intermediate complexity models do not necessarily represent all the processes that the state of the art models do, but they do allow transient simulations of the climate system and can provide important insights into feedbacks and driving mechanisms in the system. The main differences between EMICs and AOGCMs are that EMIC are of coarser spatial and temporal resolution, and possibly more processes are parametrised, rather than directly modelled. AOGCMS do not run fully-coupled with land-biosphere models, whereas some EMICs do. For the study of transient climate evolution, including feedbacks between processes, EMICs are a good tool.

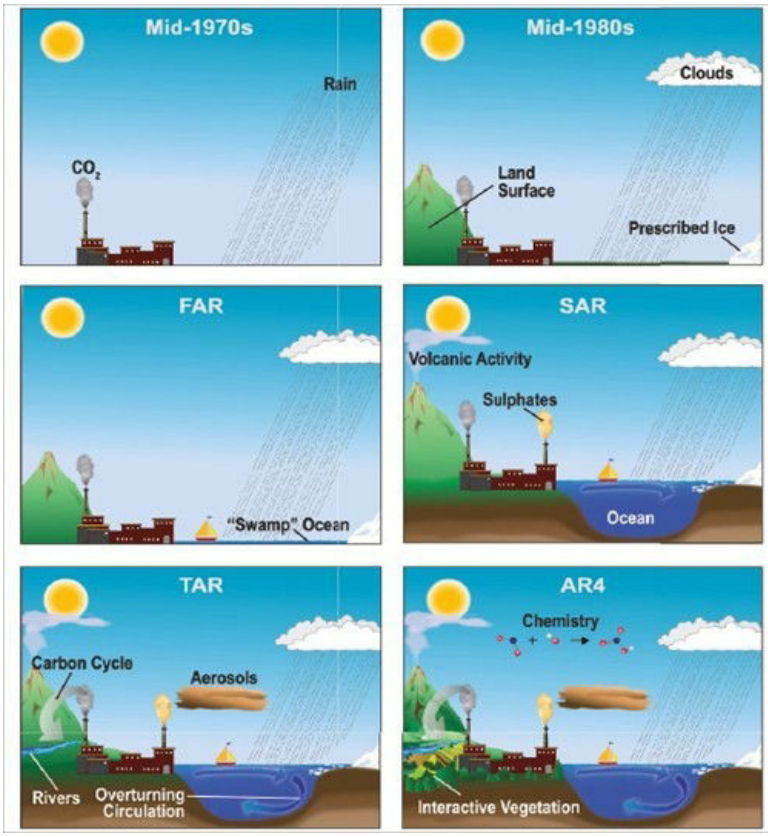

Fig 1.2: state of the art climate model development, IPCC AR4

1.3. Time-scales and carbon cycle mechanisms

Mechanisms within the carbon cycle operate on a variety of time-scales, from days to multi-millennia and longer. A diagram of mechanisms which act within and on the climate and the carbon cycle is shown in figure 1.3. The three major long-term stabilising mechanisms of the carbon cycle are the oxygen homeostat, the weathering CO_2 thermostat, and the ocean's calcium carbonate pH-stat. The Earth's orbit about the sun and the movement of tectonic plates affect the climate via setting the boundary conditions of the Earth system and carbon cycle. Other mechanisms within the system provide feedbacks on the input drivers and ultimately control and are controlled by the Earth's surface temperature and climate. Highlighted in fig 1.3 in yellow are the timescales of interest for this study, multi-centuries to multi-millennia. The mechanisms most strongly controlling these timescales are discussed in section 1.3.2.

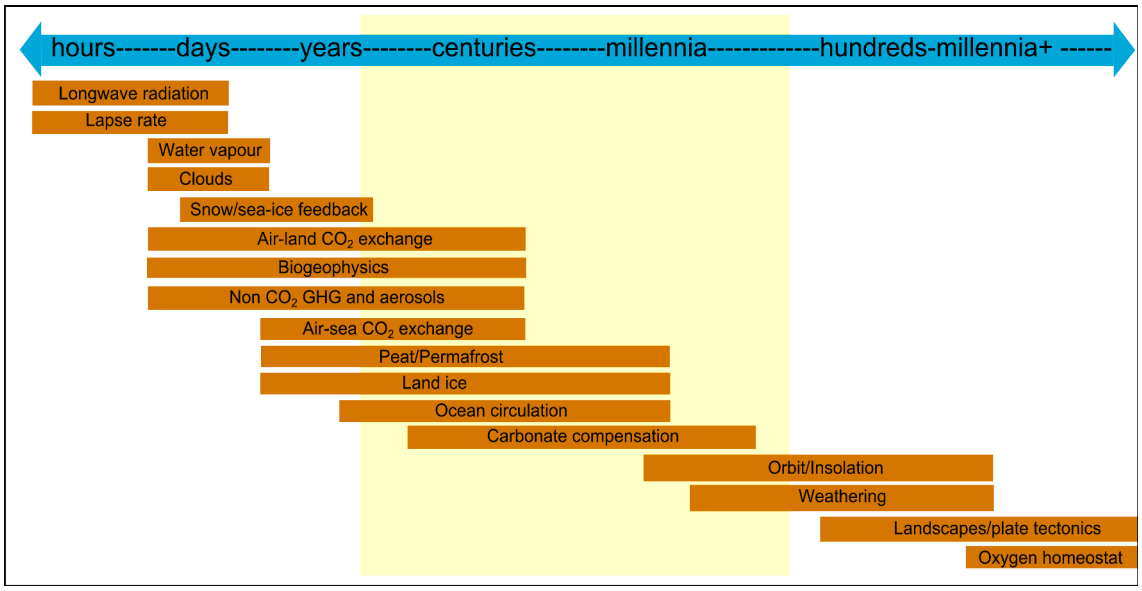

Fig 1.3: Feedbacks and Mechanisms in the climate system, with indication of the time-scales in which they act. Adapted from IPCC AR5 (Stocker et al. 2013) with longer timescale mechanisms added. Area highlighted in yellow is the timescale in which this study is interested.

1.3.1 Present-day organic carbon-cycle

Figure 1.4 shows the carbon cycle components most active on the timescales of interest in this study. The largest carbon store is the Ocean, containing around 38,000 GtC (N.B. One gigaton (Gt) of carbon is equal to one petagram (Pg)), mostly in the inorganic form; dissolved CO_2, carbonic acid H_2CO_3, bicarbonate ion HCO_3^- and carbonate ion CO_3^{2-} all of which are pH dependent. The next largest is in soils, holding an estimated 3970+-325GtC (Ciais et al 2012), of which 2370+-125GtC is considered

active in the fast carbon-cycle. This permafrost-carbon stock is not listed in figure 1.4, as it has often been neglected in carbon cycle studies. Finally, the atmosphere is presently holding around 780GtC (around 390ppmv CO_2) (Archer, 2010). The movement of carbon between these reservoirs during climatic changes and the mechanisms that control it are still subject to uncertainties. By the study of proxy, ocean and ice-cores and modelling studies, a better understanding of the function of the carbon-climate system can be approached.

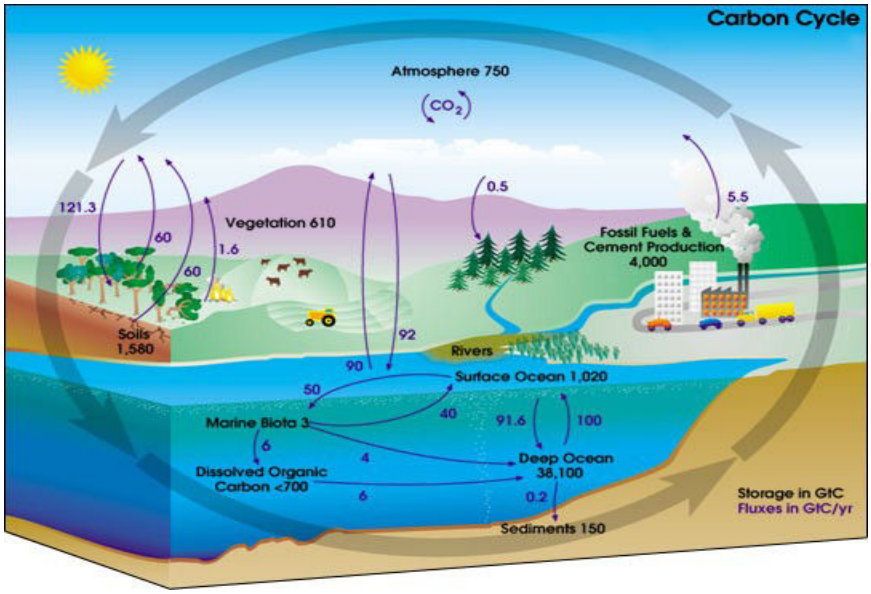

Fig 1.4: Organic carbon cycle (NASA Geo Science Enterprise). Note: this figure does not account for soil-carbon stored in the permafrost-zone.

1.3.2 Mechanisms

Oxygen homeostat

The oxidation of carbon into carbon dioxide relies on the presence of oxygen. The oxygen homeostat has the longest time-scale of the three major stabilising mechanisms, details of its operation are not well constrained but at periods in geologic time parts of the ocean have become anoxic. Due to the limited knowledge of the operation of the oxygen homeostat and the very long time-scales associated with it, it is assumed to be inactive on the time-scales that are of interest in this study.

Landscapes and plate tectonics

The position of land masses on the Earth surface has an effect on the climate system via ocean circulation patterns, albedo and atmospheric circulations. The amount of volcanism directly affects the amount of carbon dioxide in the atmosphere, as

volcanoes emit carbon otherwise buried in the Earth's crust. Landscape features such as mountain-building also effect the balance of carbon between the atmosphere and ocean (Raymo et al. 1988). With more bare land exposed the effects of weathering can increase the ocean uptake of carbon from the atmosphere. The effect of landscape changes on the time-scale of plate tectonics and mountain building is outside the scope of this study. It is assumed that these mechanisms are fixed on the multi-millennia time-scale.

Weathering

The weathering CO_2 thermostat operates on the order of tens to hundreds of thousands of years. Its most basic principle is that when the Earth warms up, the hydrological cycle speeds up (due to extra energy in the system) and increases weathering of limestone (CaO) rocks. This is via mechanical and chemical weathering and run-off to the ocean that causes the ocean to draw down the CO_2 of the atmosphere (Archer, 2010).

Urey reaction

$CaSiO_3 + CO_2 \leftrightarrow CaCO_3 + SiO_2$ eqn 1.1 (Urey, 1952)

$CaO + CO_2 \leftrightarrow CaCO_3$ eqn 1.2 (Archer, 2010)

Equations 1.1 and 1.2 give the basic constituents of the chemical process that is the weathering CO_2 thermostat. Removing silicate from both sides of the reaction leaves a very simplified process (eqn 1.2), the balance between igneous rocks, carbon dioxide and limestone, describing the action of the weathering CO_2 stat.

The set point of this weathering thermostat is also governed by the position of continents and the uplift of mountains that have an effect on the scale of tens to hundreds of millions of years. The present and glacial cycles-past are “set” colder than other time periods in Earth history (Zachos et al 2001). One theory is that the uplift of the Himalayas increased weathering of CaO and set up the conditions to push the system into the glacial – interglacial cycles (Raymo et al 1988).

Weathering of rocks occurs in two ways: mechanical and chemical weathering. Both means of weathering are accelerated in the presence of water. Generally speaking, in warm conditions chemical weathering is increased and in cold conditions mechanical weathering is increased (largely due to the effects of freezing and water-to-ice expansion).

Insolation

The orbit of the Earth about the Sun determines the total amount of energy input to the Earth system by solar radiation, as such it is the main driver of the Earth system. Figure 1.5 shows the three main components of the Earth orbit defined by Milankovitch theory. Each of these parameters has particular dominant frequencies (shown in fig 1.6) which, combined, result in a per-latitude pattern of insolation that changes with orbit.

Insolation is the only significant energy input to the Earth system, and studies which consider the statistical relationship between changes in the orbit and the proxy global temperature record gives possible clues as to controlling mechanism in the Earth system response to insolation forcing.

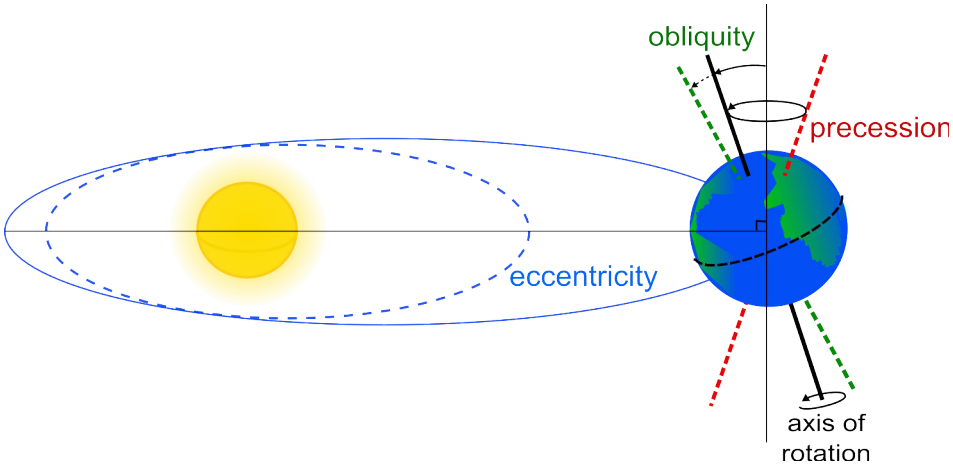

Figure 1.5: Orbital factors affecting climate on multi-millennial timescales. Eccentricity is the shape of the orbit, either more circular or more elliptical. Obliquity is the angle of tilt of the Earth rotation axis with respect to the orbital plane. Precession is the 'wobble' of the Earth's rotation axis which changes the positions of the rotation axis with respect to the distance star reference frame (the direction in which the North rotation axis is facing changes).

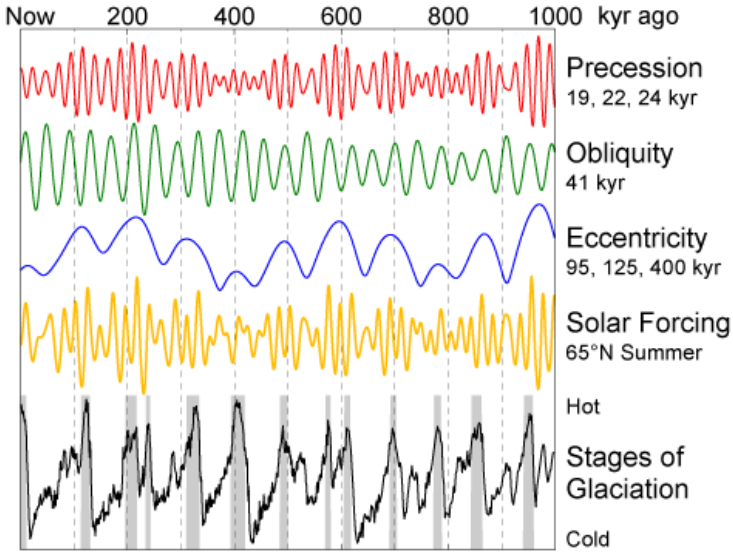

Figure 1.6: The action of each of the orbital parameters, showing dominant frequencies of each (Quinn et al 1991). Shown in yellow is the insolation (solar energy input) received at 65degN on 1st July and the black line is the ^{18}O record from Antarctic ice cores showing the climate changes over the same periods (Lisiecki and Raymo 2005) with interstadial (warmer) periods highlighted in grey. (Wikipedia 2013).

Carbonate compensation

The third of the major stabilising mechanisms is the Ocean's calcium carbonate pH stat whereby the concentration of dissolved carbon in ocean water changes the ocean pH. This in turn affects the ability of ocean water to dissolve other inorganic carbon. The net effect is that ocean carbon content is stabilised on the time-scale of a few thousand years by adjustments to the oceans pH. The carbonate compensation depth in the ocean is the point at which the input of calcium carbonate is balance out by its dissolution in the ocean water. Below this level no carbonate is deposited as sediment on the sea floor.

The changes in sea-level associated with the accumulation or melting of land ice-sheets also has an effect on the carbonate compensation mechanism. The shallow water coral reefs that would have been flooded during sea-level rise episodes are thought to be an important mechanism that increases atmospheric CO_2. By the production of carbonate in these flooded shelves, it may have reduced the Oceans ability to hold as much CO_2 in solution.

Ice sheets

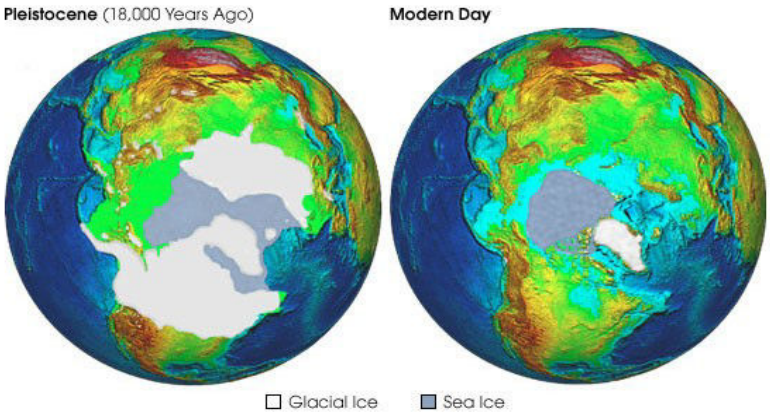

Figure 1.7: Northern hemisphere ice sheet extents for 18kyr BP and modern day (NOAA)

Evidence from landscapes and ocean and ice cores show that extensive ice sheets grew over the northern hemisphere land masses during glacial (cold) periods. The southern hemisphere ice sheet also increased during cold periods. Figure 1.7 shows a graphic representation of NH ice sheets at 18kyr BP and the modern day (NOAA, the National Oceanic and Atmospheric Administration). The presence of these large ice sheets change the surface elevation and surface energy fluxes which in turn effect atmospheric circulation. The large expanses of highly reflective ice also reduce the global albedo which results in more radiation (from insolation input) being reflected back into space and therefore a drop in global temperature. The growth of the ice sheets lock away water on the land which reduces sea-level and ocean volume.

Ocean temperature, salinity and pressure

Ocean temperature, salinity and pressure affects the waters ability to dissolve CO_2. In colder water more carbon dioxide can be held in solution. In saltier waters less carbon dioxide can be held in solution. In fresh water increasing pressure increases the ability of sea water to dissolve CO_2. During glacial periods more fresh water was locked in ice sheets and so the ocean water would have been more saline, but also colder. The relative balance of these effects are studied usually using global ocean-atmosphere models.

Ocean circulation

Ocean circulation changes are important in the control of global but also regional and local climates by changing the energy transport patterns. Ocean circulation is a combination of the Coriolis effect caused by the Earth's rotation about its axis and the combined effects of temperature and salinity on ocean water buoyancy. It is also dependent on the configuration of land masses.

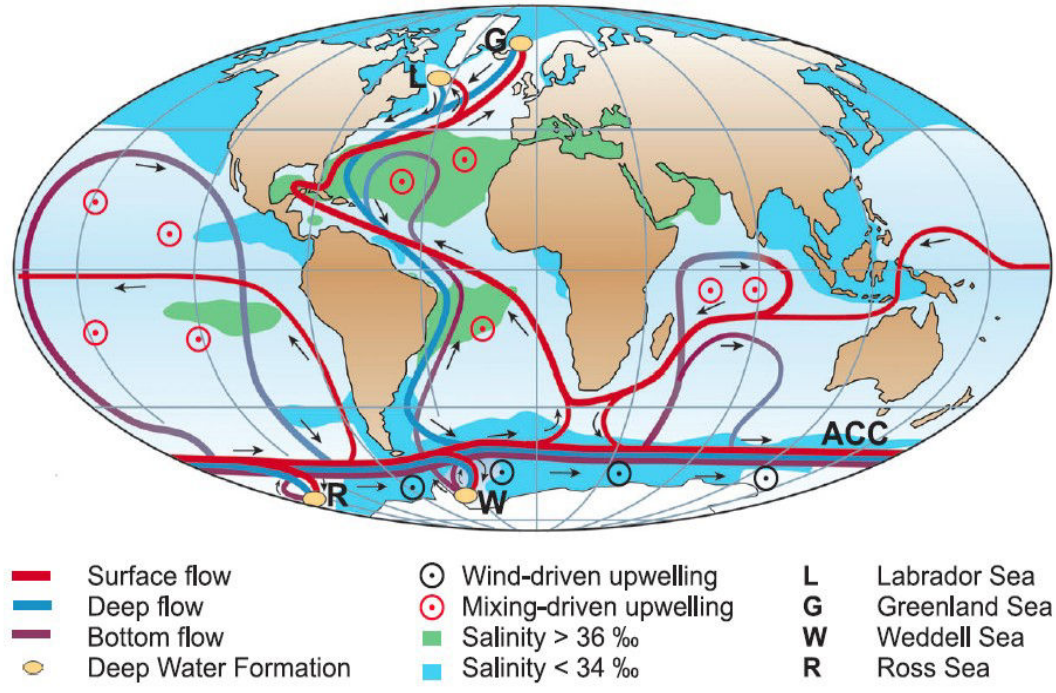

Fig 1.8: Global thermohaline circulation (Rahmstorf 2002), present day. "Schematic representation of the global thermohaline circulation. Surface currents are shown in red, deep waters in light blue and bottom waters in dark blue. The main deep water formation sites are shown in orange" ACC is Antarctic Circumpolar Current.

Figure 1.8 shows the present day global thermohaline circulation. A major driver of this circulation is the Atlantic meridional overturning circulation (AMOC) in which warm salty waters, brought to the North Atlantic via the Gulf Stream, cool and sink to the deep creating the return flow of the AMOC and North Atlantic Deep Water (NADW). During thaw periods of the northern hemisphere ice sheets, this north Atlantic region was subject to input of fresh water, which may have inhibited the ability of waters to sink to the deep (because fresh water is more buoyant than salty water). This in turn may have effected the strength of the AMOC and in turn global ocean circulation patterns.

During the glacial period it is thought that the deep southern ocean may have acted as a major store of carbon. The mechanisms which could have resulted in the high carbon storage in this location are still subjects of debate and uncertainty, but this deep ocean carbon store is a leading hypothesis for the draw-down of atmospheric CO_2 in glacial periods, after ocean temperature and carbonate compensation response to changes in ocean water pH.

Iron fertilisation

Bioproductivity in the ocean is dependent upon the availability of nutrients supplied to phyto and zooplankton to feed upon. In the glacial period there is indication that the atmosphere contained more dust particles, including iron which is a limiting nutrient for ocean productivity. If this atmospheric iron dust was made available to the ocean surface, then it may have increased ocean productivity. In terms of the carbon cycle, the increased ocean productivity may have increased the "biological pump" causing more carbon to be stored in the deep ocean via rain-down of carbon from mortality of ocean biota (Bopp et al 2003). The availability and provision of nutrients to the oceans biota can control the biological pump and therefore affect the total amount of carbon stored in the ocean. The iron fertilisation hypothesis provides a mechanism which could have resulted in the deep southern ocean carbon store.

Land carbon stocks

In response to local climate conditions, terrestrial vegetation can experience shifting biomes and a change in total carbon storage. In very cold in-hospitable conditions vegetation growth is limited, and based on pollen records it was found that at the last glacial period the terrestrial biosphere was reduced compared to the present day. With reduced input from vegetation, soil carbon accumulation would also have been affected. Carbon-13 has been used to estimate changes in land carbon stock.

Deep ocean sediment cores are considered to be largely independent of biological factors that affect ^{13}C because of the slow mixing of the deep ocean. This mean that changes in $\delta^{13}C$ seen in deep sea forams shells may be used to indicate the change in whole ocean carbon-13 content. In 1977 Shackelton, by analysing deep sea foraminifera, calculated the whole ocean change in ^{13}C from the Last Glacial Maximum ~21kyr BP (LGM) to the pre-industrial ~1850 C.E. (PI) as 0.7‰.

Method: Change in ocean $\delta^{13}C$	Delta ocean $\delta^{13}C$ (‰)	terrestrial biomass increase (GtC)
Shackelton (1977)	0.70*	1000
Duplessy et al (1984)	0.15	220
Berger and Vincent (1986)	0.40	570
Curry et al (1988)	0.46	650
Duplessy et al (1988)	0.32	450
Broecker and Peng (1993)	0.35	425
Bird et al (1994)		270-720

*from only one sediment core

Method: Palaeo and terrestrial vegetation data analysis	Range, growth in terrestrial biosphere (GtC)	Mean growth in terrestrial biosphere (GtC)
Adams et al (1990)*		1350
Van Campo et al (1993)	430-930	715
Crowley (1995)	750-1050	900

*Considered to be an overestimate

Method: Vegetation models	Details	Range, growth in terrestrial biosphere (GtC)	Mean growth in terrestrial biosphere (GtC)
Friedlingstein et al (1992)	Climate (biosphere) model		300
Peng et al (1995)	Palaeoecological data and biosphere model	470-1014	742
Francois et al (1998)	Biosphere model	134-606	370
Beerling (1999)	Biosphere model and modelled δ13C	550-680	615
Otto et al (2002)	DGVM	828-1106	967
Kaplan et al (2002)	DGVM		821

Table 1.1, estimates of total change in the terrestrial biosphere from LGM to PI period, per study type. Adapted from Maslin and Thomas 2003

Given that the whole ocean contains around 38,000Gt of carbon, it was possible to estimate how much carbon would need to have been released from the ocean since LGM to create this shift in $\delta^{13}C$. From this, and the known change in carbon content of the atmosphere from ice cores, an estimate of the growth in the terrestrial biosphere from LGM to PI was made as 1000GtC.

A review of studies on the balance between the atmosphere, ocean, and terrestrial biosphere carbon pools from the LGM to present for studies up until 2002 is shown in table 1.1 (adapted from Maslin and Thomas 2003). The interpretation of deep ocean $\delta^{13}C$ from forams is still problematic; ocean circulations and mixing affects the distribution of carbon concentrations in the ocean basins. Thus, in order to get an estimate of change in ocean carbon it is necessary to estimate (know) what these circulations were at LGM. The range of estimates for whole ocean $\delta^{13}C$ range from 0.15‰ to 0.46‰, and result in terrestrial biosphere growth estimates of 220Gt to 650Gt (see table 1.1). Another method to estimate the size of the change in the terrestrial biosphere is through the analysis of palaeo soils, fossil pollen, and sedimentology, as done by Adams et al (1990), here the estimate being 1350Gt increase in terrestrial biosphere since LGM. An update on this estimate gave a range of 900 to 1900GtC. This method is indirect, and estimates (knowledge) of plant assemblages at LGM are also necessary. From these two approaches there appears to be a mismatch between the estimate of the growth in the biosphere from pollen analysis and from the ocean's $\delta^{13}C$ changes. A major assumption made, because the ocean is the largest carbon store relevant at this timescale, is that all the carbon added to the atmosphere and biosphere since LGM was sourced from the ocean. Reassessing this assumption may be able to provide an answer to the mismatch. A region that may have provided a source of carbon to atmosphere during the last termination are thawing permafrost soils. The next section presents a review of permafrost soils and the role of permafrost in the carbon cycle.

Permafrost and Carbon Dynamics

Permafrost is defined by the IPA (International Permafrost Association) as "ground (soil or rock and including ice or organic material) that remains at or below 0°C for at least two consecutive years" (IPA website). This can include high latitude regions, or high altitude regions. For this study, high altitude, or mountain, permafrost is not the focus. The lowland higher latitude permafrost region occupies around 25% of the total land area in the northern hemisphere and it is here that high carbon soils are found. Figure 1.9 shows permafrost zonation (IPA) which defines different permafrost coverage conditions, continuous permafrost is the region where 91-100% of the land area is underlain by permafrost, discontinuous is 51-90% underlain by permafrost, sporadic is 10-50% underlain by permafrost, isolated patches are less than 10% underlain by permafrost.

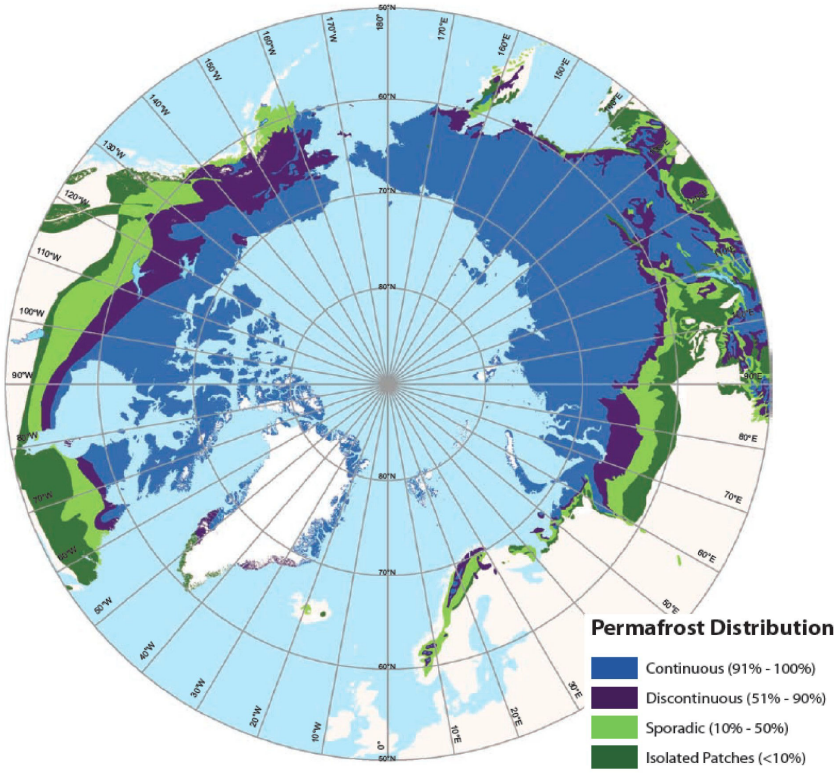

Fig 1.9: permafrost zonation, IPA (International Permafrost Association)

Figure 1.10 shows a schematic representation of permafrost landscape characteristics and of a temperature profile per depth. Frozen ground is seen in locations where surface air temperatures are below zero. The thermal conductivity in the ground, the severity (coldness) of the air temperature and the geothermal energy from depth defines the maximum depth at which the ground remains frozen. The change in temperature throughout the soil/rock column is the geothermal gradient. It takes time for the ground to warm or cool towards the air temperature and for this energy to be conducted downwards in the ground; the depth of zero annual amplitude is the point at which seasonal changes in air temperature are no longer seen in the soil/rock column. Above this zero annual amplitude depth the ground temperature changes; warming in summer and cooling in winter. When the temperature rises above zero degrees Celsius the ground is thawed and the soil becomes active. This depth marks the top of the permafrost and the bottom of the active layer depth. In this active layer soils can form from plant growth and mortality and it is here that carbon can accumulate.

Soil carbon can be moved to depths in permafrost via cryoturbation, the mixing of soils caused by freeze-thaw cycles of water in the permafrost. Also by sedimentation, the build up of organic matter on the surface increasing the height of the ground. Snow cover acts as an insulator, now the air is not in direct contact with the ground surface and the thermal gradient though the snow layer must also be taken into account. Ice and

water content of permafrost have an impact upon landscape characteristics and on thermal activity. On thawing water movement laterally to lower water-content soils can cause faster thaw of the active layer during spring. On refreeze during autumn and winter water collects in fissures, water expands on freezing to ice and this can cause ice wedges to form over time. The formation of patterned ground in permafrost regions is a result of this freeze-thaw cycling of water. A transient effect of ice wedge and ground deformation from freeze-thaw cycles are the formation of thermokarsts. These are areas of ground which used to be underlain with ice, but subsequently collapse when the ice has thawed. These depressions in the land can result in the formation of lakes, or bogs (wetlands), promoting peat-growth and high carbon accumulation.

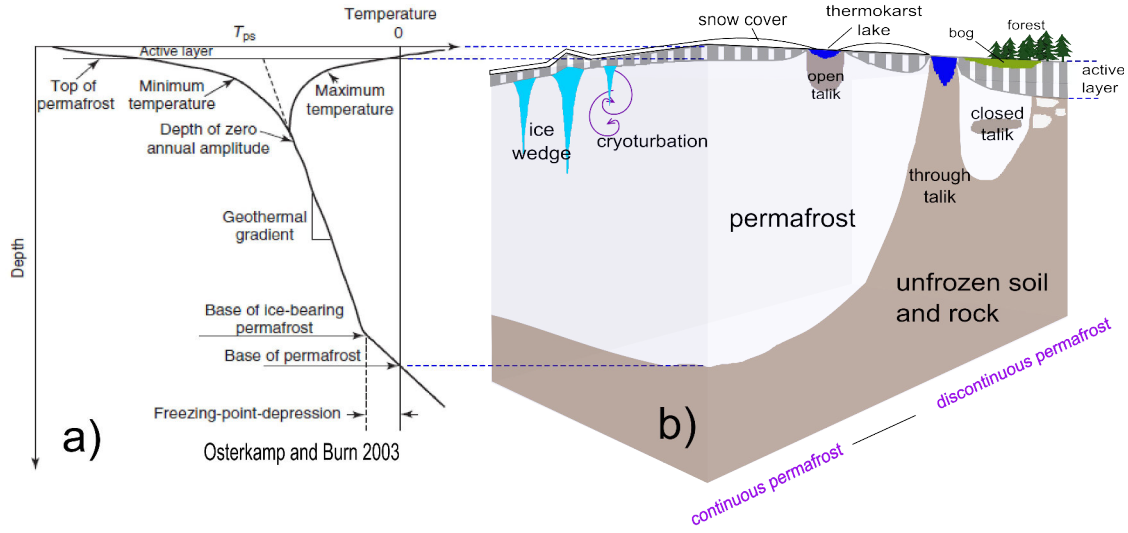

Fig 1.10:, a) permafrost schematic temperature profiles Osterkamp and Burn 2003, b) permafrost and characteristic landscape features and dynamics.

Taliks are areas of thawed ground within the permafrost, that are created by warm anomalies at the surface, such as rivers or lakes. These can be open to the ground surface, closed to the ground surface, or go through from the surface to below the base of permafrost but surrounded by continuous permafrost. Bogs and wetlands are a feature of the permafrost region, the permafrost underneath the active layer can reduce water run-off, maintaining wet soil conditions. The boreal forest is located towards the southern ranges of the continuous permafrost zone and in the discontinuous, sporadic and isolated permafrost regions. The presence of permafrost inhibits maximum rooting depth and, in areas with shallow active layers and lower soil moisture, tree and plant growth is limited.

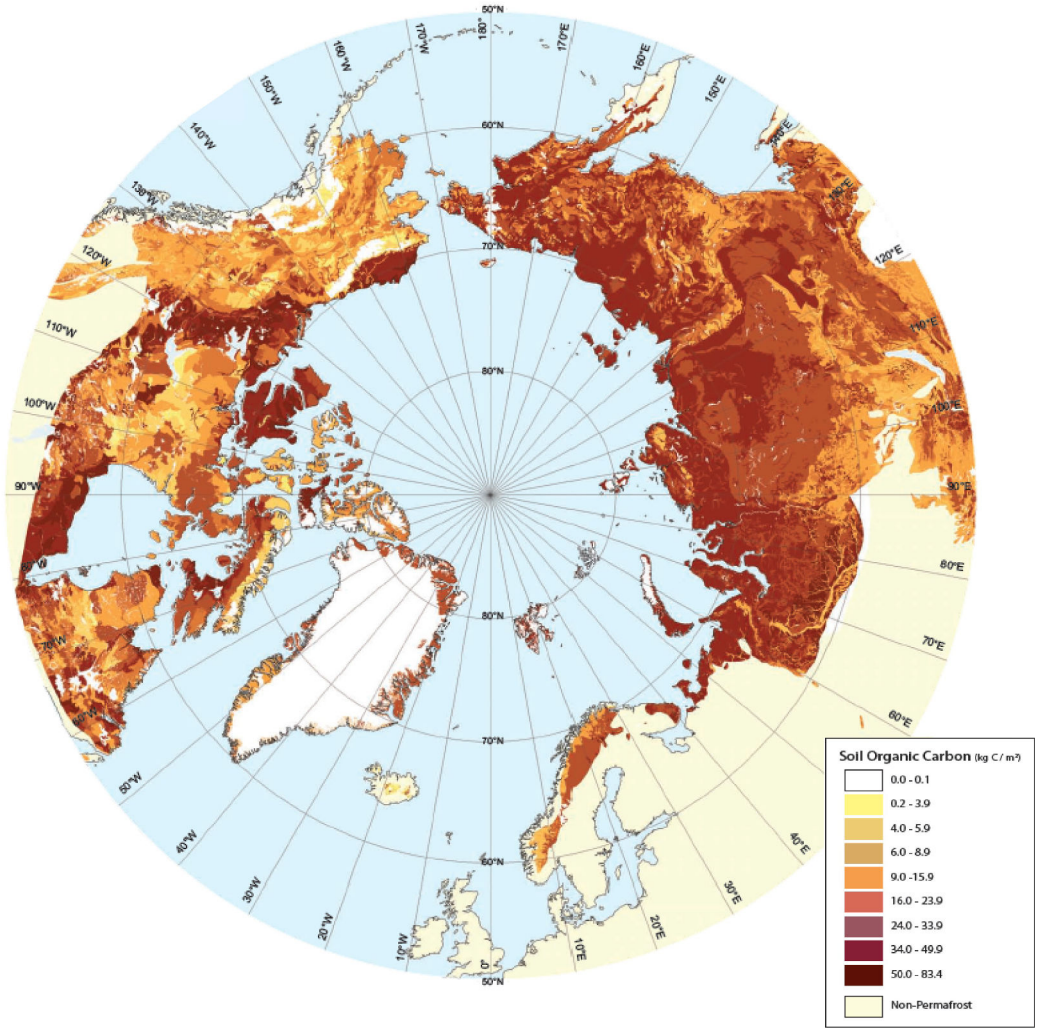

Fig 1.11: soil carbon concentrations in the permafrost region, circumpolar atlas 2007-2008 (Jones et al 2009).

High carbon soils are associated with the presence of permafrost. Figure 1.11 shows the soil carbon concentrations of the top 1m of soils in the permafrost region. Hobbie et al. (2000) looked at the controls on carbon storage and turnover in high latitude soils. Important findings included that the difference in litter decomposition that exists between growth forms is mostly due to abiotic factors e.g. temperature. However, Sphagnum mosses that dominate high latitude wetlands have a characteristic slow decomposition rate which causes high carbon in peat soils formed from these mosses. The cold temperature, anaerobiosis (bacterial decomposition of soils in low or zero oxygen conditions), and permafrost interact with substrate quality to determine the degree of organic matter stabilisation. The response of these soils to climate change and relative importance of factors controlling carbon storage and turnover is not well known. Biological activity in frozen soils can contribute to annual soil carbon fluxes, but controls on this are poorly understood. Hobbie et al. also note that fire and flood can be just as important as other processes in controlling regional carbon fluxes. Christensen

et al. (2010) summarised the possible impacts on land-atmosphere exchange of greenhouse gases for thawing permafrost. CO_2 uptake (dynamics) in permafrost regions are controlled by growing season length and timing of snow melt, with earlier snowmelt creating greater uptake of atmospheric CO_2 (by increasing the growing season length). Koven et al (2009) used the Orchidee model to simulate soil carbon accumulation in high latitude soils. They modified the soil component to include the effect of thermal insulation of soil carbon on the soil regime and also introduced diffusive vertical mixing. With these two mechanisms they modelled a 30% higher carbon stock in the top metre of permafrost soil (and also an increase below this level).

Thawing permafrost and a changing climate affect the length of the growing season. A longer growing season will increase net primary productivity (NPP), but it is the relative effects of all mechanisms that determine the carbon balance of thawing permafrost and whether a site will become a source or remain a sink of carbon in a changing climate. However, it is the relative effects' strength that is not well constrained and creates the greatest uncertainty in modelling and projections of future carbon balance in high latitude regions. Figure 1.12 shows a schematic model of thawing permafrost effect on soils' carbon balance established by Schuur et al. (2008) when looking at the vulnerability of permafrost to thawing and its possible effect on the carbon cycle. Anoxic conditions exist when decomposition occurs (generally) underwater, which for thawing soil containing ice is an expected condition. In this case methane is produced by methanogenic bacteria decomposing plant matter. In oxygenated conditions, decomposition releases carbon dioxide. In both cases it is the thawing that releases the carbon from the permafrost pool into the thawed pool and makes it available for decomposition via either pathway.

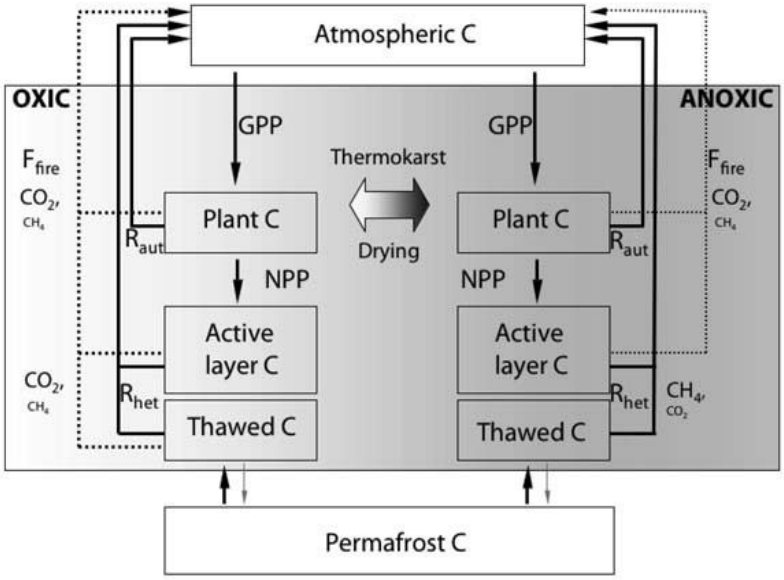

Fig 1.12, conceptual diagram of effect of permafrost thaw on a water saturation gradient, Schuur et al (2008).

Decay of organic matter within thawing permafrost (either long term or annual) can increase the soil temperature (Koven et al. 2009) and insulation of the soils from air temperature via snow cover can increase this effect (Gouttevin et al 2012). This increased soil temperature can reduce permafrost extent and increase soil carbon decay. The net result of significant snow cover insulation is a lowering of the carbon stock in the permafrost zone.

Data collected from thawing sites can help to constrain the behaviour of these soils in changing climates. Wickland et al. (2006) reported measurements of gas fluxes from black spruce forest sites subject to permafrost thaw. In the boreal forest region soil respiration, net CO_2 and CH_4 fluxes were measured May-September 2003 and March 2004. Included sites were: peat-soil underlain by permafrost at ~0.4m (PP), four thermokarst wetlands (TW) with no permafrost in upper 2.2m, and peat soils bordering the TWs with permafrost at ~0.5m depth (thermokarst edge, TE). Soil respiration was not much different between the sites, but ground vegetation photosynthesis was significantly different (TW>TE>PP). Methane emissions were 15 to 28 times higher from TW than TE and PP. Schuur et al. (2009) looked at data from a thaw gradient of tundra sites. Figure 1.13 shows the old carbon lost from these sites, where old carbon is identified with carbon-14 isotope. It shows that the longer the site has been thawing (extensive), the more old carbon is lost, and over a 3 year period a basic linear model was created relating ecosystem respiration to proportion of old carbon lost where the old carbon lost is increasing the ecosystem respiration over time. Trucco et al. (2012) presented a 7 year record from permafrost thaw sites with 3 sites representing a thaw gradient. They found the annual carbon balance to be strongly dependent on winter R_{eco} (ecosystem respiration), which is data-poor generally due to extreme environmental conditions. So they could not conclude whether increased net ecosystem exchange (NEE) in growing season is sustained annually. If winter measurements used were an underestimate then the sites were already carbon sources. Natali et al. (2011 and 2012) in an ecosystem warming experiment found that winter warming doubled the carbon loss to atmosphere during winter turning the site into a carbon source via soil respiration. Summer warming resulted in increase in both gross primary productivity (GPP) and growing season length. Again, confirming the uncertainties in the fate of high latitude regions as carbon stores in future climates.

The role of permafrost soils in surface energy exchange was highlighted by Eugster et al. (2000) on a study of arctic tundra and boreal forest surface energy balance. High latitudes are characterised by large annual changes in solar input that induce freezing in the cold season and thawing in the warm season. Permafrost provides a strong heat sink in summer due to the latent heat of thaw that reduces surface temperature and also therefore heat flux to the atmosphere. The presence of permafrost itself acts to reduce overlying air-temperature. Again, in a warming world, the energy balance associated with latent heat of thaw and the resultant surface energy balance of newly thawed regions may be important in future climate.

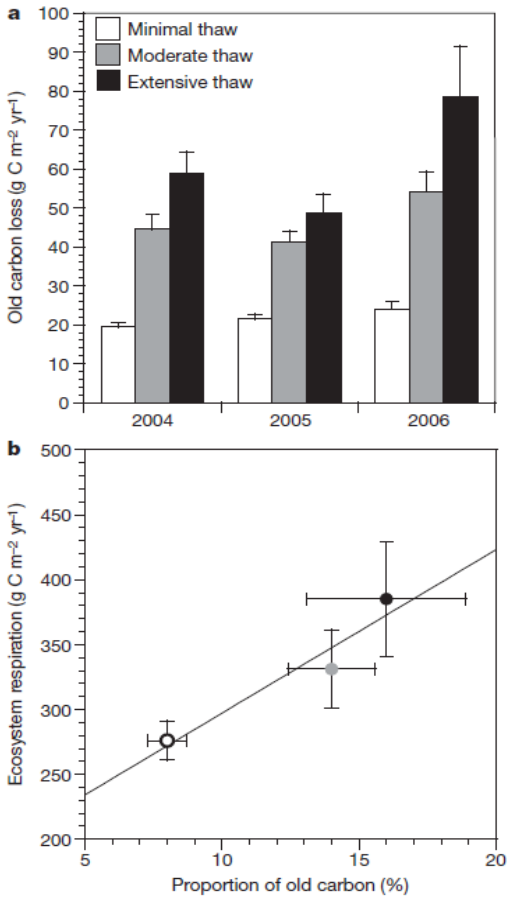

Fig 1.13: from Schuur et al. 2009, "Old Carbon loss and its relationship to total ecosystem respiration for three sites that differ in the extent of permafrost thaw. a, growing season loss of old C from deeper in the soil profile, based on statistical partitioning estimates of mean proportional old C loss multiplied by Reco flux measurements."..."b, The relationship between total Reco and proportional old C loss for the growing season across sites."

Paleosols of the Last Glacial Period

The study of paleosols, old soils, can give important information on the climate of the past. To study paleosols, sediment cores are taken from the research site and lab studies on the composition of the old soils can give an indication of the local environment at the time the soil was laid down. Figure 1.14 shows the papers that are considered in this review, given by location of the study. Although paleosol data is primarily used to reconstruct climate they may also provide hints as to soil carbon stocks. In considering the effect of permafrost and high carbon soils it must be remembered that the hypothesis is: once permafrost thaws, the carbon is relatively quickly released back into the atmosphere. As such, high carbon soil layers in the sediment core record should only be found in cooling climates if they were formed by permafrost related processes. They will only then be preserved as high-carbon if they

remain frozen. They will only be maintained in the sediment core record if sedimentation also takes place. In a warming climate and/or in an erosional condition no obvious record of paleo-permafrost-carbon soils would be preserved.

Beringia

Hofle et al. (2000) studied soils buried underneath volcanic ash around 21,500 years ago on the Seward Peninsula, Alaska. They characterise the soils that were present just before the volcanic ash burial, so represent the glacial maximum period conditions. They note minimal soil development as a result of regional loess deposition which inhibits soil formation. They found indication of a shallow active layer (average of 45cm) with evidence of a cold and seasonally dry climate. They note that no exact modern analogue soils are known, but that soils underlying dry tundra near northern Yakutia, Russia, and underlying moist non-acidic tundra soils of the Alaskan North Slope share some similar properties with the buried soils studied. They observe that the attributes of the ecosystem described by Guthrie (1990) of the Mammoth-Steppe are close to the reconstruction based on the buried soil, and also that climatic conditions would today be associated with tundra type soils. Elias and Crocker in 2008 studied fossil evidence from lowland Bering Land Bridge (BLB) organic deposits to establish the flora and fauna distributions on Beringia (current day Alaska and Northern Eastern Siberia). They recorded ecosystems of Mesic-tundra (medium moisture condition tundra) and Steppe-tundra (containing a wide variety of herbs including grasses and sedges and dwarf shrubs) for the LGM period and later. This region was likely a productive ecosystem during the glacial period with a reduction in productivity at glacial maximum conditions likely due to drier climate which inhibited vegetation growth and soil formation.

N America

Mason et al. 2008 studied a Loess record of the Pleistocene-Holocene transition on the Northern Great Plains in North America. The paleosol sequence records a broad peak of high effective moisture across the Pleistocene-Holocene boundary (the last deglaciation period), rather than well-defined climatic episodes recording Bolling-Allerod and Younger-Dryas type episodes. French and Millar reviewed studies of permafrost extents at the Last Glacial Maximum in North America (2013). Figure 1.15 shows the map created from those studies for locations which indicated the action of permafrost, and the most recent estimate of permafrost extent at the LGM for North America. To the south of the ice sheet, the region of permafrost was small compared to the ice sheet size, permafrost induced high soil carbon concentrations may have been present in this region, but compared to the Eurasian permafrost area this region likely played a smaller role in soil carbon storage than Eurasia.

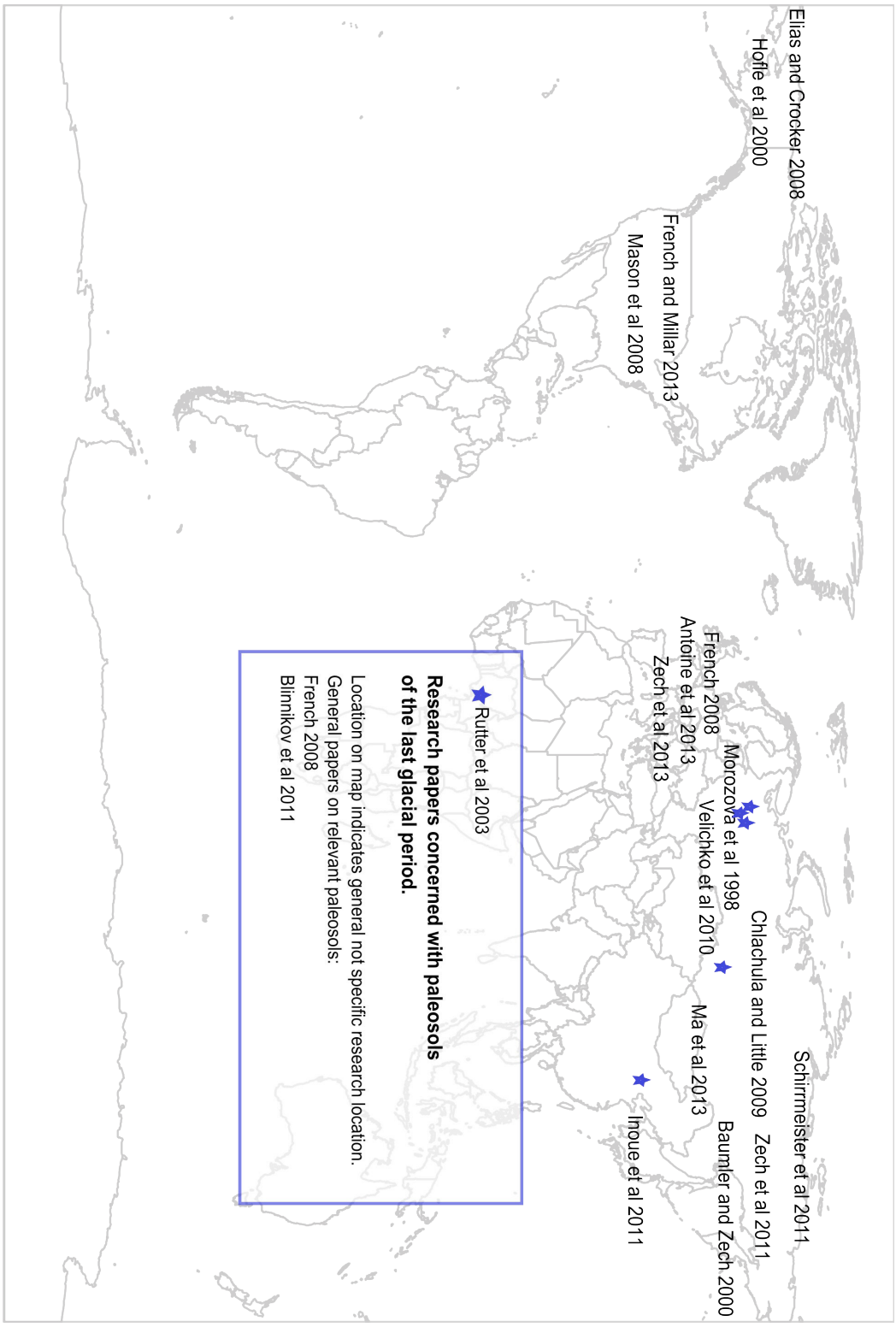

Fig 1.14: Selected scientific studies relating to paleosols covering the last glacial and glacial maximum period

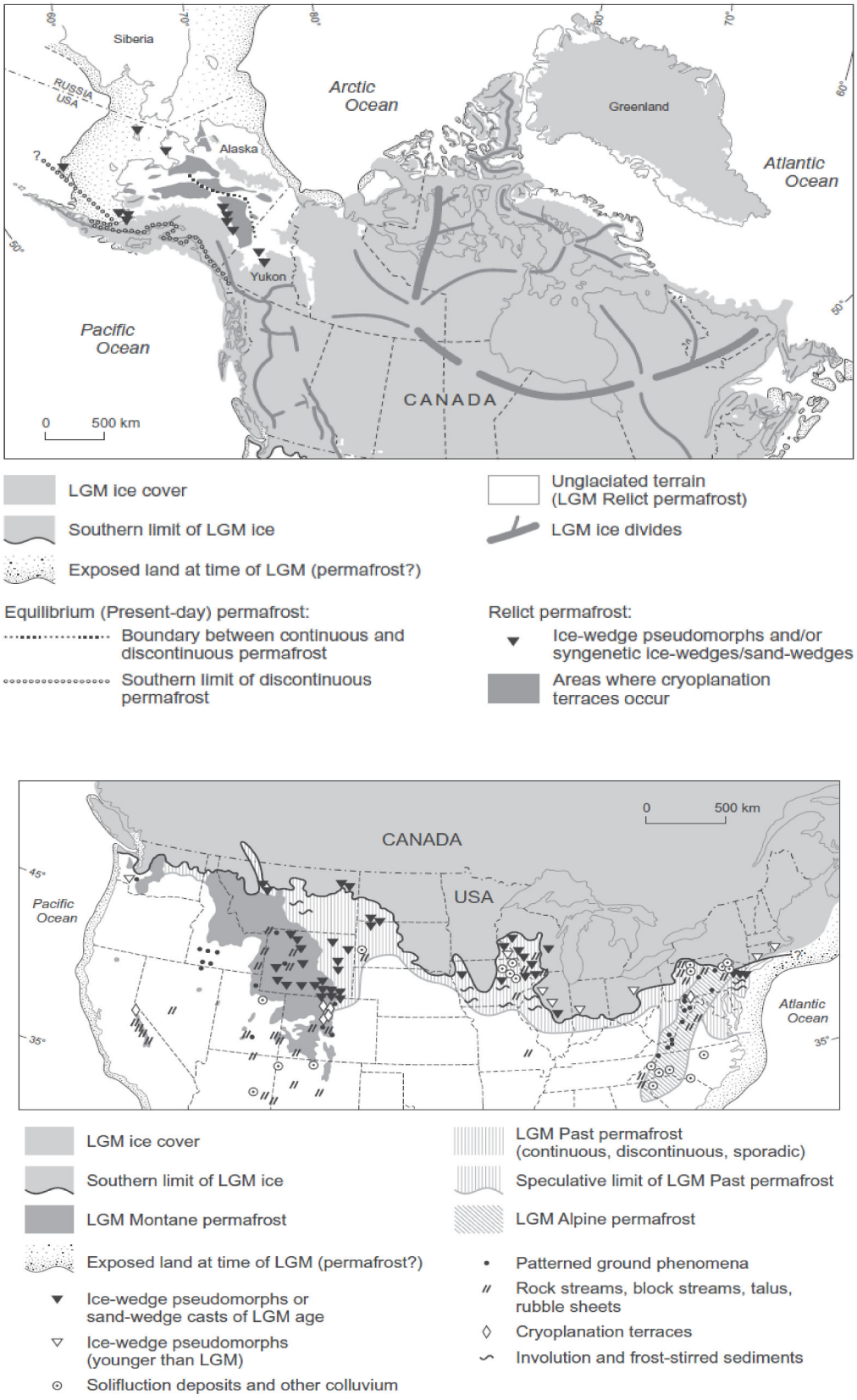

Fig 1.15: French and Millar (2013), N American continent permafrost extent and landscape features indicating the effects of permafrost.

Europe

French (2008) reviewed advances in the study of paleo-permafrost and presented results of landscape feature studies of northern Belgium and the southern Netherlands carried out by Vandenberghe (2001) and Renssen and Vandenberghe (2003). The last glacial maximum and last termination period show large reduction in permafrost coverage in the period 21-19k calyr BP, with a permafrost free climate emerging by 15.5k calyr BP. In reviewing available literature, French notes the difficulties in distinguishing between episodes of perennial frost and deep seasonal frost. A loess paleosol sequence from the Czech-Republic was studied by Antoine et al (2013). The location of the sequence is an area that at LGM was dominated by sandy Loess and Aeolian sands. They propose to use the loess record as a means of dating other paleo-proxy records. The early glacial section of the core shows humic soil complexes thereafter moving to Loess in the late glacial period. A middle pleniglacial brown soil complex of boreal-like characteristics is seen from ~55-40kyr BP, followed by a tundra gley and an upper sandy loess layer covering ~30-20kyr BP. Results confirm a climate which is strongly influenced by northern Atlantic atmospheric circulation, and also confirm periods of erosion of soils notable between 35-25kyr BP. Considering the interpretation of climate from Loess-paleosol sequences Zech et al. (2013) note that, traditionally, the presence of loess was seen as evidence of a dry climate, and the presence of paleosols to document more humid conditions, but that this does not take into account dust accumulation rates which in some regions may challenge the traditional interpretations. They consider a sediment core from Serbia which spans the last 140kyr BP years. The use of lipid biomarkers are identified as important indicators as they are less affected by changes in loess accumulation rates. They summarise that using these biomarkers seems to indicate a humid glacial period and a more arid interglacial in this region. Changing conditions throughout the glacial period appear to have been important for soil carbon storage in this region. The glacial maximum period was likely dry and combined with loess deposition may have inhibited soil carbon accumulation, but prior to this period conditions were more favourable to a productive ecosystem. Studies from different areas within the Europe region show variability in land biosphere and local climate.

Central European plain / W Russia

Morozova et al. (1998) reconstructed the organic carbon content of the late Pleistocene and Holocene fossil soils for Eastern Europe. They combined paleosol profile studies and land-cover reconstructions to make estimates of total soil carbon stored in comparison to the present day. They used estimates of soil humus carbon in the top 1m of modern type soils as analogues for the paleosols. The estimates for Arctic desert soils and for Tundra gley soils were approximately an order of magnitude lower than more recent estimates of soil carbon concentrations by Tarnocai et al. 2009. So, although they predicted that LGM soils stored around 15% of the present-day soil carbon contents in this location, the basis of their estimate was is not in agreement with data. Velichko et al. (2010) undertook a similar study to Morozova et al. in 1998. They

estimated phytomass of terrestrial vegetation and soil humus at three intervals: Last interglacial ~125ka BP, Last glacial maximum ~20-18ka BP and Holocene optimum ~5.5kaBP for Northern Eurasia. Results of their study suggested LGM phytomass was 27% of present-day content and soil humus storage was 23% of present-day content. However, they used the same data on soil carbon concentration paleo-analogues as Morozova et al. (1998), which greatly underestimate cryosols' carbon content.

Northern Siberia

Chlachula and Little (2009) studied a loess sequence from Iskitim, north of the Altai-Sayan Mountains covering the last ~250ka. The sequence provides evidence of dynamic climate change during the late Quaternary in continental North-Central Asia. The sequence seems to indicate a cooling phase from ~26ka-LGM-termination 1 period with loess deposition, which was preceded by a warmer phase associated with chernozem soil formation. The findings from this study agreed broadly with data from lake sediments of Lake Baikal (Grygar et al. 2006) and other loess sequence studies in this region. Schirrmeister et al. (2011) look at present-day carbon inventories from the NE Siberian region. They used these carbon inventories as an improvement on previous estimates on present day carbon inventories with a view to establishing vulnerability to future thawing. They present a slightly downwardly revised carbon inventory. They also note that fairly few studies of organic carbon sequestered in late quaternary soils exist and so up scaling results to represent regional estimates is problematic. Total organic carbon contents for the Early Weichselian fluvial deposits are 7.2kgCm^{-3}, for the middle Weichselian ice complex deposits 33.2kgCm^{-3}, and for the Holocene peaty deposits of 74.7kgCm^{-3}. Zech et al. 2011 studied a loess-paleosol sequence from North-East Siberia that spans two glacial cycles (~220kyr). They conclude, using δD of alkanes as a proxy for paleo-temperature to improve age-control of the sequence, that reduced biomass production during glacials may have been of second-order importance to increased soil-carbon preservation due to frozen soils and cold conditions.

Eastern and Central Asia

Baumler and Zech (2000) studied paleosols of different ages in the southern Kamchatka peninsula of Russia which were covered by multiple layers of volcanic ash. The soils were classified as Gelic Andosols and Gelic Cambisols. Dating of soil deposits was still problematic, with a 40kyr old tephra deposit from the Opala volcano (OP) being seen on the west coast but not the more eastern sites. This being attributed either to the eastern sites' deposits being younger than 40kyr, or the OP never having been deposited due to high winds, or, finally, the OP having been completely eroded before later Holocene ash deposition. Inoue et al. (2011) study buried pleistocene humic soils within a tephra-soil sequence in Japan. Total carbon content of the soils were very high for late Pleistocene soils at > 60gkg^{-1} for the oldest buried humic soils, formed from mainly grass vegetation and was relatively insensitive to climate change in the area at around 30ka. Ma et al. 2013 present a pollen-based study of vegetation and climate changes from the eolian-paleosol section in the northern Mongolia Plateau. They

concluded the area was Taiga forest between 38-30kcal BP, following a moisture level reduction between 30-23kcal BP was mainly steppe. Between 23-10kcal BP vegetation varied between forest and steppe conditions. The later phase from ~19-11kcal BP was warmer and drier than the earlier phase. These studies highlight the questions posed in paleosol studies, the Inoue study found high soil carbon concentrations compared to other late Pleistocene soils, this may be because these soils were effectively sealed off by sedimentation and volcanic deposits, and so could not experience soil carbon loss between the glacial period and today. The Baumler and Zech study highlights the issues of reconstructing a sequence of events without knowledge of what may be "missing" from a sediment sequence.

General

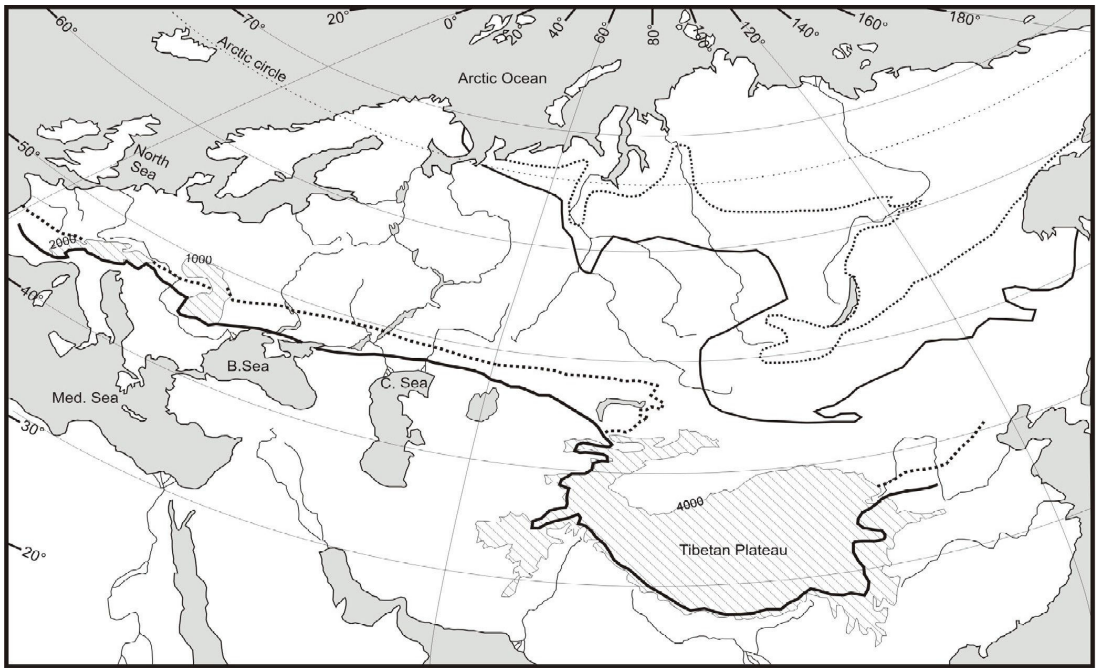

Fig 1.16: LGM and PI permafrost extent from Vandenberghe et al. 2008. Solid lines are discontinuous permafrost, dotted lines are continuous. LGM is in bold, PI thin.

Vandenberghe et al. (2008) collated a map of permafrost extent in Europe and Asia for the last glacial maximum periods and the present-day (fig 1.16), showing the LGM southern permafrost front at around the 45degreeN latitude band, and the present day front restricted to the north eastern parts of Eurasia. Rutter et al., (2003), looked at the correlation and interpretation of paleosols and loess across European Russia and Asia over the last interglacial-glacial cycle. In all sites, although they had different climates and geographical settings and loess source areas, they all had similar climate changes through the last interglacial-glacial cycle. In the Russian plain and Loess plateau, loess depositions dominated during cold periods, but in central Siberia five to seven thin paleosols were identified in the two cold stages (MIS 2 and 4). Paleosols

were more present in the warmer stage MIS3 in all sites. Blinnikov et al. (2011), reviewed evidence from multiple proxies on the character of the graminoid-dominated ecosystem of the Pleistocene Arctic. This past ecosystem, tundra-steppe (or steppe-tundra) was maintained by cold and dry conditions and grazing/disturbance by large and smaller mammals. They note that there still remains an inadequate coverage of terrestrial proxy data to resolve questions related to effects of ice sheet and coastal proximity, topography, soil heterogeneity, animal disturbance and fire regimes on ecosystems of the Pleistocene Arctic.

Summary and total land carbon stocks at LGM

Paleosols are usually used to reconstruct climate conditions, with soil carbon content reconstructions proving difficult due to the lack of analogue ecosystems and soils in the present-day compared to glacial conditions. The extent of permafrost for the coldest climate of the LGM has left landscape features still visible today, and the total area of permafrost (continuous and likely discontinuous) for the LGM and PI periods are more reliable than soil carbon stock estimates. Currently there are no reliable soil carbon estimates for the last glacial maximum period derived from proxy data and sediment core analyses. In the present-day climate the estimates of total soil carbon are already challenging, with soil carbon inventories only fairly recently also taking into account permafrost and peatland soils. The findings in the studies here do show that LGM soils in the permafrost region were not deserts, and also that the LGM soils cannot be used as a good indicator of total carbon in all soils at the end of the glacial period due to transient effects of changing climate over time and slow soil carbon accumulation rates. Ciais et al. (2012) estimated the size of the land carbon store at the LGM period by combining ocean-carbon cycle modelling studies and oxygen isotope data to infer ocean and land gross primary productivity at LGM. They found that the rate of terrestrial GPP totalled around 40+-10PgCyr^{-1}, around half that of the Holocene period. Despite the low GPP rate they estimated that total increase in the terrestrial biosphere pool between LGM to PI was 330GtC. Using these results, they propose that at LGM the terrestrial inert carbon pool, such as carbon locked up in frozen soils, was 700GtC greater than the PI. This supports the findings from paleosol studies of biome reconstruction, and also provides an explanation for the difference between pollen based terrestrial biosphere increases since LGM and ocean $\delta^{13}C$ based estimates. Pollen studies estimate changes of active land carbon pool; vegetation and non-permafrost soils of around 1000GtC (Adams et al. 1990, Van Campo et al. 1993, Crowley et al. 1995). Ocean studies indicate the total change in carbon in the land biosphere since LGM, after accounting for ocean and atmosphere pool changes, of around 400GtC to 500GtC (Duplessy et al. 1988, Broecker and Peng 1993). The difference between these estimates may be the inert carbon pool on land which would not be accounted for in pollen based estimates. Pollen-based estimates rely on soil carbon-concentration estimates that do not account for high carbon-concentration permafrost soils.

1.4. Current state of the art – Carbon cycle

1.4.1 Peatlands and permafrost-carbon

Present-day

For the present and future behaviours of the carbon cycle, there has been a lot of interest in the effects of thawing permafrost and subsequent carbon release but the mechanism is not represented in CMIP model projections (Stocker et al 2014). Complex land-surface models that make projections of future climate now include permafrost as an important mechanism, but as yet, it has not been included in palaeo-climate coupled models.

Schuur et al (2008) reviewed present day carbon stocks of previously frozen organic carbon, showing that in high latitudes there may be up to twice as much carbon stored than in the atmosphere. Increases in the land carbon sink due to a warming climate, such as extended growing season, are not thought to be able to compensate for the projected carbon release due to permafrost thaw. The effects of permafrost thaw on carbon release and net carbon exchange from tundra was considered again by Schuur et al (2009), using carbon flux data for a three year period, also measuring carbon 13 and carbon 14 content of the released CO_2 finding that the ecosystem respiration from old carbon increases over time in permafrost thaw sites. Tarnocai et al (2009) estimated that permafrost areas in circumpolar north hold around 1600PgC. Measurements of emissions from thawing permafrost effected soils is important to understand the carbon cycle effects of thawing, exactly how, and at what rate thawing permafrost releases carbon is still an area of high interest and uncertainty.

McGuire et al (2009) looked at the sensitivity of the carbon cycle to Arctic warming. A total of 1400 to 1850 PgC is estimated to be stored in soils in northern latitudes, with plant biomass estimated to be between 60 and 70 PgC. Terrestrial and marine gas-hydrates are given a total estimate of some 30 - 240 Pg of methane (CH_4). The mobilisation of even small fractions of these carbon stores with changing climate will have a significant effect on the carbon cycle.

LGM and the last glacial termination

Although the reservoirs of permafrost-carbon stocks would have likely been different at LGM, the physical processes that would affect these reservoirs would have still existed at that time. Looking specifically at the carbon storage potential of permafrost over the glacial periods Zimov et al. (2009) considered the mammoth steppe-tundra ecosystem. At the LGM steppe-tundra was the most widespread biome on Earth. They estimated the total carbon content of the steppe tundra biome by developing a carbon accumulation model together with data of present-day carbon (C) storage. With permafrost present, the model showed a steady C increase in the soil. A simulated Pleistocene/Holocene Transition (PHT) showed a loss of carbon from these soils. Their

model estimated that 1000GtC may have been released to atmosphere, ocean and other terrestrial systems during the last glacial termination.

At glacial maximum, when large ice sheets were present in the northern hemisphere and Antarctic ice sheet were at maximum, eustatic sea level was some 120m lower than present-day (Peltier 1994). This exposed the coastline, which would have been active parts of the terrestrial biosphere at the time. The Siberian shelf, now below sea level, was exposed during the glacial period and studies suggest a significant amount of carbon accumulated there (Montenegro et al 2006). During deglaciation this region was gradually inundated by the sea, but the fate of the carbon stored there is uncertain. The fate of permafrost on the shelf during the deglaciation was studied by Overduin et al (2007), who found that many processes were involved in determining whether the sediments remained frozen or thawed.

Zech et al (2011) studied two permafrost-loess palaeosol sequences from Siberia, using deuterium/hydrogen isotope ratios to identify local temperature changes. They found that on glacial timescales, the effect of reduced productive biomass may be of secondary importance to the effect of permafrost preserving soil organic matter for the total land carbon stock. Renssen et al (2000) note the importance of permafrost in modelling studies of the YD (Younger Dryas, see fig 1.18), comparing reconstructions based on palaeodata with the results of ECHAM4 atmospheric GCM experiments. In one experiment, the model was forced to maintain wet and frozen soils at high latitudes to reproduce the effect of permafrost in the model. The results were similar to palaeodata reconstructions. The depression of summer temperatures in Eurasia by 4-8 degrees and increase in precipitation. A re-evaluation of palaeoclimate simulations in which permafrost is not included was recommended. This demonstrates the possible importance of the climate-feedback of permafrost, not simply as a carbon cycle feedback.

Northern Peatlands

Beilman et al (2010) estimated carbon accumulation in peat, they found a growth of the terrestrial biosphere since the LGM to be around 270-450PgC in peatlands alone, with basal ages dating from 16kyr BP. Jones and Yu (2010) looked at the expansion of peatlands in Alaska since the LGM and more specifically during the Holocene. They found that over 75% of the peatlands sampled initiated prior to the HTM (Holocene thermal maximum) and that seasonal changes may have played a significant role in peatland growth and respiration. Yu et al, 2011, reviewed recent advances in the effect of peatland dynamics on the carbon cycle for future warming. They concluded that it is likely that sequestration of carbon by peatland expansion will continue to be a negative feedback to the carbon cycle, but they do note that uncertainties in the rate and effects of thawing permafrost on the carbon cycle mean that this conclusion is by no means definite. The lack of clear evidence of the effect of permafrost in the past was noted as an area that contributed to these uncertainties. It is worth noting again that peatland and wetland dynamics are not included in many EMICs or in state of the art CMIP GCMs.

1.4.2 Glacial-interglacial transitions

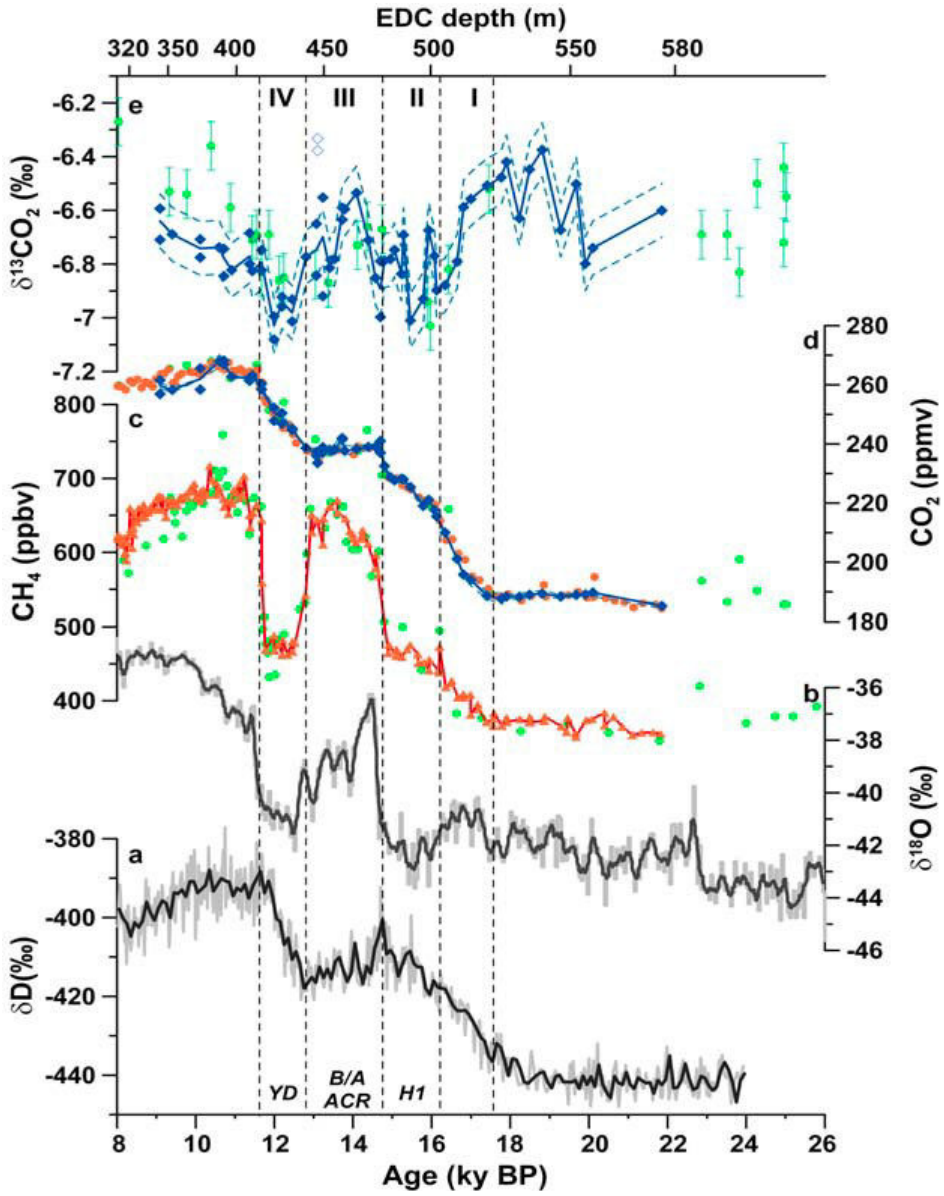

Fig 1.18: ice core data of climate indicators for the last glacial termination, EPICA dome C Antarctica (Lourantou et al 2010)

Termination 1

Figure 1.18 shows ice core measurement data from the EPICA project ice core from dome C (EDC) in Antarctica (Lourantou, 2010). From the top they show the ^{13}C isotope signature of the trapped CO_2, the CO_2 concentration, the CH_4 (methane) concentration of the air, the oxygen-18 isotope signature of the ice (water), finally, the deuterium (hydrogen isotope) signature of the ice (water). Green points are measurements from the Taylor dome ice core (Smith et al 1999). The last deglaciation

(or termination 1, T1) has several discernible periods: the H1 Heinrich event (marked on figure 1.18), the Bolling Allerod and Antarctic Cold Reversal, the Younger Dryas are events particular to the last deglaciation, where precise mechanisms causing these events at a particular time are areas of research. Figure 1.19 shows the most recent data and data mean for $\delta^{13}C$ for termination 1, and the fast drop in atmospheric $\delta^{13}C$ just as CO_2 rises.

Ice core records for the last deglaciation (from 18kyr to 12kyr BP; termination 1 or T1) show a rapid rise in atmospheric CO_2 levels from around 190ppm to 260ppm (Monnin et al. 2001). The $\delta^{13}C$ evolves simultaneously, with a drop in atmospheric $\delta^{13}C$ of 0.3‰ occurring in the first 2500years (Schmitt et al. 2012). During the deglaciation global sea-surface temperatures increased by around 4 degrees (range of 2 to 6 degrees, MARGO project members 2009), large ice sheets covering much of N America and N Europe melted (Peltier et al. 2004) and global sea-level rose by around 120m (Clark and Mix 2002).

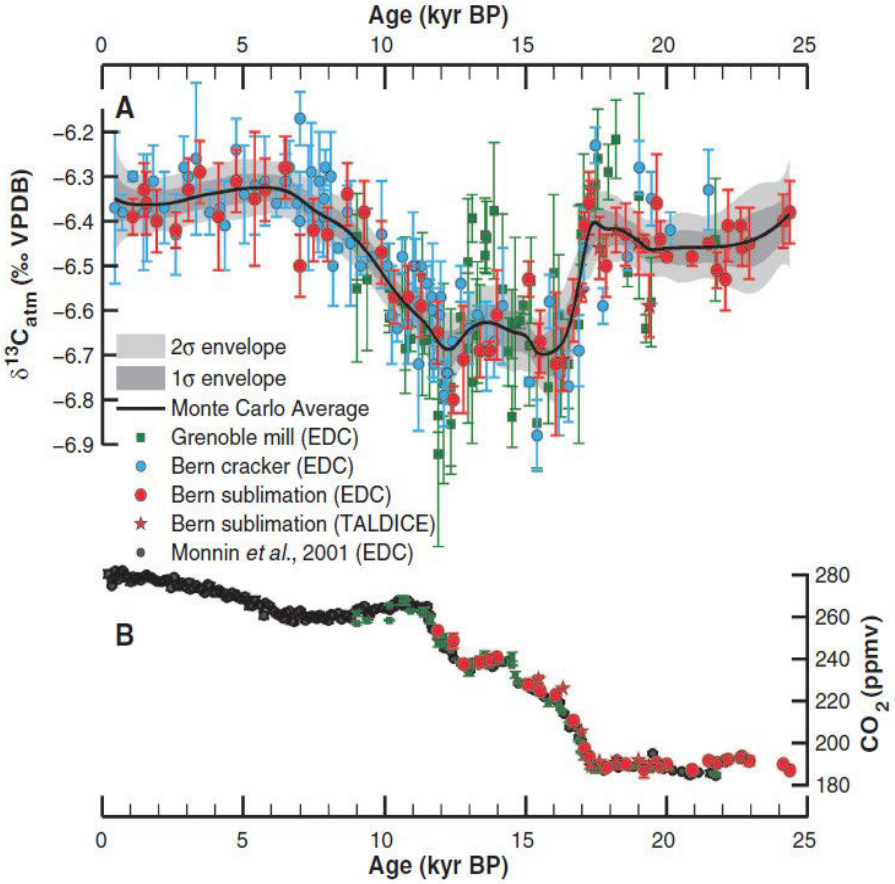

Fig 1.19: Composite ice core records for atmospheric $\delta^{13}C$ and CO_2, Schmitt et al 2012

Many studies have been carried out to investigate the causes of the rapid rise in temperatures and CO_2, including proxy-based reconstructions and modelling studies. The leading hypothesis for the onset of the deglaciation is that it starts by a similar event to the millennial scale climate oscillations, where the AMOC is in a switched-off state

during the H1 period (McManus et al 2004). The current hypotheses for the CO_2 increases lie in ocean mechanisms (Kohler et al. 2010, Kwon et al. 2011, Bouttes et al. 2012); the ocean contains around 60 to 90 times more carbon than the atmosphere and around 10 times more carbon than the land using the latest estimates (Ciais et al. 2012). The present-day estimate for total terrestrial-biosphere carbon is around 3970GtC+-325, this includes high carbon soils related to frozen ground and to wetlands which hold around 1672 GtC (Tarnocai et al. 2009). In modelling studies of the carbon cycle evolution during the last deglaciation the terrestrial biosphere had often been neglected in the past largely due to studies showing the whole-ocean $\delta^{13}C$ had become more positive since the last glacial maximum (21kyr BP) (Shackelton 1977, Broecker and Peng 1994). The mechanisms that result in the release of carbon are still subjects of study. Lourantou et al, 2010, used the box model Bicycle, and another box model, BOXKIT, to analyse data from the EPICA dome C ice core improving the $\delta^{13}C$ record of atmospheric CO_2 over the last termination. They found a characteristic W shape in the $\delta^{13}C$ record of CO_2 (atmospheric) (fig 1.18), comparing it with marine records and outputs from the two box models, to conclude that Southern Ocean ventilation drove most of the CO_2 increase in the atmosphere with contributions from marine productivity changes and then $\delta^{13}C$ increases from rapid vegetation build up during B/A (Bolling/Allerod) plateau.

Tagliabue et al (2009) used an ocean circulation model and ocean biology model looking at ocean circulation change and CO_2 changes since the LGM. They found that a reduction in ocean ventilation can explain most of the $\delta^{13}C$ and ^{14}C observations but not account for much atmospheric CO_2 change, also that biogeochemical processes can play a big role in the change in atmospheric CO_2. The lesser role for ocean circulation means that most of the necessary CO_2 changes remained to be explained. Kurahashi-Nakamura et al (2010) looked at physical ocean changes' effect on deglacial CO_2 rise. They carried out LGM experiments with an atmosphere ocean GCM (general circulation model), looking at SST (sea surface temperature), SSS (sea surface salinity) and circulation field. They found that the pCO_2 change was 30ppm over the termination, only about 1/3 of the observed variation from ice core data (~90ppm). The 30ppm change found here is smaller than those found in box models doing a similar experiment. Taking account of reduction of terrestrial carbon reservoirs, other mechanisms are required to explain the 90ppm. This model does not include ocean biological processes, already identified as important in previous studies; if a process is not included in a model, then its effects and impacts upon other systems cannot be seen.

Menviel et al (2008) looked into the southern hemisphere westerly winds' effect on the marine carbon cycle, using an EMIC to test sensitivity of atmospheric CO_2 to southern hemisphere westerlies. These westerlies are thought to be a possible mechanism effecting ocean stratification via changes in vertical mixing. They found the net response is a small atmospheric CO_2 increase of ~5ppmv. Not enough to be a main driver of CO_2 increase during the termination.

Using a different approach to analyse the forcing at deglaciation, Roche et al, 2011, use coupled transient simulations (the Loveclim EMIC model with 3D ocean),

including ocean, atmosphere and vegetation components with the slow varying forcings of the last deglaciation. They identify where and when the climate first started to warm in response to the external insolation forcing. In this transient simulation of last deglaciation the obliquity forcing seems to be responsible (as the southern and northern hemispheres see temperature increases simultaneously) firstly in sea-ice areas, thereby indicating the importance of the role of sea ice. Areas that are remote to these 'hot spots' showed a lag of around 3000 years in their deglaciation signals compared to sea-ice locations.

Brovkin et al in 2002[a], using CLIMBER-2 that includes dynamic ocean, atmosphere and land vegetation, found that ocean biology could work as an atmospheric $\delta^{13}C$ controller in a deglaciation. At the time, the assumption was that terrestrial biosphere controlled atmospheric $\delta^{13}C$ composition. By testing the sensitivity of the coupled system, they found that enhanced biological and solubility pumps considerably effects atmospheric $\delta^{13}C$ of CO_2 and therefore cannot be seen as insignificant and disregarded. In 2007 Brovkin et al, again using CLIMBER-2, looked into the atmospheric CO_2 draw down capabilities of the ocean under glacial boundary conditions. By including the carbonate compensation mechanism in which ocean waters' capability to dissolve carbonate is dependent on pH levels, ocean draw down was found to be 43ppmv in the model. Fertilizing the ocean biota in the Atlantic and Indian sectors of the southern ocean resulted in a further 37ppmv draw down. A reduction in terrestrial biosphere of 540PgC at last glacial maximum (LGM) compared to pre-industrial present (PI) gives an increase in atmospheric CO_2 of 15ppmv, increased ocean salinity (from sea level drop and reduced ocean volume) gives a further increase of 12ppmv. The model could explain a total of 65ppmv, still short of the circa 90ppmv seen from ice cores.

Bouttes et al, using the CLIMBER-2 model in 2011, tested the effect of the sinking of brines, rejected on sea-ice formation, to the deep ocean rather than their being diluted and dissipating. This mechanism was found to induce stratification, isolating the deep southern ocean and also increased the waters capacity to dissolved CO_2. They included the brines mechanism, together with iron fertilisation (from dust) and a stratification dependent diffusion as glacial ocean mechanism. By fixing the amount of brines that sink to the deep ocean at 0.6 (60%, based on previous studies and proxy data) and balancing the other mechanisms, they could explain the post glacial CO_2 rise and also the deep ocean $\delta^{13}C$ record but not the atmospheric $\delta^{13}C$ record.

The varibility of CO_2 and temperature seen on the millennial scale during the last termination is thought to be due to millennial scale climate variability, similar to that seen in the glacial period (section 1.4.3). Many studies of ice sheet melt routing and into the north Atlantic and sea level changes aim to find coincidences between this routing and events seen in the ice core and proxy records for the termination (e.g. Liu et al 1999, Standford et al 2006, Ritz et al 2013). A record for $^{231}Pa/^{230}Th$ from ocean sediments in the Atlantic ocean (McManus et al 2004) is thought to be a good indicator of the strength of the AMOC, and is interpreted to show an AMOC switch-off at the start of the deglaciation. An AMOC switch-off would result in southern hemisphere warming and provide a means of changing southern ocean conditions such that CO_2

degassing there may explain the deglacial CO_2 rise. Although the $^{231}Pa/^{230}Th$ record interpretation has been called into question (Luo et al 2010). The attribution of this millennial scale variability is a subject of great interest, as it is thought to be similar to possible future responses to fast warming caused by fossil fuel burning.

Termination II

Although there is more data on the most recent glacial termination, previous terminations can help to constrain what mechanism drive these cycles. Most recently Schneider et al (2013), studying the $\delta^{13}C_{atm}$ record for TII, concluded that mechanisms at work were likely the same as those operating during TI. For the carbon-cycle the favoured mechanism results in the release of deep southern ocean carbon via upwelling (Schmitt et al 2012). Schneider also concluded that the shift to more positive $\delta^{13}C_{atm}$ when comparing the Penultimate Glacial Maximum (PGM) to the LGM were due to changes in isotopic composition, long term peat build-up or changes in input fluxes to the ocean/atmosphere system.

1.4.3 Millennial scale climate variability

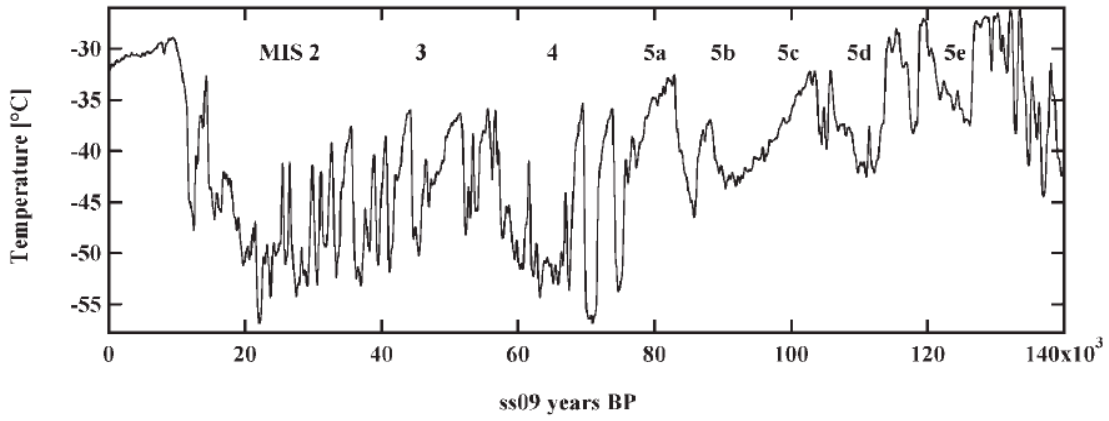

Fig 1.17: Greenland reconstructed temperature record for Summit ice core (Johnsen et al 2001) showing millennial scale climate variability

Ice core records during the glacial and deglaciation periods show millennial scale climate fluctuations and possible see-saw type variability between the climates of the Antarctic and Greenland (Bond et al. 1999, Jouzel et al 2007). Most studies point to the role of the Atlantic meridional overturning circulation (AMOC), which transports heat from the Southern to the Northern hemisphere, as being a driver of these abrupt climate changes. A slow-down of the AMOC would result in cooling of the north Atlantic region, seen in Greenland records and sea-surface temperature records during the first part of the cycle (Kageyama et al. 2010) followed by a resumption in the AMOC causing rapid temperature rises in the north Atlantic. This rapid warming in the

northern hemisphere is known as a Dansgaard-Oeschger (D/O) event. The full cycle is characterised in the Southern high latitudes as a more gradual warming (at the same time as NH cooling) then a gradual cooling, although precise dating of the Antarctic ice core record remains problematic (Wolff et al. 2010). Blunier et al. (1998) found that for 47-23kyr BP period, the ice core Antarctic temperature leads Greenland temperature by around 1 to 2.5 thousand years for the warming events. To create a slow-down in the AMOC, models employ a fresh-water forcing into the north Atlantic which reduces surface water salinity and inhibits the water mass's ability to sink to the deep ocean. This in turn reduces north Atlantic deep water (NADW) mass and reduces the strength of the AMOC, creating a more shallow overturning circulation or even switching it off altogether (Kageyama et al. 2010).

The release of fresh-water into the north Atlantic as a possible AMOC controller is supported by IRD (ice rafted debris) records in ocean sediment cores from the Atlantic (Bond et al. 1999). These high IRD layers in the cores mark the timing of Heinrich events interpreted as mass iceberg release into the Atlantic, the icebergs carrying sediments (rocks) far into the ocean before melting. The origin of the Heinrich layer IRDs has been attributed to the region around the Hudson strait (Hemming et al. 2005). D/O events and Heinrich layers are not always seen together, and D/O events are more frequent, although the presence of Heinrich layers point to instabilities in ice sheets on timescales similar to D/O events. Elliot et al. (2002) studied high resolution deep North Atlantic benthic foraminifera $\delta^{13}C$ records and temperature records, finding that drastic cooling associated with Heinrich events were related to reductions in deep water formation, but other cooling events which did not show such deep water reductions and were not a Heinrich Event (HE). They conclude that thermohaline circulation (THC) may not be the only controlling mechanism for these millennial scale oscillations or an amplifying mechanism existed which has not yet been taken into account.

1.4.4 Multi-millennial climate changes

Climate changes

The CO_2 and deuterium records for the Vostok Antarctic ice core together with the reconstructed land ice volume based on ocean $\delta^{18}O$ record are shown in figure 1.20 (Sigman and Boyle 2000) showing the co-evolution of these three data.

Petit et al (1999) using Vostok ice core data, and Jouzel et al (2007) using EDC data records for the past glacial-interglacial cycles found that deglaciations are similar and that interglacials vary in duration and temporal evolution. Fischer et al (2009) focus on the southern ocean's role in the carbon cycle. Natural CO_2 changes from last 800,000 years ice core data show remarkable correlation with southern ocean climate changes. Westerly wind speed changes are most likely too small to explain changes in atmospheric CO2, but surface buoyancy flux (related to sea ice growth and retreat) may explain high correlation of CO_2 and Antarctic temperature. Iron fertilisation seems to be

limited by other factors than total dust input such as bioavailability of iron and macronutrient supply.

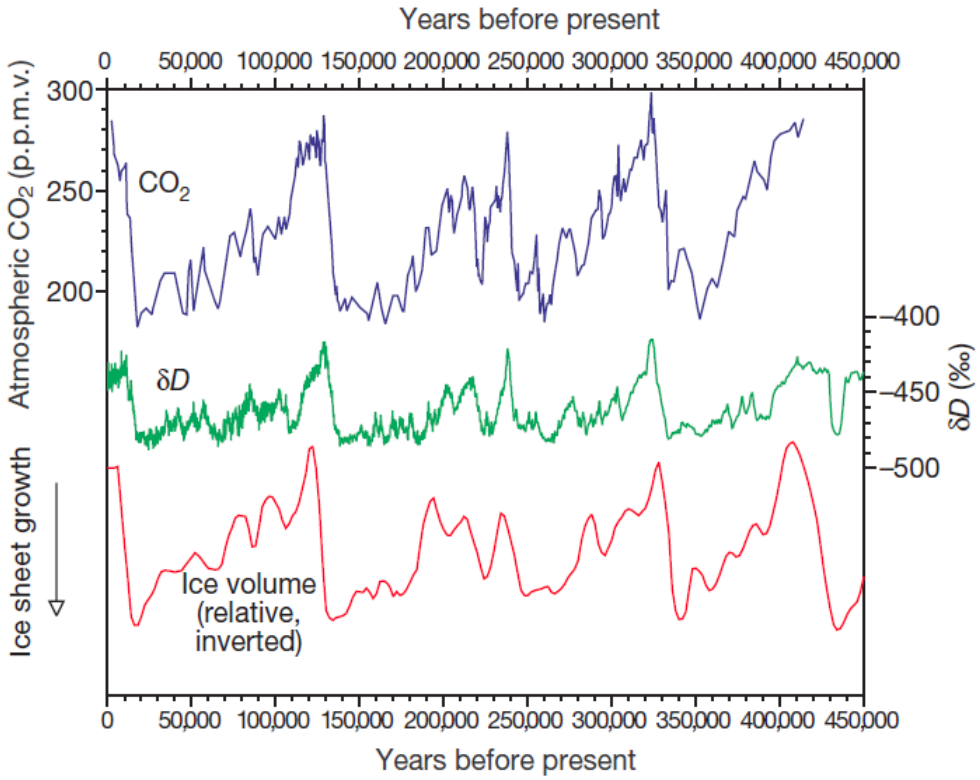

Fig 1.20: The last four glacial cycles data for CO_2 and deuterium at Vostok and total ice volume curve (Sigman and Boyle 2000).

Kohler et al's (2006) paper using the Bicycle model considered the last 740,000 years, and found that Pacific ocean $\delta^{13}C$ of DIC (dissolved inorganic carbon) and atmospheric $\delta^{13}C$ of CO_2 are controlled by different processes, suggesting a role of organic carbon and potentially a non-ocean source, or changes in Pacific ocean circulation not yet considered in previous studies.

Ikeda and Tajika in (2002) used the isotope record and a 11 layered 1D ocean model with coupled carbon biogeochemical cycle model (with diffusion and advection, atmospheric CO_2, bioproduction of particulate carbonate and organic matter in the surface ocean, regeneration of organic matter and dissolution of biogenic carbonate in the deep ocean, and carbon isotope fractionation in each process) to identify which ocean processes may be at work during glacial cycles. They found the defining mechanism for the glacial scale is the ocean pH, with vertical mixing in the ocean weakened and bioproductivity reduced. Sigman et al, 2010, reviewed the importance of polar oceans and carbon release in glacial cycles. The review paper showed mounting evidence for a Southern Ocean CO_2 'leak' being stemmed during glacial period, both increasing ocean CO_2 uptake and increasing alkalinity further driving ocean CO_2 uptake

(fig 1.21). The role of ice sheet and sea-ice extent was shown to be an important factor in reducing CO_2 leak from the Southern Ocean.

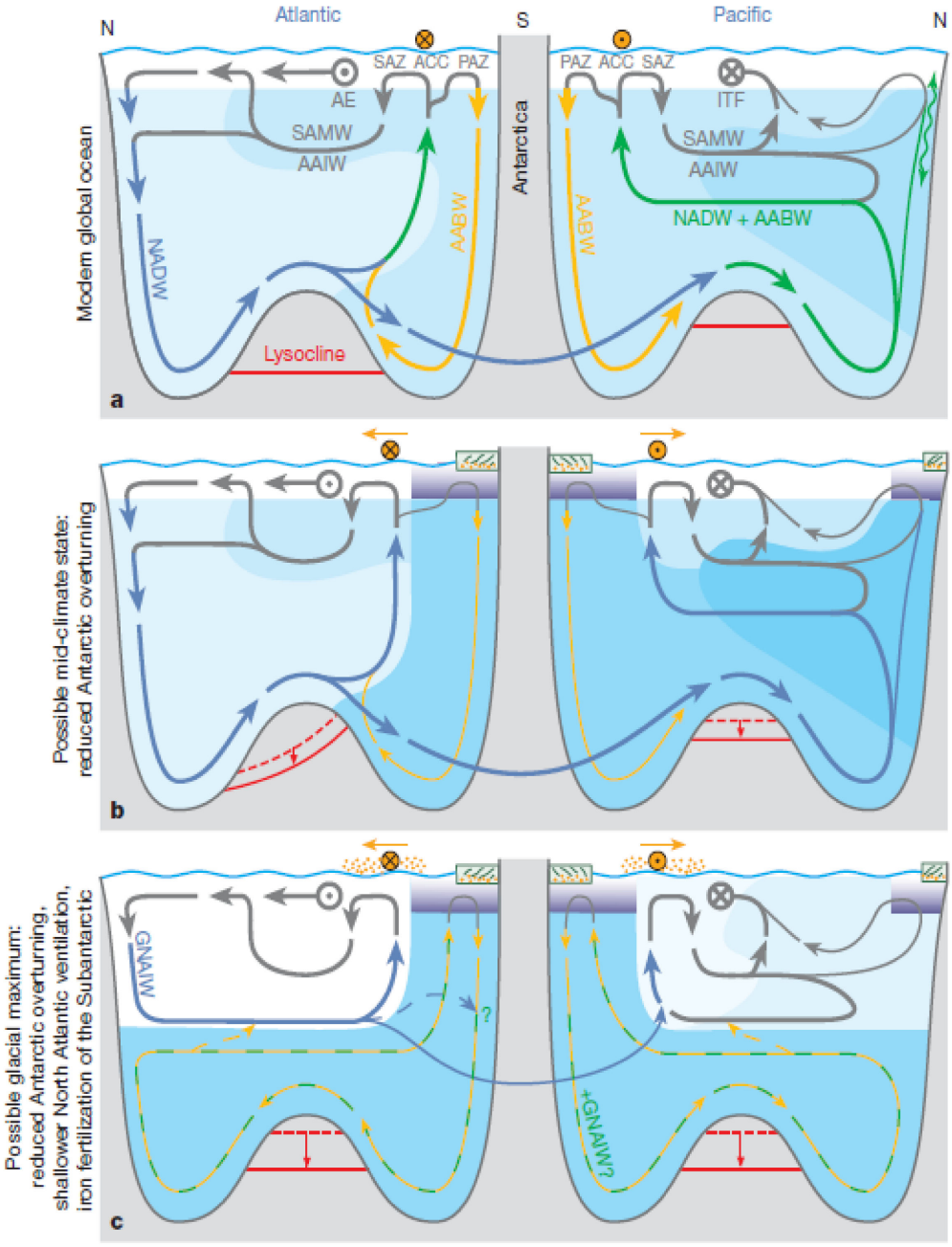

Fig 1.21: Sigman et al 2010, polar ocean control on circulation during glacial and non-glacial periods. a) modern global ocean, b) possible mid-climate state with reduced Antarctic overturning, c) possible glacial maximum state with reduced Antarctic overturning, shallow North Atlantic ventilation, iron fertilisation of the Subantarctic.

Using a comprehensive climate and ice sheet model, Abe-Ouchi et al. (2013) driving their model with insolation only, found that feedbacks between climate, ice

sheets and the lithosphere-asthenosphere system could explain the 100kyr climate cycles. A sufficiently large ice sheet becomes very sensitive to insolation forcing, but requires time to grow to a size in which the increase in NH summer insolation could start to cause an almost complete retreat with several thousand years. They noted that on this scale the atmospheric CO_2 level was involved but not determinative. The ice extent link was also found by Berger et al. 2013, studying deep sea core records. They surmised that the instability of ice masses was the chief underlying cause of changing climate states, and also provided an explanation of increased climate variability since the early Pliocene (5.3 to 2.6 Ma).

A study which tested the hypotheses for the physical mechanisms that drive glacial cycles in the Pleistocene, Kauffman and Juselius (2013) identified that sea-ice and sea-surface temperature in the southern ocean drove the large changes in atmospheric CO_2 levels and ocean biological activity. They identified that glacial variations in ice volume are driven by changes in CO_2 concentrations, global and high latitude solar insolation, latitudinal gradients in solar insolation and the atmospheric concentration of CO_2.

Weathering

On the multi-millennial timescale, the weathering CO_2 thermostat starts to potentially play a more significant role. An estimate for the contribution of weathering to the difference in CO_2 levels between PI and LGM was made by Munhoven et al (2002) as a reduction of 12.1+-1.7ppm for the maximum contribution. Using the CLIMBER-2 EMIC, Brovkin et al (2012) used the effects of weathering for their simulation of the last glacial cycle. They scaled weathering to land runoff, as Munhoven et al (2002), finding that bicarbonate flux in rivers increases as more land is exposed in the tropical regions due to ice sheet expansion and sea level drop, and thus drew down atmospheric CO_2 in glacial climates. A study of the chemical weathering in the Himalayas since the LGM by Lupker et al (2013) showed that weathering had increased since the LGM, suggesting the opposite effect to the Munhoven et al 2002 study. Another study by Hermann et al (2013) showed that mountain erosion may have accelerated in a cooling climate worldwide, which suggests that the ocean may have acted as a carbon sink in colder climate periods (glacials), the opposite of the findings by Lupker et al. Considering the balance between weathering of in-land locations to the increase in weathering due to exposed shelves at LGM sea-level lowstands was carried out by Foster and Vance (2006) using the lead isotope composition of ferromanganese crusts from the North Atlantic ocean covering the last 550k years. They found that increases in chemical weathering of exposed shelves was likely offset by decreases in weathering in the glaciated areas of the North Atlantic region. They conclude that on the time-scale of glacial-interglacial cycles chemical weathering remained largely constant. Most recently Schmitt et al (2014) studying ice core records of CF4 in polar ice for a proxy of granite weathering, found that interglacial periods saw increased weathering with respect to glacial periods.

1.4.5 Conclusions

In summary: Complex models have focussed on the ocean as the main controller of atmospheric carbon dioxide on glacial and millennial timescales. Different vegetation models used with GCMs generally show far more model spread than different ocean models, which complicates comparison of paleoclimate land biosphere studies. The deep Southern Ocean is an area of particular interest for glacial interglacial CO_2 variability, and current modelling efforts are to recreate the observed CO_2 changes using ocean mechanisms related to deep southern ocean carbon storage and release. Sea-ice extent, and its transient changes, in the southern ocean seem to be an important mechanism that may provide a control on the capability of the southern ocean to store carbon. So far the terrestrial biosphere has not been well-considered in transient simulations in Earth system models.

1.5. Foundations of this study

Evidence from the change in deep ocean carbon-13, via $\delta^{13}C$ signature of foraminifera shells in ocean sediment cores, indicated that the CO_2 draw-down in the atmosphere during glacial periods was not caused by the terrestrial biosphere carbon uptake (Broecker and Denton 1989). Fractionation of carbon during photosynthesis results in a $\delta^{13}C$ signature of terrestrial plant organic matter of around -25‰ (Maslin and Thomas 2003) with respect to the source. The estimated whole ocean change in $\delta^{13}C$ was around -0.35‰ at the glacial maximum compared to the present interglacial. In order to achieve this change, a source of carbon with $\delta^{13}C$ signature of -25‰ the size of around 500Gt is required, for example a reduction in the terrestrial biosphere. This source would increase atmospheric CO_2 by around 25ppmv (Archer 2010), the conclusion being that changes in atmospheric CO_2 between the interglacial and the glacial periods must be due to the ocean, and the uptake of carbon by the ocean in glacial periods must be strong enough to overcome the atmospheric CO_2 increase that would be caused by the carbon lost from the terrestrial biosphere. Pollen based reconstructions of the change in the size of the terrestrial biosphere and of net primary production (NPP) between the last glacial period and the present-day indicated it had grown by around 1000GtC (Crowley 1995). This seemed to confirm the $\delta^{13}C$ indication of the ocean as the carbon source during the glacial termination. However, one mechanism that is not represented in the palaeo-climate coupled modelling studies, nor in the NPP (pollen) based reconstructions of terrestrial biosphere is the effect of frozen soils. High carbon concentrations in frozen soils of the present day (Tarnocai et al 2009) and some studies of past soils (Zimov et al 2006, Ciais et al 2012) point to the importance of permafrost in climate, both directly and indirectly linked to the carbon cycle. As well as this, more recently a record of atmospheric $\delta^{13}C$ throughout the termination period shows a fast drop in $\delta^{13}C_{atm}$ then a recovery (Schmitt et al 2012). The discrepancy between ocean-based and pollen-based estimates of changes in the terrestrial biosphere, the high carbon soils in permafrost regions and the fast drop in

$\delta^{13}C_{atm}$ during the termination lead into this study: The role of permafrost soils in the global carbon-cycle on the timescales of centuries to multi-millennia.

1.6. Research questions

1. Evidence suggests that in fast-warming climates, thawing permafrost soils would release carbon to the atmosphere. Thus far modelling studies of the causes of CO_2 rise during the last deglaciation have omitted the permafrost mechanism. Could insolation driven permafrost-carbon release have contributed to the CO_2 rise between 18-12kyr BP?

2. Given that thus far the atmospheric $\delta^{13}C$ record has not been explained via ocean mechanisms, could the permafrost-carbon mechanism explain the fast drop in $\delta^{13}C_{atm}$ at the start of the last termination?

3. Can the permafrost-mechanism also explain the data from the previous termination TII?

4. If permafrost-carbon does play a significant role in rising atmospheric CO_2, does it act at each precession cycle and how strong is the effect in non-termination periods?

5. Fast climatic changes that may have effected the northern hemisphere would have an impact on the permafrost extent. Could the permafrost-carbon mechanism have played a role during these fast climatic changes?

1.7. Research method

A simplified permafrost-carbon mechanism was developed for use within the CLIMBER-2 EMIC's dynamic vegetation model. Due to large uncertainties identified in literature of the permafrost soil-carbon dynamic response to changes in climate, the carbon-cycle dynamic part of the simplified mechanism was tuned using CO_2 and $\delta^{13}C$ ice core data from the last termination period (TI), and total land carbon estimates from Ciais et al (2012). This tuning for TI included the release of carbon from the southern ocean as an important mechanism to explain deglacial CO_2 rise, that was based on the work of Bouttes et al (2012). The CLIMBER-2P model, with tuned and fully coupled permafrost mechanism in operation, was used to perform climate simulations to address the research questions above.

Chapter 2: The CLIMBER-2 model

This chapter presents the CLIMBER-2 model description. The CLIMBER-2 model is an Earth System Model of Intermediate Complexity (EMIC) which includes a carbon-13 tracer and so is suitable for comparison with CO_2 and $\delta^{13}C$ data from ice cores and for long timescale transient simulations. The dynamic global vegetation model in CLIMBER-2 represents large scale features in NPP and vegetation distributions, but without a permafrost-carbon mechanism underestimates soil carbon concentrations in high latitude soils. The model behaviour is similar to more complex model output, but due to its lower complexity level and fast simulation time it is suited for long term simulations of the Earth system response to forcings.

2. CLIMBER-2 model and performance

CLIMBER-2 is an Earth System Model of Intermediate Complexity (EMIC). It consists of a 2.5 dimensional statistical-dynamical atmosphere, a 3 basin zonally averaged ocean with biochemistry, imposed ice sheets, and a dynamic terrestrial vegetation model.

2.1 Atmosphere

The atmospheric module of CLIMBER is described in detail by Petoukhov et al. (2000). The atmosphere has a low spatial resolution of 10° in latitude and around 51° in longitude (7 equal sectors). Figure 1 shows a representation of the model. Dashed lines are the atmospheric grid, blue lines show the three ocean basins, and black lines represent the distribution of land. Land is simply defined as a fraction of a cell; it is not actually geographically distributed in the way shown in figure 2.

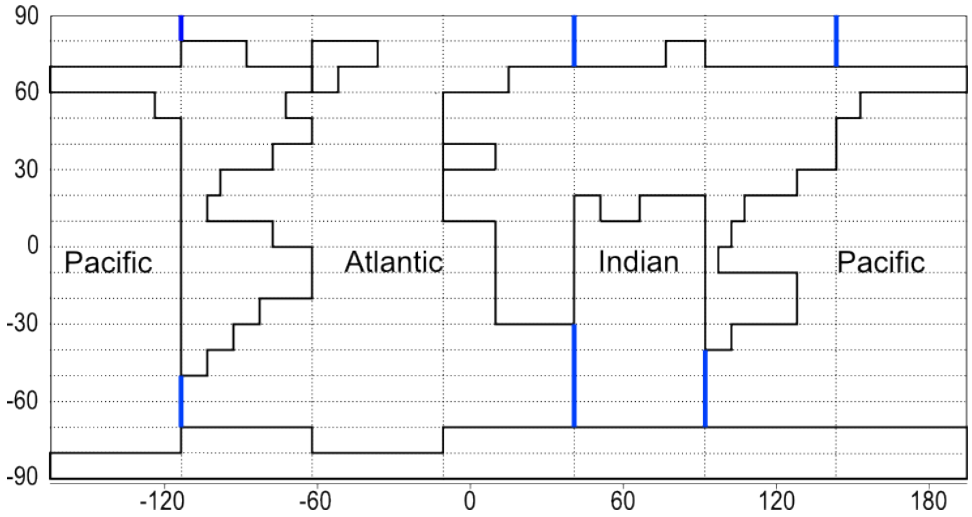

Fig 2.1, Climber atmospheric grid, land mask and ocean basins. Schematic representation

Fully described in Petoukhov et al. (2000), the atmosphere has a vertical structure made up of stratosphere, troposphere, a boundary layer and a surface layer. Stratosphere temperature is constant, lapse rate in the troposphere is considered linear and surface layer is computed using boundary layer theory. The atmospheric circulation in CLIMBER-2 is modelled according to the assumption that three pairs of cells; Hadley, Ferrel and polar cells, are robust features of circulation and exist in all climates. Zonally averaged meridional winds are calculated using the three pairs of cells assumption, and following from this temperature and sea level pressure per cell can be calculated. The surface temperature is used for computing all surface fluxes. The time-step of integration in the atmospheric model is one day. Two cloud types are represented, stratiform and cumuli, and precipitation is determined from: the total cloud

fraction, turnover time of water in the atmosphere, and specific and relative humidities. Long wave radiation (LWR) are computed by subdividing the atmospheric column into 16 levels, calculating the temperature and humidity in each level, and using integral transmission functions (ITF) of the water vapour, carbon dioxide and ozone in each layer to calculate the LWR fluxes. Clouds are treated as black body radiators and LWR fluxes are calculated in each cell as weighted sums of clear sky flux and cloudiness flux. Short wave radiation (SWR) is divided into UV-and-visible and near-infrared, and fluxes take into account water vapour, clouds, aerosols and ozone. The atmosphere interacts with the ocean and terrestrial biosphere through an atmosphere-surface interface (ASI). The ASI has six surface types: open water, sea ice, forest, grassland, desert, glacier, and different types can exist within one grid cell.

2.2 The CLIMBER-2 Carbon Cycle

The carbon cycle in CLIMBER-2 is summarised in figure 2.2. Carbon in the ocean is made up of particulate and dissolved components of organic and inorganic origin. Ocean circulation and mixing of waters between ocean layers can move dissolved carbon within the ocean. Run-off from the land forms a carbon input to the surface ocean, representing weathering effects on soils moving organic and inorganic carbon to the ocean. Marine biota in the form of phytoplankton in the surface ocean photosynthesise and use up carbon (dioxide) in the surface ocean, nutrients for phytoplankton are brought to the surface through ocean mixing. Zoo-plankton feed on the phytoplankton and mortality of both releases carbon (dioxide) on decay and causes sinking (rain down) of organic and shell (carbonate) matter to the deeper ocean. Carbonate is deposited as sediments on the ocean floor and on shelves (Brovkin et al 2002b). Below a certain depth, the carbonate compensation depth determined from ocean temperature, pressure and pH (Archer et al. 2000) carbonate dissolves back into the water and is no longer deposited as sediment (Brovkin et al 2007). At the surface ocean gas exchange with the atmosphere occurs as a result of partial pressure effects, which tends to quickly equilibrate the surface ocean with the atmospheric CO_2 concentrations (and vice versa). The ocean module includes ocean biogeochemistry in the form of zooplankton and phytoplankton (Brovkin et al. 2002[a]) and a carbon-13 tracer. The effects of iron fertilisation on marine biota in the model is described by Brovkin et al (2002[b]). Carbonate compensation is modelled in the ocean (Brovkin et al 2007) using the calcite lysocline model from Archer (1991). Ocean glacial mechanisms that account for the Atlantic ocean vertical $\delta^{13}C$ gradient indicated by paleo ocean studies (Curry and Oppo 2005) and the glacial drop in atmospheric CO_2 and are modelled (Bouttes et al 2011). These mechanisms are sinking of rejected brines from sea ice formation resulting in ocean stratification, stratification dependent diffusion in ocean layers and iron fertilisation of marine biota from atmospheric dust. The effects of ocean stratification in the CLIMBER-2 model are described by Bouttes et al. 2009. The brines mechanism accounts for sinking salt and other minerals rejected on the formation of sea-ice in the Southern Ocean and is described by Bouttes et al. 2011, together with stratification dependent diffusion and iron fertilisation in the LGM ocean. Transient

effects of ocean glacial mechanisms for the last glacial termination are described by Bouttes et al. 2012.

On the land, vegetation photosynthesises and uptakes CO_2 from the atmosphere. Vegetation respiration releases some of this CO_2 back to the atmosphere on short timescales. Through plant mortality soils are built up; over a longer time these release carbon back into the atmosphere via decay.

In the southern ocean salt rejection during the formation of sea ice can amplify ocean circulation reductions in the Atlantic in glacial periods via salinity and stratification effects, which can create very isolated Antarctic Bottom Water (AABW). Within the carbon cycle, the ocean circulation is important in determining the surface ocean carbon concentration and in turn the atmospheric CO_2 concentration.

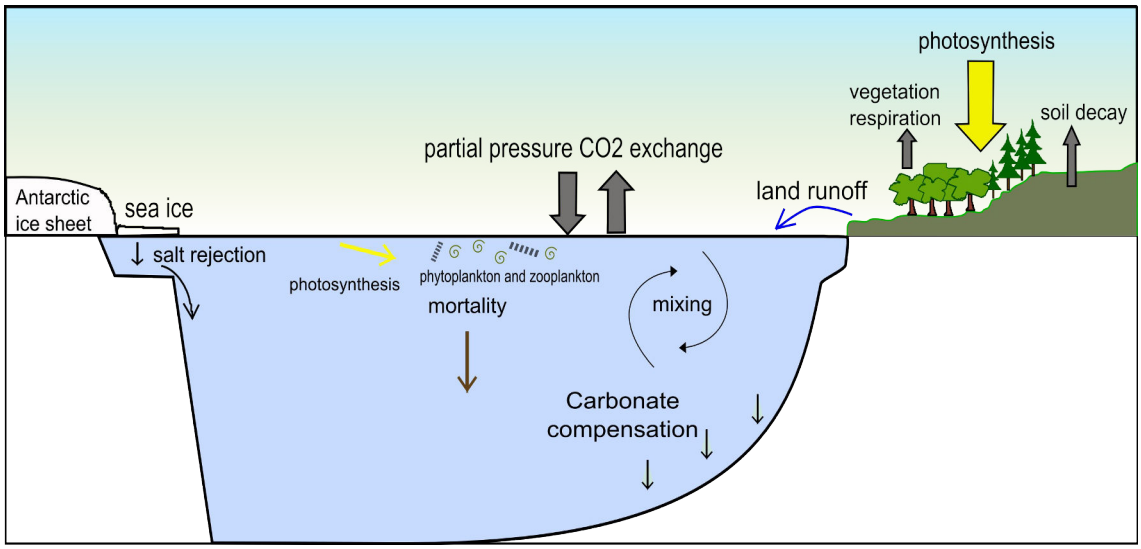

Fig 2.2, schematic of the CLIMBER-2 carbon cycle components

2.2.1 Ocean

The ocean model in CLIMBER-2 is basin-averaged, with 21 uneven vertical layers, 2.5° latitudinal resolution dynamic ocean (described by Brovkin et al. 2002[b], Petoukhov et al 2000). It models ocean dynamics and thermodynamics, sea ice and an ocean carbon cycle. Zonally averaged temperature, salinity, meridional and vertical velocities are simulated for three ocean basins: the Pacific, the Atlantic and the Indian ocean (fig 2.1). For latitude belts where continentals masses do not bound ocean basins, a zonal component of velocity is also calculated based on the density gradient between basins, and assuming a zero pressure gradient at the lower boundary (ocean floor).

Sea-ice is a one layer thermodynamic model. The fraction and thickness of sea-ice is based on a mass-balance calculation and a relationship between thickness and fraction in a grid cell. Sea-ice is modelled on the surface ocean and can appear in a grid cell when the sea surface temperature drops below 0°C. Between 0°C and -1.8°C the fraction of sea ice in a grid cell increases linearly with temperature. In the Atlantic and

Pacific basin a small northward velocity is added to sea-ice in the 70-80°S latitude band to account for conditions there where Antarctic bottom water is formed.

For this study, the ocean module is treated as Bouttes et al 2012. No changes are made to the ocean module in this study. This study focusses on the permafrost zone of the terrestrial biosphere in the northern hemisphere high-latitudes.

2.2.2 Terrestrial Biosphere

The terrestrial vegetation and soils are described with a dynamic vegetation model based on the Vecode model (Brovkin et al., 1997). It is a continuous vegetation classification using only two plant functional types (PFTs): Trees and Grass. Net primary productivity is determined from climate temperature, rainfall and CO_2 concentration. Distribution of the PFTs (and desert) is determined from climate and vegetation competition. Vegetation succession is calculated on a one year time step, with succession time determined from the growth rates of the PFTs. Vegetation is made up of two pools: leaves and stems-and-roots. Carbon dynamics in leaves are controlled via allocation factors and carbon residence time, and are a function of NPP (Net Primary Productivity). Carbon dynamics in stems and roots are controlled using residence times and NPP. Soils are split into two pools: fast and slow soils, where fast soils are made up of litter (cellulose-type matter) from plants and slow soils are humus and lignin-type plant remains. Soil have no depth, and are represented only as a carbon pool. Carbon input from dead plant matter builds the fast soil pool and the slow pool, and some input from fast soils are passed to the slow soils pool. Carbon lost from soils is determined from a residence time function; an exponential decay function based on mean annual air temperature, soil temperature (fixed in CLIMBER-2) and total carbon in the soil pool. Each vegetation and soil pool is initially calculated as a maximised carbon concentration (kg/m^2) for both PFTs then multiplied by the fraction of the cell occupied by the relevant PFT to get a cell-wide carbon concentration. This cell-wide value is used to calculate carbon fluxes to the atmosphere and carbon concentration values are multiplied by cell area to give total land carbon pool mass per grid cell.

2.5 The Carbon-13 Cycle

The CLIMBER-2 carbon cycle incorporates a ^{13}C tracer, allowing modelled outputs to be compared with ocean sediment cores and ice core data for the $^{13}C/^{12}C$ ratio. ^{13}C is a natural stable isotope of carbon, containing one extra neutron compared to ^{12}C. It is estimated to make up around 1.1% of all the carbon on Earth. When carbon moves between pools as a result of carbon cycling ^{13}C (and ^{12}C) is conserved. Fractionation, which is the process by which chemical and biochemical reactions preferentially use ^{12}C, results in different carbon pools having different signature $^{13}C/^{12}C$ ratios. Within CLIMBER-2 all carbon exchange processes are subject to fractionation of the carbon exchanged. The total amount of ^{13}C in the system is set at the start of a simulation, and can be tuned to result in an equilibrium atmospheric $\delta^{13}C$ in agreement with ice core data. The $^{13}C/^{12}C$ ratio is defined as a delta measurement from a reference ratio from a Cretaceous marine fossil of particularly high $^{13}C/^{12}C$ ratio: Pee Dee Belemnite or PDB.

The $\delta^{13}C$ is reported in parts per thousand, permil or ‰, and calculated as shown in eqn 2.1. Fractionation is the difference in ‰ of this $\delta^{13}C$ value when the carbon moves from the source pool to the sink pool.

$$\delta^{13}C_{sample} = \left(\frac{{}^{13}C/{}^{12}C_{sample}}{{}^{13}C/{}^{12}C_{PDB}} - 1 \right).1000 \qquad \text{Eqn 2.1}$$

Photosynthesis preferentially uses ^{12}C over ^{13}C, as ^{12}C is lighter atomically it is slightly more reactive. In CLIMBER-2 fractionation of terrestrial vegetation photosynthesis is -18‰ for C3 plants and -5‰ for C4 plants. C3 type plants are those that use the C3 pathway to fix carbon in photosynthesis, it is the first part of the Calvin-Benson cycle (Collister et al. 1994). C4 type plants fix carbon in the same way, but draw CO_2 out of malate into the reaction rather than CO_2 directly from the air. The C3 pathway represents around 95% of plant biomass, but the process requires more water than the C4 pathway. In hot and drier areas C4 can out-compete C3 plants. In low CO_2 environments (less than ~200ppm) C4 plants also have an advantage as they do not require as high ambient CO_2 concentrations levels. In CLIMBER-2 a fraction of grasses are C4 pathway plants, and this is determined from climate conditions and competition. Fractionation of carbon on air-sea gas exchange is dependent on temperature and fractionation increases with decreasing temperature. Surface ocean $\delta^{13}C$ is non-uniform across the globe due to temperature effects, ocean circulation effects and locations of CO_2 uptake (e.g. North Atlantic) and outgassing (e.g. the equator) (Lynch-Stieglitz et al. 1995). Within the CLIMBER-2 model, values for fractionation on air sea gas exchange are taken from Marchal et al. 1998, with carbon in the ocean approximate fractionation of +5‰ relative to the air after exchange. Fractionation of carbon from sea-water to marine biota is determined from Rau et al. 1991 and is dependent on temperature and the CO_2 concentration of the water.

2.6 The Climate and the Carbon Cycle

Up to this point, the CLIMBER-2 model has been used generally to study ocean carbon-cycle over longer time periods (centuries to millennia). The terrestrial vegetation in CLIMBER-2 has been used for some studies of vegetation dynamics in past climates. Stability analysis of vegetation in the Sahara Sahel region was carried out by Brovkin et al (1998) and of vegetation dynamics in high northern latitudes by Brovkin et al (2003). Jahn et al. (2005) consider the role of vegetation dynamics in the climatic conditions of Last Glacial Maximum (LGM). They found that for equilibrium experiments (so, assuming the climate was in equilibrium at LGM, and also in equilibrium at Pre-Industrial (PI)) of the -5.1°C change in global temperature, 0.6°C can be attributed to changes in vegetation cover (largely due to albedo). In high latitudes however, vegetation cover has a greater effect on averaged temperature change than atmospheric CO_2 radiative effect. When considering the land carbon cycle in studies of resultant atmospheric $\delta^{13}C$, the vegetation dynamics are very important, and because these are

defined by climate, the CLIMBER-2 representation of climate must be reliable. Validation and performance of the CLIMBER-2 model is available in Petoukhov et al. 2000 and Ganopolski et al. 2001.

2.7 Terrestrial Biosphere Model Performance

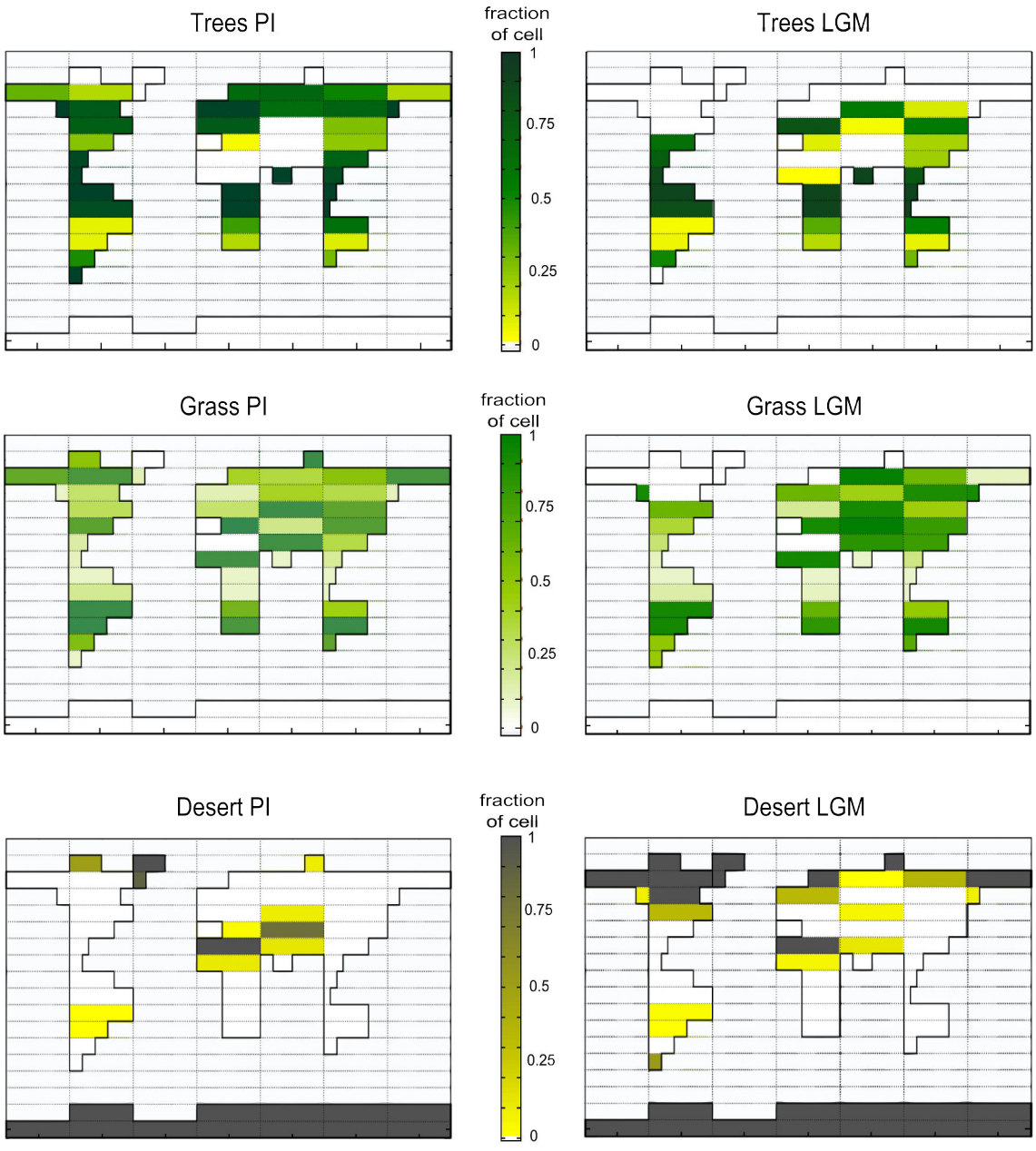

Fig 2.3, CLIMBER Fractions of PFTs for PI-equilibrium and LGM-equilibrium climate. Ice sheets are deserts in the terrestrial vegetation model.

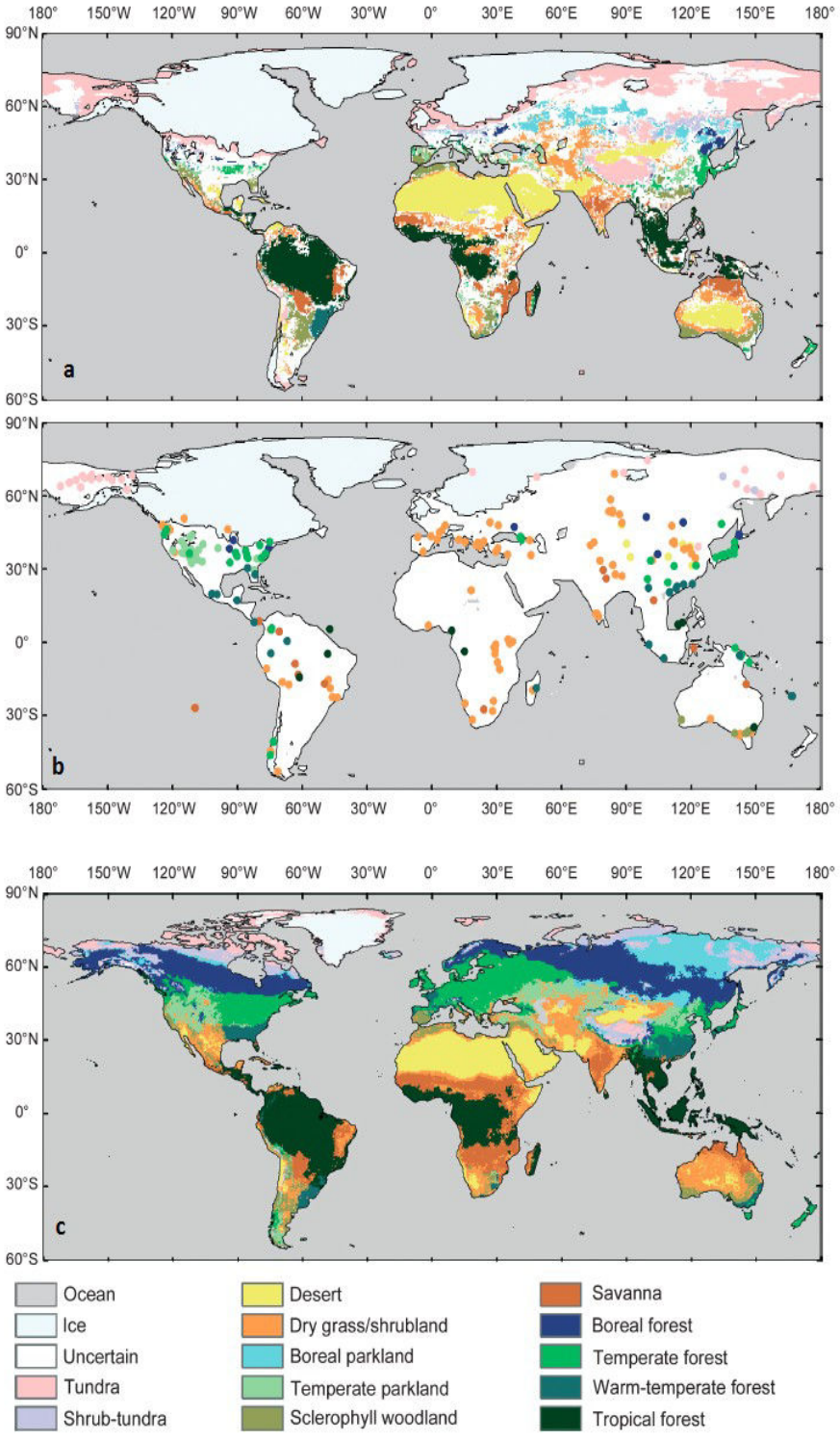

Fig 2.4, LPX model of vegetation biomes for a) LGM and c) PI. b) is pollen and plant macrofossil records (Prentice et al. 2011).

The present day large-scale vegetation patterns are reasonably well represented by the vegetation model (Brovkin, 2002[b]). An LGM simulation in which glacial mechanisms were included to obtain CO_2 and climate outputs similar to paleo-data was carried out to test the DGVM for the glacial climate. This simulation used the best-fit setting from Bouttes et al. (2011) for sinking brines, increased ocean stratification and iron fertilisation of marine biota created a glacial-like ocean. The LGM climate was created by imposing LGM ice sheets (Peltier 2004), 190ppmv CO_2 concentration, reduced ocean volume (by increasing nutrient concentration and salinity) and LGM insolation. Figure 2.3 shows the fraction of each PFT and desert fraction over the land cells for the Pre-Industrial (PI) climate and the Last Glacial Maximum (LGM) climate as Bouttes et al. (2011). Tropical and Boreal forest belts are seen in the PI, subtropical and high latitude regions are dominated by grasses, and deserts are predicted for northern Africa and in Asia over the Himalayan plateau for the PI. Forest is over-represented in northern America due to the inability of the model (coarse resolution) to show the east-west climate gradient in this region (Brovkin et al., 2002). At LGM, the model shows reduced vegetation, particularly for forests in the northern hemisphere high latitudes and increased grassland fractions for those areas. Ice sheets over Northern America and Northern Europe prevent vegetation growth in those areas. Comparing these broad scale features to the output of LPX, a higher resolution land-surface model described in Prentice et al. 2011 (fig 2.4) for the two climates shows a very general agreement in spatial patterns.

Figure 2.4 a) shows the LPX model output for the LGM simulation and figure 2.4b) shows available pollen based data to validate the model. LGM for both models and the data show a large reduction in the boreal forest coverage particularly in Asia and Siberia when compared to the PI, which is reflected in the CLIMBER-2 model output. For both climate periods the model likely overestimates the total coverage of forest in highest northern latitudes, this may be due to no representation of land-use change (deforestation) for the present-day and no representation of root depth limitations on the presence of permafrost in the LGM climate.

The NPP calculated by the model has a strong control on the carbon dynamics and pool sizes. Fig 2.5 shows the CLIMBER-2 representation of NPP (PI) compared to the MODIS dataset for global NPP patterns for the present. MODIS is the moderate resolution imaging spectrometer payload on-board the Terra and Aqua satellites, with the NPP product shown to be within around 10% of averaged published data (Pfeifer et al. 2012). CLIMBER-2 shows good overall agreement with the MODIS dataset for this climate given the limitation of grid cell size. Figure 4 also shows the LPX output of NPP (courtesy M Martin Calvo) for the LGM compared to the CLIMBER-2 output. The large scale features shown by LPX are seen in the CLIMBER-2 output; in the highest NPP areas CLIMBER-2 slightly underestimates productivity in comparison to LPX. For each of these climates it is concluded that the CLIMBER-2 spatial distribution of NPP is acceptable for long timescale simulations.

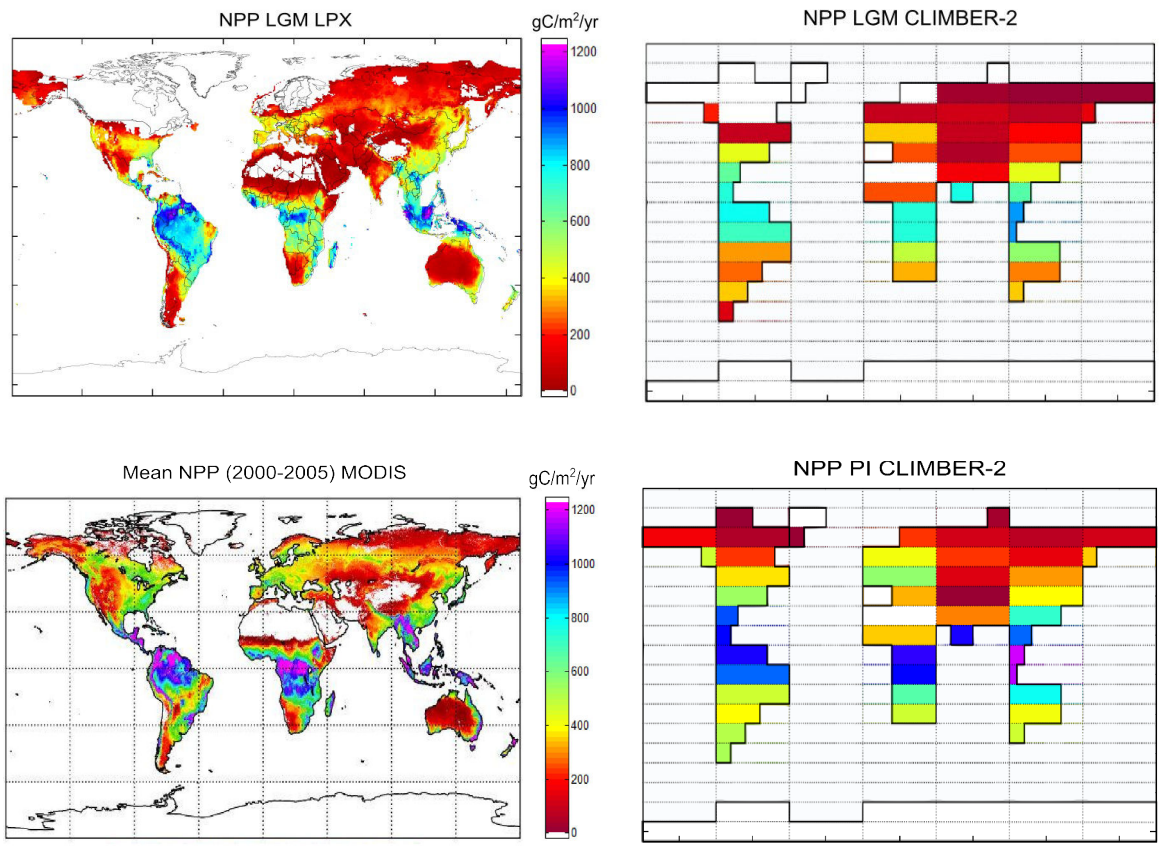

Fig 2.5, NPP in gC/m^2/yr for a) LGM LPX, b) LGM CLIMBER-2, c) 2000-2005 mean NPP MODIS, d) Pre-industrial present day CLIMBER-2.

Total terrestrial NPP for the CLIMBER-2 model at PI is 67PgC/yr and at LGM is 42PgC/yr, when glacial ocean mechanism create realistic climate conditions (settings as Bouttes et al 2011). This compares well with estimates of NPP from Ciais et al 2012, who used ^{18}O record from oxygen trapped in air bubbles in ice cores, and a global model of carbon and oxygen biogeochemical cycles to estimate NPP at LGM and PI. PI NPP_{ter} (terrestrial) was estimated to be 80±30PgC/yr. LGM NPP_{ter} was estimated to be 40±10PgC/yr (Ciais et al 2012).

The spatial distribution of carbon stored in vegetation for the two periods, LGM and PI, and stored in soils for these two periods are shown in figure 2.6 for the CLIMBER-2 standard model. In colder regions the land carbon is stored more as soils, and in warmer and tropical climates land carbon is stored more as vegetation. Total terrestrial carbon stocks at PI are 2270PgC and at LGM are 1470PgC. Ciais et al 2012 estimate 3970±325Pg for the PI and 3640±400Pg at LGM. The large differences can be accounted for as the "inert" carbon pool described by Ciais et al, with inert carbon 1600±300Pg at PI and 2300±300Pg at LGM. Compared to recent estimates of total carbon stored in permafrost region soils, the standard model underestimates high latitude full-column soil carbon concentrations by an order of magnitude for the PI simulation (Tarnocai et al. 2009). For the glacial period, physical models of land-surface

and NPP backed up by data show that cold regions were not simply deserts (see chapter 1), but soil forming vegetation was present in Siberia and Europe. As the present-day soil carbon is underestimated in these regions, it is very likely that soil carbon is also underestimated in permafrost-affected regions for the LGM simulation.

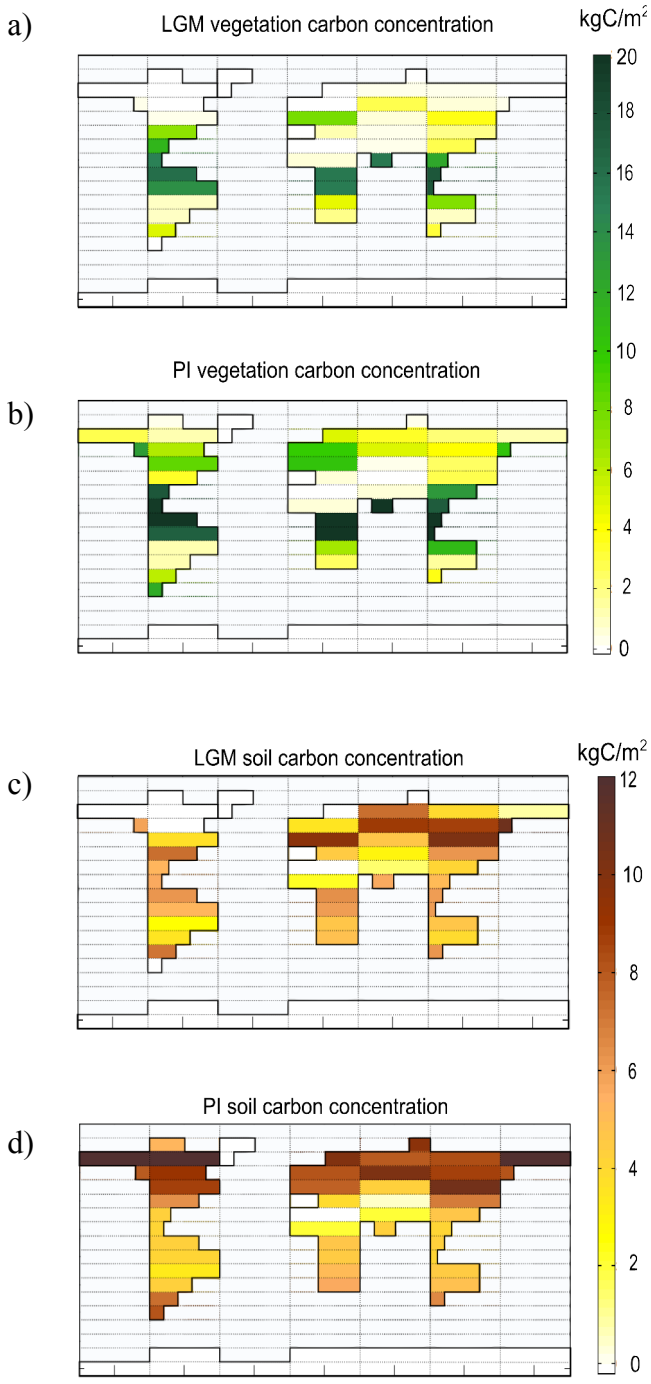

Fig 2.6, Modelled land carbon concentrations a) LGM vegetation, b) PI vegetation, c) LGM soils, d) LGM vegetation, kgC/m²

2.8 Model performance

The model is able to capture many features of the atmosphere and ocean climate fairly realistically (Pethoukov et al 2000). The model is intended as a complementary tool to study Earth system behaviour in the contexts which GCMs can not due to slower computational speeds, for example long timescales and transient simulations.

Model sensitivity experiments were carried out by Ganopolski et al. (2001) and compared to equivalent outputs generated by atmosphere, ocean and coupled GCMs. Overall the CLIMBER-2 model showed qualitative, and general quantitative, behaviour in agreement with outputs from GCMs. The sensitivity experiments were: Fresh water flux into the north Atlantic, Atmospheric CO_2 concentrations, Temporal variability of solar insolation, Vegetation cover in the boreal zone and in the tropics. The thermohaline circulations shows two stable equilibria in the model; conveyor-on and conveyor-off modes, the stability of this output is dependent upon the vertical diffusivity. For changes in CO_2 concentration the model shows equilibrium and transient responses in temperature, hydrological cycle, cryosphere and ocean characteristics. Shallow convection (or low full water-column mixing) in the Southern Ocean in the model results in relatively weak inter-hemispheric asymmetry compared to some GCMs. This means that changes in SST (sea surface temperatures) per hemisphere change at comparable rates in changing climates. Simulations for the 20th century show that the change in solar constant can explain about 0.2°C of warming, in agreement with GCM results. The deforestation experiments highlight the importance of vegetation in the climate system, and results of simulations were in agreement with GCM output with similar configurations. Atmosphere-only simulations for the deforestation experiment predicted different a sign of temperature change compared to the full model, and highlight that fully coupled modelling studies are essential for the proper understanding of the Earth system.

From the analysis in this chapter, the modelled NPP in CLIMBER-2 is similar to data and higher resolution model output, and the distribution of PFTs (trees and grass) show good agreement with LGM estimates of biomes for LPX.

Previous studies of the de-glacial and millennial timescale climate and carbon-cycle have been carried out with this version of CLIMBER-2 (Brovkin et al 2002[a,b], Jahn et al 2005, Bouttes et al 2010, 2011, 2012[a,b]). On the longer timescale of multi-millennia, the CLIMBER-2 version in this our study does not explicitly model volcanic out-gassing or changes in weathering, which would be active on the time-scale of the full glacial cycle. However, there still exists uncertainty as to the magnitude and timing of the effects of these two components (Roth and Joos 2012, Foster and Vance 2013). While they are certainly important components of the carbon cycle this study aims to focus on the role of permafrost and how it effects soil carbon in transient climate situations.

The level of complexity and completeness of components included in the CLIMBER-2 earth system model: dynamic Atmosphere, dynamic ocean, dynamic vegetation and cryosphere, make CLIMBER-2 well suited to our study for long timescales, and for the extension of the cryosphere component to include frozen soils.

Chapter 3: Permafrost-carbon model development

Based on the literature reviews and characteristics of the CLIMBER-2 model, a permafrost-carbon mechanism was created. A paper in which this model development is described and validated is provided in this chapter, the paper has been published in Geoscientific Model Development, a journal of the EGU.

Geosci. Model Dev., 7, 3111–3134, 2014
www.geosci-model-dev.net/7/3111/2014/
doi:10.5194/gmd-7-3111-2014

Geoscientific Model Development
Open Access

A simplified permafrost-carbon model for long-term climate studies with the CLIMBER-2 coupled earth system model

K. A. Crichton[1,2], D. M. Roche[3,4], G. Krinner[1,2], and J. Chappellaz[1,2]

[1]CNRS, LGGE (UMR5183), 38041 Grenoble, France
[2]Univ. Grenoble Alpes, LGGE (UMR5183), 38041 Grenoble, France
[3]CEA/INSU-CNRS/UVSQ, LSCE (UMR8212), Centre d'Etudes de Saclay CEA-Orme des Merisiers, bat. 701 91191 Gif-sur-Yvette CEDEX, France
[4]Cluster Earth and Climate, Department of Earth Sciences, Faculty of Earth and Life Sciences, Vrije Universiteit Amsterdam De Boelelaan 1085, 1081 HV Amsterdam, the Netherlands

Correspondence to: K. A. Crichton (kcrichton@lgge.obs.ujf-grenoble.fr)

Received: 27 June 2014 – Published in Geosci. Model Dev. Discuss.: 30 July 2014
Revised: 7 November 2014 – Accepted: 24 November 2014 – Published: 18 December 2014

Abstract. We present the development and validation of a simplified permafrost-carbon mechanism for use with the land surface scheme operating in the CLIMBER-2 earth system model. The simplified model estimates the permafrost fraction of each grid cell according to the balance between modelled cold (below 0 °C) and warm (above 0 °C) days in a year. Areas diagnosed as permafrost are assigned a reduction in soil decomposition rate, thus creating a slow accumulating soil carbon pool. In warming climates, permafrost extent reduces and soil decomposition rates increase, resulting in soil carbon release to the atmosphere. Four accumulation/decomposition rate settings are retained for experiments within the CLIMBER-2(P) model, which are tuned to agree with estimates of total land carbon stocks today and at the last glacial maximum. The distribution of this permafrost-carbon pool is in broad agreement with measurement data for soil carbon content. The level of complexity of the permafrost-carbon model is comparable to other components in the CLIMBER-2 earth system model.

1 Introduction

Model projections of climate response to atmospheric CO_2 increases predict that high northern latitudes experience amplified increases in mean annual temperatures compared to mid-latitudes and the tropics (Collins et al., 2013). The large carbon pool locked in permafrost soils of the high northern latitudes (Tarnocai et al., 2009) and its potential release on thaw (Schuur et al., 2008; Harden et al., 2012) make permafrost and permafrost-related carbon an important area of study. Thus far permafrost models that have been coupled within land-surface schemes have relied on thermal heat diffusion calculations from air temperatures into the ground to diagnose permafrost location and depth within soils (Koven et al., 2009; Wania et al., 2009a; Dankers et al., 2011; Ekici et al., 2014). This approach requires a good physical representation of topography, soil types, snow cover, hydrology, soil depths and geology to give a reliable output (Riseborough et al., 2008). The physically based approach lends itself to smaller grid cells and short-timescale snapshot simulations for accuracy of model output. The aim of this work is to develop a simplified permafrost-carbon mechanism that is suitable for use within the CLIMBER-2 earth system model (Petoukhov et al., 2000; Ganopolski et al., 2001), and also suitable for long-timescale experiments. The CLIMBER-2 model with a coupled permafrost-carbon mechanism, combined with proxy marine, continental and ice core data, provides a means to model the past dynamic contribution of permafrost carbon within the carbon cycle.

1.1 Physical permafrost modelling

Several land surface models diagnose permafrost and concomitant higher soil carbon concentrations (Wania et al., 2009a, b; Koven et al., 2009; Dankers et al., 2011). These models are usually driven with climatic variables output from

global climate models (GCMs), and grid cell sizes are the order of 2.5° (the order of hundreds of km) for global simulations. These models use surface air temperature and thermal diffusion calculations to estimate the soil temperature at depths, and from this the depth at which water freezes in the soil. An active layer thickness (ALT) can be determined from this, and soil carbon dynamics is calculated for the unfrozen parts of the soil. These land surface models may also include a representation of peatlands (Sphagnum-dominated areas, and wetlands), which store an estimated 574 GtC in northern peatlands (Yu et al., 2010), of which a large part are located within the permafrost region (Northern Circumpolar Atlas: Jones et al., 2009). The dynamic response of carbon in permafrost soils subject to (rapid) thaw is not well constrained (Schuur, 2011) and field studies and modelling studies still seek to better constrain this. Riseborough et al. (2008) reviewed advances in permafrost modelling, identifying that modelling of taliks (pockets or layers of thawed soil at depth that do not refreeze in winter) complicates physical modelling. The importance of soil depth (lower boundary conditions) was also highlighted; Alexeev et al. (2007) demonstrated that the longer the simulation, the larger is the soil column depth required in order to produce reliable thermal diffusion-based temperature calculations: a 4 m soil depth can produce reliable temperature predictions for a 2 year simulation, and for a 200 year simulation a 30 m soil depth would be required. Van Huissteden and Dolman (2012) reviewed Arctic soil carbon stocks estimates and the permafrost-carbon feedback. They note the processes by which carbon loss occurs from thawing permafrost including active layer thickening (also caused by vegetation disturbance), thermokarst formation, dissolved organic carbon (DOC) export, fire and other disturbances. Their conclusions are that "current models are insufficiently equipped to quantify the carbon release at rapid thaw of ice-rich permafrost", which within a model would require accurate representation of local topography and hydrology as well as a priori knowledge of the ice content in the soils. Koven et al. (2013) further highlighted the importance of soil depths and of soil and snow dynamics for the accuracy of permafrost extent in CMIP (coupled model intercomparison project) models. The high computing power requirements of physical models at grid sizes where output could be an acceptable confidence level makes these kinds of models currently unsuitable for long-timescale dynamically coupled modelling studies. Current CMIP model projections of future climate reported by the IPCC (Stocker et al., 2013) do not include a possible feedback mechanism from permafrost soils. There exist some studies of the possible future response of carbon in soils of the permafrost zone that do not rely on heat diffusion calculations down the soil column (Scheafer et al., 2011; Harden et al., 2012; Schneider von Diemling et al., 2012). However, these kinds of treatments are not suitable for the study of paleoclimate as they require a priori knowledge of soil organic carbon content (SOCC) of the soils at relatively high resolution. This is not yet feasible when considering last glacial maximum soils (for example).

1.2 Past permafrost carbon

Zimov et al. (2009) created a physical model for carbon dynamics in permafrost soils. This one-dimensional model was intended to simulate the carbon dynamics specifically in the permafrost region. Carbon input to the soil originates from root mortality and aboveground litter transport via organic carbon leaching and mixing by bioturbation and cryoturbation. Loss of carbon from the soils occurs via decomposition. The frozen soil active layer depth also determines the maximum root depth of vegetation. Modelled soil carbon profiles were similar to those found in present-day ground data for similar conditions. Results of experiments where the temperature zone was changed linearly from Temperate to Cold, then snapped back to Temperate (mimicking a glaciation then termination in Europe), demonstrated the characteristic of slow carbon accumulation in permafrost soils, and fast carbon release on thaw. An important result of this study was that the main driver of the high carbon content in the frozen soils was the low decomposition rates, which reduce further with depth in the soil column, as a result of permafrost underlying an active layer which cycles between freezing and thawing in the year. To estimate the amounts of carbon stored on the land and the ocean at Last Glacial Maximum (LGM), Ciais et al. (2012) used $\delta^{18}O$ data and carbon cycle modelling to calculate gross primary productivity (GPP) at LGM and in the present day. They estimate that the total land carbon stocks had increased by 330 GtC since LGM, but that 700 GtC less was at present stored as inert land carbon stocks compared to LGM. Zech et al. (2011), studying two permafrost-loess paleosol sequences, concluded that on glacial timescales the effect of reduced biomass productivity may be of secondary importance to the effect of permafrost preserving soil organic matter when considering total land carbon stocks. The Ciais et al. (2012) inert land carbon stock may represent this permafrost-carbon pool.

1.3 Carbon cycle responses during a deglaciation

The current leading hypothesis for the fast rise in atmospheric CO_2 in the last glacial termination (17.5 to 12 kyr BP) (Monnin et al., 2001) is that carbon was outgassed from the ocean via a reorganisation of ocean circulation that released a deep carbon store in the Southern ocean (Sigman et al., 2010; Fischer et al., 2010; Shakun et al., 2012). The Zimov et al. (2009) model, Ciais et al. (2012) and the $\delta^{13}CO_2$ record for the last termination (Lourantou et al., 2010; Schmitt et al., 2012) suggest that permafrost may have had a role to play in the dynamics of the carbon cycle during the last termination. At the start of glacial termination 1 (from the end of the last glacial period, the transition to the interglacial climate, starting at $\sim$ 17.5 kyr BP) a fast drop in the $\delta^{13}CO_2$ of

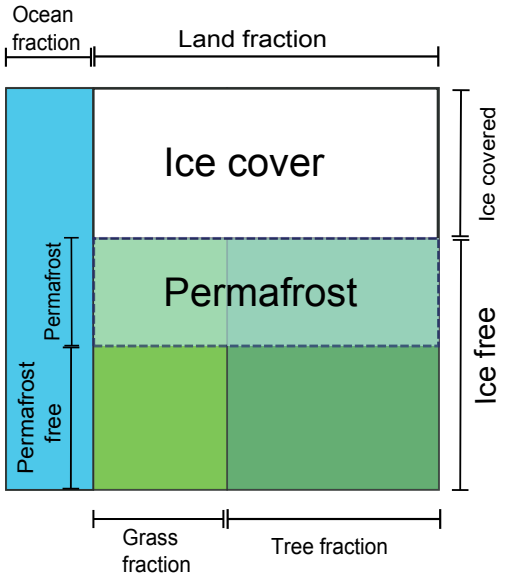

Figure 1. A CLIMBER-2P grid cell showing the distribution of different cell cover types.

the atmosphere was seen from ice core data. Soil carbon has a $\delta^{13}C$ signature depleted by around 18 ‰ compared to the atmosphere (Maslin and Thomas, 2003); a release of carbon from thawing permafrost soils is a possible explanation for the $\delta^{13}CO_2$ record.

In this study, we aim to develop a permafrost-carbon model for long-term paleoclimate studies. We present the development of the permafrost-carbon model and validate it with present-day ground measurement data for soil carbon concentrations in high northern latitude soils.

2 Model development

2.1 CLIMBER-2 standard model

The CLIMBER-2 model (Petoukhov et al., 2000; Ganopolski et al., 2001) consists of a statistical–dynamical atmosphere, a three-basin averaged dynamical ocean model with 21 vertical uneven layers and a dynamic global vegetation model, VECODE (Brovkin et al., 1997). The model version we use is as Bouttes et al. (2012) and Brovkin et al. (2007). The model can simulate around 20 kyr in 10 h (on a 2.5 GHz processor) and so is particularly suited to paleoclimate and long-timescale fully coupled modelling studies. The version of CLIMBER-2 we use (Bouttes et al., 2009, 2012) is equipped with a carbon-13 tracer, ice sheets and deep sea sediments (allowing the representation of carbonate compensation) in the ocean (Brovkin et al., 2007) as well as ocean biogeochemistry. The ice sheets are determined by scaling ice sheets' size between the LGM condition from Peltier (2004) and the Pre-Industrial (PI) ice sheet using the sea level record to determine land ice volume (Bouttes et al., 2012). The dynamic vegetation model has two plant functional types (PFTs), trees and grass, plus bare ground as a dummy type. It has two soil pools, "fast" and "slow", representing litter and humus respectively. Soils have no depth, and are only represented as carbon pools. The carbon pools of the terrestrial vegetation model are recalculated once every year. The grid cell size of the atmospheric and land surface models is approximately 51° longitude (360/7 degrees) by 10° latitude. Given the long-timescale applications of the CLIMBER-2 model and the very large grid size for both atmosphere and land, none of the existing approaches of modelling permafrost carbon are suitable. Thermal diffusion-based physical models would produce results with unacceptable uncertainties (error bounds) compounding over long timescales. To create the permafrost model for CLIMBER-2, the driving mechanism creating high soil carbon concentrations is a reduced soil decomposition rate in the presence of permafrost, identified by Zimov et al. (2009) as the primary driver in soil carbon accumulation for these soils.

2.2 Permafrost-carbon mechanism

CLIMBER-2 grid cells for the land surface model are very large. Two options are available to diagnose permafrost location: either by creating a sub-grid within the land grid or by diagnosing a fraction of each grid cell as permafrost, which is the approach followed here. Conceptually the sub-grid model represents keeping permafrost carbon separate from other soil carbon, and the remixing model represents mixing all soil carbon in a grid cell. Figure 1 shows a schematic representation of a CLIMBER-2 grid cell, and how the permafrost fraction of the land is defined relative to other cell parameters when permafrost is diagnosed as a fraction of each cell. For the carbon cycle the calculations of carbon fluxes between atmosphere and land grid cells are for the cell mean. Each grid cell contains cell-wide soil carbon pools (fast soil or slow soil, per plant functional type), so to account for permafrost soils either a new permafrost-soil pool needs to be created for each grid cell, or permafrost soils can be mixed back into the standard soil pools at every time-step (Fig. 2a). If the land grid is downscaled a third option is available, where each sub-grid cell maintains an individual soil carbon pool (Fig. 2b). This, however, requires an increase in computational time which slows down the run speed of the model.

The soil carbon in CLIMBER-2 is built from vegetation mortality and soil carbon decomposition is dependent on surface air temperature, the total amount of carbon in the pool and the source of carbon (i.e. trees or grass). Equation (1) shows how carbon content of each pool is calculated in CLIMBER-2. The pool is denoted by C_i, where pool C_1 is plant green phytomass (leaves), C_2 is plant structural biomass (stems and roots), C_3 is a soil pool made of litter and roots residue and C_4 is a soil pool made of humus and residues of woody-type stems and roots. Hereafter, the soil pools will be referred to as $Soil_{fast}$ for C_3 and $Soil_{slow}$ for C_4.

The equations (Eq. 1) are numerically solved in the model with a time-step of one year.

$$\frac{dC_1^p}{dt} = k_1^p N - m_1^p C_1^p$$
$$\frac{dC_2^p}{dt} = (1 - k_1^p) N - m_1^p C_2^p$$
$$\frac{dC_3^p}{dt} = k_2^p m_1^p + k_3^p m_2^p C_2^p - m_3^p C_3^p$$
$$\frac{dC_4^p}{dt} = k_4^p m_2^p C_2^P + k_5^p m_3^p C_3^p - m_4^p C_4^p, \quad (1)$$

where C is the carbon content in the pool (kgC m^{-2}); k is allocation factors ($0 < ki < 1$); N is net primary productivity (NPP; kgC m^{-2} yr^{-1}); m_i is decomposition rates for the carbon in each pool (yr^{-1}); p is the plant functional type (trees or grass).

The residence time of carbon in soil pools is $1/m$; we call this τ. For residence times corresponding to decomposition rates m_3 and m_4, τ is:

$$\tau_i = n_i^p \cdot e^{(-\mathrm{ps5}(T_{\mathrm{mat}} - T_{\mathrm{ref}}))}, \quad (2)$$

where i is the soil pool, n is a multiplier dependent on the pool type, ps5 is a constant, $= 0.04$, T_{mat} is mean annual temperature at the surface–air interface, °C, T_{ref} is a reference soil temperature, fixed in CLIMBER-2 at 5 °C.

The value of n is dependent on the soil carbon type, being 900 for all slow soils, 16 for fast tree PFT soil and 40 for fast grass PFT soil. The decomposition rates for organic residue in the soils are most strongly based on soil microbial activity and the relative amount of lignin in the residues (Aleksandrova, 1970; Brovkin et al., 1997). Increasing the residence time of carbon in permafrost-affected soils reduces the decomposition rates and results in higher soil carbon concentrations. We modify the residence time, $\tau_{3,4}$, in the presence of permafrost using:

$$\tau_{(\mathrm{permai})} = \tau_i (a F_{\mathrm{sc}} + b), \quad (3)$$

where a and b are tuneable dimensionless constants and F_{sc} is frost index, a value between 0 and 1, which is a measure of the balance between cold and warm days in a year, and is shown in Eq. (4) where DDF is degree-days below 0 °C and DDT is degree-days above 0 °C in a year for daily average surface air temperature (Nelson and Outcalt, 1987). DDF and DDT have units of °C days yr^{-1}. Snow cover acts to insulate the ground against the coldest winter temperatures and reduces permafrost extent (Zhang, 2005; Gouttevin et al., 2012). The subscript sc in Eqs. (3) and (4) indicates that these values are corrected for snow cover and represent the ground–snow interface conditions, not the snow surface–air interface conditions.

$$F_{\mathrm{sc}} = \frac{\mathrm{DDF}_{\mathrm{sc}}^{(1/2)}}{\mathrm{DDF}_{\mathrm{sc}}^{(1/2)} + \mathrm{DDT}^{(1/2)}} \quad (4)$$

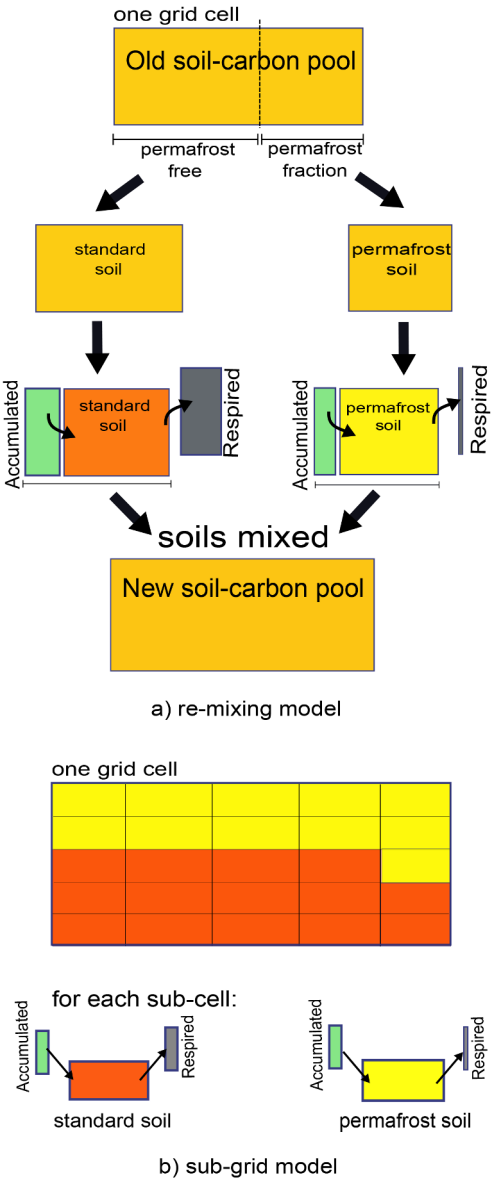

Figure 2. Schematic of a CLIMBER-2P grid cell showing how carbon is accumulated at each time-step. Remixing model **(a)** separates grid cell into permafrost or non-permafrost, calculates the change in carbon pool and remixing all carbon in the cell back together. Sub-grid model **(b)** separates the grid cell into 25 sub-grid cells, calculates change in carbon pool in each individually and does not remix any carbon between sub-grid cells.

Including the frost index as a multiplier (in Eq. 3) for the permafrost soils' carbon residence time was needed to allow the correct tuning of the model and allow for total land carbon stocks to be in agreement with data estimates. Therefore, the decomposition rates of soil carbon in permafrost-affected cells are dependent on: mean annual temperature (as with non-permafrost soils), the fractional cover of permafrost in the cell and the frost index (a measure of the severity of cold-

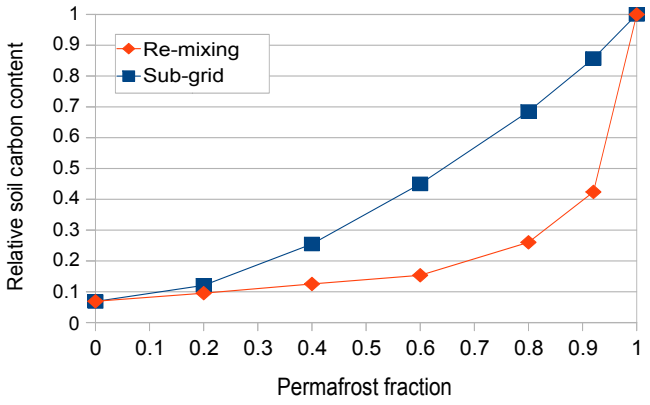

Figure 3. Comparison of sub-grid to remixing approach for relative soil carbon contents of a grid cell for increasing permafrost fraction. The variables of mean annual temperature and frost index vary with permafrost fraction according to data relationships upscaled to CLIMBER-2 grid relationships (see Appendix A and Fig. A2).

ness in a year). This $\tau_{\text{perma}\,i}$ (Eq. 3) is only applied to the soils that are diagnosed as permafrost. The remainder of the carbon dynamics in land carbon pools was unaltered from the standard model.

2.3 1-D model

We test a one-dimensional model to compare the effect the different assumptions made for the model design. The total carbon stock in a grid cell using each method (sub-grid and remixing) was compared for equilibrium soil carbon content by running the 1-D model for 100 000 simulation years. The carbon input from vegetation mortality is the same for the remixing and the sub-grid model, as is rainfall. The variables of permafrost fraction, mean annual air–surface interface temperature (MAT) and frost index are varied one at a time to compare the model outputs. The constants a and b for Eq. (3) were set to 20 for $\text{Soil}_{\text{fast}}$ and 2 for $\text{Soils}_{\text{slow}}$ (so a and b have matching values) for the permafrost soils, and as the standard model for the non-permafrost soils. These values for a and b were chosen to compare the performance of the two methods, not for accurate soil carbon concentrations. They result in total carbon in the $\text{Soil}_{\text{fast}}$ and the $\text{Soil}_{\text{slow}}$ carbon pools being approximately equal, which studies suggest is appropriate (Harden et al., 2012; Zimov et al., 2009).

Figure 3 shows the output for carbon content along a permafrost gradient, taking account of the relationship between permafrost fraction, frost index and mean annual temperature. More detail on this figure is available in Appendix A. The relationship between permafrost fraction and frost index is defined as that determined in this study for the CLIMBER-2 model in Sect. 3.2. As shown in Eq. (1), NPP exerts a control on soil carbon content via input from plant material, although note that Fig. 3 shows model output for fixed NPP. For both approaches, carbon content increases non-linearly

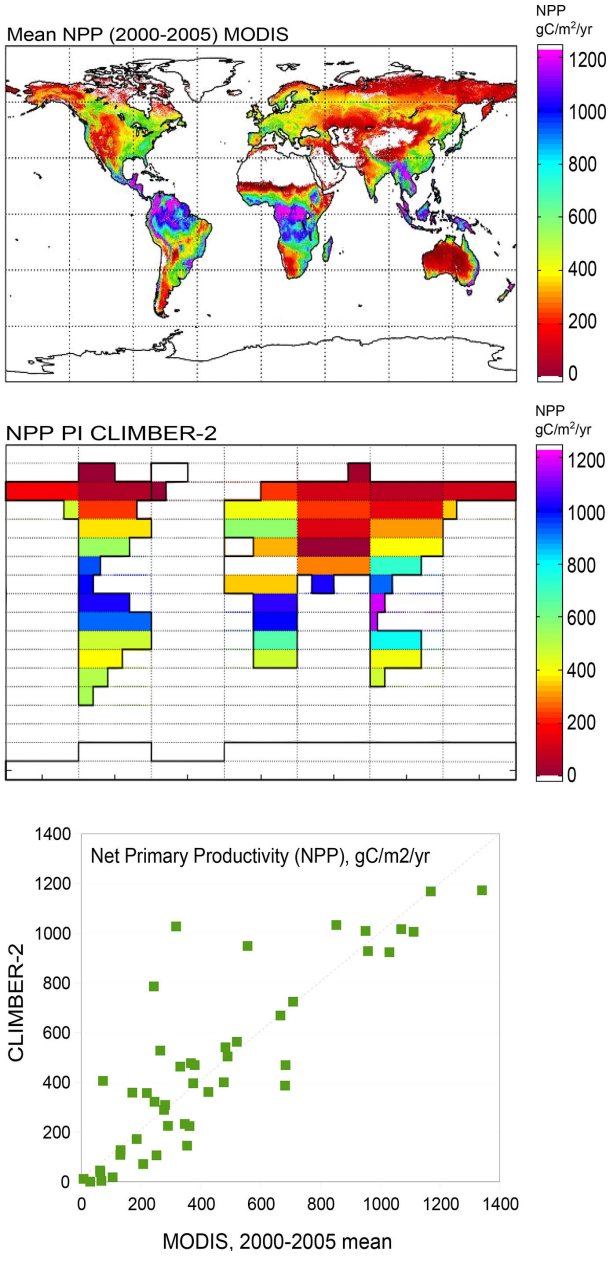

Figure 4. Comparison of NPP, which has a control on carbon input to soils, for MODIS data set (top, mean 2000–2005) and CLIMBER-2 model for PI(eq) (modelled year 1950) plotted on the same scale ($\text{gC}\,\text{m}^{-2}\,\text{yr}^{-1}$). MODIS data upscaled to CLIMBER-2 grid scale are shown against equivalent points for CLIMBER-2 NPP.

along the permafrost gradient (increasing permafrost fraction of the grid cell). The remixing model shows stronger non-linear behaviour than the sub-grid model.

2.4 CLIMBER-2 modelled NPP

The comparisons of the sub-grid to remixing approaches shown in Fig. 3 take no account of reductions in input to soils

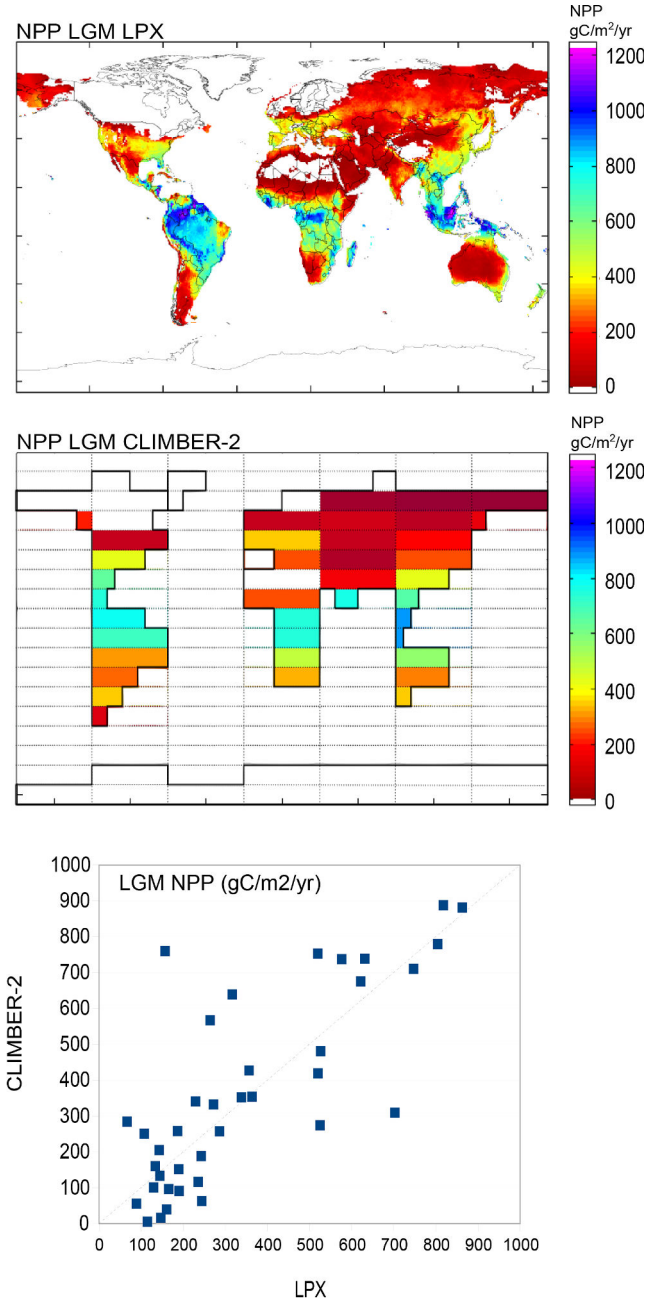

Figure 5. Comparison of NPP, which has a control on carbon input to soils, for LPX model (top, courtesy of M. Martin-Calvo, average of an ensemble model output) and CLIMBER-2 model for LGM(eq) (at 21 kyr BP) plotted on the same scale ($gC\,m^{-2}\,yr^{-1}$), and the same scale as Fig. 4. LPX output upscaled to CLIMBER-2 grid and plotted against equivalent CLIMBER-2 NPP is shown also.

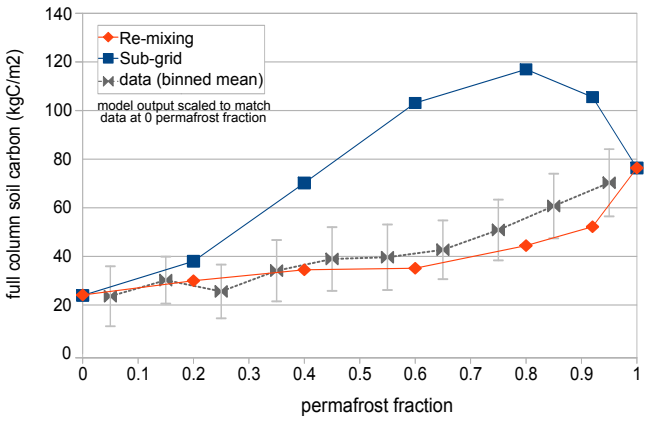

Figure 6. Modelled output for 1-D models along a permafrost gradient, with correction for NPP and initial value (at 0 % permafrost). Overlaid on 1° data for SOCC binned into 0.1 permafrost fraction mean values ±1 sigma (Hugelius et al., 2013), permafrost fraction is calculated using relationship identified in Sect. 3.2.

via NPP in colder climates. Figure 4 shows the CLIMBER-2 modelled NPP and the MODIS 2000–2005 mean NPP product (Zhao et al., 2011) for the present day (PI, pre-industrial for CLIMBER output). The CLIMBER-2 vegetation model shows NPP patterns similar to the MODIS data set. The boreal forest belt seen at around 60° N in the MODIS data set is not clearly seen in the CLIMBER-2 model, mainly due to the large grid cell size. In Siberia and Alaska the NPP in CLIMBER-2 is not overestimated. The reduced NPP in the coldest regions would tend to reduce soil carbon accumulation via reduced input from plant mortality. Also shown in Fig. 4 are the upscaled data points plotted against CLIMBER-2 model output. The MODIS data set represents the earth system already subject to anthropogenic forcing, where the CLIMBER-2 model output represents the natural system only. However, the use of measurement-based data to validate CLIMBER-2 NPP was preferred due to the quite large model spread seen in output for numerical global dynamic vegetation models of higher complexity than CLIMBER-2. The fact that MODIS is for the present-day "perturbed" system (due to deforestation, for example) may also explain some of the model–data mismatch, although we consider this less significant for the permafrost zone low-NPP soils in which we are interested . In order to test the applicability of the CLIMBER-2 model for the glacial climate, a comparison of NPP for the LGM with a more complex model can be done (as measurement data are not available). Figure 5 shows LGM(eq) NPP for LPX (data courtesy of M. Martin-Calvo, Prentice et al., 2011) and for CLIMBER-2 for an LGM climate. At LGM the NPP in Siberia and the coldest permafrost regions is non-zero in both models, and CLIMBER-2 follows the same general patterns as LPX predicts. CLIMBER-2 shows slightly lower NPP in the southern parts of Russia, possibly similar to the boreal forest belt that is not well represented in the PI climate background NPP due to the large grid cell size. Again, the upscaled LPX data are shown plotted against CLIMBER-2 output, showing reasonable agreement on this scale. Overall at both periods, PI and LGM, CLIMBER-2 represents NPP reasonably well.

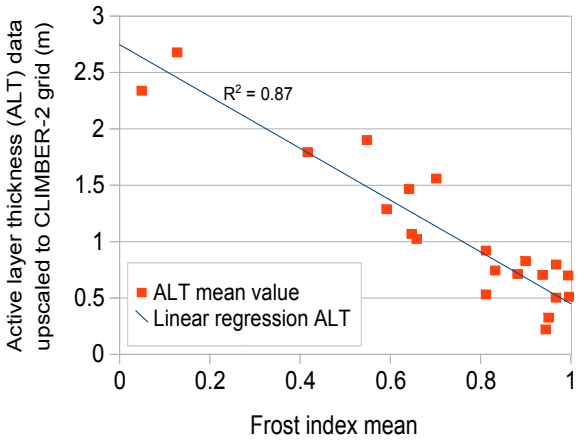

Figure 7. Measurement data for active layer thickness (CALM network, Brown et al., 2003) and frost index (Zhang, 1998) upscaled to the CLIMBER-2 grid scale, showing the distinct relationship of reducing active layer with increasing frost index at this scale. Note that permafrost fraction is calculated from frost index in our model (see Sect. 3.2).

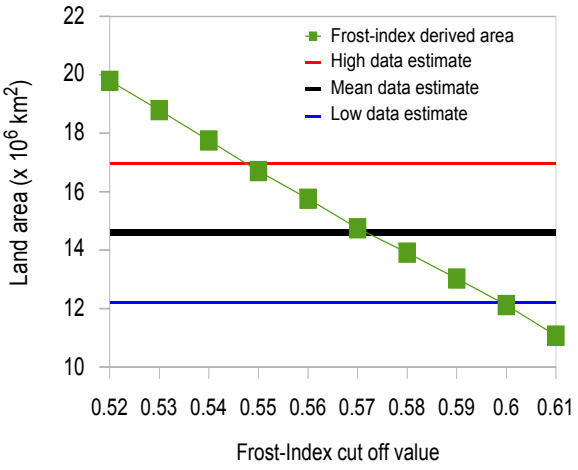

Figure 8. Total land area with a frost index higher (colder) than the x axis cut-off value, for frost-index data from Zhang (1998) (NSIDC). Horizontal lines show the Zhang et al. (2000) data estimates for area of land underlain by permafrost.

When the soil carbon content shown in Fig. 3 is adjusted to compensate for the reduction in NPP along a permafrost gradient and for the 0 % permafrost SOCC data value (by multiplying relative value by 350), the resultant outputs are shown in Fig. 6 (more details are available in Appendix A). Now the remixing model shows a slight increase in total carbon along a permafrost gradient, where the sub-grid model shows a peak value at around 80 % permafrost coverage. Figure 6 shows a comparison between these 1-D model outputs and data for SOCC. The unadjusted data are for the top 1 m of soils, whereas model output represents the full soil column. As in Sect. 4.4, the model–data comparison is carried out by assuming that 40 % of total soil carbon is located in the top 1 m for permafrost soils (and is fully described in Appendix A). From this comparison, the change in SOCC along a permafrost gradient is relatively small, due to the combined effects of reducing soil decomposition rate and reducing NPP. Here, the remixing model represents these changes quite well. It may be possible to improve the performance of the sub-grid model by, for example, downscaling the climate variables also. However, this would represent a more significant change of the land biosphere model in CLIMBER-2, and increase the complexity and therefore reduce the computational efficiency of the model.

For the remixing model: at each time-step a proportion of carbon that is accumulated in the permafrost part is then sent back to decompose as standard soil. This occurs because the high-carbon permafrost soil is mixed with the lower carbon standard soil in a grid cell at each time-step. This can be seen as similar to that which occurs in the active layer. The active layer is the top layer of the soil that thaws in warm months and freezes in cold months. In warm months the carbon in this thawed layer is available to be decomposed at "standard" soils rates, determined by local temperature. In the remixing model, the relative proportion of the permafrost soil carbon that is sent to decompose as standard soil carbon reduces along a permafrost gradient. This reduction can be seen as mimicking the characteristic of a reducing active layer thickness along a permafrost gradient, which is shown in Fig. 7 for active layer thickness data upscaled to the CLIMBER-2 grid size. Here active layer thickness mean is shown plotted against mean frost index (and permafrost fraction is directly calculated from frost index in CLIMBER-2). It must be noted that on smaller spatial scales the relationship between the mean active layer thickness and the extent of permafrost in a location may be less clear. The local conditions determine both permafrost extent and active layer thickness. Our treatment for permafrost relies entirely on the relationships between climate characteristics and soil carbon contents on the CLIMBER-2 grid scale.

3 CLIMBER-2 permafrost-carbon model

We implemented Eq. (3) into CLIMBER-2 using the remixing model. In order to study the effect of different carbon accumulation and release rates (the permafrost-carbon dynamics) in later modelling studies, the soil carbon residence times can be tuned to distribute the carbon more into the $\text{Soil}_{\text{fast}}$ pool (making a quickly responding soil carbon pool) or more into the $\text{Soil}_{\text{slow}}$ pool (making a more slowly responding soil carbon pool). A total of four dynamic settings are retained for later coupled climate studies (described in Sect. 3.5).

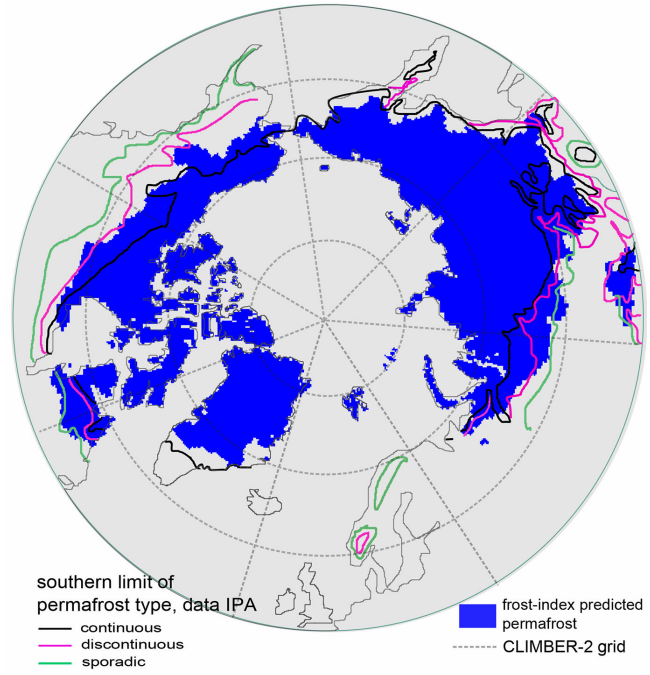

Figure 9. Map of land with frost index greater than 0.57 (frost index predicted permafrost) shown in blue with southern limit of permafrost boundaries for the present day defined by IPA overlaid. Black line: continuous permafrost, pink line: discontinuous permafrost, green line: sporadic permafrost. Grey dotted lines are the CLIMBER-2 grid.

3.1 Simulated climates to tune the permafrost-carbon model

Three simulated climates were used to tune and validate the permafrost-carbon model: an LGM equilibrium climate, LGM(eq); a PI equilibrium climate, PI(eq); and a PI transient climate, PI(tr) obtained at the end of a transient deglaciation from the LGM climate. These three climates allow the total soil carbon to be tuned to the estimates of Ciais et al. (2012) for the LGM and PI climate conditions; these are described in Table 1.

3.2 Calculating permafrost extent

In order to obtain a relationship between calculated frost index and the permafrost fraction of a grid cell, measurement and ground data for frost index and permafrost location were used. For present-day mean daily surface air temperatures, the freeze and thaw indices values on a 0.5° global grid were obtained from the National Snow and Ice Data Centre (NSIDC) database (Zhang, 1998). Using these values for freeze and thaw index, a global frost-index data set on a 0.5° grid scale was created using Eq. (4). The present-day estimates of land area underlain by permafrost are provided by Zhang et al. (2000), using the definition of zones: "continuous" as 90–100 % underlain by permafrost, "discontinuous" as 50–90 %, "sporadic" as 10–50 % and "isolated" as less than 10 %. Zhang et al. (2000) used these zonations to provide area estimates of the total land area underlain by permafrost. Summing the total land area that has a frost index higher than a particular value and comparing this to the Zhang et al. (2000) estimate can identify the appropriate boundary between permafrost and non-permafrost soils. Figure 8 shows the Zhang et al. (2000) permafrost areas for the high, medium and low ranges defined by the high, medium and low % estimates of permafrost zones marked as horizontal lines. The land area indicated by green squares is the total land surface in the northern hemisphere that has a frost-index value higher (where higher indicates a colder climate) than the cut-off value shown on the x axis. Here the frost-index cut-off value of 0.57 shows good agreement with the medium (mean) estimate of the Zhang et al. (2000) total area of land underlain by permafrost.

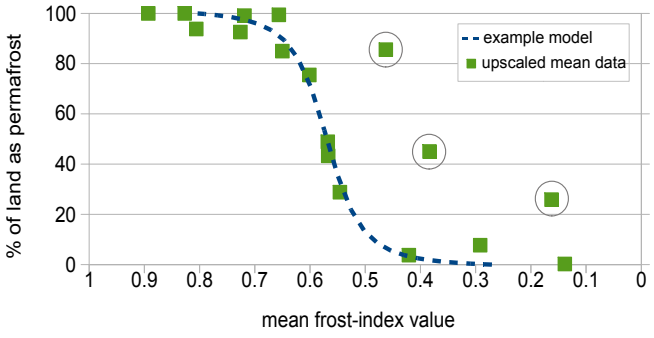

Figure 10. Frost-index-predicted permafrost fraction of land from Fig. 8 upscaled to the CLIMBER-2 grid and plotted against mean frost index for the same CLIMBER-2 grid cell. Circled points are where the total fraction of land vs. ocean in the grid cell is small (land is less than 25 % of the grid cell) and ocean temperatures pull frost index lower (warmer). The dashed line is a representative relationship between frost index and permafrost land fraction.

3.3 Geographic permafrost distribution for the present-day

Figure 9 shows, coloured in blue, the land grid cells with a frost-index higher than 0.57 for 0.5° grid, with the north located at the centre of the map. Overlaid on this map area are the limits of the permafrost zones defined by the International Permafrost Association (IPA) (Jones et al., 2009). The frost-index value cut-off at 0.57 results in a southern limit of permafrost that represents approximately the middle of the discontinuous zone with some areas showing better agreement than others.

Figure 10 represents the upscaling of the 0.5° data sets for mean frost index and permafrost coverage to the CLIMBER-2 land grid scale. It shows the percentage of land in each CLIMBER-2 size grid cell defined as permafrost (according to the 0.57 frost-index cut-off value shown in Fig. 8) plotted against the mean value of frost index for the same grid cell.

Table 1. Simulated climates used in this study.

Date	Event
LGM (equilibrium)	Obtained after an 80 kyr spin-up with glacial CO_2 levels of 190 ppmv, reduced ocean volume, LGM ice sheets, LGM insolation, LGM runoff. Carbonate compensation in the ocean (Brovkin et al., 2002). Sea-level effects on coast lines are not included; land area is as PI (equilibrium). The continental shelves exposed at LGM are not accounted for in this model set-up because the fate of any carbon that may have accumulated on these shelves is not well constrained. The long time of spin-up, 80 kyr, is required to allow the soil carbon pools to equilibrate.
PI (equilibrium)	Obtained after 40 kyr spin-up with pre-industrial CO_2 levels of 280 ppmv, present-day ocean volume, present-day ice sheets, insolation, and land run-off. The 40 kyr spin-up time allows soil carbon pools to equilibrate.
PI (transient)	End of a 21 kyr simulation of a transient deglaciation that has the LGM equilibrium climate as a start point at 21 kyr BP. The PI (transient) is the climate at 0 yr BP. The transient deglaciation has evolving ice sheets scaled to sea-level, increasing ocean volume, insolation changes (seasonality), carbonate compensation and LGM runoff. This transient PI climate is required to account for the long time to equilibrium of the permafrost-affected soil carbon pools. In order to compare model output with ground-data the PI(transient) provides a more realistic model output.

Circled points in Fig. 9 are where the grid cell has a large fraction of ocean (more than 75 %), and the milder ocean temperatures in winter reduce the mean frost-index value of the whole grid cell. The dashed line shows a well-defined sigmoid function that relates frost index to permafrost percentage of the land. We employ this relationship to predict permafrost area in CLIMBER-2, as the frost index can be calculated within the model from modelled daily temperatures. Permafrost fraction is thus modelled as:

$$P_{\text{landfraction}} = A(0.976 + \frac{\beta}{\sqrt{(1+\beta^2)}}) - 0.015, \quad (5)$$

where A and β are defined in Table 2 and the model described in Sect. 3.5. Frost index is calculated from modelled daily surface temperatures and corrected for snow cover. The snow correction in our model is achieved using a simple linear correction of surface–air temperature, using snow thickness to estimate the snow–ground interface temperature. This correction is based on data from Taras et al. (2002). The snow correction performs reasonably well in CLIMBER-2 compared to measurement data from Morse and Burn (2010) and Zhang (2005). This is because the large grid-cell size results in non-extreme snow depths and air surface temperatures. The snow correction is described in Appendix B. Equation (6) shows this linear model for snow correction, which is only applied for daily mean surface air temperatures lower than −6 °C. This snow–ground interface temperature is used to calculate the freeze index (DDF_{sc}) in Eq. (4).

$$T_{\text{g.i}} - T_{\text{surf}} - \frac{(T_{\text{surf}} + 6) \cdot \text{SD}}{100}, \quad (6)$$

where $T_{\text{g.i}}$ is ground interface temperature (°C), T_{surf} is surface air temperature (°C) and SD is snow depth (cm). Overall the effect of the snow correction within the model produced a maximum decrease in permafrost area of 8 % (compared to the uncorrected version) in the most affected grid cell for the PI(eq) simulation and is therefore significant.

Table 2. Permafrost area model settings for Eq. (5).

	A	β
HIGH	0.58	$22(F_{sc} - 0.58)$
MED	0.555	$21(F_{sc} - 0.59)$
LOW-MED	0.54	$20.5(F_{sc} - 0.595)$
LOW	0.53	$20(F_{sc} - 0.6)$

3.4 Permafrost extent tuning

Using the snow-corrected frost-index value, four permafrost extent models representing the range of values for permafrost area from Zhang et al. (2000) were determined. The model settings are shown in Table 2 and refer to A and β from Eq. (5). $P_{\text{landfraction}}$ is limited between 0 and 1, and the functions are plotted in Fig. 11. These settings were identified by adjusting the sigmoid function to obtain total permafrost area values at the PI(eq) simulation similar to the Zhang et al. (2000) areal estimates of permafrost and to maximise the difference in area between the PI(eq) and LGM(eq) simulations permafrost extent. More complex models underestimate permafrost extent at LGM (Levavasseur et al., 2011; Saito et al., 2013) quite significantly, and so by maximising the difference between PI and LGM permafrost, we reduce the underestimate as far as possible for LGM permafrost extent.

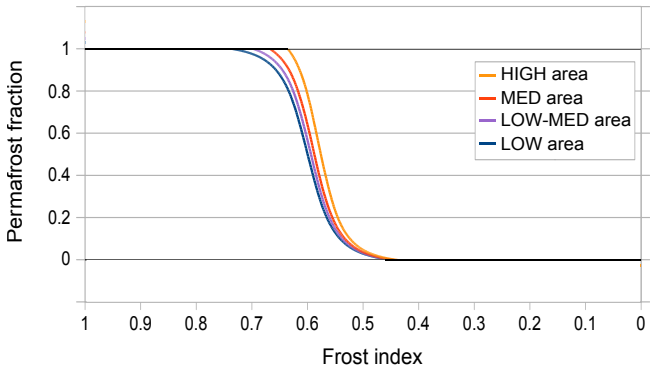

Figure 11. CLIMBER-2P model for permafrost fraction of the land in a grid cell from frost index (snow corrected). Range of areas is within the range of estimates for present-day land area underlain by permafrost by Zhang et al. (2000). Permafrost fraction is limited between 0 and 1. Zhang estimate for total permafrost area is 12.21 to 16.98×10^6 km^2. Listed from HIGH to LOW, model output is 16.35, 14.87, 14.00 and 13.21×10^6 km^2.

3.5 Tuning the soil carbon model

Soil carbon content is controlled by the balance between soil carbon uptake and soil carbon decomposition. There are four soil carbon pools in CLIMBER-2: $\text{Soil}_{\text{fast}}$: trees derived and grass derived; $\text{Soil}_{\text{slow}}$: trees derived and grass derived (Eq. 1). $\text{Soil}_{\text{fast}}$ have shorter carbon residence times than $\text{Soil}_{\text{slow}}$, so soil decays more quickly in $\text{Soil}_{\text{fast}}$ pools. The tunable constants a and b (Eq. 3) are independently applied for $\text{Soil}_{\text{fast}}$ and $\text{Soil}_{\text{slow}}$, so carbon can be placed relatively more in the $\text{Soil}_{\text{fast}}$ ($\text{Soil}_{\text{slow}}$) pool as required in model tuning. Carbon is lost from permafrost soils as the permafrost fraction of a grid cell reduces. If there is relatively more (less) carbon in the $\text{Soil}_{\text{fast}}$ pool, this results in carbon that decays more quickly (more slowly) when the permafrost thaws.

At LGM, the area of permafrost on land was larger than today (Vandenberghe et al., 2012), but not much information on soil carbon has been conserved, especially if it has long since decayed as a result of permafrost degradation during the last termination. To constrain the total carbon content in permafrost soils we use the estimates of Ciais et al. (2012); for total land carbon these are 3640 ± 400 GtC at LGM and 3970 ± 325 GtC at PI, with a total change of $+330$ GtC between LGM and PI. The standard CLIMBER-2 model predicts total land carbon stocks of 1480 GtC at LGM and 2480 GtC at PI, showing good agreement with the active-land-carbon estimates of Ciais et al. (2012) (of 1340 ± 500 GtC LGM and 2370 ± 125 GtC PI). Any "new" soil carbon is created via the permafrost-carbon mechanism and is assumed to be equivalent to the inert land carbon pool estimates of Ciais et al. (2012). However, the dynamic behaviour of permafrost-carbon in changing climates is not well constrained and it is for this reason that a set of four dynamic settings were sought. Here the "speed" of the dynamic setting is determined by the ratio of total $\text{Soil}_{\text{fast}}$ pool to $\text{Soil}_{\text{slow}}$ pool carbon (fp / sp), with the "slow" dynamic being fp / sp < 0.5, "medium" being fp / sp 0.5 to 1, "fast" being fp / sp 1 to 1.5 and "extra-fast" being fp / sp > 1.5 for the PI-equilibrium simulation. The variables "a" and "b" shown in Eq. (3) were set and each setting used to run a PI(equilibrium), LGM(equilibrium) and PI(transient) simulation to identify the settings that resulted in total land carbon pools in agreement with the Ciais et al. (2012) estimates.

Table 3. Selected settings for permafrost decomposition function, where subscript indicates the soil pool. Permafrost area model is LOW-MEDIUM for all.

	Constants' settings for Eq. (3)			
Dynamic settings	a fast	b fast	a slow	b slow
Slow	10	10	10	10
Medium	20	40	1	3
Fast	60	50	0	1
Xfast	60	80	0.1	0.1

The LGM is conventionally defined as being the period around 21 kyr BP, when large parts of north America were underneath the Laurentide ice sheet. According to their time-to-equilibrium (the slow carbon accumulation rate), soils in this location now free of ice may not yet have reached equilibrium. Furthermore, climate has changed significantly since the LGM so permafrost soils anywhere may not be currently in equilibrium (Rodionov et al., 2007), again due to their slow carbon accumulation rates. Due to this the PI(tr) simulation model output for total land carbon was used to tune the total land carbon stocks, as it includes a receding Laurentide ice sheet. At LGM, ice sheets were at maximum extent, so the problem of land being newly exposed does not occur in the model. For this reason, the LGM(eq) simulation is used to tune total land carbon for the LGM.

Details of the tuning for total land carbon stocks are available in Appendix C. It was found that only one permafrost area setting, the LOW-MEDIUM area, provided an acceptable range of dynamic settings, as defined by the ratio of fast to slow soil carbon. The four selected dynamics settings are shown in more detail in Fig. 12 for total land carbon stock, atmospheric CO_2 and ratio of fast to slow soil carbon pool. The a and b values for these settings are shown in Table 3.

To evaluate the effect of the different dynamic settings we ran an equilibrium PI simulation for all four selected settings for 40 kyr, followed by a permafrost switch-off for a further 10 kyr. Figure 13 shows the global total land carbon stocks for this experiment. The period between 0–40 k simulation years demonstrates the transient effects of the slow accumulation rates in permafrost soils. Depending on the dynamic setting, the total land carbon takes more than 40 kyr to fully equilibrate in PI climate conditions. On permafrost switch-off, from 40 k simulation years, the soil carbon pre-

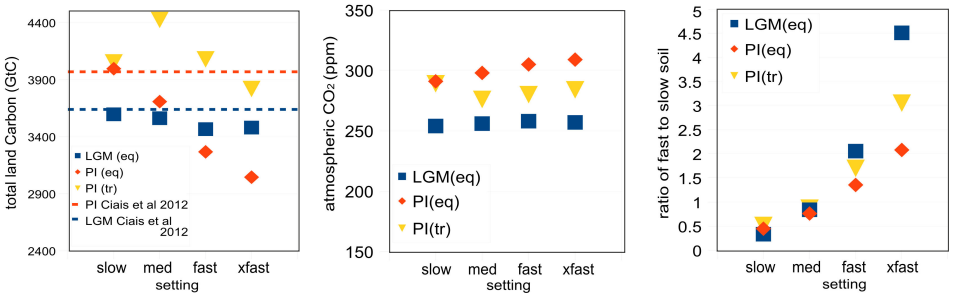

Figure 12. Chosen dynamic settings for the range of permafrost-carbon dynamics. Left: total land carbon with Ciais et al. (2012) estimates as dashed lines. Middle: atmospheric CO_2 (ppm). Right: ratio of all fast to all slow soil pools, indicating the speed of response of the soil carbon to changing climate.

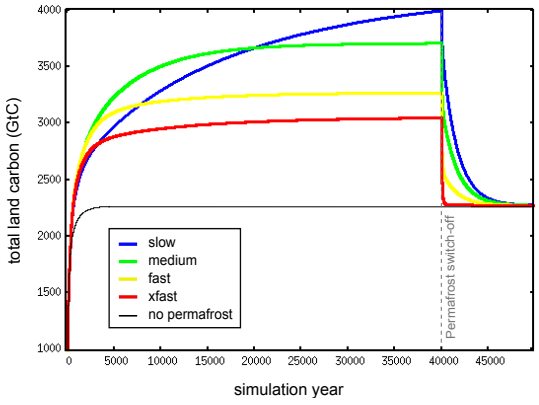

Figure 13. Total land carbon (GtC) for the PI(eq) simulation followed by a permafrost switch-off at 40 k simulation years representing a complete and immediate permafrost thaw, demonstrating the different dynamic behaviour of each dynamic setting.

viously held in permafrost soils is quickly released to the atmosphere, at a rate dependent on the dynamic setting. The xfast setting entails releasing all excess carbon within hundreds of years and the slow setting around 8000 years after total permafrost disappearance. Currently, the most appropriate carbon dynamic setting is unconstrained by measurement data. It is for this reason that the permafrost-carbon dynamics settings cover a large range. They are intended to be used in transient model simulations to better constrain permafrost-carbon dynamics in changing climate. It should be noted that the PI(eq) simulation was not used to tune the model, i.e. was not used to compare model output to Ciais et al. (2012) PI total land carbon stocks. Figure 13 demonstrates only the range of dynamic response for all four settings. This PI(eq) simulation also demonstrates the difference between transient vs. equilibrium PI simulations. The slow dynamic equilibrates (after more than 40 kyr) at far higher total carbon stocks than the xfast dynamic, but for the PI(tr) simulation these two settings show very similar total land carbon stocks (we selected them for this behaviour).

4 Model performance

Hereafter, "CLIMBER-2P" denotes the model in which the permafrost-carbon mechanism operates fully coupled within the dynamic vegetation model.

4.1 Permafrost areal coverage and spatial distribution

Figure 14a shows the spatial pattern of permafrost as predicted in CLIMBER-2P with the snow correction included for the LOW-MEDIUM area setting. The modelled PI(tr) permafrost extent estimates fairly well the location of the present-day southern boundary of the discontinuous permafrost zone (Jones et al., 2009), with overestimate of permafrost extent in the western Siberian grid cell, and underestimate over the Himalayan plateau. Total permafrost area extent is shown in Table 4.

Comparing this to performance of other models (Levavasseur et al., 2011), the PI(eq) total permafrost area is closer to Zhang et al. (2000) estimates, but it must be kept in mind that for CLIMBER-2P the area was tuned to be in agreement with a mean estimate from Zhang et al. (2000). The PI(tr) total permafrost area is higher by around 4×10^6 km^2 compared to the PI(eq). This is due to the North Pacific region being colder in PI(tr) than that of the PI(eq) simulation, and may be related to the land run-off, which is kept at LGM settings for the transient simulations. For the LGM period, the best PMIP2 model in the Levavasseur study (interpolated case) underestimated total permafrost area by 22 % with respect to data estimates (of 33.8×10^6 km^2), and the "worst" model by 53 %, with an all-model-median value of 47 % underestimate. The LOW-MEDIUM CLIMBER-2P setting gives an LGM total permafrost area underestimate of around 40 %, slightly better than the median for PMIP2 models' permafrost area.

Figure 14b shows the LGM CLIMBER-2P permafrost extent with the reconstructed continuous and discontinuous southern boundaries (Vandenberghe et al., 2012; French and Millar, 2013) overlaid. In the LGM simulation for CLIMBER-2P, coastlines do not change so the Siberian Shelf

Table 4. Modelled permafrost-affected land area and data-based estimates.

	Permafrost area ($\times 10^6$ km^2) (land underlain by permafrost)		
Permafrost model area setting	Pre-industrial climate (equilibrium)	Pre-industrial climate (transient)	Glacial climate
LOW-MEDIUM	14.0	18.4	20.7
Data estimate	12.21 to 16.98 (Zhang et al., 2000)		33.8 (Levavasseur et al., 2011) 40 (Vandenberghe et al., 2012)

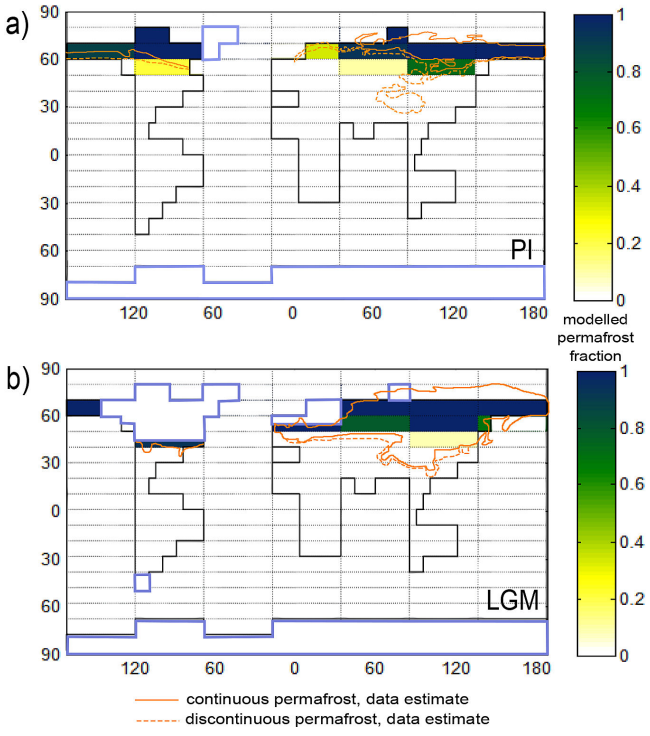

Figure 14. Modelled permafrost area for **(a)**: PI(tr) simulation, **(b)** LGM(eq) simulation for LOW-MEDIUM permafrost area. Overlaid in orange are data estimates from Circumpolar Atlas (Jones et al., 2009) for the present day, Vandenberghe et al. (2008) for LGM Eurasia, French and Millar (2013) for LGM N. America.

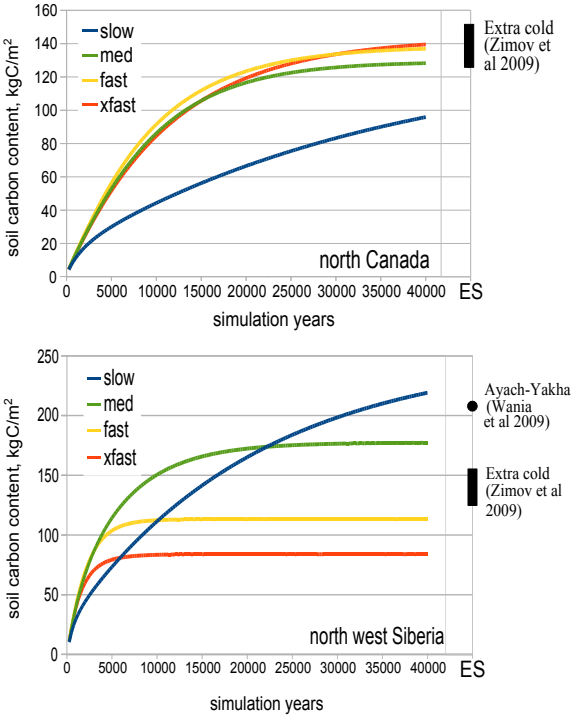

Figure 15. Modelled PI(eq) simulation output for total soil column carbon content for two grid cells. ES is equilibrium state (> 50 kyr).

and other exposed coastlines in the northern polar region are not included in the CLIMBER-2P permafrost area estimate. These coastal shelves cover an estimated area of 5 to 7×10^6 km^2. Another area that is not diagnosed as permafrost in CLIMBER-2P is the Tibetan plateau, which would be an additional estimated 6×10^6 km^2. If these two regions were added (totalling around 12×10^6 km^2) to the LGM area estimate it would bring the modelled permafrost area (then totalling around 33×10^6 km^2) much closer to the data estimate as reported in the Levavasseur et al. (2011) study. The permafrost extent model is dependent on the CLIMBER-2P modelled climate. The very large grid cell size of CLIMBER-2P means that modelled mountainous regions such as the Tibetan plateau are problematic, resulting in a possible too-warm climate (compared to the real world) in this region.

4.2 Soil carbon dynamics

Accumulation rates show general agreement with the Zimov et al. (2009) model and the Wania et al. (2009b) (LPJ) model, although the fast and xfast dynamic settings accumulate carbon faster than these comparison models. Figure 15 shows output for all permafrost dynamics for the PI (equilibrium) spin-up. The north-west Siberia site can be compared to the the Ayach-Yakha location from Wania et al. (2009b) and to the extra-cold conditions from Zimov et al. (2009). The Ayach-Yakha modelled site in Wania et al. (2009b) has a time to equilibrium of greater than 80 kyr and soil carbon content of greater than 200 kg m^{-2}; the Zimov model predicts

that 200 kg m^{-2} soil carbon content can be reached within 10 kyr in the top layer of the soil and 150 kg m^{-2} for the full soil column taking longer than $\sim$ 50 kyr to reach equilibrium. The N. Canada (Fig. 15) location takes a longer time to reach equilibrium than soils in the NW Siberia grid cell. NPP in the N Canada grid cell is less than one third of that for the NW Siberia grid cell. Due to the lower soil carbon input there is a lower range in the output between the different carbon dynamic settings for the N Canada grid cell. Northern Canada was underneath the Laurentide ice sheet at LGM. Since the demise of the Laurentide ice sheet around 13 kyr ago (Denton et al., 2010) there has not been enough time for these soils to equilibrate, which takes longer than 40 kyr according to our model. As well as this, this region has very high water contents (and islands) that are not represented in CLIMBER-2P, which may modify soil carbon concentrations. Although we do not account for water content, we can take account of the demise of the Laurentide ice sheet and the time that these soils have had to accumulate carbon. The PI climate condition and soil carbon content that we applied to tune and validate the model are the PI(tr), the transient simulation, which includes ice sheet evolution.

4.3 Soil carbon stocks

The total land carbon stocks were tuned using data from Ciais et al. (2012). An assumption made in this study is that all "extra" soil carbon, relative to the standard model, in the Arctic region is located in permafrost soils and only by the mechanism of increased soil carbon residence time in frozen soils. Table 5 shows the Ciais et al. (2012) land carbon pools values that have been used to tune this model. The standard model total land carbon (tlc) values are similar to the active land carbon stocks, with PI tlc at 2199 GtC and LGM tlc at 1480 GtC (shown in Table 7).

The soil types that are found in the continuous and discontinuous permafrost zone are the Cryosols (circumpolar atlas) or Gelisols (soil taxonomy). Within this group are subgroups: Turbels, which are subject to cryoturbation and characterise the continuous permafrost zone; Orthels, which are less affected by cryoturbation and are related to discontinuous permafrost; and Histels, which relate to peat growth (histosols) and have permafrost at less than 2 m depth. Histels are not directly represented in the simplified model, as they are dominated by peat growth (Sphagnum), a distinct PFT not represented in CLIMBER-2P.

The Tarnocai et al. (2009) SOCC estimates for the present day for relevant soils are shown in Table 6. Summing "All soils" with loess soils and Deltaic deposits gives the 1672 GtC estimated total SOCC for the permafrost region. The extra land carbon stocks created in our model in permafrost soils range between 1620 to 2226 GtC (Table 8) compared to Tarnocai et al. (2009) at 1672 GtC and to Ciais et al. (2012) at 1600 ± 300 GtC for inert land carbon for the present day. For the LGM climate, the model shows a range of 1987 to 2117 GtC for extra soil carbon compared to the Ciais estimate of 2300 ± 300 GtC for inert land carbon. The "medium" dynamic setting shows total land carbon stocks in the present day outside the range estimated by Ciais et al. (2012), However, during tuning (see Appendix C) this overestimate could not be improved upon.

4.4 Soil carbon contents validation

The carbon content of Orthels and Turbels decreases with depth, but high carbon contents are still found at depths of 3 m and more (Tarnocai et al., 2009). For Orthels (with alluvium), around 80 % of their carbon content was found in the top 200 cm, and for Turbels 38 % of carbon content was found in the top 100 cm. Based on these values, to compare the CLIMBER-2P output with ground spatial data, it is assumed that 40 % of the modelled total soil-column carbon is located in the top 100 cm for all permafrost-affected soils.

Soil carbon data from Hugelius et al. (2013) were used to compare against the CLIMBER-2P output. The Orthels and Turbels dominate the continuous and coldest permafrost areas, with Histels and other soils becoming more dominant towards the southern parts of the permafrost region. As no peatlands or wetlands are represented in our simplified model, only Orthel and Turbel soils were used as comparison points for SOCC. SOCC data from Hugelius et al. (2013), for grid cells with 50 % or more Orthel and Turbel soils, were upscaled to the CLIMBER-2P grid. These mean SOCC data values for the top 1 m of soil were plotted against CLIMBER-2P model output for matching grid cells; this is shown in Fig. 16. Also shown in Fig. 16 is the standard model output, which has no permafrost mechanism. Two grid cells show very much higher SOCC than data suggest, with around a 3-fold overestimate, and are located in Siberia. All other grid cells are within a range of $\pm$80 %, heavily dependent on the soil carbon dynamic setting. The standard model shows progressively worse performance as mean SOCC increases in the data. The permafrost model shows an increasing SOCC trend more similar to data. The spatial location of SOCC can be compared to data using Fig. 17. The two grid cells with very high SOCC compared to data are central and eastern Siberia. These grid cells are both 100 % permafrost and have had a total of 101 kyr (80 k for LGM(eq) plus 21 k to PI(tr)) to accumulate carbon. This is in contrast to the North American continent grid cells, which were underneath the ice sheet until the deglaciation so have had less time to accumulate carbon.

The assumption that all permafrost region soil carbon acts as Turbels and Orthels has an impact on the physical location of the SOCC with respect to data. Turbels and Orthels are located in the northern parts of the permafrost zone, with Histels and other soils becoming more dominant to the south. Compared to SOCC in ground data (Fig. 17), a northern bias in SOCC is seen in model output, as expected. Histels (peatland soils) and other soil types of the permafrost zone, with

Table 5. Total land carbon stock estimates from Ciais et al. (2012).

Period	Total land carbon (GtC)	Active land carbon (GtC)	Inert land carbon (GtC)
Present day	3970 ± 325	2370 ± 125	1600 ± 300
LGM	3640 ± 400	1340 ± 500	2300 ± 300

Table 6. Permafrost region soil carbon stock estimates from Tarnocai et al. (2009).

Soil type	Depth		Soil carbon (GtC)
Gelisols	To 1 m	Turbels	211.9
		Orthels	51.3
		Histels	88.0
		All	351.5
	To 3 m	Turbels	581.3
		Orthels	53.0
		Histels	183.7
		All	818.0
All soils	To 1 m		495.8
	To 3 m		1024.0
Pleistocene loess	> 3 m		407
Deltaic	> 3 m		241

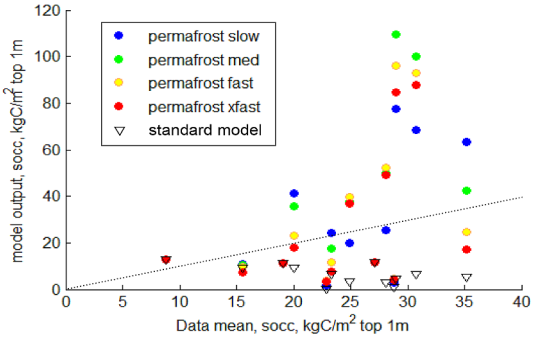

Figure 16. Modelled SOCC ($\mathrm{kgC\,m^{-2}}$) for the top 1 m plotted against SOCC data for the top 1 m of soil upscaled to the CLIMBER-2 grid scale. Circles are for the permafrost-carbon model (CLIMBER-2P); triangles are for the standard model (CLIMBER-2). Dotted line shows the 1 : 1 position. Points are SOCC $\mathrm{kgC\,m^{-2}}$.

an estimated 390 GtC (Tarnocai et al., 2009), are not represented in our model. If these were modelled they should increase SOCC in model output in the more southern part of the permafrost region, and parts of Canada. Large river deltas, which contain deltaic deposits of 241 GtC (Tarnocai et al., 2009), are also not represented in our model. One example of this is the Ob River and Gulf of Ob, located in western Siberia, which, combined with dominance of Histels in this region (Hugelius et al., 2013), cause a high SOCC in data. The model does not represent well the boreal forest belt (see Fig. 4), which is also located in the southern region of the permafrost zone. This results in carbon input to soils in this region being underestimated in our model.

Figure 18 shows the model outputs for the LGM climate. No soil carbon is present underneath ice sheets and the highest carbon concentrations are seen in present-day southeastern Russia and Mongolia, with quite high soil carbon concentrations in present-day northern Europe and northwestern Russia. Comparing this output to the permafrost extent model (Fig. 14), the SOCC is likely located too far north for the same reasons as the PI(tr) SOCC but also because permafrost extent is underestimated for the LGM(eq) climate. The northern China region, according to data, was continuous permafrost at LGM, as was the southwest Russia region. These regions would have higher SOCC in model output if the modelled permafrost area were closer to data estimates. The same would be true of the Siberian shelf. This means that the extra soil carbon tuned to the Ciais et al. (2012) estimate (Table 5) is more concentrated in a central band in Eurasia than the model would predict if permafrost extent were more like the data estimate for LGM.

5 Model applications and limitations

5.1 Applications

The simplified permafrost mechanism is intended to be used for the study of carbon-cycle dynamics on timescales of centuries/millennia and longer. It represents an improvement on the previous terrestrial carbon cycle model in CLIMBER-2, which did not include any effects of frozen soils. It is not intended for the study of carbon cycle dynamics on scales shorter than centuries due to the simplifications made and many processes not accounted for. The permafrost-carbon mechanism is dependent on the relationship between climate, soil carbon content and active layer thickness on the CLIMBER-2 grid scale. To apply this parameterisation of permafrost-carbon to other grid scales, the relationship of active layer thickness and climate variables would need to be reassessed. The relationship between permafrost fraction of a grid cell and SOCC is non-linear. The values for "a" and "b" would need to be retuned in order to output total land carbon stocks in agreement with Ciais et al. (2012) for grid scales different to the CLIMBER-2 grid.

The permafrost-carbon mechanism is fully dynamic and responds to changes in: insolation (orbit), atmospheric CO_2

Table 7. Modelled total land carbon stocks per model setting.

Total land carbon (GtC)	Standard model	With permafrost, per dynamic setting			
		Slow	Medium	Fast	Xfast
PI (transient)	2199	4052	4425	4079	3819
LGM (eq)	1480	3597	3563	3467	3481

Table 8. Modelled permafrost-region extra land carbon stocks with respect to standard model per model setting.

Extra soil carbon (GtC)	Standard model	With permafrost, per dynamic setting			
		Slow	Medium	Fast	Xfast
PI (transient)	0	1853	2226	1880	1620
LGM (eq)	0	2117	2083	1987	2001

(via changes in NPP and climate), and land area in response to coverage by ice sheets extending or contracting. This could not be easily achieved if a box model representation of permafrost-carbon were applied as the model response to the drivers (orbit, CO_2 and ice sheet) are dependent on spatial location.

5.2 Simplifications and limitations

The permafrost model does not make any changes to soil carbon based on hydrology or ice contents. Precipitation only affects vegetation growth, not soil formation.

No account is taken of the effect of peatland soils in permafrost regions as the PFT for Sphagnum species, which accounts for most of peat soil vegetation cover, is not included in the model. The effect of frozen ground inhibiting root growth (to depth) is not accounted for, which may have an impact on the GPP and soil formation in very cold regions.

During glacial climates, no extra land is exposed as sea level drops in the CLIMBER-2P model; all the carbon used to tune the carbon dynamics for the LGM period is located on land that is at present above sea-level.

Wetlands and river deltas increase the spatial spread of the soil carbon in the real world, and these are not represented in CLIMBER-2P. Therefore, it is also not intended that the spatial location of the highest soil carbon concentrations should be used as a very good indicator of the real world case.

Slow accumulation rates in permafrost soils result in the characteristic that in the real world during thaw (or deepening of the active layer) the youngest soils would decompose first. In CLIMBER-2P all soil is mixed, so the age of carbon down the soil column cannot be represented. This age of the soils is important for the correct modelling of ^{14}C then seen in the atmosphere. The model has no soil "depth" (only a carbon pool) so ^{14}C cannot be used as a useful tracer as part of CLIMBER-2P in its current configuration. The CLIMBER-2P model does have a ^{13}C tracer within the carbon cycle which is intended to be used in conjunction with the permafrost model to constrain carbon cycle dynamics.

The possible impact of high dust concentrations on soil formation during glacial climates is not accounted for in the model. Loess soils, those created by wind-blown dust or alluvial soils, are not represented. For our study it is assumed that the ratio of loess to non-loess soils is the same in the present day as it was during glacial climates. This is not the case in the real world, where high dust concentrations in the dry atmosphere increased loess deposition at LGM (Frechen, 2011). However, the LGM climate is only representative of the coldest and driest part of the last glacial period. Evidence suggests that soils were productive in cold conditions in the permafrost region of the last glacial period, with loess accumulation only more widely significant towards the harsh conditions of the LGM (Elias and Crocker, 2008; Chlachula and Little, 2009; Antoine et al., 2013; Willerslev et al., 2014).

No changes were made to the vegetation model or to controls on soil input, which are only dependent on temperature and NPP; the mammoth-steppe biome is not explicitly modelled (Zimov et al., 2012).

Underneath ice sheets soil carbon is zero; as an ice sheet extends over a location with soil carbon (and vegetation), that carbon is released directly into the atmosphere. As an ice sheet retreats and exposes ground, the vegetation (and soil) can start to grow again. So, our model does not account for any carbon that may have been buried under ice sheets (Wadham et al., 2012).

6 Conclusions/summary

This permafrost-carbon model is a simplified representation of the general effect of frozen ground on soil carbon decomposition. In the presence of frozen ground the soil carbon decays more slowly. The method by which permafrost is diagnosed relies only on the balance between warm (above

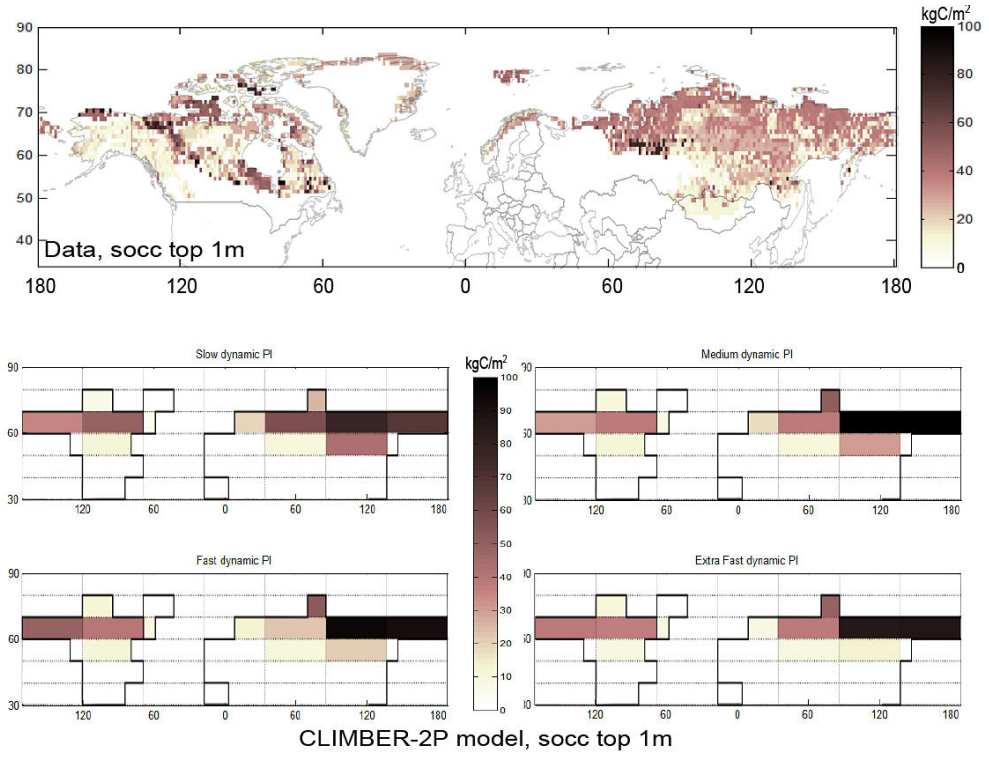

Figure 17. SOCC data (kgC m^{-2}) for the top 100 cm of soils, Hugelius et al. (2013) (top panels). Modelled PI(tr) SOCC (kgC m^{-2}) in permafrost soils for top 100 cm (lower panels).

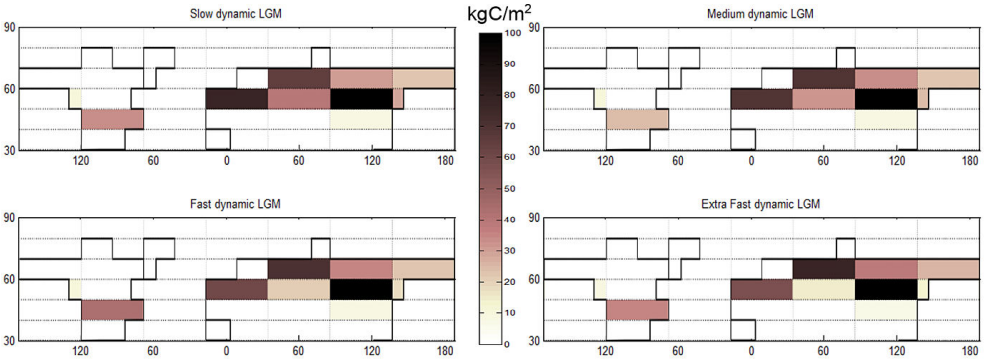

Figure 18. Modelled LGM(eq) SOCC (kgC m^{-2}) in permafrost soils for top 100 cm.

0 °C) and cold (below 0 °C) days, which removes the problem of compounding errors in thermal diffusion calculations (for example). As such, the permafrost-carbon model would perform just as well in distant past climates as it does in pre-industrial climate. In order to account for uncertainties in carbon accumulation and release rates in frozen (and thawing) soils, a range of dynamic settings are retained that agree with total land carbon estimates of Ciais et al. (2012). Due to the slow accumulation in permafrost soils, soil carbon has a long time to equilibrium and therefore the present-day climate must be treated as a transient state, not as an equilibrium state. We showed that the model performs reasonably well at pre-industrial and present-day conditions. The permafrost-carbon model creates a mechanism that slowly accumulates soil carbon in cooling or cold climates and quickly releases this high soil carbon in warming climates, caused either by changes in insolation patterns or by global increases in temperature and climatic changes due to greenhouse gas feedbacks and ocean circulation changes. It can thus be used to quantitatively evaluate the role of permafrost dynamics on the carbon build-up and release associated with this specific physical environment, over supra-centennial to glacial–interglacial timescales.

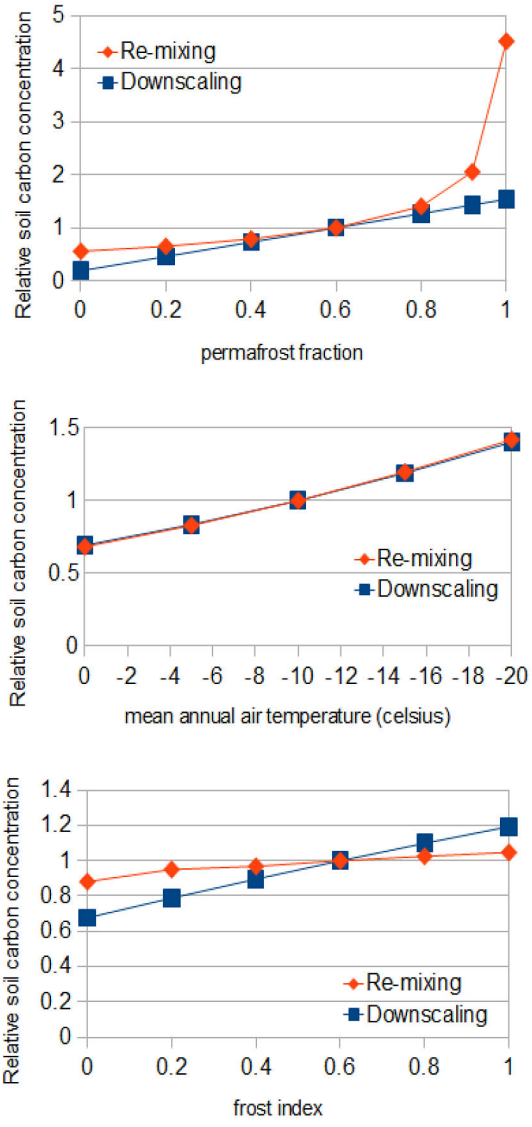

Figure A1. 1-D model output to compare the performance of the remixing (diamonds) and the sub-grid (squares) approaches. Top: MAT and frost index are constant, permafrost fraction is variable. Middle: frost index and permafrost fraction are constant, MAT is variable. Bottom: permafrost fraction and MAT are constant, frost index is variable. Input to soils from plant mortality and rainfall are constant for all.

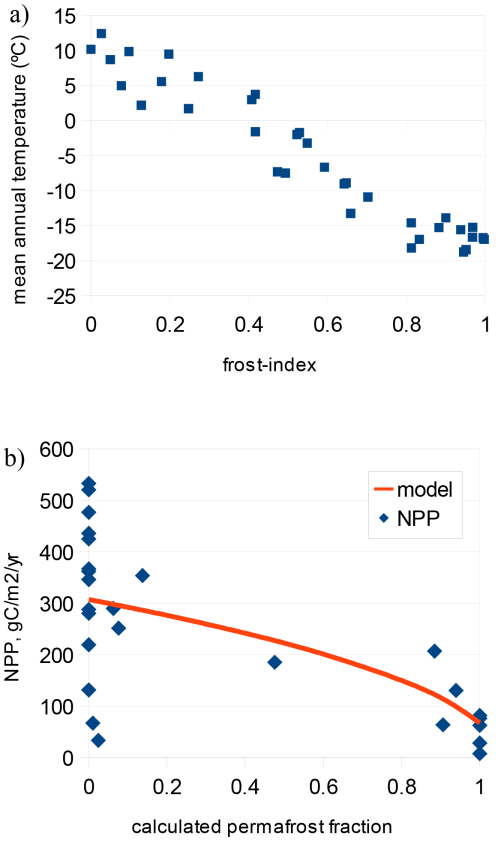

Figure A2. Relationships between frost index and MAT on the CLIMBER-2 grid scale (data from Zhang, 1998; Jones et al., 1999). Frost index determines permafrost fraction according to the model described in Sect. 3.2 (main text). NPP data for the permafrost zone from MODIS plotted against permafrost fraction (calculated from frost index values of Zhang, 1998) on the CLIMBER-2 grid scale.

Appendix A: 1-D models

Figure A1 shows the results of sensitivity experiments comparing these two approaches for one CLIMBER-2 land grid cell. Baseline settings of permafrost fraction = 0.6, frost index = 0.6 and mean annual air temperature = −10 °C have a relative soil carbon concentration of 1. The sub-grid method outputs a linear-type relationship between permafrost fraction and soil carbon stored. The remixing model outputs lower soil carbon concentration for lower fractional permafrost coverage rising quickly when permafrost fraction approaches 1. For the air temperature as variable, the two approaches show a similar response. For higher frost index the soil carbon concentration increases, with the sub-grid method showing slightly more sensitivity than the remixing model.

The variables of permafrost fraction, frost index and mean annual temperature are interrelated, and covary. The relationships between these variables are shown in Fig. A2a. For permafrost fraction to frost index, the relationship is defined as that determined in the main text for the CLIMBER-2 grid scale in Sect. 3.2.

When the effect of NPP is included, the equilibrium total carbon contents are scaled according to the relationship between NPP and permafrost fraction. Figure A2b shows MODIS data for NPP plotted against frost index (calculated from data from Zhang (1998) for freeze (DDF) and thaw (DDT) values to be used in Eq. (4) from the main text). These data are upscaled to the CLIMBER-2 grid and plotted against

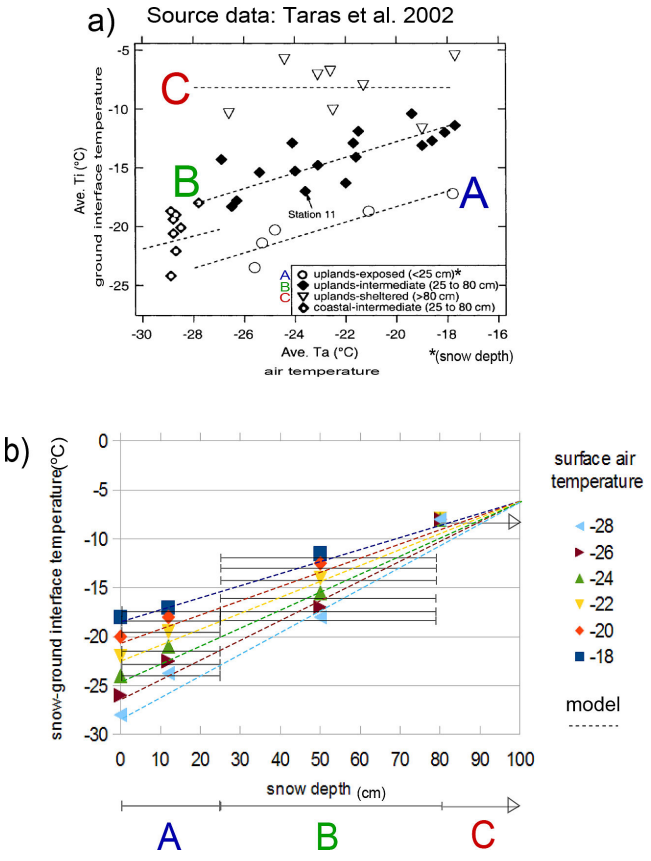

Figure B1. Snow correction model. Linear regressions of data points in **(a)** (dashed lines) are re-plotted as ground interface temperature per snow depth and shown in **(b)**. For each surface air temperature, a linear model based on snow depth predicts the snow–ground interface temperature.

permafrost fraction (calculated from the frost-index value). The values are only for NPP in the high northern latitudes.

To compare the model to data, it is assumed that 40 % of total soil column carbon is located in the top 1 m for permafrost soils (Tarnocai et al., 2009). To convert SOCC (top 1 m) to full column, the SOCC data are multiplied by (2.5· permafrost_fraction). This soil carbon content is plotted against calculated permafrost fraction; that is, using the model from Sect. 3.2 to get permafrost fraction from frost-index data. These SOCC data are then binned into 0.1 increases in permafrost fraction and the mean value is shown with ±1 sigma in Fig. 7 (main text).

Appendix B: Snow correction

B1 Linear model

In more complex physical models, snow correction of ground temperature is achieved by modelling the thermal diffusion characteristics of the snow cover, a function of snow depth

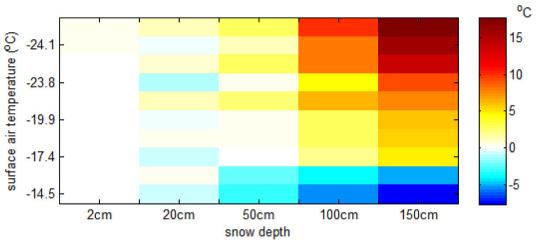

Figure B2. Model error when the linear snow correction model is used to predict temperatures at snow-depth or snow–ground interface for data from Morse and Burn (2010) (measurement data are down snow column temperatures). Positive numbers indicate that the linear model output is too warm compared to data.

and snow type (for example snow density). A thermal diffusion model is used to make an estimate of the snow–ground interface temperature using the surface air temperature; the thermal gradient is also dependent on the initial snow–ground interface temperature. Within the CLIMBER-2 model, snow is already modelled (Petoukhov et al., 2000) as it has a significant effect on overall climate (Vavrus, 2007). Snow depth in CLIMBER-2 is available as well as snow fraction per cell, but snow type and snow density are not individually modelled. Attempting to model the thermal diffusion in the snow does not make sense for CLIMBER-2, as with permafrost location. Rather the approach is to use measurement data to create a general relationship between air temperature and snow–ground interface temperature based only on the snow depth.

The snow correction linear model is based on data from Taras et al. (2002) giving a correction for snow–ground interface temperature from snow depth and air temperature. Figure B1a shows the data from Taras et al. (2002) and the linear regressions (labelled as A, B and C) of these data re-plotted per snow depth (Fig. B1b). Equation (B1) shows this linear model for snow correction, which is only applied for surface air temperatures lower than −6 °C. This snow–ground interface temperature is used to calculate the freeze index (DDF_{sc}) in Eq. (4) in the main text.

$$T_{gi} = T_{surf} - \frac{(T_{surf} + 6) \cdot SD}{100}, \quad \text{(B1)}$$

where T_{gi} is ground interface temperature (°C), T_{surf} is surface air temperature (°C) and SD is snow depth (cm).

B2 Snow correction validation

This simple snow correction was tested against data from Morse and Burn (2010). Figure B2 shows the error made by the linear model when used to predict the snow–ground interface temperature (or snow depth temperature) from Morse and Burn measurement data. In the more extreme conditions, the error of the linear model is far higher, for example in deep snow and cold temperatures. Figure B3 shows the

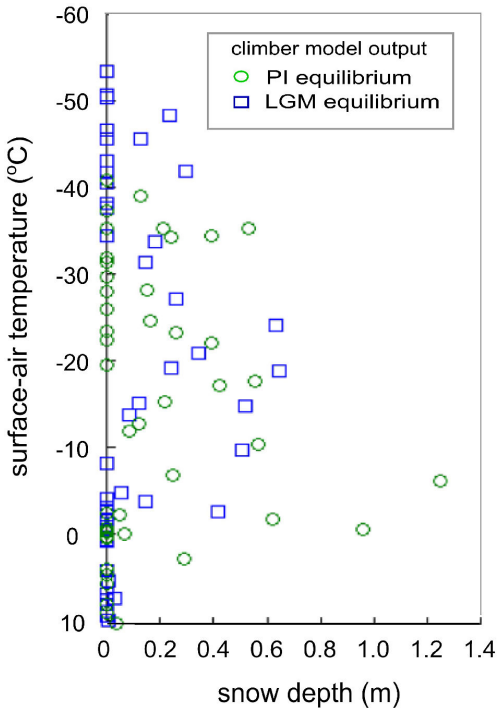

Figure B3. CLIMBER-2 model output for snow depth (m) plotted against surface air temperature (°C) for the PI(eq) (green circles) and LGM(eq) (blue squares) climates. Model output does not show extreme conditions for snow cover due to the very large grid-cell size.

outputs from CLIMBER-2 for snow depths plotted against surface air temperatures for the PI(eq) pre-industrial climate and LGM(eq) glacial climate, for all grid cells. The large CLIMBER-2 grid size means that extreme conditions are not present in the model output. Comparing Figs. B2 and B3 shows that the linear correction can provide an estimated confidence within ±8 °C for the deepest snow cover and highest temperatures of CLIMBER-2P data output, and within ±2 °C for the majority of CLIMBER-2P data outputs. A similar performance is found when comparing to snow thickness and snow–ground interface temperatures from Zhang (2005) for a site in Zyryanka, Russia. The most extreme temperatures and snow conditions produce a larger error from the linear model, but the intermediate conditions, those seen in CLIMBER-2P data points, agree better with the data. Overall the effect of the snow correction within the model produced a maximum decrease in permafrost area of 8 % (compared to the uncorrected version) in the most affected grid cell for the PI(eq) simulation and is therefore significant.

Appendix C: Tuning for total land carbon at the LGM and PI

Table C1 shows all the settings for "*a*" and "*b*" per soil pool (Eq. (3), main text) that were tested to obtain total soil carbon contents for the LGM and the PI simulations. Figure C1 shows the modelled total land carbon (GtC) for all simulations sorted by permafrost area function. Green dashed lines on the LOW-MEDIUM area setting indicate the dynamic settings chosen to represent the "slow", "medium", "fast" and "extra-fast" permafrost-carbon dynamic settings. The total land carbon content is clearly very sensitive to permafrost area, and despite many simulation tunings only the LOW-MEDIUM area setting provided a good enough range of dynamics that could be used to later investigate the permafrost-carbon dynamics. Within the settings chosen, the "medium" dynamic setting overestimated the present-day total land carbon estimate from Ciais et al. (2012), but further tuning experiments did not improve this overestimate.

Table C1. All settings for Eq. (3) (main text) used to tune total land carbon and permafrost-carbon dynamics.

Area: LOW				
	a fast	*b* fast	*a* slow	*b* slow
1	30	30	2	2
2	40	30	2	2
3	50	50	2	2
4	50	50	3	3
5	20	20	10	10
6	10	10	20	20
7	55	45	3	2
8	70	60	0	1
9	60	70	2	2
10	80	70	0	1
11	100	90	0	1
12	150	100	0	0.5
13	100	150	0	0.5
14	75	200	0	0.5
15	20	20	2	2
16	60	50	0	1

Area: LOW-MED				
	a fast	*b* fast	*a* slow	*b* slow
1	50	40	0	0.5
2	21	20	2	2
3	10	10	10	10
4	60	50	0	1
5	50	60	0	1
6	10	30	1	3
7	20	40	1	3
8	5	50	1	3
9	30	70	0	1
10	50	5	3	1
11	45	30	3	2
12	45	25	3	2
13	40	20	3	2
14	60	80	0.1	0.1
15	10	40	1	4
16	5	55	1	2

Area: MED				
	a fast	*b* fast	*a* slow	*b* slow
1	50	40	0	0.5
2	20	20	2	2
3	10	10	10	10
4	30	50	0	0.5
5	60	50	0	1

Area: HIGH				
	a fast	*b* fast	*a* slow	*b* slow
1	30	30	2	2
2	15	30	1	2
3	15	15	15	15
4	10	30	0	1
5	5	45	0	2
6	4	8	12	16
7	8	35	0	1
8	3	8	12	16
9	1	35	1	2
10	30	10	1	1
11	0.5	40	0.5	2.5
12	3	7	11	15
13	0.2	45	0.2	3
14	1	100	0	1
15	20	30	0	1
16	70	40	0	0.5
17	20	20	2	2
18	60	50	0	1

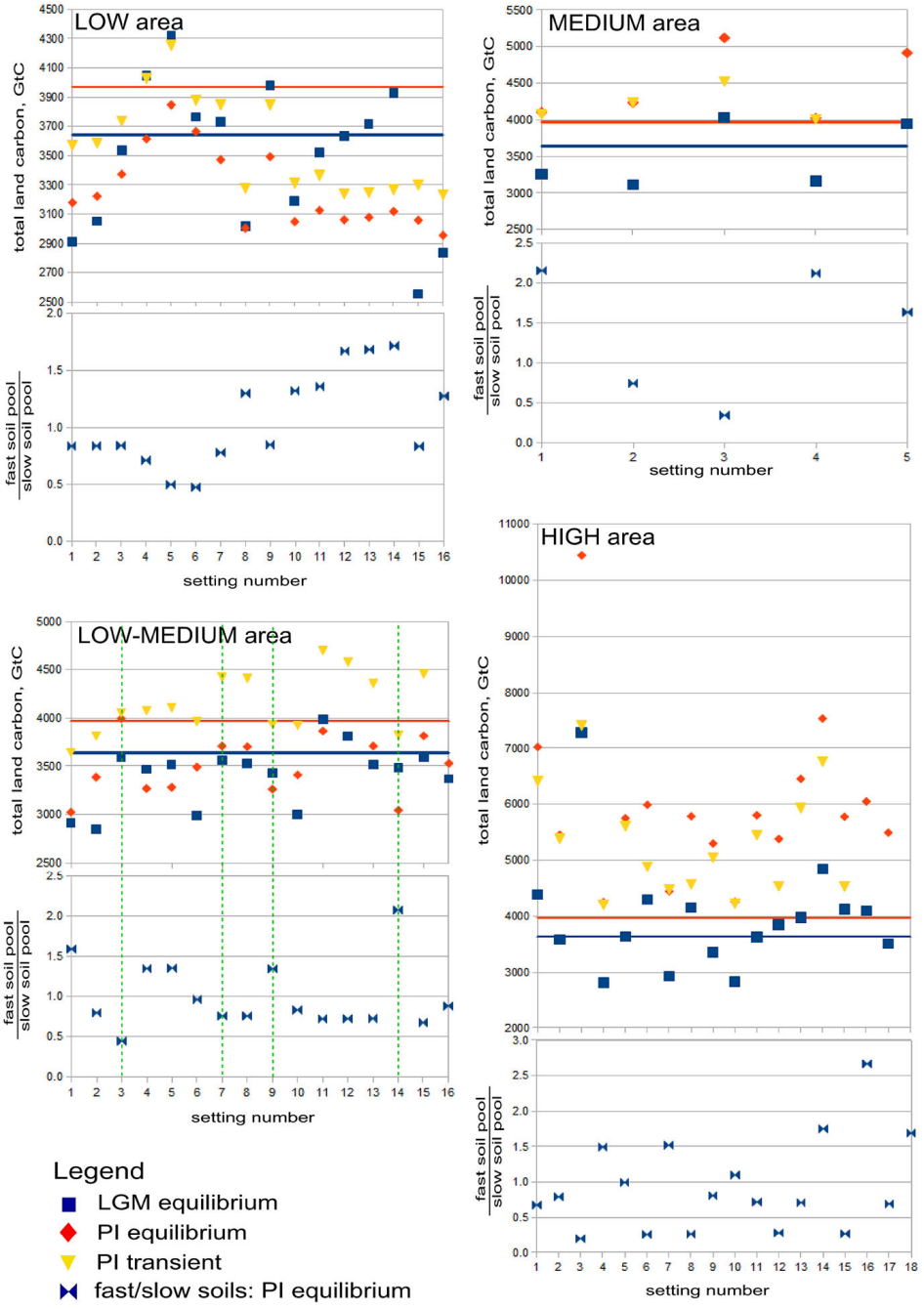

Figure C1. Modelled total land carbon stocks, and ratio of fast soils to slow soils for all settings used to tune the permafrost-carbon dynamics. Blue squares are for the LGM(eq) simulation, red diamonds are for the PI(eq) simulation and yellow triangles are for the PI(tr) simulation. Horizontal lines show the total land carbon estimates of Ciais et al. (2012). Green dashed lines indicate the chosen dynamic settings where LGM(eq) and PI(tr) show best agreement with Ciais et al. (2012) estimates.

Acknowledgements. The research leading to these results has received funding from the European Community's Seventh Framework Programme (FP7 2007–2013) under Grant 238366 (GREENCYCLES II) and under grant GA282700 (PAGE21, 2011–2015). D. M. Roche is supported by INSU-CNRS and by NWO under project no. 864.09.013.

Edited by: A. Stenke

References

Aleksandrova, L. N.: Processes of humus formation in soil, Proceedings of Leningrad Agricultural Institute, Leningrad, 142, 26–82, 1970 (in Russian).

Alexee, V. A., Nicolsky, D. J., Romanovsky, V. E., and Lawrence, D. M.: An evaluation of deep soil configurations in the CLM3 for improved representation of permafrost, Geophys. Res. Lett., 34, L09502, doi:10.1029/2007GL029536, 2007.

Antoine, P., Rousseau, D. D., Degeai, J. P., Moine, O., Lagroix, F., Fuchs, M., and Lisá, L.: High-resolution record of the environmental response to climatic variations during the Last Interglacial–Glacial cycle in Central Europe: the loess-palaeosol sequence of Dolní Věstonice (Czech Republic), Quaternary Sci. Rev., 67, 17–38, 2013.

Bouttes, N., Roche, D. M., and Paillard, D.: Impact of strong deep ocean stratification on teh glacial carbon cycle, Paleooceanography, 24, PA3202, doi:10.1029/2008PA001707, 2009.

Bouttes, N., Paillard, D., Roche, D. M., Waelbroeck, C., Kageyama, M., Lourantou, A., Michel, E., and Bopp, L.: Impact of oceanic processes on the carbon cycle during the last termination, Clim. Past, 8, 149–170, doi:10.5194/cp-8-149-2012, 2012.

Brovkin, V., Ganopolski, A., and Svirezhev, Y.: A continuous climate-vegetation classification for use in climate-biosphere studies, Ecol. Model., 101, 251–261, 1997.

Brovkin, V., Ganopolski, A., Archer, D., and Rahmstorf, S.: Lowering of glacial atmospheric CO_2 in repsonse to changes in oceanic circulation and marine biogeochemistry, Paleoceanography, 22, PA4202, doi:10.1029/2006PA001380, 2007.

Brown, J., Hinkel, K., and Nelson, F.: Circumpolar Active Layer Monitoring (CALM) Program Network, Boulder, Colorado USA: National Snow and Ice Data Center, 2003.

Chlachula, J. and Little, E.: A high-resolution Late Quaternary climatostratigraphic record from Iskitim, Priobie Loess Plateau, SW Siberia, Quaternary Int., 240, 139–149, 2011.

Ciais, P., Tagliabue, A., Cuntz, M., Bopp, L., Scholze, M., Hoffman, G., Lourantou, A., Harrison, S. P., Prentice, I. C., Kelley, D. I., Koven, C., and Piao, S. L.: Large inert carbon pool in the terrestrial biosphere during the Last Glacial Maximum, Nat. Geosci., 5, 74–79, doi:10.1038/NGEO1324, 2012.

Collins, M., Knutti, R., Arblaster, J., Dufresne, J.-L., Fichefet, T., Friedlingstein, P., Gao, X., Gutowski, W. J., Johns, T., Krinner, G., Shongwe, M., Tebaldi, C., Weaver, A. J., and Wehner, M.: Long-term Climate Change: Projections, Commitments and Irreversibility, in: Climate Change 2013: The Physical Science Basis. Contribution of Working Group I to the Fifth Assessment Report of the Intergovernmental Panel on Climate Change, edited by: Stocker, T. F., Qin, D., Plattner, G.-K., Tignor, M., Allen, S. K., Boschung, J., Nauels, A., Xia, Y., Bex, V., and Midgley, P. M., Cambridge University Press, Cambridge, United Kingdom and New York, NY, USA, 2013.

Dankers, R., Burke, E. J., and Price, J.: Simulation of permafrost and seasonal thaw depth in the JULES land surface scheme, The Cryosphere, 5, 773–790, doi:10.5194/tc-5-773-2011, 2011.

Denton, G. H., Anderson, R. F., Toggweiler, J. R., Edwards, R. L., Schaefer, J. M., and Putnam, A. E.: The last glacial termination, Science, 328, 1652–1656, 2010.

Ekici, A., Beer, C., Hagemann, S., Boike, J., Langer, M., and Hauck, C.: Simulating high-latitude permafrost regions by the JSBACH terrestrial ecosystem model, Geosci. Model Dev., 7, 631–647, doi:10.5194/gmd-7-631-2014, 2014.

Elias, S. A. and Crocker, B.: The Bering Land Bridge: a moisture barrier to the dispersal of steppe–tundra biota?, Quaternary Sci. Rev., 27, 2473–2483, 2008.

Fischer, H., Schmitt, J., Lüthi, D., Stocker, T. F., Tschumi, T., Parekh, P., and Wolff, E.: The role of Southern Ocean processes in orbital and millennial CO_2 variations – A synthesis, Quaternary Sci. Rev., 29, 193–205, 2010.

Frechen, M.: Loess in Eurasia, Quaternary Int., 234, 1–3, 2011.

French, H. M. and Millar, S. W. S.: Permafrost at the time of the Last Glacial Maximum (LGM) in North America, Boreas, 43, 667–677, doi:10.1111/bor.12036, 2013.

Ganopolski, A., Petoukhov, V., Rahmstorf, S., Brovkin, V., Claussen, M., Eliseev, A., and Kubatzki, C.: CLIMBER-2: a climate system model of intermediate complexity, Part II: model sensitivity, Clim. Dynam., 17, 735–751, 2001.

Gouttevin, I., Menegoz, M., Dominé, F., Krinner, G., Koven, C., Ciais, P., Tarnocai, C., and Boike, J.: How the insulating properties of snow affect soil carbon distribution in the continental pan-Arctic area, J. Geophys. Res.-Biogeo., 117, G02020, doi:10.1029/2011JG001916, 2012.

Harden, J. W., Koven, C. D., Ping, C. L., Hugelius, G., McGuire, A. D., Cammill, P., Jorgenson, T., Kuhry, P., Michaelson, G. J., O'Donnell, J. A., Schuur, E. A. G., Tarnocai, C., Johnson, K., and Grosse, G.: Field information links permafrost carbon to physical vulnerabilities of thawing, Geophys. Res. Lett., 39, L15704, doi:10.1029/2012GL051958, 2012.

Hugelius, G., Tarnocai, C., Broll, G., Canadell, J. G., Kuhry, P., and Swanson, D. K.: The Northern Circumpolar Soil Carbon Database: spatially distributed datasets of soil coverage and soil carbon storage in the northern permafrost regions, Earth Syst. Sci. Data, 5, 3–13, doi:10.5194/essd-5-3-2013, 2013.

Jones, A., Stolbovoy, V., Tarnocai, C., Broll, G., Spaargaren, O., and Montanarella, L.: Soil Atlas of the Northern Circumpolar Region, European Commission, Office for Official Publications of the European Communities, Luxembourg, 142 pp., 2009.

Koven, C., Friedlingstein, P., Ciais, P., Khvorostyanov, D., Krinner, G., and Tarnocai, C.: On the formation of high-latitude soil carbon stocks: Effects of cryoturbation and insulation by organic matter in a land surface model, Geophys. Res. Lett., 36, L21501, doi:10.1029/2009GL040150, 2009.

Koven, C. D., Riley, W. J., and Stern, A.: Analysis of permafrost thermal dynamics and response to climate change in the CMIP5 Earth System Models, J. Climate, 26, 1877–1900, 2013.

Levavasseur, G., Vrac, M., Roche, D. M., Paillard, D., Martin, A., and Vandenberghe, J.: Present and LGM permafrost from climate simulations: contribution of statistical downscaling, Clim. Past, 7, 1225–1246, doi:10.5194/cp-7-1225-2011, 2011.

Lourantou, A., Lavric, J. V., Kohler, P., Barnola, J. M., Paillard, D., Michel, E., Raynaud, D., and Chappelaz, J.: Constraint of the CO_2 rise by new atmospheric carbon isotopic measurements during the last deglaciation, Global Biogeochem. Cy., 24, BG2015, doi:10.1029/2009GB003545, 2010,

Maslin, M. A. and Thomas, E.: Balancing the deglacial global carbon budget: the hydrate factor, Quaternary Sci. Rev., 22, 1729–1736, 2003.

Monnin, E., Indermühle, A., Dällenbach, A., Flückiger, J., Stauffer, B., Stocker, T. F., Raynaud, D., and Barnola, J. M.: Atmospheric CO_2 concentrations over the last glacial termination, Science, 291, 112–114, 2001.

Morse, P. D. and Burn, C. R.: Ground temperature variation with snow, Kendall Island Bird Sanctuary, outer Mackenzie Delta, Northwest Territories, GEO2010, 2010.

Nelson, F. E. and Outcalt, S. I.: A computational method for perdiction and regionalization of permafrost, Arctic Alpine Res., 19, 279–288, 1987.

Peltier, W. R.: Global glacial isostasy and the surface of the ice-age Earth: The ICE-5G (VM2) Model and GRACE, Ann. Rev. Earth Planet. Sci., 32, 111–149, doi:10.1146/annurev.earth.32.082503.144359, 2004.

Petoukhov, V., Ganopolski, A., Brovkin, V., Claussen, M., Eliseev, A., Kubatzki, C., and Rahmstorf, S.: CLIMBER-2: a climate system model of intermediate complexity, Part 1: model description and performance for present climate, Clim. Dynam., 16, 1–17, 2000.

Prentice, I. C., Harrison, S. P., and Bartlein, P. J.: Global vegetation and terrestrial carbon cycle changes after the last ice age, New Phytol., 189, 988–998, 2011.

Riseborough, D., Shiklomanov, N., Etzelmuller, B., Gruber, S., and Marchenko, S.: Recent advances in permafrost modelling, Permafr. Periglac. Proc., 19, 137–156, 2008.

Rodionov, A., Flessa, H., Grabe, M., Kazansky, O. A., Shibistova, O., and Guggenberger, G.: Organic carbon and total nitrogen variability in permafrost?affected soils in a forest tundra ecotone, Euro. J. Soil Sci., 58, 1260–1272, 2007.

Saito, K., Sueyoshi, T., Marchenko, S., Romanovsky, V., Otto-Bliesner, B., Walsh, J., Bigelow, N., Hendricks, A., and Yoshikawa, K.: LGM permafrost distribution: how well can the latest PMIP multi-model ensembles perform reconstruction?, Clim. Past, 9, 1697–1714, doi:10.5194/cp-9-1697-2013, 2013.

Schaefer, K., Zhang, T., Bruhwiler, L., and Barrett, A. P.: Amount and timing of permafrost carbon release in response to climate warming, Tellus, 63, doi:10.1111/j.1600-0889.2011.00527.x, 2011.

Schmitt, J., Schneider, R., Elsig, J., Leuenberger, D., Lourantou, A., Chappellaz, J., Kohler, P., Joos, F., Stocker, T. F., Leuenberger, M., and Fischer, H.: Carbon isotope constraints on the deglacial CO_2 rise from ice cores, Science, 336, 711–714, 2012.

Schneider von Deimling, T., Meinshausen, M., Levermann, A., Huber, V., Frieler, K., Lawrence, D. M., and Brovkin, V.: Estimating the near-surface permafrost-carbon feedback on global warming, Biogeosciences, 9, 649–665, doi:10.5194/bg-9-649-2012, 2012.

Schuur, E. A.: High risk of permafrost thaw, Nature, 480, 32–33, 2011.

Schuur, E. A. G., Bockheim, J., Canadell, J. G., Euskirchen, E., Field, C. B., Goryachkin, S. V., Hagemann S., Kuhry,P., Lafleur, P. M., Lee, H., Mazhitova, G., Nelson, F. E., Rinke, A., Romanovsky, V. E., Shiklomanov, N., Tarnocai, C., Venevsky, S., Vogel, J. G., and Zimov, S. A.: Vulnerability of permafrost carbon to climate change: Implications for the global carbon cycle, BioScience, 58, 701–714, 2008.

Schuur, E. A. G., Vogel, J. G., Crummer, K. G., Lee, H., Sickman, J. O., and Osterkamp, T. E.: The effect of permafrost thaw on old carbon release and net carbon exchange from tundra, Nature, 459, 556–559, doi:10.1038/nature08031, 2009.

Shakun, J. D., Clark, P. U., He, F., Marcott, S. A., Mix, A. C., Liu, Z., and Bard, E.: Global warming preceded by increasing carbon dioxide concentrations during the last deglaciation, Nature, 484, 49–54, 2012.

Sigman, D. M., Hain, M. P., and Haug, G. H.: The polar ocean and glacial cycles in atmospheric CO_2 concentration, Nature, 466, 47–55, 2010.

Stocker, T. F., Qin, D., Plattner, G.-K., Tignor, M., Allen, S. K., Boschung, J., Nauels, A., Xia, Y., Bex, V., and Midgley, P. M. (Eds.): IPCC, 2013: Climate Change 2013: The Physical Science Basis. Contribution of Working Group I to the Fifth Assessment Report of the Intergovernmental Panel on Climate Change Cambridge University Press, Cambridge, United Kingdom and New York, NY, USA, 1535 pp., 2013.

Taras, B., Sturm, M., and Liston, G. E.: Snow-ground interface temperatures in the Kupuruk River Basin, Arctic Alaska: measurements and model, J. Hydrometeorol., 3, 377–394, 2002.

Tarnocai, C., Canadell, J. G., Schuur, E. A. G., Kuhry, P., Mazhitova, G., and Zimov, S.: Soil organic carbon pools in the northern circumpolar permafrost region, Global Biogeochem. Cy., 23, GB2023, doi:10.1029/2008GB003327, 2009.

Vandenberghe, J., Renssen, H., Roche, D. M., Goosse, H., Velichko, A. A., Gorbunov, A., and Levavasseur, G.: Eurasia permafrost instability constrained by reduced sea-ice cover, Quaternary Sci. Rev., 34, 16–23, doi:10.1016/j.quascirev.2011.12.001, 2012.

van Huissteden, J. and Dolman, A. J.: Soil carbon in the Arctic and the permafrost carbon feedback, Environ. Sustain., 4, 545–551, 2012.

Vavrus, S.: The role of terrestrial snow cover in the climate system, Clim. Dynam., 29, 73–88, doi:10.1007/s00382-007-0226-0, 2007.

Wadham, J. L., Arndt, S., Tulaczyk, S., Stibal, M., Tranter, M., Telling, J., Lis, G. P., Lawson, E., Ridgwell, A., Dubnick, A., Sharp, M. J., Anesio, A. M., and Butler, C. E. H.: Potential methane reservoirs beneath Antarctica, Nature 488, 633–637, 2012.

Wania, R., Ross, I., and Prentice, I. C.: Intergrated peatlands and permafrost into a dynamic global vegetation model: 1. Evaluation and sensitivity of physical land surface processes, Global Biogeochem. Cy., 23, GB3014, doi:10.1029/2008GB003412, 2009a.

Wania, R., Ross, I., and Prentice, I. C.: Intergrated peatlands and permafrost into a dynamic global vegetation model: 2. Evaluation and sensitivity of vegetation and carbon cycle processes, Global Biogeochem. Cy., 23, GB3015, doi:10.1029/2008GB003413, 2009b.

Willerslev, E., Davison, J., Moora, M., Zobel, M., Coissac, E., Edwards, M. E., Lorenzen, E. D., Vestergård, M., Gussarova, G., Haile, J., Craine, J., Gielly, L., Boessenkool, S., Epp, L. S., Pearman, P. B., Cheddadi, R., Murray, D., Bråthen, K. A., Yoccoz, N., Binney, H., Cruaud, C., Wincker, P., Goslar, T., Alsos, I. G.,

Bellemain, E., Brysting, A. K., Elven, R., Sønstebø, J. H., Murton, J., Sher, A., Rasmussen, A., Rønn, R., Mourier, T., Cooper, A., Austin, J., Möller, P., Froese, D., Zazula, G., Pompanon, F., Rioux, D., Niderkorn, V., Tikhonov, A., Savvinov, G., Roberts, R. G., MacPhee, R. D. E., Gilbert, M. P. T., Kjær, K. H., Orlando, L., Brochmann, C., and Pierre Taberlet, P.: Fifty thousand years of Arctic vegetation and megafaunal diet, Nature, 506, 47–51, 2014.

Yu, Z., Loisel, J., Brosseau, D. P., Beilman, D. W., and Hunt, S. J.: Global peatland dynamics since the Last Glacial Maximum, Geophys. Res. Lett., 37, L13402, doi:10.1029/2010GL043584, 2010.

Zech, R., Huang, Y., Zech, M., Tarozo, R., and Zech, W.: High carbon sequestration in Siberian permafrost loess-paleosols during glacials, Clim. Past, 7, 501–509, doi:10.5194/cp-7-501-2011, 2011.

Zhang, T.: Global Annual Freezing and Thawing Indices, Boulder, Colorado USA, National Snow and Ice Data Center, 1998.

Zhang, T.: Influence of the seasonal snow cover on the ground thermal regime. An overview, Rev. Geophys., 43, RG4002, doi:8755-1209/05/2004RG000157, 2005.

Zhang, T., Heginbottom, J. A., Barry, R. G., and Brown, J.: Further statistics on the distribution of permafrost and ground ice in the Northern Hemisphere, Polar Geography, 24, 126–131, doi:10.1080/10889370009377692, 2000.

Zhao, M., Running, S., Heinsch, F. A., and Nemani, R.: MODIS-derived terrestrial primary production, in: Land Remote Sensing and Global Environmental Change, 635–660, Springer New York, 2011.

Zimov, N. S., Zimov, S. A., Zimova, A. E., Zimova, G. M., Chuprynin, V. I., and Chappin III, F. S.: Carbon storage in permafrost and soils of the mammoth tundra-steppe biome: Role in the global carbon budget, Geophys. Res. Lett., 36, L02502, doi:10.1029/2008GL036332, 2009.

Zimov, S. A., Zimov, N. S., Tikhonov, A. N., and Chapin III, F. S.: Mammoth steppe: a high-productivity phenomenon, Quaternary Sci. Rev., 57, 26–45, 2012.

Relevant Model Code

Included on the next pages are the codes associated with the permafrost-carbon model development that was implemented into CLIMBER-2. This code is available also from the Geoscientific Model Development journal's website. Locating permafrost in the model is carried out in the PERMA_LOC subroutine. The permafrost dynamics are implemented into the model in the CCDYN subroutine.

```
**********************************************************************
       SUBROUTINE PERMA_LOC
ckc:   Purpose: Routine to calculate permafrost fraction using Frost Index
ckc:            from monthly surface temperature. From Nelson and Outcalt
ckc:            1987 for Frost index.
ckc:
ckc:   Initially no snow correction
ckc:
ckc:   K. CRICHTON - 13/06/2012
**********************************************************************
        use declar_mod
        use svat_mod
        use params_mod
        use buffer_mod
        use bio_mod


        INTEGER :: month

c reset indices

        freeze(lat,lon)=0.
        thaw(lat,lon)=0.

ckc sum degree-months above zero for thaw index and below zero for freeze
index
c corrected for snow fraction and height, linear model based on Taras et
al
c 2002 measurement data


ckc Version: No snow correction
c *************************
c
c        DO month=1,12
c         IF (TATMSMON2(lat,lon,month).LT.0) THEN
c          freeze(lat,lon)=freeze(lat,lon)+TATMSMON2(lat,lon,month)
c         ELSE IF (TATMSMON2(lat,lon,month).GT.0) THEN
c          thaw(lat,lon)=thaw(lat,lon)+TATMSMON2(lat,lon,month)
c         ENDIF
c        ENDDO
c
c *************************
ckc end of no snow correction
```

```
ckc Version: Snow corrected
c *************************

ckc        IF (NYR.eq.1) THEN
ckc        p_frac(lat,lon)=FRPRM(lat,lon)
ckc        ELSE
        DO month=1,12

ckc        print *, "temp_month : ", TATMSMON2(lat,lon,month)
           IF (TATMSMON2(lat,lon,month).LT.0) THEN
            IF (TATMSMON2(lat,lon,month).GT.-180.) THEN !-6*30 is -180
ckc             IF (TATMSMON2(lat,lon,month).GT.-0.) THEN
             cold(lat,lon)=TATMSMON2(lat,lon,month)/30.
             ELSE
             cold(lat,lon)=FRSNWMON2(lat,lon,month)*((0.01*(-6.
     >         -(TATMSMON2(lat,lon,month)/30.))*HSNWMON2(lat,lon,month))
     >            +(TATMSMON2(lat,lon,month)/30.))
ckc              IF (cold(lat,lon).GT.-6.) THEN
ckc                 cold(lat,lon)=-6.
ckc               ENDIF
             ENDIF
ckc         print *, "original temp ", TATMSMON2(lat,lon,month)/30.
ckc         print *, "corrected temp ", cold(lat,lon)
             freeze(lat,lon)=freeze(lat,lon)+cold(lat,lon)
           ELSE IF (TATMSMON2(lat,lon,month).GT.0) THEN
             thaw(lat,lon)=thaw(lat,lon)+(TATMSMON2(lat,lon,month)/30.)
           ENDIF
        ENDDO
ckc        ENDIF

c ***************************
ckc end of snow corrected


ckc for magnitude of freeze
        freeze(lat,lon) = -1*(freeze(lat,lon))

ckc Calculate frost index, snow corrected

        fr_ndx(lat,lon)=SQRT(freeze(lat,lon))/(SQRT(freeze(lat,lon))
     >    +SQRT(thaw(lat,lon)))

c        print *,"frost index : ", fr_ndx(lat,lon)
```

```
ckc use frost index to permafrost fraction relationship developed by k
crichton
c for CLIMBER-2

ckc If using permafrost lag function, uncomment the next line
c       p_frac_old(lat,lon)=p_frac(lat,lon)


ckc permafrost function "LOW"
c       b(lat,lon) = 20*(fr_ndx(lat,lon)-0.6)
c       p_frac_pred(lat,lon) = 0.53*(0.976+(b(lat,lon)/
c     >       (SQRT(1+(b(lat,lon)**2)))))-0.015


ckc permafrost function "LOW-MED" !for deglaciation paper
       b(lat,lon) = 20.5*(fr_ndx(lat,lon)-0.595)
       p_frac_pred(lat,lon) = 0.54*(0.976+(b(lat,lon)/
     >       (SQRT(1+(b(lat,lon)**2)))))-0.015


ckc permafrost function "MED"
c       b(lat,lon) = 21*(fr_ndx(lat,lon)-0.59)
c       p_frac_pred(lat,lon) = 0.555*(0.976+(b(lat,lon)/
c     >       (SQRT(1+(b(lat,lon)**2)))))-0.015


ckc permafrost function "HIGH"
ckc    function "3" 25 oct 2012
c        b(lat,lon) = 22*(fr_ndx(lat,lon)-0.58)
ckc        print *,"B(lat,lon) : ", b(lat,lon)
c        p_frac_pred(lat,lon) = 0.58*(0.976+(b(lat,lon)/
c     >       (SQRT(1+(b(lat,lon)**2)))))-0.015

        IF(p_frac_pred(lat,lon).GT.1) THEN
            p_frac_pred(lat,lon) = 1
        ELSE IF(p_frac_pred(lat,lon).LT.0) THEN
            p_frac_pred(lat,lon) = 0
        ENDIF

ckc for no permafrost lag
        p_frac(lat,lon)=p_frac_pred(lat,lon) !no lag
ckc for permafrost lag function
c        p_frac(lat,lon)=0.5*(p_frac_old(lat,lon)+p_frac_pred(lat,lon))

        w_frac(lat,lon) = 1-p_frac(lat,lon)
```

```
c        print *,"perma frac PERM i : ", p_frac(lat,lon), lat
        FRPRM(lat,lon)=p_frac(lat,lon)
        FRWRM(lat,lon)=w_frac(lat,lon)
        FROST(lat,lon)=fr_ndx(lat,lon)
c        print *, "FRPRM : ", FRPRM(lat,lon)
ckc calculate the area of permafrost in each cell
c       parea(lat,lon)=carea(lat,lon)*p_frac(lat,lon)*FRGLC(lat,lon)

       return

       END SUBROUTINE PERMA_LOC
```

```
c*********************************************************************
              SUBROUTINE CCDYN
c*********************************************************************
       use declar_mod
       use params_mod
       use bio_mod
       use buffer_mod

cscript Les declarations suivantes ont ete faite par un script
      REAL G4D
csript ---
c*********************************************************************
c temporal var*/
        REAL tempor1,tempor2,tempor3,tempor4,db2,fd,dst,dd,nld,
     >        dstime,tempor5,tempor6,dsg,dsd,temp_sg,temp_st,
     >         b4t_hold, b4g_hold, b4t14_hold, b4g14_hold,
     >          b4t13_hold, b4g13_hold, b3t_hold, b3g_hold,
     >           b3t14_hold, b3g14_hold, b3t13_hold, b3g13_hold


c calculation of current carbon cycle parameters

        call CCPARAM

cnb        print*, 'npp',lat, lon, npp
cnb        npp_tot=npp_tot+npp
cnb        print*,'npp_tot',npp_tot

cnb - Test sur le carbone pris par la veget
cnb - S il est trop important on divise npp par 2
cnb - et on recalcul tous les reservoirs

cnb - Initialisation pour entrer dans la boucle
      anup(lat,lon)=co2_max+10
cnb      print *, "initialisation reussie, anup =",anup(lat,lon)
      test_veget=0

      do while (anup(lat,lon) .gt. co2_max)
cnb ---

c calculation of fraction dynamic variables

        fd=forshare_st-st(lat,lon)
        dd=desshare_st-sd(lat,lon)
        nld=nlshare_st-snlt(lat,lon)
        g4d=g4share_st-sg4(lat,lon)
        temp_st=st(lat,lon)
```

```
        temp_sg=sg(lat,lon)

c calculation of forest dynamics; exponential filtre
        dst=forshare_st-fd*exp(-1./t2t)-st(lat,lon)
        st(lat,lon)=st(lat,lon)+dst
        snlt(lat,lon)=nlshare_st-nld*exp(-1./t2t)

c desert dynamics; exponential filtre
        dsd=desshare_st-dd*exp(-1./t2g)-sd(lat,lon)
        tempor1=sd(lat,lon)+dsd+st(lat,lon)

c calculation of characteristic time of desert propagation
        if (tempor1.gt.0.9) then
             dstime=t2g*(1-tempor1)*10.+t2t*(tempor1-0.9)*10
             dsd=desshare_st-dd*exp(-1./dstime)-sd(lat,lon)
        endif

        sd(lat,lon)=sd(lat,lon)+dsd
        dsg=-dst-dsd

        sg(lat,lon)=1.-st(lat,lon)-sd(lat,lon)
        sg4(lat,lon)=g4share_st-g4d*exp(-1./t2g)

        if (sg(lat,lon).lt.0) sg(lat,lon)=0
        if (st(lat,lon).lt.0) st(lat,lon)=0
        if (sd(lat,lon).lt.0) sd(lat,lon)=0


c calculation of dynamics of storages

c calculation of changes of storages due to conservation law

c correction for trees

        tempor1=b4t(lat,lon)
        tempor2=b3t(lat,lon)
        tempor3=b4t14(lat,lon)
        tempor4=b3t14(lat,lon)
        tempor5=b4t13(lat,lon)
        tempor6=b3t13(lat,lon)


        if(st(lat,lon).gt.0) then
          if(dst.gt.0) then

            b4t(lat,lon)=(b4t(lat,lon)*temp_st
     >         +b4g(lat,lon)*dst)/st(lat,lon)
```

```
            b3t(lat,lon)=(b3t(lat,lon)*temp_st
     >         +b3g(lat,lon)*dst)/st(lat,lon)

            b4t14(lat,lon)=(b4t14(lat,lon)*temp_st
     >         +b4g14(lat,lon)*dst)/st(lat,lon)
            b3t14(lat,lon)=(b3t14(lat,lon)*temp_st
     >         +b3g14(lat,lon)*dst)/st(lat,lon)

            b4t13(lat,lon)=(b4t13(lat,lon)*temp_st
     >         +b4g13(lat,lon)*dst)/st(lat,lon)
            b3t13(lat,lon)=(b3t13(lat,lon)*temp_st
     >         +b3g13(lat,lon)*dst)/st(lat,lon)


          endif

          b2t(lat,lon)=b2t(lat,lon)*temp_st/st(lat,lon)
          b1t(lat,lon)=b1t(lat,lon)*temp_st/st(lat,lon)

          b2t14(lat,lon)=b2t14(lat,lon)*temp_st/st(lat,lon)
          b1t14(lat,lon)=b1t14(lat,lon)*temp_st/st(lat,lon)

          b2t13(lat,lon)=b2t13(lat,lon)*temp_st/st(lat,lon)
          b1t13(lat,lon)=b1t13(lat,lon)*temp_st/st(lat,lon)

        endif

c correction for grass

        if(sg(lat,lon).gt.0) then
                if(dst.gt.0) then

                 b4g(lat,lon)=b4g(lat,lon)*(temp_sg-dst)
     >           /sg(lat,lon)
                 b3g(lat,lon)=b3g(lat,lon)*(temp_sg-dst)
     >           /sg(lat,lon)

                 b4g14(lat,lon)=b4g14(lat,lon)*(temp_sg-dst)
     >           /sg(lat,lon)
                 b3g14(lat,lon)=b3g14(lat,lon)*(temp_sg-dst)
     >           /sg(lat,lon)

                 b4g13(lat,lon)=b4g13(lat,lon)*(temp_sg-dst)
     >           /sg(lat,lon)
                 b3g13(lat,lon)=b3g13(lat,lon)*(temp_sg-dst)
     >           /sg(lat,lon)
```

```
                else

              b4g(lat,lon)=(b4g(lat,lon)*temp_sg-tempor1*dst)
     >        /sg(lat,lon)
              b3g(lat,lon)=(b3g(lat,lon)*temp_sg-tempor2*dst)
     >        /sg(lat,lon)

              b4g14(lat,lon)=(b4g14(lat,lon)*temp_sg
     >        -tempor3*dst)/sg(lat,lon)
              b3g14(lat,lon)=(b3g14(lat,lon)*temp_sg
     >        -tempor4*dst)/sg(lat,lon)

              b4g13(lat,lon)=(b4g13(lat,lon)*temp_sg
     >        -tempor5*dst)/sg(lat,lon)
              b3g13(lat,lon)=(b3g13(lat,lon)*temp_sg
     >        -tempor6*dst)/sg(lat,lon)

                endif

           b2g(lat,lon)=b2g(lat,lon)*temp_sg/sg(lat,lon)
           b1g(lat,lon)=b1g(lat,lon)*temp_sg/sg(lat,lon)

           b2g14(lat,lon)=b2g14(lat,lon)*temp_sg/sg(lat,lon)
           b1g14(lat,lon)=b1g14(lat,lon)*temp_sg/sg(lat,lon)

           b2g13(lat,lon)=b2g13(lat,lon)*temp_sg/sg(lat,lon)
           b1g13(lat,lon)=b1g13(lat,lon)*temp_sg/sg(lat,lon)

          endif


c slow soil organic matter

ckc place holder for b4 terms

          b4t_hold=b4t(lat,lon)
          b4g_hold=b4g(lat,lon)
          b4t14_hold=b4t14(lat,lon)
          b4g14_hold=b4g14(lat,lon)
          b4t13_hold=b4t13(lat,lon)
          b4g13_hold=b4g13(lat,lon)

ckc for non permafrost affected fraction

          b4t(lat,lon)=w_frac(lat,lon)*(b4t_hold
     *               +k3t/t3t*b3t(lat,lon)-b4t_hold/t4t)
```

```
        b4g(lat,lon)=w_frac(lat,lon)*(b4g_hold+k4g/t2g*b2g(lat,lon)
     *              +k3g/t3g*b3g(lat,lon)-b4g_hold/t4g)

ckc for permafrost fraction of cell for b4 and c14 and c13

        b5t(lat,lon)=p_frac(lat,lon)*(b4t_hold+k3t/t3t*b3t(lat,lon)
     >              -b4t_hold/t5t)
        b5g(lat,lon)=p_frac(lat,lon)*(b4g_hold+k4g/t2g*b2g(lat,lon)
     >              +k3g/t3g*b3g(lat,lon)-b4g_hold/t5g)


        b4t14(lat,lon)=w_frac(lat,lon)*(b4t14_hold+k3t/t3t*
     >                b3t14(lat,lon)-b4t14_hold/t4t)
        b4g14(lat,lon)=w_frac(lat,lon)*(b4g14_hold+k4g/t2g*
     >                b2g14(lat,lon)+k3g/t3g*b3g14(lat,lon)-
     >                 b4g14_hold/t4g)


        b5t14(lat,lon)=p_frac(lat,lon)*(b4t14_hold+k3t/t3t*
     >                b3t14(lat,lon)-b4t14_hold/t5t)
        b5g14(lat,lon)=p_frac(lat,lon)*(b4g14_hold+k4g/t2g*
     >                b2g14(lat,lon)+k3g/t3g*b3g14(lat,lon)-
     >                 b4g14_hold/t5g)



        b4t13(lat,lon)=w_frac(lat,lon)*(b4t13_hold+k3t/t3t*
     >                b3t13(lat,lon)-b4t13_hold/t4t)
        b4g13(lat,lon)=w_frac(lat,lon)*(b4g13_hold+k4g/t2g*
     >                b2g13(lat,lon)+k3g/t3g*b3g13(lat,lon)-
     >                 b4g13_hold/t4g)



        b5t13(lat,lon)=p_frac(lat,lon)*(b4t13_hold+k3t/t3t*
     >                b3t13(lat,lon)-b4t13_hold/t5t)
        b5g13(lat,lon)=p_frac(lat,lon)*(b4g13_hold+k4g/t2g*
     >                b2g13(lat,lon)+k3g/t3g*b3g13(lat,lon)-
     >                 b4g13_hold/t5g)



ckc add permafrost carbon back in to b4 components

        b4t(lat,lon)=b4t(lat,lon)+b5t(lat,lon)
        b4g(lat,lon)=b4g(lat,lon)+b5g(lat,lon)
```

```
        b4t14(lat,lon)=b4t14(lat,lon)+b5t14(lat,lon)
        b4g14(lat,lon)=b4g14(lat,lon)+b5g14(lat,lon)

        b4t13(lat,lon)=b4t13(lat,lon)+b5t13(lat,lon)
        b4g13(lat,lon)=b4g13(lat,lon)+b5g13(lat,lon)


*        b4t14(lat,lon)=b4t14(lat,lon)+k3t/t3t
*     *                 *b3t14(lat,lon)
*     *                 -b4t14(lat,lon)/t4t
*        b4g14(lat,lon)=b4g14(lat,lon)+k4g/t2g
*     *                 *b2g14(lat,lon)+k3g/t3g*
*     *  b3g14(lat,lon)-b4g14(lat,lon)/t4g

*        b4t13(lat,lon)=b4t13(lat,lon)+k3t/t3t
*     *                 *b3t13(lat,lon)
*     *                 -b4t13(lat,lon)/t4t
*        b4g13(lat,lon)=b4g13(lat,lon)+k4g/t2g
*     *                 *b2g13(lat,lon)+k3g/t3g*
*     *  b3g13(lat,lon)-b4g13(lat,lon)/t4g


c   fast soil organic matter
ckc place holder for fast soil terms
        b3t_hold=b3t(lat,lon)
        b3g_hold=b3g(lat,lon)
        b3t14_hold=b3t14(lat,lon)
        b3g14_hold=b3g14(lat,lon)
        b3t13_hold=b3t13(lat,lon)
        b3g13_hold=b3g13(lat,lon)

ckc non-permafrost fraction of cell, b3, permafrost affected b6

        b3t(lat,lon)=w_frac(lat,lon)*(b3t_hold+b1t(lat,lon)
     >           /t1t*k0t+k2t/t2t*b2t(lat,lon)-b3t_hold/t3t)
        b3g(lat,lon)=w_frac(lat,lon)*(b3g_hold+b1g(lat,lon)
     >           /t1g*k0g+k2g/t2g*b2g(lat,lon)-b3g_hold/t3g)


        b6t(lat,lon)=p_frac(lat,lon)*(b3t_hold+b1t(lat,lon)
     >           /t1t*k0t+k2t/t2t*b2t(lat,lon)-b3t_hold/t6t)
        b6g(lat,lon)=p_frac(lat,lon)*(b3g_hold+b1g(lat,lon)
     >           /t1g*k0g+k2g/t2g*b2g(lat,lon)-b3g_hold/t6g)


        b3t14(lat,lon)=w_frac(lat,lon)*(b3t14_hold+b1t14(lat,lon)
     >         /t1t*k0t+k2t/t2t*b2t14(lat,lon)-b3t14_hold/t3t)
```

```
      b3g14(lat,lon)=w_frac(lat,lon)*(b3g14_hold+b1g14(lat,lon)
     >         /t1g*k0g+k2g/t2g*b2g14(lat,lon)-b3g14_hold/t3g)
      b6t14(lat,lon)=p_frac(lat,lon)*(b3t14_hold+b1t14(lat,lon)
     >         /t1t*k0t+k2t/t2t*b2t14(lat,lon)-b3t14_hold/t6t)
      b6g14(lat,lon)=p_frac(lat,lon)*(b3g14_hold+b1g14(lat,lon)
     >         /t1g*k0g+k2g/t2g*b2g14(lat,lon)-b3g14_hold/t6g)

      b3t13(lat,lon)=w_frac(lat,lon)*(b3t13_hold+b1t13(lat,lon)
     >         /t1t*k0t+k2t/t2t*b2t13(lat,lon)-b3t13_hold/t3t)
      b3g13(lat,lon)=w_frac(lat,lon)*(b3g13_hold+b1g13(lat,lon)
     >         /t1g*k0g+k2g/t2g*b2g13(lat,lon)-b3g13_hold/t3g)
      b6t13(lat,lon)=p_frac(lat,lon)*(b3t13_hold+b1t13(lat,lon)
     >         /t1t*k0t+k2t/t2t*b2t13(lat,lon)-b3t13_hold/t6t)
      b6g13(lat,lon)=p_frac(lat,lon)*(b3g13_hold+b1g13(lat,lon)
     >         /t1g*k0g+k2g/t2g*b2g13(lat,lon)-b3g13_hold/t6g)

ckc sum b3 components back together

      b3t(lat,lon)=b3t(lat,lon)+b6t(lat,lon)
      b3g(lat,lon)=b3g(lat,lon)+b6g(lat,lon)
      b3t14(lat,lon)=b3t14(lat,lon)+b6t14(lat,lon)
      b3g14(lat,lon)=b3g14(lat,lon)+b6g14(lat,lon)
      b3t13(lat,lon)=b3t13(lat,lon)+b6t13(lat,lon)
      b3g13(lat,lon)=b3g13(lat,lon)+b6g13(lat,lon)

ckc Soil respiration

     rsoil_g(lat,lon)=w_frac(lat,lon)*((-b3g_hold/t3g)+(-b4g_hold/t4g))
     >               +p_frac(lat,lon)*((-b3g_hold/t6g)+(-b4g_hold/t5g))
     rsoil_t(lat,lon)=w_frac(lat,lon)*((-b3g_hold/t3t)+(-b4g_hold/t4t))
     >               +p_frac(lat,lon)*((-b3g_hold/t6t)+(-b4g_hold/t5t))

ckc Veg respiration

     rveg_g(lat,lon)=-b2g(lat,lon)/t2g
     rveg_t(lat,lon)=(-b1t(lat,lon)/t1t)+(-b2t(lat,lon)/t2t)


c leaves biomass


      b1t(lat,lon)=b1t(lat,lon)+k1t*npp-b1t(lat,lon)/t1t
      b1g(lat,lon)=k1g*npp*t1g


      b1t14(lat,lon)=b1t14(lat,lon)+k1t*npp*c14atm
     *               -b1t14(lat,lon)/t1t
```

```
              b1g14(lat,lon)=k1g*npp*c14atm*t1g


         b1t13(lat,lon)=b1t13(lat,lon)+k1t*npp*c13atm*
      *                 c13frac-b1t13(lat,lon)/t1t


         b1g13(lat,lon)=k1g*npp*c13atm*(c13frac*(1-sg4(lat,lon))+
      *                 c13frac4*sg4(lat,lon))*t1g

c    stems and roots biomass

         b2t(lat,lon)=b2t(lat,lon)+(1-k1t)*npp-b2t(lat,lon)/t2t
         b2g(lat,lon)=b2g(lat,lon)+(1-k1g)*npp-b2g(lat,lon)/t2g


         b2t14(lat,lon)=b2t14(lat,lon)+(1-k1t)*npp*c14atm
      *                 -b2t14(lat,lon)/t2t

         b2g14(lat,lon)=b2g14(lat,lon)+(1-k1g)*npp*c14atm
      *                 -b2g14(lat,lon)/t2g

         b2t13(lat,lon)=b2t13(lat,lon)+(1-k1t)*npp*c13atm
      *                 *c13frac-b2t13(lat,lon)/t2t

         b2g13(lat,lon)=b2g13(lat,lon)+(1-k1g)*npp*c13atm
      *                 *(c13frac*(1-sg4(lat,lon))+
      *                 c13frac4*sg4(lat,lon))-b2g13(lat,lon)/t2g

c    c14 annual decay
         b1t14(lat,lon)=b1t14(lat,lon)*(1-c14tdec)
         b2t14(lat,lon)=b2t14(lat,lon)*(1-c14tdec)
         b3t14(lat,lon)=b3t14(lat,lon)*(1-c14tdec)
         b4t14(lat,lon)=b4t14(lat,lon)*(1-c14tdec)
         b1g14(lat,lon)=b1g14(lat,lon)*(1-c14tdec)
         b2g14(lat,lon)=b2g14(lat,lon)*(1-c14tdec)
         b3g14(lat,lon)=b3g14(lat,lon)*(1-c14tdec)
         b4g14(lat,lon)=b4g14(lat,lon)*(1-c14tdec)

         call CLIMPAR

cnb --- Ze Test sur le carbone pris par la veget
cnb --- S il est trop important on divise npp par 2
cnb --- et on recalcul tous les reservoirs
```

```
ckc  should also be for KLSR is 2 for seds restart?
cam: This test is not done if KLSR=1:
        IF (KLSR.EQ.1) anup(lat,lon)=co2_max
cnb        do while (anup(lat,lon) .gt. co2_max)
          if (anup(lat,lon) .gt. co2_max) then
cnb            print *,"lat,lon",lat,lon,"anup",anup(lat,lon)
            npp=npp/2
            test_veget=1
cnb          print*,'passe dans test veget'
          endif

      enddo !fin du test


        return
        end
```

Chapter 4: Glacial-interglacial transitions and tuning the permafrost-carbon model dynamics

This chapter presents, in three sections, the experiments and results to investigate the possible role of permafrost-carbon during the glacial terminations 1 and 2. The first section presents equilibrium-background tests in which carbon is released into the CLIMBER-2 atmosphere (without permafrost-carbon module) at various rates to study the atmospheric $\delta^{13}C$ response. The second section is a draft research paper in which results of transient simulations of the last termination, which include the permafrost-carbon module, are presented and the best fit permafrost-carbon dynamics are selected. The third section investigates the penultimate termination period for which atmospheric $\delta^{13}C$ data have recently become available.

4.1 Emissions tests with the CLIMBER-2 model without permafrost-carbon module

Using a carbon cycle model and oxygen-18 isotope measurements of water in ice cores, Ciais et al (2012) estimated than the terrestrial biosphere had lost 700GtC of inert carbon since the LGM. If we assume than this inert carbon is stored in permafrost, then a first look at the response of the Earth system to a permafrost-carbon release is possible. In order to investigate this, CLIMBER-2 (without permafrost) was forced with a release of 700GtC with a $\delta^{13}C$ signature of -25‰ (Maslin and Thomas 2003) into the atmosphere, at various rates, and the model was allowed to run for 6000 years with an equilibrium Last Glacial Maximum (LGM), 21kyr BP, climate background. The LGM climate is achieved by forcing the radiative code (and vegetation module) with CO_2 of 190ppm, LGM ice sheets, increased concentration of salinity and nutrients in the ocean by 3.3% to account for the reduced ocean volume (Bouttes et al. 2011), 21kyr orbital parameters for insolation and glacial runoff.

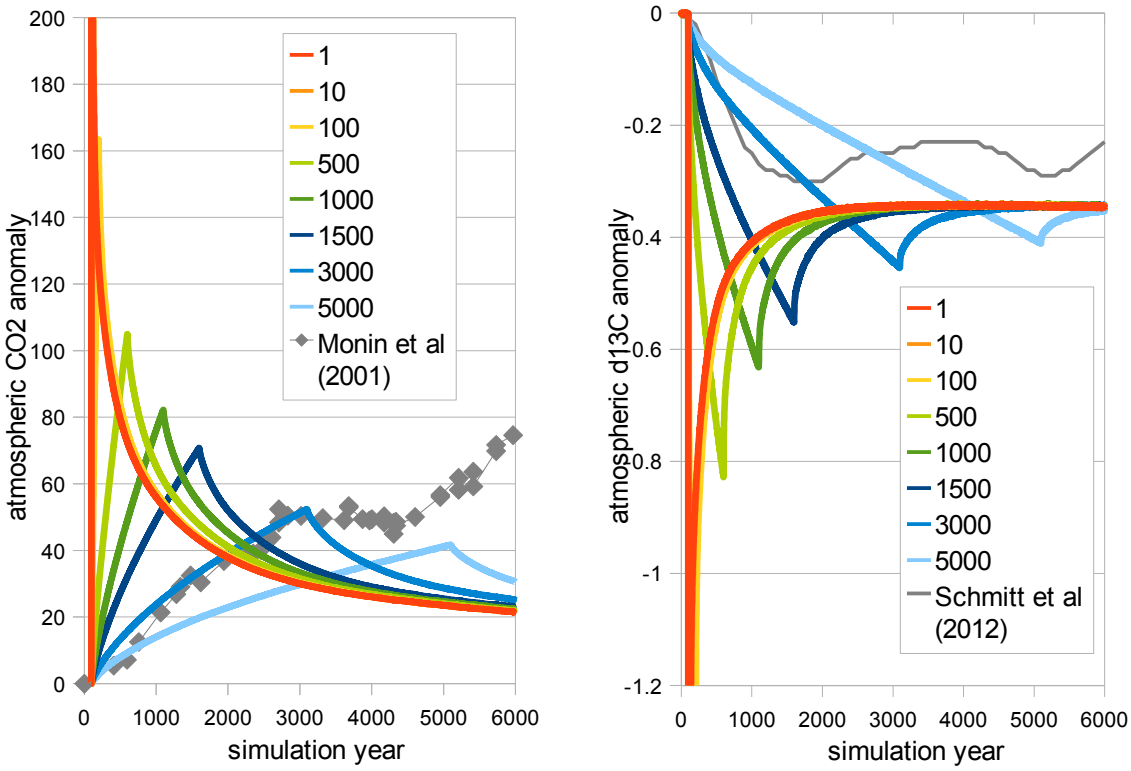

Fig 4.1, Evolution of atmospheric CO_2 (ppm) and $\delta^{13}C$ (‰) in the test simulations with a release of 700GtC spread over 1 year to 5000 years (shown per colour as legend). Left: atmospheric CO_2 anomaly and Monnin et al. (2001), Right: atmospheric $\delta^{13}C$ anomaly (per mil) and Schmitt et al. (2012) $\delta^{13}C$ data. Anomalies are with respect the the initial value.

The emission of 700GtC at various rates shows the response of the standard CLIMBER-2 model to a possible carbon release from a permafrost-soils source. The timescale of the carbon emission varies from 1 year to 5000 years, and carbon is released as a step function, with carbon release evenly distributed over the release period. Figure 4.1 shows the atmospheric CO_2 and $\delta^{13}C$ anomalies for each release rate, together with the data for CO_2 and $\delta^{13}C$. The data anomaly is with respect to the year 17.3kyrs BP. By comparing model output to data and interpreting this in terms of permafrost-carbon, we are assuming that only permafrost-carbon contributed to the changes in CO_2 and $\delta^{13}C$ at the start of the last termination. The rate of CO_2 rise matches the data for the release of 700GtC over 3000 years, corresponding to 0.233GtC/yr. The atmospheric $\delta^{13}C$ anomaly is also closer to the data for the 3000 year release period, although the complex evolution of $\delta^{13}C$ is not expected to be correctly reproduced with a simple constant carbon release and a steady state LGM climate. The lowest value of $\delta^{13}C$ modelled anomaly for this release rate is -0.45‰, which is around 1.5 times more than the (smoothed) data suggests (Schmitt et al. 2013).

The data shows an increase in $\delta^{13}C$ from around 2000 years after the initial drop. At 2000 years from simulation start in the simulation, total carbon released is 470GtC at the 0.233GtC/yr release rate. After 2000 years, the $\delta^{13}C$ record indicates a possible change of source. At this point $\delta^{13}C$ starts to become more positive indicating a $\delta^{13}C$ source more positive than the atmosphere for the continued rise in CO_2 and possibly a preferential uptake of Carbon-12 by land biosphere increases. After the emission of the 700GtC for each of the simulations, the atmospheric CO_2 declines and stabilises at around +20ppm. The emission tests do not represent a real deglaciation, and comparison with data is only to compare rates of change. However, the rise in CO_2 coupled with the fast drop in $\delta^{13}C$ of the atmosphere indicates a possible role of the permafrost-carbon mechanism in the CO_2 and $\delta^{13}C$ changes, which is more thoroughly investigated with CLIMBER-2 including the permafrost-carbon model (described in chapter 3) and a transient background climate in the next section.

4.2 Draft paper: The contribution of permafrost in the carbon-cycle evolution during the last termination

The draft paper presents the results of transient deglaciation simulations with the CLIMBER-2P model. A realistic deglaciation, in which LGM CO_2 and Atlantic ocean $\delta^{13}C$ vertical gradient is in agreement with data, was achieved by employing the glacial ocean mechanisms developed by Bouttes et al (2011, 2012). In this paper I have tested the role of permafrost in the context of the deglaciation by running transient simulations. The addition of the permafrost-carbon model improves the evolution of simulated atmospheric $\delta^{13}C$ during the termination and provides an alternative source of carbon to the atmosphere, while the ocean remains a major contributor for the rest of the deglaciation.

The contribution of permafrost in the carbon-cycle evolution during the last termination

K.A. Crichton 1,2
N. Bouttes 3
D. Roche 4,5
J. Chappellaz 1,2
G. Krinner 1,2

1 CNRS, LGGE (UMR5183), F-38041 Grenoble, France
2 Univ. Grenoble Alpes, LGGE (UMR5183), F-38041 Grenoble, France.
3 NCAS-Climate, University of Reading, Reading RG6 6BB, UK
4 CEA/INSU-CNRS/UVSQ, LSCE (UMR8212), Centre d'Etudes de Saclay CEA-Orme des Merisiers, bat. 701 91191 Gif-sur-Yvette Cedex, France
5 Cluster Earth and Climate, Department of Earth Sciences Faculty of Earth and Life Sciences, Vrije Universiteit Amsterdam De Boelelaan 1085, 1081 HV Amsterdam, The Netherlands

Abstract

The last glacial period ended around 17.5 thousand years ago, with conditions going from glacial cold to interglacial warm climate within 8 thousand years. A leading hypothesis to explain the fast rise in atmospheric CO_2 in this period is ocean circulation reorganisation leading to fast out-gassing of CO_2, likely from a deep southern ocean source. Paleoclimate modelling studies used to investigate the causal mechanisms for the fast CO_2 rise consider the land biosphere to be a carbon sink during this time. However, these studies can not correctly simulate the evolution of atmospheric $\delta^{13}C$. Additionally, they do not account for the role of permafrost (frozen soil) which can contain large amounts of carbon with a negative $\delta^{13}C$ signature. Here we use the fully coupled model CLIMBER-2P equipped with a simplified permafrost-carbon mechanism to explore the role of permafrost in the carbon cycle evolution during the last deglaciation. CLIMBER-2P also includes glacial ocean mechanisms causing deep southern ocean stratification and carbon storage during glacial periods. We show that CLIMBER-2P can reproduce the magnitude and timing of onset of the rise seen in the CO_2 record, and is in agreement with the atmospheric $\delta^{13}C$ record during the termination. A permafrost-thaw carbon-release mechanism appears to be a plausible source for the initial rise in atmospheric CO_2 from 18kyr BP. In our simulation the ocean only becomes a carbon source after 15kyr BP. The permafrost-carbon release from around 18kyr BP is in response to increases in summer insolation in the permafrost zone, and provides a direct carbon-cycle link to high latitude insolation as a driver of glacial terminations, in support of Milankovitch theory.

1. Introduction

Ice core data for the last deglaciation (from 18kyr to 11.5kyr BP; termination 1 or T1) show a rapid rise in atmospheric CO_2 levels from around 190ppm to 260ppm (Monnin et al. 2001). The $\delta^{13}C$ evolves simultaneously, with a drop in atmospheric $\delta^{13}C$ of 0.3‰ occurring in the first 2500 years (Lourantou et al 2010, Schmitt et al. 2012). During the deglaciation global sea-surface temperatures increased by around 4 degrees (range of 2 to 6 degrees, MARGO project members 2009), large ice sheets covering much of North America and Northern Europe melted (Peltier et al. 1994) and global sea-level rose by around 120m (Clark and Mix 2002). Furthermore the Atlantic $\delta^{13}C$ vertical gradient was found to be higher at LGM at around 1.4‰ compared to ~0.5‰ in the Holocene (Curry and Oppo 2005).

Many studies have been carried out to investigate the causes of the rapid rise in temperatures and CO_2, including proxy-based reconstructions and modelling studies. Most current hypotheses for the CO_2 increases lie in ocean mechanisms (Kohler et al. 2010, Kwon et al. 2011, Bouttes et al. 2012); the ocean contains around 60 to 90 times more carbon than the atmosphere and around 10 times more carbon than the land using the latest estimates (Ciais et al. 2012). The present-day estimate for total terrestrial-biosphere carbon is around 3970GtC+-325, this includes high carbon soils related to frozen ground and to wetlands which hold around 1672 GtC (Tarnocai et al. 2009). In transient modelling studies of the carbon cycle evolution during the last deglaciation the terrestrial biosphere had often been neglected. This was due to the much larger pool size of the ocean, and also due to earlier studies showing that the whole-ocean $\delta^{13}C$ had become more positive since the last glacial maximum (21kyrBP) (Shackelton 1977, Duplessy et al 1988, Broecker and Peng 1993). The ratio of carbon-12 to carbon-13 can give information about the source of inputs and outputs via fractionation processes (Kump and Arthur 1999). The photosynthesis process preferentially assimilates the carbon-12 isotope causing a fractionation of around -18‰ (Maslin and Thomas 2003) compared to the carbon source. Photosynthesis taking up atmospheric CO_2 (with $\delta^{13}C$ = -6.45‰ at PI, Lourantou et al. 2010) results in a $\delta^{13}C$ signature of ~-25‰ for the terrestrial biosphere. While the whole ocean $\delta^{13}C$ signature is closer to 0‰ (Maslin and Thomas 2003). As the ocean was more positive in $\delta^{13}C$ at the Pre-Industrial compared to the LGM, it was thought that the CO_2 source could not be from land-carbon, which would have shown up in the ocean as a $\delta^{13}C$ more negative than LGM. Another reason why land carbon was not considered as a source for the CO_2 increase during T1 was that until quite recently the high latitude soils were thought to store very little carbon (Adams et al. 1990). It resulted in an estimation of the total global increase of carbon stored in the terrestrial biosphere of around 700 to 900GtC (Van Campo et al. 1993, Crowley 1995), or more (Adams et al. 1990). All these factors seemed to discount the terrestrial biosphere as a source of CO_2 increase and indicated that it acted as a sink of carbon during terminations instead.

Recently, the importance of large carbon stores in soils in high latitude permafrost regions has been acknowledged (Tarnocai et al., 2009) and its role in the context of the future climate change (Schuur et al 2008). If these permafrost areas thaw, then large amounts of carbon could be released into the atmosphere, creating a positive feedback that could cancel out any sink due to increasing NPP (Net Primary Production) (Koven et al. 2011, Schaefer et al. 2011, Schneider von Diemeling et al. 2012, Harden et al. 2012, Schaphoff et al. 2013). For the LGM, studies show that rather than being deserts, frozen soils probably stored more (inert) carbon than they do in the present day (Zimov et al. 2009, Ciais et al. 2012). This increased carbon storage was partly due to lower sea level: continental shelves were exposed during glacial periods, further increasing the area of land that would be permafrost affected, particularly the Siberian shelf which was ice-free. The carbon content also increased because the long timescale of the glacial period allowed it to progressively accumulate carbon in the cold climate.

This study aims to evaluate the role of permafrost in the change of CO_2 and atmospheric $\delta^{13}C$ recorded during the last termination using transient deglaciation experiments within an earth system model. The model includes the carbon-13 tracer and has been improved to account for the evolution of permafrost, using a simplified representation of the carbon content in permafrost (Crichton et al. 2014). On top of this permafrost-carbon mechanism, we also consider additional processes such as the sinking of brines and increased ocean stratification which was found to effectively reduce atmospheric CO_2 to the LGM levels (Bouttes et al. 2009, Bouttes et al. 2011). Other studies suggest the importance of iron fertilisation in strengthening the biological pump in glacial periods (Bopp et al. 2003), which we also account for.

2. Methods

The CLIMBER-2 model is an Earth System Model of Intermediate Complexity (EMIC). It includes a 2.5D statistical dynamical atmosphere with resolution of 10° latitude and around 51° longitude, a 21 layer basin-averaged dynamic ocean model with ocean biology and resolution of 2.5 degree latitude, and a dynamic vegetation model matching the atmospheric model resolution (Petoukhov et al. 2000, Ganopolski et al. 2001, Brovkin et al. 2002, 2007). The CLIMBER-2P version includes a simplified permafrost mechanism within the dynamic vegetation model. The driving principle of the permafrost-carbon model for CLIMBER-2P is that frozen soils result in a reduction in annual soil carbon respiration and therefore increase soil carbon concentrations (Zimov et al. 2009). Locating permafrost is achieved using a frost-index, an index indicating the balance between above 0°C and below 0°C days in a year, and as such permafrost is sensitive to insolation changes (seasonality), local climate and CO_2 related temperature changes. The permafrost model is fully described in Crichton et al. (2014).

An LGM climate is achieved in the model in an 80kyr simulation using LGM ice sheets, atmospheric CO_2 levels of 190ppm, reduced ocean volume based on the relative sea-level record (Peltier et al 1994) achieved by increasing salinity and nutrient concentrations by 3.3%, 21kyr BP insolation and LGM runoff levels. The model was spun-up for 80,000 years to allow the terrestrial land carbon to equilibrate when permafrost-carbon is included. The transient deglaciation is created using CO_2 data (Monnin et al. 2001) to drive the radiative model and CO_2 levels seen by the terrestrial vegetation model, evolving ice sheets based on relative sea-level record which indicates total land-ice volume (Peltier 2004), insolation according to orbital changes, ocean volume increase indicated by sea-level record and modelled by reducing nutrient and salinity concentrations back to PI levels. The model calculates the carbon-cycle atmospheric CO_2, which is the balance between the ocean and land carbon pools fluxes to the atmosphere. Comparing the data CO_2 to the carbon-cycle modelled CO_2 allows an appraisal of the carbon-cycle components and controllers. The permafrost-carbon mechanism was tuned using the Ciais et al. 2012 estimates of 3640+-400GtC at LGM and 3970+-325 GtC at PI for total land carbon. Four dynamic settings are available for testing in the model, and are defined by the ratio of the total fast soil carbon pool to the slow carbon pool (determined by permafrost soils). Four ocean mechanisms are also included in the simulation: carbonate compensation, the sinking of brines as a result of salts rejected on sea-ice formation in the Southern ocean, stratification dependent diffusion in the Southern ocean and iron fertilisation of marine biota. The effects of iron fertilisation on marine biota from high dust contents of the atmosphere during the last glacial period in the CLIMBER-2 model is described by Brovkin et al. 2007. The effects of the sinking of brines is described in Bouttes et al., 2011, while its impact in conjunction with interactive diffusion, carbonate compensation and iron fertilization is studied at the LGM in Bouttes et al., 2011 and during the deglaciation in Bouttes et al., 2012.

Name	**Evolving drivers and mechanisms**	**Permafrost**
Clim	CO_2, insolation, ice sheet	
Perm	CO_2, insolation, ice sheet	✓
Sed	Clim plus carbonate compensation	
Perm Sed	Clim plus carbonate compensation	✓
Sed Brines	Sed plus glacial ocean mechanisms	
Perm Sed Brines	Perm Sed plus glacial ocean mechanisms	✓

Table 1: simulation settings

Three simulations conditions are studied which included drivers and mechanisms identified in table 1. Each simulation is carried out for the standard CLIMBER-2 model and the CLIMBER-2P model which includes the permafrost-carbon mechanism in order to study to role of the permafrost-carbon in the carbon cycle. For simulations with

permafrost included for the carbon cycle, each of the dynamic settings is tested resulting in 4 outputs per simulation. These permafrost-carbon dynamic settings are described in Crichton et al (2014) and are named to give a qualitative description, relative to the other settings, of the rate of carbon accumulation and carbon release on thaw in modelled permafrost soils.

3. Results

3.1 LGM equilibrium

Atmospheric CO_2 and vertical $\delta^{13}C$ gradient in the Atlantic ocean for the LGM equilibrium simulations are shown in figure 1. The Clim simulation shows CO_2 levels of 309ppm. This is because the land biosphere has reduced with respect to PI (pre-industrial present-day), releasing carbon dioxide to the atmosphere and pushing atmospheric CO_2 higher. Without carbonate compensation or other glacial ocean mechanisms operating, this "excess" atmospheric CO_2 is not all taken up by the ocean. The inclusion of permafrost results in a CO_2 decrease from 309ppm (Clim simulation) to 197-204ppm (Perm simulation). Data points on figure 1 represent all permafrost-carbon dynamic settings; permafrost-carbon is equilibrated and LGM model outputs are very similar for all permafrost-carbon settings because LGM stocks are all tuned to the Ciais et al (2012) estimate. In this equilibrium spin-up experiment, the permafrost land-carbon uptake appears to, alone, explain all the LGM CO_2 draw-down. However, we know important mechanisms are missing because the Atlantic vertical $\delta^{13}C$ gradient is far too low in the Perm simulation. When the carbonate compensation is included but not the permafrost (Sed experiment) the LGM CO_2 becomes 281ppm (from 309ppm in Clim) because this mechanism amplifies ocean carbon uptake in glacial conditions. In the Perm Sed experiment, which includes both carbonate compensation and the permafrost mechanism, the LGM CO_2 level becomes 250-255ppm. The combined effects of permafrost-carbon and ocean carbonate compensation in Perm Sed act to *increase* atmospheric CO_2 with respect to the Perm simulation. The inclusion of permafrost reduces atmospheric CO_2 at the LGM by only around 30ppm when carbonate compensation is included.

None of the simulations without the glacial ocean mechanisms can reproduce the data indications of $\delta^{13}C$ distribution in the Atlantic ocean (Curry and Oppo 2005). The vertical $\delta^{13}C$ gradient in the Atlantic ocean shows better agreement with data when the glacial ocean mechanisms are included (Bouttes et al 2011). These mechanisms are the sinking of brines on sea-ice formation, ocean diffusion responding to stratification changes and the fertilisation of marine biota in response to increased atmospheric dust. The brines mechanism is based on the conceptual idea that the bottom water formation around Antarctica partly depends on the conditions above the continental shelves, in particular the position of the Antarctic ice sheet, the sea level (related to the volume of the Northern Hemisphere ice sheets) and rate of sea ice formation. These mechanisms are fully described by Bouttes et al (2009, 2011, 2012) including the temporal evolution

of sinking brines as a fraction of salt rejected on sea-ice formation during the last glacial termination. Dashed lines in figure 1 indicate the data range from ice core (CO_2, Monnin et al 2001) and ocean core (Atlantic $\delta^{13}C$ vertical gradient, Curry and Oppo 2005) studies. Model output points which are numbered 1 to 4 show the model settings that provide the best agreement with data and these settings are shown in the table in figure 1. Two of the four settings include the fertilisation of marine biota in response to atmospheric dust (1 and 3), and two of the settings do not (2 and 4). When compared to the Bouttes et al (2011) results, the model settings that show agreement with data are very similar to ours. This suggests that the permafrost-carbon mechanism does not have a strong impact on deep ocean $\delta^{13}C$ distribution, which is mainly controlled by ocean mechanisms.

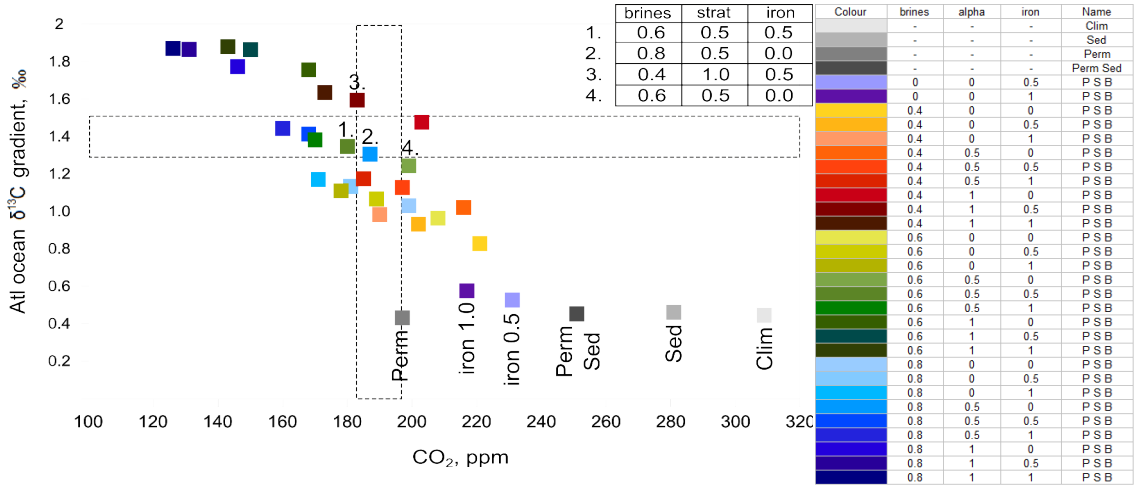

	brines	strat	iron
1.	0.6	0.5	0.5
2.	0.8	0.5	0.0
3.	0.4	1.0	0.5
4.	0.6	0.5	0.0

Colour	brines	alpha	iron	Name
	-	-	-	Clim
	-	-	-	Sed
	-	-	-	Perm
	-	-	-	Perm Sed
	0	0	0.5	P S B
	0	0	1	P S B
	0.4	0	0	P S B
	0.4	0	0.5	P S B
	0.4	0	1	P S B
	0.4	0.5	0	P S B
	0.4	0.5	0.5	P S B
	0.4	0.5	1	P S B
	0.4	1	0	P S B
	0.4	1	0.5	P S B
	0.4	1	1	P S B
	0.6	0	0	P S B
	0.6	0	0.5	P S B
	0.6	0	1	P S B
	0.6	0.5	0	P S B
	0.6	0.5	0.5	P S B
	0.6	0.5	1	P S B
	0.6	1	0	P S B
	0.6	1	0.5	P S B
	0.6	1	1	P S B
	0.8	0	0	P S B
	0.8	0	0.5	P S B
	0.8	0	1	P S B
	0.8	0.5	0	P S B
	0.8	0.5	0.5	P S B
	0.8	0.5	1	P S B
	0.8	1	0	P S B
	0.8	1	0.5	P S B
	0.8	1	1	P S B

Fig 1, Modelled atmospheric CO_2 plotted against vertical $\delta^{13}C$ gradient in the Atlantic ocean. Outlined in dashed lines are data ranges for each indicated by Monnin et al 2001 for LGM CO_2, Curry and Oppo 2005 for Atlantic vertical $\delta^{13}C$ gradient. Modelled Atlantic vertical $\delta^{13}C$ gradient is calculated as Bouttes et al 2011, as the difference between the "surface" (0-2000m) and deep (3000-5000m) mean Atlantic ocean $\delta^{13}C$.

3.2 Last deglaciation transient simulation

The settings and drivers for the transient deglaciations are shown in figure 2 (CO_2, sea-level, fraction of sinking brines) and figure 3. Figure 3 shows insolation at 60ºN in June (Berger and Loutre 1991) and the model-calculated permafrost area; demonstrating the sensitivity of the permafrost model to summer insolation at high latitudes. The variability of insolation in summer at 60°N is larger than the winter variability and as such it is the summer insolation that determines the southern limit of permafrost more than the winter insolation.

To isolate the contribution of each mechanism in a realistic transient deglaciation, where "realistic" denotes modelled atmospheric CO_2 levels and Atlantic $\delta^{13}C$ vertical gradient in agreement with data, the model outputs that do not include glacial ocean mechanisms are discussed first.

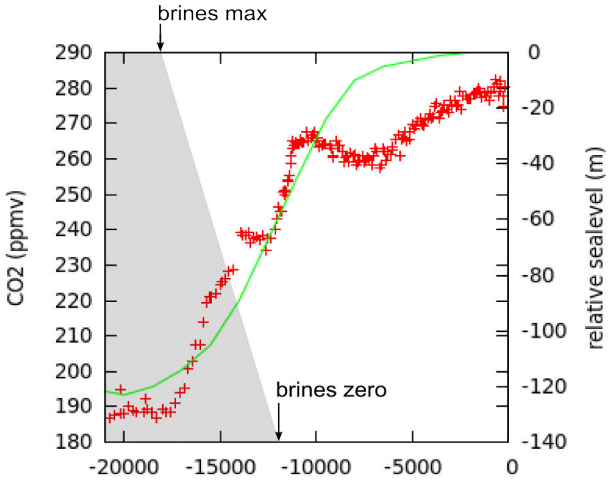

Fig 2, Drivers for the last deglaciation, red crosses: atmospheric CO_2 to drive the radiative code (Monnin et al 2001), green line: relative sea-level for ocean volume and ice sheet extent (Peltier 1994), grey shaded: brines controller, maximum at 18kyr BP with linear reduction to zero at 12kyr BP, as Bouttes et al (2012).

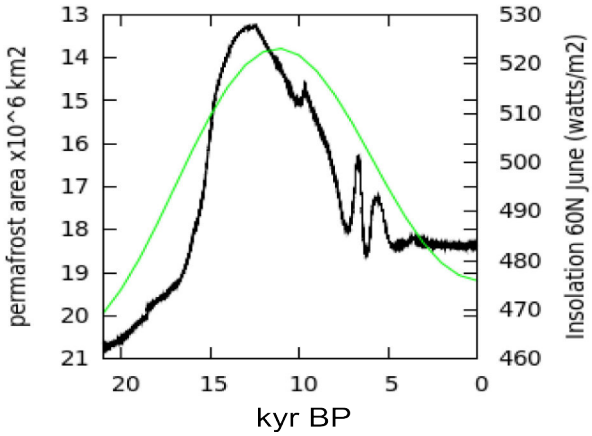

Fig 3, Modelled permafrost area (black line) on inverted scale overlaid on insolation at 60°N June, Berger and Loutre (1991).

3.2.1 Impact of permafrost-carbon mechanism

The Clim and Perm transient deglaciations, for all permafrost-carbon dynamic settings are shown in figure 4. Features will be discussed chronologically from LGM to PI. For all settings the simulation outputs which include the permafrost-carbon model starts to move away from the standard (Clim) model at around 19kyr BP, indicating a possible significant contribution of permafrost soils to the deglaciation CO_2 dynamics. For the medium, fast and xfast settings CO_2 starts to increase, and for the slow setting remains constant,. The xfast setting shows a good agreement with ice core data for both the CO_2 and the $\delta^{13}C$ values from 18kyr to 14kyr BP, but it starts to rise around 1000 years sooner than data.

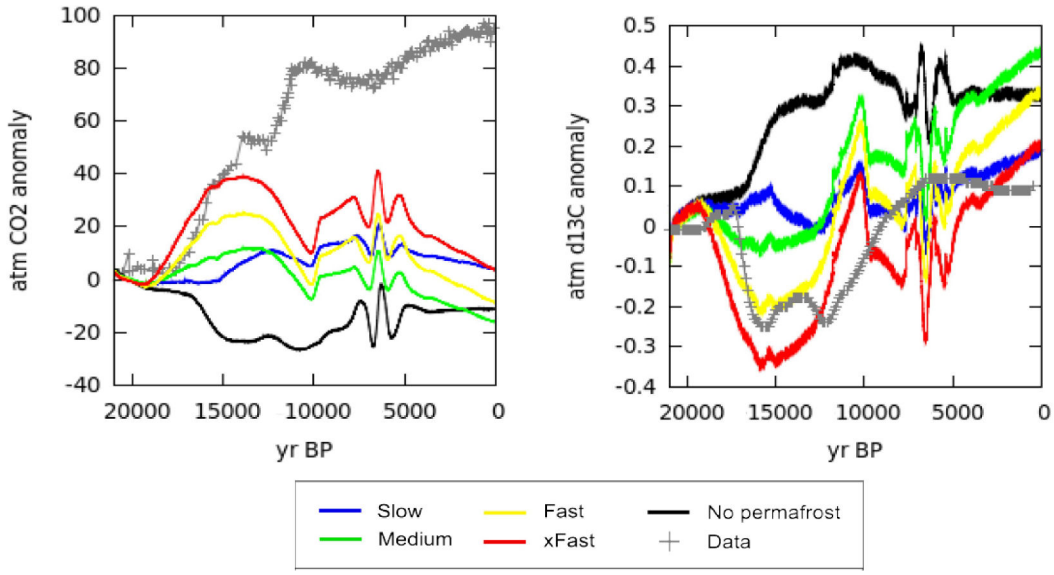

Fig 4, Clim and Perm modelled atmospheric CO_2 (left) and $\delta^{13}C$ (right). Data for CO_2 is Monnin et al (2001), $\delta^{13}C$ is Schmitt et al (2012). All data plotted with respect to the LGM value.

The total area available for permafrost is not only determined by frost-index, but also by the land area that is ice-free. The retreat of the northern hemisphere ice sheets increases the land area available for permafrost to exist. The total amount of carbon in these permafrost-soils is, in turn, not only determined from area, but also from carbon input from plant mortality and the rate of decay of carbon in soils. These characteristics can be seen in figures 3 and 5, the low for permafrost land carbon coincides with a minimum in total area of permafrost at around 12.5kyr BP.

All permafrost settings display a drop or dip in atmospheric CO_2 just before 10kyr BP, at this point the CO_2 data (a driver for vegetation model and radiative code) starts to drop, as has the insolation at northern high latitudes. Figure 5 shows model output for the land carbon, as permafrost and non-permafrost carbon. From 10kyr BP it shows land carbon has plateaued or is reducing. This pattern, together with the rise in modelled CO_2 seen in the Clim and Perm experiment, shows the rise in CO_2 after 10kyr BP must be due to an ocean carbon release. Just after 10kyr BP there is a short-lived decrease in permafrost area (fig 3) causing a land carbon release which combined with the ocean out-gassing results in a jump in atmospheric CO_2.

The model does not include peatlands, presently storing around 547GtC in northern peatlands (Yu et al 2010) or 278GtC in peat soils of the permafrost region (Tarnocai et al. 2009). From basal dating of peat cores (Yu et al. 2010) after 10kyr BP peatland initiation and growth created a land-carbon sink. In model output, the total land carbon

plateaus from around 10kyr BP with a later increase from 5kyr BP resulting from the stabilisation of permafrost area and accumulation of carbon in permafrost soils of up to 400GtC. The large fluctuations in model output from 7.5kyrBP to 5kyrBP are due to the instability and then the total collapse of vegetation in the Sahara/Sahel region causing feedbacks for the carbon cycle directly from land carbon stocks, but also feedbacks via albedo and thermal balance of the earth surface. The maximum CO_2 fluctuation is less than 20ppm, although not easily seen in the CO_2 data plot here, Luthi et al (2008) shows fluctuations of a maximum 10ppm around this time. There is evidence of vegetation collapse in the Sahara during this period from data and modelling studies (Brovkin et al 1998, Foley et al 2003, Kröpelin et al 2008, Janssen et al, 2008) but in its current configuration, CLIMBER-2 possibly exaggerates its effect on the carbon cycle.

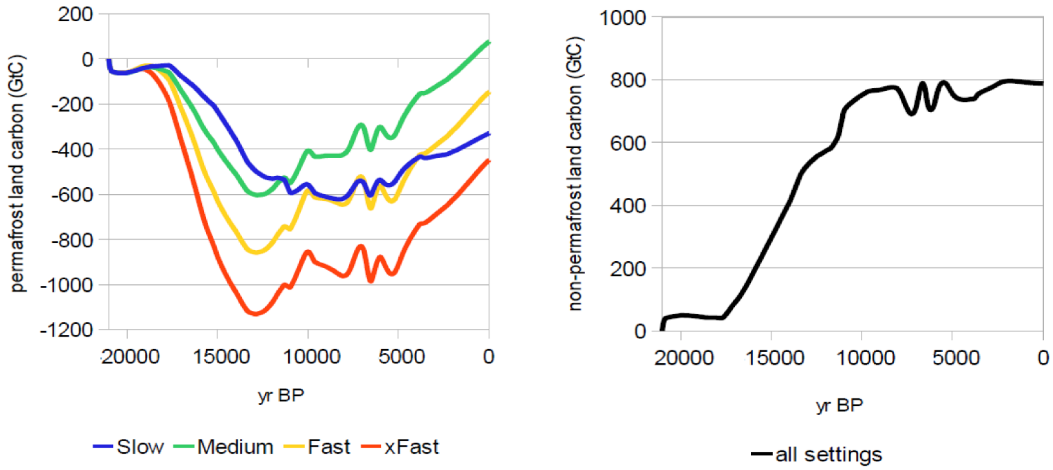

Fig 5, CLIMBER-2P Perm experiment, left: permafrost associated land carbon, right: non-permafrost land carbon. Permafrost land carbon is defined as the difference between model output with the permafrost-carbon and without the permafrost-carbon mechanism.

At the end of the deglaciation (0kyr BP) the total permafrost area is lower than at LGM and permafrost land carbon ranges from +80GtC to -420GtC depending on dynamic setting. The Ciais et al. 2012 estimate for the total change in inert land carbon stocks (here seen as equivalent to the modelled permafrost land carbon) is -700GtC from LGM to PI. The closest modelled amount is closer to -400GtC (for the tuning with greatest change). The Ciais et al (2012) estimate for active land carbon change is +1030GtC from LGM to PI, whilst the CLIMBER-2P modelled is +800GtC, this can account for some of the missing inert carbon change (as the model was tuned for *total* land carbon). As well as this, the transient deglaciation at 0kyr BP shows a slightly colder north Pacific region compared to a PI equilibrium simulation, this results in total permafrost area being higher than for the model tuning (Crichton et al. 2014, Zhang et al. 2000).

Without the inclusion of carbonate compensation in the ocean or any other ocean mechanism the CO_2 levels at the end of the deglaciation (0kyr BP) are rather similar to

the start values (21kyr BP). The range of the CO_2 levels between model output per permafrost-carbon dynamics settings at the end of the deglaciation is due to the differences in total land carbon for each setting and the 'speed' of the response of carbon in the permafrost soils (Crichton et al. 2014).

3.2.2 Impact of permafrost-carbon mechanism and carbonate compensation

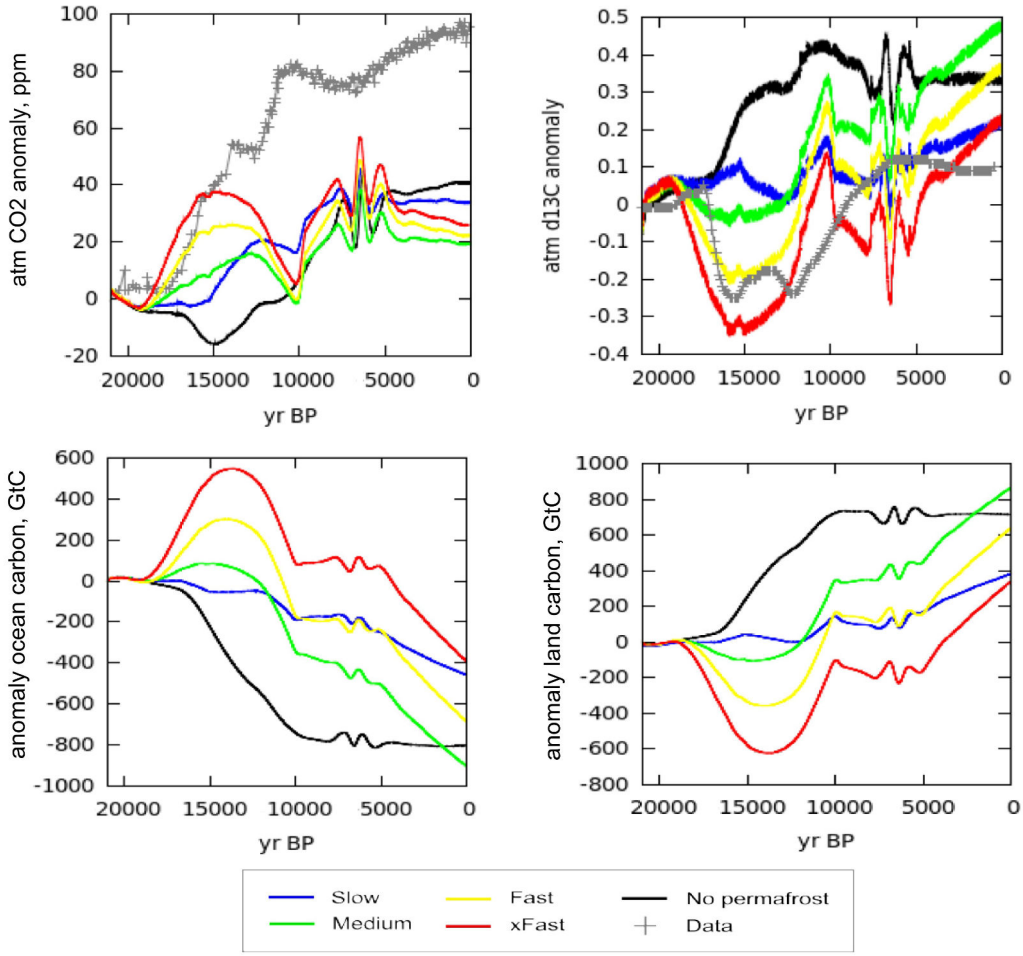

Fig 6, Sed and Perm Sed modelled atmospheric CO_2 (top left) and $\delta^{13}C$ (top right), ocean carbon anomaly wrt. LGM value (bottom left) and land carbon anomaly wrt. LGM (bottom right). Data for CO_2 is Monnin et al (2001), $\delta^{13}C$ is Schmitt et al (2012).

The Sed and Perm Sed experiment output is shown in figure 6. The mechanism causes the atmospheric CO_2 concentration to rise more between around 15kyr to 8kyr BP compared to the Clim (and Perm) simulation. The overall contribution of carbonate compensation to the final CO_2 change depends on whether permafrost-carbon is also included in the model, and on the dynamics of the permafrost carbon, but in all cases the contribution is reduced when permafrost is included in the model. Like the Perm experiment output the "xfast" permafrost setting has the best fit for rate and magnitude of the CO_2 increase from 18kyr to 15kyr BP and also for the $\delta^{13}C$ record from 18kyr to

around 10kyr BP. Figure 6 also shows the ocean and land carbon pools for the Sed and Perm Sed simulations. The effect of the carbon release from thawing permafrost causes the ocean to take-up carbon during the first half of the termination for the "medium" to "xfast" dynamic settings, and only to become a source of carbon after most of the land carbon release is completed. This is a significantly different profile to the standard model Sed experiment (shown as a black line), and to the general idea of the attribution of the rise in CO_2 during deglaciations. The permafrost-carbon mechanism included in the model does not, however, result in an atmospheric CO_2 value at LGM in agreement with data, with 250ppm rather than around 190ppm, nor with a rise in CO_2 by PI of around 90ppm. To be able to have a realistic deglaciation, glacial ocean mechanisms need to be invoked.

3.2.3 Impact of permafrost-carbon with all ocean mechanisms included

For the simulation which includes glacial ocean mechanisms (Perm Sed Brines or PSB, and Sed Brines) the fraction of sinking brines is linearly decreased from 18k yr to 12kyr BP (fig 2), and iron fertilisation, if included, depends on the dust record (Bouttes et al., 2012). The permafrost carbon mechanism provides an explanation for the initial rise in CO_2, seen in the Perm and Perm Sed simulations, which in the Bouttes et al. (2012) was reproduced by rapid reduction in the sinking brines. The scenario here, a linear reduction to zero between 18kyr and 12kyr BP, is a gradual change of conditions during the deglaciation towards a situation less favourable for the formation of very dense water on the shelves susceptible to sink to the abyss in the southern ocean.

Two of the ocean settings identified in figure 1 were used to run deglaciation simulations. These represent the closest matches for the data indications of CO_2 and Atlantic vertical $\delta^{13}C$ gradient, one which includes iron fertilisation and one which does not. Here-on-in setting 1 is discussed as “AllMechs” as it includes all the glacial ocean mechanisms, and setting 2 is discussed as “NoFert” as it does not include iron fertilisation of marine biota. The results for atmospheric CO_2 and atmospheric $\delta^{13}C$ for these two settings are shown in figure 7 as anomalies from LGM.

Deglaciation

During the deglaciation the deep ocean releases carbon due to the gradual reduction of the sinking of brines and increasing ocean mixing. This causes atmospheric CO_2 to continue to rise from 15kyr BP onwards compared to the Perm Sed modelled CO_2 output. The circulation re-organisation also speeds up the rate of northern high latitudes temperature rise compared to the Perm Sed simulation. This carbon from the ocean, which has a low $\delta^{13}C$ signature, also contributes to a drop in atmospheric $\delta^{13}C$, compared to the Perm Sed experiment and the faster warming causes carbon to be released more quickly from thawing permafrost soils. Due to this, the best-fit permafrost carbon dynamic setting now becomes the "medium" dynamic for $\delta^{13}C$. The overall best-

fit modelled rise in CO_2 is also the "medium" dynamic setting compared to the CO_2 data. Between the two ocean settings, NoFert shows a better model output fit with atmospheric $\delta^{13}C$ data. With the AllMechs, the $\delta^{13}C$ has final values lower than data show, and for the "medium" permafrost dynamic setting $\delta^{13}C$ is too low from 15kyr BP compared to data.

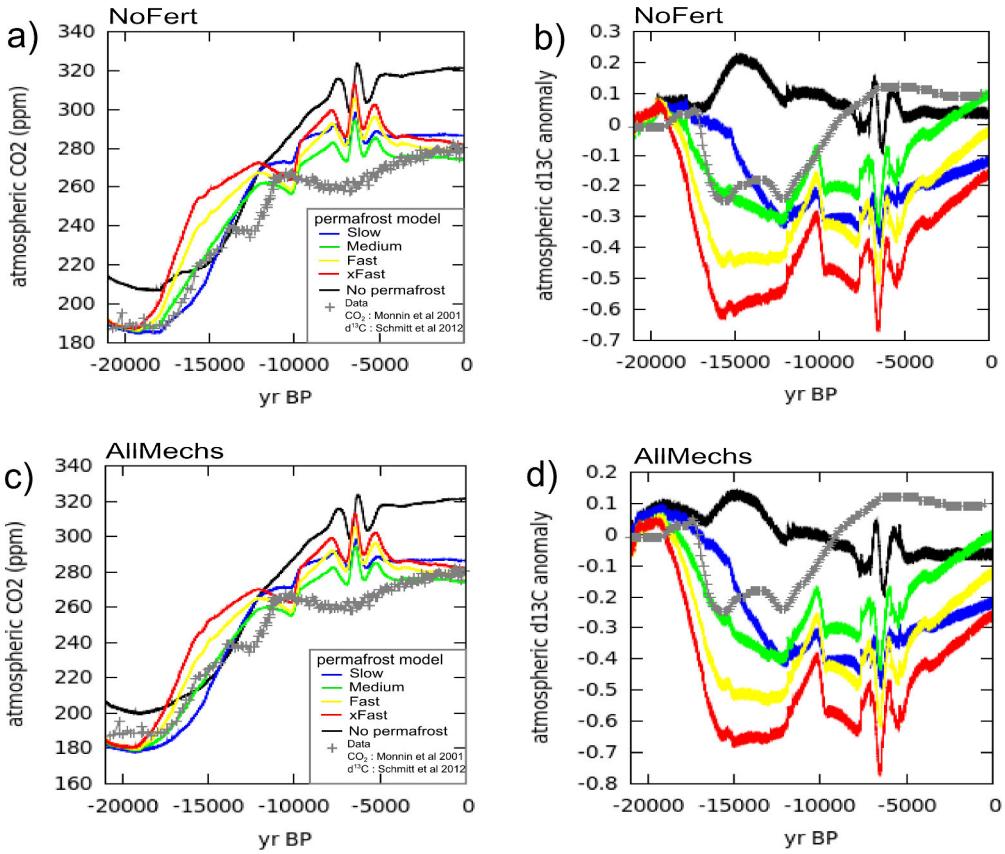

Fig 7, Modelled atmospheric CO_2 (left) and $\delta^{13}C$ (right) for Sed Brines and Perm Sed Brines experiments, for two settings identified in fig 5, NoFert (2. fig 5) 1. All mechs (1. fig 5). Data for CO_2 is Monnin et al (2001), $\delta^{13}C$ is Schmitt et al (2012).

The best fit "NoFert" setting, with "medium" permafrost-carbon dynamic is shown more closely in figure 8 for all simulations. The glacial ocean mechanism causes a cooler climate, and more carbon is stored on land in NoFert than in Perm Seds (for the medium carbon dynamic). Total ocean carbon anomaly shows that until around 15kyr BP the ocean is a sink, not a source of carbon for the Perm Sed Brines (PSB) simulation. The carbon released from permafrost increases the partial pressure of CO_2 in the atmosphere and causes the ocean to take-up carbon, this would have implications for surface ocean $\delta^{13}C$ values for region which take-up carbon-dioxide from the atmosphere.

The period between 14 to 12.5kyr BP, the Bolling Allerod to Younger Dryas (YD), the CO_2 record is not naturally reproduced by the model (figure 8), no fresh water forcing is represented in the model which has been identified as important for the strength of the

Atlantic Meridional Overturning Circulation (AMOC) (e.g. Tarasov and Peltier 2005, Kageyama et al. 2010). The AMOC transports heat to the northern hemisphere which, if reduced, would have an effect on total permafrost area and therefore atmospheric carbon according to this study.

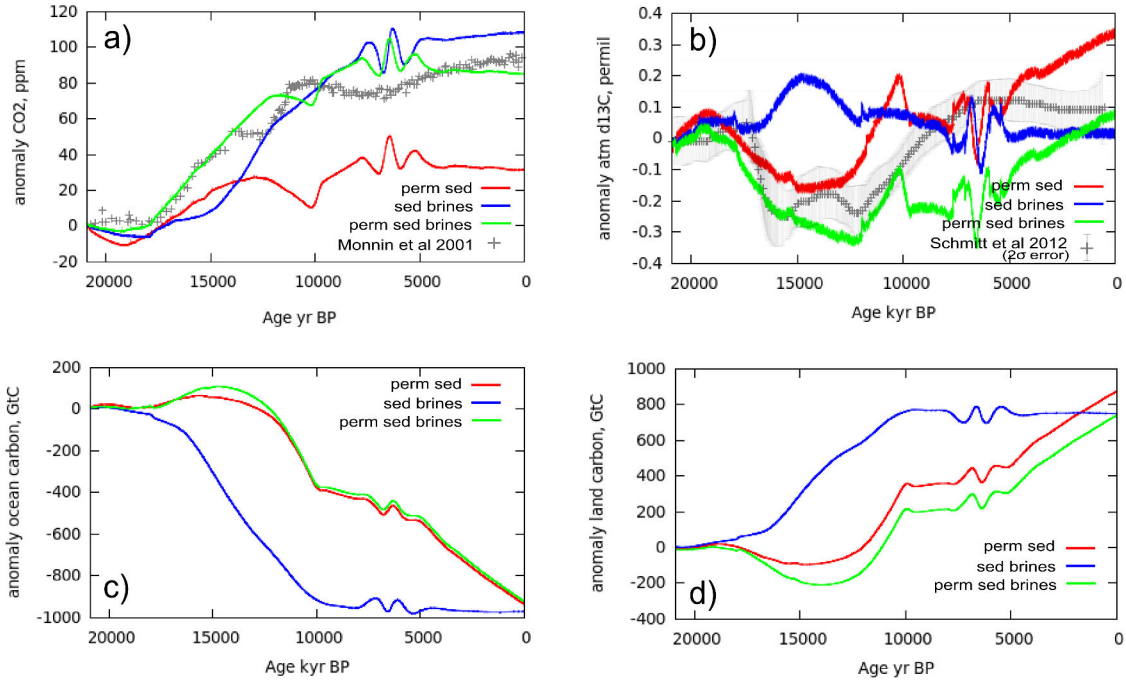

Fig 8, Modelled output comparing included mechanisms, red Perm Sed, blue Sed Brines, green Perm Sed Brines. Permafrost dynamic setting is "medium". Ocean settings are "NoFert". a) CO_2 ppm, b) atmospheric $\delta^{13}C$, c) anomaly ocean carbon wrt LGM value GtC, d) anomaly land carbon wrt LGM GtC.

Holocene trends

At 10kyr BP the modelled $\delta^{13}C$ diverges from the data, where data continues to rise the model shows a fast short term drop, a plateau then a rise. The $\delta^{13}C$ drop coincides with a fast modelled CO_2 rise, both a result of a short-term fast decrease in permafrost area (fig 3). At the same time the atmospheric CO_2 data has reached a plateau and starts to drop; the CO_2 data is used to drive the vegetation model and the radiative code for climate which combine to cause a plateauing of global NPP. The reduction in CO_2 seen in data from 10kyrBP has been attributed to peatland initiation and carbon accumulation (Yu et al. 2010) and the subsequent gradual increase from 7.5kyrBP has been explained in some studies as being due to post Holocene-maximum reduction in NPP (Brewer et al. 2007) or carbonate compensation (Elsig et al. 2009); although it is interesting to note this kind of pattern of gradual and steady increase in CO_2 is not clearly seen in CO_2 records of previous interglacials (Ruddiman 2003, Luthi et al. 2008).

At around 6kyr BP the permafrost area is too large (compared to present-day estimates).

As it responds to insolation changes and gradual CO_2 rise this causes carbon to accumulate in the frozen ground which in turn causes a gradual increase in modelled atmospheric $\delta^{13}C$. The permafrost carbon model (Crichton et al. 2014) was tuned using present-day estimates of permafrost affected ground for the pre-industrial equilibrium simulation, however, at the end of the transient deglaciation permafrost area is too high by around 4 to $5x10^6$ km^2. The north Pacific region in the transient simulation of pre-industrial period is colder than the PI equilibrium simulation. This may point to transient effects in ocean circulation, or may be related to land runoff and increased weathering at PI, which for the transient simulation is kept at LGM levels. The effect of this can be seen from around 7kyr BP in the increasing total land carbon stocks, resulting in the reduction in atmospheric CO_2 and the decreasing total ocean carbon.

The "medium" permafrost dynamic setting in NoFert creates a final total land carbon amount higher than estimated by Ciais et al. 2012 (Crichton et al. 2014), however, the $\delta^{13}C$ anomaly at 0kyrBP is in agreement with the data. If the land uptake was smaller, then this $\delta^{13}C$ anomaly would be more negative, moving further away from the data. CLIMBER-2P takes no account of methane, which has an effect on $\delta^{13}C$ of the atmosphere with a $\delta^{13}C$ signature on the order of -50‰ (-25‰ to -100‰ depending on source, Maslin and Thomas 2003), which with higher atmospheric methane levels at PI from data may also tend to pull atmospheric $\delta^{13}C$ more negative, the "wrong" direction according to the model. The model was tuned to fit $\delta^{13}C$ data for the present day (Crichton et al, submitted), but according to our analysis of the transient changes and the mechanisms we know are missing, it shouldn't fit the data both at LGM and at the present-day. This hints that important mechanisms that drove the atmospheric $\delta^{13}C$ changes in the real World are missing from our model, for example northern peatlands/wetlands (Yu et al 2010) and possibly a perturbed carbon cycle (for example Ruddiman 2007).

Comparison with marine data

Modelled ocean $\delta^{13}C$ and data from benthic foraminifera are shown in figure 9. The standard model, the no-permafrost case, shows agreement with mean data in the deep South Atlantic ocean. When permafrost is included in the model, the deep South Atlantic ocean $\delta^{13}C$ still shows good agreement still with data but now the ocean carbon uptake (from the atmosphere) from 17.5 to 15 kyrBP delays the deep ocean $\delta^{13}C$ rise. This result, compared to the data mean, suggests that the ocean glacial mechanism controller (sinking brines in this case) may have started to evolve sooner in the deglaciation than 18kyrBP (as we have modelled). It also suggests that the time taken for this evolution may have been even longer than the 6000 years brines evolution imposed in the simulations (from 18 to 12kyr BP). The CLIMBER-2(P) basin averaged Atlantic ocean model has been shown to be representative of the western Atlantic current, where the data shown in figure 9 is for any North Atlantic surface ocean location. In the North Atlantic surface ocean, a region of carbon uptake from the

atmosphere, the standard model shows fairly poor agreement with data patterns for both simulations. When permafrost is included the $\delta^{13}C$ shows a stronger negative shift, larger than the data range. This may be a result of using the mean data from all North Atlantic locations (Oliver et al 2010), not just from the west Atlantic current. In any case, the surface $\delta^{13}C$ data shows characteristics more similar to atmospheric data, a net drop during the termination period (from 18-13kyr BP) and a rise net thereafter (from 12-5kyrBP). Although the model with permafrost overestimates the initial drop, the general pattern is better than when permafrost is not included in the model.

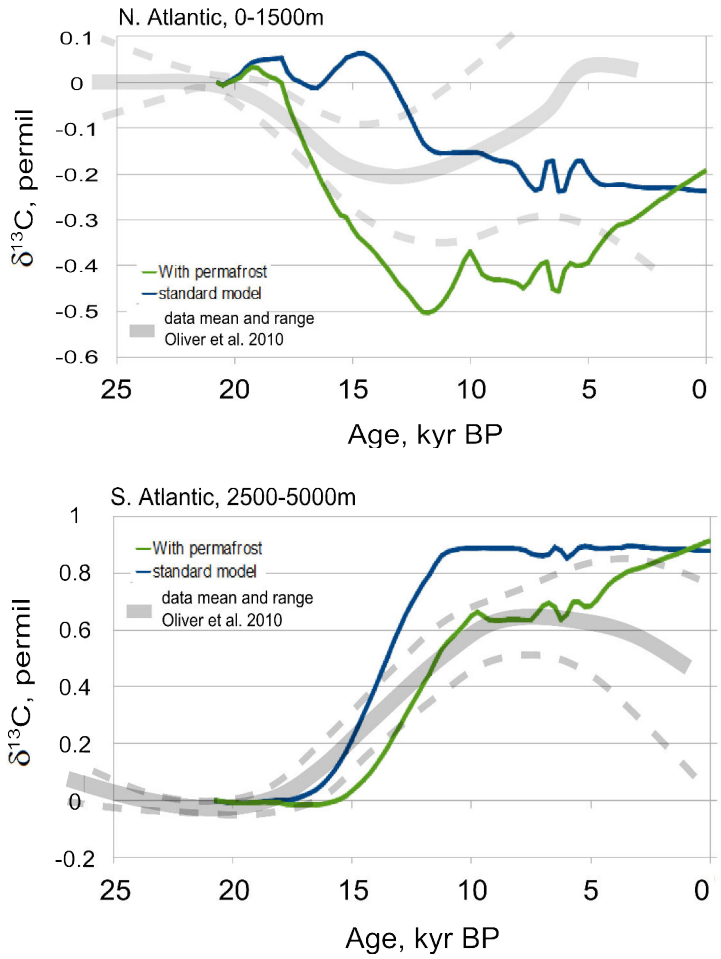

Fig 9, Modelled ocean $\delta^{13}C$ for surface North Atlantic and deep South Atlantic ocean overlaid on data for benthic $\delta^{13}C$ (Oliver et al 2010). Model output for standard model is without permafrost-carbon with matching ocean glacial mechanisms evolution, linear reduction in fraction of sinking brines from 18kyr to 12kyr BP.

Continental carbon change spatially

The changes in the amount of carbon stored in soil during the modelled deglaciation are shown in figure 10, plotted per grid cell for 40°N to 70°N and positioned per latitude and longitude. The cell that is the major contributor to the loss of soil carbon during the

first part of the deglaciation is southern-eastern Russia, with northern Europe and northern USA also contributing. Northern western Russia contributes carbon loss a little later in the deglaciation, the remaining of the northern-most cells do not lose carbon during the deglaciation, but rather accumulate carbon as NPP increases due to more favourable conditions for plant growth and as carbon input to soils increase, and also as the ice sheet retreats exposing new land surface for plant growth.

The permafrost-carbon model is a very simplified representation of the effect of freezing on soil decay. Currently for the PI it predicts too-high soil carbon concentrations in the coldest regions of northern Siberia. The presence of permafrost does not affect NPP in the model or rooting depth. In the real world, permafrost limits the maximum depth at which roots can grow, which reduces carbon input to the soils. As well as this, the model does not have a wetlands plant communities representation which increase the soil carbon concentration in high soil moisture conditions, which would include the southern boundaries of the Eurasian permafrost region, and also a large part of N.America (Tarnocai etal 2009).

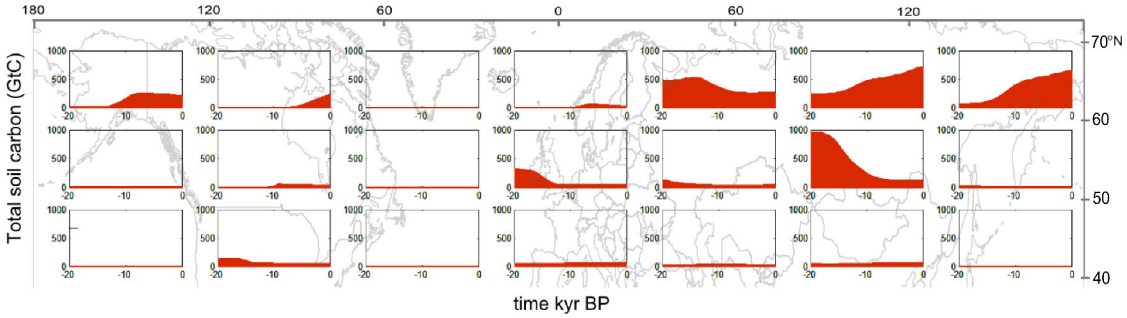

Fig 10, CLIMBER-2P PSB, NoFert "medium" permafrost dynamic experiment change in total soil carbon from LGM to pre-industrial plotted per grid cell overlaid on map, 40N to 70N, to show the location of each cell.

During a deglaciation the Western Northern Russia, Scandinavian and Northern European grid cells should show an increased carbon storage from around 10k yrBP due to peatland initiation and growth (Yu et al. 2010), which the model does not show. The modelled Alaska, Southern Canada and Northern Canada grid cells already show some increases in soil carbon storage from 10kyr BP, but it is expected that the Alaskan and Southern Canada cells should have even more carbon accumulation from around 10kyr BP again due to peatland initiation and growth. The model takes no account of the Siberian shelf which would have been exposed during the glacial period, it is likely there was significant carbon storage on this exposed land (Sher et al. 2005). An LGM equilibrium simulation using the NoFert medium dynamic setting with two extra grid cells exposed north of Siberia (an extra 4.1×10^6 km^2 of permafrost affected land) was carried out. This resulted in a total land carbon storage of 3765GtC, some 80GtC more

compared to the no-shelf case. This compares to around 113GtC to 202GtC according to reconstructions of Montenegro et al. (2006). As well as this, the model is known to underestimate permafrost extent at LGM. With the glacial ocean mechanisms an extra 0.13 $x10^6$ km^2 of permafrost is modelled due to the colder climate compared to the no glacial ocean mechanisms case. Although this is still an underestimate compared to data (Crichton et al. 2014). The South-western Russia and Northern China regions would likely have contributed more significantly to carbon losses from land at the start of the termination if it was modelled as 100% permafrost at LGM, as data suggests (Vandenberghe et al 2008).

4. Discussion

Measurements of the $\delta^{13}C$ signature of CO_2 bubbles trapped in ice cores indicate a clear drop in atmospheric $\delta^{13}C$ around the start of the last deglaciation at the same time as a fast rise in atmospheric CO_2 (Lourantou et al. 2010, Schmitt et al. 2012). A permafrost-carbon mechanism, in which slow accumulation of carbon in permafrost affected soils causes high soil carbon concentration by the end of the glacial period that is released quickly on thaw, reproduces a $\delta^{13}C$ drop and initial CO_2 rise as seen in the data. This result is found when only climate; obtained with ice sheets, ocean volume, CO_2 radiative code drivers and insolation patterns drive CLIMBER-2P to simulate a deglaciation. The release of land carbon via the permafrost-carbon mechanism from around 18kyr BP is directly in response to the changes in insolation at high northern latitudes. Previous qualitative studies which addressed the possible impact of a land-carbon source for the CO_2 rise since LGM rejected the hypothesis on the grounds that whole ocean $\delta^{13}C$ had become more positive since LGM, and the land biosphere had increased in size. The results from the current study support the conclusion that permafrost-carbon is not responsible for the full rise in atmospheric CO_2 during the deglaciation, but they do suggest that, with fresh water forcing influencing AMOC strength, the $\delta^{13}C$ record may be able to be reproduced. In our model with no fresh water forcing, atmospheric $\delta^{13}C$ dropped from around 18kyrBP, a few hundred years too early according to data. However, without the permafrost mechanism, no drop on the scale of that shown in data could be reproduced, as Bouttes et al (2012). The full rise in CO_2 and the general pattern of $\delta^{13}C$ in the atmosphere and in the ocean can be reasonably well reproduced by combining permafrost-carbon with carbonate compensation and glacial ocean mechanisms. These mechanisms operating along with reducing ice sheet area, increasing ocean volume and changing insolation can explain the deglaciation.

A possible argument against the contribution of northern hemisphere soils to the CO_2 rise between 17.5kyr BP to 15kyr BP are records which suggest relatively small increasing temperatures in this period in Europe and the European plain (Clark et al. 2012), and particularly in the Greenland temperature record (Johnsen et al. 2001). Not many land-based proxy records for temperature are available for regions which may have been permafrost and high-soil-carbon affected at the LGM period (Clark et al.

2012), especially in the southern Russian and Siberian region. The attribution of the lag of temperature increase (Shakun et al. 2012) in the northern hemisphere in general has been thought to be the result of reduction in the strength of the AMOC, which transports heat to the northern Atlantic, and northern hemisphere, from the Southern hemisphere. Relative sea level records for the H1 (Heinrich 1) event, ice-berg discharge and fresh water flushing to the north Atlantic which is thought to be the cause of AMOC switch-off, do not show a consensus for a large sea-level rise at this time (Carlson and Clark 2012). Ocean carbon-14 ages from sediment cores covering the deglaciation (Stern and Lisiecki 2014) suggest an AMOC reduction during H1. An increase in radiocarbon age of these waters is considered to represent the increased influence of older polar waters on the water mass, caused by an AMOC reduction and a southward shift in the Northern Polar Front. However, this neglects the possibility that the north Atlantic acted as a carbon sink for "old" permafrost land carbon during this period, as we suggest in our study, whereby reductions in ocean water radiocarbon may have been due to uptake of the atmospheric signal, which was increasing in age (Broecker and Barker 2007) due to "old" carbon released from permafrost. Considering these arguments, the release of permafrost carbon cannot be disqualified by existing data records. The results from the experiments in this study suggest that the permafrost mechanism accounts for around 20 to 30ppm CO_2 rise during the first 6000 years of the deglaciation. Here 20 to 30ppm is the difference between experiments with and without permafrost for the "medium" dynamic setting. The "medium" dynamic output, when combined with ocean mechanisms has the overall best agreement with the range of CO_2 and $\delta^{13}C$ variations seen in ice core records (figure 7) representing a carbon release rate of around 0.15GtC per year from 17.5kyr BP to 13kyr BP. This release rate in comparison with the Perm and Perm Sed simulations, which showed ~0.23GtC (xfast dynamic) per year as best fit for data, demonstrate the importance of including all driving mechanisms in modelling studies. Without the ocean mechanisms, which cause changes in ocean circulation and deep ocean carbon storage and explain a large proportion of the low glacial CO_2 levels seen in data, the best fit permafrost carbon release rates would have appeared to be twice as fast. The 'best-fit' NoFert setting presented in figure 8 does not include a contribution from iron fertilisation. Although previous studies show that during glacial periods an iron fertilisation of marine biota effectively reduced atmospheric CO_2 (to a maximum of around 30ppm), other studies indicate no change in productivity in the ocean between glacial and interglacial conditions (Wolff et al. 2006). Our study suggests that iron fertilisation of marine biota is not required to explain low glacial CO_2 data or atmospheric $\delta^{13}C$ data for the termination.

5. Conclusions

The results of this study suggest that permafrost is an important mechanism acting within the carbon cycle. Modelled outputs with best agreement with $\delta^{13}C$ and CO_2 atmospheric data from ice cores show that a land carbon sourced release starting at around 18kyr can explain the onset of the CO_2 rise at the start of the deglaciation. The

carbon release rate of 0.15GtC/yr mean between 17.5kyr and 13.5kyr BP from the land combined with deep southern ocean sourced carbon out-gassing starting a few thousand years later explain the CO_2 rise and its timing. The initiator of the carbon release from land is changes in insolation at high northern latitudes, which have previously been identified as a driver of glacial cycles (Milankovitch 1941, Imbrie et al. 1992), that increase summer temperatures. At the same time the reduction of sinking of brines, caused by salts rejected on ice formation in the southern ocean, starts to change deep ocean circulation. This results in the ocean out-gassing CO_2 from 15kyr BP that contributes to CO_2 rise in the atmosphere. The carbon release from the land would have effected the ocean $\delta^{13}C$ signal. A re-analysis of surface and mid-ocean $\delta^{13}C$ data may be able provide more evidence for the appraisal of this permafrost-carbon hypothesis.

Acknowledgements
The research leading to these results has received funding from the European Community's Seventh Framework Programme (FP7 2007-2013) under Grant 238366 (GREENCYCLES II) and under grant GA282700 (PAGE21, 2011-2015). D.M. Roche is supported by INSU-CNRS and by NWO under project no. 864.09.013.

References

Adams, J.M., Faure, H., Faure-Denard, L., McGlade, J.M., Woodward, F.I. 1990. 'Increases in terrestrial carbon storage from the Last Glacial maximum to the present'. Nature 348, 711–714.

Berger A. and Loutre M.F., 1991, Insolation values for the climate of the last 10 million of years. Quaternary Sciences Review, Vol. 10 No. 4 pp. 297-317.

Bopp, L., Kohfeld, K.E., Le Quere, C. 2003. Dust impact on marine biota and atmospheric CO_2 during glacial periods. Paleoceanography 18: 2, 1046, doi: 10.1029/2002PA000810

Bouttes, N., Roche, D.M., Paillard, D. 2009. Impact of strong deep ocean stratification on the glacial carbon cycle. Paleoceanography 24: PA3203, doi:10.1029/2008PA001707

Bouttes, N., Paillard, D., Roche, D.M., Brovkin, V., Bopp, L. 2011. 'Last glacial maximum CO_2 and δ13C successfully reconciled', Geophysical Research Letters, 38, doi:10.1029/2010GL044499.

Bouttes, N., Paillard, D., Roche, D.M., Waelbroeck, C., Kageyama, M., Lourantou, A., Michel, E., Bopp, L. 2012. 'Impact of oceanic processes on the carbon cycle during the last termination', Climate of the Past, 8, p149-170.

Brewer, S., Guiot, J., Torre, F. 2007. Mid-Holocene climate change in Europe: a data-model comparison. Climate of the Past: 3, 499-512.

Broecker, W.S., Peng, T-H., 1993. 'What caused the glacial to interglacial CO_2 change.' In: Heimann, M. (Ed.), The Global Carbon Cycle, NATO ASI Series, Vol. 15. Springer, Berlin.

Brovkin, V., Claussen, M., Petoukhov, V., & Ganopolski, A. 1998. On the stability of the

atmosphere-vegetation system in the Sahara/Sahel region. Journal of Geophysical Research: Atmospheres (1984–2012), 103(D24), 31613-31624.

Brovkin, V., M. Hofmann, J. Bendtsen, and A. Ganopolski. 2002. 'Ocean biology could control atmospheric δ13C during glacial interglacial cycle,' Geochem. Geophys. Geosyst., 35, 10.1029/2001GC000270

Brovkin, V., A. Ganopolski, D. Archer, and S. Rahmstorf. 2007. 'Lowering of glacial atmospheric CO_2 in response to changes in oceanic circulation and marine biogeochemistry,' Paleoceanography, 22, PA4202, doi:10.1029/2006PA001380.

Carlson, A. E., and P. U. Clark. 2012. Ice sheet sources of sea level rise and freshwater discharge during the last deglaciation, Rev. Geophys., 50, RG4007, doi:10.1029/2011RG000371.

Ciais, P., Tagliabue, A., Cuntz, M., Bopp, L., Scholze, M., Hoffman, G., Lourantou, A., Harrison, S.P., Prentice, I.C., Kelley, D.I., Koven, C., Piao, S.L. 2012. 'Large inert carbon pool in the terrestrial biosphere during the Last Glacial Maximum', Nature Geoscience, DOI: 10.1038/NGEO1324

Clark, P.U., and Mix, A.C. 2002. Ice sheets and sea level of the Last Glacial Maximum. Quaternary Science Reviews. 21: 1-7

Clark, P.U., Shakun, J.D., Baker, P.A., Bertlein, P.J., Brewer, S., Brook, E., Carlson, A.E., Cheng, H., Kaufman, D.S., Liu, Z., Marchitto, T.M., Mix, A.C., Morrill, C., Otto-Bliesner, B.L., Pahnke, K., Russell, J.M., Whitlock, C., Adkins, J.F., Blois, J.L., Clark, J., Colman, S.M., Curry, W.B., Flower, B.P., He, F., Johnson, T.C., Lynch-Stieglitz, J., Markgraf, V., McManus, J., Mitrovica, J.X., Moreno, P.I., Williams, J.W. 2012. Global climate evolution during the last deglaciation. PNAS. Doi:10.1073/pnas.1116619109

Crichton, K.A., Chappellaz, J., Krinner, G., Roche, D. 2014. A simplified Permafrost-Carbon model for long-term long term climate studies with the CLIMBER-2 coupled Earth system model. Accepted for review, Geoscientific Model Development Discussions.

Crowley, T.J., 1995. 'Ice age terrestrial carbon changes revisited.' Global Biogeochemical Cycles 9, 377–389.

Curry, W. B. and Oppo, D. W. 2005: Glacial water mass geometry and the distribution of $\delta^{13}C$ of SUM CO_2 in the western Atlantic Ocean, Paleoceanography, 20, PA1017, doi:10.1029/2004PA001021.

Duplessy, J.-C., Shackleton, N.J., Fairbanks, R.J., Labeyrie, L.D., Oppo, D., Kallel, N., 1988. 'Deep water source variations during the last climatic cycle and their impact on the global deep water circulation.' Paleoceanography 3, 343–360

Elsig, J., Schmitt, J., Leuenberger, D., Schneider, R., Eyer, M., Leuenberger, M., Joos, F., Fischer, H., Stocker, T.F. 2009. Stable isotope constraints on Holocene carbon cycle changes from an Antarctic ice core. Nature. 461, doi: 10.1038/nature08393

Foley, J. A., Coe, M. T., Scheffer, M., & Wang, G. 2003. Regime shifts in the Sahara and Sahel: interactions between ecological and climatic systems in Northern

Africa. Ecosystems, 6(6), 524-532.

Ganopolski A., Petoukhov V., Rahmstorf S., Brovkin V., Claussen M., Eliseev A., Kubatzki C. 2001. CLIMBER-2: a climate system model of intermediate complexity. Part II: model sensitivity. Climate Dynamics. 17: 735-751

Harden, J.W., Koven, C.D., Ping, C., Hugelius, G., McGuire, A.D., Camill, P., Jorgenson, T., Kuhry, P., Michaelson, G.J., O'Donnell, J.A., Schuur, E.A.G, Tarnocai, C., Johnson, K., Grosse, G. 2012. Field Information links permafrost carbon to physical vulnerabilities of thawing. Geophysical Research Letters. 39, L15704, doi: 10.1029/2012GL051958

Imbrie, J., Boyle, E. A., Clemens, S. C., Duffy, A., Howard, W. R., Kukla, G., ... & Toggweiler, J. R. 1992. On the structure and origin of major glaciation cycles 1. Linear responses to Milankovitch forcing. Paleoceanography, 7(6), 701-738.

Janssen, R.H.H., Meinders, M.B.J., Van Nes, E.H. and Scheffer, M. 2008. Microscale vegetation-soil feedback boosts hysteresis in a regional vegetation–climate system. Global Change Biology, 14: 1104–1112. doi: 10.1111/j.1365-2486.2008.01540.x

Johnsen, S. J., Dahl-Jensen, D., Gundestrup, N., Steffensen, J. P., Clausen, H. B., Miller, H., Masson-Delmotte, V., Sveinbjo¨ rnsdottir, A. E. and White, J. 2001. Oxygen isotope and palaeotemperature records from six Greenland ice-core stations: Camp Century, Dye-3, GRIP, GISP2, Renland and NorthGRIP J. Quaternary Sci., Vol. 16, pp. 299–307. ISSN 0267-8179.

Kageyama, M., Paul, A., Roche, D.M., Van Meerbeeck, C.J. 2010. Modelling glacial climatic millenial-scale variability related to changes in the Atlantic meridional overturning circulation:a review. Quaternary Science Reviews. 29: 2931-2956

Koven, C.D., Ringeval, B., Friedlingstein, P., Ciais, P., Cadule, P., Khvorostyanov, D., Krinner, G., Tarnocai, C. 2011. Permafrost carbon-climate feedbacks accelerate global warming. PNAS. 108, 14769-14774

Kröpelin, S., Verschuren, D., Lézine, A. M., Eggermont, H., Cocquyt, C., Francus, P., ... & Engstrom, D. R. (2008). Climate-driven ecosystem succession in the Sahara: the past 6000 years. science, 320(5877), 765-768.

Kump, L.R and Arthur, M.A. 1999. Interpreting carbon-isotope: carbonates and organic matter. Chamical Geology. 161: 181-198.

Lourantou, Lavric, J.V., Kohler, P., Barnola, JM., Paillard, D., Michel, E., Raynaud, D., Chappelaz, J. 2010. 'Constraint of the CO_2 rise by new atmospheric carbon isotopic measurements during the last deglaciation', Global Biogeochemical Cycles, 24, BG2015, doi:10.1029/2009GB003545.

Lüthi, D., Le Floch, M., Bereiter, B., Blunier, T., Barnola, J. M., Siegenthaler, U., ... & Stocker, T. F. (2008). High-resolution carbon dioxide concentration record 650,000–800,000 years before present. Nature, 453(7193), 379-382.

MARGO Project Members: Constraints on the magnitude and patterns of ocean cooling at the Last Glacial Maximum, Nature Geoscience., 2, 127–132,

doi:10.1038/ngeo411, 2009.
Maslin, M.A., Thomas, E. 2003. 'Balancing the deglacial global carbon budget: the hydrate factor', Quaternary Science Reviews, 22, 1729-1736
Milankovitch, M. 1941. Kanon der Erdbestrahlung und seine Anwendung auf das Eiszeitproblem. Akad. R. Serbe 133, 1–633 (1941).
Monnin, E., Indermuhle, A., Daellenbach, A., Flueckiger, J., Stauffer, B., Stocker, T. F., Raynaud, D., and Barnola, J.-M.: Atmospheric CO_2 concentrations over the Last Glacial Termination, Science, 291, 112–114, 2001.
Montenegro, A., Eby, M., Kaplan, J.O., Meissner, K.J., Weaver, A.J. 2006. Carbon storage on exposed continental shelves during the glacial-interglacial transition. Geophysical research Letters. 33, L08703, doi: 10.1029/2005GL025480
Oliver, K. I. C., Hoogakker, B. A. A., Crowhurst, S., Henderson, G. M., Rickaby, R. E. M., Edwards, N. R. and Elderfield, H. 2010. A synthesis of marine sediment core 13C data over the last 150 000 years. Climate of the Past, 6, pp. 645–67
Peltier WR. 1994. Ice Age Paleotopography. Science. 265 (5169): 195-201
Peltier, W. R. 2004. Global glacial isostasy and the surface of the ice-age Earth: the ICE-5G (VM2) model and GRACE. Annu. Rev. Earth Planet. Sci., 32, 111-149.
Petoukhov V., Ganopolski A., Brovkin V., Claussen M., Eliseev A., Kubatzki C., Rahmstorf S. 2000. CLIMBER-2: a climate system model of intermediate complexity. Part 1: model description and performance for present climate. Climate Dynamics. 16:1-17
Ruddiman, W.F. 2003. The anthropogenic greenhouse era began thousands of years ago. Climatic Change, 61, 261-293.
Ruddiman, W.F. 2007. The early anthropogenic hypothesis: Challenges and Responses. Reviews of Geophysics, 45, RG4001, doi: 10.1029/2006RG000207
Schaefer K., Zhang T., Bruhwiler L., Barrett AP. 2011. Amount and timing of permafrost carbon release in response to climate warming. Tellus. Doi: 10.1111/j.1600-0889.2011.00527.x
Shakun, J.D., Clark, P.U., He, F., Marcott, S.A., Mix, A.C., Liu, Z., Otto-Bliesner, B., Schmittner, A., Bard. 2012. Global warming preceded by increasing carbon dioxide concentratons during the last deglaciation. Nature. 484. doi:10.1038/nature10915
Schaphoff S., Heyder U., Ostberg S., Gerten D., Heinke J., Lucht W. 2013. Contribution of permafrost soils to the global carbon budget. Environmental Research Letters. 8: 014026. doi: 10.1088/1748-9326/8/1/014026
Schmitt, J. et al. 2012. Carbon isotope constraints on the deglacial CO_2 rise from ice cores, Science, 336, 711, DOI: 10.1126/science.1217161
Schneider von Diemling T., Ganopolski A., Held H., Rahmstorf S. 2012. How cold was the Last Glacial Maximum? Geophysical Research Letters. 33. L14709. Doi: 10.1029/2006GL026484
Schuur, E., Bockheim, J., Canadell, J., Euskirchen, E., Field, C.B., Goryachkin, S.V.,

Hagemann, S., Kuhry, P., Lafleur, P.M., Lee, H., Mazhitova, G., Nelson, F.E., Rinke, A., Romanovsky, V.E., Shiklomanov, N., Tarnokai, C., Venevsky, S., Vogel, J.G., Zimov, S.A. 2008. 'Vulnerability of permafrost to climate change: Implications for the global carbon cycle', BioScience, 588, 701-714.

Shackleton, N.J. 1977. Carbon 13 in Uvigerina: tropical rain forest history and the equatorial Pacific carbonate dissolution cycles. In: Anderson, R.L.N. and Malaho, A. (eds), The Fate of Fossil Fuel CO_2 in the Oceans, pp. 401-427. Plenum, New York.

Sher, A.V., Kuzmina, S.A., Kuznetsova, T.V., Sulerhutsky, L.D. 2005. New insights into the Weichselian environment and climate of the East Siberian Arctic, derived from fossil insects, plants and mammals. Quaternary Science Reviews. 24: 533-569

Tarasov, L. and Peltier, W.R. 2005. Arctic freshwater forcing of the Younger Dryas cold reversal. Nature. 435. doi:10.1038/nature03617.

Tarnocai C., Canadell JG., Schuur EAG., Kuhry P., Mazhitova G., Zimov S. 2009. Soil organic carbon pools in the northern circumpolar permafrost region. Global Biogeochemical Cycles. 23. GB2023. Doi: 10.1029/2008GB003327

Van Campo, E., Guiot, J., Peng, C.H. 1993. 'A data-based re-appraisal of the terrestrial carbon budget at the last glacial maximum.' Global and Planetary Change 8, 189–201.

Vandenberghe, J., Velichko, A., and Gorbunov, A. 2008: Forcing factors of permafrost retreat: a comparison between LGM and present-day permafrost extent in Eurasia, edited by: Kane, D. L. and Hinkel, K. M., 9th Int. Conf. Permafrost Fairbanks, 327–328.

Wolff, E. W.; Fischer, H.; Fundel, F.; Ruth, U.; Twarloh, B.; Littot, G.; Mulvaney, R.; Röthlisberger, R.; de Angelis, M.; Boutron, C.; Hansson, M.; Jonsell, U.; Hutterli, M.; Bigler, M.; Lambert, F.; Kaufmann, P.; Stauffer, B.; Steffensen, J. P.; Siggaard-Andersen, M. L.; Udisti, R.; Becagli, S.; Castellano, E.; Severi, M.; Wagenbach, D.; Barbante, C.; Gabrielli, P.; Gaspari, V. 2006. Southern Ocean sea-ice extent,productivity and iron flux over the pasteight glacial cycles. Nature. 440:doi:10.1038/nature04614

Yu, Z., Loisel, J., Brosseau, D.P., Beilman, D.W., Hunt, S.J. 2010. Global peatland dynamics since the Last Glacial Maximum. Geophysical Research Letters. 37, L12402, doi: 10.1029/2010GL043584

Zhang T., Heginbottom JA., Barry RG., Brown J. 2000. Further statistics on the distribution of permafrost and ground ice in the Northern Hemisphere. Polar Geography. 24:2, 126-131. doi 10.1080/10889370009377692

Zimov, N.S., Zimov, S.A., Zimova, A.E., Zimova, G.M., Chuprynin, V.I., Chapin III, F.S. 2009. 'Carbon storage in permafrost and soils of the mammoth tundra-steppe biome: Role in the global carbon budget', Geophysical Research Letters, 36, L02502, doi:10.1029/2008GL036332.

4.3 Termination 2

Atmospheric $\delta^{13}C$ data for termination 2 has recently become available from Schneider et al. (2013). Using this data it is possible to further test the hypothesis that permafrost-carbon plays a role during termination periods. The termination 1 simulations presented in the previous section utilise the glacial ocean dynamic settings from Bouttes et al. (2012). A linear reduction in the sinking of brines between 18-12kyr BP within the Earth system that included the permafrost-carbon mechanism resulted in modelled atmospheric CO_2 and $\delta^{13}C$ in general agreement with data measurements until around 10kyrBP. In order to test the model for termination 2, the glacial ocean mechanism evolution first needs to be defined. Two settings were tested, the first based on the change in deep Atlantic ocean benthic $\delta^{13}C$ data presented by Lisiecki and Raymo (2008), and the second based on the $\delta^{13}C$ data combined with the benthic $\delta^{18}O$ stack (as a proxy for land ice volume). The first tested setting is a linear reduction of sinking brines between 140k to 125kyr BP, and the second a linear reduction between 135k to 125kyr BP. The termination period simulation is run with evolving nutrient concentration for ocean volume, insolation, ice sheet and CO_2 to drive the radiative and vegetation model. Here the ice sheets are modelled as the same extent as LGM for PGM period, with land ice volume scaled according to sea-level change.

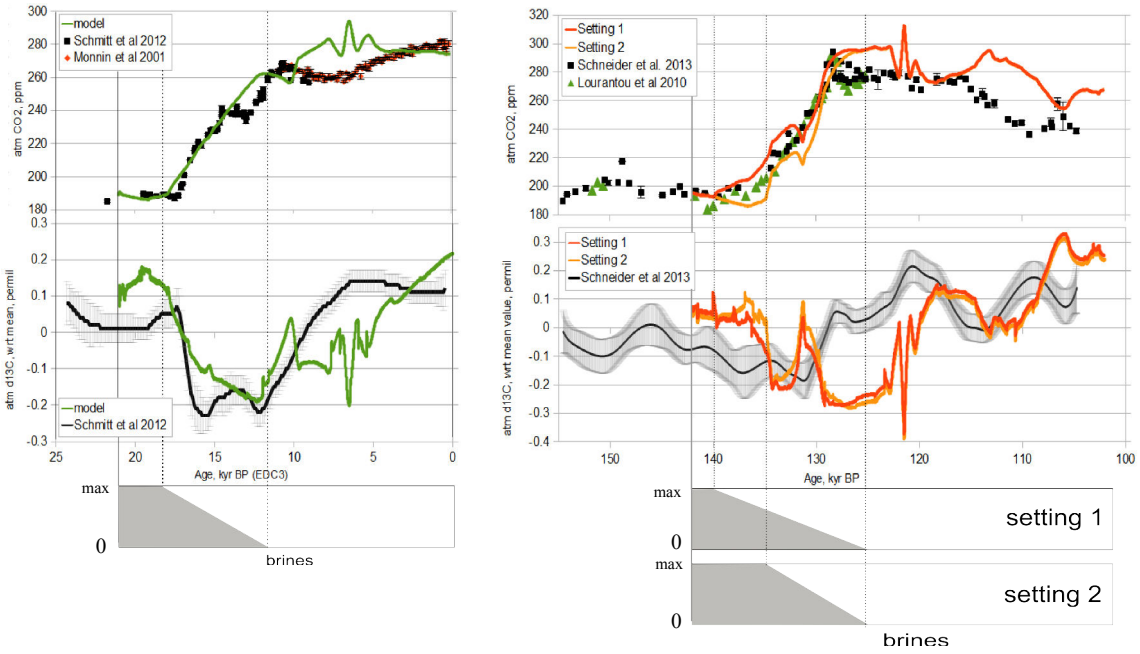

Fig 4.2: Atmospheric CO_2 and $\delta^{13}C$ model output overlaid on data for terminations 1 (left) and 2 (right). Data for atmospheric $\delta^{13}C$ plotted with respect to its mean value. Permafrost dynamic setting is "medium". Ocean settings are "NoFert".

Model results for termination 1 and termination 2 are shown in figure 4.2, here CO_2 is plotted as ppm and $\delta^{13}C$ plotted with respect to its mean value over the

simulation. The model output is overlaid on measurement data. The rate of CO_2 rise during termination 2 and total anomaly with respect to PGM (penultimate glacial maximum) is in reasonable agreement with data. The amplitude of $\delta^{13}C$ changes over the simulated termination 2 period (here covering also the Last Interglacial, LIG) also agrees with data measurements amplitude. The onset of CO_2 rise at termination 2, from 137kyrBP, does not appear to be associated with an obvious drop in atmospheric $\delta^{13}C$ in the data. At around 140kyrBP there is a drop in atmospheric $\delta^{13}C$, although less sudden than in termination 1. The dynamics of permafrost are dependent upon insolation forcing, climate and ice sheet dynamics on the land surface. For the termination 2 simulation, the timing of changes in insolation and ice sheet area in northern high latitudes are subject to uncertainty, as is the ice core age model for CO_2 data. When analysing the $\delta^{13}C$ and CO_2 model outputs this must be kept in mind. In the model output, the rise in CO_2 from 137kyrBP is created largely from permafrost-thaw so a drop in $\delta^{13}C$ is seen in model output, at a time when data suggests a rise in $\delta^{13}C$. Thereafter, from 130kyrBP the fast rise in $\delta^{13}C$ seen in data occurs when the model is showing a fast drop in $\delta^{13}C$. The sustained rising trend in $\delta^{13}C$ in data between 130kyrBP to 120kyrBP is also not seen in model output, that only rises starting from around 125kyrBP. The peaks and troughs in atmospheric $\delta^{13}C$ data occurring from 120kyr to 105kyr BP are similar in length and amplitude to the changes seen in model output at this time, but appear to be shifted in timing by around 3000 years.

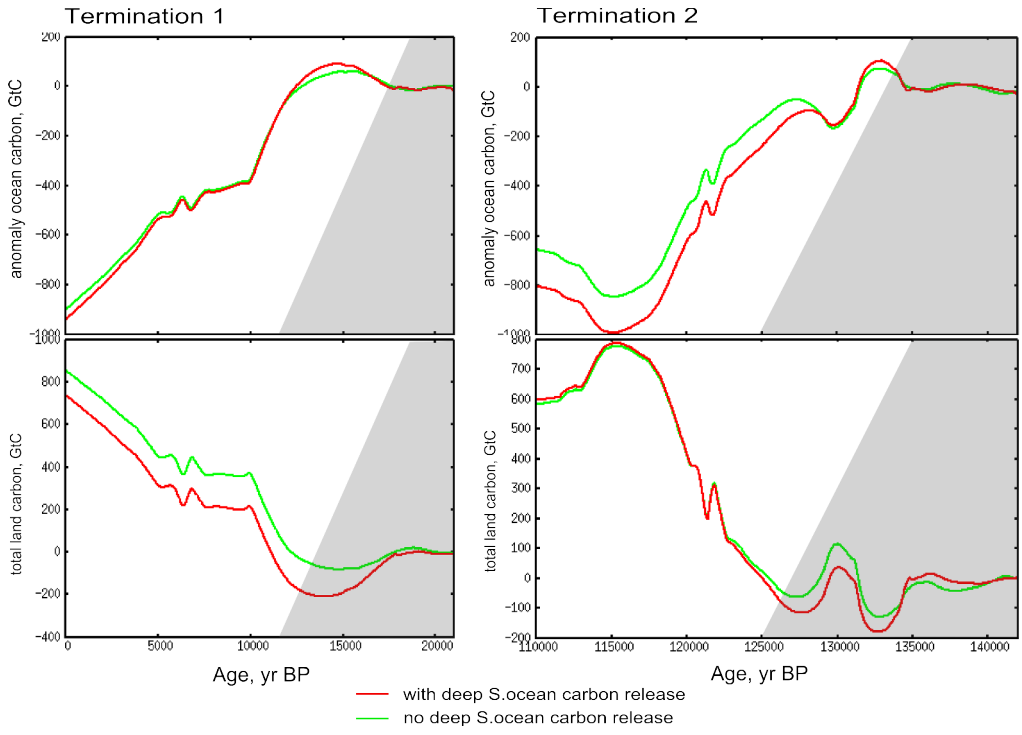

Fig 4.3: Ocean carbon anomaly and total land carbon plotted for termination 1 and termination 2. Green line is Perm Sed, red line is Perm Sed Brines. Termination 2 brines is setting 2. Shaded is brines controller from maximum value to zero. Permafrost dynamic setting is "medium". Ocean settings are "NoFert".

Changes in modelled ocean and land carbon stocks for both terminations are shown in figure 4.3, where model output that includes the glacial ocean mechanisms of sinking brines and stratification dependent diffusion (in red) is compared to model output without these mechanisms (in green). The shaded region indicates the reduction in the sinking of brines occurring through the termination period. In both cases, the changes in ocean circulation caused by the reduction in sinking brines causes the land to lose carbon faster than in the case without glacial ocean mechanisms. From 135kyr to 128kyr BP the changes in ocean carbon between model output with or without glacial ocean mechanisms is not very different for both simulations. For termination 1 this is also the case through the deglaciation period. The two terminations show differing distributions of carbon between land and ocean during the interglacial period relative to the glacial maximum. When glacial ocean mechanisms are included, relatively less carbon is stored in the ocean by the start of the Eemian interglacial (~129kyr BP) compared to termination 1.

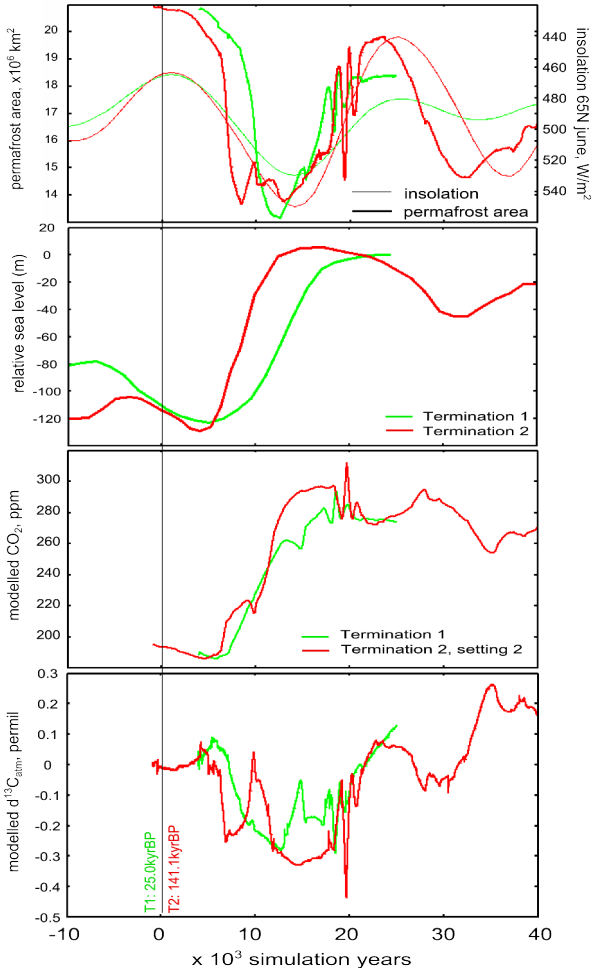

Fig 4.4: Comparing model output for termination 1 and termination 2. Insolation 65N maximum and minimum values matched for deglaciation periods to compare model output. a) Insolation and modelled permafrost area, b) relative sea level showing T2 sea level rise occurring sooner in the insolation cycle than for T1, c) CO_2 ppm, d) atmospheric $\delta^{13}C$ ‰.

Modelled output from the last two terminations are plotted together by matching 65ºN summer insolation maxima and minima (Lascar et al 2004) shown in figure 4.4. Plotting the two outputs like this allows the comparison of the timing of events and drivers of the terminations. The most obvious difference is the timing between the rise in sea-level and insolation increases. For T2 relative sea-level rises faster and sooner with respect to insolation forcing, occurring on average around 6k years sooner than for T1. The combined effect of this is that permafrost area falls sooner (with respect to insolation) at T2 compared to T1 by around 4-5kyrs. The ocean glacial mechanisms controller for T2 in fig 6.4 is a linear reduction in sinking brines from 135kyr to 125kyr BP. Relative to the insolation change, T2 CO_2 begins to rise sooner than at T1 as a result of the drop in permafrost area occurring sooner in T2 than T1. However, data CO_2 starts to rise even sooner than this (figure 6.2), being ahead of modelled (brines setting 2) CO_2 rise. It is possible that error or offsets in age models used to interpret measurement data (for sea-level, insolation or CO_2) has resulted in an offset in model output at T2 compared to data. The age model used for the CO_2 and $\delta^{13}C$ gas age dating by Lourantou et al (2010) and Schneider et al (2013) is the EDC3 age model (Parrenin et al 2007). This age model shows agreement with Vostok and Dome Fuji age scales within 1kyr back to 100kyr BP, but shows discrepancies to those age scales larger than 3kyrs during MIS 5.4, 5.5 and 6 (Parennin et al 2007). These are the periods covering termination 2 and the Eemian interglacial.

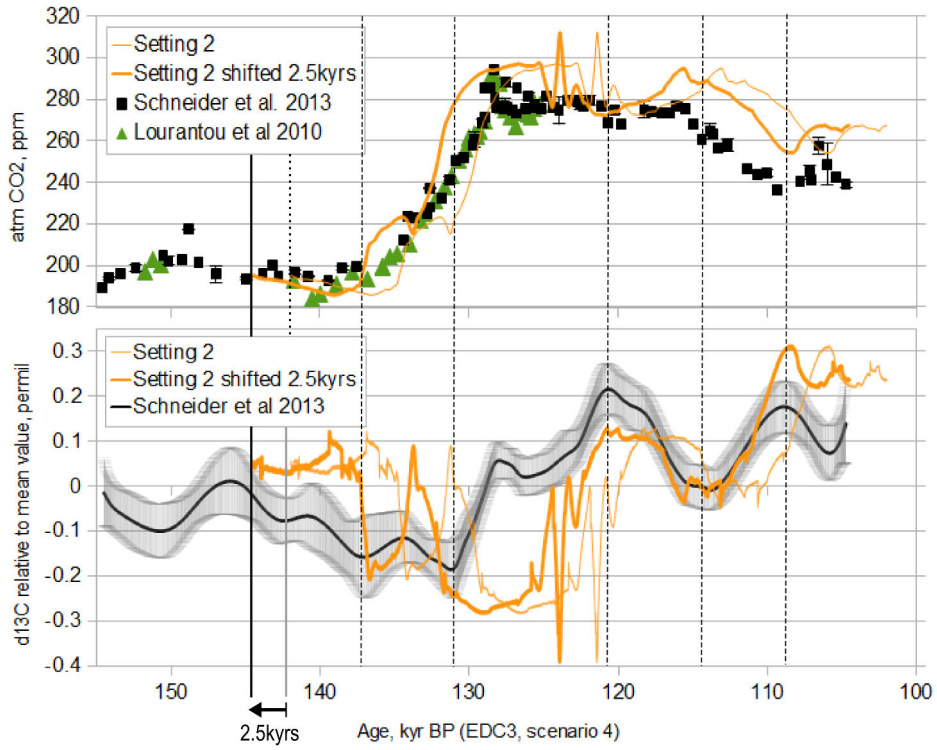

Fig 4.5: Termination 2 CO_2 and $\delta^{13}C$ model output overlaid on data. Model output shifted 2.5kyrs to give a closer fit to Schneider et al (2013) $\delta^{13}C$ data.

The modelled T2 output is shown in figure 4.5, here model output is shifted by 2.5kyrs with respect to the data's age model, which we know is likely less reliable at this time, to better fit dynamics seen in the data. Now the shifts in modelled $\delta^{13}C$ show better agreement with shifts in data and CO_2 rise, although occurring faster and in two steps, is similar to data. Dashed lines in figure 4.5 indicate periods where modelled $\delta^{13}C$ and data $\delta^{13}C$ match for minima and maxima and changes in sign of trends. The overestimate in the $\delta^{13}C$ drop seen at 138kyrBP coincides with an overestimate in CO_2. This indicates that, possibly, too much carbon is lost via the permafrost-carbon mechanism in the model. This may be explained via the simplification of the ice sheet evolution in the model. At PGM the ice sheet extended further over the Siberia/N.W.Russia land mass than at LGM (Svendsen et al 2004), although in the CLIMBER-2P model the ice sheet extent at PGM and LGM are very the same. This land area that would have actually been covered in ice holds around 200GtC in the modelled PGM period. The case in N. America may have been similar, resulting in an overestimate of permafrost carbon there as well. As well as this, data suggests a colder and even less hospitable climate during PGM with less vegetation (e.g. Roucoux et al 2011). Modelled NPP at PGM is 44GtC/yr and at LGM is 43GtC/yr. The model, if with a larger ice sheet at PGM, and climate system feedbacks, would likely result in a lower global NPP. This would in turn result in lower carbon stocks globally, affecting both the non-permafrost and permafrost vegetation and soils. This reduced terrestrial carbon pool in non ice sheet areas and the reduced permafrost-carbon pool (due to ice cover) may be enough to explain the lower $\delta^{13}C$ in the atmosphere at PGM. According to the emission tests (section 4.1) an estimated reduction of around 600GtC would result in an equilibrium drop of ~0.3‰ in atmospheric $\delta^{13}C$, -0.3‰ being the absolute difference between mean $\delta^{13}C$ at PGM compared to LGM (Schneider et al 2013, Schmitt et al 2012). Further studies would need to be done in order to test this hypothesis.

With a reduced permafrost land area, and a lower permafrost carbon stock at PGM, the amount of carbon released on termination of the glacial period would also be reduced compared to model output. This may explain why the $\delta^{13}C$ drop seen in data for T1 is greater and more defined than for T2. Between 137kyr and 130kyr BP the rise then fall in $\delta^{13}C$ data is also seen in (shifted) model output, although far more defined in the model. This $\delta^{13}C$ change is a result of permafrost area change (fig 6.4) and the more exaggerated response of the model may be a combined effect of the simplified permafrost-carbon model and the overestimate of permafrost land carbon at PGM.

From 130kyrBP the modelled and data $\delta^{13}C$ diverge, and model $\delta^{13}C$ rises late, lagging data. This is very similar to the pattern seen in T1 from 12kyr BP where $\delta^{13}C$ starts to rise in the data, modelled output initially rises then falls and later rises lagging the $\delta^{13}C$ data rise. The rise in model $\delta^{13}C$ from after 12kyrBP is attributable to a fast increase in permafrost area and carbon accumulation in newly frozen soils. The lag in model $\delta^{13}C$ with respect to data is similar to the lag seen in termination 2. As discussed for T1 in the previous section, this may be attributed to the lack of peatland and wetland dynamics in CLIMBER-2P. Basal dating of peat columns show accumulation of carbon in peat would have created a land carbon sink from around 10kyrBP. Atmospheric CO_2

levels at the time of $\delta^{13}C$ rise in T1 at 12kyrBP are 240 to 245ppm. CO_2 levels during T2 when $\delta^{13}C$ data starts to rise from 129kyrBP are also 240ppm. Climate conditions at these two points were likely similar for each termination, stimulating peatland expansion, and so the peatland/wetland dynamic may also explain the model-data mismatch from 129kyr BP at termination 2. From 120kyrBP model and data output are very similar for both $\delta^{13}C$ and CO_2 when the model output is shifted as fig 6.5. The CO_2 drop from 117kyr BP is a result of ocean carbon uptake in the model and a more stable total land carbon stock (fig 6.3). The total drop in CO_2 at this time is underestimated in the model, but at this point no glacial ocean mechanisms are operating. If they had started to operate again in the cooling climate then the ocean draw-down may be stronger and the CO_2 record may be better reproduced.

4.3.1 Conclusions

The simulation of termination 2 shows that the hypothesis of the role of permafrost-carbon during termination periods is not invalidated by T2 $\delta^{13}C$ and CO_2 data. The model output is strongly dependent on the accuracy of age models used to create drivers such as ice sheet extent, insolation and CO_2. During termination 2 the combined results of data and model output suggest that total land carbon, in the permafrost zone and elsewhere, was probably lower at PGM than at LGM. The onset of CO_2 rise at the termination can be partly explained as a loss of permafrost carbon, but the $\delta^{13}C$ data suggest that this was less strong than for T1 or it was more strongly compensated for during T2 compared to T1, for example a land carbon uptake via increasing NPP. The total increase in CO_2 from PGM to LIG (the Last Inter-Glacial, the Eemian) is overestimated in the model output, again this may be due to an overestimate of permafrost land-carbon at PGM which then releases too much carbon to the atmosphere, or may be due to a pre-industrial present-day CO_2 anomaly (with respect to the natural system) with which the model was tuned, creating a high CO_2 at LIG. The length of the LIG is well reproduced when permafrost-carbon is accounted for in the model and when no glacial ocean mechanisms operate between 125kyr to 115kyrBP (the cold summer in the southern hemisphere). According to the mean data mismatch with model output, the role of peatland initiation and carbon accumulation in these soils is also likely an important mechanism to explain both CO_2 and atmospheric $\delta^{13}C$ dynamics from glacial to interglacial conditions. Further studies using CLIMBER-2P for termination 2 should be carried out, investigating more thoroughly the role played by permafrost independently of ocean settings and vice versa. It should also include a system sensitivity study to the model drivers of sea-level, ice sheet extent, CO_2 record age model and insolation changes.

Chapter 5 Modelling glacial cycles

The chapter presents results of long time-scale experiments with the permafrost-carbon mechanism coupled with CLIMBER-2. The first set of experiments are for the last glacial cycle running from 142kyr BP to the pre-industrial present day and shows model sensitivity to the drivers of ice sheet, CO_2 and insolation. The second experiment is a long time-scale simulation from 432kyr BP to pre-industrial climate using the CLIMBER-2P model with the best-fit medium permafrost dynamic, but without any glacial ocean mechanisms operating. The permafrost model is sensitive to insolation changes, as expected, and to CO_2 as an amplifier. It is also particularly sensitive to ice sheet dynamics which determine the area of land available for permafrost to exist.

5.1. Introduction and Background

5.1.1 Climate

In 1941 Milankovitch linked the changes in summer insolation at high latitudes (65° North) to glacial-interglacial oscillations. In 1976, Hays, Imbrie and Shackleton used two ocean sediment cores to test the veracity of Milankovitch's orbital-paced glacial cycles theory. They used oxygen-18 isotope of foraminifera shells recorded in the deep sea sediments to reconstruct global ice volume, subantarctic radiolarieans to reconstruct temperature and the percentage of C.divisiana down the cores to reconstruct local ocean conditions. They performed frequency domain tests and time-domain tests on the results to find the dominant pacings of climate changes. They confirmed that orbital geometry were the drivers of glacial cycles and also predicted that in the absence of anthropogenic forcings the trend would be for extensive northern hemisphere glaciation in the next few thousand years.

In 2004 EPICA community members published a 740kyr CO_2 record from Antarctica's Dome C core, identifying a slightly different pattern in CO_2 from 740kyr to 430kyr BP. Prior to 430kyr BP Antarctic temperatures were less warm in the interglacial periods, but these interglacials lasted longer than those after 430kyr BP. They found that the interglacial period following termination V (430kyr BP) was especially long and postulated that the present interglacial warm period may extent well into the future even in the absence of any anthropogenic forcing. Also in 2004, the northern Greenland ice coring project members (NGRIP) published a 123kyr record of Greenland temperature, allowing the comparison of northern and southern hemisphere climate responses on longer timescales. In 2006 Wolff et al. published a continuous chemical proxy data record for EPICA dome C, finding that on millennial time-scales, maximum sea-ice extent was closely tied to Antarctic temperature. They found no change in internal feedbacks that explain the changes in amplitude seen in data after 440kyr BP. In 2007 the EPICA dome C deuterium, a proxy for temperature, record was extended back to 800k years (Jouzel et al. 2007).

The questions posed by the original geological studies are still subjects of research. The question of timing and pacing of glacial scale climate changes and Milankovitch theory and controlling mechanisms are subjects of study. Kawamura et al. 2007 used the ratio of oxygen to nitrogen molecules trapped in air in ice cores to determine a proxy for local summer insolation. They found that on the orbital scale Antarctic climate change lags northern hemisphere change by a few millennia, and increasing CO_2 occurred within the rising phase of NH temperature during the last four terminations, supporting Milankovitch theory. However, Ganopolski and Roche, 2009, used an EMIC to study lead-lag relationships during glacial-interglacial transitions concluded that lead-lag studies of data records alone were not sufficient to understand the system. Considering the synchronicity of local summer insolation in Antarctica and the ice-core temperature record, Laepple et al. 2011 concluded that seasonal cycles in snow accumulation, and its effect on the ice core record, meant that the Antarctic

temperature record could not be used to support or contradict a norther hemisphere climate controller.

5.1.2 Carbon cycle

Although Milankovitch theory links increasing high northern latitudes' summer insolation to the onset of terminations, the carbon cycle component currently most widely believed to be responsible for rising CO_2 at these times lies in the Southern ocean. In 1995 Sowers and Bender published a chronology for the GISP (Greenland), Vostok and Byrd (Antarctica) ice cores using $\delta^{18}O$ of molecular oxygen trapped in ice. They found that CO_2 began to rise 2000 to 3000 years before warming began in Greenland, and with timing closely linked to the warming in Antarctica. They conclude that it was the CO_2 rise that then resulted in deglaciation and warming of temperate and boreal regions in the northern hemisphere. Sigman and Boyle in 2000 identified that the biological and physical mechanisms in the ocean surrounding Antarctica in a glacial state could explain a significant part of the difference in atmospheric CO_2 compared to interglacial periods.

Updating the southern hemisphere sourced carbon hypothesis, Sigman et al. in 2010 reviewed data and studies that supported the deep Southern Ocean (SO) as being an important part of the explanation of atmospheric CO_2 changes. Evidence particularly from Opal flux, an indicator for ocean upwelling, supported the hypothesis that on glacial timescales the Southern Ocean (SO) played an important role. Fischer et al. 2010 presented a synthesis of the SO processes and their role in atmospheric CO_2 variations on orbital and millennial timescales. They compiled the most recent ice core and marine core records on atmospheric CO_2, temperature and environmental change in the SO region along with carbon cycle experiments to quantify the SO's effect on the carbon cycle. They note that the waxing and waning of sea ice and it's subsequent effect on the surface buoyancy flux may go some way to explain the high correlation of CO_2 and Antarctic temperature. Iron fertilisation of marine biota in the SO, which was previously a favoured explanation of CO_2 drawdown during glacial periods (Bopp et al 2003) was determined to have only a small effect on CO_2 drawdown, as it is likely limited by factors such as bioavailability of iron or other nutrients. Bouttes et al. 2010 proposed that the sinking of brines, rejected on sea-ice formation, produces a stratification which provided an amplifier of the effect of sea ice formation and ice sheet extent on CO_2 drawdown in the southern ocean.

Modelling the last full glacial cycle and biogeochemical cycle using CLIMBER-2 coupled with a dynamic ice sheet model SICOPOLIS (Ganopolski et al 2010), Brovkin et al (2012) found that modelled changes could fairly well reproduce data for atmospheric CO_2 and deep ocean indicators . They concluded that “changes in sea surface temperatures and in the volume of bottom water of southern origin control atmospheric CO_2 during the glacial inception and deglaciation; changes in carbonate chemistry and marine biology are dominant during the first and second parts of the glacial cycle, respectively”. They included changes in weathering in their study, which

were increased during glacial periods and accounted for some of the atmospheric CO_2 drop (by increased ocean carbon uptake).

A 160kyr record of climate for the Lake Baikal was reconstructed by Grygar et al (2006). They found a dry intermediate (relative to interglacial vs glacial) climate existed between 76-66kyr BP followed by a dramatic climate deterioration during 66-60kyr BP. Millennial scale variability in climate was identified by Grygar et al (2006) studying the Lake Baikal sediment records. They found that events coinciding with Heinrich events (iceberg discharge) in the north Atlantic were seen in the Lake Baikal record, suggesting a teleconnection between North Atlantic and central eastern Asia climate. This finding further supports the idea that permafrost-carbon, which is sensitive to climate changes, may have a role to play in fast changing climates during glacial periods.

5.1.3 Climate and ice sheets

A full glacial cycle was modelled by Ganopolski et al (2010) using the CLIMBER-2 model that included the dynamic ice sheet model SICOPOLIS. They were able to successfully model the temporal and spatial dynamics of northern hemisphere ice sheets. The timing of ice sheet collapse (deglaciations) in glacial cycles using the same model relied on the mechanism of dust deposition on the ice sheet reducing albedo and resulting in sustained melt (Ganospolski and Calov 2011). This atmospheric dust was caused by ice sheets extending over terrestrial sediments in northern continents. They provided a possible explanation of the Pliocene-Pleistocene transition as due to the removal of terrestrial sediments in northern high latitudes (in N.America) allowing the growth of larger ice sheets. They found that temporal atmospheric CO_2 concentration changes were required as an amplifier in the 100kyr glacial cycles, but that the cycles themselves could be achieved with a fixed CO_2 background climate.

Using a comprehensive climate and ice sheet model, Abe-Ouchi et al. 2013, driving their model with insolation only, found that feedbacks between climate, ice sheets and the lithosphere-asthenosphere system could explain the 100kyr climate cycles. A sufficiently large ice sheet becomes very sensitive to insolation forcing, but requires time to grow to a size in which the increase in NH summer insolation could start to cause an almost complete retreat within several thousand years. They noted that on this scale the atmospheric CO_2 level was involved but not determinative. Berger et al. 2013, studying deep sea core records surmised that the instability of ice masses was the chief underlying cause of changing climate states.

5.1.4 Weathering for glacial timescales

On the glacial timescale the effects of weathering on ocean/atmosphere CO_2 drawdown capability via the carbonate compensation mechanism is no longer negligible. As described in chapter 1, there exists uncertainty as to the magnitude and timing of changes in chemical weathering over glacial cycles of the Pleistocene. The

conclusions of Foster and Vance (2006), in which increased weathering on continental shelves due to lowered sea-level is offset by reduced weathering on continental interiors, so that weathering rates remained fairly constant through the glacial cycle will be adopted for our glacial cycles simulations. The version of CLIMBER-2P used in this study does not account for any changes in chemical weathering and so over all simulations, described in the next section, chemical weathering rates are constant.

5.2 Last glacial cycle simulation

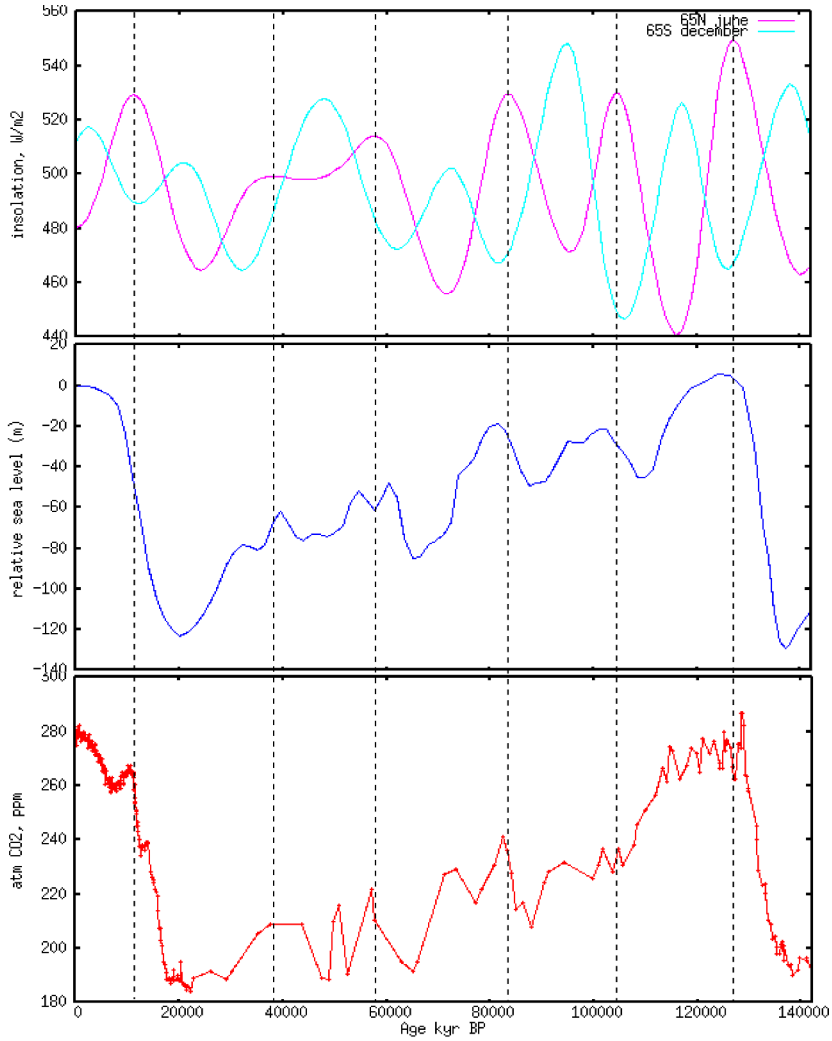

Fig 5.1, drivers for simulations. Top: insolation at 65°S Dec and 65°N June (Laskar et al 2004), middle: relative sealevel (Peltier 1994), bottom: atmospheric CO_2 (Luthi et al 2008). Dashed lines mark insolation maxima at 65°N June.

In order to study the effect of the permafrost-carbon dynamics on long timescales, a full glacial cycle is simulated which includes the permafrost mechanism (medium permafrost-carbon dynamic, chapter 4) and various "driver" settings. These

drivers are insolation, ice sheets and CO_2 concentration. Insolation controls the spatial distribution of solar energy input over the globe and is dependent upon orbital configuration. Ice sheets exert a strong control on climate (Clark et al. 1999) and on the land available in the high northern latitudes for permafrost. Atmospheric CO_2 concentration is a driver for the radiative code of CLIMBER-2P, so exerts control on the overall climate. It also controls the CO_2 levels which are experienced by the vegetation model which in turn influence NPP and therefore carbon accumulation rates. This CO_2 value will be denoted as CO_{2_RAD}. CLIMBER-2P also calculates a carbon cycle atmospheric CO_2, which in our model configuration does not drive the radiative code (or vegetation) but rather indicates the balance between the ocean and the land carbon fluxes. This CO_2 value will be denoted as CO_{2_CC}. Comparing CO_2 data (or CO_{2_RAD}) to CO_{2_CC} allows us to appraise the performance of the mechanisms and dynamics modelled in the CLIMBER-2P carbon cycle. By considering the drivers of insolation, ice sheet and CO_{2_RAD} one at a time the system response with permafrost carbon can be studied. Drivers are shown in figure 5.1, relative sea level controls prescribed ice sheet extent in the model. Table 5.1 describes the simulations carried out and the start CO_{2_CC} values, arrived at after an equilibrium spin-up simulation of 80kyrs at 190ppm for fixed CO_{2_RAD} simulation, or 193ppm 142kyrBP orbital configuration, ice sheet extent determined from the relative sea-level record, LGM runoff and increased nutrient and salinity concentration in the ocean to represent reduced ocean volume. The ice sheet extent is determined using the same method as for the LGM simulation. The sea level record is used to determine land ice volume, and maximum land ice extent is the same as the LGM ice sheet (because sea-level is lower at PGM than at LGM). When sea level rises it is assumed that all the water is sourced from the northern hemisphere ice sheet, as Antarctica's ice sheet is fixed in CLIMBER-2P. This is a very coarse model of the ice sheet, although as a simplification it allows us to represent the action of a dynamic ice sheet, without using a computationally expensive ice sheet model, and therefore allows us to carry out long timescale simulations.

Simulation start and length (kyr BP)	Simulation drivers	Start model CO_{2_CC} values (ppm)	Data CO_2 start (ppm)
142	Insolation, PI ice sheet (fixed), fixed CO_{2_RAD} 190ppm	268	193
142	Insolation, evolving ice sheet, fixed CO_{2_RAD} 190ppm		
142	Insolation, CO_{2_RAD} (Luthi et al 2008), PI ice sheet (fixed)		
142	Insolation, evolving ice sheets, CO_{2_RAD} (Luthi et al 2008)		

Table 5.1, simulation set-ups for model including carbonate compensation and Permafrost-carbon mechanisms.

At this stage the CLIMBER-2P model has no way of determining the transient behaviour of the deep Southern Ocean carbon pool over a full glacial cycle. However, simulations in which the permafrost-carbon mechanism is included in the Earth system can give some valuable information on the possible carbon cycle response on glacial scale forcings. So far, modelling studies and data-interpretation have relied on the assumption that in a cooling climate the land loses carbon and the ocean takes-up carbon. With the permafrost mechanism responding strongly to northern high latitude insolation this pattern is likely altered.

5.2.1 Results

The modelled global mean temperature and permafrost area are shown in figure 5.2. After each insolation peak in the northern hemisphere the model displays some fast variability lasting around 2-3kyrs, as already observed in our simulations covering the last deglaciation and the Holocene (chapter 4). This is due to an instability of the modelled vegetation in the Sahara/Sahel grid cell and is a feature of each insolation cycle. When insolation-only is used to drive the model (plotted in pink), global temperature remains within a range of less than 1°C. Permafrost-area is controlled by high latitude insolation forcing only and so follows closely the 65°N insolation changes, with higher variability in the first half of the glacial period (130k to 70kyrBP) and lower variability in the second part of the glacial period (70k to 20k yr BP). The addition of CO_2 data to drive the radiative and vegetation models (imposed CO_{2_RAD}) increases the amplitude of temperature changes to around 2°C and the glacial cycle pattern starts to emerge. The modelled permafrost area reflects this, with reduced area in the warmer periods and the cooling trend from 130kyr BP to 20kyr BP superimposed on the insolation driven area variability. The combined ice sheets and insolation driven simulation (in blue, with fixed LGM CO_{2_RAD} levels) also shows the glacial cycle pattern. The temperature change between LGM (21kyr BP) and PI (0kyr BP) is around 1.8°C. The northern hemisphere ice sheet has a control on permafrost area not only via climate (temperature) but also as area available for permafrost to exist. At around 72kyr BP the strong summer insolation minimum (fig 5.1) results in an increase in permafrost area (pink line fig 5.2). This peak in area is delayed when CO_2 in included as a driver (red line fig 5.2, $CO_{2\_RAD} = CO_2$ data) because a high CO_2 reduces permafrost area via a warmer climate. When the ice sheet is added as a driver with insolation this peak occurs earlier than the insolation minimum because now the ice sheet, extending over the land, reduces the permafrost area. With all the three drivers, in green in figure 2 shows the combined effect. Now the global temperature varies up to 3.6°C between glacial maxima and interglacials. The permafrost area for all drivers is most similar to the insolation-plus-icesheet simulation between 110kyr BP and 17kyr BP indicating that the ice sheet extending (and retreating) over the land has a strong control on permafrost area and therefore on the carbon cycle.

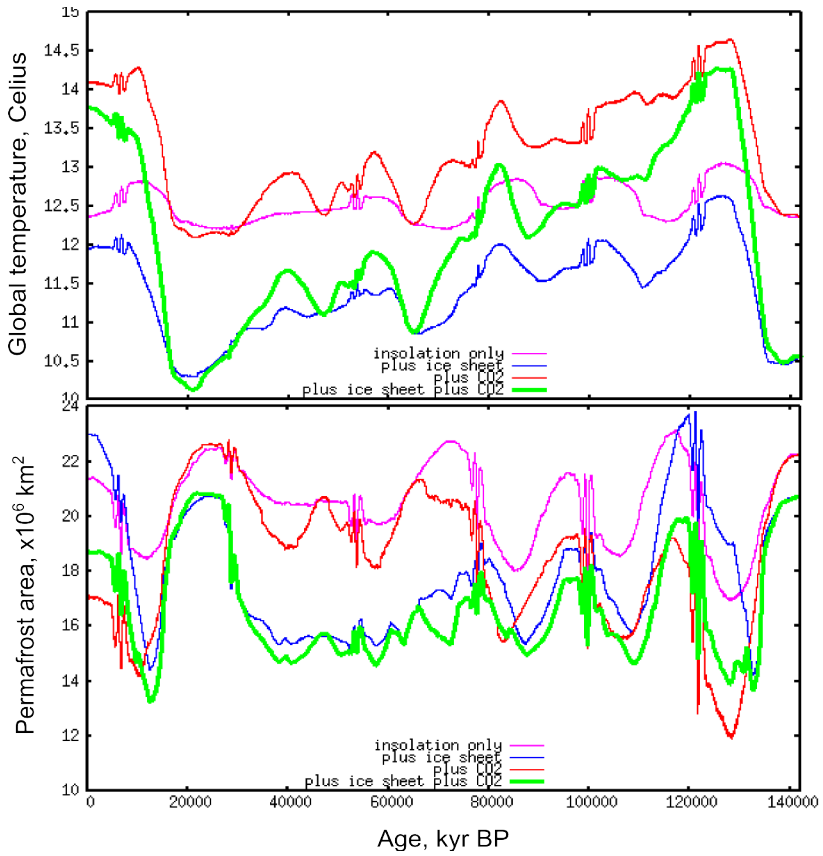

Fig 5.2, Modelled global mean temperature (top) and modelled permafrost area (bottom) for all 142k yr simulations.

The carbon cycle output results for modelled CO_{2_CC} for the 142k yr simulations are shown in figure 5.3. The modelled CO_{2_CC} represents the combined carbon-cycle response of the terrestrial biosphere and the ocean to the forcings imposed. The insolation-plus-icesheet simulation demonstrates the importance of ice sheet extent on permafrost area and therefore on carbon dynamics in the permafrost zone. Relative to the insolation-only forcing there is higher variability and CO_{2_CC} peaks no longer necessarily coincide with insolation forcing CO_{2_CC} peaks. This is in contrast to the insolation-plus-CO_2 simulation with accentuates the 65°N insolation cycle. In this case the reduction in permafrost area which causes a loss of land carbon is accentuated by the increase in global temperatures via the CO_2/greenhouse effect.

The range of CO_{2_CC} when all forcings are included is around 40ppm (green line fig 5.3). During termination periods the data CO_2 indicates increases in the order of 90ppm. As discussed in chapter 4, the absence of any glacial ocean mechanisms does not produce CO_{2_CC} model output that agrees with data. The variability in CO_{2_CC} for the insolation plus CO_2 is far greater than in other simulations. This can be explained via the terrestrial biosphere, shown in figure 5.4 as total land carbon. The peaks and troughs in land carbon contents for the insolation-plus-icesheet and insolation-plus-CO_2 simulations are out of phase during termination periods. This causes a delay in land carbon loss for the combined simulation (green line) relative to insolation forcing. The

pattern of changes in total land carbon in the combined simulation is most similar to the insolation-plus-icesheet simulation. The insolation-plus-CO_2 simulation shows the highest amplitude changes because it is only the southern limit of permafrost that determines permafrost area, and the northern limit is fixed (by coastline and the fixed ice sheet). During cold summers (low summer insolation) permafrost expands to the south. When the ice sheet is included in the model, during cold summers the ice sheet also expands to the south, over the permafrost, reducing total permafrost area from the north. This again confirms the important role of the ice sheet on the carbon cycle response when permafrost is accounted for.

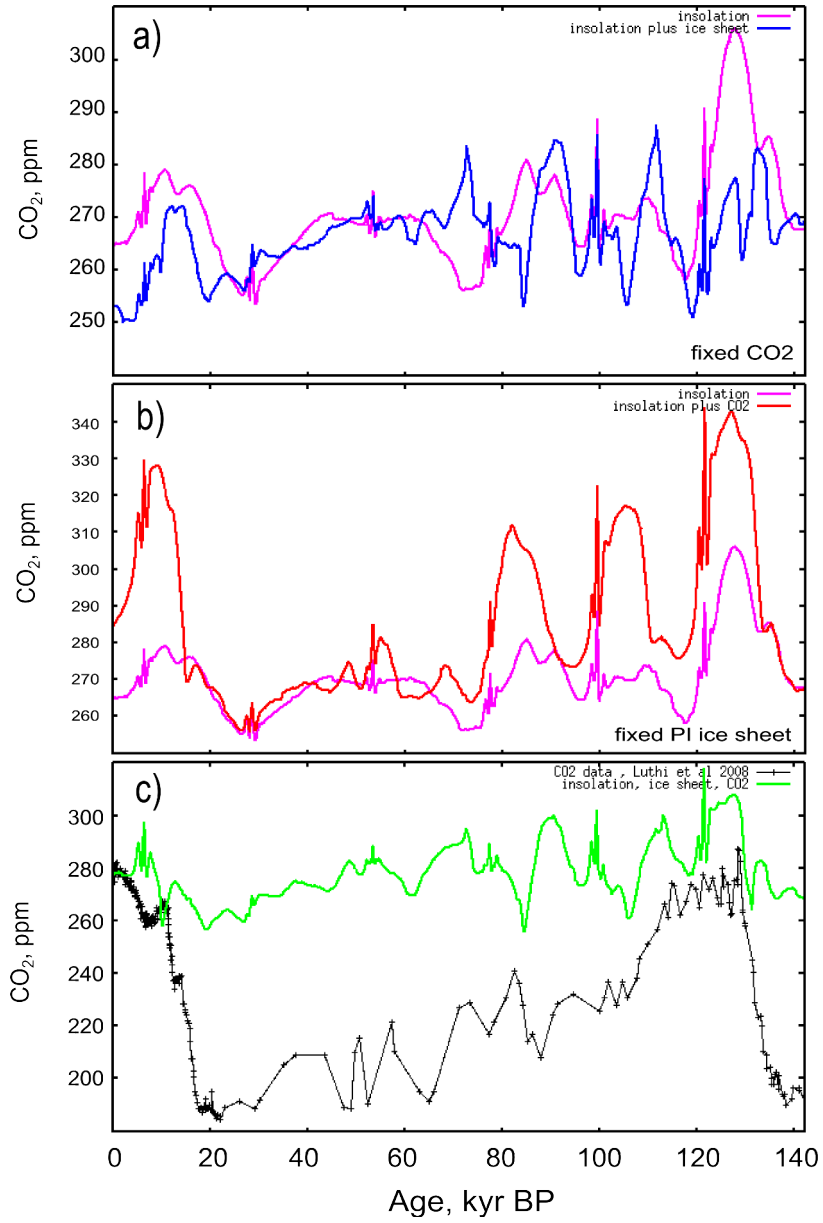

Fig 5.3, Modelled atmospheric CO_{2_CC} per simulation. a) insolation only and insolation plus ice sheet, b) insolation only and insolation-plus-CO_2, c) insolation, ice sheet and CO_2 (combined) simulation, with CO_2 data from Luthi et al 2008.

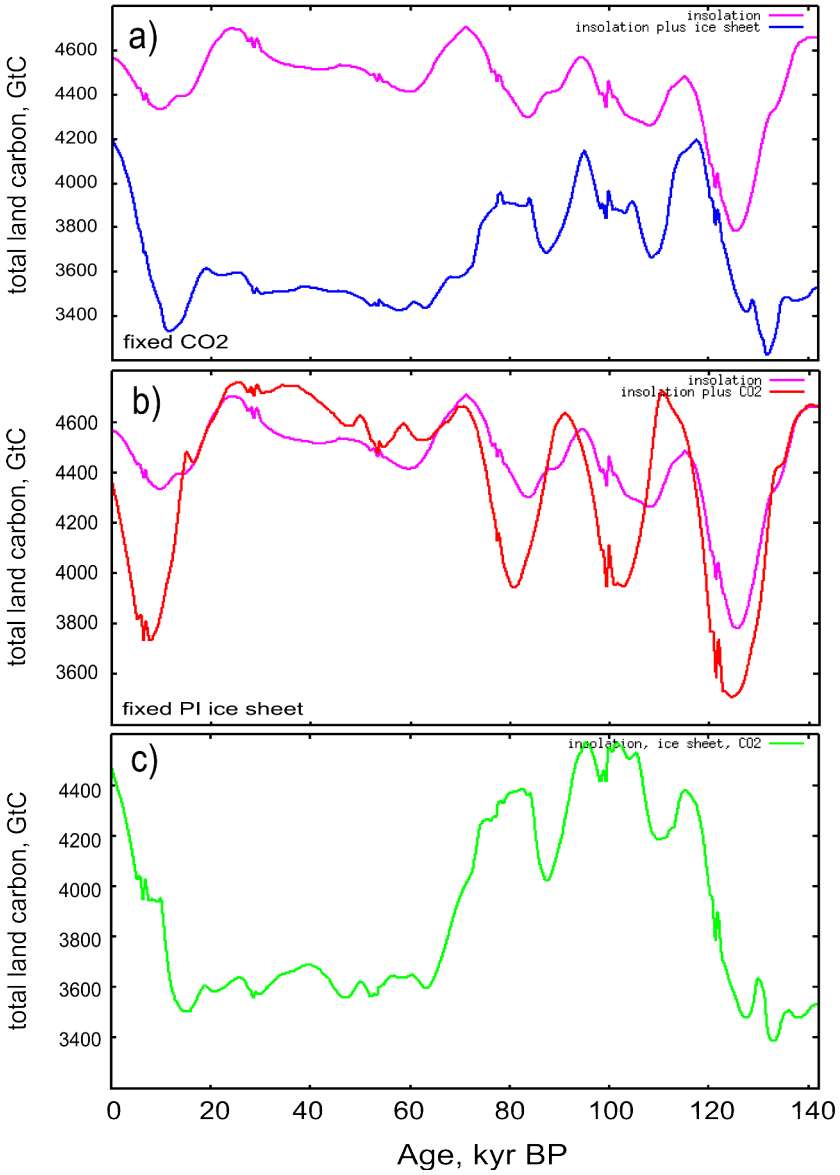

Fig 5.4, Modelled total land carbon anomaly per simulation setting. a) insolation only and insolation-plus-icesheet. b) insolation only and insolation-plus-CO_2, c) insolation, ice sheet and CO_2 (combined) simulation.

A comparison of a high resolution CO_2 record for the glacial period and model output for the combined simulation is presented in figure 5.5. The CO_2 variability seen in data is not fully represented in model output. The CO_2 variability seen during this period in the data is thought to be due to millennial scale climate variability caused by fast changes in the Atlantic Meridional Overturning Circulation (AMOC) (Kageyama et al. 2010). This is not represented in the simulations here so modelled CO_2 is not expected to match data CO_2. However, some characteristics of the data record are seen also in the model output. The underlying reducing atmospheric CO_2 trend is seen in the model, with a reduction of around 25ppm between 50kyr BP to LGM. Between 30 to 15 kyr BP, the period covering the glacial maximum and the first part of the deglaciation,

the pattern of changes in CO_2 is seen in model output. A drop in CO_2 from 29kyr BP to 27kyr BP, a rise after this point followed by a drop to low CO_2 after 20kyr BP. This shows that some of the scale of the CO_2 variability during this period can be explained without any AMOC changes.

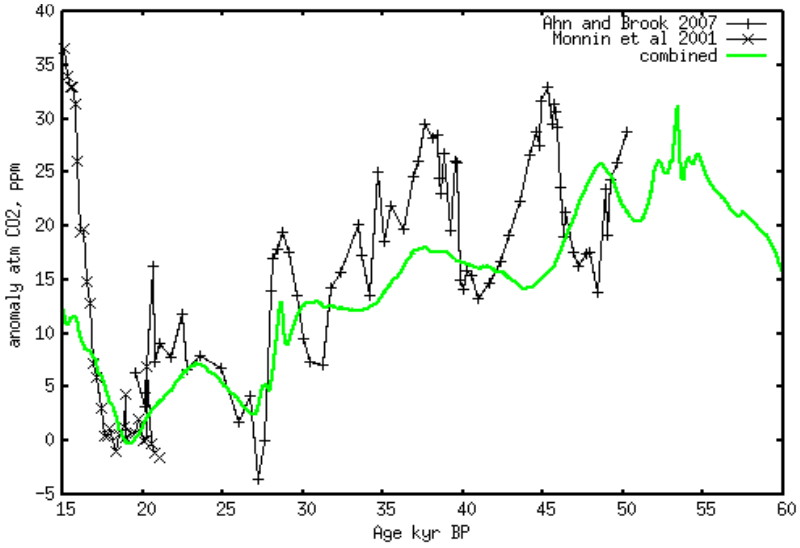

Fig 5.5, Modelled CO_2 anomaly overlaid on high resolution CO_2 record (Ahn and Brook 2007) showing some variability, but not all, can be reproduced when permafrost is included.

5.3 Four glacial cycles long simulation

Using the combined forcings of insolation, ice sheet and CO_2 (for the model CO_{2_RAD}) a simulation of the last 4 glacial cycles was carried out. This allows a comparison of glacial cycles in which differing insolation forcing is seen by the Earth system. The model set up is as the 142k simulation that includes insolation, ice sheet, CO_2 shown in table 5.2. The equilibirum spin-up that creates the start point for the transient simulation is CO_{2_RAD} 200ppm, as data, and 432kyr insolation, LGM maximum extent for ice sheet.

Simulation start and length (kyr BP)	Simulation drivers	Start model CO_{2_CC} values (ppm)	Data CO_2 start (ppm)
432	Insolation, evolving ice sheets, CO_{2_RAD} (Luthi et al 2008)	255	200

Table 5.2, simulation four cycles set-up including the carbonate compensation and Permafrost-carbon mechanisms.

5.3.1 Results

Permafrost extent

Modelled permafrost area for the 432kyr simulation is shown in figure 5.6 overlaid on June insolation at 65°N (inverted scale). The very clear link between summer insolation and permafrost response is evident throughout the simulation. During periods in which the insolation forcing is not the dominant driver for permafrost area, it is ice sheet extent (determined via sea-level) that affects permafrost area. This is the same effect as seen in the 142tr simulations.

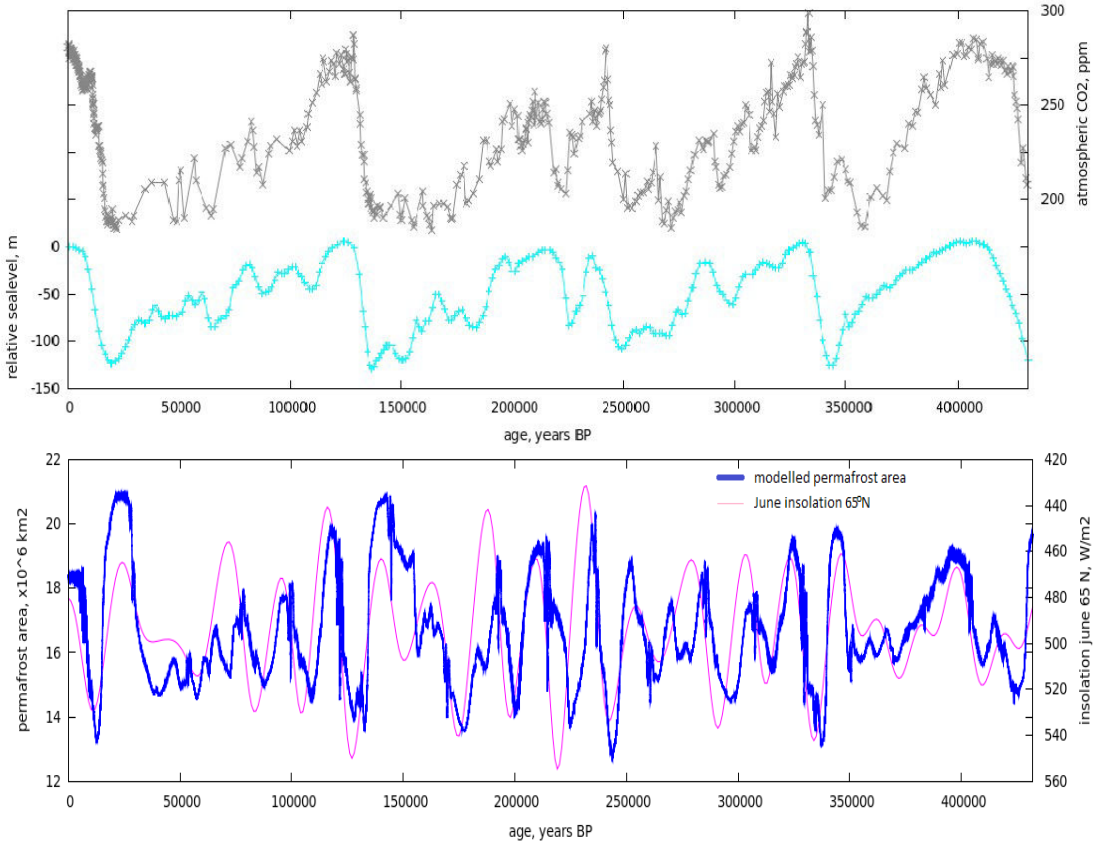

Fig 5.6, Top: model drivers for CO_{2_RAD} (Luthi et al 2008) and relative sea-level (Peltier 1994). Bottom: Modelled permafrost area for the 432kyr simulation, overlaid on June insolation 65°N (Laskar et al 2004), inverted scale.

During glacial maximum periods, particularly PGM and LGM, the cold background climate results in the largest permafrost areas. The low amplitude in insolation changes during 430-350kyr BP (MIS 11 and 10) and low sea level variability result in low variability in permafrost area changes, with both sea level and permafrost area showing a fairly steady falling/cooling trend from 400kyr to ~350kyrBP. On the scale of insolation forcing (~20kyr variability) the highest fluctuations in permafrost area are seen between 240kyr to 190kyrBP (MIS 7 and 6), this coincides with the largest amplitude in insolation changes at 65°N June.

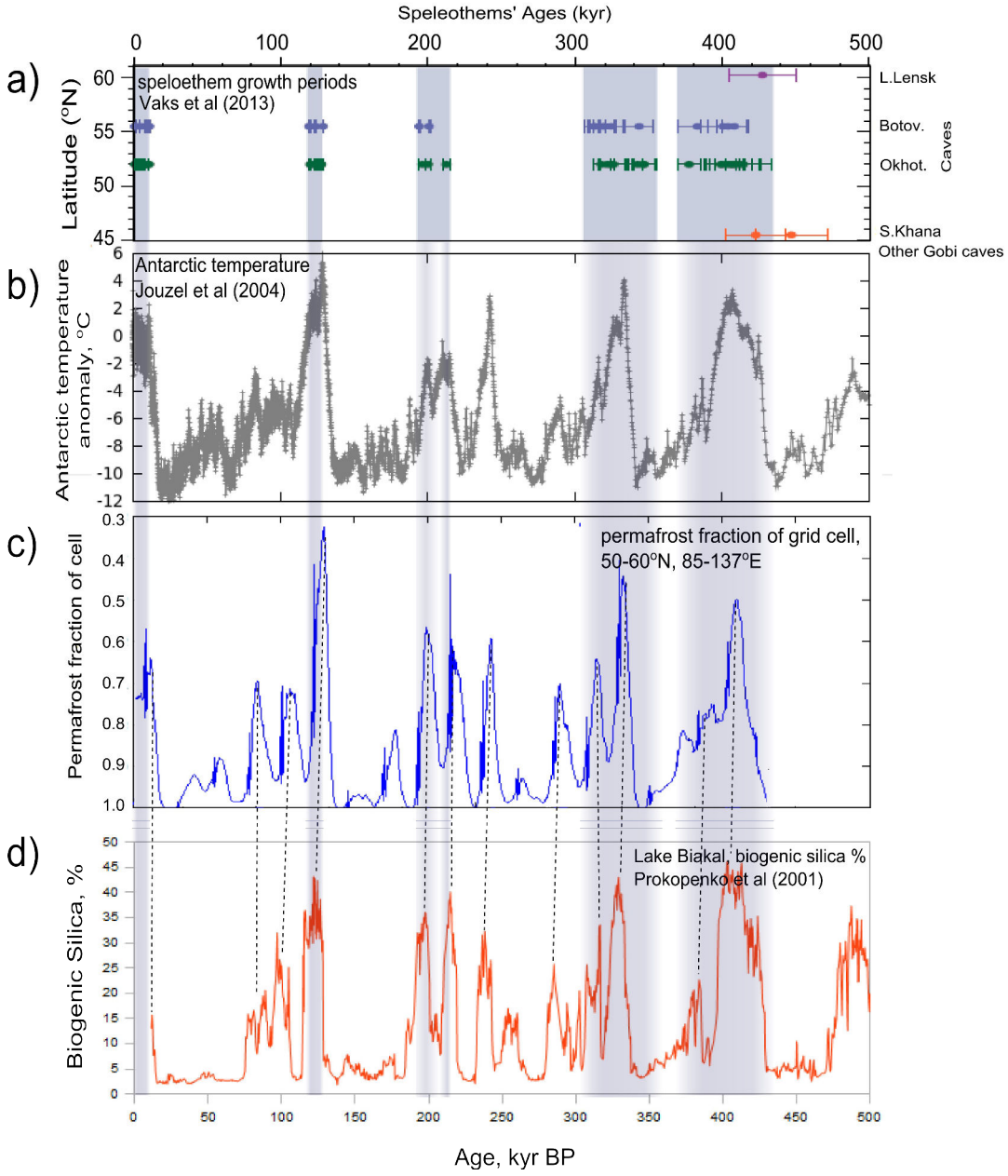

Fig 5.7, a) Speleothem growth periods indicating thawed permafrost conditions at caves near Lake Baikal (Vaks et al 2013), b) Reconstructed Antarctic temperature anomaly from the present (Jouzel at al 2004), c) modelled permafrost fraction of grid cell 50-60N, 85-137E in which Lake Baikal would be located, d) biogenic Silica content of sediments in Lake Baikal (Prokopenko et al. 2001).

Looking closer at one grid cell, model output for the permafrost fraction of the southern east Russian grid cell (50-60°N, 55-137°E) is compared with the speleothem indicator for permafrost thaw and the biogenic Silica record from lake Baikal (Prokopenko et al. 2001) located at 53°3'N 108°E in figure 5.7. The biogenic silica contents of sediments from lake Baikal have been used as a climate indicator for the region (Carter and Colman 1994). There is good agreement between the biogenic silica

record and the permafrost fraction of the grid cell which would contain the Lake Baikal site. This indicates that the frost-index based calculation of permafrost fraction, so the local climate conditions, calculated in the model are good with respect to the data indicated conditions for this grid cell. Extensive permafrost thaw occurs, according to the speleothem record, during warm interglacial periods with the exception of termination 3 and the warm peak at around 240kyrBP. In our model these thaw periods coincide with periods in which permafrost fractions of less than 0.6 are seen in the grid cell. The 240kyr warm interval is not associated with permafrost thaw according to the speleothems, and the lake Baikal biogenic silica % is lower in this interval than in the subsequent warm periods at ~220kyr and ~190kyr BP.

Carbon pools

Modelled CO_{2_CC} output overlaid on CO_2 data is shown in figure 5.8. Throughout the simulation the difference between glacial and interglacial periods' CO_2 levels are underestimated in model output. Again this is likely due to the lack of any glacial-ocean mechanisms (see chapter 4) operating in the model. The scale of variability in CO_{2_CC} on the millennial scale during glacial periods shows some agreement with the CO_2 record. During MIS 6 the amplitude of variability in CO_{2_CC} is of a lower magnitude compared to MIS 4 and 3. The end of MIS 9 going into MIS 8 shows high variability whereas MIS 11 to MIS 10 variability on the millennial scale is lower. This variability is not solely caused by insolation forcing, but by the coupled effects of insolation, CO_2 and ice sheet dynamics. Some changes in CO_2 show similar patterns to the data in scale but are offset in the model with respect to the data. The model outputs at MIS 4 and MIS 8 are similar to data but occur 5k to 10k years later in the model output. As identified in the 142kyr simulations the ice sheet extent in the northern hemisphere has a strong effect on the carbon cycle response. The relative sea level record controls ice sheet extent, however, the sea level record is the result of a combination of both southern and northern hemisphere ice sheet reductions and increases. Therefore, some error is produced by applying all sea-level changes to the northern hemisphere ice sheet, this may particularly affect timing of ice sheet changes and may explain some of the model-data mismatch. As well as this, the sea level record and subsequent ice sheet extent likely do not hold a direct relationship as modelled in CLIMBER-2P. Wilschut et al (2006) found that ice sheet extent shows a hysteresis behaviour with global temperature caused by ice volume redistribution (a consequence of the processes of merging and separation of ice sheets) in changing climates when employing a 3D ice sheet model. The modelled CO_2 output, and climate, may show better agreement with data if the northern hemisphere ice sheet extent model was more realistic.

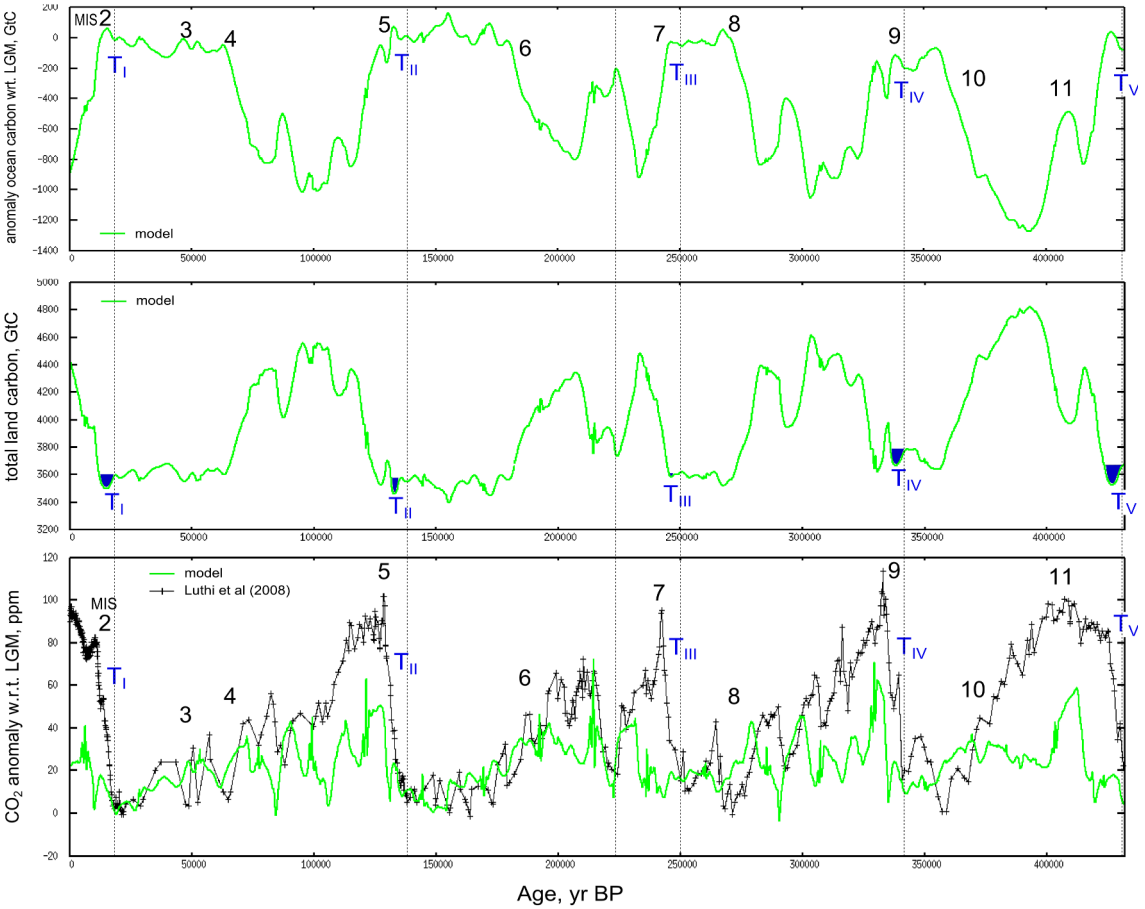

Fig 5.8, Top: Modelled ocean carbon anomaly (wrt LGM). Middle: modelled total land carbon for the 432kyr simulation. Marine isotope stages marked for ocean and termination periods marked for both. Bottom: Modelled CO_2 output for the 432kyr simulation overlaid on CO_2 data from Luthi et al (2008). Marked on are terminations (Tn) and marine isotope stage (MIS) datings.

The onset of terminations I and II for the 142kyr simulation are seen in the land carbon pool as a drop in carbon content on the order of 50 to 100GtC and the CO_2 rise seen in the atmosphere is 15 to 20ppm (shaded in blue in figure 5.8). This does not hold for all terminations. Figure 5.8 shows the land carbon pool anomaly and the ocean carbon pool anomaly from the model. Termination III shows no significant drop in land carbon at the onset of deglaciation where all other termination periods show this drop. The CO_2 rise between MIS 7 and MIS 6 (~220kyr BP) does coincide with a drop in land carbon (marked as a dashed line). From these results, termination III appears to be a two-stage termination, with two short interglacial periods (figure 5.7).

According to results from chapter 4, the deep ocean carbon pool at glacial maximum periods results in atmospheric CO_2 levels in agreement with data estimates. At 21kyr BP (LGM) modelled CO_{2_CC} is 188ppm data is 185ppm (Monnin et al 2001), and at 142kyr BP, penultimate glacial maximum (PGM) modelled CO_{2_CC} is 195ppm and data 193 ppm (Luthi et al 2008). The change in the deep Southern Ocean causes

changes in ocean circulation patterns which, combined with permafrost, results in atmospheric CO_2 levels increasing at rates in agreement with data estimates for terminations 1 and 2. However, comparing the total change in ocean carbon content with a simulation in which no glacial ocean mechanisms were employed showed a contribution of an extra 100GtC for termination 2, and 0GtC for termination 1 from the deep southern ocean carbon pool. This suggests that the carbon contents for the ocean and land plotted in figure 5.8 would be similar (±140GtC) to the model output if a mechanism causing carbon accumulation (and release) in the deep southern ocean were present. According to model output, carbon is preferentially stored on the land during interglacial and the start of glacial periods. When extending northern hemisphere ice sheet reduces land area and cools the climate, and therefore reduces carbon stored on land, carbon is preferentially stored in the ocean. With the exception of MIS 3, full MIS stages mark strong carbon transfer periods between the land biosphere and the ocean.

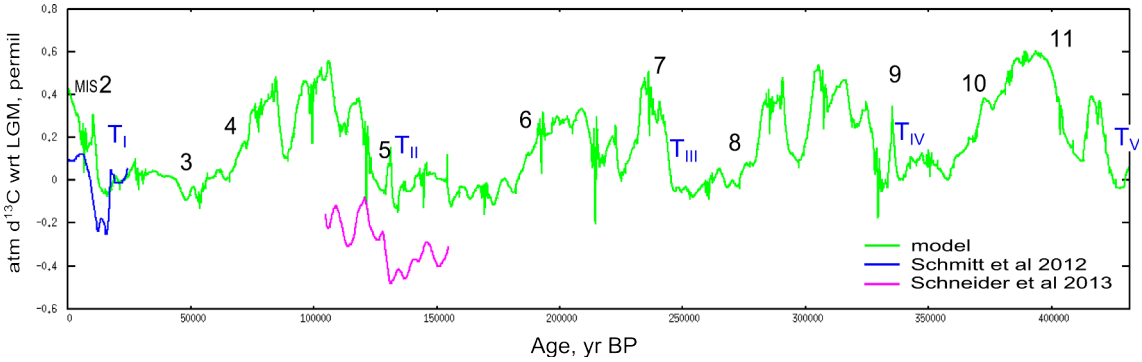

Fig 5.9, Modelled atmospheric $\delta^{13}C$ anomaly (wrt LGM) with $\delta^{13}C$ data overlaid. Marine isotope stages are marked, as are termination periods

The timing of these large scale transfers of carbon between land and ocean coincide with changes in the deep Atlantic $\delta^{13}C$ record (Lisiecki and Raymo 2008), indicating a possible role for land carbon in ocean $\delta^{13}C$. The deep ocean $\delta^{13}C$ data show that it was different for each glacial maximum period. For example, more negative at PGM than at LGM by 0.2 to 0.3‰. Figure 5.9 shows the modelled atmospheric $\delta^{13}C$ with measured data from Antarctic ice cores overlaid. During PGM the model shows $\delta^{13}C$ values around 0.3‰ higher than data. These two pieces of evidence suggest that at this period the model over-predicts the amount of carbon stored on land and under-predicts the amount stored in the deep ocean (chapter 4). Land carbon has a strongly negative $\delta^{13}C$ value (~-25‰) so a reduction in total land carbon would shift atmospheric $\delta^{13}C$ more negative. If this signal is transferred to the ocean, it would also reduce ocean $\delta^{13}C$. A possible explanation as to why the model may over-predict total land carbon at PGM is the simplified ice sheet representation. Geological evidence and modelling studies have found that ice sheet extent at the PGM was far greater than at LGM (Svendsen et al 2004, Jakobsson et al 2010). As already discussed, the ice sheet extent has a strong control on permafrost carbon contents via the land area available for carbon accumulation.

Ice sheet representation

The modelled northern hemisphere ice sheet in CLIMBER-2P at the LGM period (21kyrBP) and the PGM (142kyrBP) shows very little difference, as does permafrost extent. If the ice sheet model were more realistic then total land carbon at PGM would be likely reduced and so would atmospheric $\delta^{13}C$ values. The PGM ice sheet estimate from Svendsen et al (2004) if applied to the PGM CLIMBER-2P model simulation would result in at least a full grid cell being removed from the permafrost available land (as figure 5.10). The grid cells identified as ice sheet by Svendsen et al estimate holds (174GtC + 1/3*125GtC) 216GtC at PGM in the current model configuration. If this land was actually under the ice sheet at this time, then the extra carbon would need to be stored elsewhere. As identified in the previous chapter, land carbon was also likely reduced, also in the non-ice sheet permafrost and non-permafrost regions (see section 4.3).

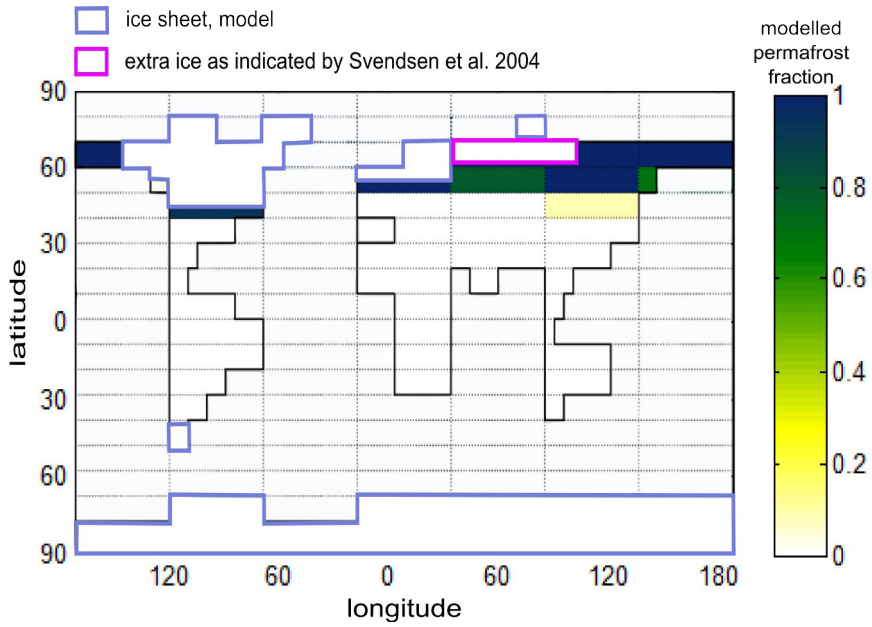

Fig 5.10, Ice sheets on land (outlined in blue) and permafrost fraction of cells for CLIMBER-2P at 142kyrBP. Ice sheet outlined in pink is extra ice that would bring model into line with data estimate (Svendssen et al. 2004).

This ice sheet-permafrost factor may be able to provide part of an explanation as to why deep ocean $\delta^{13}C$ is not the same for all maximum glacial periods seen in the record, with a range of up to 0.5‰ for the last 5 cycles (Lisiecki et al 2008). At PGM, both atmosphere and deep ocean $\delta^{13}C$ was more negative than at LGM. Similarly, it may be that ice sheet extent on the land was at its greatest at MIS 8. This would have the effect of reducing permafrost area, and reducing global NPP even more so than for PGM. Although the relative sea level record suggests that land ice volume was less at MIS 8 than at LGM (MIS 2) or PGM (MIS 5), there is evidence that the largest ice sheet area extending over the west Siberian plain dates to around MIS 8 (Svendsen et al

2004). During MIS 8 deep Atlantic $\delta^{13}C$ records are at their most negative, and the "rejected" land carbon caused by a large ice sheet may be able to explain some of this low $\delta^{13}C$. In this sense it is the location and extent of the ice sheet on land, not just the global volume of ice, that has more impact on the permafrost-carbon dynamics and the carbon cycle. This hypothesis would require further study including a more representative ice sheet model, and including glacial ocean mechanisms.

5.4 Conclusions

The results discussed in this chapter suggest that permafrost-carbon plays a role in the carbon cycle not only during termination periods, as found in chapter 4, but also during other periods. The combined action of the land ice sheet in the northern hemisphere and the accumulation of carbon in permafrost affected soils creates variability in atmospheric CO_2 on a similar scale to that seen in the data record. During modelled terminations 1, 2, 4 and 5 the thawing of permafrost caused a release of carbon from the land to the atmosphere and may have been responsible for the onset of CO_2 rise seen in the records during these periods. Termination 3 was not associated with a loss of land carbon, and so for this termination all the carbon was sourced from the ocean. The CO_2 rise following termination 3, occurring around 225kyrBP is associated with a loss of carbon from permafrost thaw. Data for $\delta^{13}C$ for this period may be able to constrain this feature.

The role of the ice sheet was found to be particularly important for the total size of the land carbon pool. The CLIMBER-2P ice sheets are determined from relative sea level record to calculate total ice sheet volume. This simplification results in an ice sheet at LGM very similar to that at PGM. An increased land ice sheet extent in west Siberia may be able to explain why the atmospheric $\delta^{13}C$ data record is 0.3‰ more negative at PGM with respect to LGM. The increased ice sheet would reduce permafrost area and therefore reduce total permafrost carbon. It may also have reduced global NPP, therefore affecting the remaining permafrost and non-permafrost region. This carbon, released to the atmosphere would reduce atmospheric $\delta^{13}C$. Further than this, a more realistic ice sheet may be able to improve the timing of rises and drops during MIS 4 and MIS 8 in modelled CO_2 with respect to data, and possibly in other periods too. These findings suggest that not all CO_2 variability during glacial periods needs to be explained via millennial scale climate variability caused by collapse and resumption of AMOC strength.

Considering current hypotheses for drivers of glacial cycles, the results here support Milankovitch theory, with the permafrost carbon creating a direct carbon cycle link to high northern latitude insolation but with ice sheet dynamics an important factor controlling permafrost extent. The deep Southern Ocean carbon store is required in order to explain the timing and extent of rises in CO_2 in terminations, but variability already present in the model CO_2 suggests that this deep pool may be more stable on the millennial scale than other studies suggest. The CLIMBER-2 model is known to have a CO_2 outgassing in the Southern Ocean lower than present day data estimates (Brovkin et

al 2012). In a full glacial experiment carried out by Brovin et al (2012) increasing the background vertical diffusivity in the Southern Ocean increased atmospheric pCO_2 sensitivity to sea-ice cover in the Southern Ocean. Over a deglaciation simulation this increased vertical diffusivity caused atmospheric CO_2 between LGM and PI to increase by 10ppm in their model set-up compared to the standard model. This increased sensitivity would reduce the gap between modelled and data CO_2 levels if it was applied in the CLIMBER-2P model. If pCO_2 responded to ice sheet cover more strongly, then a retuning of the model for total glacial-interglacial CO_2 change (like chapter 4) would result in the glacial ocean mechanism being slightly less-strong, for example a maximum brines fraction of 0.6 and not 0.8.

The modelled atmospheric CO_2 anomaly is too low during interglacial periods compared to data due to the lack of glacial ocean mechanisms in this model set-up. However, indications from the changes in land and ocean carbon content over the last two deglaciations (chapter 4) show that the glacial ocean mechanism more strongly controls the rate of climate change, rather than directly the carbon cycle. The greatest anomaly between simulations with and without glacial ocean mechanisms was 140GtC for the termination periods. If terminations represent the fastest changing ocean conditions, then we may assume that 140GtC is the maximum anomaly possible. Considered from this point of view, the dynamics in the land and ocean carbon pools modelled in the 432kyr simulation (fig 5.9) are considered to be robust, to an error of ±140GtC maximum, if millennial scale climate variability is neglected.

Chapter 6 Millennial scale climate variability

This chapter presents experiments in which millennial scale climate variability with the permafrost-carbon mechanism and ocean glacial mechanisms are studied. Millennial scale climate variability is created via fresh water hosing into the north Atlantic ocean. Experimental results are broken into three section. Firstly equilibrium climate background experiments' results are presented which demonstrate the strong effect that permafrost-carbon has on the carbon cycle during AMOC switch-off and resumption events. Secondly a transient deglaciation for termination 1 is presented in which fresh water forcing magnitudes and timing is based on existing literature estimates. Finally a transient deglaciation in which fresh water forcing has been inverted to obtain a CO_2 profile in which the BA/YD (Bolling-Allerod/Younger Dryas) plateau is produced. Model output shows good agreement with $\delta^{13}C$ data for the deglaciation, and no AMOC switch-off occurred during the first part of the last deglaciation.

6.1 Introduction and Background

Ice core records during the glacial and deglaciation periods show millennial scale climate fluctuations and possible see-saw type variability between the climates of the Antarctic and Greenland (Bond et al. 1999, Jouzel et al 2007). Most studies point to the role of the Atlantic meridional overturning circulation (AMOC), which transports heat from the Southern to the Northern hemisphere, as being a driver of these abrupt climate changes. A slow-down of the AMOC would result in cooling of the north Atlantic region, seen as a drop in Greenland records and sea-surface temperature records during the first part of the cycle (Kageyama et al. 2010) followed by a resumption in the AMOC causing rapid temperature rises in the north Atlantic. This rapid warming in the northern hemisphere is known as a Dansgaard-Oeschger (D/O) event. The full cycle is characterised in the Southern high latitudes as a more gradual warming (at the same time as NH cooling) then a gradual cooling, although precise dating of the Antarctic ice core record remains problematic (Wolff et al. 2010). Blunier et al. (1998) found that for 47-23kyr BP period, the ice core Antarctic temperature leads Greenland temperature by around 1 to 2.5 thousand years for the warming events. To create a slow-down in the AMOC, models employ a fresh-water forcing into the north Atlantic which reduces surface water salinity and inhibits the water mass's ability to sink to the deep ocean. This in turn reduces north Atlantic deep water (NADW) mass and reduces the strength of the AMOC, creating a more shallow overturning circulation or even switching it off altogether (Kageyama et al. 2010).

The release of fresh-water into the north Atlantic as a possible AMOC controller is supported by IRD (ice rafted debris) records in ocean sediment cores from the Atlantic (Bond et al. 1999). These high IRD layers in the cores mark the timing of Heinrich events interpreted as mass iceberg release into the Atlantic, the icebergs carrying sediments (rocks) far into the ocean before melting. The origin of the Heinrich layer IRDs has been attributed to the region around the Hudson strait (Hemming et al. 2005). D/O events and Heinrich layers are not always seen together, and D/O events are more frequent, although the presence of Heinrich layers point to instabilities in ice sheets on timescales similar to D/O events. Elliot et al. (2002) studied high resolution deep North Atlantic benthic foraminifera $\delta^{13}C$ records and temperature records, finding that drastic cooling associated with Heinrich events were related to reductions in deep water formation, but other cooling events which did not show such deep water reductions and were not a Heinrich Event (HE). They conclude that thermohaline circulation (THC) may not be the only controlling mechanism for these millennial scale oscillations or an amplifying mechanism existed which has not yet been taken into account.

Considering the last deglaciation as part of a similar mechanism to the millennial scale oscillations seen during the glacial period, Stanford et al. (2006) found that melt-water pulse 1a (MWP 1a), which saw rapid sea level rise, coincided with cooling in the northern Atlantic of the Older Dryas (~14kyr BP). Their study, which looked at the

ocean sediment core of Eirik's drift, south of Greenland, and coral records to more precisely date the timing of MWP1a contradicted earlier studies which associated it with an earlier warming period. They noted the importance of the location of fresh water forcing in the north Atlantic, that NADW shut-down (AMOC reduction or switch-off) was likely a trigger of the Younger Dryas cooling (12.8 to 11.6kyr BP) but saw no major sea level change at the same time. In 2011 Stanford et al., using the Eirik's Drift record again, determined the timing of H1 event to ~19 to 14.6k BP seeing it as not a short event but a series of events resulting from large scale northern hemisphere ice sheet melting and calving. Again the importance of location of the fresh water forcing on the AMOC strength was highlighted, this indicates that a Heinrich layer seen in ocean sediments may not always be associated with a major reduction in AMOC strength. Liu et al., 2009, used a modelled shut-down and subsequent resumption of the AMOC to explain the warming of the Bolling-Allerod (BA, ~14.5kyr BP). They used the NCAR CCSM3 climate system model combined with melt water forcing (MWF) loosely based on eustatic sea-level records (although they require more sea level rise than the record shows to produce enough fresh water forcing during HE1). They compared the modelled NADW with a commonly used proxy for AMOC strength, the $^{231}Pa/^{230}Th$ record measured from an Atlantic ocean core (McManus et al. 2004) located at around 4300m depth below sea-level. This proxy is currently used in other studies to compare model outputs, but its validity as an AMOC proxy has been called into question (Luo et al. 2010). Ritz et al. (2013) estimate the AMOC strength for the H1 and YD periods, finding that both periods saw a significant reduction in strength, however they also rely on the Pa/Th records to validate the model findings. They found that the AMOC strength during the LGM and the Holocene period were almost indistinguishable. This is in contradiction to other modelling studies, and also to the understanding of the role of Southern ocean sea-ice extent and related buoyancy forcing which during the glacial period is expected to result in a reduced AMOC strength (Gersonde et al. 2005, Fischer et al. 2010, Lund et al. 2011, Marshall and Speer 2012).

These ocean based studies of the millennial scale variability focusses on climate records and temperature proxies rather than the carbon cycle. Attribution of atmospheric carbon dioxide concentrations changes are problematic. Ice core records were until quite recently at low resolution for glacial periods due to low snow accumulation rates, and models for changes in vegetation patterns for warming and cooling periods show more model spread than for ocean models of physical ocean circulation changes, making earth system modelling difficult.

The role of the terrestrial biosphere during these millennial scale climate variations was the subject of a Quaternary Science Reviews special issue in 2010. This special issue combined new land-based records spanning these cycles, as well as vegetation modelling studies, an ocean modelling study and evidence from ice cores. The introduction to the special issue addressed questions of nomenclature for this millennial scale variability and also established datings of Heinrich stadials, here defined as the maximum length of IRD deposition. They used the GICC05 chronology to date events in the ice core and compared them to the timing and length of D/O cycles

(Sanchez-Goñi 2010). Harrison and Sanchez-Goñi (2010), considered 94 land based records presenting the responses of vegetation and fire to the millennial scale variability during the glacial period. They found strong vegetation responses to D/O warming and subsequent cooling events to be most pronounced in the northern extra-tropics. They found that vegetation and fire regimes responded immediately to the climate change. In the extra-tropical regions vegetation responses were largely determined by winter temperatures, in the tropics vegetation response was largely determined by plant-available water. Kageyama et al. (2010) reviewed literature from modelling studies of the millennial scale variability and performed simulations with two Earth system models of intermediate complexity (EMIC). They found that there were similarities in model response to forcing, but also significant differences. They note the importance of proxy data to better constrain the behaviour of the system during these climate variations. On reviewing previous modelling studies they note the variation in experimental set-ups between models, resulting in great difficulty making a comparison between models. One important characteristic that can determined however is that the model outputs are very different depending on the climate background state.

6.2 Equilibrium background climate experiments

6.2.1.Model and simulation settings

The equilibrium background climate experiments show how the permafrost-carbon mechanism strongly effects the carbon cycle response to FWF compared to the standard CLIMBER-2 model. Two forcing profiles are applied, first a step function at two magnitudes and two climate backgrounds (PI and LGM). Step simulations for PI start from an equilibrium background climate, with atmospheric CO_2 at 280ppmv, PI runoff, PI ice sheet, PI insolation. For LGM with 190ppmv, LGM runoff, LGM ice sheet, reduced ocean volume and LGM insolation for the LGM. Each simulation is run for 5000 model years, with fresh water forcing starting at 500 model years as a step function then ceasing at 1000 model years as shown in figure 6.1. The permafrost-carbon settings used here are the 'best-fit' settings from the deglaciation experiment in chapter 4, with the fraction of brines that sink set to 0.8 for the LGM, stratification dependent diffusion parameter alpha set to 0.5 and no iron fertilisation of marine biota. Model settings and forcings are shown in table 1. A further test, a series of forcing is applied to the LGM background climate case to (figure 6.2) mimic a series of Daansgaard-Oeschger events with progressively diminished forcing magnitudes.

Climate background	Forcing (Sv)	Model settings and mechanisms	Name
PI	0.15	Climate forcings, plus standard ocean and standard land model	Clim
	0.15	Clim plus carbonate compensation in the ocean	Seds
	0.15	Seds plus permafrost-carbon mechanism	Perm Seds
LGM	0.15	Climate forcings only	Clim
	0.15	Clim plus carbonate compensation in the ocean	Seds
	0.15	Seds plus permafrost-carbon mechanism	Perm Seds
	0.15	Perm Seds with ocean glacial mechanisms: sinking brines and increased ocean stratification	Perm Seds Brines
LGM	0.3	Perm Seds with ocean glacial mechanisms: sinking brines and increased ocean stratification	Perm Seds Brines

Table 6.1 Simulations for fresh water release into the north Atlantic

Climate background	Forcing (Sv)	Model settings and mechanisms	Name
LGM	0.15	Climate forcings, plus standard ocean and standard land model	Clim
	0.15	Clim plus carbonate compensation in the ocean	Seds
	0.15	Seds plus permafrost-carbon mechanism	Perm Seds
	0.15	Perm Seds with ocean glacial mechanisms: sinking brines and increased ocean stratification	Perm Seds Brines
LGM	0.3	Perm Seds with ocean glacial mechanisms: sinking brines and increased ocean stratification	Perm Seds Brines

Table 6.2 Simulations for fresh water release into the south Atlantic

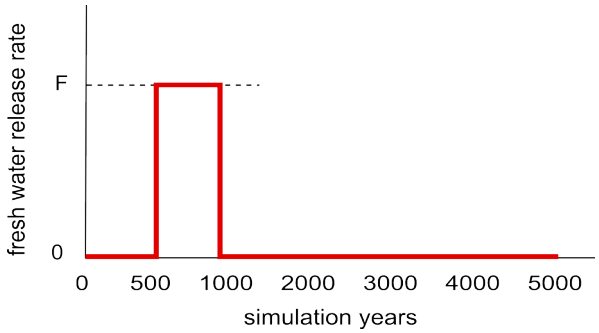

Fig 6.1: Fresh water forcing for equilibrium background climate experiments

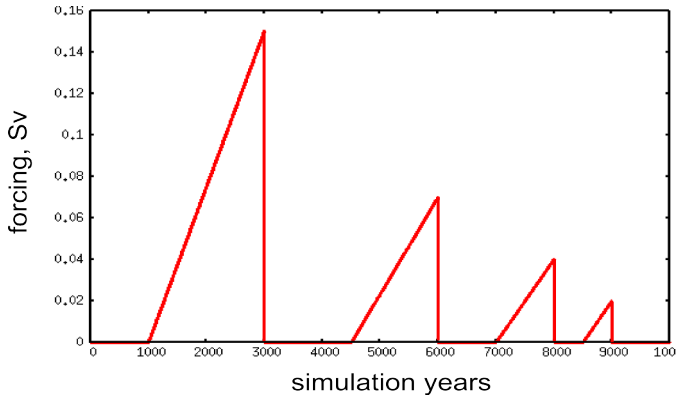

fig 6.2 Series of forcing in the north Atlantic applied to the Sed Brines (without permafrost) and the Perm Sed Brines model settings for an equilibrium LGM climate background

6.2.2 Results

Step function fresh water forcing

The pre-industrial climate background 0.15Sv northern hemisphere freshwater forcing (FWF) mechanisms comparison is shown in figure 6.3. There is a clear difference in model output when the permafrost mechanism is included. The cooling of the northern hemisphere associated with a reduction the strength of the AMOC causes the total permafrost area to increase significantly. This in turn increases the total land carbon amount, via accumulation in frozen soils, by 250GtC before the end of the FWF period. After the forcing has ceased land carbon continues to increase by another 100GtC before the AMOC recovers fully. On AMOC overshoot, the land loses around 100GtC due to a permafrost thaw. After the AMOC has stabilised the total land carbon amount continues to rise because total permafrost area stabilises at a greater area than at the start of the experiment.

The uptake from permafrost soils causes a large drop in atmospheric CO_2 of 57ppm occurring just after the fresh water forcing ceases. The CO_2 then recovers to a level around 17ppm lower than at the start of the experiment. This result is significantly

different from the model outputs when permafrost is not included. Without the permafrost the atmospheric CO_2 levels stabilise around 17ppm higher than at the start. It is important to note than in all the experiments any changes in atmospheric CO_2 from the carbon cycle output are not transferred to the thermal balance of the system. That is to say, the atmospheric CO_2 drops as a result of permafrost related land carbon uptake, but the temperatures, shown in the bottom two graphs in figure 6.3, do not show any difference between the outputs with or without permafrost. If the CO_2 feedback was taken into account then the permafrost would tend to amplify a lowering of temperature.

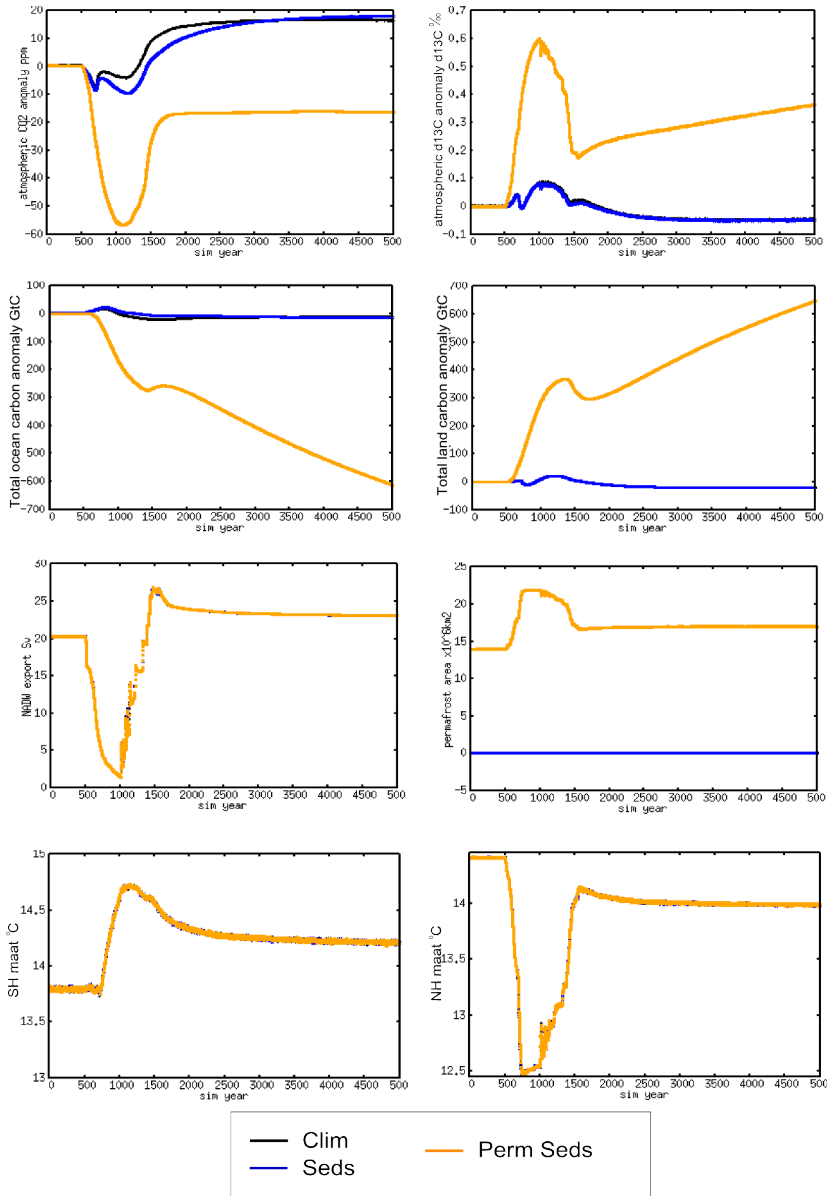

Fig 6.3: Model output for PI equilibrium background climate with 0.15Sv constant FWF in the north Atlantic between 500 and 1000 sim years.

The source of the carbon which transfers into the land carbon pool after the AMOC has recovered is from the ocean, which loses carbon. The pre-industrial background experiment can be seen as the interglacial case, where fresh water forcing could be from melting of the Greenland ice sheet. All model outputs show a shift to a more positive $\delta^{13}C$ during the forcing period, with a subsequent drop when the AMOC recovers. The major difference is that the maximum increase without permafrost is around 0.1‰, but with permafrost is 0.6‰. An increase of this magnitude would be visible in the atmospheric $\delta^{13}C$ record if a fast Greenland ice sheet thaw occurred and caused an AMOC response.

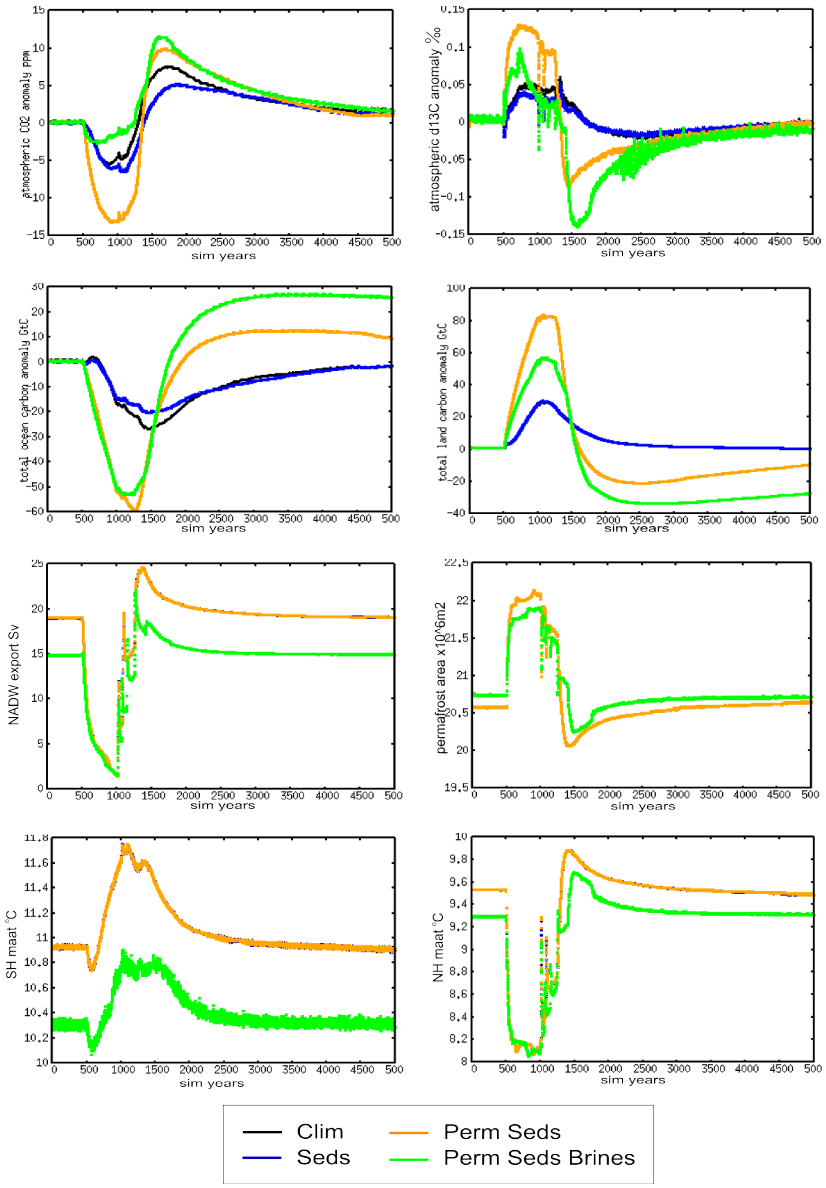

Fig 6.4, Model output for LGM equilibrium background climate with 0.15Sv constant FWF in the north Atlantic between 500 and 1000 sim years. Outputs for included mechanisms identified in table 1

The equivalent experiment output using an LGM climate background is shown in figure 6.4. Already it is clear that the system shows a very different behaviour than in the PI case. The atmospheric CO_2 level shows an initial drop followed by a recovery then an overshoot, eventually stabilising more than 400 years after the forcing has ceased. The total magnitude of the changes are smaller than those seen in the PI case when permafrost is included, but higher than PI for the other settings (without permafrost). The land carbon profile when permafrost is included is somewhat different to the PI case, for LGM climate the initial rise in total land carbon is followed by a drop then a loss of carbon compared to the initial condition. The final total amount of carbon stored on land is less than at the start even though the total permafrost area is approximately the same. This can be explained by an AMOC overshoot that causes a permafrost thaw, releasing carbon from the soils. When the AMOC overshoot has finished, around 0.5-1kyr later, the soils start to slowly accumulate carbon once again in the newly frozen soils, but from a lower carbon ceoncentration than at the start.

The extra mechanism acting in the glacial condition is the sinking of brines and a stratification-dependent ocean diffusion. By adding these mechanism along with permafrost the CO_2 output is significantly different compared to the no-brines/strat case. Now rather than an initial drop in atmospheric CO_2 of 13ppm, the drop essentially disappears (2ppm). This is a significant difference between the glacial and interglacial case. With the carbon cycle mechanisms that create a realistic LGM climate (Bouttes et al. 2011, chapter 4) a northern hemisphere fresh-water forcing appears as an increase in CO_2 after AMOC recovery at LGM, but the same forcing causes a drop in atmospheric CO_2 at PI during the forcing period.

The inclusion of the brines and ocean stratification mechanism also has an effect on the initial AMOC strength. In initial conditions with brines sinking, the NADW export is 5Sv lower. This reduction also already has an initial effect on the global temperature which is colder compared to the other model conditions. The 'disappearance' of the initial drop in CO_2 when brines is added can be explained due to a more limited increase in total land carbon during the forcing period associated with a smaller total permafrost area increase, but a relatively unchanged ocean out-gassing.

The modelled atmospheric $\delta^{13}C$ for the LGM (glacial) case is an initial rise in $\delta^{13}C$ of a maximum of 0.1‰, followed by a drop of around the same magnitude coinciding with AMOC overshoot (which causes a fast permafrost thawing). In order to test the sensitivity of the system to the magnitude of fresh water forcing, the results from the 0.15Sv forcing experiment for brines/strat and permafrost mechanisms are shown together with a 0.3Sv forcing in figure 6.5 for the Perm Seds Brines setting. In both cases the AMOC is reduced to almost zero before the end of the forcing period, but with the 0.3Sv forcing AMOC switch-off happens faster, and the recovery takes longer. The overshoot for the 0.3Sv case is, however, not greater in magnitude to the 0.15Sv FWF. The overall effect of the increased forcing is an amplification and a delaying of the maximum (or minimum) values. An exception to this is the northern hemisphere temperature which is slightly lowered for the 0.3Sv forcing by around 0.3°C, and the southern hemisphere is slightly warmer by around 0.4°C.

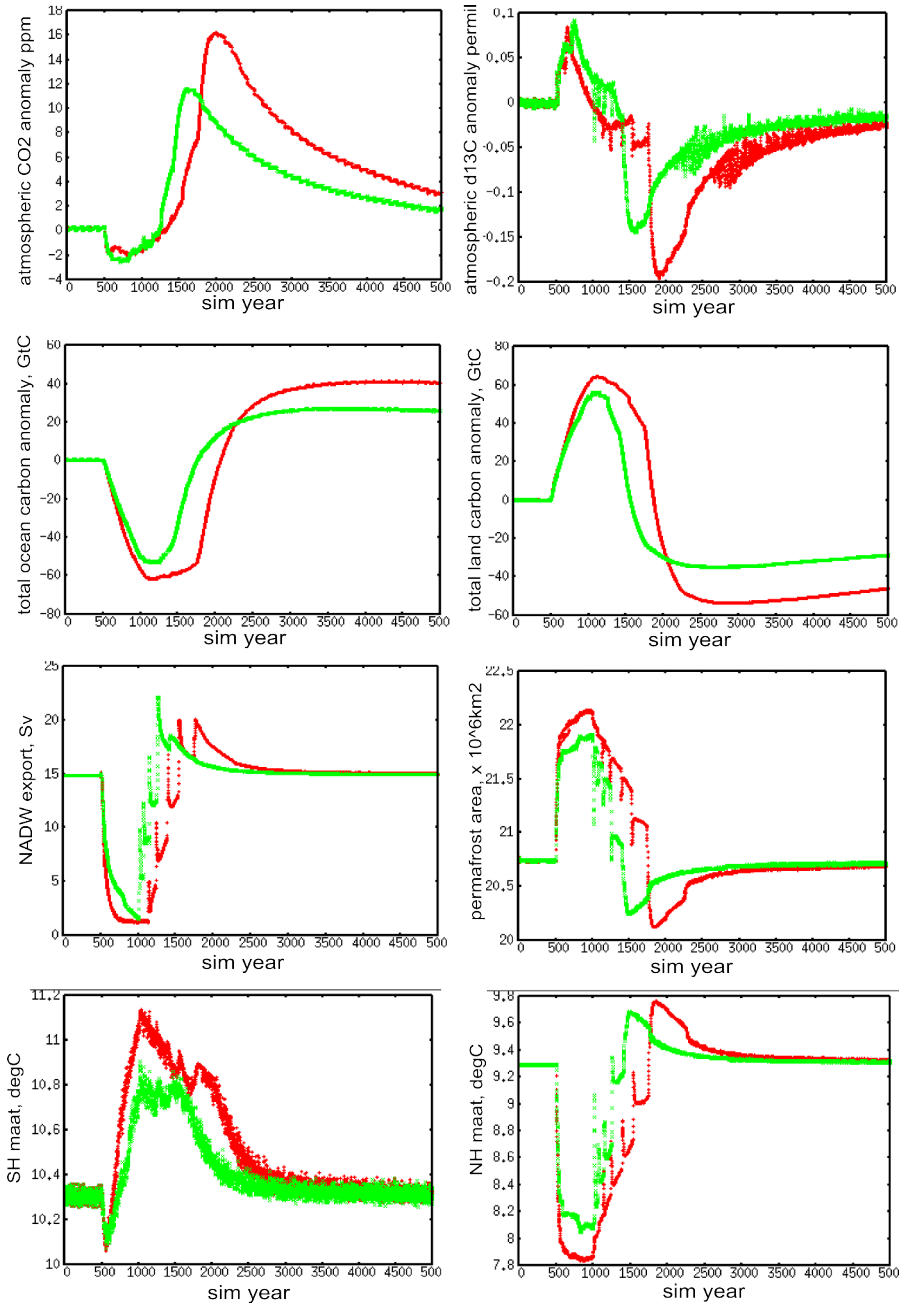

Fig 6.5, Model output for LGM equilibrium background climate with 0.15Sv and 0.3Sv constant FWF in the north Atlantic between 500 and 1000 sim years. For Perm Seds Brines setting

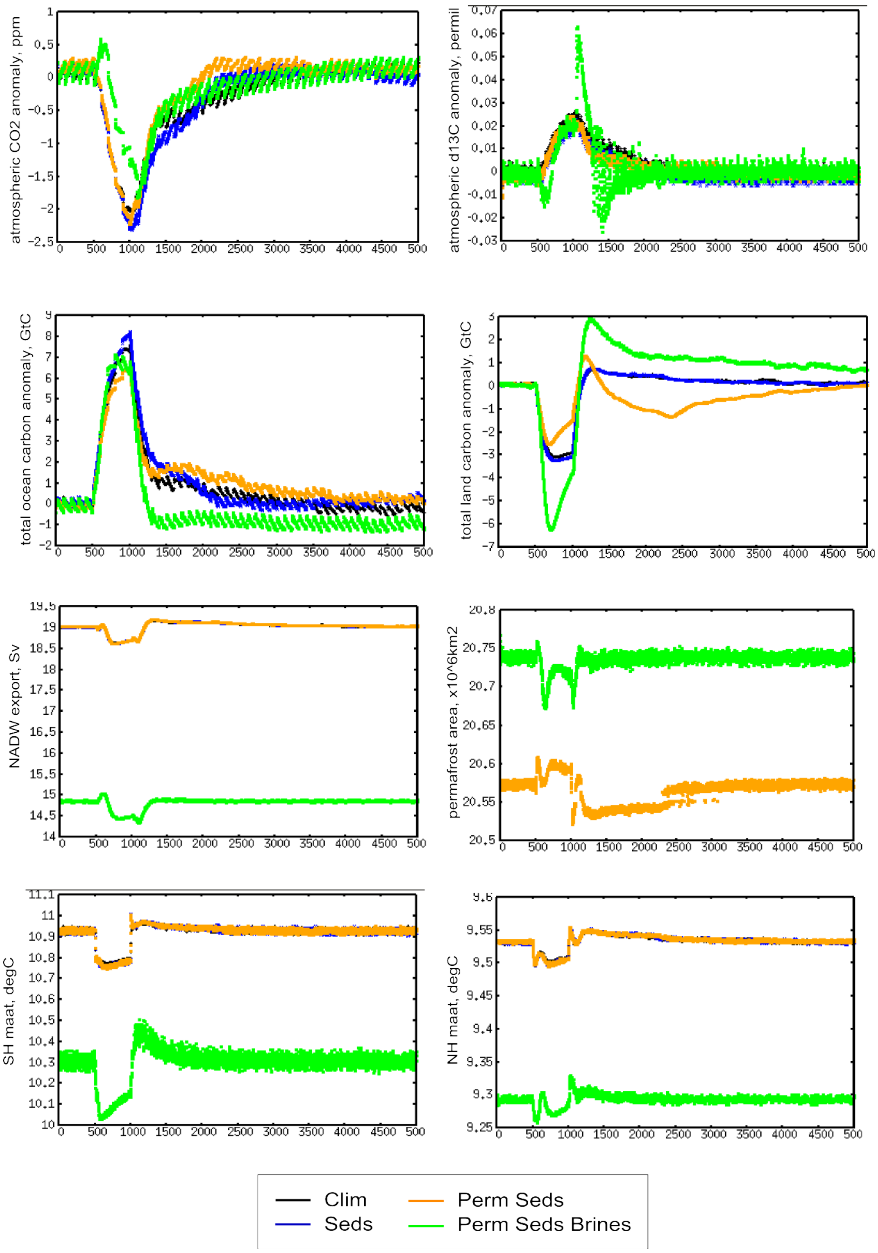

Fig 6.6, Model output for LGM equilibrium background climate with 0.15Sv constant FWF in the Southern Ocean Atlantic sector between 500 and 1000 sim years.

The forcing for a S. Atlantic sourced fresh water is shown in figure 6.6. In this case the forcing also causes a slight reduction in AMOC strength by around 0.5Sv. However, the other outputs are not simply reduced duplicates of the northern hemisphere forcing case. Despite the reduction in AMOC, the southern hemisphere temperature still reduces, as does the northern hemisphere temperature. There is a small reduction in total land carbon, which is accentuated when brines is also present. For 0.15Sv forcing a drop in atmospheric CO_2 of 2ppm is seen, followed by essentially a stabilisation of the system back to the initial condition after around 400 years.

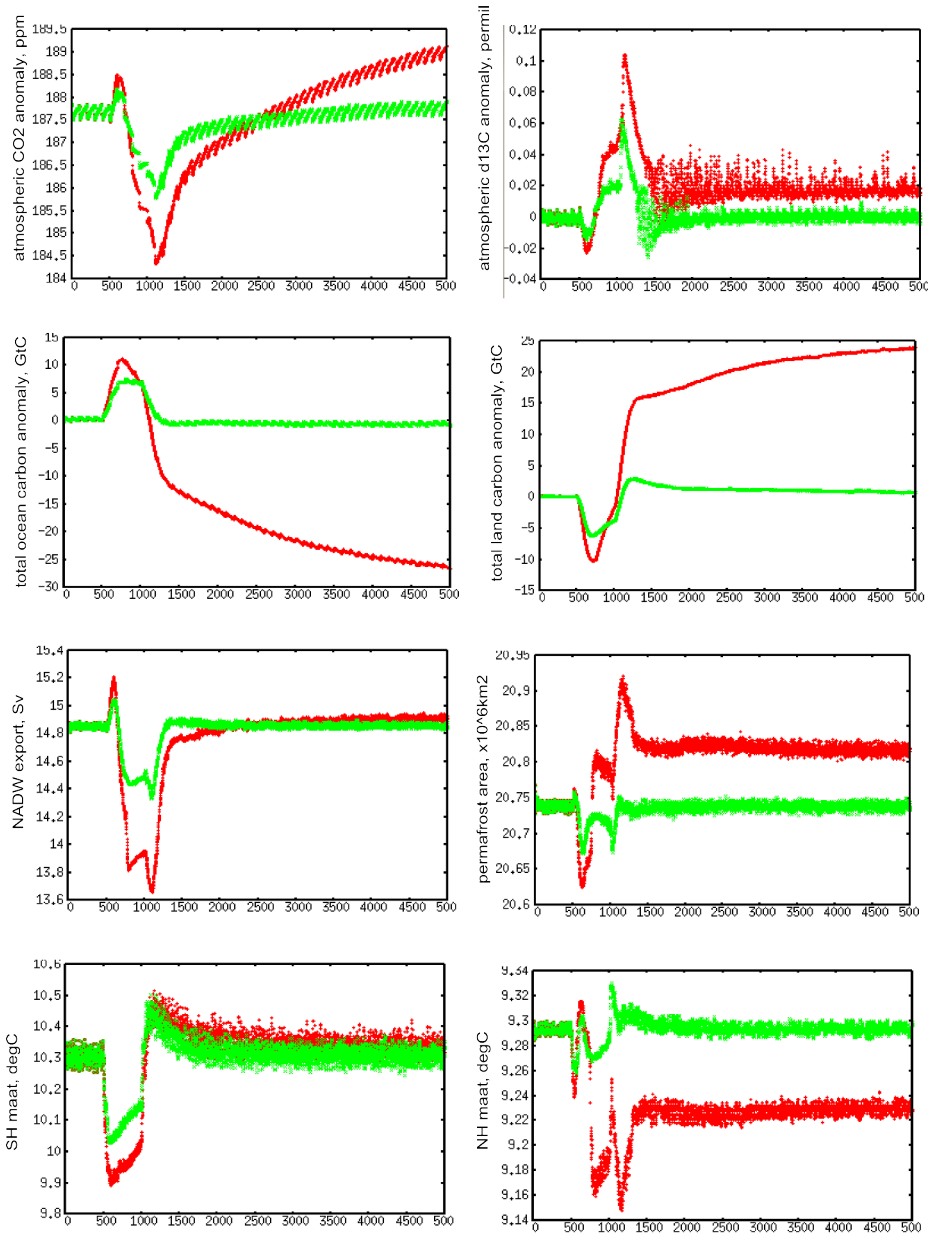

Fig 6.7, Model output for LGM equilibrium background climate with 0.15Sv (green) and 0.3Sv (red) constant FWF in the Southern Ocean Atlantic sector between 500 and 1000 sim years. For Perm Seds Brines setting

By contrast to the 0.15Sv south Atlantic forcing, a 0.3Sv forcing (figure 6.7) causes a change in the system, after the forcing has finished total land carbon continues to increase due to increased permafrost area. The ocean out-gasses carbon into the atmosphere, which cannot be caused solely due to land uptake, because atmospheric CO_2 rises at the same time. The experiment is halted at 4500 years after the forcing has finished, at this stage CO_2 is around 1.5ppm higher than the initial condition, but the final stabilised value has not been reached. The $\delta^{13}C$ record shows an increase of around 0.1‰ coinciding with the lowest strength of the AMOC.

Series of fresh water forcing events

The results for the series of fresh water forcings are shown in figure 6.8, here with "Sed Brines" compared with "Perm Sed Brines" to look at the affect that permafrost has on the system. Without permafrost the increase in atmospheric CO_2 from the start of the first forcing period is around 10ppm peaking at the same time as the AMOC overshoot. The subsequent FWFs do not have a great effect on CO_2. When permafrost is included the CO_2 peak is increased to a total of ~22ppm relative to the CO_2 low. The combined effect of land carbon uptake in cooling periods and ocean carbon release at the same time causes an initial drop in CO_2 during the first forcing period. A fast rise in atmospheric CO_2 occurs just after AMOC resumption and is sourced from carbon released from thawing soils. Subsequent forcing periods have a similar effect on the land carbon contents but of reducing magnitude due to the reducing AMOC response.

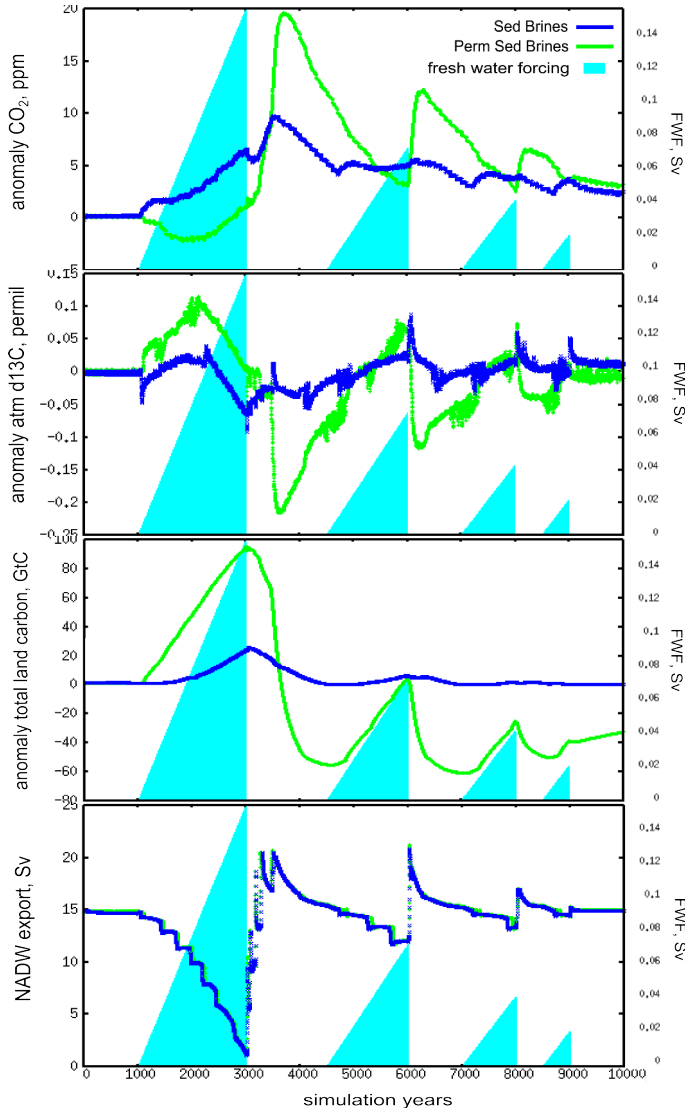

Fig 6.8, Model output for a series of fresh water forcing profiles comparing without permafrost (Sed Brines, blue) to with permafrost (Perm Sed Brines, green).

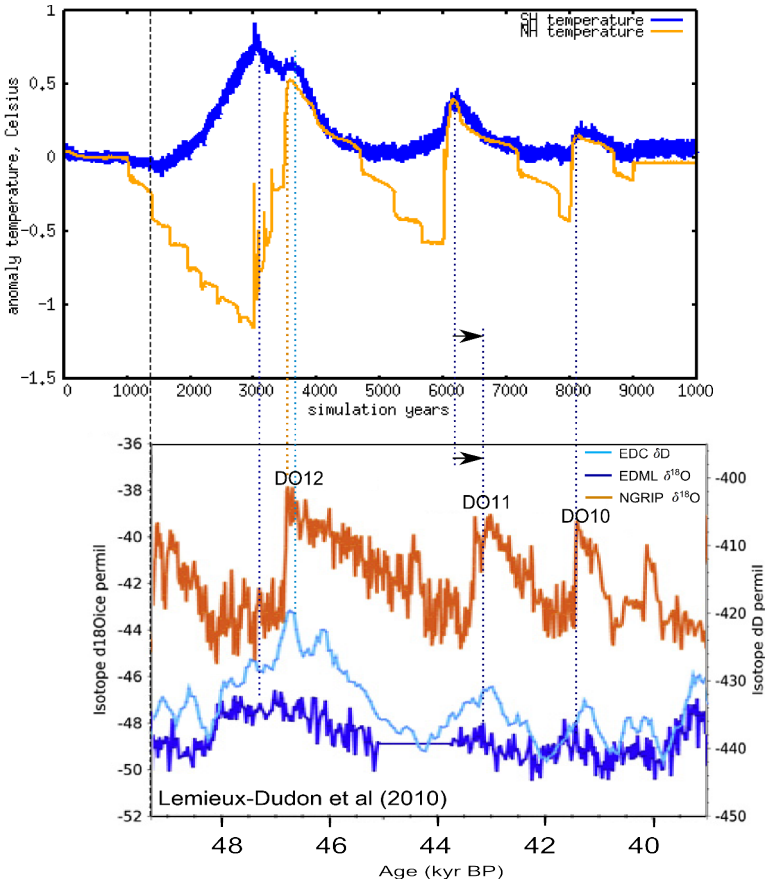

Fig 6.9, Top: Modelled northern (orange) and southern (blue) hemispheric temperatures for series of FWF forcings. Bottom: Ice core data for temperature proxy on the Lemieux-Dudon et al 2010 synchronised age scale to compare DO events 12 to 10 with model output.

Modelled hemispheric temperatures for the series of forcings are shown in figure 6.9. The southern hemisphere peak warming occurs just prior to the northern hemisphere peak for the first forcing period, thereafter the peaks coincide. Only the first forcing period has a strong effect on the ocean, because it is only this forcing that reduces the AMOC significantly (fig 6.8). Further forcings affect the northern hemisphere more strongly than the southern. If this series is compared to D/O events 12, 11 and 10 the timings of peak warming relative to the Antarctic and Greenland temperatures are in good agreement (Lemieux-Dudon et al. 2010) (fig 6.9). The modelled CO_2 does not have a good agreement with data pattern, which is more similar to the Seds Brines model settings of a CO_2 rise (blue line fig 6.8) occurring only 1000 years after peak Antarctic warming (Ahn and Brook 2008), and subsequent rises coinciding with D/O 11 and D/O 10 not seen clearly in the data. The total magnitude of the rise seen in data for D/O 12 is ~20ppm which is reproduced when permafrost-carbon is included in the model. However, it should be noted that this is an equilibrium LGM background climate simulation, which is not representative of real world conditions in which changes in CO_2 forcing, insolation and ice sheets have a strong effect on the carbon cycle.

A schematic representation of the behaviour of the permafrost-carbon dynamics during a series of cooling-warming events is shown in figure 6.10. The slow accumulation rate in permafrost soils combined with the progressively reducing magnitude of the forcing causes the CO_2 to peak more strongly during the first forcing and progressively less strongly during subsequent forcing. This model is very simplified and does not include dynamics from some fast-changing vegetation communities and fire regimes, which according to Harrison and Sanchez-Goñi (2010) responded very quickly during this type of climate variability. During cold periods (forcing periods) conditions for plant growth were less favourable, precipitation was likely reduced as well as temperature. During warming phases this quickly changed creating conditions far more favourable. Peatland dynamics, not present in CLIMBER-2P, may have acted to dampen the carbon cycle response from permafrost-carbon. Peatlands may have lost carbon in cold dry periods, and expanded during warm and wet periods and acting as a carbon sink.

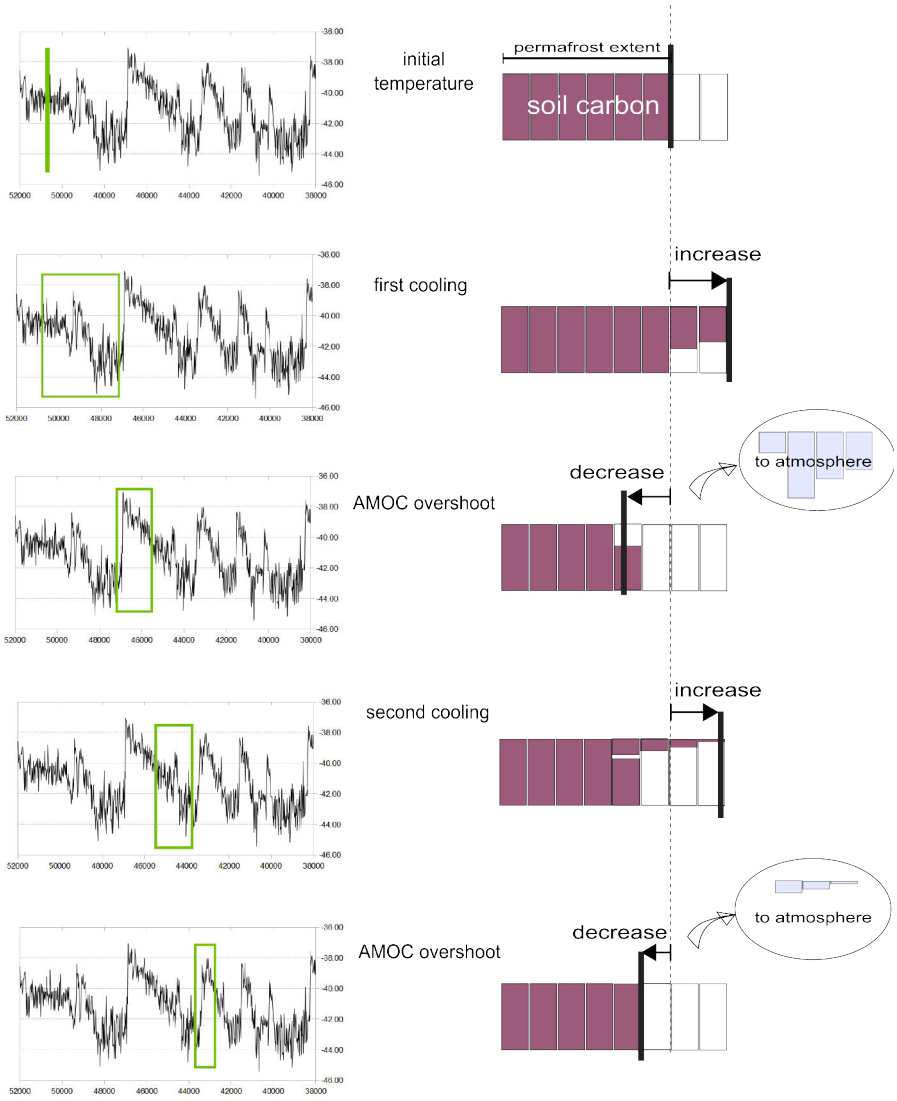

Fig 6.10, Schematic of permafrost-carbon dynamic during a series of cooling and warming events.

During the series of FWF events, only the first one caused a strong response from the ocean. Land carbon uptake dynamics that are absent from the model may have gone some way to offset losses from thawing permafrost carbon during warming phases. This could provide an explanation as to why the CO_2 record indicates that not every D/O event seen in the Greenland record is associated with a rise in atmospheric CO_2. A high resolution $\delta^{13}C$ record for this period would be able to identify whether CO_2 rise during AMOC fluctuation periods was sourced from the land or the ocean.

6.3: Transient deglaciation – forcing of varying magnitude

6.3.1 Model and simulation settings

The transient simulation sets employ a step function then a triangle (fig 6.11) function (here called "StT"). This pattern is based on Tarasov and Peltier (2005) for the Arctic drainage chronology, identified as being of particular importance for AMOC strength. These fresh water forcings are applied in the North Atlantic sector during a transient deglaciation in which ice sheets, ocean volume, insolation forcing and CO_2 forcing for radiative code are all evolving. The model settings are all for "Perm Seds Brines". The ocean glacial mechanisms are controlled as a linear reduction in their magnitude of forcing from 18kyr to 12kyr BP as chapter 4. Th permafrost dynamic is “medium”. These settings produced the best-fit output for the deglacial records for atmospheric $\delta^{13}C$ and CO_2. The deglaciation with no fresh-water forcing shows that the model cannot reproduce a Younger-Dryas type CO_2 plateau from 13.5kyrBP (chapter 4) and the initial CO_2 rise is slightly less-fast than the data suggests. The transient simulations allow to explore the affect of timing and magnitude of northern hemisphere fresh-water forcing on the carbon cycle. The applied forcings are shown in figure 6.12 and table 3.

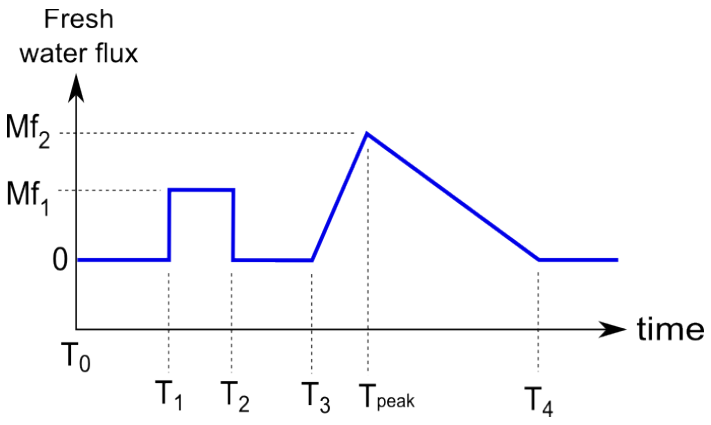

Fig 6.11, StT experiment settings for transient deglaciation experiments. Timings shown in table 3.

	Step forcing			Triangle forcing			
name	T1 (kyr BP)	T2 (kyr BP)	Mf1 (Sv)	T3 (kyr BP)	T_{peak}(kyr BP)	T4 (kyr BP)	Mf2 (Sv)
taras[1]	-20	-17	0.3	-13	-12.8	-11.5	1.2
StT 2	-19	-17	0.1	-13	-12.8	-12	0.5
StT 1	-20	-17	0.05	-15	-12.8	-11	0.05

Table 3 StT FWF settings

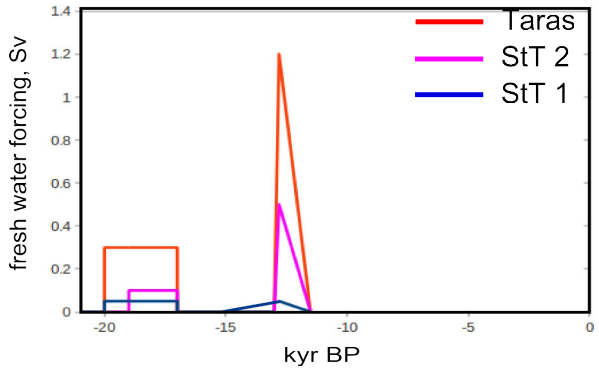

Fig 6.12, Step Triangle forcings applied for the transient deglaciation as table 3.

6.3.2 Results

Applying a fresh water forcing similar to Tarasov and Peltier (2005) results in the timing of the initial rise in CO_2 showing a better-fit with data (fig 6.13). However, the subsequent rise is far too great and too fast compared to the data. The effect of the fresh water forcing from 18kyr BP is to increase total land carbon and reduce total ocean carbon, as with the LGM equilibrium experiment. After the forcing ceases and the AMOC recovers the land releases carbon due to permafrost thaw and causes a large part of the fast CO_2 rise. For this transient simulation, the permafrost thaw from AMOC overshoot acts in addition to the thaw that is being driven by high latitude summer insolation increases between 20 to 10kyr BP. The lowest forcing from 21kyr BP (the step part of the forcing, StT 1) shows the best agreement with data for timing and rate of CO_2 rise, but is still too fast compared to data. With permafrost-carbon included in the model set-up the rise in CO_2 is almost all due to the system response to insolation, and does not require an AMOC switch-off to induce a CO_2 rise (from the southern ocean).

The second forcing period (the triangle part) has a similar effect on the AMOC to the first forcing period in the 'taras' simulation. The effect seen in the land and ocean carbon pools is somewhat different. Although there is a small increase in total land carbon (compared to the no FWF case), and decrease in ocean carbon, the magnitude is far smaller than for the first forcing period. The maximum increase in land carbon for period 1(step) is around 400GtC, but for period 2 (triangle) is 150GtC. This is because

1 Since writing I realised these values from the Tarasov and Peltier study have been misread from their paper as Sv. They used dSv (tenths of Sv) rather than Sv. Consequently the "taras" set forcing is ten times too strong compared to their reconstruction.

at this stage the land carbon pool is already on a rising trend and the uptake of carbon on the land is limited by the maximum accumulation rate in (permafrost) soils. The CO_2 output for the second forcing period shows a large drop when the AMOC strength is at minimum, rather similar to the PI equilibrium case (fig 6.3), with a maximum decrease of 30ppm. The lower forcing, StT 2 shows a similar magnitude change in CO_2 to the taras setting but of a shorter duration. The lowest forcing, StT1 shows poor agreement with data, producing only a slight slow-down in CO_2 rise relative to the no-forcing case.

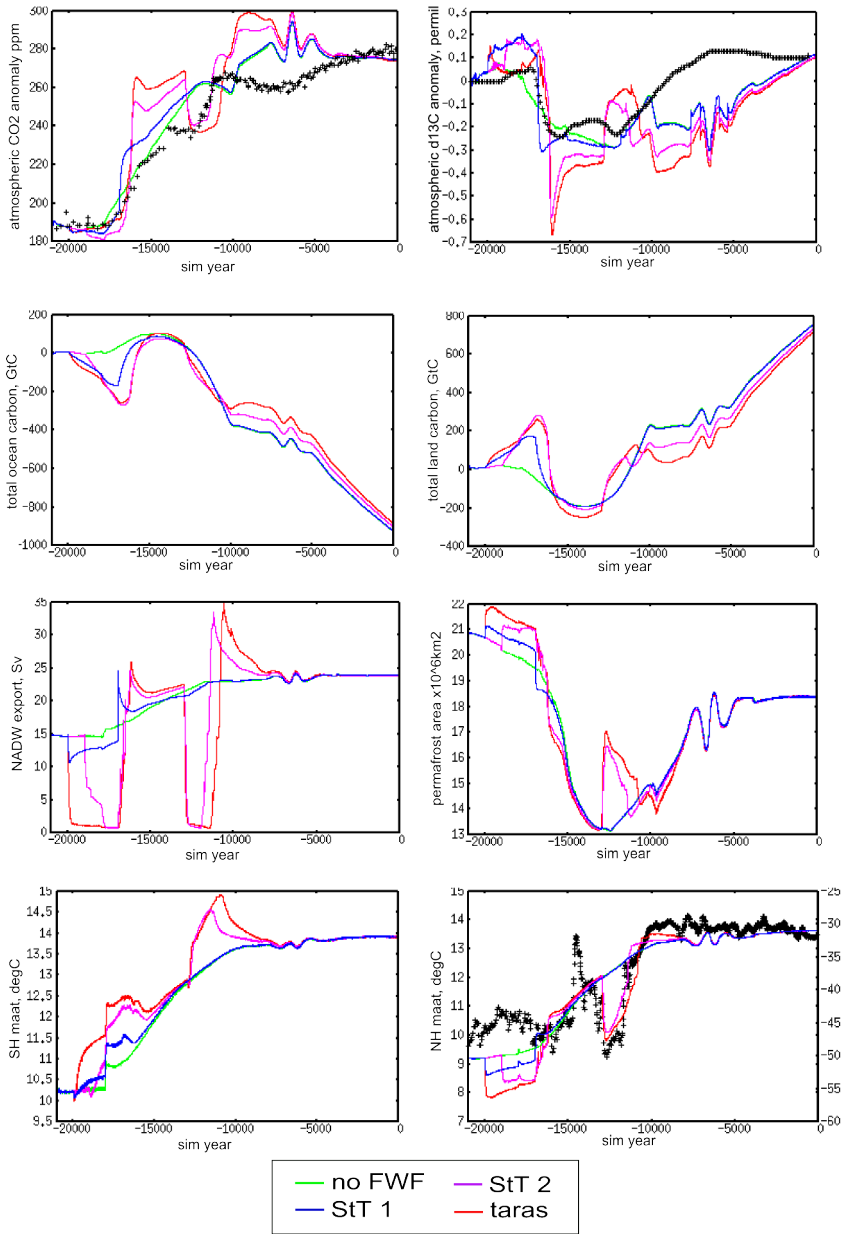

Fig 6.13, StT transient deglaciation experiment outputs for FWF forcing in the North Atlantic shown in figure 6.12. Model settings are Perm Seds Brines (linear).[2]

2 The "taras" set forcing is ten times stronger than the Tarasov Peltier 2005 reconstruction due to a misreading of their paper. Consequently this output is not a good representation of their actual proposed discharge forcing, it is ten times too strong.

The results from the Step Triangle experiments suggest that with permafrost, an AMOC switch-off just prior to the deglaciation followed by a recovery and overshoot causes atmospheric CO_2 to rise too fast and too far in the absence of any other forcing between 17.5kyr BP and 12.5kyr BP. The drop in $\delta^{13}C$ for the first part of the deglaciation is also overly negative compared to data if AMOC switch-off and overshoot is induced. The B-A/YD forcing (~13.5 to 11.5 kyrBP) results show that a significant reduction in AMOC strength is required to explain the CO_2 record, the lowest forcing in which no real AMOC reduction is produced does not create a B-A/YD-like CO_2 plateau or drop. The northern hemisphere temperature output shows a drop which is comparable in timing to the Greenland temperature record when the AMOC is significantly reduced (fig 6.13).

6.4 Transient deglaciation – inverted FWF

6.4.1 Model and simulation settings

A fresh water forcing profile was created based on the results from the previous section and a transient deglaciation simulation was carried out using this profile. Using these first results the forcing profile was adjusted and the deglaciation was re-run and these results were used to improve the FWF profile. This process was carried out until a CO_2 profile similar to data was obtained. Full results of this process are available in the Appendix. The only driver for adjusting the profile was how well the CO_2 record fitted data from Monnin et al 2001 (using the synchronised age scale from Lemieux-Dudon et al. (2010)). The drivers for the deglaciation are presented in figure 6.14. The sinking of brines is again a linear reduction from 18kyr BP to zero at 12kyr BP. Insolation in the high northern latitudes has a strong control over the timing of permafrost thaw.

6.4.2 Results

Fresh water forcing and sea level

The fresh water forcing profile (FWF profile) that was identified is shown in figure 6.14. The modelled AMOC response to that forcing and modelled atmospheric CO_2 is shown in figure 6.15. A record of sea level rise compiled by Carlson and Clark is shown in figure 6.16, along with the FWF forcing and modelled NH temperature. As expected after results for the non-FWF forced deglaciation in chapter 4, no large fresh water forcing at the onset of deglaciation is required to correctly model CO_2 rise. Comparing this to the sea level record, between 20kyr to 19kyr BP of around 5 to 10m is seen, being sourced from northern hemisphere ice sheets. Our FWF starts later than this, with a maximum release of 0.03Sv by 17.5 kyr BP. This causes a very small drop in AMOC and slight delay in CO_2 rise.

A second FWF period peaking at ~14.8kyrBP causes another slow down in the rate of AMOC strength rise, and a slowing in CO_2 rise. When this forcing reduces it results in a faster AMOC strength increase and faster CO_2 rise. Comparing this to sea level rise data, no obvious rise is seen in this period (fig 6.16). However, Licciardi et al (1999) reconstructed the routing of the Laurentide ice sheet and identified a continental run-off routed through the Hudson river causing a strong flux of more than 0.12Sv occurring between ~16kyr and ~15.1kyrBP. This LIS release may coincide with our forcing period starting from 16kyr and rising to peak at 14.8kyr BP.

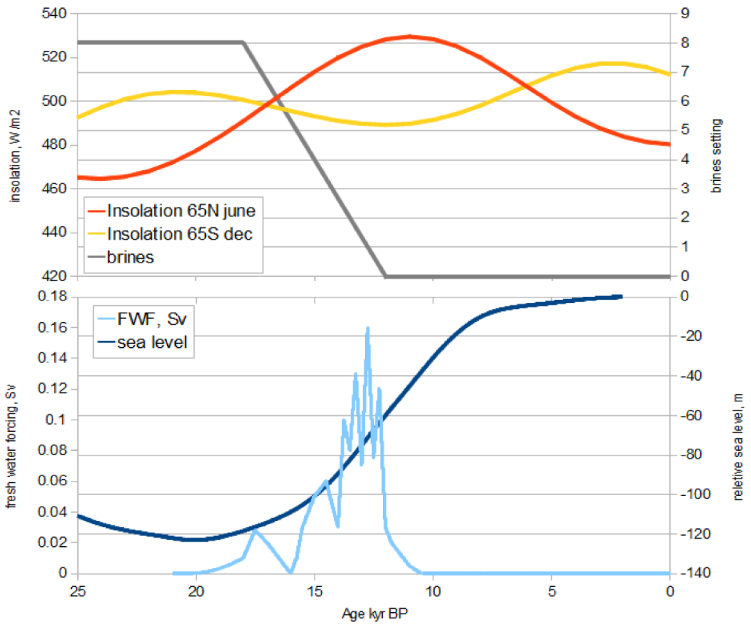

Fig 6.14, Model forcing used for the transient deglaciation, inverted FWF simulation. Brines reduce as chapter 4, from 0.8 at 18kyrBP then linearly reduce to 0 at 12kyrBP. Insolation evolves with orbital changes. Relative sea level controls ocean volume (and salinity and nutrient concentrations) as well as ice sheet extent.

The forcing required to produce a plateau/slight drop in CO_2 and a subsequent NH cooling for the B-A/YD period is a strong fluctuating fresh water forcing into the North Atlantic. This causes a gradual drop in AMOC strength to a low at 12.5kyr BP, but not a sudden switch-off (figure 6.15). According to sea level records, a fast rise is seen apparently occurring earlier than our B-A/YD (third) forcing period (in figure 6.16). A closer look at this sea level rise by Carlson and Clark (2012) shows that the fastest rate of sea-level rise in this period, Melt Water Pulse 1 a (MWP1a), occurred after 14kyr BP, as does our FWF. The source of this MWP1a has been modelled in various studies with findings assigning it variously to either N American or European ice sheets flushing water into the Pacific, the Atlantic or the Arctic oceans[3], or sourced from southern hemisphere ice sheets.

3 According to the discharge chronology from Tarasov and Peltier (2005) our forcing period shows agreement with the Arctic ocean drainage chronology for both timing and magnitude of forcing (0.13Sv to 0.2Sv max), although with a later and stronger MWP1a than they report.

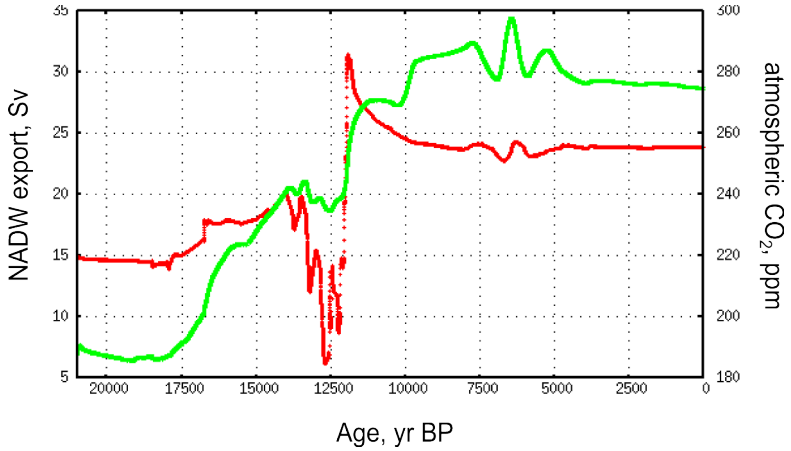

Fig 6.15, Model NADW export, Sv (red), and modelled CO_2, ppm (green) for transient deglaciation FWF inverted.

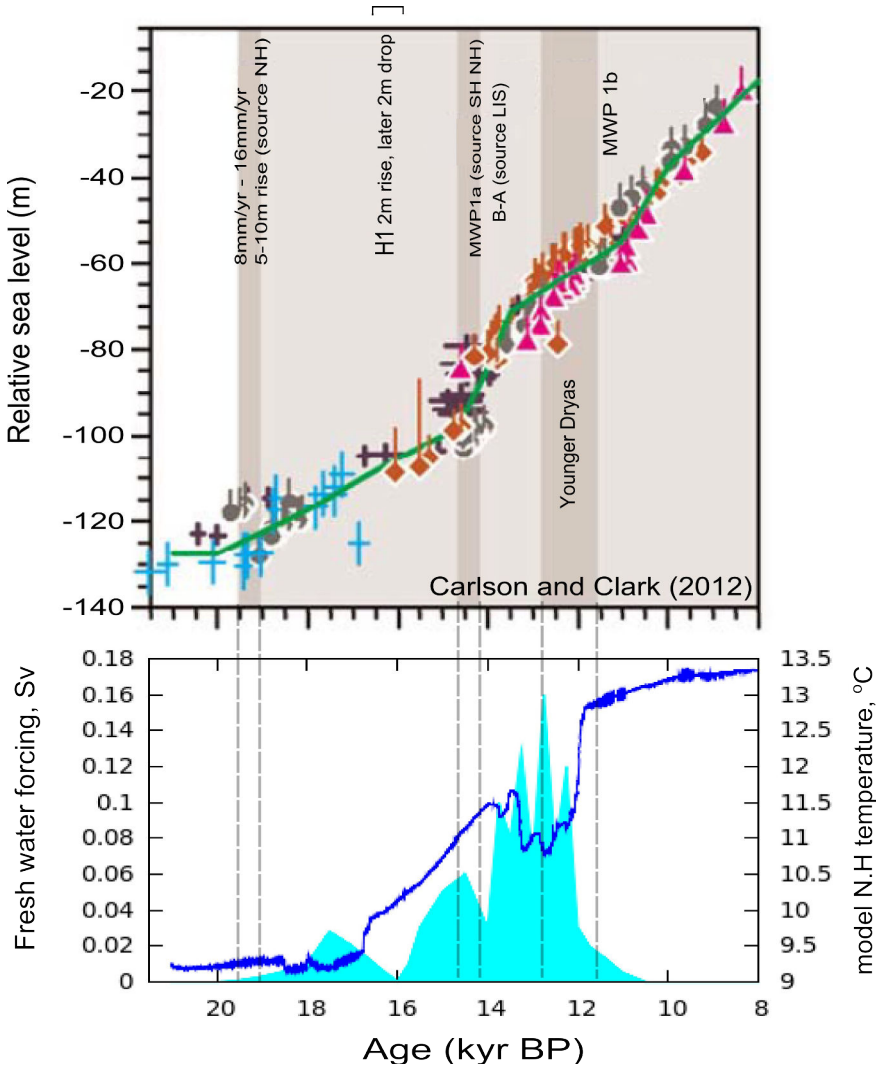

Figure 6.16, Top: Sea level records from Carlson and Clark (2012) for the deglaciation with major periods discussed marked ontop. Bottom: Modelled northern hemisphere temperature and fresh water forcing applied.

After 12kyr BP no more forcing is applied in our FWF profile. This is largely because the initial focus was to recreate the CO_2 plateau during the B-A/YD. From 12 kyr BP a further 60m of sea level rise was still to come, being sourced from the Laurentide, the European and the Antarctic ice sheets (Carlson and Clark 2012). With more iterations of the technique used here to recreate the CO_2 record, fresh water forcing from 12kyrBP may be able to explain some of the remaining model-data mismatches in the CO_2 and temperature records.

Our fresh water input into the north Atlantic is only carried out to control AMOC response. As such we do not consider other runoff areas and therefore can not provide a modelled sea-level rise history to compare with the full sea-level rise record. However, the periods which we do propose as strong fresh water forcings are not disqualified by the sea-level record.

Carbon cycle and temperature evolution

Model output compared with data for CO_2 and $\delta^{13}C$ is shown in figure 6.17. With a small FWF period occurring between 19 to 16kyr BP (but having only a small effect on AMOC strength), the modelled $\delta^{13}C$ matches almost exactly the mean $\delta^{13}C$ data between 19kyr to 16.5kyr BP.

The $\delta^{13}C$ output as a result of the AMOC strength-drop from 13.5 kyr BP shows a positive shift as with the StT experiments and the equilibrium experiments (particularly the PI and the no brines/strat LGM case, fig 6.3 and 6.4). The smoothed $\delta^{13}C$ data (Schmitt et al. 2012) does not show a large positive excursion at this time (~-13kyrBP), but the measured data (Lourantou et al. 2010) shows an increase occurring around the same time (a few hundred years before). The drop in CO_2 seen in data also occurs a few hundred before modelled CO_2, so in principal the mechanism causing these changes is consistent with data output.

The AMOC recovery in the CLIMBER-2P model is very fast after the forcing ceases (order of 200 years), in other modelling studies the AMOC takes a longer time to recover, or requires forcing to switch back on (Kageyama et al. 2010). In order to create a CO_2 output similar to data for the B-A/YD, the fresh water forcing in CLIMBER-2P continues until the end of the CO_2 plateau, the fast AMOC recovery results in a fast drop in $\delta^{13}C$ in the modelled atmosphere. If the AMOC took a longer time to recover, this drop may be less fast. The $\delta^{13}C$ data from Lourantou et al. 2010 does show a positive shift at the start of the B-A/YD period followed by a large negative excursion coinciding with the CO_2 rise of the Younger Dryas. During the B-A/YD period of cold northern hemisphere, the modelled permafrost area increased but the permafrost soils had only a few thousand years to accumulate carbon and therefore the $\delta^{13}C$ drop at the start of the subsequent warming is not as large as for the initial deglaciation (17.5kyr BP).

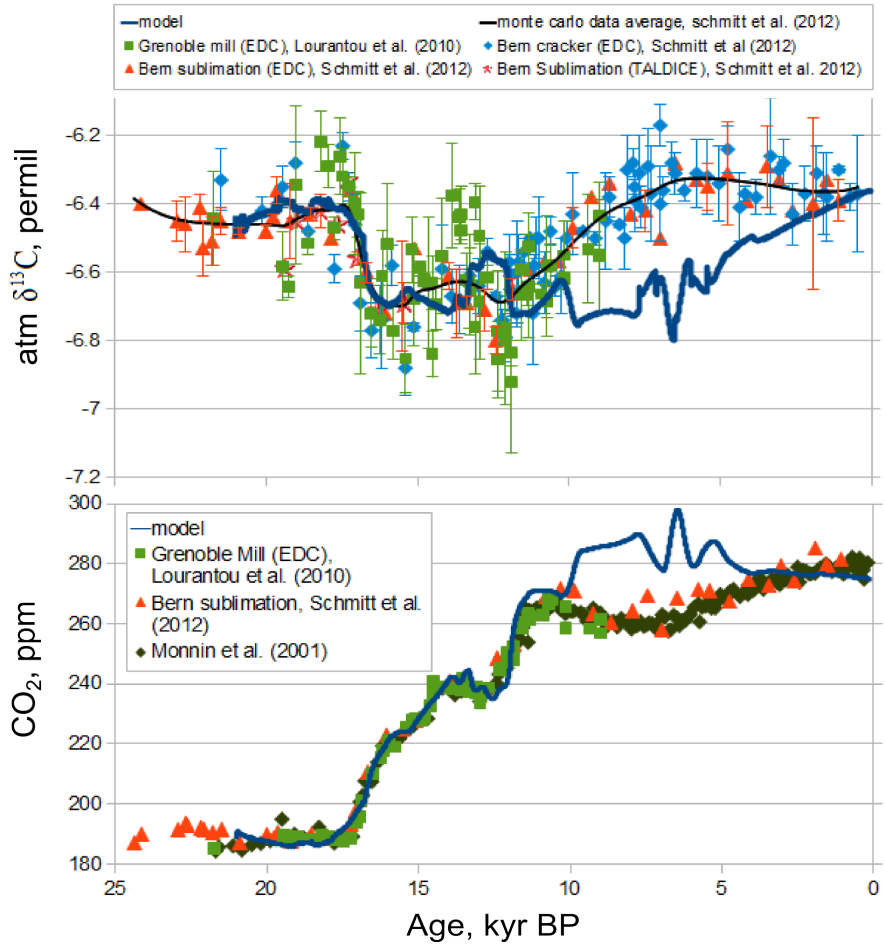

Fig 6.17, Model output and data for atmospheric $\delta^{13}C$, ‰ (top) and CO_2, ppm (bottom) for the transient deglaciation applying the FWF profile (fig 6.14). All data records plotted on the synchronised timescale (Lemieux-Dudon et al. 2010) as Schmitt et al (2012).

The model output for Antarctic and Greenland temperature through the deglaciation overlaid on ice core data reconstructions is shown in figure 6.18. The model output shows the mean annual surface temperatures for the grid cells where the respective ice cores would be located, with the summer temperature mean included for the Greenland location to account for possible seasonality effects in the water isotope thermometer (Krinner and Werner 2003). The initial temperature rise seen in Greenland data from around 22kyr BP is not reflected in the model output, although the simulation only starts from a 21kyr BP equilibrium climate which is likely not realistic enough. The freshwater forcing causes a slight drop in modelled temperature from 19kyr BP lasting until the forcing ceases, which shows some similarities to data. The very fast warming seen during the B/A peaking at almost interglacial values is not seen in model output. This can either be attributed to uncertainties in the interpretation of the Greenland data (Krinner and Werner 2003, Liu et al. 2012), or the level of complexity and large grid cell size of the CLIMBER-2P model which does not capture climate

fluctuations on this spatial and temporal scale, or that we miss the mechanism causing it. This fast warming seen in data is associated with a fast rise in atmospheric CO_2 in data, so conceptually is in agreement with a permafrost-carbon mechanism even though it has not been reproduced in the FWF inverted simulation. Liu et al (2009) modelled the deglaciation and proposed an AMOC control on the B-A warming, as being a result of AMOC resumption after the H1 AMOC quasi-shutdown. As was discussed previously, in our model no AMOC switch-off is seen during H1, so this explanation can not be easily applied for the B-A fast warming. The same principle is as Liu et al (2009) is applied by Shakun et al (2012) in explaining the proxy data per-latitude for temperature changes during the deglaciation. However, by employing yhe AMOC shut-down the modelled northern hemisphere temperature is much too large compared to their data indicators. The Liu et al study comparison for sea-level changes shows that their model overestimates the increase in sea-level during H1, and rather a faster rise is seen (as Carlson and Clark 2012, in figure 6.16) at around 19.5kyr BP. The data for the Iberian margin sea surface temperature drop (shown in Liu et al 2009) cannot be easily explained in our scenario, where data indicates a fall of around 7°C between 18kyr and 17.5kyr BP. To freshen the N. Atlantic in the model, salinity is reduced in surface waters, but no actual cold water input is seen by the ocean model. This may go some way to explaining model-data mismatch, as we neglect the thermal effects of glacial meltwater runoff.

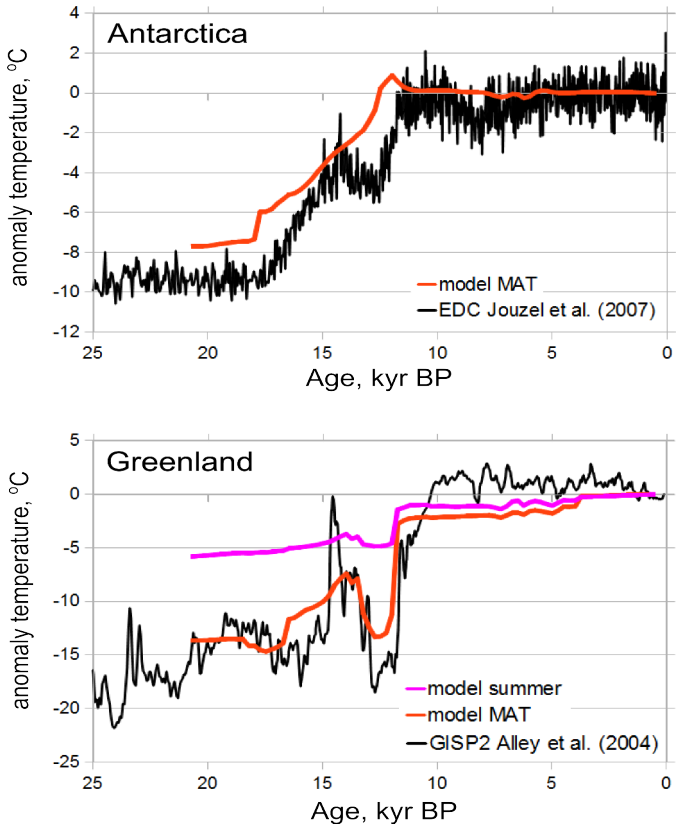

Fig 6.18, Modelled Antarctic and Greenland temperatures overlaid on data reconstruction for transient deglaciation FWF inverted.

Modelled Greenland temperature shows good agreement for the B-A/YD temperature drop between 14 to 12.5kyr BP. The fresh water forcing that is applied all occurs in the north Atlantic, and it may be for this reason that the Antarctic Cold Reversal (ACR) is not seen in the modelled Antarctic temperature output. The hemispheric temperature output can be compared against the data reconstruction from Shakun et al 2012, and this is showed in figure 6.19. The southern hemisphere reconstruction does not show a strong cooling coinciding with the ACR. The Shakun et al. temperature reconstruction is based on many proxy sources located globally, although Siberia and the permafrost zone is not represented in these datasets. Despite this, the model output shows similar characteristics to data reconstructions. The southern hemisphere starts to warm sooner than the northern hemisphere and shows a steady rise in temperature throughout the deglaciation. The model shows warming a little faster in the northern hemisphere than data estimates at the start of the deglaciation from 17.5kyr BP, although the CO_2 rise (fig 6.16) is not faster than data indication. This can be attributed either to the lack of proxy data for temperature in the permafrost region, or the simplified permafrost-carbon dynamics. The model tuning was achieved by assessing data for the deglaciation without any fresh water forcing (chapter 4), so there is a margin of error that may explain why the CO_2 record shows a good match during the start of the termination but the temperature rise is too fast in the northern hemisphere. If the permafrost dynamics were "faster" then a reduced warming rate may produce the same CO_2 rise rate, and the carbon would be lost sooner (therefore not overshooting the data indication). Testing this hypothesis would require further sensitivity studies with CLIMBER-2P carbon dynamics and fresh water scenarios.

The northern hemisphere mean temperature shows the B-A/YD cooling also seen in the Greenland output (fig 6.17) and the fast warming afterwards, as the model reflects these characteristics. Again the warming following the AMOC recovery is faster than the data suggests, and at this point the modelled CO_2 rise (fig 6.17) is also faster than data suggests. As discussed, the modelled AMOC recovery is fast in CLIMBER-2P compared to some other models, and this may be an explanation for the fast temperature rise and related CO_2 rise. Alternatively, the lack of a fresh water forcing after 12kyr BP may explain some of the mismatch.

A generic fresh water forcing study with CLIMBER-2 (without permafrost) was carried out by Ganopolski and Roche (2009) in their analysis of lead lag relationships during the last glacial termination. Their simulation of an AMOC drop and quasi switch-off lasting around 7 thousands years could reproduce a pattern of Antarctic temperature rise lead over Greenland temperature by around 1000yrs, a pattern seen in deglaciation data. In our set-up a fresh water forcing is also responsible for this lag of Greenland temperature rise, but the forcing is a much smaller extent and affects mainly the start point of the respective temperature rise. By reducing the fresh water input rate, Ganopolski and Roche were able to create a B-A type warming and ACR type event, as the AMOC recovered more quickly to forcing (than in the increased fresh water input rate simulation). In our simulation, as no AMOC switch-off is seen during H1, seen in data can, conceptually not be the result of a large AMOC overshoot (on resumption after

forcing has ceased).

Modelled southern hemisphere temperature shows warming slightly faster and starting around 500 years later than data suggests at the onset of deglaciation. This can be due to the brines controller, which reduces the fraction of sinking brines from 18kyr BP. If this occurred sooner then the southern hemisphere temperature would also start to rise sooner. The full length of southern hemisphere warming can be controlled by the brines controller. In the setting used here all brines sinking has stopped by 12kyr BP, but if this was extended to around 10kyrBP the full length of warming may be better represented compared to the data. This longer and slower southern hemisphere warming would also reduce some of the CO_2 rise rate, and may bring model output closer to data from 12kyr to 10kyr BP. After 10kyrBP all fresh water forcing has ceased and the model output resembles the deglaciation from chapter 4. As stated there, the lack of peatland dynamics in the model and possibly the simplified vegetation model itself are likely responsible for the divergence between modelled CO_2 and data CO_2. This hypothesis is supported by comparing the atmospheric $\delta^{13}C$ data with model output because a land carbon uptake would shift atmospheric $\delta^{13}C$ more positive.

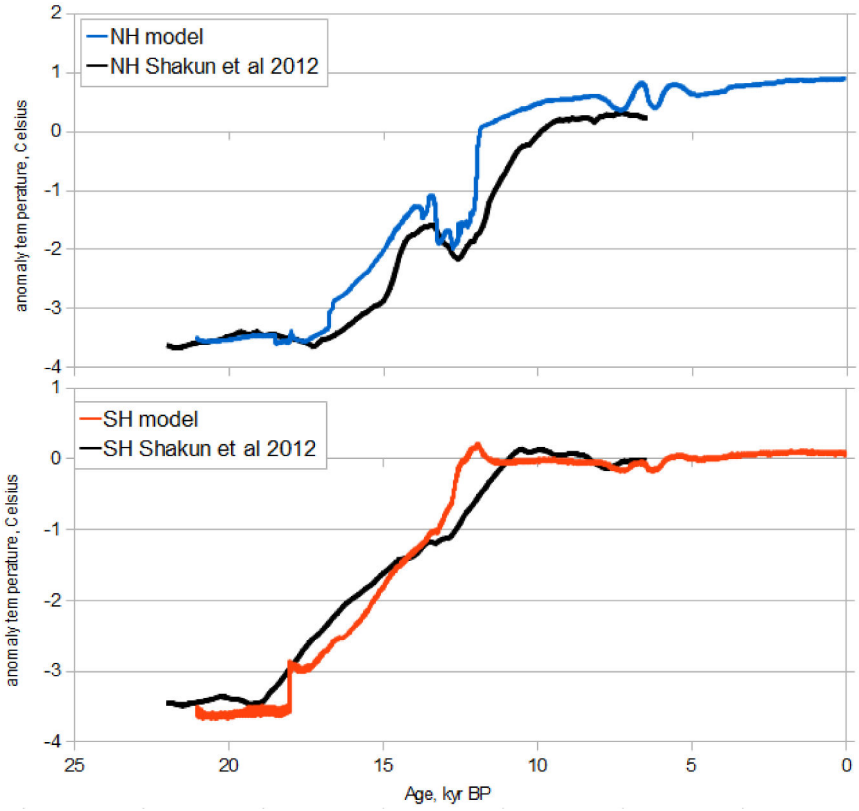

Fig 6.19, Hemispheric temperature mean for model output overlaid on data-based reconstruction from Shakun et al (2012). Top is northern hemisphere, bottom is southern hemisphere.

Atlantic ocean stream function, Younger Dryas

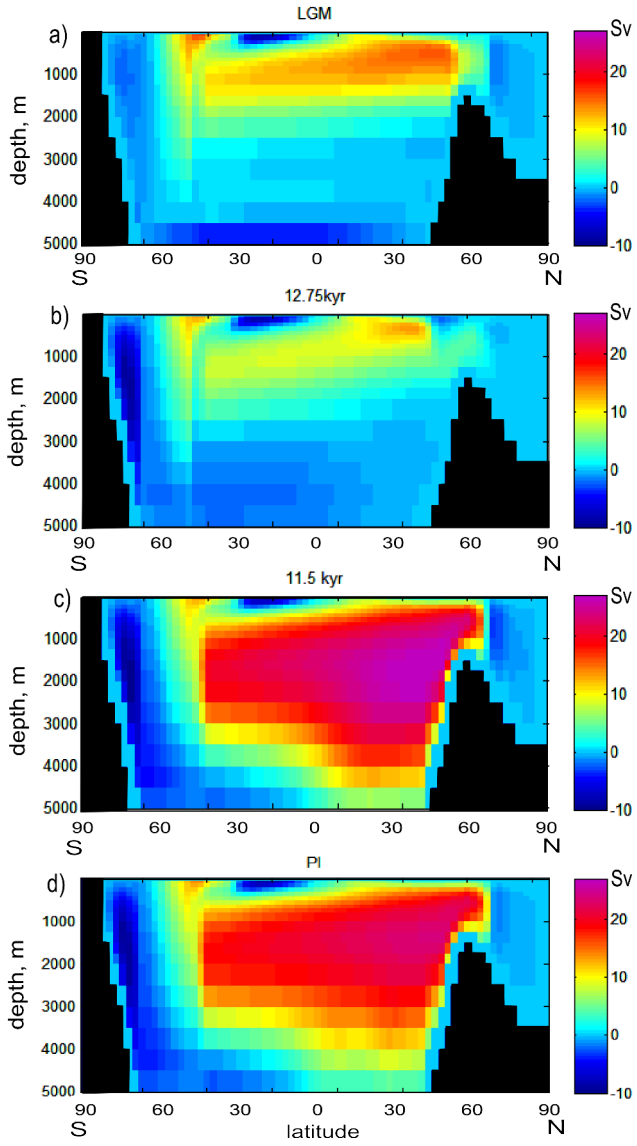

Fig 6.20, Atlantic ocean stream function, Sv, snapshots for inverted FWF transient deglaciation simulation. a) LGM, b)12.75kyr BP at AMOC strength minimum, c)11.5kyrBP at AMOC strength maximum during overshoot period, d) PI.

The model set-up that reproduces a good fit CO_2 and $\delta^{13}C$ data does not show an AMOC switch-off between 17.5 and 15kyr BP, unlike some data based reconstructions, but does suggest a switch off from around 14k to 12kyr BP. Figure 6.20 shows four time slices of the stream function in the Atlantic basin through the model simulations to illustrate this: at LGM, 12.75kyr BP at AMOC minimum, 11.5kyr BP at AMOC maximum and at PI (0kyr BP). Positive numbers show a clockwise rotation and negative numbers an anti-clockwise rotation. At LGM there is a large amount of AABW and more shallow AMOC. It is this configuration at LGM, with permafrost-carbon and

glacial ocean, that the model can recreate the glacial climate with an atmospheric CO_2 and $\delta^{13}C$ levels in agreement with data. At AMOC minimum when fresh water forcing in the north Atlantic is strong, the AMOC strength reduces although does not switch off entirely. When AMOC recovery and overshoot occurs, the AMOC not only strengthens but deepens, at this period the sinking of brines from Antarctic sea ice has ceased and so AABW is also reduced. The AMOC overshoot is what creates a fast northern hemisphere warming (the Younger Dryas warming) and concurrent permafrost thaw and CO_2 rise, as well as a drop in atmospheric $\delta^{13}C$.

Ocean and Land carbon pools

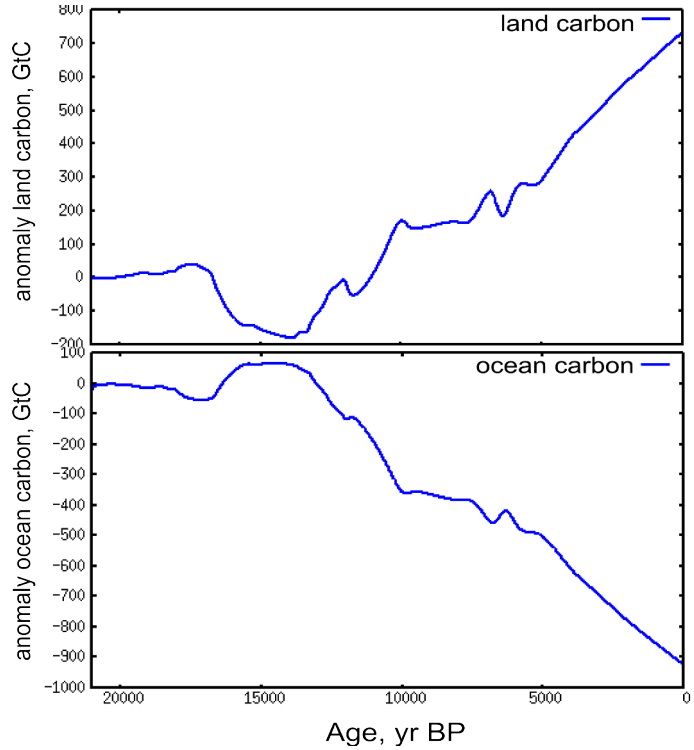

Fig 6.21, Anomalies from LGM for total land carbon pool, and total ocean carbon pool. The ocean only becomes significant carbon source to the atmosphere from around 15kyr BP.

Changes in land and ocean carbon pools are shown in figure 6.21. Just prior to deglaciation, when a small fresh water forcing is applied in the N.Atlantic (fig 6.14) a small cooling in the northern hemisphere causes permafrost area to increase and land to take up <50GtC. This uptake reduces atmospheric CO_2 and partly causes outgassing from the ocean in response to the partial pressure reduction at the ocean surface. The onset of atmospheric CO_2 rise from 17.5kyr BP occurs when the land starts to lose carbon, reflected in the $\delta^{13}C$ record and model output. The ocean at this time takes-up some of the carbon released to the atmosphere due to the partial pressure increase at the

ocean surface. During this time the fraction of sinking brines in the model southern ocean is reducing and ocean circulation is slowly reorganising gradually reducing the capacity of the surface ocean to dissolve carbon dioxide. From 13.5kyr BP the land starts to become a carbon sink, when the loss of carbon from thawing soils is overtaken by the growth in the terrestrial biosphere in response to more favourable growing conditions. The ocean starts to become a strong source of carbon to the atmosphere around the same time. During the northern hemisphere cooling period from 13.5 to 12.5kyr BP an extra ~50GtC are accumulated in permafrost which has expanded due to the B-A/YD cooling. After AMOC resumption this carbon is released back to the atmosphere. The total land carbon pool continues to rise after this and the model atmospheric $\delta^{13}C$ reflects this land carbon uptake. The $\delta^{13}C$ data from 10kyr BP shows a continued rising trend, where the data does not. In the model the total land carbon pool shows a near-plateauing trend 10kyr BP to 7kyr BP. Data from pollen reconstruction suggests that this period saw a large increase in tree growth, the Pre-Boreal and Boreal period, which is not clearly seen in modelled vegetation. As well as this, peatland initiation and growth indicated by basal dating of peat columns occurred around the same period (Yu et al 2011), which is not modelled in CLIMBER-2P. These combined carbon uptakes on land would cause an increase in atmospheric $\delta^{13}C$, which is seen in data.

6.5 Summary

Millennial scale climate variability is seen in climate proxy and ice core records during the last glacial period, and possibly during the last deglaciation. A hypothesis for the cause of this variability is by AMOC reduction in response to strong freshening of the North Atlantic surface ocean region, caused by ice melt from the NH (Northern Hemisphere) ice sheets. This study employs the CLIMBER-2P model equipped with a permafrost-carbon mechanism to study the behaviour of the Earth system in response to fresh water forcing. Equilibrium-climate experiments demonstrate the system response's sensitivity to background climate state. Including ocean mechanisms which successfully create glacial climate conditions by stratifying the southern ocean in a glacial climate background result in a very different system response compared to the same forcing applied in a pre-industrial background climate state. The permafrost-carbon mechanism creates a strong land carbon sink in cooling NH periods (when FWF is applied and AMOC strength reduced), and a fast carbon release in fast NH warming conditions (when FWF ceases and AMOC recovers). A transient deglaciation simulation in which FWF was tuned to create a CO_2 model output to match data for the last glacial termination confirmed the hypothesis that permafrost thaw and carbon release could have been responsible for the onset of CO_2 rise at the start of the deglaciation, and for the fast rise during the Younger Dryas. Model findings suggest that there was no AMOC switch-off during H1, but a strong AMOC reduction or switch-off during B-A/YD resulting in a CO_2 plateau and strong northern hemisphere cooling during this period.

Chapter 7: Future Projections

The CLIMBER-2P model was able to model output which fairly well reproduced ice core data for CO_2 and climate for glacial scale and climate transition states. This chapter presents results from future projections using the same model settings employed for the paleoclimate simulations. In the future projection studies the glacial ocean mechanisms do not operate. Emission profiles from the RCP database were used to drive the CLIMBER-2P model in a fully coupled set-up, in which modelled CO_2 was used to drive the radiative code and the vegetation model. These experiments were intended to determine the amount of carbon lost from thawing permafrost soils since 1850 and into the future. These estimates are then compared with other modelling and measurement studies.

Future Projections

Evidence from $\delta^{13}C$ of atmospheric CO_2 for the last two terminations appear to support the case for the importance of the permafrost-carbon feedback in fast-warming climates. CMIP model projections of future climate response to anthropogenic forcings as reported by IPCC do not include a permafrost-carbon feedback (Ciais et al 2013, Collins et al 2013). Given the long term stability of the CLIMBER-2P model and the possibility to drive climate within the model using carbon emission to the atmosphere, future projections driven with RCP emissions scenarios can be undertaken.

7.1 Methods

Representative concentration pathways (RCPs) are a series of scenarios ranging from a reduction in emissions with a final net negative emission to a high emission scenario rising to $28PgCyr^{-1}$ from human sources. The four RCPs are summarised in table 1, with descriptions from the RCP database.

RCP	Description
2.6	The RCP 2.6 is developed by the **IMAGE** modelling team of the Netherlands Environmental Assessment Agency. The emission pathway is representative for scenarios in the literature leading to very low greenhouse gas concentration levels. It is a so-called "peak" scenario: its radiative forcing level first reaches a value around 3.1 W/m2 mid-century, returning to 2.6 W/m2 by 2100. In order to reach such radiative forcing levels, greenhouse gas emissions (and indirectly emissions of air pollutants) are reduced substantially over time. The final RCP is based on the publication by Van Vuuren et al. (2007).
4.5	The RCP 4.5 is developed by the **MiniCAM** modelling team at the Pacific Northwest National Laboratory's Joint Global Change Research Institute (JGCRI). It is a stabilization scenario where total radiative forcing is stabilized before 2100 by employment of a range of technologies and strategies for reducing greenhouse gas emissions. The scenario drivers and technology options are detailed in Clarke et al. (2007). Additional detail on the simulation of land use and terrestrial carbon emissions is given by Wise et al (2009).
6.0	The RCP 6.0 is developed by the **AIM** modelling team at the National Institute for Environmental Studies (NIES), Japan. It is a stabilization scenario where total radiative forcing is stabilized after 2100 without overshoot by employment of a range of technologies and strategies for reducing greenhouse gas emissions. The details of the scenario are described in Fujino et al. (2006) and Hijioka et al. (2008).
8.5	The RCP 8.5 is developed by the **MESSAGE** modelling team and the IIASA Integrated Assessment Framework at the International Institute for Applies Systems Analysis (IIASA), Austria. The RCP 8.5 is characterized by increasing greenhouse gas emissions over time representative for scenarios in the literature leading to high greenhouse gas concentration levels. The underlying scenario drivers and resulting development path are based on the A2r scenario detailed in Riahi et al. (2007).

Table 1 description of RCP and emission scenarios descriptions from RCP database webpage http://tntcat.iiasa.ac.at:8787/RcpDb

Each RCP is associated with an emission of carbon from human sources which would result in the defined atmospheric CO_2 concentration projection (RCP database). Each emission projection is given for a range of greenhouse gases up to the year 2100 with an extension of emission projections until 2300 (Extended concentration pathways, ECPs). In CLIMBER-2P these emissions per year are used to drive the fully coupled model. Figure 7.1 shows the emission scenarios for carbon (including fossil fuel emissions of CO_2 and equivalent CO_2 emission from land use change) that were used to drive the CLIMBER-2P model. These emission rates in fig 7.1a are hereafter referred to as Extended Emission Pathways (EEP) to distinguish them from ECPs and RCPs. Like the real world case the model responds to carbon released to the atmosphere. After the year 2100 emissions for EEPs 2.6, 4.5 and 6.0 were linearly reduced to zero by 2200 and EEP 8.5 was held constant until 2200 then reduced linearly to zero by 2300. Using these extended emission scenarios the CO_2 output of CLIMBER-2P shows similar profile forms to the CO_2 concentrations provided for each RCP and ECP (up to 2300). It must be noted that CLIMBER-2P does not model all the mechanisms which affect climate sensitivity in future projection scenarios. The carbon emissions in the EEPs do represent terrestrial carbon lost as a result of land use change, but this land use change itself is not implemented into the CLIMBER-2P terrestrial vegetation model. A control (or no emissions) simulation was also run, which represents the natural Earth system response to insolation forcing without fossil fuel or land use change emissions.

The permafrost-carbon mechanism is dynamic on long timescales and likely not in equilibrium, so the use of an equilibrium simulation as the start point is not appropriate. The CLIMBER-2P future projections used the termination 1 simulation (fig 7.2, from chapter 4) as a start point, with the year 1850 marking the year in which emission forcings were initiated. For the paleoclimate simulations CO_2 data from ice cores was used to drive the radiative code and the dynamic vegetation model. In order to drive the CLIMBER-2P model via emissions of carbon to the atmosphere all components of the system must be fully coupled. For the future scenario simulations the model calculated CO_2 (CO_{2_CC}) is used to drive the radiative code and the dynamic vegetation model. The model set-up includes the carbonate compensation mechanism and the permafrost-carbon mechanism. The model does not include any glacial mechanisms; it does not include any fertilisation of marine biota from airborne dust, it does not include the sinking of brines to the deep southern ocean and it does not include changes in diffusion in the deep ocean responding to changes in ocean stratification. The brines and diffusion mechanisms are conceptually related to a colder world in our model, and are not likely to be in effect in a future warming world.

Future simulations are run for 1000 years from 1850 for all four EEP scenarios. The EEP 4.5 and EEP 8.5 scenario are run for a further 10,000 years. The EEP 4.5 scenario represents an emission stabilised by 2100 achieved via active mitigation strategies, followed by emission reductions (in this simulation). The EEP 8.5 scenario represents a world in which no mitigation of carbon emissions takes place, and according to estimates of total fossil fuel reserves and future discoveries represents a maximised output scenario (Riahi et al 2007).

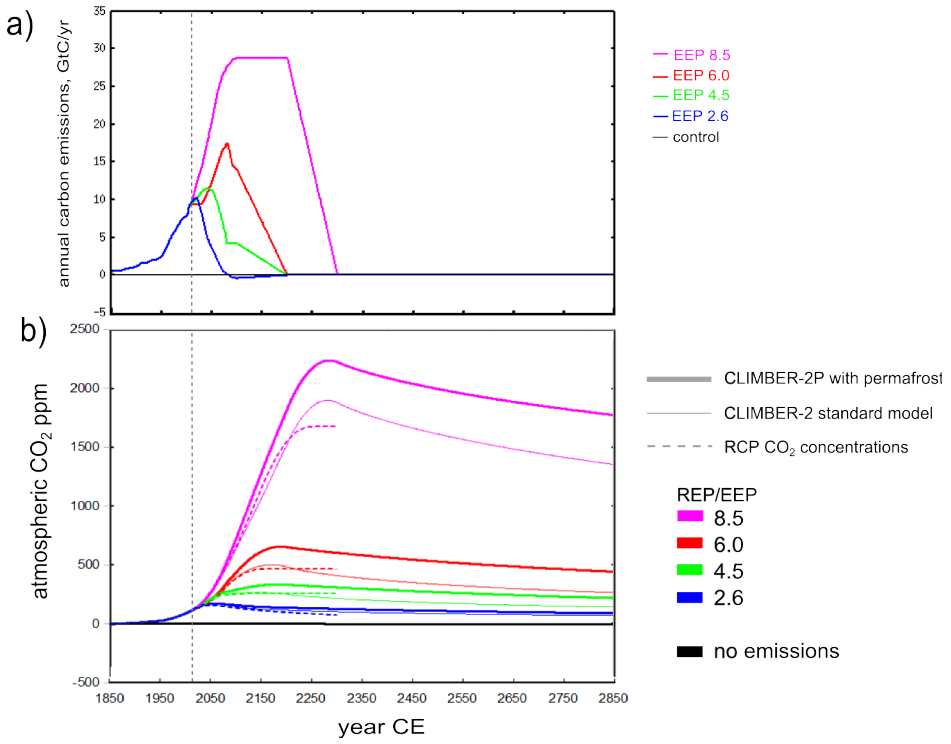

Fig 7.1, RCP based carbon emission drivers for CLIMBER-2P future scenarios. a) "EEP" emissions used to drive simulations. b) fully coupled modelled atmospheric CO_2 comparison with REP CO_2 concentrations per scenario, dashed line is 2013

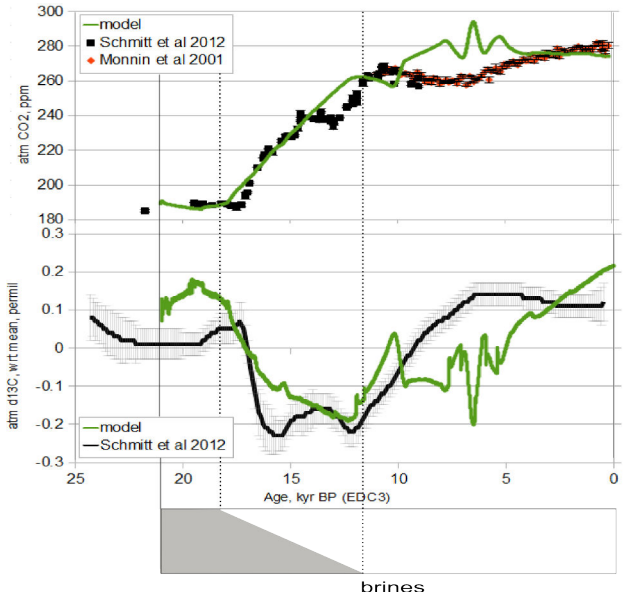

Fig 7.2, CLIMBER-2P model with glacial ocean mechanisms and permafrost-carbon for termination 1. Future projection simulations are started from 1850CE (100 yr BP) in a fully coupled model-set up where carbon-cycle calculated CO_{2_CC} drives the radiative and vegetation model code.

7.2 Results

Emissions per year used to drive the simulations are shown in fig 7.1 a). The modelled CLIMBER-2P atmospheric CO_2 levels are shown in figure 7.1 b) together with the RCP database projected CO_2 concentrations and the CLIMBER-2 standard model (no permafrost) output. When permafrost is included in the model, atmospheric CO_2 peaks at higher values, and remains higher throughout the simulations for all EEPs. The increased CO_2 at peak temperature for the EEP 8.5 scenario is over 400 ppm higher than the standard model and the RCP projection.

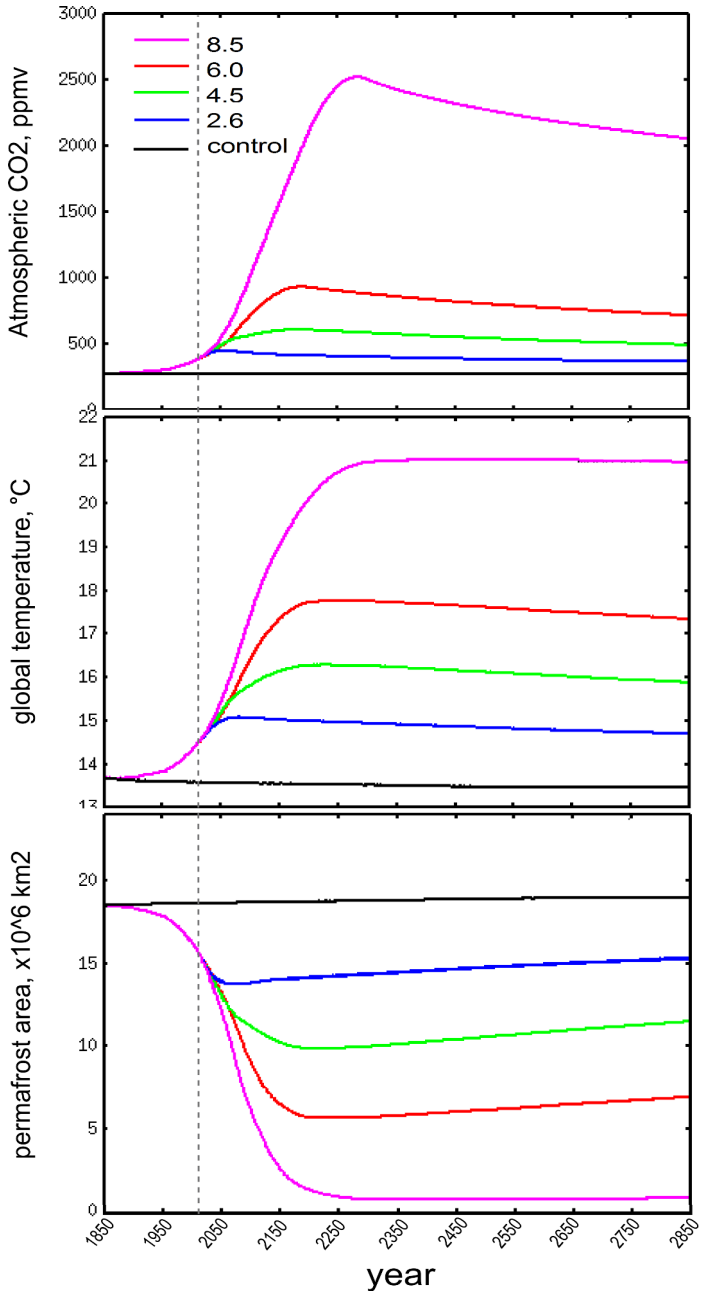

Fig 7.3, a) modelled atmospheric CO_2, b) modelled global temperature, c) modelled permafrost area. Dashed line marks 2013. 'Control' is the no-emission scenario.

Figure 7.3 shows the 1000 year experiment outputs for atmospheric CO_2, global surface air temperature and permafrost area. Included in the plotted output is the no emissions scenario labelled as 'control', in which the CLIMBER-2P model was allowed to run with no emission forcing. The dashed line shows the present-day (2013), with an atmospheric CO_2 of 395ppm, showing good agreement with measurements for the 2008-2012 mean of 390ppm (CO2now.org). With historical emissions, the predicted permafrost area is currently (in 2013) around $3x10^6 km^2$ less than the natural system prediction. The global mean temperature is 0.8°C higher at 2013 than the 1850 level, which is in agreement to measurement data estimate of Morice et al (2012). With the no-emission control simulation, the global mean temperature and atmospheric CO_2 is predicted to be presently on a slow downwards trend, and the permafrost area a slow upward trend. Clearly with the EEP forcing all these trends are reversed for the present-day (2013).

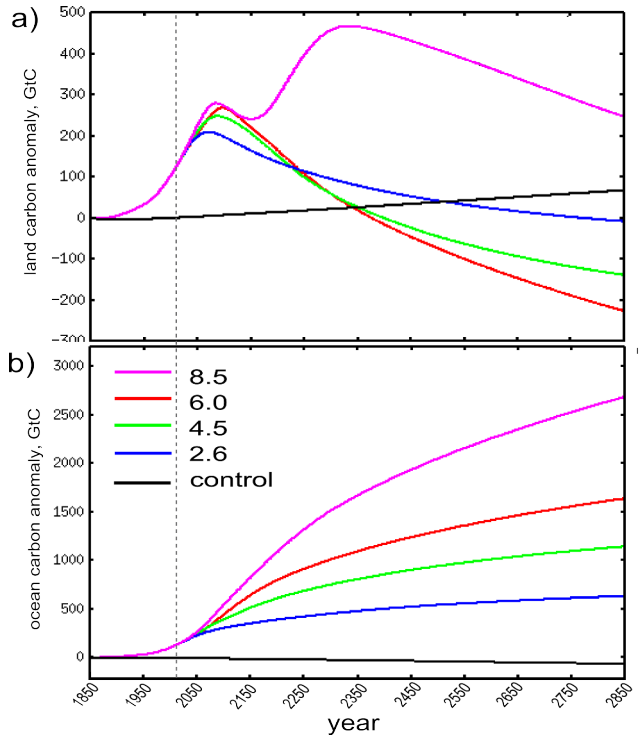

Fig 7.4, a) modelled land carbon anomaly, b) modelled ocean carbon anomaly. Dashed line marks 2013.

The land and ocean carbon pools projections are shown in figure 7.4. The total land carbon anomaly shows that since 1850 the land has taken up around 130GtC, and the ocean around 140GtC. After the year 2050 the differences between the emission scenarios start to become more clear, but in all cases the long tail in ocean carbon uptake is evident; after emissions have gone to zero the ocean continues to take up carbon. For the EEP 2.6, EEP 4.5 and EEP 6.0 scenarios land carbon uptake starts to reduce after peak emissions, for the EEP 8.5 scenario a double land carbon peak is seen,

responding first to the point where carbon lost from permafrost outweighs vegetation uptake. The second peak because in EEP 8.5 almost all fast-soil (easily decomposed) permafrost carbon has been lost and continued vegetation uptake outweighs total soil carbon losses for around 100 years.

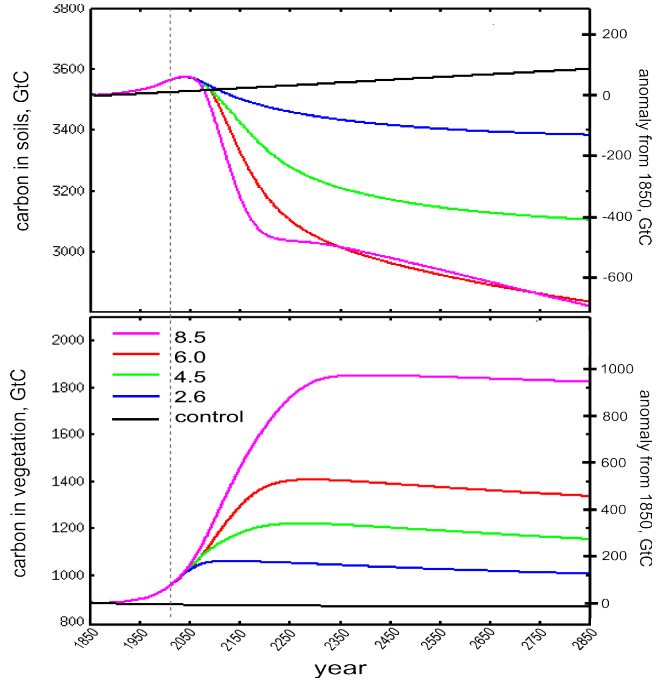

Fig 7.5, a) modelled total soil carbon content GtC, b) modelled total ocean carbon content GtC. Dashed line marks 2013.

The land carbon pool is plotted separately as vegetation and soil carbon in figure 7.5. Until around the year 2070 both soil and vegetation carbon show positive anomalies relative to the natural system (control) and the year 1850. After 2070 carbon is still accumulating in vegetation, and soils start to lose carbon, both at a rate dependent on the emission scenario. However, CLIMBER-2P takes no account of human land-use changes in the vegetation model which would affect the vegetation carbon sink. The no emissions control simulation predicts that soils would be currently on an up-taking trend and vegetation a slow downward trend. Figure 7.6a shows the total carbon which is presently located in the permafrost zone, here defined as all latitudes north of 60°N. The no emissions control projection shows this region to be on a rising trend, and indeed up until the present day when emissions are included this region is currently taking up carbon. Plotted with modelled outputs are other studies which concentrate on the permafrost-carbon feedback. The CLIMBER-2P model does not include peatland dynamics, which according to results on the last two termination periods (chapter 4) and peatland carbon studies may play an important role in land carbon uptake in warming climate (Yu et al 2010, Wania et al 2009a,b). Other modelling studies of future projections of carbon change in permafrost simulate losses around half that of the CLIMBER-2P projection (figure 7.6). None of the models in figure 7.6 actively model

peatland carbon dynamics. Plotted on fig 7.6b) are results from the Harden et al. (2012) study that identifies carbon which would be vulnerable to thaw in a warmer world. They calculate new active layer thickness' to find how much soil carbon, currently permanently frozen, would then find itself in the active layer. The CLIMBER-2P output suggests that it would take about 30-40 years (depending on emission scenario) for all the excess carbon to be released from thawed permafrost. The Schneider Von Deimling et al (2012) projection predicts it would take around 3 to 4 times longer for this carbon to be released, with other models in this range or longer. An estimate of the future carbon losses from permafrost soils from a group of around 40 permafrost experts (Schuur et al 2011) is shown with figure 7.6a. For the highest warming scenario, the CLIMBER-2P model shows carbon losses in very good agreement with the expert estimates, and supports the view that more complex models may be underestimating the permafrost carbon feedback.

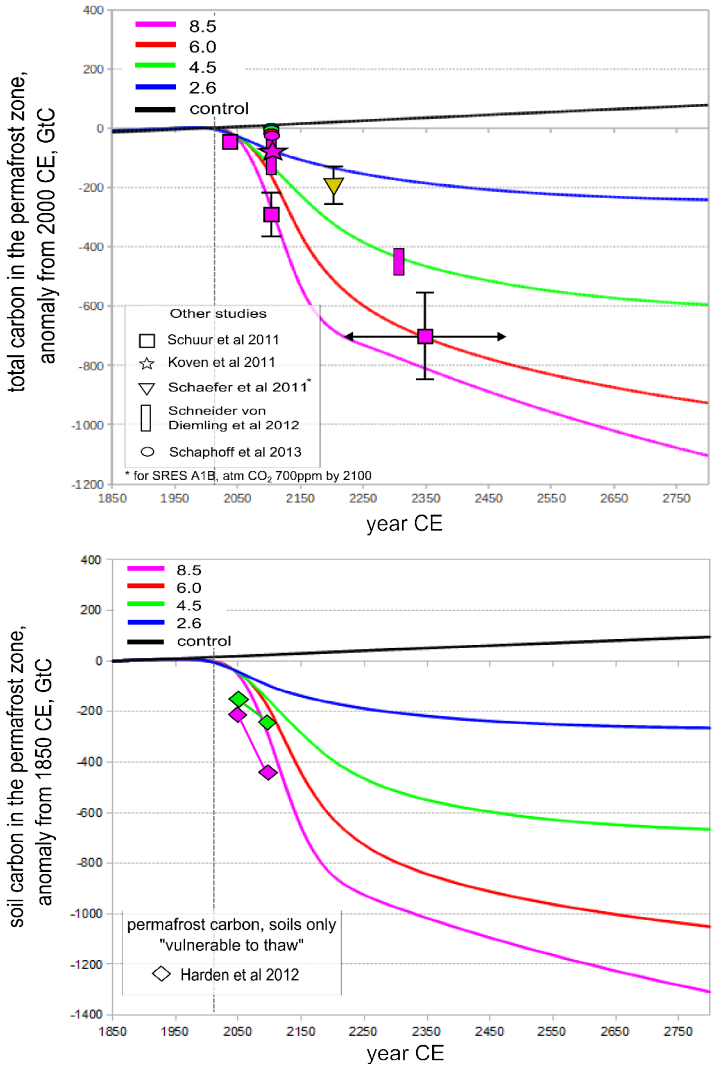

Fig 7.6, total carbon and soil carbon in the present-day permafrost zone, dynamic response to RCP emission scenarios (lines). Comparison to other modelling studies of permafrost-carbon response to future climates.

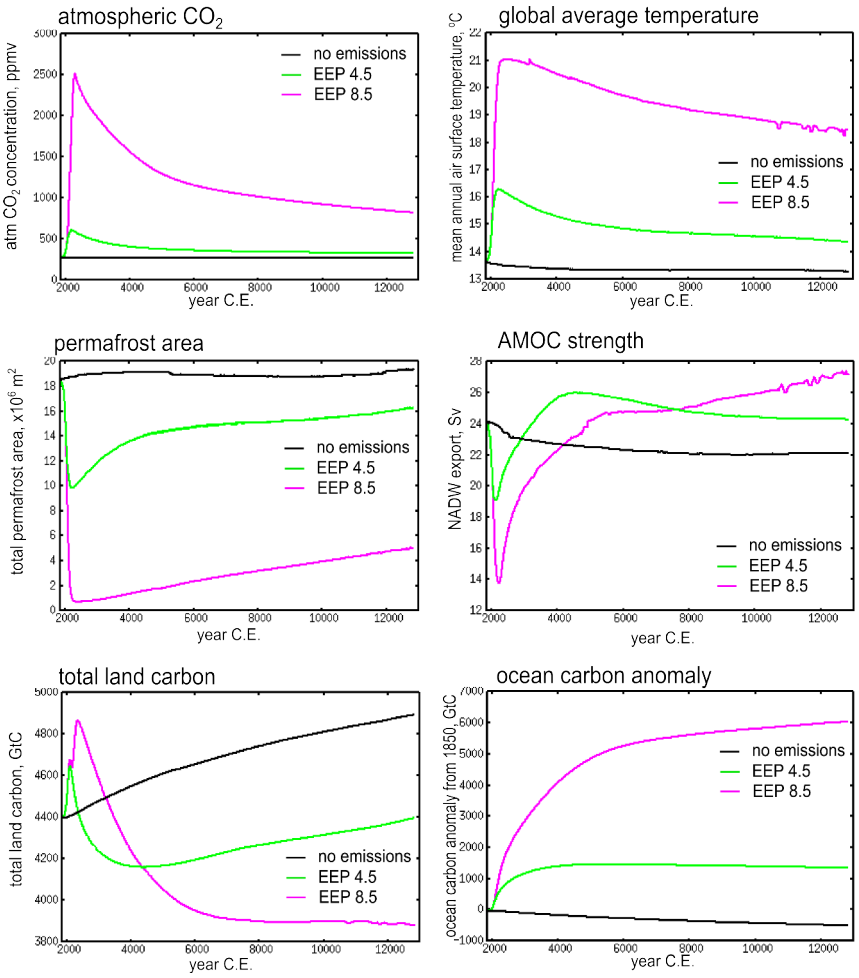

Fig 7.7, modelled outputs for extended post-RCP simulations for "EEP 8.5", "EEP 4.5" and no-emissions forcing.

Two scenarios, the EEP 4.5 and the EEP 8.5 emission scenario, and the no emissions (control) case were extended for a further 10k years. The results are shown in figure 7.7. In both emission cases the system has not returned to initial conditions by 10k years after the CO_2 peak. Average global temperatures also remain high at 12kyr CE, the EEP 8.5 scenario results in mean global annual temperatures only around 2.5°C lower than peak temperature, over 5°C warmer than no emissions control case. Total land carbon stocks for the EEP 4.5 scenario has recovered to 1850 levels by around 13kyr CE. For EEP 8.5 total land carbon falls and remains somewhat stable at around 700GtC lower than 1850 levels from 8000yr CE. Ocean carbon anomaly in the EEP 4.5 scenario has plateaued and starts to reduce around 6000yr CE, whereas the EEP 8.5 scenarios see increasing ocean carbon stock even after 13kyr CE. In the no emission control scenario ocean carbon stocks are falling in response to uptake in the terrestrial biosphere throughout the simulation period. Both EEP scenarios have changed the system for a period of longer than 10k years. It is worth noting that the modelled output

takes no account of ice sheet melt, and related albedo feedbacks. These would effect the Earth system response. It also takes no account of possible increased weathering from the hydrological cycle response to warming. There are no land-use changes taken into account, as already mentioned, which would be determining factors in the terrestrial carbon cycle response.

7.4 Comparison with Ground Measurement Studies

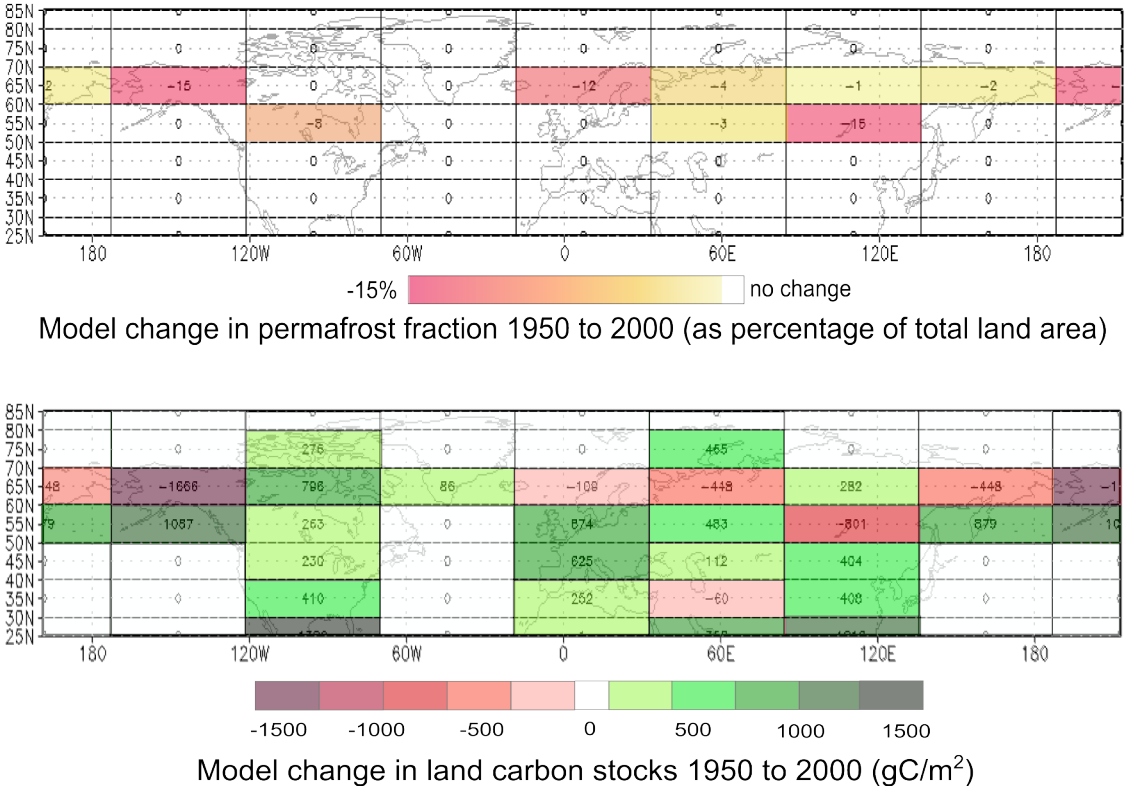

Fig 7.8, High latitudes spatial distribution of the change in permafrost area between 1950 and 2000 (top), and the change in land carbon stocks between 1950 to 2000 (bottom). The carbon stocks do not take any account of land use changes.

Ground studies have addressed the question of the present-day carbon release rates from thawing permafrost sites and so CLIMBER-2P model output can be compared with these. Figure 7.8 shows the modelled change in permafrost area and terrestrial carbon between the period 1950 to 2000. The greatest losses are seen in the Alaska (north) grid cell (175- 125W, 60-70N) and the south east Russia/Asia grid cell (86-137E, 50-60N), with 15% of the land area changing from permafrost in 1950 to non-permafrost by 2000. Largest modelled soil carbon concentration losses are from North Alaska. A comparison for the Alaska grid cell with ground studies demonstrates that the CLIMBER-2P model is likely not overestimating the permafrost carbon losses. In 2009 Schuur et al studied the carbon fluxes on a thaw gradient over several years for

an Alaska site. They found an average R_{eco} (ecosystem respiration) of around 380gCm^{2}yr^{-1} for all sites, with a NEE (Net Ecosystem Exchange) of the extensive thaw site of 32+-22 gC/m^{2}yr^{-1}, but with significant variability over the study period (3 years). Ecosystem respiration is the carbon lost (respired) from soils and vegetation, net ecosystem exchange is the difference between ecosystem respiration and carbon uptake via photosynthesis in plants. Natali et al in 2011 performed a warming experiment of permafrost soils in an Alaska site, producing a winter temperature increase of around 1.5°C, which compares well with the increase modelled winter temperature in CLIMBER-2P for the period between 1950 to 2013 for the Alaska grid cell. The Natali et al. results showed an increase in R_{eco} of 90gC/m^{2}yr^{-1} from the ambient condition, to a total of 364gC/m^{2}yr^{-1}. The NEE fell to -119gC/m^{2}yr^{-1} from -69gC/m^{2}yr^{-1} (a loss), it is worth noting that their control (ambient) site was already a net carbon source without any enforced warming. Trucco et al in 2012 presented the results of a seven year study of carbon fluxes from permafrost thaw sites in Alaska. R_{eco} over the three thaw condition sites averaged at around 350gC/m^{2}yr^{-1} with NEE at around 100gC/m^{2}yr^{-1} (so a carbon uptake). For the Schuur et al and Trucco et al study sites the increases in NPP (Net Primary Production, the photosynthesis carbon uptake in plants) offset soil carbon losses during the study period, whereas at the Natali et al study site they did not. The CLIMBER-2P output, for all EEP scenarios, predicts a mean NEE for the Alaska grid cell of -103gC/m^{2}yr^{-1} for the year 2000 and -190gC/m^{2}yr^{-1} for the year 2013 (so, a loss of land carbon to the atmosphere). Modelled R_{eco} for the Alaska grid cell is 338gC/m^{2}yr^{-1} for the year 2000, showing a very good agreement with the ground measurement studies. So, increases in photosynthesis do not offset carbon losses from soils in CLIMBER-2P.

To re-iterate, the CLIMBER-2P model does not include peatland dynamics, which represent an important ecosystem component in the permafrost region. In order for the Alaska grid cell to be currently carbon neutral within the CLIMBER-2P model, a peatland dynamic would need to be accumulating carbon at a rate of 103gC/m^{2}yr^{-1} for year 2000, and 190gC/m^{2}yr^{-1} for year 2013. For the Holocene period, a maximum carbon accumulation rate in a natural Finland bog was around 90gC/m^{2}yr^{-1} (Strack 2008), and for a re-wetted/restored bog (previously cut-over) in Sweden of a maximum 100-250gC/m^{2}yr^{-1} (Strack 2008) although carbon flux studies results showed a large range, including sites being carbon sources even as natural peatlands. These figures suggest that peatland carbon accumulation, in favourable accumulation conditions, could currently be compensating for losses of old carbon from permafrost thaw.

7.5 The Permafrost Carbon Feedback

The permafrost carbon anomalies per emission and per degree change in global temperature are shown in figures 7.9 and 7.10. Figure 7.9 shows the carbon released from the permafrost region per degree change in global temperature from 1850. The change in high latitude land-carbon is non-linear, and is dependent on EEP emission rate. Release of carbon from soils in the permafrost zone continues after peak

temperatures have passed and EEP emissions are at zero. The slow-accumulation and fast-release characteristic of carbon in permafrost and permafrost thaw soil conditions results in a hysteresis response in the carbon stock changes per temperature change. The higher emission scenarios result in a stronger feedback from permafrost soils via warmer global temperatures, and the higher the emissions the longer it will take for permafrost extent and soil carbon concentrations to return to natural levels. In the EEP 8.5 scenario there is almost no recovery seen in permafrost soil carbon stocks , permafrost area is less than 10% at 2850 compared to the 1850 extent.

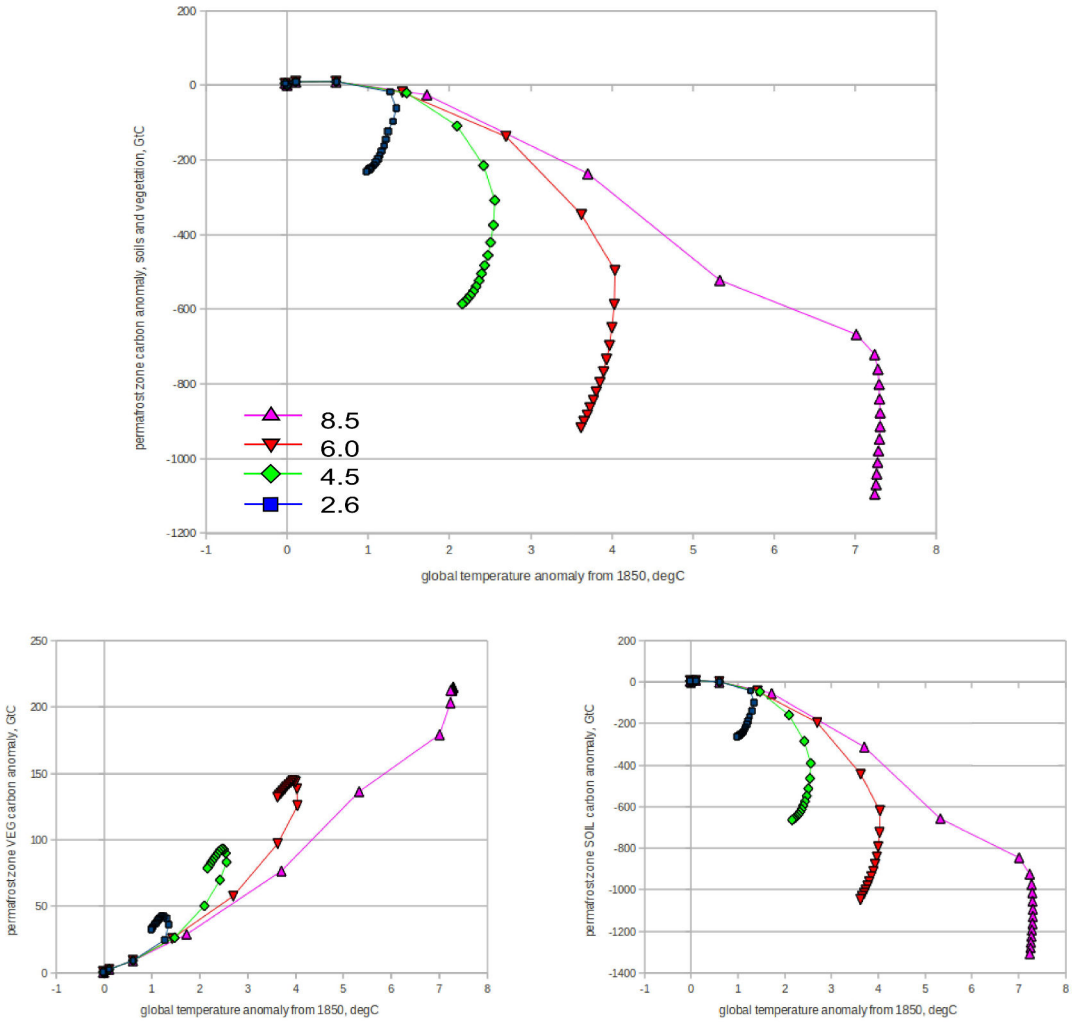

Fig 7.9, Modelled change in carbon from the permafrost zone per degree of global temperature change. For top, total carbon change 60-90deg N. Bottom left, vegetation carbon change in 60-90deg N, bottom right, soil carbon change in 60-90deg N.

Figure 7.9 b) and c) demonstrate that in this CLIMBER-2P model configuration, increases in vegetation in the permafrost region do not offset carbon losses from soils. The highest emission scenarios show the largest increases in vegetation due to the combined effects of climate and CO_2 fertilisation. When emissions stop the CO_2 fertilisation becomes less strong (because the CO_2 concentration starts to fall) and

vegetation carbon stocks start to reduce. Figure 7.10 shows the high latitude carbon anomaly plotted against cumulative emissions from EEP scenarios. Again the carbon lost from the permafrost zone is dependent upon EEP emission rates, each EEP has a distinctly different permafrost-carbon response. A closer look at the period 1850 to 2050 shows that the anomaly is relatively small in this time period. Before around 2020 the increases in NPP outweigh losses from soils. Emission scenarios start to diverge at 2013 (where emissions before this date are data and not projections) and between 2000 and 2050 the difference in permafrost soil carbon release between the lowest, EEP 2.6, and highest, EEP 8.5, emissions are only around 10GtC. By 2100 the difference becomes 180GtC, and the projected total permafrost carbon losses by 2850 for the EEP 2.6 scenario are less than the losses at 2100 for the EEP 8.5 scenario.

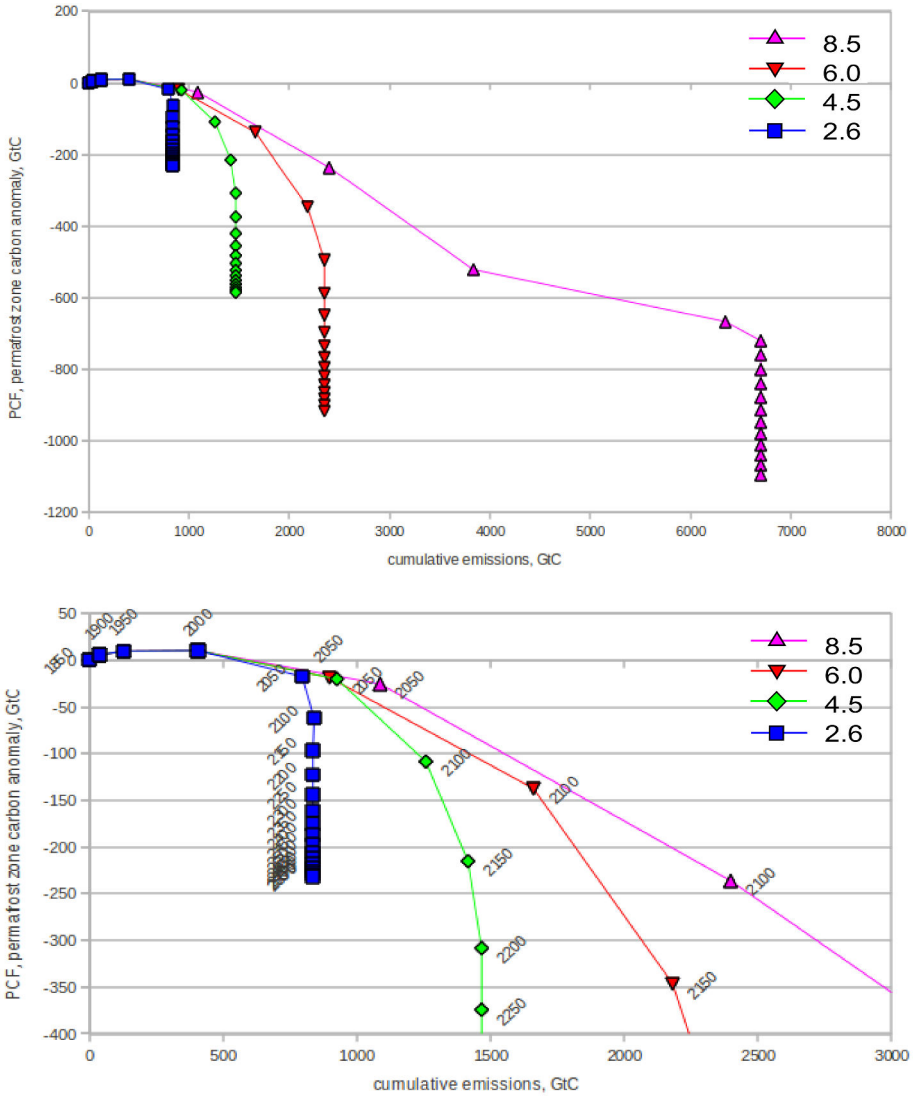

Fig 7.10 Modelled change in carbon from the permafrost zone plotted against cumulative emissions. Top, emissions until 2850. Bottom, close-up of top up to 400GtC release from the permafrost zone.

7.6 Comparison with other Earth system studies

Our results can be compared to those from Zickfeld et al 2013, a model inter-comparison for a series of EMICs' responses to future forcings. Comparable results are for the Zickfeld PIEM-CO_2 experiment (pre-industrial CO_2 emission commitment) which shows most similar emission forcing patterns to those used in this study. Figure 7.3 shows the 1000 year experimental outputs for atmospheric CO_2, global surface air temperature and permafrost area. Compared to Zickfeld et al. the first difference to notice is that the two higher emissions forcings predict higher atmospheric CO_2 concentrations in our CLIMBER-2P study, and this is due to the permafrost-carbon feedback. Only one of the EMICs in the Zickfeld study includes the permafrost carbon feedback: Bern3D-LPJ. The lowest emissions scenario, EEP 2.6, our study shows a total loss of around 240GtC from high latitude regions by 2800 and a total (global) land carbon loss of 130GtC by 2800. The Bern3D-LPJ estimates around 200GtC loss globally with respect to 1850 for scenario 2.6. For the EEP 4.5 scenario (which includes re-forestation in the Zickfeld study) Bern3D-LPJ predicts total land carbon loss of slightly less than 200GtC by year 3000 CE, CLIMBER-2P estimates around 260GtC lost by 2850 CE. For the ECP 6.0 scenario Bern3D-LPJ gives land carbon losses of around 400GtC by 3000CE, CLIMBER-2P around 350GtC lost by 2850CE. Finally for the ECP 8.5 scenario Bern3D-LPJ predicts losses of 1300GtC by 3000CE, whereas CLIMBER-2P predicts an uptake of around 120GtC by 2850CE. The Zickfeld study models include land cover changes dependent on the scenario, which is not taken into account in the CLIMBER-2P model. Extensive deforestation is included in the ECP 8.5 scenario, and because this is not modelled in our study CLIMBER-2P predicts a vegetation uptake of around 850GtC, and a loss of soil carbon of around 700GtC. If deforestation were taken into account in the model, vegetation increases would be greatly reduced, and more soil carbon would probably also be lost.

7.7 Model uncertainties

The permafrost dynamics used in this model were identified based on selection of the best-fit-dynamic to data from the last termination (chapter 4). This dynamic predicted total land carbon stock changes of +800GtC, as opposed to 330GtC estimated by Ciais et al (2012), between the LGM and pre-industrial present day. This overestimate may result in an overestimate of the permafrost carbon losses identified in this study. The location of this excess land carbon accumulated was found to be in northern Siberia and may be due to the lack of a root depth limitation mechanism and/or accounting for ice content in soils. If the carbon loss from permafrost soils is over-estimated in this study, it also suggests that peatlands need not be compensating as much as was identified in section 7.2 and 7.4. However, from model outputs of transient simulations during termination periods and fresh water forcing, the peatland dynamic is likely an important mechanism controlling CO_2 evolution during fast warming. This complicates the understanding of the permafrost carbon loss estimate from this chapter. Peatland dynamics were not included when tuning the model with data from termination

1. If peatlands may have started compensating for a soil carbon loss from permafrost thaw at that time, then the permafrost carbon losses may have been underestimated at the start. The output from the model shown in figure 7.6 is a composite of the possible original underestimate of the carbon loss, and the possible overestimate of the carbon loss due to excess carbon in the very cold soils in Siberia. For this reason no weighting correction has been applied to land carbon losses for future projections, even though the model is known to overestimate Siberian soil carbon concentrations.

The Siberian grid cells contribute to soil carbon losses, especially in the EEP 6.0 and EEP 8.5 simulations. On the order of centuries, the CLIMBER-2P model predicts higher soil carbon losses than the Schuur et al (2011) experts' estimates. This can be due to the overestimate of the total carbon stored in the Siberian grid cell soils, and amounts to around 100-200GtC in total if compared to Schuur et al (2011). None of the models, or the Schuur et al. estimate, shown in figure 7.6 include the possible land carbon uptake due to peatland dynamics. Peatland expansion and carbon accumulation could offset a significant amount of soil carbon loss from thawing permafrost soils, and require further study.

7.8 Summary and Conclusions

The permafrost-carbon feedback (PCF) amplifies the effects of anthropogenic CO_2 forcings via fossil fuel burning. For the highest forcing scenario, EEP 8.5, peak CO_2 is around 400ppm higher than studies without the PCF, and around 500ppm higher than the Zickfeld et al. (2013) model studies and CMIP projections for IPCC. The anomaly between CLIMBER-2 model projections with and without permafrost-carbon increase after peak CO_2, as permafrost soils continue to lose carbon after peak warming and even when emissions are zero. For EEP 4.5 (RCP 4.5) and EEP 8.5 (RCP 8.5) permafrost area has not returned to pre-industrial levels by 10k years after emission forcing has ceased. This is attributed to atmospheric CO_2 remaining higher than pre-industrial levels and global mean temperature in response remaining higher, which keep permafrost area reduced. This study has not included the effect of peat forming plants in high latitude biosphere systems, but results here provide a means of isolating the relative effects of frozen ground from peatland dynamics. Peat formation and carbon accumulation likely offset carbon losses from permafrost thaw to some extent. In future climates the sink provided by peat formation is dependent on climate conditions. In unfavourable climate, particularly drought conditions, the carbon sink from peat would be inhibited. In peatland disturbances, peat can turn from a carbon sink to a carbon source quickly via drying and soil decay (Martikainen et al 1995, Strack et al 2009). Land carbon stocks are particularly sensitive to land use changes affected by human activity. In high deforestation scenarios the land carbon sink would be greatly inhibited compared to the modelled natural system response that has been shown in this chapter. Including land use change and disturbances in terrestrial biosphere models is essential in future projections of earth system response to anthropogenic forcing. The permafrost carbon feedback is dependent on the rate of emissions, carbon released from thawed

permafrost continues for many centuries after forcing ceases and global temperature has peaked, in all EEP emission scenarios.

The results here suggest that the permafrost carbon feedback may be strong enough to affect the emissions pathways that would result in the projected warming scenarios described in the RCP database. According to our permafrost-carbon dynamics that were tuned using data for CO_2 and $\delta^{13}C$ for the last termination period, the feedback on global temperature is an extra ~15% to 25% of the total warming predicted by the model in which no permafrost is represented (fig 7.11). If this potential feedback is not accounted for in model projections then it is possible they underestimate future temperature rises in response to carbon emissions from man-made sources. In order to limit global mean temperature rises to a set level, the extra carbon released from permafrost would result in estimates of human based emissions via fossil fuel burning and land use changes having to be reduced, as some of the those emissions now come from permafrost-carbon as well.

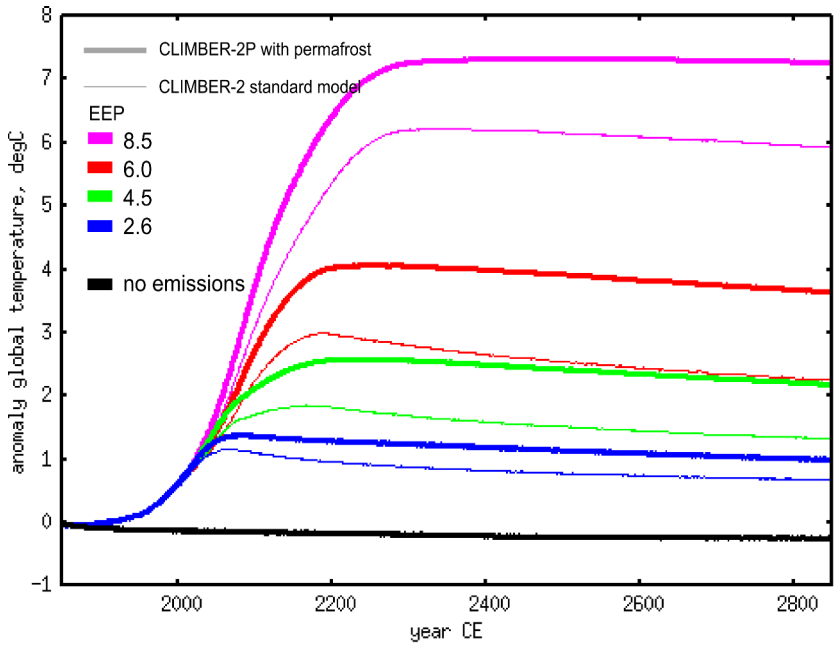

Fig 7.11, Modelled global mean temperature for the standard CLIMBER-2 and the CLIMBER-2P model. The permafrost carbon mechanism amplifies global mean temperature per anthropogenic emission of carbon.

The energy required to thaw large areas of permafrost is currently not accounted for in the CLIMBER-2P model. The total area of permafrost already thawed, according to this study, since 1850 is $2.95 \times 10^6 km^2$, and from 2000 to 2013 is $0.7 \times 10^6 km^2$. In order to turn water from its solid to its liquid phase (the latent heat of thaw) the energy required is 334kJ/kg. Assuming that permafrost soils are 25% water (ice) content (Jones et al 2009) and that, as a conservative estimate, permafrost thaw has occurred in the top

1m over the thaw area it is possible to estimate to total energy required to thaw (water in) the permafrost. From 1850 to 2013 our model predicts that this is $254x10^{15}$ kJ, and from 2000 to 2013 some $58x10^{15}$kJ. This energy requirement would all be sourced from the air above the thaw sites and would act to reduce surface temperatures, and therefore may retard permafrost thaw to some extent. Compared to the total atmospheric volume, these energy requirements represent around 6% of the total energy increase in the atmosphere (as temperature) globally over the same periods.

As already stated, no peatlands or wetlands dynamics are represented in the CLIMBER-2P model. In a World which is getting warmer and wetter the role of northern peatlands may be as a strong sink of atmospheric CO_2. Currently the increases in NPP may be offsetting, or masking, losses of carbon as a result of permafrost thaw. In order to better understand the peatland dynamics and future fate of this land carbon sink it is essential to include it in future modelling studies.

Chapter 8: Discussion and Conclusions

This chapter discusses the main findings from the experiments carried out in this study. The implications of these findings are discussed in terms of the understanding of the Earth system responses to insolation forcing and Earth system feedbacks. Further areas of study, which build on the findings here, are suggested and the main conclusions on the contribution of permafrost-carbon within the Earth system are summarised.

8.1. Research questions discussion

In the following section each of the research questions posed in chapter 1 will be addressed individually. In considering the answer the CLIMBER-2P model proposes for each question the findings from the simulations are discussed first followed by a discussion of limitations of both the model and/or data, and their implication for the interpretation of our modelling results..

8.1.1 The CO_2 evolution during the last glacial termination

> 1. Evidence suggests that in fast-warming climates, thawing permafrost soils would release carbon to the atmosphere. Thus far modelling studies of the causes of CO_2 rise during the last deglaciation have omitted the permafrost mechanism. Could insolation driven permafrost-carbon release have contributed to the CO_2 rise between 18 to 12kyr BP?

In order to answer this question, a simplified permafrost-carbon mechanism was developed and is presented in chapter 3. The mechanism relies on the first order controller for high carbon soils in permafrost-affected ground: reduced soil decay. The CLIMBER-2 model has no soil depth and carbon decay in soils is only controlled by temperature and total carbon stocks in a grid cell. This allowed us to model reduced soil decay by increasing residence time with a multiplier for permafrost-affected soils in each grid cell in CLIMBER-2P. The "re-mixing" model described in chapter 3 was found to better represent the combined effects of a reducing active layer depth and a reducing growing season length along a permafrost gradient. These two characteristics create a non-linear relationship between permafrost fraction of a grid cell and equilibrium soil carbon concentration. The permafrost-carbon model was tuned for total land carbon stocks at LGM and PI with estimates from Ciais et al (2012). A total of four dynamic settings, that determine the rate of carbon accumulation and release in soils associated with permafrost and permafrost-thaw, were retained for use in simulations of T1 (termination 1).

T1 was simulated in chapters 4 and 6. Chapter 4 presented the T1 simulations with four permafrost dynamic settings and an evolving background climate of ice sheets, CO_2, orbital changes and a reducing deep glacial ocean carbon storage. The release of fresh water into the north Atlantic region that affected AMOC circulation was included in the simulation of T1 in chapter 6.

Termination 1 events

The CLIMBER-2P model, with permafrost mechanism incorporated, was used to run simulations of the last termination (chpt 4). Ocean glacial mechanism that were developed and tested by Bouttes et al (2011) were applied in conjunction to find an LGM climate and carbon cycle set-up that showed agreement with data for

atmospheric CO_2, atmospheric $\delta^{13}C$ and ocean $\delta^{13}C$ data. Using a relatively slow release of the deep ocean carbon pool, the findings suggested that permafrost-thaw carbon release may have had an important role to play in deglacial CO_2 rise.

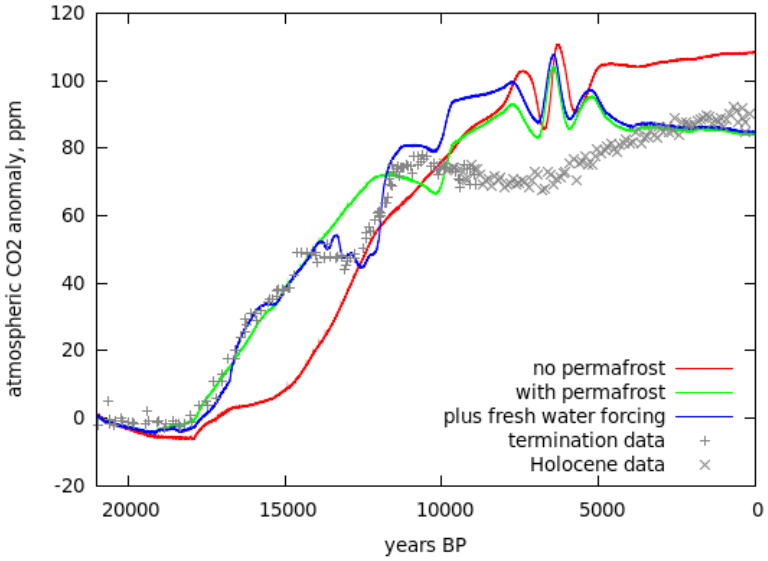

Fig 8.1, Atmospheric carbon dioxide concentrations for termination 1 simulations, standard model no-permafrost (red), with permafrost (green) and with permafrost and fresh water forcing (blue). Data from Monnin et al 2001 plotted on Parrenin et al 2013 age scale.

21kyr BP to 14kyr BP

The increases in summer insolation at mid and high-northern latitudes resulted in a reduction in permafrost area and a release of carbon from the land to atmosphere from around 18kyr BP. This in turn resulted in a net uptake of carbon between 18k to 15kyr BP in the ocean despite the re-organisation of ocean circulation at the same time (and a release of carbon from deep ocean waters via the reduction in the sinking of brines). When the same simulation was carried out in chapter 6, this time with fresh-water release into the north Atlantic, the first part of the termination was not greatly affected. No AMOC (Atlantic Meridional Overturning Circulation) switch-off, as was proposed by McManus et al (2004), was required to induce a rise in atmospheric CO_2 from 18kyr to 14kyr BP. The modelled atmospheric CO_2 are shown in figure 8.1.

14kyr BP to 10kyr BP

From 14kyr BP the ocean was found to be a carbon source to the atmosphere. From ~13kyr BP the permafrost affected soils started to become a net carbon sink, driven by increasing NPP and slightly later by a permafrost area increase. This permafrost area increase was the result of new land being exposed as ice sheets retreated, and later in response to falling summer insolation (from around 11kyr BP). The permafrost carbon uptake combined with increasing size of the land biosphere, driven by improving climate and increasing NPP, turned the land biosphere from a

carbon source to a carbon sink. Now that the land biosphere had started to remove carbon from the atmosphere, the ocean was the sole contributor to atmospheric CO_2 rise seen in the model output with no fresh water forcing.

The CO_2 plateau, seen in the data record between 14kyr and 12kyr BP (the Bolling-Allerod/Younger Dryas or B-A/YD), was simulated in chapter 6 by forcing the north Atlantic ocean with fresh water. This fresh water forcing reduced the strength of the AMOC which resulted in a cooling of the northern hemisphere. This cooling resulted in an increase in permafrost area and an increase in the rate of carbon uptake in the land biosphere. When fresh water forcing had ceased, the AMOC recovery and overshoot caused a fast warming in the northern hemisphere, a permafrost thaw, and a short lived land biosphere carbon release. This caused a fast rise in atmospheric CO_2 after the plateau.

An earlier period of fast CO_2 increase during the Bolling-Allerod (B-A) just before 14kyr BP was not explicitly modelled in chapter 6. According to Lourantou et al (2010) this CO_2 rise is a jump of over 10ppm in the space of tens to hundreds of years. In their record this CO_2 jump is preceded by a slowing down in the rate of CO_2 rise. According to the simulation in chapter 6, it is possible that this B-A CO_2 jump may have been caused by a similar mechanism as the B-A/YD: an AMOC increase causing a permafrost thaw and land carbon release, although we do not propose an extensive AMOC shut-off preceding it.

Post 10kyr BP

From around 10kyr BP the model can no longer well reproduce the data record. It is likely a result of model simplifications and the lack of a peatlands/wetlands mechanism. According to Yu et al (2011) northern peatlands started to accumulate significant amounts of carbon from around 10kyrBP. If this dynamic were included in the model then it would likely explain the model-data mismatch currently seen.

In all model outputs the destabilisation and later collapse of vegetation in the Sahara region causes a strong perturbation in the carbon cycle. The permafrost-carbon mechanism amplifies the effect of this perturbation slightly.

Discussion of T1, model and data

The proxy temperature reconstruction for the last termination (Clarke et al 2012, Shakun et al 2012) is lacking in data for the continental permafrost locations, as shown in figure 8.2. The 30 to 60 degrees North band, which in Eurasia likely held large quantities of soil carbon locked up in permafrost, is heavily biased towards north Atlantic climate and oceanic locations in general. According to Clark et al (2012) the Beringia locations (around present data Alaska) saw temperature rises from 18kyr BP lasting throughout the termination period. There is currently not enough proxy temperature data to discount an Eurasian sourced permafrost-thaw-induced land carbon release. Indeed according to global reconstructions currently used to assign lead-lag relationships, there is no data at all for continental Eurasia.

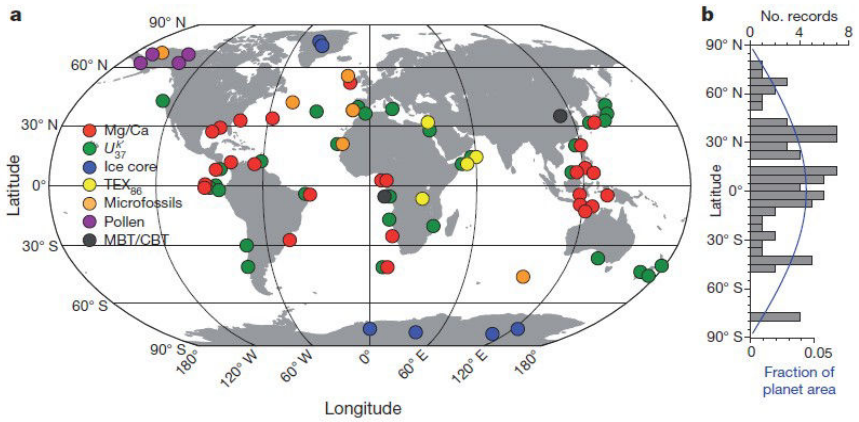

Fig 8.2, a) Locations and types of proxy temperature records used by Shakun et al (2012) to reconstruct global temperature changes during the last termination. There is no data for continental Eurasia, where likely large soil carbon stocks were present at LGM (chapter 3), b) number of records per latitude band. (from Shakun et al 2012).

The operation of the permafrost-carbon mechanism developed in chapter 3 is very simplified with respect to the real world. As a parametrisation it does not specifically model thaw dynamics that depend on local conditions (Riseborough et al 2008). However, the carbon cycle dynamics tuned to data from termination 1 provide an indication of the possible general response of permafrost-carbon. Although permafrost extent is in instantaneous equilibrium with climate in the CLIMBER-2P model, the carbon cycle dynamics result in a lag in the loss of carbon (with respect to climate) from previously-permafrost soils. This mimics the combined real-world mechanisms such as talik formation, rate of active layer thickening, thermal conduction through permafrost and the rate of soil carbon decay itself. Another major simplification is that coastlines are fixed. The dynamics of carbon on continental shelves and is a mechanism that needs further study. The role of peatland and wetland formation was also identified in all chapters as important and would be linked to the permafrost-carbon dynamics.

In order to simulate termination 1 the ocean contribution was chosen as the linear reduction in sinking of brines between 18kyr to 12kyrBP (Bouttes et al 2012). According to the model output when no glacial ocean mechanisms were operating, a release of carbon from thawing permafrost could explain the initial rise in CO_2 in the atmosphere, removing this requirement from the glacial ocean mechanism. Throughout all simulations this 18kyr to 12kyr BP linear brines reduction was not changed. Different start/end points and different functions (e.g. exponential, parabolic, controlled by another model parameter, etc.) for the reduction in brines would have an impact on the carbon cycle. According to the comparison with the data reconstruction by Shakun et al (2012) (chapter 6, figure 6.18) for the southern hemisphere, the model shows the onset of temperature rise occurring around 1k years later than data suggests. It also shows a peak temperature occurring around 2k years sooner than data suggests. This may hint that the controller for the southern ocean glacial mechanism should have been slower than the one used, perhaps from 19kyr to 10kyrBP. If this were the case

then the implication is that the carbon loss from permafrost thaw would need to be slightly faster from 18kyr to 14kyr BP to reproduce the data record. The deep south Atlantic ocean $\delta^{13}C$ record also suggests that release of carbon from the deep ocean storage may have started sooner than 18kyr BP by several thousand years (chapter 4, figure 9).

The dynamics settings determined in chapter 3 were intended to give a broad range with which to perform simulations of termination 1 carbon cycle dynamics. Of the four settings the "medium" dynamic, where the size of the total fast soil pool was approximately the same size as the total slow soil pool, provided the best-fit for data. As discussed in the previous paragraph in relation to the ocean mechanisms, the dynamic setting of the permafrost carbon mechanism may be subject to adjustment in future studies. The fresh water forcing simulation in chapter 6 relies on the underlying dynamics of the carbon cycle, both ocean and land, to produce a best-fit CO_2 record. If the permafrost-carbon dynamics were "faster" (i.e. carbon release occurs more quickly on thaw) then this would have implications for the response of the system on AMOC switch off and re-start events.

In chapter 4 the combined roles of the ocean and land carbon cycles were investigated. It was found that increased productivity of marine biota in the southern ocean was not necessary to recreate the LGM climate or the CO_2 record for the last termination. The selected "best fit" combination of mechanisms was an 80% sinking of brines created on ice formation which reduced linearly from 18k to 0% at 12k yrBP during the termination. This was combined with the "medium" permafrost carbon dynamic to result in a good match for the changes in CO_2 seen in data. According to other studies (Haarpainter et al 2001, Bouttes et al 2011) the maximum amount of sinking brines should be closer to 60%. It is known that CLIMBER-2 carbon cycle is less sensitive to ice cover in the southern ocean than the observational data suggests (Brovkin et al 2012). If it was more sensitive, then the fraction of rejected brines that sink need not be as high as 80%. Brovkin et al (2012) found that improving the model sensitivity to sea ice cover for southern ocean outgassing resulted in an increase of 10ppm of CO_2 in the atmosphere at the end of a glacial termination, compared to the standard model. This extra 10ppm would bring the required maximum brines sinking fraction to around 60% according to the LGM equilibrium simulations in chapter 4. Here the ocean settings of 0.6 as maximum fraction sinking brines and 0.5 ocean stratification setting "alpha" resulted in an LGM climate of ~200ppm, where data shows ~190ppm, so 10ppm difference.

The simulation of the B-A/YD CO_2 plateau did not take account of changes in ocean glacial mechanisms in response to a changing climate. The Antarctic Cold Reversal seen in ice core data is not seen in model output in chapter 6. If the glacial ocean mechanism was coupled to the climatic changes caused by a freshening of the north Atlantic ocean, and AMOC response, this cold reversal may be able to be modelled. The ocean brines controller remained a linear reduction between 18kyr and 12kyrBP. It may be that changing sea-ice extent in the southern ocean would have had a stronger effect on the deep ocean carbon stock via sinking brines.

8.1.2 The $\delta^{13}C$ evolution during the last termination

2. Given that thus far the atmospheric $\delta^{13}C$ record has not been explained via ocean mechanisms, could the permafrost-carbon mechanism explain the fast drop in $\delta^{13}C_{atm}$ at the start of the last termination?

As for the atmospheric CO_2 record data comparison, termination 1 model settings for permafrost dynamics and glacial ocean settings were selected to agree best with data. So, the assumption is that no other mechanisms than those modelled were responsible or played a major role in the atm $\delta^{13}C$ record evolution.

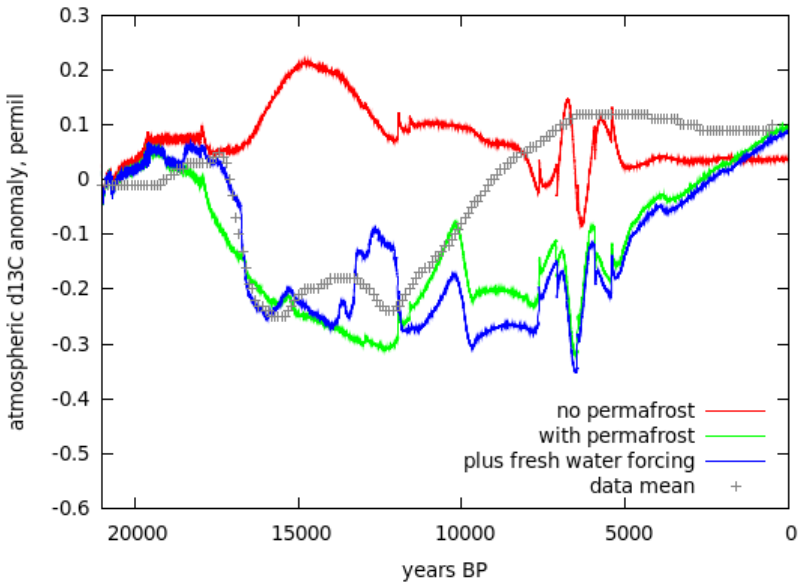

Fig 8.3, Atmospheric $\delta^{13}C$ of carbon dioxide for termination 1 simulations, standard model no-permafrost (red), with permafrost (green) and with permafrost and fresh water forcing (blue). Data mean as Schmitt et al 2013.

21kyr to 14kyr BP

The drop in $\delta^{13}C$ seen in the data record between 18kyr to 16kyr BP could be well modelled when permafrost-carbon was included as a carbon source to the atmosphere at this time (figure 8.3). When no fresh water forcing was applied in the north Atlantic region the drop in atmospheric $\delta^{13}C$ occurred sooner than the data shows (green line). Applying a small fresh water input that delayed AMOC strength increase until 17.5kyrBP resulted in the rise in $\delta^{13}C$ matching data (blue line), and the modelled CO_2 record matching data (fig 8.1 blue line). For the fresh-water forcing input only the CO_2 record was used to adjust the forcing profile (chapter 6), so the fact that it fits the $\delta^{13}C$ record very well is good evidence in support of the permafrost-carbon release hypothesis.

14-10kyr BP

From 14kyr BP, when fresh water forcing is applied and the CO_2 record is better modelled (fig 8.1) the variability shown in the modelled $\delta^{13}C$ data is not seen in the mean $\delta^{13}C$ data. In chapter 6 all the data points from measured atmospheric $\delta^{13}C$ are plotted together with model output (figure 6.17). As CO_2 starts to plateau, the data from Lourantou et al (2010) shows a rise in $\delta^{13}C$ as does our model output. As CO_2 starts to rise quickly again after the plateau, data from Lourantou et al (2010) shows a fast drop in $\delta^{13}C$, as does our model output. The fresh water forcing profile was arrived at by adjusting it until the CO_2 record could be well reproduced, a total of 10 iterations. In figure 8.1 we can see that modelled CO_2 changes show a slight lag with respect to data. This lag is also seen in modelled $\delta^{13}C$ output when compared to Lourantou et al's data. If the forcing profile were further refined then the timing of CO_2 and $\delta^{13}C$ changes could very likely be better modelled.

Post 10kyr BP

After around 10kyr BP, the modelled $\delta^{13}C$ diverges significantly from data. Where data shows a sustained rise, model output shows a drop followed by a rise only 5kyrs later. As for the CO_2 output, this discrepancy can be explained via the lack of a peatland/wetlands dynamic in the model. Another issue may be the vegetation dynamics, which do not show a strong mid-Holocene climate maximum response, as data suggests was vegetation expansion (Prentice et al 1998, Gallimore et al 2005) were the model vegetation carbon has plateaued. Destabilisation and collapse of vegetation in the Sahara before 5kyrBP is also evident in model output but less clear from $\delta^{13}C$ mean data.

Discussion for T1, model and data

The discussion of termination 1 model settings and simplifications considering the CO_2 record also hold when considering the $\delta^{13}C$ record comparison. If the ocean carbon release occurred over a longer period than that modelled in our study, as suggested by data, then it would have an impact on the $\delta^{13}C$ record. In model simulations in which no glacial ocean mechanism operated (chapter 4) the best-fit for the $\delta^{13}C$ record was a much faster responding permafrost land carbon dynamic. A linear reduction of sinking of brines between 18kyr to 12kyr BP resulted in a match for the CO_2 and $\delta^{13}C$ record with the "medium" permafrost dynamic. A slower acting glacial ocean mechanism would need to be combined with a faster permafrost dynamic in order to match CO_2 and $\delta^{13}C$ data.

There are mechanisms that may have affected the atmospheric $\delta^{13}C$ record which are not included in our simulation. These include: destabilisation of gas hydrates in the ocean; flooding of the continental shelves on sea level rise; changes in methane release on the land; changes in ocean biota productivity; peatlands/wetlands dynamic. As discussed, the peatlands/wetlands dynamic likely affected the $\delta^{13}C$ record from

around 10kyrBP and is a significant carbon sink estimated at more than 500GtC growth since the start of the present interglacial period. Changes in ocean productivity may have had some effect on $\delta^{13}C$, but according to Fischer et al (2009) this is likely only a small effect, in agreement with results in our study (chapter 4). The ice core methane record indicates fast changes in atmospheric concentration of methane through the glacial termination (Chappellaz et al 1990). Methane is strongly depleted in carbon-13 and changes in sources would be enough to affect atmospheric $\delta^{13}C$ of CO_2. According to Melton et al (2012), who measured $\delta^{13}C$ of CH_4 in ice cores, the sources of methane rise seen in data during the Younger Dryas warming period was most likely dominated by biomass burning, followed by thermokarst lakes (indicating permafrost thaw). They suggest that contribution from tropical wetlands or from methane gas-hydrates in the ocean did not play a large role. Fischer et al (2008) also conclude that methane gas hydrates did not play a large role in the full termination methane record. The flooding of the continental shelves may have resulted in release of carbon to the rest of the system and have affected atmospheric $\delta^{13}C$, CO_2 and CH_4.

The ice core record of $\delta^{13}C$ represents what has been recorded of the true atmospheric $\delta^{13}C$ signal in the ice. It is dependent upon rates of change, because the firn closure process allows gas exchanges between snow/ice and atmosphere until its completion. Kohler et al (2011) considered the B-A warming between 15 and 14 kyrBP and jump in atmospheric CO_2 for fast-acting processes in which the ice core record would not represent the true scale of changes that occurred. Firn closure processes would also attenuate the $\delta^{13}C$ signal. They conclude that around 125GtC was released resulting in a CO_2 rise of 20-35ppm, or 2 to 3.5 times higher than ice core records showed, during a period of less than 200 years. At the time of their study the high resolution $\delta^{13}C$ records were not available and they could not conclude whether the rise in atmospheric CO_2 was largely from an ocean or a land source, but suggest the flooding of continental shelves at this time may have caused the 125GtC release. In fast changing climates this attenuation of the atmospheric signal in ice cores must be kept in mind when performing model-data comparisons.

The Lourantou et al (2010) data set appears to show more variability than other datasets presented by Schmitt et al (2012). Between the period 16kyr to 12kyr BP the Grenoble Mill dataset has many more data points than the Bern Sublimation set. The Bern sublimation set is used by Schmitt et al as the reference set to perform residual analyses for other sets, and determine these residuals by comparing data at the same point in time. Given that Lourantou et al's Grenoble Mill data is higher resolution, this comparison with matching-in-time points to Bern sublimation data is problematic. As described in the previous paragraph, fast changes in $\delta^{13}C$ in the atmosphere may not all be captured in ice core data records. A higher resolution ice core should give datapoints that are closer to reality, although, the Bern sublimation method is more accurate than the Grenoble Mill and Bern Cracker methods. However, age models of ice core measurements are a very important factor to consider when creating time series data, especially for fast changing data. Creating residuals by comparing datapoints that are not from the same point in time may have resulted in a false smoothing for the Monte

Carlo average for $\delta^{13}C$ data reported by Schmitt et al (2012). Our results show that very fast changes in atmospheric $\delta^{13}C$ can be caused in response to AMOC related events (chapter 6), the ±200 years between datapoints reported by Schmitt et al for calculating residuals is likely far too long a period. For this reason, the variability shown in the modelled output when the system is effected by AMOC strength changes are not considered to be invalidated based on the monte carlo mean $\delta^{13}C$ dataset.

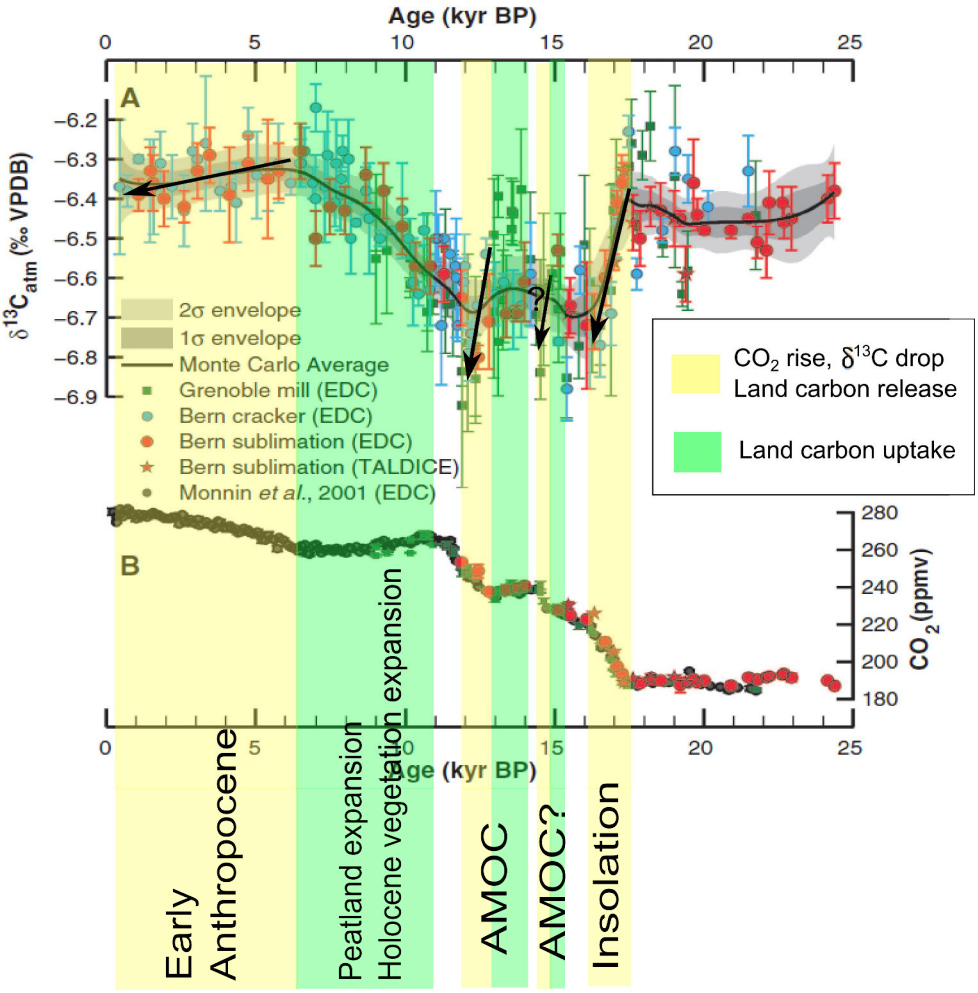

Fig 8.4, Data for CO_2 and $\delta^{13}C$ as reported by Schmitt et al (2012) with proposed mechanisms overlaid. Arrows show general trend that may be seen in data

According to the CLIMBER-2P modelled results and comparison with data, a proposed explanation for the CO_2 and $\delta^{13}C$ records is presented in figure 8.4. The increase in summer insolation in high northern latitudes caused a permafrost thaw that resulted in soil decay and carbon released to the atmosphere resulting in the onset of CO_2 rise at around 17.5kyrBP. This occurred while changes in the southern ocean were slowly causing the reduction of Antarctic bottom water mass. Between 17.5 to 15kyrBP, despite this ocean circulation change, the ocean was a net carbon sink. From around 16kyrBP the loss of carbon from land slowed, and from 13kyrBP the land

became a carbon sink as biosphere expansion outweighed any losses from permafrost-thaw. Also occurring around 15kyr BP, ice sheet melt into the ocean may have slowed northern hemisphere temperature increases via the AMOC response. During the B-A warming event occurring from 14.7kyrBP, a fast increase in AMOC may have caused a faster thaw in permafrost releasing new fast-decaying carbon soils seen as a CO_2 rise and $\delta^{13}C$ drop. The CO_2 plateau seen just after this fast rise and lasting several thousand years was likely a result of a stronger ice sheet melt event that caused drastic reduction in AMOC strength and a short term re-expansion of permafrost. On AMOC resumption after this event the very fast warming of the northern hemisphere caused a fast permafrost thaw and carbon release, via soil carbon decay, increasing CO_2 in the atmosphere and reducing $\delta^{13}C$. Throughout these events the slow rearrangement of ocean circulation resulted in a CO_2 rising trend in the atmosphere in periods when the land was a carbon sink. Peatlands started to establish and expand significantly from 11kyrBP and together with vegetation expansion approaching the Holocene climate optimum caused a long term slow fall in CO_2 and rise in $\delta^{13}C$. From 10kyr BP, insolation in the northern hemisphere high latitude summer started to fall again and permafrost area started to expand in response. From around 6kyr BP the data records for CO_2 and $\delta^{13}C$ may be recording the perturbed earth system already responding to human impacts on the carbon cycle and climate system. This will be discussed further in section 8.3.

8.1.3 Termination II CO_2 and $\delta^{13}C$ evolution

> 3. Can the permafrost-mechanism also explain the data from the previous termination TII?

Termination II (T2) data for CO_2 could be generally fairly well reproduced but relied also on ocean glacial mechanisms, as termination 1, to produce CO_2 rise of around 100ppm by the end of the deglaciation. For $\delta^{13}C$ (and also CO_2) the patterns of changes could be reproduced but only if model output was shifted by around 2.5kyrs. This may be due to uncertainties in the age model used to date CO2 and $\delta^{13}C$ data. This shift was a simple means of explaining the apparent mismatch between model and data. To properly model T2 the simulation should be carried out again using a shifted age model for CO_2 data to drive CLIMBER-2P. If this were carried out then the $\delta^{13}C$ model output may show a better fit with data than the shifted data shown in chapter 4. Another possibly contributing explanation is that initial sea level rises were caused by ice sheet melt in the southern hemisphere, not just the northern hemisphere (see section 8.5.1). Age models and sychronisation of very different datasets, even for termination 1, are still a non-trivial exercise. In this sense it is considered reasonable to suggest shifted model output can well represent measured data for termination 2.

Prior to T2 the land may have stored less carbon in permafrost than at T1, due to a larger Eurasian ice sheet, and this may be able to explain why a fast drop in $\delta^{13}C$ at

the onset of insolation increases is not seen as clearly in T2 as in T1 data. This is discussed in more detail in section 8.5, Model simplifications and their implication. No fresh water forcing experiments were carried out for the T2 period, but as with T1 it may be that ice sheet melt and fresh water input to the north Atlantic had an impact on the carbon cycle principally via the land biosphere.

As with T1, the importance of peatlands/wetlands for carbon cycle dynamics was identified. For both terminations when CO_2 levels reached around 250ppm modelled $\delta^{13}C$ diverged from data and modelled CO_2 rose too fast. This suggests a land carbon uptake mechanism missing from the model: northern peatlands and wetlands. The discussions of simulations for T1 concerning the interdependence between ocean and land carbon cycle responses in reproducing data also hold for termination 2.

8.1.4 Permafrost dynamics on glacial timescales

> 4. If permafrost-carbon does play a significant role in rising atmospheric CO_2, does it act at each precession cycle and how strong is the effect in non-termination periods?

The permafrost-carbon mechanisms significantly changed the land carbon dynamics compared to the standard model. The total land carbon stocks modelled over the last glacial cycle period are shown in figure 8.5, and the permafrost carbon for the same simulation is shown in figure 8.6. In the standard version model the terrestrial biosphere response was only really sensitive to CO_2 and mean annual temperature. This led it to act only as a negetive feedback to climatic changes, where warming and CO_2 increase induced land carbon stock increases. With the permafrost mechanism responding to insolation forcing the land carbon stock is now far more sensitive to ice sheet extent and changes in summer insolation in high latitudes.

Permafrost area was sensitive to insolation forcing at all insolation cycles, but was also strongly influenced by ice sheet area on the land, as well as CO_2 levels' control on climate. Not all terminations, as they are defined, are associated with a drop in permafrost area and a release of land carbon according to model output. At T3 (~250kyr BP) carbon increase was all sourced from the ocean in model output. During terminations (excepting T3) the permafrost thaw contributed to the initial rise in atmospheric CO_2. However, larger drops in total land carbon stocks are seen in periods other than terminations. The expansions of ice sheets in cooling phases, associated with insolation cycles, caused losses in permafrost area and losses of permafrost soil carbon. This occurred at the same time as climate conditions become more unfavourable for vegetation growth and so the loss of land carbon was compounded via NPP reductions. For the last glacial cycle a drop in the order of 800GtC was seen between 80kyr to 65kyrBP, this kind of drop would be apparent in $\delta^{13}C$ data. The longest and fastest drops in permafrost-carbon stocks all occurred during termination periods.

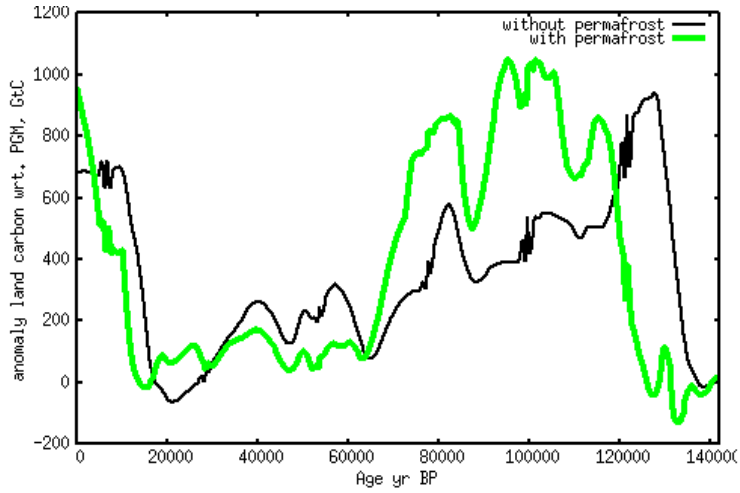

Fig 8.5, Land carbon anomaly with respect to PGM for CLIMBER-2P (green line) and the CLIMBER-2 standard model (black line, no permafrost carbon).

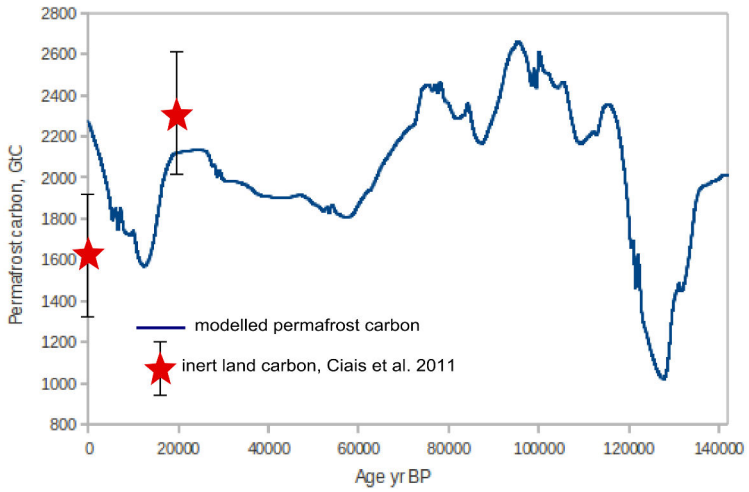

Fig 8.6, Modelled permafrost carbon stock (found by subtracting standard model land carbon stock from CLIMBER-2P land carbon stock) for last glacial cycle. Estimate of inert land carbon stock of Ciais et al (2012) marked as red stars.

The simulations presented in chapter 5 did not include any contribution from a glacial ocean mechanism. This is the reason why the CO_2 record could not be reproduced in model output. However, the results from the simulations of termination 1 and 2 suggest that the glacial ocean mechanism produces rather slow-responding changes in ocean carbon stocks. For termination 2, the inclusion of the ocean mechanism produced a maximum anomaly of 140GtC in ocean or land carbon stocks with respect to the simulation without glacial ocean mechanisms (chapter 4, fig 4.3). According to ice core records, termination periods represent the largest and fastest changes in climate over a glacial cycle, possibly with the exception of millennial scale climate variability for speed. For these reasons, the land carbon and ocean carbon stocks changes/dynamics in figure 5.8 (chapter 5) are considered reliable to an

estimated confidence of ±140GtC for the insolation driven system response. No fresh water forcing was included in the simulations for full glacial cycles, so the ice sheet melt/AMOC system response is not represented in the results. Glacial ocean mechanisms would result in longer term underlying trends not shown in our model simulations (but seen in data). Peatland/wetland dynamics, not included in our model, would have an effect on land carbon stocks. According to the terminations model-data comparison it may be that peatlands and wetlands are more important in warmer climates only, where CO_2 is above ~250ppm, this idea is supported by basal age dates from present-day peatlands (Yu et al 2010).

8.1.5 Millennial scale climate variability

> 5. Fast climatic changes that may have affected the northern hemisphere would have an impact on the permafrost extent. Could the permafrost-carbon mechanism have played a role during these fast climatic changes?

No data is yet available for $\delta^{13}C$ for millennial scale climate variability, but comparison with the CO_2 record and temperature records could be done. In model results in chapter 6 for equilibrium climate AMOC switch-off-recovery events, the modelled CO_2 rose faster and later than data suggests for equivalent real world events. The simulations carried out were very simplified and an equilibrium climate background is not representative of the real world case. However, as with other studies of AMOC driven fast climatic changes, the importance of background climate on system response was very obvious. During a series of fresh water forcing events of diminishing magnitude implemented into the model, the modelled CO_2 mismatch with data may be explained via a lack of peatlands, fire and glacial ocean mechanism response in the model. If permafrost-carbon, or a land carbon source, had a role to play during these millennial scale events then it would be visible in $\delta^{13}C$ data. For our model settings an AMOC switch-off-recovery event lasting 1500 years resulted in a $\delta^{13}C$ drop of 0.3‰ from maximum to minimum value. Cooling in the northern hemisphere resulted in a land carbon uptake and a rise in $\delta^{13}C$ later, warming caused a land carbon release and a fast drop in $\delta^{13}C$ for the LGM background simulations.

8.2 Future projections for anthropogenic carbon emission scenarios

As well as the initially posed research questions on paleoclimate, the fully coupled CLIMBER-2P model was used to simulate future climate changes based on carbon dioxide emissions from human sources. Driving the model with emission

projections from the RCP database allowed a first estimate of the magnitude of the permafrost-carbon feedback for future scenarios in chapter 7. Identified from the long timescale simulations, during interglacial periods the model is not driven by glacial ocean mechanisms so these were not considered in model output. Modelled CO_2 for 1850 CE in the model was 274ppm, within 5ppm of data. This allowed the model to be fully coupled and atmospheric CO_2 calculated within the model carbon cycle to drive the radiative code and the vegetation model.

Comparing CLIMBER-2P outputs to CMIP models and EMIC model ensembles (Zickfeld et al 2013), calculated CO_2 was higher due to the carbon release from the permafrost zone. For the highest forcing, RCP 8.5, this amounted to around 500ppm higher CO_2 concentration at peak temperature. The emission rate from permafrost-thaw was dependent upon the rate of temperature rise and was non-linear. This is a feature of mechanisms with a long time to equilibrium, and makes the Permafrost Carbon Feedback (PCF) difficult to compare with IPCC description of feedbacks that are considered linear and fast acting in future projections. The PCF also creates a longer 'tail' in climate system response, the atmospheric CO_2 remains higher in the atmosphere over longer timescales.

Again as with other simulations, peatlands and wetlands in northern latitudes are likely an important dynamic for future response of the Earth system to forcing. The CLIMBER-2P model represents only the response for frozen ground, not the strongly linked peatland PFTs, in high latitudes. When compared to other models outputs, CLIMBER-2P projects far greater land carbon losses. Model output shows good agreement with the estimates from Schuur et al (2011) for permafrost carbon release and Harden et al (2012) for soil carbon vulnerable to thaw. It may be that the difference between CLIMBER-2P projections and other models can be largely explained via increasing carbon uptake in peatlands. Our model was tuned to data from termination 1, as such it represents all thaw dynamics such as talik formation, active layer thickening and carbon release rates in permafrost thaw. In order to determine whether all the difference between our model and more complex land surface models' outputs are due to peatland uptake, the sphagnum/wetland communities PFT should be incorporated in the CLIMBER-2P model for further studies.

The treatment of permafrost in our model only considers its role in the carbon cycle, not in the surface energy fluxes. The freezing and thawing of material would have an impact on the energy budget throughout the year and in changing climates. This latent heat of thaw for the cryosphere, including permafrost which represents a significant amount of energy according to the estimate in chapter 7, needs to be considered in complex GCMs when calculating the energy budget.

The simulations for future projections considered only the impact of increasing CO_2 on the present-day system including fixed ice sheets. In the real world case, and especially for the longer timescales and strongest forcings, the impact of ice sheet melt would be important in Earth system response. These effects would be via albedo changes, land area both via new land exposed (presently under ice sheets) and sea-level rises, and via the AMOC response. Recent evidence suggests a slow down in

AMOC strength already since the 1990s (Robson et al 2014), which coincides with Greenland ice sheet melt (Hanna et al 2008). Strong fresh water forcing in the north Atlantic ocean may induce a strong AMOC reduction (according to chapter 6) which may temporarily cool the northern hemisphere and affect atmospheric CO_2 concentration. Further studies of future system response to forcing that include ice sheet melt as well as CO_2 forcing and land use change will better represent possible future system response than current projections do.

8.3 Early Anthropocene

The model results from the long timescale simulations (chapter 5) and the future projections (chapter 7) indicated that permafrost area in the Holocene and pre-industrial climate may be anomalous with respect to the "natural" system. When cryosphere area is plotted against insolation at 65°N mid-summer (fig 8.8), only in the Holocene does cryosphere size continue to fall when insolation is also falling. In all other interglacial periods (marked in light orange) cryosphere size is either plateaued or increasing when insolation falls due to ice sheet inception and/or permafrost expansion.

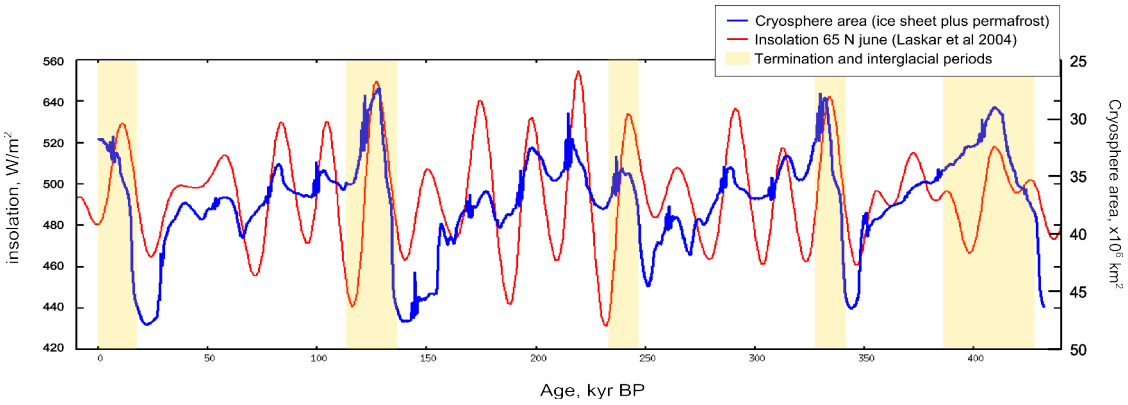

Figure 8.8, Cryosphere area (inverted scale), including ice sheets and permafrost, plotted with summer insolation at 65°N. Only in the Holocene does cryosphere size fall strongly when insolation in high latitudes in summer is also is falling.

Based on this observation a fully coupled simulation for the last deglaciation was carried out, where the carbon cycle model calculated the atmospheric CO_2 and drove the radiative code with this (CO_{2_RAD} = CO_{2_CC} rather than data CO_2). The Holocene period modelled total permafrost area for this fully coupled "natural" system simulation is shown in figure 8.9, together with the CO_2 driven system (as chapter 4) and the recent emissions (1850-present) fully coupled system up to the year 2014 (as chapter 7). The permafrost area change is given with respect to the -6000year C.E. value, where a possible CO_2 anomaly may be seen in the atmospheric data (Ruddiman 2007). These results show that the pre-industrial permafrost area, when CO_2 data is used to drive the model, is already reduced compared to the natural system permafrost

area. Since the start of the pre-industrial period, here modelled from 1850 C.E, permafrost area has lost a further 2.6x10^{6}km^2. This brings present-day permafrost area to 15.1x10^{6}km^2 compared to a data estimate in 2000 of 12.21 to 16.98x10^{6}km^2 (a mean of 14.55x10^{6}km^2). This indicates that the present-day extent of permafrost may be around 4 to 5 x10^{6}km^2 less than the natural system, responding to insolation forcing, would produce. The pre-industrial and post-industrial changes in permafrost area affected by human perturbation of the climate system would have a feedback effect in the carbon cycle, and are in support of the Early Anthropocene hypothesis where the 20ppm rise in CO_2 since the mid-Holocene is considered anomalous with respect to the natural system.

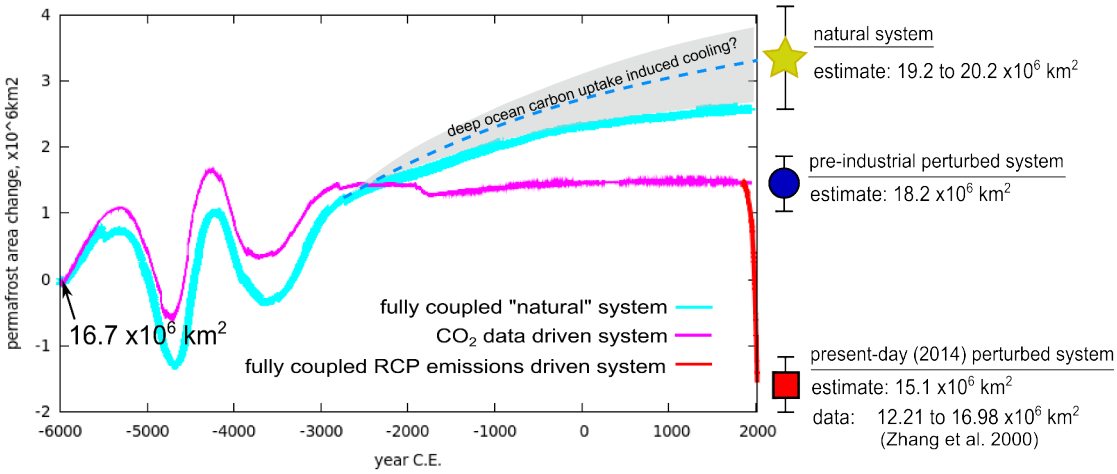

Fig 8.9, Modelled permafrost area for the Holocene period for the fully coupled "natural" system, the CO_2 data driven system and the full coupled emission driven industrial period. Permafrost area estimates for each period are given on the right.

8.3.1 CO_2 and $\delta^{13}C$ change since the mid Holocene maximum

By comparing the fully coupled "natural" system to the CO_2 data driven system output, an estimate of carbon anomaly in land is ~100GtC and -0.06‰ in atmospheric $\delta^{13}C$. If 85% of carbon emitted to the atmosphere ends up in the ocean reservoir and 15% remains in the atmosphere, this equates to an equilibrium contribution of ~7ppm. Figure 8.10 shows the total difference between the two simulations (CO_2 data driven to fully coupled) as 15-20ppm, although this is also a result of the overestimate for CO_{2_CC} levels in both simulations, but amplified in the fully coupled simulation because this drive the radiative code too resulting in a 40ppm overestimate compared to data. This can also be seen in figure 8.9 where the fully coupled system initially simulates lower permafrost area than the CO_2 driven system between -6000 to -2500C.E. If modelled CO_2 (and temperature) in the fully coupled simulation were as data for 7kyrBP, permafrost area would be greater. For this reason the differences between the fully coupled simulation and the CO_2 data driven simulation by the present-day (2014 C.E.) for permafrost land-carbon are considered to be a minimum

anomaly case. A comparison of the model outputs for CO_2 and $\delta^{13}C$ against data is shown in figure 8.10. Clearly there are differences and these will be discussed in the next section. Hereafter the general trend (shown as a dashed line) in coupled model output for the natural system and data measurements will be considered.

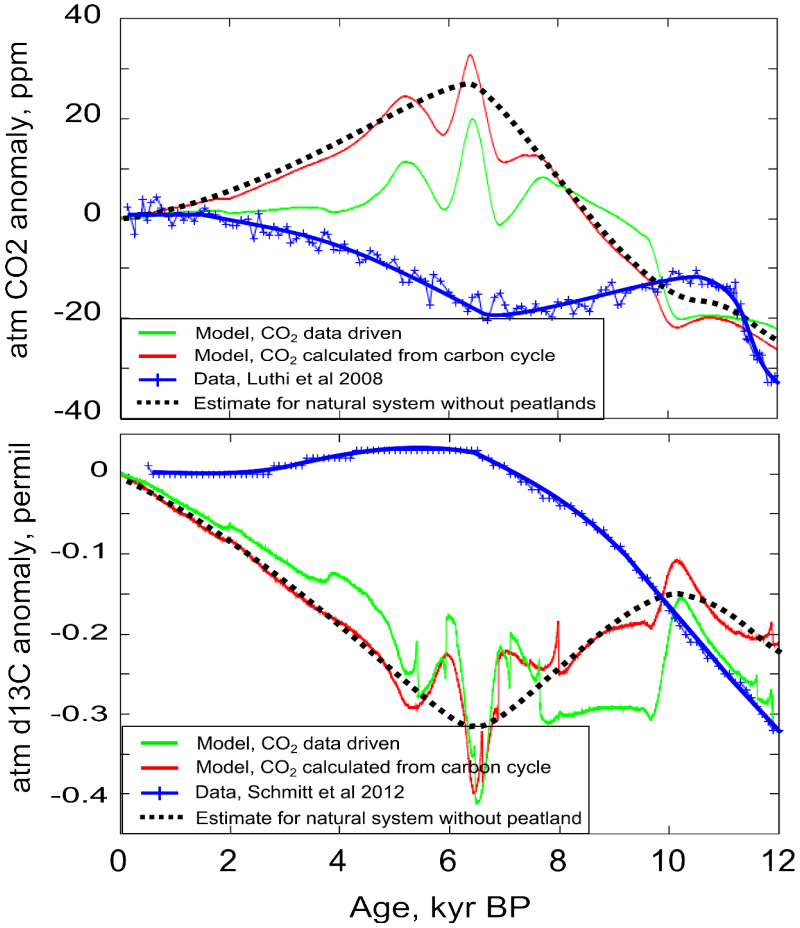

Figure 8.10, Holocene CO_2 and $\delta^{13}C$ anomalies with respect to pre-industrial present-day values. Model outputs for CO_2 data driven system and for fully coupled system plotted with data. Dashed line is trend for fully coupled "natural" system.

One argument against the early anthropocene hypothesis is the atmospheric $\delta^{13}C$ record. This record indicates that since the onset of farming, $\delta^{13}C$ has only dropped by around 0.05‰ in the last 7000 years (see figure 8.10). At the same time CO_2 has risen by around 20ppm. This would seem to indicate that deforestation and biomass burning could not have been responsible for a possible 35ppm CO_2 anomaly with respect to the natural system (Ruddiman 2007, Elsig et al 2009). However, since the last termination period some 547GtC have accumulated in northern peatland soils, and 612GtC globally (Yu et al 2011). In the last 7000 years this peatland stock is estimated to have grown by at least 250GtC. This means that in the last 7000years, a loss of terrestrial land carbon of at least 250GtC at the same rate as peatland uptake would have had to occur to keep atmospheric $\delta^{13}C$ stable (assuming that land carbon

stocks all have the same $\delta^{13}C$ signature of -25‰ and neglecting any ocean induced $\delta^{13}C$ changes). Ruddiman (2007) estimates the total biomass lost via anthropogenic deforestation in the pre-industrial period as 120 to 137GtC, leaving 113 to 130GtC to lose from the land biosphere just to keep the $\delta^{13}C$ record stable. As it has dropped by around 0.05‰, then it indicates there has been a net drop in land carbon stocks over this period, and greater than 130GtC not including human induced deforestation/biomass burning.

Since the mid-Holocene, the CLIMBER-2P CO_2 driven model predicts increases in the southern hemisphere temperature of 0.2ºC, whereas the fully coupled model shows a decrease of 0.4ºC from a peak at 6kyr BP. This warming since the mid-Holocene can likely explain some of the CO_2 rise in the atmosphere via ocean processes, for example sea ice reduction. The anomaly from the natural system, at least 0.6°C in the southern hemisphere or ~2°C in high latitudes, can explain more of the apparent CO_2 anomaly with respect to the projected trends for the natural system. As described in Ruddiman (2007) these are feedbacks on the ocean carbon cycle are as a result of unusually high global temperature.

8.3.2 CO_2 and $\delta^{13}C$ anomaly with respect to the possible natural system

The 35ppm anomaly as estimated by Ruddiman (2007) is given with respect to the natural system, not with respect to the 7000yr BP value. The CO_2 anomaly from 7000yr BP is around 20ppm. The proposed natural system $\delta^{13}C$ for the Holocene period can be compared with data from termination II and the Eemian (chapter 4, fig 4.5 where the shifted model output fits well with changes in trends seen in the data). For termination II the enrichment of Carbon-13 in the atmospheric pool continues for around 9000 years after peak CO_2 levels have been seen in the atmosphere. Where the peak CO_2 is associated with peak summer insolation in the northern hemisphere. For termination 1 the peak enrichment in $\delta^{13}C$ occurs only 4000 years after the peak CO_2 (with peak insolation). The CLIMBER-2P model predicts that presently $\delta^{13}C$ should be on an enriching trend. The timing of peak $\delta^{13}C$ is correctly predicted for the Eemian period by CLIMBER-2P. In the CLIMBER-2P future projection simulation, shown in chapter 7 (as “control” or “no emissions”), the predicted $\delta^{13}C$ by the model continues on a positive trend. The simulation in chapter 7 does not include any glacial ocean mechanisms or ice sheet nucleation or growth. In order to explain the drop in $\delta^{13}C$ seen in the record, another mechanism needs to be invoked. Here, the calculations of Ruddiman (2007) for the total land deforested as a result of agriculture in the pre-industrial Holocene can start to explain the $\delta^{13}C$ drop.

If the Holocene was similar to the Eemian then insolation driven onset of glaciation would have started to happen around 1000 years ago, or around 9000 years after peak CO_2 (after peak insolation) (see fig 5.1 chapter 5), as seen in the sea-level record for the Eemian. In the present interglacial period the insolation forcing is less pronounced than for the last interglacial. The peak CO_2 level (at ~11kyrBP) of 260ppm is around 30ppm lower than the Eemian peak of 290ppm. So for a cooler climate

interglacial we may expect glaciation onset to happen sooner, as the threshold (determined by thermal balance) is crossed sooner. In this case a climate cooling may begin to induce carbon uptake in the ocean via the glacial ocean mechanisms (increasing sea-ice cover in the southern ocean, brines rejection and increasing ocean stratification). An ocean induced climate cooling, caused mainly by ocean carbon uptake, would have the effect of increasing permafrost area and possibly increasing the permafrost land carbon stocks in the natural system. In the pre-industrial perturbed system, this cooling did not occur. This is as Ruddimans hypothesis (2003, 2007) of delayed glaciation. In this case the permafrost-carbon contribution to the pre-industrial perturbed system carbon anomaly relative to the natural system is likely higher than the 7ppm estimated earlier.

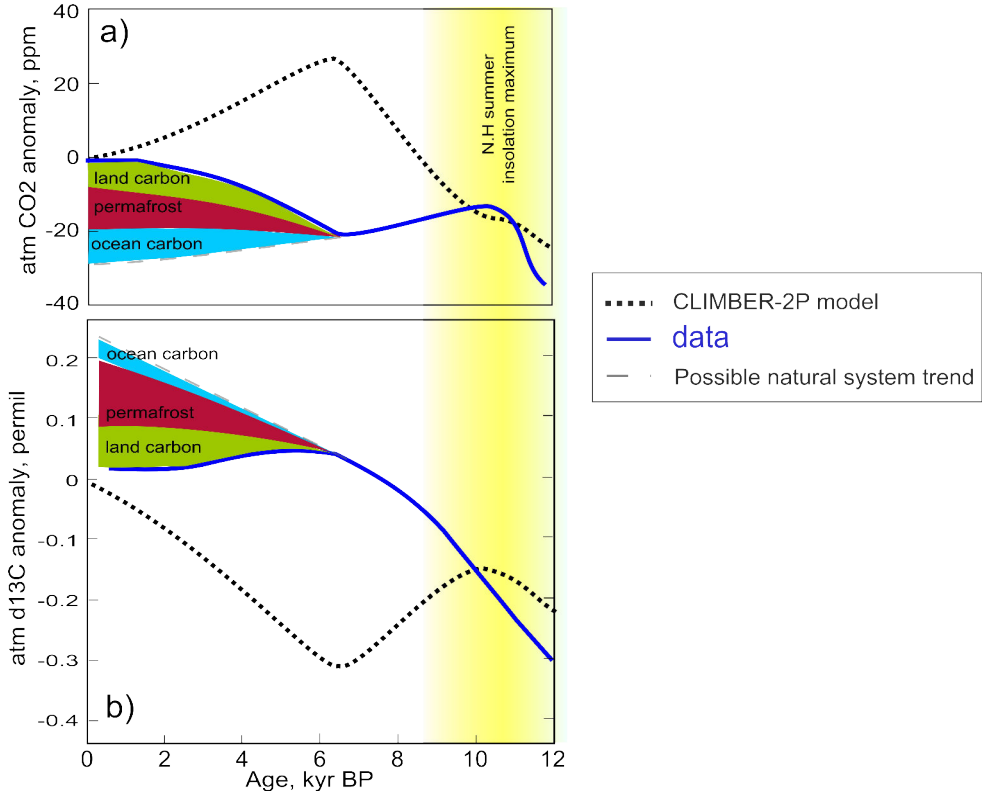

Fig 8.11, Modelled and data trends for atmospheric CO_2 and $\delta^{13}C$, with possible natural system trend marked as dashed lines. Mechanisms explaining the data-natural system mis-match are marked ontop.

This analysis of the perturbed pre-industrial system is shown schematically in figure 8.11. Here the three perturbed mechanisms are removed from the data in turn in order to reach the proposed natural system trend. The ocean carbon contribution is given a $\delta^{13}C$ anomaly to represent the possible role of the deep glacial ocean carbon store, which is depleted in carbon-13 (chapter 4). Clearly there is a discrepancy between the proposed natural system and the CLIMBER-2P model output. This is addressed next.

In fig 8.12 the CLIMBER-2P model output for the trends seen in the fully

coupled model are compared with data. As has been discussed many times, the absence of the peatland dynamics is the likely main cause for model-data mismatches for interglacials. A schematic representation of the difference a long lasting carbon sink in peatland soils may make to the model output if it agreed with Yu et al (2011) peatland carbon accumulation rates is shown in fig 8.12. The mid-Holocene climatic optimum saw greater expansion of forests in the northern hemisphere (which most of the land mass lies), that have since reduced in response to reducing summer insolation. This is not clearly seen in the CLIMBER-2P vegetation model, so it is represented schematically and added to the CLIMBER-2P plus peatlands curve in figure 8.12. To agree with the previous estimate for the $\delta^{13}C$ anomaly explanation, these land carbon changes amount to a total of 20ppm of CO_2 and around 0.2‰ $\delta^{13}C$ of the pre-industrial anomaly compared to the natural system. This 0.2‰ is the shift that would be seen in model output if an extra 560GtC were accumulated in peatlands. The remaining anomaly of around 10 to 15ppm relative to the natural system trend may be found in the ocean carbon cycle.

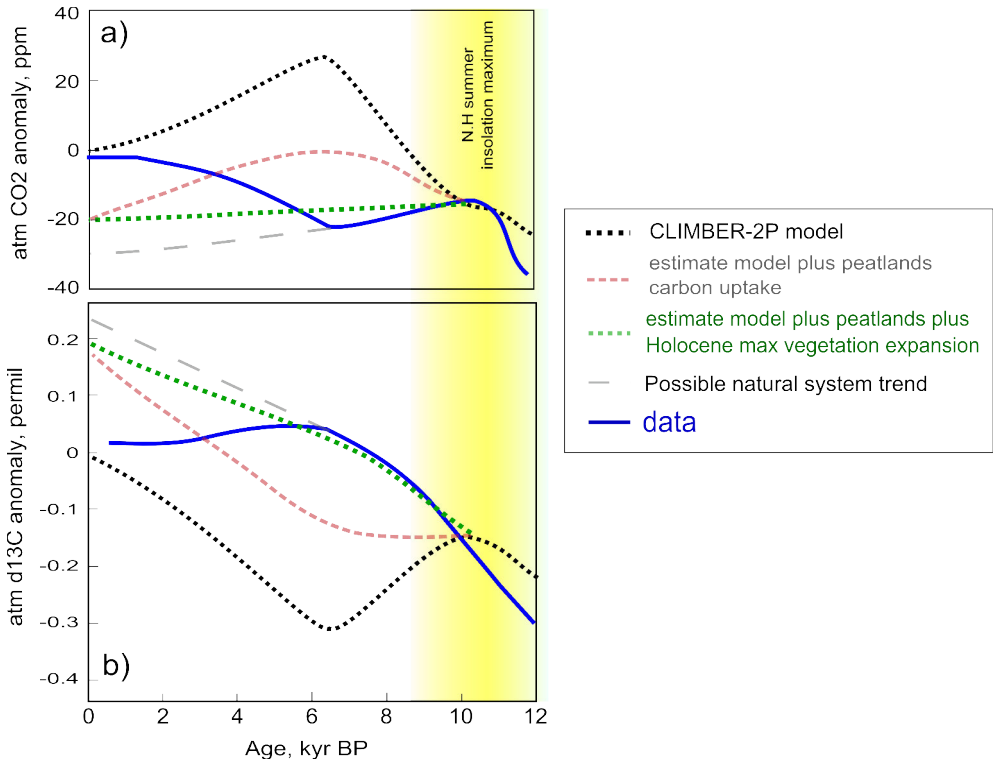

Figure 8.12, Modelled and data trends for atmospheric CO_2 and $\delta^{13}C$, with possible natural system trend marked as dashed lines. Mechanisms explaining the model-natural system mis-match are marked ontop.

The early anthropocene changes in land carbon stocks were simulated by Stocker et al (2011) using BernCC carbon cycle model and the Lund-Potsdam-Jena dynamic global vegetation model (LPJ-DGVM, Sitch et al 2003) with a land use change representation based on Strassman et al (2008). Northern latitudes were treated as Wania (2007 PhD thesis). Stocker et al concluded that changes in land use by

humans did not create any CO_2 increase in the atmosphere outside natural variability before the year 1000 C.E. A limitation of their conclusion lies in their methodology. They kept the background climate constant for their simulations, which is unlike the real-world case in which summer insolation in northern latitudes was falling over this Holocene period. In our model this fall in summer insolation results in permafrost expansion and carbon uptake in soils. It also results in carbon loss from vegetation post-mid-Holocene maximum (Menviel and Joos 2012).

Obviously the figure 8.12 is only a qualitative representation, but it demonstrates the importance of insolation changes, at least two of these dynamics; mid-Holocene forest expansion and permafrost extent are strongly dependent on insolation changes on this timescale. As such, the Stocker et al (2011) study, which keeps climate constant, cannot be considered a reliable representation of the land carbon cycle over the last 10k years. They also assume that peat and permafrost related carbon stocks would be little affected by biomass burned and agricultural clearance of forest, on the basis that these regions are outside the areas which were cultivated before 1000C.E. This ignores the climate feedback on permafrost area that an increase in atmospheric CO_2 levels would have. It also ignores the use of peat as a fuel (Deforce et al 2007) in regions where forest was more sparse, and that cutting of peat can create a feedback which releases more carbon from the soil than was contained in the removed section (Waddington et al 2002). The size of this feedback may turn out to be negligible for the earliest periods of agricultural expansion, but it should be included in studies which address more recent total land carbon losses via human activities.

Menviel and Joos (2012) modelled the termination and Holocene carbon cycle using estimates from literature to determine the relative contribution of each mechanism possibly acting in these time periods. They successfully recreated the CO_2 and $\delta^{13}C$ record for the last 10kyrs. Their land carbon representation was a total uptake of 658GtC since LGM, 404GtC land carbon increase during the termination (as Menviel et al 2011), and 290-36GtC since the Holocene maximum (as the lower estimate of Elsig et al 2009). They conclude that carbonate compensation in response to earlier land carbon uptake, shallow water carbonate deposition and changes in land carbon stocks contributed equally to the 20ppm change in CO_2 since the start of the Holocene. One of their scenarios in which peatland carbon accumulation is included in the land carbon dynamics estimates supports the $\delta^{13}C$ anomaly as proposed here. When including the peatland uptake the total increase in land carbon is too high (according to the $\delta^{13}C$ record). In order to counteract this an extra land carbon loss is needed, for example anthropogenic based deforestation. This is also argued by Ruddiman et al (2011). When the peatland dynamic is included by Menviel and Joos (2012), atmosphere $\delta^{13}C$ shows an anomaly of around 0.2‰ with respect to data, the same as proposed in our study in fig 8.12. As a conclusion, with permafrost as a feedback to climate changes, the door remains open for further investigation of the Early Anthropocene hypothesis, that land use changes created feedbacks in the carbon cycle and climate system that altered the system well before 1000 C.E. The pre-industrial climate (~1750 C.E.) was already perturbed and Earth system models that are tuned to

pre-industrial climate conditions are not in fact representing the truly "natural" Earth system. This may have implications when mechansims, such as permafrost that have a long response time are included in modelling studies.

8.4 Earth system on longer timescales

A comparison of the Earth system responses during glacial time scale and millennial time scale experiments showed a pattern linking these timescales. In both cases, glacial and millennial scale, the instability of large ice sheets are a driving mechanism and the heat input gradient between the two hemispheres creates the variability in the Earth system. In glacial terminations the heat input gradient is via insolation forcing, where seasonality results in anti-phase maximum forcing between the hemispheres. During millennial scale climate variability the AMOC response to fresh water forcing provides the heat input gradient, creating increased input to the southern hemisphere during AMOC reduction episodes and increased input to the northern hemisphere during AMOC resumption and overshoot episodes. The long timescales associated with equilibration time for the glacial ocean and permafrost-carbon mechanisms are essential in re-creating paleoclimate variability seen in data. This response of the system is dependent upon the location of continents for ocean circulation, and on the presence of ice sheets. It is also dependent upon the location of continents in high latitudes, or where cold conditions exist, for the presence of permafrost.

8.5 Model simplifications and their implication

8.5.1 Ice sheet

Chapter 5 identified the role that ice sheet dynamics plays in determining the total area available on land for permafrost (and vegetation) in the high latitudes. The current simplified ice sheet representation cannot distinguish between northern high-latitudes or southern high-latitudes when determining where the ice should go if a sea-level drop is present in the sea level record. The land-ice area in Antarctica is fixed for all simulations, so any changes in sea-level will affect the North American and European ice sheet areas. In the real world not all sea-level changes had their cause in the northern hemisphere ice sheets. Any sea-level changes that were in fact due to southern hemisphere ice sheets will create errors in the northern hemisphere ice sheet representation in the model. This would change the land area available in the northern hemisphere for vegetation and affect permafrost and non-permafrost land carbon uptake, and therefore also the atmospheric CO_2 and $\delta^{13}C$ levels.

The simplified ice sheet is based on a scaling between LGM and PI ice sheet extent. As discussed in chapter 5, other glacial periods had different ice sheet extents and locations (even if the sea level record indicates the same ice volume) compared to

LGM. This affects the land area available for vegetation and permafrost to exist, which as above will also affect atmospheric CO_2 and $\delta^{13}C$ levels. It would also affect ocean $\delta^{13}C$ levels. Evidence of this may be seen in the benthic $\delta^{13}C$ record by comparing the absolute values from the LGM to those of the penultimate glacial maximum (PGM or MIS 5). Atmospheric and ocean $\delta^{13}C$ may have been more depleted in carbon-13 simply because less carbon-12 was stored on the land at PGM. If this is correct then analysis of ocean $\delta^{13}C$ may be able to provide an indication of the extent of land-ice during glacial maximum periods.

8.5.2 Sea level and coastlines

Land was exposed on glacial sea level lowstands and land was inundated on interglacial highstands as a result of sea-level changes. For all time periods and transitions in climate this dynamic likely played a role in the carbon cycle, although it is not represented in CLIMBER-2 because coastlines are fixed. During the last termination period, the Siberian shelf began to experience inundation from around 13kyr BP (Overduin et al. 2007) from sea-level rise. Models suggest that at LGM the Siberian shelf landscape would have stored significant amounts of carbon. Permafrost still exists beneath the sea-floor (Overduin et al. 2007) and this permafrost "lid" is thought to be preventing the release of large amounts of methane stored in sediments of the East Siberian Arctic Shelf (ESAS) (Shakova et al. 2010). The source of the methane stored, and currently being released from the ESAS, is likely from organic carbon accumulated when the shelf was above sea-level. This is a similar mechanism to that described by Ridgewell et al. (2012) but occurring far more slowly due to the presence of permafrost and cold climate in the Arctic location. This in turn is a strong indication that not all the carbon present on the shelf at LGM was quickly released to the atmosphere when this land was flooded during the deglaciation. Further modelling and ground data studies would be required in order to determine how much of a role these flooded shelves may have played during termination periods.

As ice sheets grow and sea-level slowly drops land is exposed on the coastline. This new land would then be available for vegetation growth. Contrary to the flooding of shelves in the opposite case, newly exposed land (in the permafrost zone) would immediately start to play a role in the carbon cycle. Provided of course that the growth of vegetation is viable. This may to some extent offset the loss of permafrost-available land occurring as the ice extends over land at the same time.

In chapter 5 the question of the anomaly between LGM and PGM atmospheric $\delta^{13}C$ values was addressed. I proposed the answer lay in the different size and location of the Eurasian ice sheet between LGM and PGM. With less land available for carbon accumulation in permafrost at PGM, more carbon-12 is seen in the atmosphere-ocean part of the system. This large ice sheet likely also had a role to play during the Eemian interglacial, where atmospheric $\delta^{13}C$ is still more depleted in carbon-13 (so, enriched in carbon-12) compared to the current interglacial, the Holocene. After the termination period, global sea-level was higher during the Eemian than in the Holocene by an

estimated at least 6m (Kopp et al 2009). This combined with the depression of the crust from the weight of ice (now melted) resulted in the appearance of the Eemian sea to the south of present-day Scandinavia and parts of north western Siberia. This land would not have been available for permafrost or peatland carbon uptake during the Eemian. These locations in the present day have high soil carbon contents, around 40kgC/m2 on average (Soil organic carbon map, USDA Natural Resources Conservation Centre) . In model output this Eemian sea area represents around 150GtC to 200GtC, although our model does not include peatlands and wetlands which would increase soil carbon in this area.

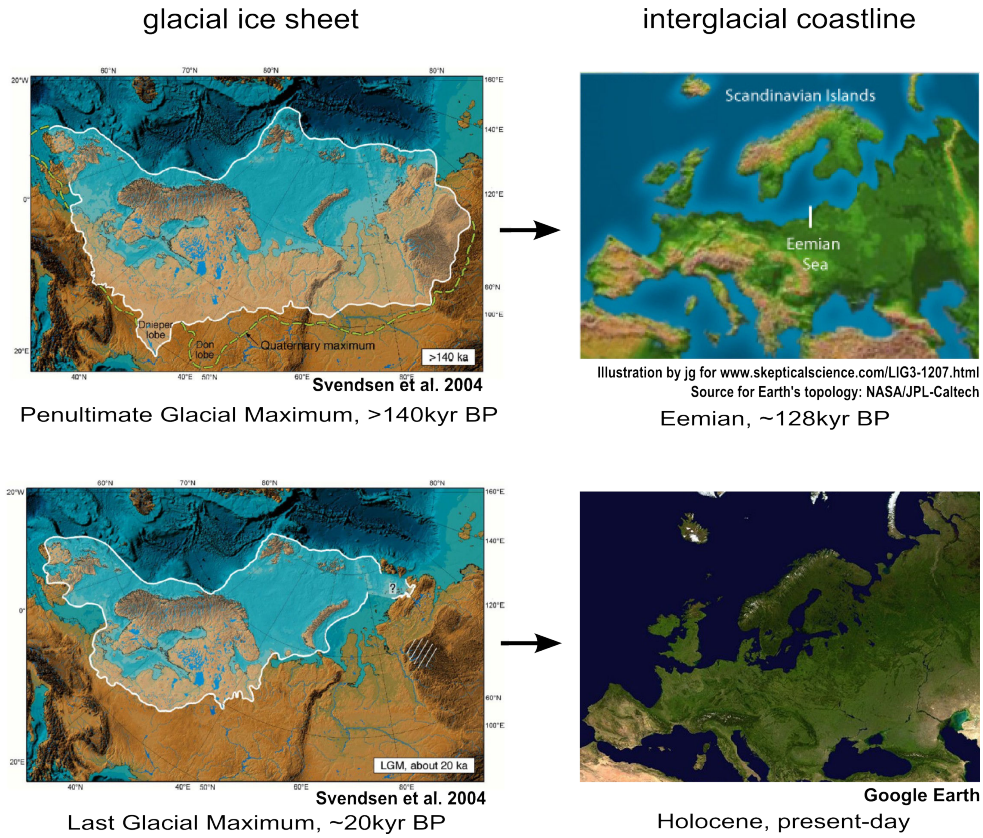

Figure 8.13, Glacial maximum ice sheet extent in Eurasia and following interglacial coastlines.

The total modelled permafrost area minimum in the Holocene is $13.2 \times 10^6 km^2$, and at Eemian $13.5 \times 10^6 km^2$. For a warmer Eemian period we would expect permafrost area to be lower. This indicates that CLIMBER-2P may also be overestimating total permafrost carbon for the Eemian. Total land carbon would very likely have been smaller at the Eemian compared to the Holocene, and this may be able to explain the interglacial $\delta^{13}C$ anomaly between the Eemian and the Holocene. Isostatic rebound would have very slowly acted to push the Eemian sea-bed back up after the removal of the weight of ice, slowly exposing new land. This new land would have then become available for carbon accumulation and atmospheric $\delta^{13}C$ would have become more enriched in carbon-13, perhaps approaching Holocene mean values. The rate of this

uplift to test this hypothesis would need to be the subjects of further study. This explanation for $\delta^{13}C$ difference between PGM and LGM (and Eemian and Holocene) does not consider the North American ice sheet dynamics and land carbon stocks, which would also need to be taken into account in further testing.

8.6 Model uncertainties and permafrost-carbon model dependencies

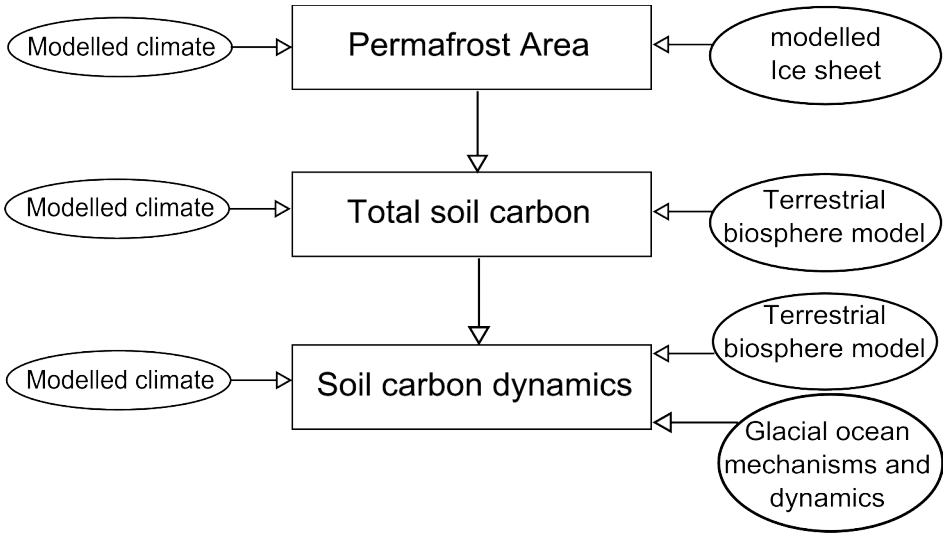

Fig 8.14 model and model development interdependencies.

The permafrost-carbon model relies on the first order controller; reduced soil carbon decay in the presence of permafrost, which leads to higher soil carbon concentrations (Zimov et al 2009). The location of permafrost within the model is acheived by using the Frost-index, an indicator of permafrost location (Nelson and Outcalt 1987), calculated within the model climate to diagnose the fraction of each grid cell that is likely permafrost affected. The total amount of carbon stored in soils was tuned to obtain estimates in line with Ciais et al 2011, and is dependent upon the modelled NPP and vegetation to determine soil carbon input which is itself dependent upon modelled climate. The soil carbon dynamics used for long timescale and millenial scale variability simulations were determined from model-data comparisons of the last termination. The last termination dynamics were sensitive to the ocean glacial mechanisms dynamics and the terrestrial biosphere dynamic responses to modelled climate changes. The climate dynamics also directly affect the permafrost extent calculation so provide indirect and direct controls on the permafrost soil carbon dynamics. Figure 8.3 shows these model dependencies throughout the model development.

8.6.1 Proposed model sensitivity tests

The permafrost-carbon model used here is very simplified and does not account for all processes at work in permafrost-affected soils. It also works with CLIMBER-2's standard terrestrial vegetation model, without altering any of its parameters. Sensitivity tests may be conducted with the model in order to provide an envelope of model responses accounting for these simplifications.

Frost-index control on decay rates

Extensive tuning experiments were done during model development to create a total land carbon stock at LGM and PI-transient which agreed with estimates from Ciais et al 2012. These relied on the use of a Frost-index multiplier to create the greatest reduction in soil decay in the coldest regions. It also meant that the model was more tuneable. Reducing or increasing the magnitude of this extra 'coldness' effect on soil carbon decay would help to constrain its role on longer timescales.

NPP/Rooting depth limitation

Currently the model produces soil carbon concentrations that are too high in the coldest regions. This may be related to the Frost-index decay rate controller (see above) or that the model transfers too much vegetation (via vegetation mortality) to the soils. Either reducing the NPP to recreate root depth limitations (or vice versa) would identify the soil carbon concentrations' sensitivity to NPP, and may also produce concentrations in better agreement with data for the coldest regions. There is also no nitrogen limitation in CLIMBER-2P, which if present may reduce NPP in these cold regions.

Soil temperature

Soil temperature is fixed in CLIMBER-2(P), and soil decay depends on air temperature. However, studies show that carbon decay in permafrost-affected soils can increase soil temperature (Khvorostyanov et al. 2008a,b, Koven et al. 2009). Adjusting the soil temperature in permafrost soils could identify the models sensitivity to this parameter via the rate of carbon decay and release to the atmosphere.

Snow cover thermal diffusion

Snow cover is an important factor for both permafrost-extent and soil carbon decay via insulation from cold air temperatures (Gouttevin et al 2012). The snow correction used in the CLIMBER-2P permafrost model is linear, simply using air temperature and snow depth to predict ground temperature. Adjusting the linear model can give the sensitivity of permafrost-extent to a more or less insulating snow cover. Combining this and the soil temperature tests may be able to estimate the envelope of possible soil carbon decay rates for the model and account for these mechanisms.

Combined brines and fresh water forcing

The deep southern ocean carbon store hypothesis relies on the idea that in cold climates more carbon is stored in the deep ocean, and during warming this carbon can be released back to the rest of the system. During the fresh water forcing experiments, the fraction of brines was kept constant for equilibirum climate experiments, and linear for the termination 1 with fresh water forcing experiment (chapter 6). In the real world case the change in AMOC strength affects the temperature in the southern hemisphere and high southern latitudes. It is very likely that this would have an impact on a deep southern ocean carbon storage mechanism. Further experiments that combine the fresh water forcing and changes in the deep southern ocean carbon store (via the brines controller) should be carried out.

8.6.2 Data validation of model findings

In its current configuration, CLIMBER-2P is not ideally suited to model ^{14}C. Because soils have no depth, all the soil in each grid cell would have the same ^{14}C signature. In the real world case, the most likely scenario for soil carbon is "last in, first out". The first soil carbon stocks to be released on thawing would likely be the youngest and least depleted in ^{14}C. In CLIMBER-2P the first soils to be released would simply be a mix of all the soil-carbon ^{14}C ages in a thawing grid cell. The grid cell size is 10° latitude by 51° longitude, so this represents a very large range of 'real-world' ^{14}C ages. Although this may still give a very rough and first order indication of whether model outputs agree with data (or not), it should be treated with extreme caution.

At the time of writing, $\delta^{13}C_{atm}$ records at high resolution were only available for the last two termination periods from Schmitt et al 2012 (termination 1) and Schneider et al 2013 (termination 2). In order to support or contest the role of permafrost-carbon in time periods other than terminations, especially for millennial scale variability, a high resolution $\delta^{13}C_{atm}$ record for these periods is needed. During the last glaciation, millennial scale variability is seen from around 90kyr BP. Snow accumulation rates at this period should mean that $\delta^{13}C_{atm}$ data is available with the temporal resolution necessary to identify whether data confirms model findings.

Currently, the Greenland ice core does not provide any robust atmospheric CO_2 data due to issues with separating the original atmospheric CO_2 from in-situ derived CO_2. If CO_2 data from Greenland were available, the interhemispheric CO_2 gradient would be able to identify a significant release of carbon from high northern latitudes.

Proxy data for temperature in the permafrost region (particularly Siberia and Mongolia) for the termination period would aid in assessing whether the model findings can be backed up with temperature data. Current proxies for temperature in the Northern hemisphere may be biased to the North Atlantic, and oceanic climates, disimilar to the (probable) locations of high soil carbon storage at the LGM. Borehole data may be able to confirm whether temperature changes in the more recent past may have effected permafrost extent, as proposed in the future projections using CLIMBER-2P.

8.7 Proposed model developments and applications

8.7.1 Peatland and wetland dynamics

Throughout this study the role of peatlands in high latitude terrestrial carbon cycle dynamics has been highlighted as mechanism that may provide answers to model-data mismatch during terminations. Adding a new PFT for wetland plant communities and employing a soil moisture parameter may improve the model dynamics. Adding this PFT would certainly provide a means to make the model more realistic considering the strong accumulation seen in northern peatlands since the end of the last termination. If this dynamic were added to the model then the permafrost-carbon dynamics would have to be re-tuned, as chapter 3 and 4. This is because the peatland dynamics would have a strong effect on total carbon contents in permafrost soils.

8.7.2 Continental shelves

For the simulations carried out here, the land masses retained the same coastlines throughout. Sea-level fluctuations of around 120m are seen between LGM lowstands and interglacial periods. These exposed shelves would have very likely been productive land during sea-level lowstands. The Siberian shelf, now under sea-level, very likely still retains organic matter that was accumulated during the glacial period, and is currently a source of methane due to anerobic decomposition. Experiments to test the sensitivity of the CLIMBER-2P model may be able to help in the understanding of the fate of carbon on this shelf during the deglaciation. It is possible to increase the land fraction of the Siberian grid cells for LGM simulations. It may also be possible to calculate the land fraction based on the eustatic sea-level. However, it would also be necessary to create a new carbon pool per grid cell to account for carbon that is stored under sea-level. If this were not done then any land that becomes sea (submerged) would immediately loose all its carbon stocks to the atmosphere, which is not the real world case for the Siberian shelf. This new "under-sea" carbon pool may also be adapted to test the Glacial Burial hypothesis (Zeng 2003).

8.7.3 Holocene and Future projections

As highlighted in this chapter, it appears the early anthropocene hypothesis is supported by model output. In order to test this a land use change module could be created that adjusts the tree-fraction to grass-fraction in a grid cell. For CLIMBER-2P, with only 2 PFTs, this could be a relatively simple experiment to test the sensitivity of the modelled system to land use change. Although previous modelling studies have discounted land use change as the cause of Holocene CO_2 rise before 1750CE, there is still uncertainty surrounding estimates of population growth, and of land use change estimates (Boyle et al 2011). The permafrost-carbon mechanism is a positive feedback

that would may amplify the CO_2 rise effects of biomass burning.

The future projections carried out in this study did not include any ice sheet melt or related ocean circulation and albedo effects. According to the results from the fresh water forcing studies, fast fresh water input to the Northern Atlantic and Southern Ocean Atlantic sector has an impact on the carbon-cycle and climate. Future projections which take account of these mechanisms would be possible with CLIMBER-2P and may provide a more realistic future projection.

Conclusions

This study aimed to develop a permafrost-carbon dynamic model to incorporate into the CLIMBER-2 Earth system model and to carry out simulations with a view to contributing to the knowledge of the carbon cycle. The work would, for the first time, allow a fully coupled modelling study with an earth system model which included dynamic atmosphere, ocean, vegetation and cryosphere components including frozen land to study paleoclimates. The availability of recent ice core data for CO_2 and $\delta^{13}C$ of atmospheric CO_2 was to provide a means of validating model findings to identify whether a permafrost-carbon dynamic could have played a significant role in past changing climates.

A simplified permafrost-carbon mechanism was developed and validated (chapter 3) and tuned using data from termination 1 (chapter 4). It was found that in order to reproduce atmospheric CO_2 and $\delta^{13}C$ data (for atmosphere and ocean) during the termination, a combination of glacial ocean mechanisms and the permafrost-carbon mechanism was required. Following this finding, several glacial cycles were modelled to study the sensitivity of the permafrost-carbon mechanisms to CO_2, ice sheets and insolation (chapter 5). Ice sheet extent was found to be particularly important in controlling the land area available for permafrost and therefore the carbon dynamics of permafrost-carbon. The permafrost-carbon mechanism, via carbon release from thawing soils responding to increasing summer insolation in higher northern latitudes, was found to very likely be the source of initial rises in CO_2 on glacial terminations.

Termination 1 CO_2 data could be well reproduced, including the B-A/YD CO_2 plateau, when fresh water forcing was applied to the north Atlantic. Freshening the north Atlantic in the B-A/YD period resulted in northern hemisphere cooling and a permafrost advance and soil carbon uptake. On AMOC resumption fast heat transport to the northern hemisphere caused permafrost thaw and a fast rise in atmospheric CO_2. It was found that the rise in CO_2 at the start of the termination did not require an AMOC switch-off and resumption event as the source of the initial CO_2 rise was from the land, and the ocean only became a carbon source after around 15kyrBP.

Fresh water forcing experiments pointed to the importance of the permafrost-carbon mechanism in fast changing climates. Very fast increases in atmospheric CO_2 levels may be explained by fast soil-carbon release responding to increased heat transport to the northern hemisphere on AMOC resumption following an AMOC

switch-off/reduction event, such as D/O events seen in the Greenland $\delta^{18}O$ record. Future climate change projections represent fast warming events. Driving the model by emissions projections (RCP database) predicted increased peak CO_2 and much longer term elevated CO_2 levels relative to model outputs which did not include the permafrost carbon feedback.

Analysis of ocean $\delta^{13}C$ must take into account the dynamics of permafrost and land carbon in general and its effect on atmospheric $\delta^{13}C$ levels. If this is not taken into account then ocean circulation may be over-invoked in attempting to explain changes in ocean $\delta^{13}C$ and atmospheric CO_2. The Earth system is not simply atmosphere and ocean. The findings in this work highlight that it is essential to consider land carbon dynamics when interpreting paleo-indicators for the carbon cycle.

The permafrost-carbon mechanism reacts to temperature changes and amplifies the carbon cycle's response. It is stongly dependent not only on energy input (that determines soil temperature and permafrost location), but also on the area of land available globally on which it can exist. In order to properly model and understand the Earth system response to forcing in both future and past climates, the permafrost-carbon feedback mechanism is an important system component. This work has been a first step to address the role that the land cryosphere plays in the carbon cycle and climate system on long timescales, and further studies are essential.

Bibliography

Abe-Ouchi, A., Saito, F., Kawamura, K., Raymo, M.E., Okuno, J., Takahashi, K., Blatter, H. (2013). 'Insolation-driven 100,000-year glacial cycles and hysteresis of ice-sheet volume'. *Nature*, 500, doi: 10.1038/nature12374

Adams, J.M., Faure, H., Faure-Denard, L., McGlade, J.M., Woodward, F.I. (1990). 'Increases in terrestrial carbon storage from the Last Glacial maximum to the present.' *Nature* 348, 711–714.

Ahn, J., Brook, E.J. (2008). 'Atmospheric CO2 and climate on millennial time scales during the last glacial period.' *Science*, 322, 83. doi: 10.1126/science.1160832

Aleksandrova, L.N. (1970), 'Processes of humus formation in soil', *Proceedings of Leningrad Agricultural Institute*. Leningrad. 142, 26-82, 1970. In Russian

Alexeev VA., Nicolsky DJ., Romanovsky VE., Lawrence DM. (2007). 'An evaluation of deep soil configurations in the CLM3 for improved representation of permafrost.' *Geophysical Research Letters*. 34. L09502, doi:10.1029/2007GL029536

Antoine,P., Rousseau, DD., Degeai, JP., Moine O., Lagroix, F., Kruetzer, S., Fuchs, M., Hatte, C., Gauthier, C., Svoboda, J., Lisa, L. (2013). 'High Resolution record of the environmental response to climatic variations during the Last Interglacial-Glacil cycle in Central Europe: The loess-paleosol sequence of Dolni Vestonice (Czech Republic).' *Quaternary Science Reviews*, 67, 17-38

Archer, D. (2010) '*The Global Carbon Cycle*.' Princeton Primers in Climate, pub. Princeton University Press, 2010

Arrhenius, S. (1896). XXXI. 'On the influence of carbonic acid in the air upon the temperature of the ground.' *The London, Edinburgh, and Dublin Philosophical Magazine and Journal of Science*, 41(251), 237-276.

Baumler, R. and Zech, W. (2000). 'Quaternary paleosols, tephra deposits and landscape history in South Kamchatka, Russia.' *Catena*, 41, 199-215

Beerling, D.J., (1999), 'New estimates of carbon transfer to terrestrial ecosystems between the last glacial maximum and the Holocene.' *Terra Nova* 11, 162–167.

Berger, W.H., Vincent, E., (1986), 'Deep-sea carbonates: reading the carbon isotope signal.' *Geologische Rundschau* 75, 249–269.

Berger A. and Loutre M.F., (1991), 'Insolation values for the climate of the last 10 million of years.' *Quaternary Sciences Review*, Vol. 10 No. 4 pp. 297-317.

Berger, W. H. (2013). 'On the Milankovitch sensitivity of the Quaternary deep-sea record.' *Climate of the Past*, 9(4), 2003-2011.

Bethke, I., Camille, L., Nisancioglu, K.H. (2012). 'Can we use ice sheet reconstruction to constrain meltwater for deglacial simulations?' *Paleoceanography*. 27. PA2205, doi:10.1029/2011

Bird, M.I., Lloyd, J., Farquhar, G.D., (1994). 'Terrestrial carbon storage at the LGM.' *Nature* 371, 566.

Blinnikov, M., Gaglioti, B.V., Walker D.A., Wooller, M.J., Zazula, G.D. (2011). 'Pleistocene graminoid-dominated ecosystems in the Arctic.' *Quaternary Science Reviews*, 30, 2906-2929

Blunier, T., Chappellaz, J., Schwander, J., Dallenbach, A., Stauffer, B., Stocker, T.F, Raynaud, D., Jouzel, J., Clausen, H.B., Hammer, C.U., Johnsen, S.J. (1998). 'Asynchrony of Antarctic and Greenland climate change during the last glacial period.' *Nature*. 394. 739-743

Bond, G.C., Showers, W., Elliot, M., Evans, M., Lotti, R., Hajdas, I., Bonani, G., Johnson, S. (1999). 'The North Atlantics 1-2 kyr climate rhythm: Relation to Heinrich events, Dansgaard/Oeschger cycles and Little Ice Age'. *Geophysical Monograph* 112, 35-58

Bopp, L., Kohfeld, K.E., Le Quere, C. (2003). 'Dust impact on marine biota and atmospheric CO2 during glacial periods.' *Paleoceanography* 18: 2, 1046, doi: 10.1029/2002PA000810

Bouttes, N., Roche DM., Paillard D. (2009). 'Impact of strong deep ocean stratification on the glacial carbon cycle.' *Paleooceanography*. 24. PA3202. Doi: 10.1029/2008PA001707

Bouttes N., Paillard D., Roche DM., Brovkin V., Bopp L. (2011). 'Last Glacial Maximum CO2 and δ13C succesfully reconciled.' *Geophysical Research Letters*. 38, L02705, doi:10.1029/2010GLO44499

Bouttes, N., Paillard, D., Roche, D.M., Waelbroeck, C., Kageyama, M., Lourantou, A., Michel, E., Bopp, L. and Siddall, M., (2012) 'Impact of oceanic processes on the carbon cycle during the last termination.' *Climate of the Past*. 8, 1.

Bouttes, N., Roche, D.M., Paillard, D. (2012). 'Systematic study of the impact of fresh water fluxes on the glacial carbon cycle.' *Climate of the Past*. 8, 589-607

Boyle, J. F., Gaillard, M. J., Kaplan, J. O., & Dearing, J. A. (2011). 'Modelling prehistoric land use and carbon budgets: A critical review.' *The Holocene*, 0959683610386984.

Brewer, S., Guiot, J., Torre, F. (2007). 'Mid-Holocene climate change in Europe: a data-model comparison.' *Climate of the Past*: 3, 499-512.

Broecker, W.S. and Denton, G.H. (1989). 'The role of ocean-atmosphere reorganizations in glacial cycles.' *Geochimica et Cosmocimica Acta*, 53, 2465-2501.

Broecker, W.S., Peng, T-H., (1993). 'What caused the glacial to interglacial CO2 change.' In: Heimann, M. (Ed.), *The Global Carbon Cycle*, NATO ASI Series, Vol. 15. Springer, Berlin.

Brovkin V., Ganopolski A., Svirezhev Y. (1997). 'A continuous climate-vegetation classification for use in climate-biosphere studies.' *Ecological Modelling*. 101: 251-261

Brovkin, V., Claussen, M., Petoukhov, V., & Ganopolski, A. (1998). 'On the stability of the atmosphere-vegetation system in the Sahara/Sahel region.' *Journal of Geophysical Research: Atmospheres* (1984–2012), 103(D24), 31613-31624.

Brovkin, V., Bendtsen, J., Claussen, M., Ganopolski, A., Kubatzki, C., Patoukhov, V., Andreev, A., (2002a), 'Carbon cycle, Vegetation and climate dynamics in the Holocene: Experiments with the CLIMBER-2 model', *Global Biogeochemical Cycles*, 164, 1139, doi:10.1029/2001GB001662.

Brovkin, V., M. Hofmann, J. Bendtsen, and A. Ganopolski, (2002b), 'Ocean biology could control atmospheric δ13C during glacial interglacial cycle,' *Geochem. Geophys. Geosyst.*, 35, 10.1029/2001GC000270.

Brovkin, V., Levis, S., Loutre, M. F., Crucifix, M., Claussen, M., Ganopolski, A., Kubatzki, C., Petoukhov, V. (2003). 'Stability analysis of the climate-vegetation system in the northern high latitudes.' *Climatic Change*, 57(1-2), 119-138.

Brovkin, V., A. Ganopolski, D. Archer, and S. Rahmstorf. (2007), 'Lowering of glacial atmospheric CO2 in response to changes in oceanic circulation and marine biogeochemistry,' *Paleoceanography*, 22, PA4202, doi:10.1029/2006PA001380.

Brovkin, V., Ganopolski, A., Archer, D., & Munhoven, G. (2012). 'Glacial CO 2 cycle as a succession of key physical and biogeochemical processes.' *Climate of the Past*, 8(1), 251-264.

Carlson, A. E., and P. U. Clark (2012), 'Ice sheet sources of sea level rise and freshwater discharge during the last deglaciation', *Rev. Geophys*., 50, RG4007, doi:10.1029/2011RG000371.

Carter and Colman, (1994) 'Biogenic Silica in Lake Baikal Sediments: Results From 1990–1992 American Cores.' *Journal of Great Lakes Research*, Volume 20, Issue 4, Pages 751-760

Chappellaz, J., Barnola, J.M., Raynaud, D., Korotkevich, Y.S., Lorius, C. (1990). 'Ice-core record of atmospheric methane over the past 160,000 years.' *Nature*, 345:127-131

Chlachula, J., & Little, E. (2011): 'A high-resolution Late Quaternary climatostratigraphic record from Iskitim, Priobie Loess Plateau, SW Siberia.' *Quaternary International*, 240(1), 139-149,.

Christensen, T.R., Mastepanov, M., Johansson, M., Charman, D., 2010, 'Peatland exchanges of CO2 and CH4: The importance of presence or absence of permafrost', Pages, 181, 29-31.

Ciais P., Tagliabue A., Cuntz M., Bopp L., Scholze M., Hoffman G., Lourantou A., Harrison SP., Prentice IC., Kelley DI., Koven C., Piao SL. (2012). 'Large inert carbon pool in the terrestrial biosphere during the Last Glacial Maximum.' *Nature Geoscience*. 5: 74. doi: 10.1038/NGEO1324.

Ciais, P., C. Sabine, G. Bala, L. Bopp, V. Brovkin, J. Canadell, A. Chhabra, R. DeFries, J. Galloway, M. Heimann, C. Jones, C. Le Quéré, R.B. Myneni, S. Piao and P. Thornton. (2013) 'Carbon and Other Biogeochemical Cycles.' In: *Climate Change 2013: The Physical Science Basis. Contribution of Working Group I to the Fifth Assessment Report of the Intergovernmental Panel on Climate Change* [Stocker, T.F., D. Qin, G.-K. Plattner, M. Tignor, S.K. Allen, J. Boschung, A. Nauels, Y. Xia, V. Bex and P.M. Midgley (eds.)]. Cambridge University Press, Cambridge, United Kingdom and New York, NY, USA.

Clark, P. U., Alley, R. B., & Pollard, D. (1999). 'Northern Hemisphere ice-sheet influences on global climate change.' *Science*, 286(5442), 1104-1111.

Clark, P.U., and Mix, A.C. (2002). 'Ice sheets and sea level of the Last Glacial Maximum.' *Quaternary Science Reviews*. 21: 1-7

Clark, P.U., Shakun, J.D., Baker, P.A., Bertlein, P.J., Brewer, S., Brook, E., Carlson, A.E., Cheng, H., Kaufman, D.S., Liu, Z., Marchitto, T.M., Mix, A.C., Morrill, C., Otto-Bliesner, B.L., Pahnke, K., Russell, J.M., Whitlock, C., Adkins, J.F., Blois, J.L., Clark, J., Colman, S.M., Curry, W.B., Flower, B.P., He, F., Johnson, T.C., Lynch-Stieglitz, J., Markgraf, V., McManus, J., Mitrovica, J.X., Moreno, P.I., Williams, J.W. (2012). 'Global climate evolution during the last deglaciation.' *PNAS*. Doi:10.1073/pnas.1116619109

Clarke, L., J. Edmonds, H. Jacoby, H. Pitcher, J. Reilly, R. Richels, (2007). 'Scenarios of Greenhouse Gas Emissions and Atmospheric Concentrations.' Sub-report 2.1A of *Synthesis and Assessment Product 2.1* by the U.S. Climate Change Science Program and the Subcommittee on Global Change Research. Department of Energy, Office of Biological & Environmental Research, Washington, 7 DC., USA, 154 pp.

Claussen, M., Mysak, L., Weaver, A., Crucifix, M., Fichefet, T., Loutre, M. F., ... & Wang, Z. (2002). 'Earth system models of intermediate complexity: closing the gap in the spectrum of climate system models.' *Climate Dynamics*, 18(7), 579-586.

Collins, M., R. Knutti, J. Arblaster, J.-L. Dufresne, T. Fichefet, P. Friedlingstein, X. Gao, W.J. Gutowski, T. Johns, G. Krinner, M. Shongwe, C. Tebaldi, A.J. Weaver and M. Wehner, (2013): 'Long-term Climate Change: Projections, Commitments and Irreversibility.' In: *Climate Change 2013: The Physical Science Basis. Contribution of Working Group I to the Fifth Assessment Report of the Intergovernmental Panel on Climate Change* [Stocker, T.F., D. Qin, G.-K. Plattner, M. Tignor, S.K. Allen, J. Boschung, A. Nauels, Y. Xia, V. Bex and P.M. Midgley (eds.)]. Cambridge University Press, Cambridge, United Kingdom and New York, NY, USA, 2013.

Crichton, K.A., Chappellaz, J., Krinner, G., Roche, D. (2014). 'A simplified Permafrost-Carbon model for long-term long term climate studies with the CLIMBER-2 coupled Earth system model.' *Geoscientific Model Development Discussions*. 7, 4931-4992, 2014

Crowley, T.J., (1995). 'Ice age terrestrial carbon changes revisited.' *Global Biogeochemical Cycles,* 9, 377–389.

Curry, W.B., Duplessy, J.-C., Labeyrie, L.D., Shackleton, N.J., (1988). 'Changes in the distribution of δ13C of deep water SCO2 between the last glacial and the Holocene.' *Paleoceanography,* 3, 317–341.

Curry, W. B. and Oppo, D. W. (2005): 'Glacial water mass geometry and the distribution of δ13C of SUM CO2 in the western Atlantic Ocean', *Paleoceanography*, 20, PA1017, doi:10.1029/2004PA001021.

Dankers R., Burke EJ., Price J. (2011). 'Simulation of permafrost and seasonal thaw depth in the JULES land surface scheme.' *The Cryosphere*. 5:773-790. doi: 10.5194/tc-5-773-2011

DeConto, R. M., Galeotti, S., Pagani, M., Tracy, D., Schaefer, K., Zhang, T., ... & Beerling, D. J. (2012). 'Past extreme warming events linked to massive carbon release from thawing permafrost.' *Nature*, 484(7392), 87-91.

Denton, G. H., Anderson, R. F., Toggweiler, J. R., Edwards, R. L., Schaefer, J. M., & Putnam, A. E. (2010). 'The last glacial termination.' *Science*, 328(5986), 1652-1656.

Duplessy, J.-C., Shackleton, N.J., Matthews, R.K., Prell, W., Ruddiman, W.F., Caralp, M., Hendy, C.H., (1984). '13C record of benthic foraminifera in the last interglacial ocean: implications for the carbon cycle and the global deep water circulation.' *Quaternary Research* 21, 225–243.

Duplessy, J.-C., Shackleton, N.J., Fairbanks, R.J., Labeyrie, L.D., Oppo, D., Kallel, N., (1988). 'Deep water source variations during the last climatic cycle and their impact on the global deep water circulation.' *Paleoceanography* 3, 343–360

Ekici, A., Beer, C., Hagemann, S., Boike, J., Langer, M., and Hauck, C. (2014). 'Simulating high-latitude permafrost regions by the JSBACH terrestrial ecosystem model', *Geosci. Model Dev.*, 7, 631-647, doi:10.5194/gmd-7-631-2014, 2014.

Elias, S.A and Crocker, B. (2008). 'The Bering land-bridge: a moisture barrier to the dispersal of steppe-tundra biota?' *Quaternary Science Reviews*. 27, 2473-2483

Elliot, M., Labeyrie, L., Duplessy, J.-C. (2002). 'Changes in North Atlantic deep-water formation associated with the Dansgaard-Oeschger temperature oscillations (60-10ka).' *Quaternary Science Reviews*, 21, 1153-1165.

Elsig, J., Schmitt, J., Leuenberger, D., Schneider, R., Eyer, M., Leuenberger, M., Joos, F., Fischer, H., Stocker, T.F. (2009). 'Stable isotope constraints on Holocene carbon cycle changes from an Antarctic ice core.' *Nature*. 461, doi: 10.1038/nature08393

EPICA community members, (2004), 'Eight glacial cycles from an Antarctic ice core.' *Nature*. 429, 623-628.

Eugster, W., Rousem W.R., Peilke Sr, R.A., McFadden, J.P., Baldocchi, D.D., Kittle, T.G.F., Chapin III, F.S., Liston, G.E., Vidale, P.L., Vaganov, E., Chambers, S. (2000). 'Land-atmosphere energy exchange in Arctic tundra and boreal forest: available data and feedbacks to climate.' *Global Change Biology*. 6 Suppl.1, 84-115

Fischer, H., Behrens, M., Bock, M., Richter, U., Schmitt, J., Loulergue, L., ... & Stocker, T. F. (2008). 'Changing boreal methane sources and constant biomass burning during the last termination.' *Nature*, 452(7189), 864-867.

Fischer, H., Schmitt, J., Luthi, D., Stocker, T.F., Tschumi T., Parekh, P., Joos, F., Kohler, P., Volker, C., Gersonade, R., Barbante, C., Le Floch, M., Raynaud, D., Wolff, E. (2010). 'The role of Southern Ocean processes in orbital and millennial CO2 variations – A synthesis.' *Quaternary Science Reviews*, 29, 193-205

Foley, J. A., Coe, M. T., Scheffer, M., & Wang, G. (2003). 'Regime shifts in the Sahara and Sahel: interactions between ecological and climatic systems in Northern Africa.' *Ecosystems*, 6(6), 524-532.

Foster, G. L., & Vance, D. (2006). 'Negligible glacial–interglacial variation in continental chemical weathering rates.' *Nature*, 444(7121), 918-921.

Francois, L.M., Delire, C., Warnant, P., Munchoven, G., (1998). 'Modelling the glacial-interglacial changes in continental biosphere.' *Global Planetary Change,* 16–17 1–4, 37–52.

Frechen, M. (2011). 'Loess in Eurasia.' *Quaternary International*, 234(1), 1-3.

French, H. (2008). 'Recent contributions to the study of past permafrost.' *Permafrost and Periglacial processes*, 19, 179-194.

French, H.M. and Millar, SWS. (2013). 'Permafrost at the time of the Last Glacial Maximum (LGM) in North America.' *Boreas*, doi:10.1111/bor.12036.

Friedlingstein, C., Delire, C., Muller, J.F., Gerard, J.C., (1992). 'The climate induced variation of the continental biosphere: a model simulation of the last glacial maximum.' *Geophysical Research Letters.* 19, 897–900.

Fujino, J., R. Nair, M. Kainuma, T. Masui, Y. Matsuoka, 2006. Multi-gas mitigation analysis on stabilization scenarios using AIM global model. Multigas Mitigation and Climate Policy. The Energy Journal Special Issue.

Gallimore, R., Jacob, R., & Kutzbach, J. (2005). 'Coupled atmosphere-ocean-vegetation simulations for modern and mid-Holocene climates: role of extratropical vegetation cover feedbacks.' *Climate Dynamics*, 25(7-8), 755-776.

Ganopolski A., Petoukhov V., Rahmstorf S., Brovkin V., Claussen M., Eliseev A., Kubatzki C. (2001). 'CLIMBER-2: a climate system model of intermediate complexity. Part II: model sensitivity.' *Climate Dynamics*. 17: 735-751

Ganopolski, A., Roche, D.M., (2009), 'On the nature of lead-lag relationships during glacial-interglacial climate transitions.' *Quaternary Science Reviews*. 28, 2261-2278.

Ganopolski, A., Calov, R., & Claussen, M. (2010). 'Simulation of the last glacial cycle with a coupled climate ice-sheet model of intermediate complexity.' *Climate of the Past*, 6(2), 229-244.

Ganopolski, A., & Calov, R. (2011). 'The role of orbital forcing, carbon dioxide and regolith in 100 kyr glacial cycles.' *Climate of the Past*, 7(4), 1415-1425.

Gersonde, R., Crosta, X., Abelmann, A., Armand, L., (2005). 'Sea-surface temperature and sea ice distribution of the Southern Ocean at the EPILOG Last Glacial Maximum – a circum-Antarctic view based on siliceous microfossil records.' *Quaternary Science Reviews*, 24, 869–896.

Godwin, H. (1962). 'Half-life of radiocarbon.' *Nature* 195, 984. Doi:10.1038/195984a0

Gouttevin, I., Menegoz, M., Dominé, F., Krinner, G., Koven, C., Ciais, P., Tarnocai, C..,and Boike, J. (2012). 'How the insulating properties of snow affect soil carbon distribution in the continental pan-Arctic area.' *Journal of Geophysical Research: Biogeosciences* (2005–2012), 117(G2), 2012.

Grygar, T., Kadlec, J., Pruner, P., Swann, G., Bezdicka, P., Hradil, D., Lang, K., Novotna, K., Oberhansli, H. (2006). 'Paleoenvironmental record in Lake Baikal sediments: Environmental changes in the last 160 kyr.' *Palaeogeography, Palaeoclimatiology, Palaeoecology*, 237, 240-254

Guthrie, R.D. (1990) *Frozen fauna of the mammoth steppe. The story of Blue Babe*. Univ. of Chicago Press, Chicago.

Haarpaintner, J., J. C. Gascard, and P. M. Haugan (2001), 'Ice production and brine formation in Storfjorden, Svalbard,' *J. Geophys. Res*., 106, 14,001–14,013.

Harden, J.W., Koven, C.D., Ping, C., Hugelius, G., McGuire, A.D., Camill, P., Jorgenson, T., Kuhry, P., Michaelson, G.J., O'Donnell, J.A., Schuur, E.A.G, Tarnocai, C., Johnson, K., Grosse, G. (2012). 'Field Information links permafrost carbon to physical vulnerabilities of thawing.' *Geophysical Research Letters*. 39, L15704, doi: 10.1029/2012GL051958

Harrison, S.P., and Sanchez Goni, M.F. (2010). 'Global patterns of vegetation response to millennial-scale variability and rapid climate change during the last glacial period.' *Quaternary Science Reviews*, 29, 2957-2980.

Hays, J.D., Imbrie, J., Shackelton, N.J., (1976), 'Variations in the Earth's orbit: Pacemaker of the Ice Ages.' *Science, New Series*. 194 (4270), 1121-1132.

Hemming, S.R. (2005). 'Heinrich events: Massive later Pleistocene detritus layers of the north Atlantic and their global imprint.' *Review of Geophysics*, 42, RG1005, 2003RG000128.

Hijioka, Y., Y. Matsuoka, H. Nishimoto, M. Masui, and M. Kainuma, (2008). 'Global GHG emissions scenarios under GHG concentration stabilization targets.' *Journal of Global Environmental Engineering* 13, 97-108.

Hobbie, S.E., Schimel, J.P., Trumbore, S.E. (2000). 'Controls over carbon storage and turnover in high-latitude soils.' *Global Change Biology*. 6 Suppl.1, 1960210

Hofle, C., Edwards, M.E., Hopkins, D.M., Mann, D.H. (2000). 'The full-glacial environment of the northern Seward peninsula Alaska, reconstruction from the 21,500-year-old Kitluk Paleosol.' *Quaternary Research*, 53, 143-153.

Hugelius, G., Tarnocai, C., Broll, G., Canadell, J. G., Kuhry, P., and Swanson, D. K. (2013). 'The Northern Circumpolar Soil Carbon Database: spatially distributed datasets of soil coverage and soil carbon storage in the northern permafrost regions', *Earth System Science Data*, 5, 3-13, doi:10.5194/essd-5-3-2013

Ikeda, T., Tajika, E., (2002), 'Carbon cycling and climate change during the last glacial cycle inferred from the isotope records using an ocean biogeochemical carbon cycle', *Global and Planetary Change*, 35, 131-141.

Imbrie, J., Boyle, E. A., Clemens, S. C., Duffy, A., Howard, W. R., Kukla, G., ... & Toggweiler, J. R. (1992). 'On the structure and origin of major glaciation cycles 1. Linear responses to Milankovitch forcing.' *Paleoceanography*, 7(6), 701-738.

Inoue, Y., Nagaoka, S., Sugiyama, S. (2011). 'Late Plesitocene buried humic soils within a tephra-soil sequence near Unzen volcan, Kyushu, Japan.' *Quaternary International*, 246, 233-238.

IPA website, http://ipa.arcticportal.org/

Jahn, A., Claussen, M., Ganopolski, A., & Brovkin, V. (2005). 'Quantifying the effect of vegetation dynamics on the climate of the Last Glacial Maximum.' *Climate of the Past Discussions*, 1(1), 1-16.

Jakobsson, M., Nilsson, J., O'Regan, M., Backman, J., Löwemark, L., Dowdeswell, J. A., ... & Wallin, Å. (2010). 'An Arctic Ocean ice shelf during MIS 6 constrained by new geophysical and geological data.' *Quaternary Science Reviews*, 29(25), 3505-3517.

Jamieson T.F, (1862). 'On the Ice-worn rocks of Scotland.' *Quarterly Journal of the Geological Society*, February 1862, v.18, 164-184. doi: 10.1144/GSL.JGS.1862.018.01-02.30

Janssen, R.H.H., Meinders, M.B.J., Van Nes, E.H. and Scheffer, M. (2008). 'Microscale vegetation-soil feedback boosts hysteresis in a regional vegetation–climate system.' *Global Change Biology*, 14: 1104–1112. doi: 10.1111/j.1365-2486.2008.01540.x

Johnsen, S. J., Dahl-Jensen, D., Gundestrup, N., Steffensen, J. P., Clausen, H. B., Miller, H., Masson-Delmotte, V., Sveinbjo¨ rnsdottir, A. E. and White, J. (2001). 'Oxygen isotope and palaeotemperature records from six Greenland ice-core stations: Camp Century, Dye-3, GRIP, GISP2, Renland and NorthGRIP'. *J. Quaternary Sci*., Vol. 16, pp. 299–307. ISSN 0267-8179.

Jones, A., V. Stolbovoy, C. Tarnocai, G. Broll, O. Spaargaren and L. Montanarella (eds.), (2009) *Soil Atlas of the Northern Circumpolar Region*. European Commission, Office for Official Publications of the European Communities, Luxembourg. 142 pp.

Jones, M.C., Yu, Z., (2010), 'Rapid deglacial and early holocene expansion of peatlands in Alaska', *PNAS*, 107 16, 7347-7352.

Jouzel, J. et al. (2007). 'Orbital and millenial Antarctic climate variability over the past 800,000 years.' *Science*. 317, 793-796

Kageyama, M., Paul, A., Roche, D.M., Van Meerbeeck, C.J. (2010). 'Modelling glacial climatic millenial-scale variability related to changes in the Atlantic meridional overturning circulation:a review.' *Quaternary Science Reviews*. 29: 2931-2956

Kaplan, J., Prentice, I.C., Knorr, W., Valdes, P.J., (2002). 'Modeling the dynamics of terrestrial carbon stroage since the LGM.' *Geophysical Research Letters* 29, 2074, doi:10.1029/2002GL015230.

Kaufmann, R. K., & Juselius, K. (2013). 'Testing hypotheses about glacial cycles against the observational record.' *Paleoceanography*, 28(1), 175-184.

Kawamura, K. et al.. (2007). 'Northern Hemisphere forcing of climatic cycles in Antarctica over the past 360,000 years.' *Nature*, 448, doi: 10.1038/nature06015

Khvorostyanov, D. V., Krinner, G., Ciais, P., Heimann, M., & Zimov, S. A. (2008)a. 'Vulnerability of permafrost carbon to global warming. Part I: model description and role of heat generated by organic matter decomposition.' *Tellus B*, 60(2), 250-264.

Khvorostyanov, D. V., Ciais, P., Krinner, G., Zimov, S. A., Corradi, C., & Guggenberger, G. (2008)b. 'Vulnerability of permafrost carbon to global warming. Part II: sensitivity of permafrost carbon stock to global warming.' *Tellus B*, 60(2), 265-275.

Köhler, P., & Fischer, H. (2006). 'Simulating low frequency changes in atmospheric CO2 during the last 740 000 years.' *Climate of the Past*, 2(2), 57-78.

Kohler, P., Fischer, H., Schmitt, J., (2010) 'Atmospheric δ13CO2 and its relation to pCO2 and deep ocean δ13C during the late Pleistocene', *Paleoceanography*, 25, doi:10.1029/2008PA001703.

Köhler, P., Knorr, G., Buiron, D., Lourantou, A., & Chappellaz, J. (2011). 'Abrupt rise in atmospheric CO2 at the onset of the Bølling/Allerød: in-situ ice core data versus true atmospheric signal.' *Climate of the Past*, 7(2), 473-486.

Kopp, R. E., Simons, F. J., Mitrovica, J. X., Maloof, A. C., & Oppenheimer, M. (2009). 'Probabilistic assessment of sea level during the last interglacial stage.' *Nature*, 462(7275), 863-867.

Koven C., Friedlingstein P., Ciais P., Khvorostyanov D., Krinner G., Tarnocai C. (2009). 'On the formation of high-latitude soil carbon stocks: Effects of cryoturbation and insulation by organic matter in a land surface model.' *Geophysical Research Letters*. 36. L21501. Doi: 10.1029/2009GL040150

Koven, C. D., Riley, W. J., & Stern, A. (2013). 'Analysis of permafrost thermal dynamics and response to climate change in the CMIP5 Earth System Models.' *Journal of Climate*, 26(6), 1877-1900.

Koven, C.D., Ringeval, B., Friedlingstein, P., Ciais, P., Cadule, P., Khvorostyanov, D., Krinner, G., Tarnocai, C. (2011). 'Permafrost carbon-climate feedbacks accelerate global warming.' *PNAS*. 108, 14769-14774

Krinner, G., & Werner, M. (2003). 'Impact of precipitation seasonality changes on isotopic signals in polar ice cores: a multi-model analysis.' *Earth and Planetary Science Letters*, 216(4), 525-538.

Kröpelin, S., Verschuren, D., Lézine, A. M., Eggermont, H., Cocquyt, C., Francus, P., ... & Engstrom, D. R. (2008). 'Climate-driven ecosystem succession in the Sahara: the past 6000 years.' *Science*, 320(5877), 765-768.

Kump, L.R and Arthur, M.A. (1999). 'Interpreting carbon-isotope: carbonates and organic matter.' *Chemical Geology*. 161: 181-198.

Kurahashi-Nakamura, T., Abe-Ouchi, A., Yamanaka, Y., (2010), 'Effects of physical changes in the ocean on the atmospheric pCO2: glacial-interglacial cycles', *Climate Dynamics*, 35, 713-719.

Kwon, E. Y., Sarmiento, J. L., Toggweiler, J. R., & DeVries, T. (2011). 'The control of atmospheric pCO2 by ocean ventilation change: The effect of the oceanic storage of biogenic carbon.' *Global Biogeochemical Cycles*, 25(3).

Laskar, J., Robutel, P., Joutel, F., Gastineau, M., Correia, A. C. M., & Levrard, B. (2004). 'A long-term numerical solution for the insolation quantities of the Earth.' *Astronomy & Astrophysics*, 428(1), 261-285.

Laepple, T., Werner, M., Lohmann, G. (2011). 'Synchronicity of Antarctic temperatures and local solar insolation on orbital timescales.' *Nature*. Doi:10.1038/nature09825

Lemieux-Dudon, B., Blayo, E., Petit, J., Waelbroeck, C., Svensson, A., Ritz, C., Barnola, J., Narcisi, B M., Parrenin, F. (2010). 'Consistent dating for Antarctic and Greenland ice cores.' *Quaternary Science Reviews*. 29, 8-20.

Levavasseur G., Vrac M., Roche DM., Paillard D., Martin A., Vandenberghe J. (2011). 'Present and LGM permafrost from climate simulations: contribution of statistical downscaling.' *Climate of the Past*. 7: 1225-1246. doi: 10.5194/cp-7-1225-2011

Lisiecki, L. E., & Raymo, M. E. (2005). 'A Pliocene-Pleistocene stack of 57 globally distributed benthic δ18O records.' *Paleoceanography*, 20(1).

Lisiecki, L., Raymo, M.E., Curry, W.B. (2008). 'Atlantic overturning responses to Late Pleistocene climate forcings.' *Nature*. 464. doi:10.1038/nature07425

Liu, Z., et al. (2009). 'Transient simulation of last deglaciation with a new mechanism for the Bolling-Allerod warming.' *Science*, 325, 310. doi: 10.1126/science.1171041.

Liu, Z., Carlson, A. E., He, F., Brady, E. C., Otto-Bliesner, B. L., Briegleb, B. P., ... & Zhu, J. (2012). 'Younger Dryas cooling and the Greenland climate response to CO2.' *Proceedings of the National Academy of Sciences*, 109(28), 11101-11104.

Lourantou, Lavric, J.V., Kohler, P., Barnola, JM., Paillard, D., Michel, E., Raynaud, D., Chappelaz, J. (2010). 'Constraint of the CO2 rise by new atmospheric carbon isotopic measurements during the last deglaciation', *Global Biogeochemical Cycles*, 24, BG2015, doi:10.1029/2009GB003545.

Lourantou, A., Chappellaz, J., Barnola, J-M., Masson-Delmotte, V., Raynaud, D., (2010), 'Changes in atmospheric CO2 and its carbon isotope ratio during the penultimate deglaciation.' *Quaternary Science Reviews*, 29, 1983-1992.

Lourens, L. J., Sluijs, A., Kroon, D., Zachos, J. C., Thomas, E., Röhl, U., ... & Raffi, I. (2005). 'Astronomical pacing of late Palaeocene to early Eocene global warming events.' *Nature*, 435(7045), 1083-1087.

Licciardi, J. M., Teller, J. T., & Clark, P. U. (1999). 'Freshwater routing by the Laurentide Ice Sheet during the last deglaciation.' *Mechanisms of global climate change at millennial time scales*, 177-201.

Lund, D. C., Adkins, J. F., & Ferrari, R. (2011). 'Abyssal Atlantic circulation during the Last Glacial Maximum: Constraining the ratio between transport and vertical mixing.' *Paleoceanography*, 26(1).

Luo, Y., Francois, R., Allen, S.E. (2010). 'Sediment 231Pa/230Th as a recorder of the rate of the Atmatic meridional overturning circulation: insights from a 2-D model.' *Ocean Science*. 6, 381-400.

Lupker, M., France-Lanord, C., Galy, V., Lavé, J., & Kudrass, H. (2013). 'Increasing chemical weathering in the Himalayan system since the Last Glacial Maximum.' *Earth and Planetary Science Letters*, 365, 243-252.

Lüthi, D., et al.. (2008). EPICA Dome C Ice Core 800KYr Carbon Dioxide Data. IGBP PAGES/World Data Center for Paleoclimatology Data Contribution Series # 2008-055. NOAA/NCDC Paleoclimatology Program, Boulder CO, USA

Lüthi, D., Le Floch, M., Bereiter, B., Blunier, T., Barnola, J. M., Siegenthaler, U., ... & Stocker, T. F. (2008). 'High-resolution carbon dioxide concentration record 650,000–800,000 years before present.' *Nature*, 453(7193), 379-382.

Lynch-Stieglitz, J., Stocker, T.F., Broecker, W.S., Fairbanks, R.G. (1995). 'The influence of air-sea exchange in the isotopic composition oc oceanic carbon: Observations and modeling.' *Global Biogeochemical Cycles*. 9 4, 653-665.

Ma, Y., Liu, K. B., Feng, Z., Meng, H., Sang, Y., Wang, W., & Zhang, H. (2013). 'Vegetation changes and associated climate variations during the past～ 38,000 years reconstructed from the Shaamar eolian-paleosol section, northern Mongolia.' *Quaternary International*, 311, 25-35.

Marchal, O., Stocker, T. F., & Joos, F. (1998). 'A latitude-depth, circulation-biogeochemical ocean model for paleoclimate studies. Development and sensitivities.' *Tellus B*, 50(3), 290-316.

MARGO Project Members (2009). 'Constraints on the magnitude and patterns of ocean cooling at the Last Glacial Maximum.' *Nature Geoscience*., 2, 127–132, doi:10.1038/ngeo411.

Marshall, J., & Speer, K. (2012). 'Closure of the meridional overturning circulation through Southern Ocean upwelling.' *Nature Geoscience*. doi:10.1038/ngeo1391

Martikainen, P. J., Nykänen, H., Alm, J., & Silvola, J. (1995). 'Change in fluxes of carbon dioxide, methane and nitrous oxide due to forest drainage of mire sites of different trophy.' *Plant and Soil*, 168(1), 571-577.

Maslin, M.A., Thomas, E. (2003). 'Balancing the deglacial global carbon budget: the hydrate factor', *Quaternary Science Reviews*, 22, 1729-1736

Mason, J.A., Miao, X., Hanson, P.R., Johnson, W.C., Jacobs, P.M., Goble, R.J. (2008). 'Loess record of the Pleistocene-Holocene transition on the northern and central Great Plains, USA.' *Quaternary Science Reviews*, 27, 1772-1783.

McGuire, A.D., Anderson, L., Christensen, T.R., Dallmore, S., Guo, L., Hayes, D.J., Loresnson, T.D., Macdonald, R.W., Roulet, N., (2009), 'Sensitivity of the carbon cycle in the Arctic to climate change', *Ecological Monographs*, 794, 523-555.

McManus, J.F., Francois, R., Gherardi, J.-M., Keigwin, L.D., Brown-Leger, S. (2004). 'Collapse and rapid resumption of Atlantic meridional circulation linked to deglacial climate changes.' *Nature*. 428, 834-837

Melton, J. R., Schaefer, H., & Whiticar, M. J. (2012). 'Enrichment in 13 C of atmospheric CH 4 during the Younger Dryas termination.' *Climate of the Past*, 8(4), 1177-1197.

Menviel, L., Timmermann, A., Mouchet, A., Timm, O., (2008), 'Climate and marine carbon cycle response to changes in the strength of the southern hemispheric westerlies', *Paleoceanography*, 23, PA 4201, doi:10.1029/2008PA001604

Menviel, L., Timmermann, A., Timm, O. E., & Mouchet, A. (2011). 'Deconstructing the Last Glacial termination: the role of millennial and orbital-scale forcings.' *Quaternary Science Reviews*, 30(9), 1155-1172.

Menviel, L., & Joos, F. (2012). 'Toward explaining the Holocene carbon dioxide and carbon isotope records: Results from transient ocean carbon cycle-climate simulations.' *Paleoceanography*, 27(1).

Milankovitch, M. (1941). 'Kanon der Erdbestrahlung und seine Anwendung auf das Eiszeitproblem'. *Akad. R. Serbe* 133, 1–633

Monnin, E., Indermühle, A., Dällenbach, A., Flückiger, J., Stauffer, B., Stocker, T. F., Raynaud, D.,and Barnola, J. M. (2001). 'Atmospheric CO2 concentrations over the last glacial termination.' *Science*, 291(5501), 112-114.

Montenegro, A., Eby, M., Kaplan, J.O., Meissner, K.J., Weaver, A.J. (2006). 'Carbon storage on exposed continental shelves during the glacial-interglacial transition.' *Geophysical Research Letters*. 33, L08703, doi: 10.1029/2005GL025480

Morice, C. P., Kennedy, J. J., Rayner, N. A., & Jones, P. D. (2012). 'Quantifying uncertainties in global and regional temperature change using an ensemble of observational estimates: The HadCRUT4 data set.' *Journal of Geophysical Research: Atmospheres (1984–2012)*, 117(D8).

Morozova, T.D., Velichko A.A., Dlussky, K. (1998). 'Organic carbon content in the late Pleistocene and Holocene fossil soils reconstruction for Eastern Europe.' *Global and Planetary Change*. 16-17, 131-151.

Morse PD., Burn CR. (2010). 'Ground temperature variation with snow, Kendall Island Bird Sanctuary, outer Mackenzie Delta. Northwest Territories.' *GEO2010*.

Munhoven, G. (2002). 'Glacial–interglacial changes of continental weathering: estimates of the related CO2 and HCO3− flux variations and their uncertainties.' *Global and Planetary Change*, 33(1), 155-176.

Natali, S.M., Schuur, E.A.G., Trucci, C., Hicks Pries, C.E., Crummer, K.G., Lopez, A.F.B. (2011). 'Effects of experimental warming of air, soil and permafrost on carbon balance in Alaskan tundra.' *Global Change Biology*. 17, 1394-1407. doi: 10.1111/j.1365-2486.2010.02303.x

Natali SM., Schuur EAG., Rubin RL. (2012). 'Increased plant productivity in Alaskan tundra as a result of experimental warming of soil and permafrost.' *Journal of Ecology.* 100: 488-498. doi: 10.1111/j.1365-2745.2011.01925.x

Nelson FE., Outcalt SI. (1987). 'A computational method for perdiction and regionalization of permafrost.' *Arctic and Alpine Research*. 19(3): 279-288.

NGRIP members. (2004). 'High-resolution record of northern hemisphere climate extending into the last interglacial period.' *Nature*. 431, 147-151

Oliver, K. I. C., Hoogakker, B. A. A., Crowhurst, S., Henderson, G. M., Rickaby, R. E. M., Edwards, N. R. and Elderfield, H. (2010). 'A synthesis of marine sediment core 13C data over the last 150 000 years.' *Climate of the Past*, 6, pp. 645–673.

Osterkamp, T. E., and C. R. Burn (2003), 'Permafrost', in *Encyclopedia of Atmospheric Sciences*, edited by J. R. Holton, pp. 1717–1729, Academic, Oxford, U. K., doi:10.1016/B0-12-227090-8/00311-0.

Otto, D., Rasse, D., Kaplan, J., Warnant, P., Francois, L., (2002). 'Biospheric carbon stocks reconstructed at the last glacial maximum.' *Global and Planetary Change* 33, 117–138.

Overduin, P. P., Hubberten, H. W., Rachold, V., Romanovskii, N., Grigoriev, M., & Kasymskaya, M. (2007). 'The evolution and degradation of coastal and offshore permafrost in the Laptev and East Siberian Seas during the last climatic cycle.' *Geological Society of America Special Papers*, 426, 97-111.

Parrenin, F., Barnola, J. M., Beer, J., Blunier, T., Castellano, E., Chappellaz, J., ... & Wolff, E. (2007). 'The EDC3 chronology for the EPICA Dome C ice core.' *Climate of the Past*, 3(3), 485-497.

Parrenin, F., Masson-Delmotte, V., Köhler, P., Raynaud, D., Paillard, D., Schwander, J., ... & Jouzel, J. (2013). 'Synchronous change of atmospheric CO2 and Antarctic temperature during the last deglacial warming.' *Science*, 339(6123), 1060-1063.

Peltier WR. (1994). 'Ice Age Paleotopography.' *Science*. 265 (5169): 195-201

Peltier, W. R. (2004). 'Global glacial isostasy and the surface of the ice-age Earth: The ICE-5G (VM2) Model and GRACE.' *Ann. Rev. Earth Planet*. Sci., 32, 111–149, doi:10.1146/annurev.earth.32.082503.144359.

Peng, C.H., Guiot, J., Van Campo, E., (1995). 'Reconstruction of the past terrestrial carbon storage of the Northern Hemisphere from the Osnabrueck biosphere model and palaeodata.' *Climate Research* 5, 107–118.

Petit, J.R., Jouzel, J., Raynaud, D., Barkov, N.I., Barnola, JM., Basile, I., Benders, M., Chappelaz, J., Davis, M., Delaygue, G., Delmotte, M., Kotlyakov, V.M., Legrand, M., Lipenkov, V.Y., Lorius, C., Pepin, L., Ritz, C., Saltzman, E., Stievenard, M., 1999, 'Climate and atmospheric history of the past 420,000 years from the Vostok ice core, Antarctica.', Nature, 399, 429-439.

Petoukhov V., Ganopolski A., Brovkin V., Claussen M., Eliseev A., Kubatzki C., Rahmstorf S. (2000). 'CLIMBER-2: a climate system model of intermediate complexity. Part 1: model description and performance for present climate.' *Climate Dynamics*. 16:1-17

Pfiefer, M., Disney, M., Quaife, T., Marchant, R. (2012). 'Terrestrial ecosystems from space: a review of earth observation products for macroecology applications.' *Global Ecology and Biogeography.* 21, 603-624.

Prentice, I.C, Harrison, S. P., Jolly, D., & Guiot, J. (1998). 'The climate and biomes of Europe at 6000 yr BP:: comparison of model simulations and pollen-based reconstructions.' *Quaternary Science Reviews*, 17(6-7), 659-668.

Prentice, I.C., Harrison, S.P., Bartlein, P.J. (2011). 'Global vegetation and terrestrial carbon cycle changes after the last ice age.' *New Phytologist*. 189, 988-998. doi: 10.1111/j.1469-8137.2010.03620.x

Prokopenko, et al. (2001). 'Biogenic silica record of the lake Baikal response to climatic forcing during the Brunhes.' *Quaternary Research*. 55, 123-132.

Quinn, T. R., Tremaine, S., & Duncan, M. (1991). 'A three million year integration of the Earth's orbit.' *The Astronomical Journal*, 101, 2287-2305.

Rahmstorf, S. (2002). 'Ocean circulation and climate during the past 120,000 years.' *Nature*, 419(6903), 207-214.

Rau, G.H., Riebesell, U., Wolf-Gladrow, D. (1991). 'A model of photosynthetic 13C fractionation by marine phytoplankton based on diffusive molecular CO2 uptake.' *Marine Ecology*. Doi: 10.3354/meps133275.

Raymo, M. E., Ruddiman, W. F., & Froelich, P. N. (1988). 'Influence of late Cenozoic mountain building on ocean geochemical cycles.' *Geology*, 167, 649-653.

RCP database http://www.iiasa.ac.at/web-apps/tnt/RcpDb

Renssen, H., Isarin, R., Vendenberghe, J., Lautenschlager, M., Schlese, U., (2000), 'Permafrost as a critical factor in paleoclimate modelling: the Younger Dryas case in Europe', *Earth and Planetary Science Letters*, 176, 1-5.

Renssen, H., Vendenberghe, J. (2003). 'Investigation of the relationship between permafrost distribution in NW Europe and extensive winter sea-ice cover in the North Atlantic Ocean during the cold phases of the Last Glacial.' *Quaternary Science Reviews*, 22, 209-223

Riahi, K. Gruebler, A. and Nakicenovic N. (2007). 'Scenarios of long-term socio-economic and environmental development under climate stabilization.' *Technological Forecasting and Social Change* 74, 7, 887-935.

Ridgwell, A., Maslin, M., & Kaplan, J. O. (2012). 'Flooding of the continental shelves as a contributor to deglacial CH4 rise.' *Journal of Quaternary Science*, 27(8), 800-806.

Riseborough D., Shiklomanov N., Etzelmuller B., Gruber S., Marchenko S. (2008). 'Recent advances in permafrost modelling.' *Permafrost and Periglacial Processes*. 19: 137-156

Ritz, S.P., Stocker, T.F., Grimalt, J.O., Menviel, L., Timmermann, A. (2013). 'Estimated strength of the Atlantic overturning circulation during the last deglaciation.' *Nature Geoscience*, doi: 10.1038/NGEO1723.

Roche, D.M., Renssen, H., Paillard, D., Levavasseur, G., (2011), 'Deciphering the spatio-temporal complexity of climate change of the last deglaciation: a model analysis', *Climate of the Past*, 7, 591-602.

Rodionov, A., Flessa, H., Grabe, M., Kazansky, O.A., Shibistova, O., and Guggenberger, G. (2007). 'Organic carbon and total nitrogen variability in permafrost-affected soils in a forest tundra ecotone.' *European journal of soil science*, 58, no. 6, 1260-1272.

Rodionow, A., Flessa, H., Kazansky, O., & Guggenberger, G. (2006). 'Organic matter composition and potential trace gas production of permafrost soils in the forest tundra in northern Siberia.' *Geoderma*, 135, 49-62.

Rose, K.A., Sikes, E.L., Guilderson, T.P., Shane, P., Hill, T.M., Zahn, R., Spero, H.J., (2010), 'Upper-ocean-to-atmosphere radiocarbon offsets imply fast deglacial carbon dioxide release', *Nature*, doi:10.1038/nature09288.

Roth, R., F. Joos, (2012) 'Model limits on the role of volcanic carbon emissions in regulating glacial-interglacial CO2 variations', *Earth and Planetary Science Letters*, 329-330, 141-149.

Roucoux, K. H., Tzedakis, P. C., Lawson, I. T. and Margari, V. (2011), 'Vegetation history of the penultimate glacial period (Marine isotope stage 6) at Ioannina, north-west Greece.' *J. Quaternary Sci.*, 26: 616–626. doi: 10.1002/jqs.1483

Ruddiman, W.F. (2003). 'The anthropogenic greenhouse era began thousands of years ago.' *Climatic Change*, 61, 261-293.

Ruddiman, W.F. (2007). 'The early anthropogenic hypothesis: Challenges and Responses.' *Reviews of Geophysics*, 45, RG4001, doi: 10.1029/2006RG000207.

Ruddiman, W. F., Kutzbach, J. E., & Vavrus, S. J. (2011). 'Can natural or anthropogenic explanations of late-Holocene CO2 and CH4 increases be falsified?'. *The Holocene*, 0959683610387172.

Rutter, N.W., Rokosh, D., Evans, M.E., Little, E.C., Chlachula, J., Velichko, A. (2003). 'Correlation and interpretation of paleosols and loess across European Russia and Asia over the last interglacial-glacial cycle.' *Quaternary Research*, 60, 101-109.

Saito, K., T. Sueyoshi, S. Marchenko, V. Romanovsky, B. Otto-Bliesner, J. Walsh, N. Bigelow, A. Hendricks, and K. Yoshikawa. (2013). 'LGM permafrost distribution: how well can the latest PMIP multi-model ensembles perform reconstruction?' *Climate of the Past*. 9, 4.

Sanchez-Goñi. (2010). 'Millennial-scale climate variability and vegetation changes during the last glacial: Concepts and terminology.' *Quaternary Science Reviews*. 29, 2823-2827.

Schaefer K., Zhang T., Bruhwiler L., Barrett AP. (2011). 'Amount and timing of permafrost carbon release in response to climate warming.' *Tellus*. Doi: 10.1111/j.1600-0889.2011.00527.x

Shakhova, N., Semiletov, I., Salyuk, A., Yusupov, V., Kosmach, D., & Gustafsson, Ö. (2010). 'Extensive methane venting to the atmosphere from sediments of the East Siberian Arctic Shelf.' *Science*, 327(5970), 1246-1250.

Schaphoff S., Heyder U., Ostberg S., Gerten D., Heinke J., Lucht W. (2013). 'Contribution of permafrost soils to the global carbon budget.' *Environmental Research Letters*. 8: 014026. doi: 10.1088/1748-9326/8/1/014026

Schirrmeister, L., Grosse, G., Wetterich, S., Overduin, P.P., Strauss, J., Schuur, E.A.G., Hubberten, HW. (2011). 'Fossil organic matter characteristics in permafrost deposits of the northeast Siberian Arctic.' *Journal of Geophysical Research*. 116. G00M02, doi: 10.1029/2011JG001647

Schmitt, J., Schneider, R., Elsig, J., Leuenberger, D., Lourantou, A., Chappellaz, J., Kohler, P., Joos, F., Stocker, T.F., Leuenberger, M. and Fischer, H. (2012). 'Carbon isotope constraints on the deglacial CO2 rise from ice cores.' *Science*, 336(6082), 711-714.

Schmitt, J., Seth, B., Köhler, P., Willenbring, J., & Fischer, H. (in prep). 'Atmospheric CF4 trapped in polar ice–A new proxy for granite weathering.' Presented at Goldschmidt conference 2013

Schneider von Diemling T., Ganopolski A., Held H., Rahmstorf S. (2012). 'How cold was the Last Glacial Maximum?' *Geophysical Research Letters*. 33. L14709. Doi: 10.1029/2006GL026484

Schneider von Diemling, T., Meinhausen, M., Levermann, A., Huber, V., Frieler, K., Lawrence, D.M., Brovkin, V. (2012). 'Estimating the near-surface permafrost-carbon feedback on global warming.' *Biogeosciences*. 9, 649-665

Schneider, R., Schmitt, J., Köhler, P., Joos, F., and Fischer, H. (2013). 'A reconstruction of atmospheric carbon dioxide and its stable carbon isotopic composition from the penultimate glacial maximum to the last glacial inception.' *Clim. Past*, 9, 2507-2523, doi:10.5194/cp-9-2507-2013.

Schuur, E., Bockheim, J., Canadell, J., Euskirchen, E., Field, C.B., Goryachkin, S.V., Hagemann, S., Kuhry, P., Lafleur, P.M., Lee, H., Mazhitova, G., Nelson, F.E., Rinke, A., Romanovsky, V.E., Shiklomanov, N., Tarnokai, C., Venevsky, S., Vogel, J.G., Zimov, S.A., (2008), 'Vulnerability of permafrost to climate change: Implications for the global carbon cycle', *BioScience*, 588, 701-714.

Schuur EAG., Vogel JG., Crummer KG., Lee H., Sickman JO., Osterkamp TE. (2009). 'The effect of permafrost thaw on old carbon release and net carbon exchange from tundra.' *Nature*. 459. doi: 10.1038/nature08031

Schuur, E. A. (2013). 'High risk of permafrost thaw.' *Nature*, 480, 32-33, 2011.

Shackleton, N.J. (1977). 'Carbon 13 in Uvigerina: tropical rain forest history and the equatorial Pacific carbonate dissolution cycles.' In: Anderson, R.L.N. and Malaho, A. (eds), *The Fate of Fossil Fuel CO2 in the Oceans*, pp. 401-427. Plenum, New York.

Shakun, J.D., Clark, P.U., He, F., Marcott, S.A., Mix, A.C., Liu, Z., Otto-Bliesner, B., Schmittner, A., Bard. (2012). 'Global warming preceded by increasing carbon dioxide concentratons during the last deglaciation.' *Nature*. 484. doi:10.1038/nature10915

Sher, A.V., Kuzmina, S.A., Kuznetsova, T.V., Sulerhutsky, L.D. (2005). 'New insights into the Weichselian environment and climate of the East Siberian Arctic, derived from fossil insects, plants and mammals.' *Quaternary Science Reviews*. 24: 533-569

Sigman, D.M. and Boyle, E.A. (2000). 'Glacial/interglacial variations in atmospheric carbon dioxide.' *Nature*. 407, 859-869

Sigman, D.M., Hain, M., Haug, G.H., (2010), 'The polar ocean and glacial cycles in atmospheric CO2 concentration', *Nature*, 446, doi:10.1038/nature09149

Sitch, S., Smith, B., Prentice, I. C., Arneth, A., Bondeau, A., Cramer, W., ... & Venevsky, S. (2003). 'Evaluation of ecosystem dynamics, plant geography and terrestrial carbon cycling in the LPJ dynamic global vegetation model.' *Global Change Biology*, 9(2), 161-185.

Skinner, L.C., Fallon, S., Waelbroeck, C., Michel, E., Barker, S., (2010), 'Ventilation of the deep southern ocean and deglacial CO2 rise', *Science*, 328,1147, DOI: 10.1126/science.1183627

Smith, H. J., Fischer, H., Wahlen, M., Mastroianni, D., & Deck, B. (1999). 'Dual modes of the carbon cycle since the Last Glacial Maximum.' *Nature*, 4006741, 248-250.

Smith, S.J. and T.M.L. Wigley, (2006). 'Multi-Gas Forcing Stabilization with the MiniCAM.' *Energy Journal Special Issue #3* pp 373-391.

Sowers, T., and Bender, M. (1995). 'Climate records covering the last deglaciation.' *Science*, 269 (5221), 210-214.

Stanford, J.D., Rohling, E.J., Bacon, S., Roberts, A.P., Grousset, F.E., Bolshaw, M. (2011). 'A new concept for the paleoceanographic evolution of Heinrich event 1 in the North Atlantic.' *Quaternary Science Reviews*. 30. 1047-1066.

Stanford, J.D., Rohling, E.J., Hunter, S.E., Roberts, A.P., Rasmussen, S.O., Bard, E., McManus, J., Fairbanks, R.G. (2006). 'Timing of meltwater pulse 1a and climate responses to meltwater injections.' *Paleoceanography*. 21. PA4103. Doi: 10.1029/2006PA001340

Stocker, B. D., Strassmann, K., and Joos, F. (2011). 'Sensitivity of Holocene atmospheric CO2 and the modern carbon budget to early human land use: analyses with a process-based model', *Biogeosciences*, 8, 69-88, doi:10.5194/bg-8-69-2011.

Stocker, T.F., D. Qin, G.-K. Plattner, M. Tignor, S.K. Allen, J. Boschung, A. Nauels, Y. Xia, V. Bex and P.M. Midgley (eds.), IPCC, (2013): 'Climate Change 2013: The Physical Science Basis.' Contribution of Working Group I to the Fifth Assessment Report of the Intergovernmental Panel on Climate Change Cambridge University Press, Cambridge, United Kingdom and New York, NY, USA, 1535 pp, 2013.

Strack, M. Ed, (2008). *Peatlands and Climate Change*, International Peat Society, Vapaudenkatu 12, 40100 Jyväskylä, Finland

Strack, M., & Price, J. S. (2009). 'Moisture controls on carbon dioxide dynamics of peat-Sphagnum monoliths.' *Ecohydrology*, 2(1), 34-41.

Strassmann, K. M., Joos, F., & Fischer, G. (2008). 'Simulating effects of land use changes on carbon fluxes: past contributions to atmospheric CO2 increases and future commitments due to losses of terrestrial sink capacity.' *Tellus B*, 60(4), 583-603.

Svendsen, J. I., Alexanderson, H., Astakhov, V. I., Demidov, I., Dowdeswell, J. A., Funder, S., ... & Stein, R. (2004). 'Late Quaternary ice sheet history of northern Eurasia.' *Quaternary Science Reviews*, 23(11), 1229-1271.

Tagliabue, A., Bopp, L., Roche, D.M., Bouttes, N., Dutay, J.-C., Alkama, R., Kageyama, M., Michel, E., Paillard, D., (2009), 'Quantifying the roles of ocean circulation and biogeochemistry in governing ocean carbon-13 and atmospheric carbon dioxide at the last glacial maximum', *Climate of the Past*, 5, 695-706.

Taras B., Sturm M., Liston GE. (2002). 'Snow-ground interface temperatures in the Kupuruk River Basin, Arctic Alaska: measurements and model.' *Journal of Hydrometeorology*. 3: 377-394

Tarasov, L. and Peltier, W.R. (2005). 'Arctic freshwater forcing of the Younger Dryas cold reversal.' *Nature*. 435. doi:10.1038/nature03617.

Tarnocai C., Canadell JG., Schuur EAG., Kuhry P., Mazhitova G., Zimov S. (2009). 'Soil organic carbon pools in the northern circumpolar permafrost region.' *Global Biogeochemical Cycles*. 23. GB2023. Doi: 10.1029/2008GB003327

Trucco C., Schuur EAG., Natali SM., Belshe EF., Bracho R., Vogel J. (2012). 'Seven-year trends of CO2 exchange in a tundra ecosystem affected by long-term permafrost thaw.' *Journal of Geophysical Research*. 117. G02031. Doi: 10.1029/2011JG001907

Vaks, A., Gutareva, O.S, Breitenbach, S.F.M., Avirmed, E., Mason, A.J., Thomas, A.L., Osinzev, A.V., Kononov, A.M., Henderson, G.M. (2013). 'Speleothems reveal 500,000 year history of Siberian permafrost.' *Science*, 340, 183, doi: 10.1126/science.1228729.

Van Campo, E., Guiot, J., Peng, C.H. (1993). 'A data-based re-appraisal of the terrestrial carbon budget at the last glacial maximum.' *Global and Planetary Change* 8, 189–201.

Van Huissteden J., Dolman AJ. (2012). 'Soil carbon in the Arctic and the permafrost carbon feedback.' *Environmental Sustainability*. 4: 545-551.

Van Vuuren, D., M. den Elzen, P. Lucas, B. Eickhout, B. Strengers, B. van Ruijven, S. Wonink, R. van Houdt, (2007). 'Stabilizing greenhouse gas concentrations at low levels: an assessment of reduction strategies and costs.' *Climatic Change*, doi:10.1007/s/10584-006-9172-9.

Vandenberghe, J. (2001). 'Permafrost during the Pleistocene in north west and central Europe.' In *Permafrost response on economic development, environmental security and natural resources* (pp. 185-194). Springer Netherlands.

Vandenberghe, J., Velichko, A., and Gorbunov, A. (2008). 'Forcing factors of permafrost retreat: a comparison between LGM and present-day permafrost extent in Eurasia.' edited by: Kane, D. L. and Hinkel, K. M., 9th Int. Conf. Permafrost Fairbanks, 327–328.

Vavrus S. (2007). 'The role of terrestrial snow cover in the climate system.' *Climate Dynamics*. 29: 73-88. doi: 10.1007/s00382-007-0226-0

Velichko, A.A., Borisova, O.K., Zelikson, E.M., Morozova, T.D. (2010). 'Dynamics of carbon storage in phytomass and soil humus in Northern Eurasia during the last climatic macrocycle.' *Global and Planetary Change*. 72, 257-264.

Wadham, J. L., S. Arndt, S. Tulaczyk, M. Stibal, M. Tranter, J. Telling, G. P. Lis et al. (2012). 'Potential methane reservoirs beneath Antarctica.' *Nature* 488, 7413, 633-637.

Wania R., Ross I., Prentice IC. (2009a). 'Intergrated peatlands and permafrost into a dynamic global vegetation model: 1. Evaluation and sensitivity of physical land surface processes.' *Global Biogeochemical Cycles*. 23. GB3014. Doi: 10.1029/2008GB003412

Wania R., Ross I., Prentice IC. (2009b). 'Intergrated peatlands and permafrost into a dynamic global vegetation model: 2. Evaluation and sensitivity of vegetation and carbon cycle processes.' *Global Biogeochemical Cycles.* 23. GB3015. Doi: 10.1029/2008GB003413

Wickland, K.P., Striegl, R.G., Neff, J.C., Sachs, T. (2006). 'Effects of permafrost melting on CO2 and CH4 exchange of a poorly drained black spruce lowland.' *Journal of Geophysical Research*. 111. G02011, doi: 10.1029/2005JG000099

Willerslev, E., Davison, J., Moora, M., Zobel, M., Coissac, E., Edwards, M.E., Lorenzen, E.D., et al. (2014). 'Fifty thousand years of Arctic vegetation and megafaunal diet.' *Nature*, 506, 7486 47-51.

Wilschut, F., Bintanja, R., & Van de Wal, R. S. (2006). 'Ice-sheet modelling characteristics in sea-level-based temperature reconstructions over the last glacial cycle.' *Journal of glaciology*, 52(176), 149-158.

Wise, MA, KV Calvin, AM Thomson, LE Clarke, B Bond-Lamberty, RD Sands, SJ Smith, AC Janetos, JA Edmonds. (2009). 'Implications of Limiting CO2 Concentrations for Land Use and Energy.' *Science*. 324:1183-1186. May 29, 2009.

Wolff, E. W.; Fischer, H.; Fundel, F.; Ruth, U.; Twarloh, B.; Littot, G.; Mulvaney, R.; Röthlisberger, R.; de Angelis, M.; Boutron, C.; Hansson, M.; Jonsell, U.; Hutterli, M.; Bigler, M.; Lambert, F.; Kaufmann, P.; Stauffer, B.; Steffensen, J. P.; Siggaard-Andersen, M. L.; Udisti, R.; Becagli, S.; Castellano, E.; Severi, M.; Wagenbach, D.; Barbante, C.; Gabrielli, P.; Gaspari, V. (2006). 'Southern Ocean sea-ice extent,productivity and iron flux over the pasteight glacial cycles.' *Nature*. 440:doi:10.1038/nature04614

Yu, Z., Loisel, J., Brosseau, D.P., Beilman, D.W., Hunt, S.J. (2010). 'Global peatland dynamics since the Last Glacial Maximum.' *Geophysical Research Letters*. 37, L12402, doi: 10.1029/2010GL043584

Yu, Z., Beilman, D.W., Frolking, S., MacDonald, G.M., Roulet, N.T., Camill, P., Charman, D.J., (2011), 'Peatlands and their role in the global carbon cycle', *EOS*, 9212, 97-98.

Zachos, J., Pagani, M., Sloan, L., Thomas, E., Billups, K. (2001). 'Trends, Rhythms and Aberrations in the global climate 65Ma to present.' *Science*, 292, 686-693

Zech, R., Huang, Y., Zech, M., Tarozo, R., Zech, W., (2011), 'High carbon sequestration in Siberian permafrost loess-paleosols during glacials', *Climate of the Past*, 7, 501-509.

Zeng, N. (2003). 'Glacial-interglacial atmospheric CO2 change—The glacial burial hypothesis.' *Advances in Atmospheric Sciences*, 20(5), 677-693.

Zech, R., Zech, M., Markovic, S., Hambach, U., Huang, Y. (2013). 'Humid glacials, arid interglacials? Critical thoughts in pedogenesis and paleoclimate based on multi-proxy analyses of the loess-paleosol sequence Crvenka, Northern Serbia.' *Palaeogeography, Palaeoclimatology, Palaeoecology.* 387, 165-175.

Zhang T. (1998). *Global Annual Freezing and Thawing Indices*. Boulder, Colorado USA: National Snow and Ice Data Center.

Zhang T., Heginbottom JA., Barry RG., Brown J. (2000). 'Further statistics on the distribution of permafrost and ground ice in the Northern Hemisphere.' *Polar Geography*. 24:2, 126-131. doi 10.1080/10889370009377692

Zhang T. (2005). 'Influence of the seasonal snow cover on the ground thermal regime. An overview.' *Reviews of Geophysics*. 43. RG4002. Doi: 8755-1209/05/2004RG000157

Zhao, M., Running, S., Heinsch, F. A., & Nemani, R. (2011). 'MODIS-derived terrestrial primary production.' In: *Land Remote Sensing and Global Environmental Change* (pp. 635-660). Springer New York.

Zimov, S.A., Schuur, E., Chapin III.,F.S., (2006), 'Permafrost and the global carbon budget', *Science*, 312, 1612-1613.

Zimov NS., Zimov SA., Zimova AE., Zimova GM., Chuprynin VI., Chappin III FS. (2009). 'Carbon storage in permafrost and soils of the mammoth tundra-steppe biome: Role in the global carbon budget.' *Geophysical Research Letters*. 36. L02502. Doi:10.1029/2008GL036332.

Zimov, S. A., Zimov, N. S., Tikhonov, A. N., & Chapin III, F. S. (2012). 'Mammoth steppe: a high-productivity phenomenon.' *Quaternary Science Reviews*, 57, 26-45.

Zickfeld, K. et al. (2013). 'Long term climate change commitment and reversibility: An EMIC intercomparison.' *Journal of Climate*. 26, doi: 10.1175/JCLI-D-12-00584.1

Chapter 6 supplemetary material

The transient fresh water forcing to create the best-fit for the CO_2 record was identified from a series of deglaciation simulations in which different forcing profiles were applied. A first forcing profile was based on the Bethke et al. 2012 paper which estimates fresh water release from ice sheet melt (using ice 5G model) for the deglaciation period. Further forcing profiles were based on the results from the first experiment and results from the StT experiment output. From the CO_2 output of the previous, a new forcing was created and deglaciation simulation was carried out with the new forcing profile. A series of ten forcings were applied as NH fresh water input before the forcing profile used in the paper was identified. Six forcings were also applied during the deglaciation employing southern hemisphere fresh water hosing. For selected forcing settings the no permafrost case was tested and the the brines switch-off at 18kyrBP was tested with and without the permafrost mechanism.

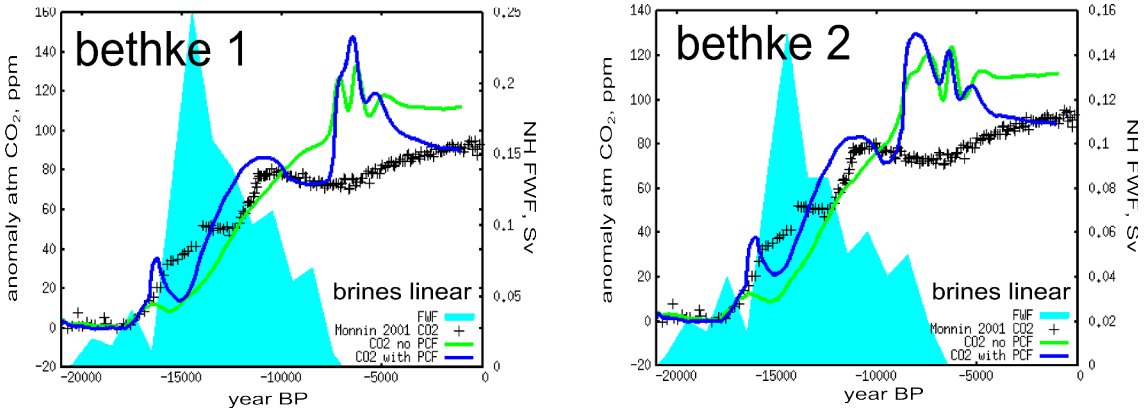

Fig 1, Bethke et al. 2012 based estimates of fresh water input forcing to the Arctic, applied in the N Atlantic region.

The Bethke et al 2012 based output, figure 1, suggests that fresh water forcing of this magnitude is too high, resulting in a large CO_2 overshoot after forcing ceases. This is the case for both the model with and without permafrost-carbon operating. This is in agreement with studies in which the location of fresh-water forcing is particularly important for AMOC response.

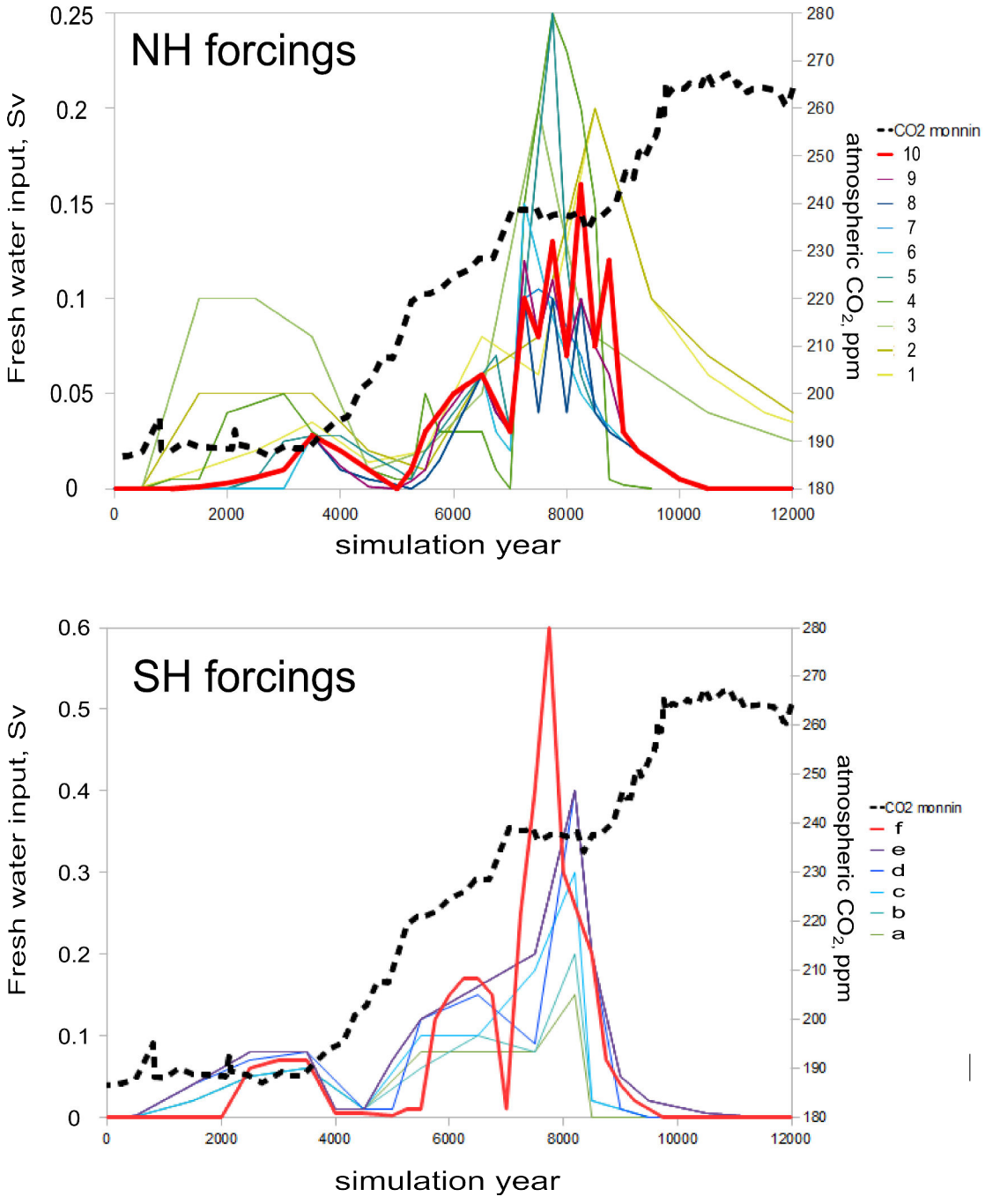

Fig 2, Forcing profiles plotted per hemisphere forcing. The CO_2 record is a a comparison to show the timing of maximum FWFs.

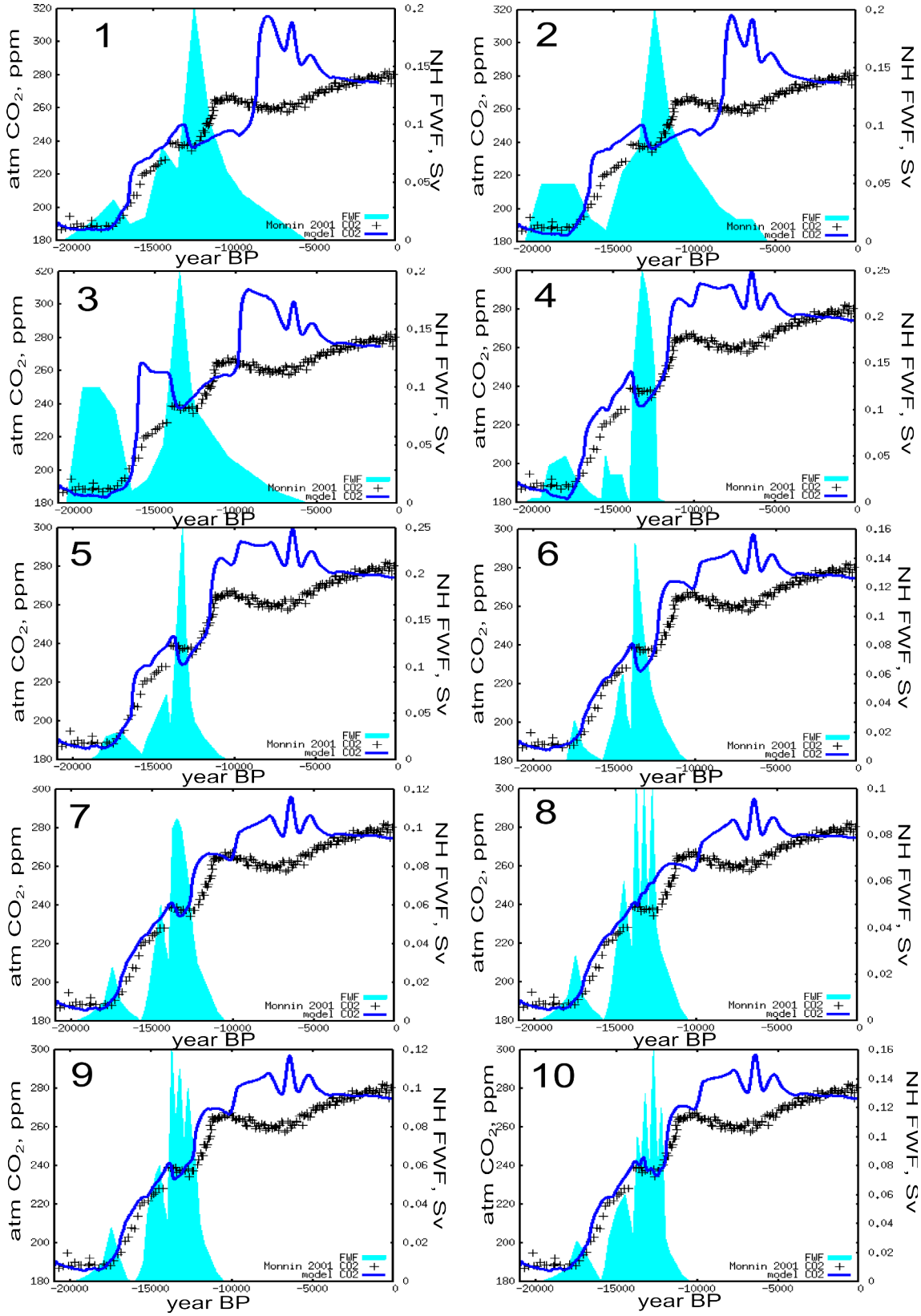

Fig 3, Northern Hemisphere FWF experiment outputs for the linear brines with permafrost-carbon operating.

Tuning the FWF profiles (figure 2) for the NH hemisphere resulted in a setting (10) in which the CO_2 record for the period between 21kyrBP to 10kyrBP can be quite well reproduced (figure 3). The SH FWF (figure 4) can also produce a good fit with data for the period 21kyrBP to 12kyrBP, but requires far higher fresh water input, which does not have a good agreement with rates and total fresh water release into the southern hemisphere from the Bethke et al. 2012 study.

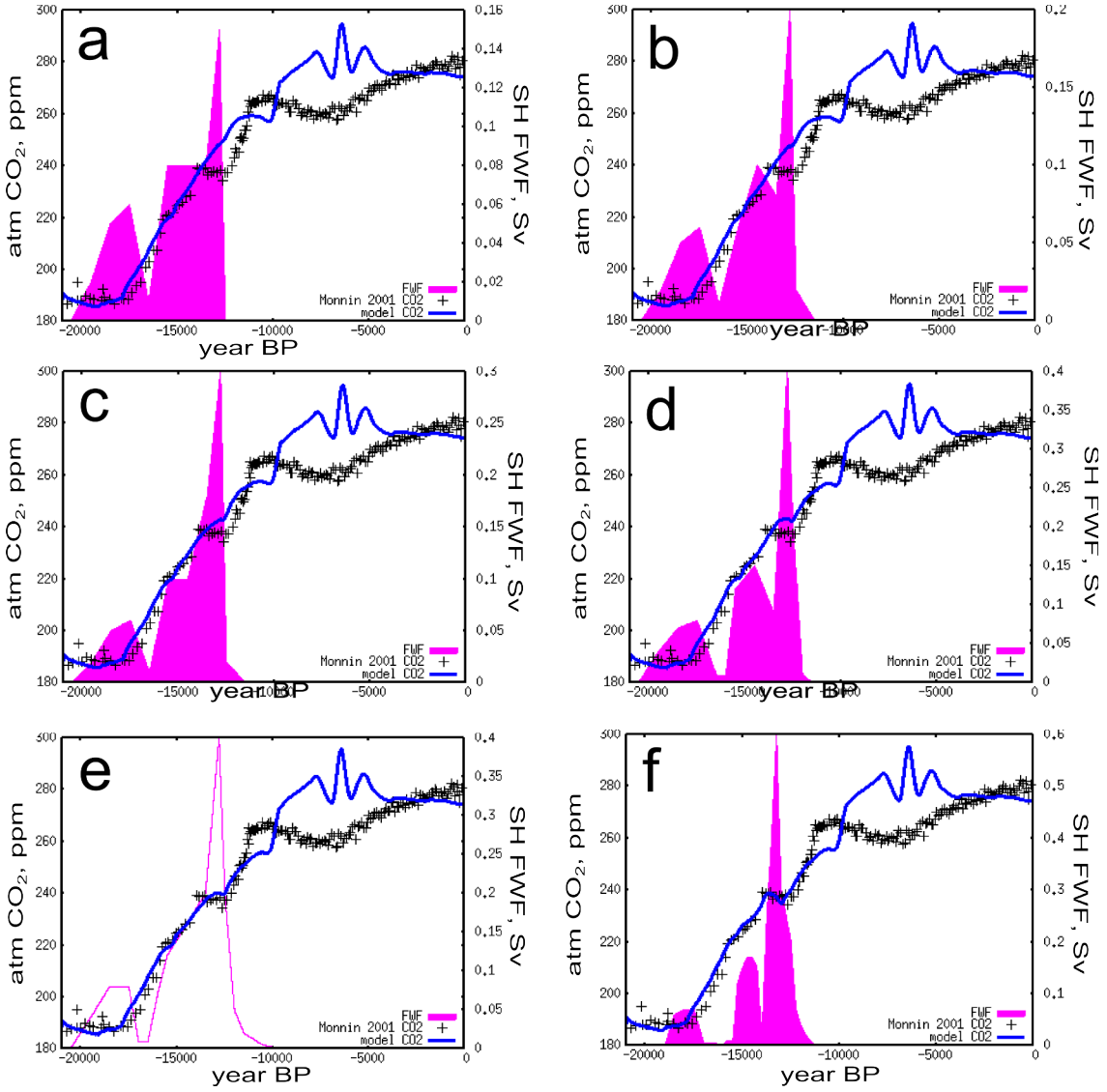

Fig 4, Southern Hemisphere FWF experiment outputs for the linear brines with permafrost-carbon operating

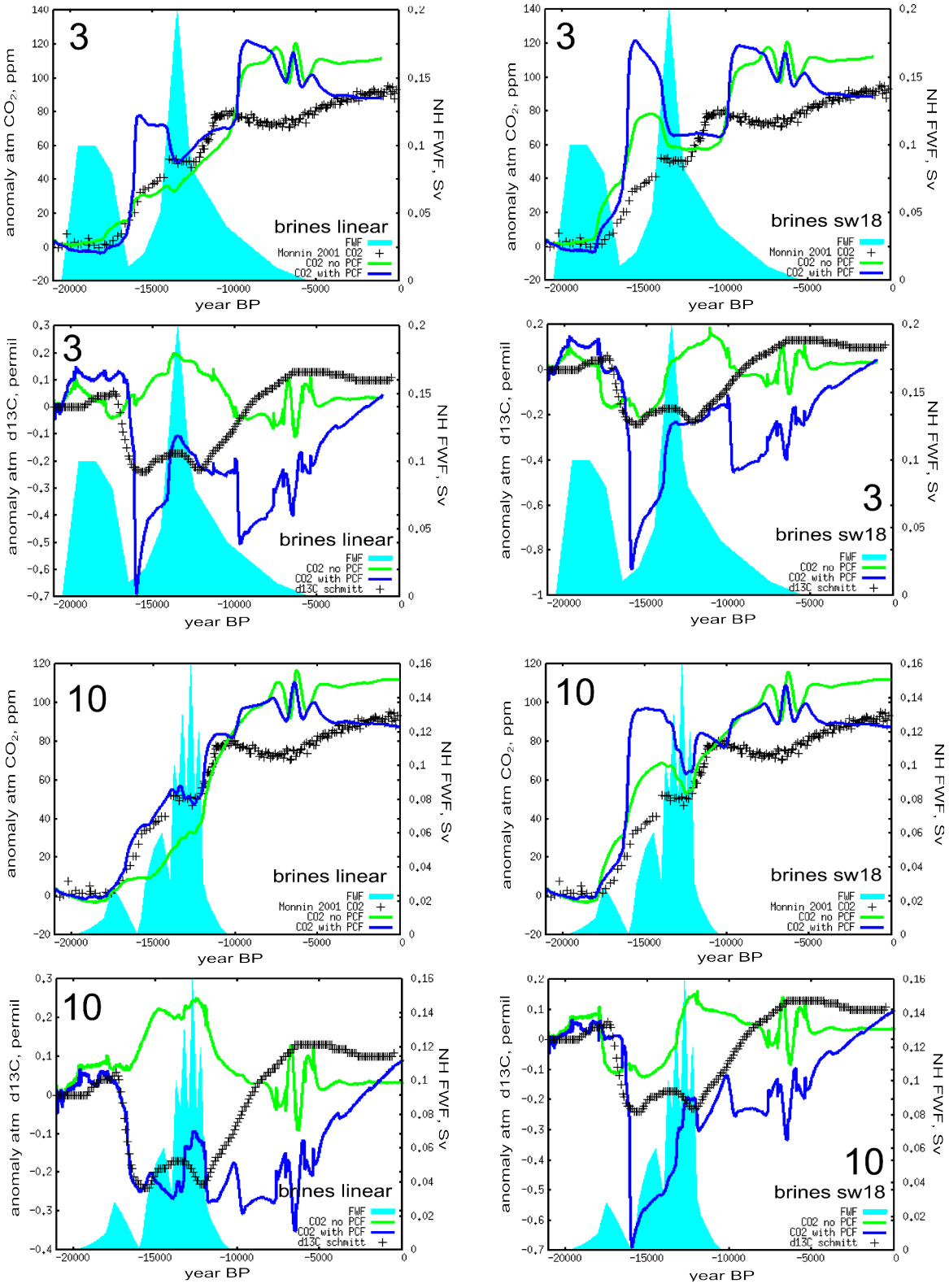

Fig 5, two NH FWF profile outputs comparing model with (blue) and without (green) permafrost for left: linear brines. Right: brines switch-off at 18kyrBP

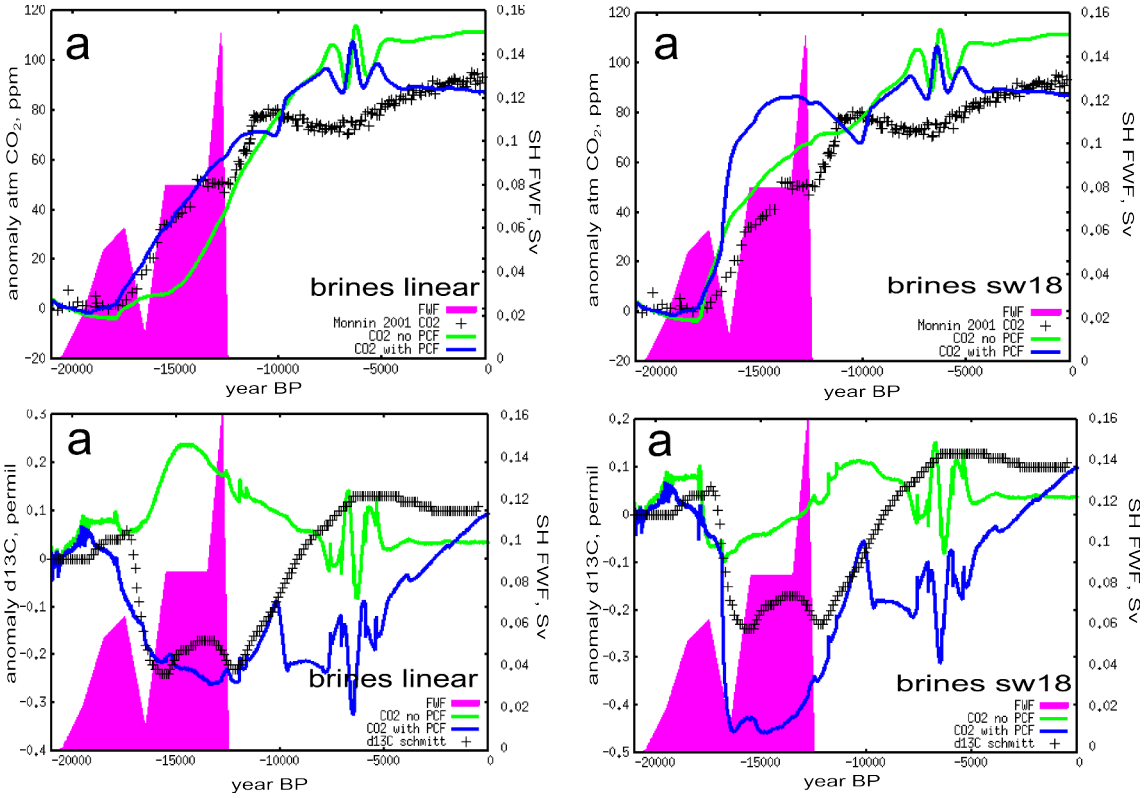

Fig 6, SH forcing a) profile outputs comparing model with (blue) and without (green) permafrost for left: linear brines. Right: brines switch-off at 18kyrBP.

Adjusting the model mechanisms and settings resulted in significant changes in CO_2 output for the same forcings applied. In experiments without permafrost-carbon, but with linear brines, the CO_2 record lagged data except when a very large FWF forcing was applied before 17kyrBP then ceased. This is similar to the standard view of the causes of CO_2 rise at the start of the termination period, where AMOC switch-off plays an important role during H1 and all carbon release comes from the ocean. When the brines setting is a sudden switch-off at 18kyrBP, the CO_2 overshoots the data at the onset of CO_2 rise and particularly just before the Bolling-Allerod for both a high FWF forcing around H1 or a relatively low forcing, not causing AMOC switch-off. In the SH forcing and mechanisms experiment (figure 4 and figure 6), the adjustments made do not show a higher sensitivity to the ceasing in FWF like NH experiment outputs show. It suggests that by adjusting the brines controller and the FWF forcing at H1, the onset of CO_2 rise, the model may be able to reproduce data. The more realistic scenario, where forcing occurs both in the northern and southern hemisphere, should be tested for in future studies. This is because AMOC response is sensitive to forcing in both hemispheres.